University of Nottingham
UK | CHINA | MALAYSIA

Novel complementation biosensors to investigate G protein-coupled receptor kinetics and signalling bias.

Nicola C Dijon, MSci (Hons)

Thesis submitted to the University of Nottingham for the degree of Doctor of Philosophy

March 2022

UKRI Biotechnology and Biological Sciences Research Council

COMPARE
CENTRE OF MEMBRANE PROTEINS AND RECEPTORS

Declaration of Own Work

This thesis is entirely the candidate's own work. The experiments described in this thesis were performed by the author between October 2017 and August 2021 in the Cell Signalling Research Group at the Centre of Membrane Proteins and Receptors, University of Nottingham, UK. No part of this material has been submitted previously for a degree or any other qualification at any University.

i. Abstract

G protein coupled receptors (GPCRs) signal through a complex cellular network, with a range of temporally variable signalling responses generated by GPCR activation. Characterisation of GPCR ligands is generally taken from the ligand "affinity", the ability to bind the receptor, and the ligand "efficacy", the ability to activate signalling from the receptor. Often single timepoints are used to quantify ligand affinity and efficacy by being applied to pharmacological models. Biased ligands, which have been suggested to preferentially activate one signalling pathway over another, are often identified from comparisons of concentration response data of an agonist between single timepoints of assays measuring the activation of different signalling proteins. Existing pharmacological models, which estimate ligand potencies, efficacies and ligand bias, such as the Black and Leff operational model, from functional data assume system equilibrium, yet often concentration response data at early timepoints are taken from hemi-equilibrium conditions. More recently, appreciation of agonist binding kinetics and signalling kinetics at GPCRs has increased, enhancing the extent of ligand characterisation and used to investigate discrepancies in ligand bias between different experimental systems. The origin of ligand bias has been suggested to be conformational, where the agonist binds the receptor to allosterically promote the formation of a conformation which preferentially activates one signalling pathway over another. It has also been suggested that bias originates from different receptor binding kinetics, which produce different profiles of signalling and can confound comparisons of bias – especially when bias is compared from a single timepoint. In this thesis we investigate how signalling kinetics and binding kinetics can influence measures of ligand affinities, efficacy and bias using experimental system monitoring dynamic protein:protein and ligand-receptor interactions.

Firstly, we established a NanoBiT complementation assay to monitor agonist-stimulated recruitment of effector proteins, either β-arrestin2 or a synthetic mini Gαs protein, at β adrenoceptor subtypes. Recruitment profiles of β-arrestin2 recruitment produced a transient "rise and fall to plateau" profile, peaking at 3 minutes, whilst the mini Gαs protein was recruited to the receptor rapidly in the first 1-5 minutes and then plateaued and/or steadily increased over the timecourse. This experimental system allowed for dynamic agonist-stimulated recruitment profiles to be monitored over time and concentration response data to be gathered from multiple timepoints. Concentration response data from each

timepoint was then applied to the Black and Leff operational models to compare how direct comparisons of ligand bias can change in magnitude and direction over time. Full kinetic signalling profiles were then applied to a kinetic operational model, which takes hemi-equilibrium conditions into account, to estimate agonist affinities and efficacies from β-arrestin2 recruitment data. Agonist affinities estimated from the kinetic operational model were strongly correlated with values obtained in a time-resolved fluorescence resonance energy transfer (TR-FRET) binding assays, highlighting the model's value in obtaining drug potency and affinity from a single functional recruitment assay.

Secondly, we investigated the value of the NanoBiT complementation assays in monitoring receptor antagonism and how the kinetic context may misrepresent the mechanism of action of the antagonist ligands: propranolol, ICI-118,551 and CGP-12177. Schild-Gaddum based experiments were applied and monitored over a 61 minute timecourse, at β_2 adrenoceptors. All antagonists at early timepoints (3 minutes) produced insurmountable antagonism of the formoterol response, with only propranolol demonstrating surmountable antagonism at 61 minutes. The extent of insurmountability correlated with a decreased dissociation rate (k_{OFF}) of the antagonist, with k_{OFF} estimated from a kinetic TR-FRET assay. The signalling profiles of antagonism of mini Gαs protein recruitment at the β_2 adrenoceptor were applied to an antagonist form of the kinetic operational model, to provide similar estimates of antagonist affinity in comparison to values obtained in Schild-based and TR-FRET assays. The kinetic operational model also provided estimates of antagonist association (k_{ON}) and k_{OFF}, though these were not comparable to estimates from the kinetic TR-FRET assay and highlight the need for model modification for accurate estimates of kinetic values.

Lastly, this thesis investigated how the conformation of the receptor can influence binding properties of β_2 adrenoceptor ligands. High affinity variants of the NanoBiT complementation fragments (LgBiT and HiBiT) were used to stabilise the β_2 adrenoceptor in complex with an effector protein to form effector driven receptor conformations. Initially, high affinity NanoBiT fragments were genetically tagged to the β_2 adrenoceptor and either β-arrestin2 or mini Gαs and expressed in dual-expression cell lines. However, unbalanced expression of the proteins resulted in insufficient formation of NanoBiT stabilised receptor-effector conformations. To resolve this issue, the HiBiT-tagged mini Gαs protein was bacterially expressed and purified and added to membranes expressing LgBiT-tagged β_2 adrenoceptors, saturating the receptor population. The complimented

NanoBiT fragments were used as the donor species to excite an extracellular fluorescent ligand bound to the receptor, to establish a novel transmembrane bioluminescence resonance energy transfer (TM-BRET) assay. In TM-BRET assays, β_2 adrenoceptor-mini Gαs protein "high affinity" conformations were shown to have increase affinity for agonist ligands, compared to the receptor alone, whilst antagonist ligands were unchanged. Kinetic TR-FRET assays were used to monitor the kinetic binding properties of β_2 adrenoceptor ligands and demonstrated that the increase in agonist affinity at receptor-mini Gαs protein complexes was driven by a decrease in agonist k_{OFF} and that the extent of the decrease in k_{OFF} rate was correlated with ligand efficacy.

The findings presented in this thesis highlight the value of kinetic signalling data and binding kinetics in assessing ligand pharmacology, including measures of ligand bias. This thesis went onto to highlight how differences in receptor conformation drive changes in agonist k_{OFF}, combining conformational and kinetic explanations of ligand bias.

ii. Publications Arising from Doctoral Studies

Publications

- Dijon, N. C., Nesheva, D. N., & Holliday, N. D. (2021). Luciferase Complementation Approaches to Measure GPCR Signaling Kinetics and Bias. In G Protein-Coupled Receptor Screening Assays (pp. 249-274). Humana, New York, NY.
- Hoare, B. L., Kaur, A., Dijon, N. C., Holliday, N. D., Sykes, D. A., & Veprintsev, D. (2020). Measurement of non-purified GPCR thermostability using the homogenous ThermoBRET assay. bioRxiv.
- Dijon, N., Holliday, N., & Charlton, S. (2020). Investigating the Kinetics of β_1 and β_2 Adrenoceptor Effector Recruitment using Luciferase Complementation Assays. The FASEB Journal, 34(S1), 1-1.

Conference Proceedings

- Dijon NC, Holliday ND, Charlton SJ (2020) Use of a kinetic operational model to predict binding affinities from functional data at β_1 and β_2 adrenoceptors.
  (Oral Communication at Pharmacology 2020, Virtual Conference)
- Dijon NC, Holliday ND, Charlton SJ (2020) Use of a kinetic operational model to predict binding affinities from functional data at β_1 and β_2 adrenoceptors.
  (Oral Communication at GDR3545 GPCR 2020, Virtual Conference)
- Dijon NC, Lockington H, Charlton SJ, Holliday ND (2019) Investigating the relationship between binding kinetics and antagonist action at the β_2 adrenoceptor, using luciferase complementation effector recruitment assays.
  (Oral Communication at Pharmacology 2019, Edinburgh, UK)
- Dijon NC, Holliday ND, Charlton SJ (2018) Real time kinetic analysis of β_2 adrenoceptor "mini" G and arrestin recruitment, using NanoBiT® luciferase complementation.
  (Oral Communication at Pharmacology 2018, London, UK)
- Dijon NC, Holliday ND, Charlton SJ (2018) Using NanoBiT luciferase complementation in real-time kinetic monitoring of effector recruitment.
  (Poster presentation at ELRIG: Drug Discovery 2018, London, UK)
- Dijon NC, Nesheva DN, Holliday ND (2018) Real-time kinetic analysis of β_2 adrenoceptor β-arrestin2 recruitment using NanoBiT luciferase complementation.
  (Poster presentation at 7th BPS Focused Meeting on Cell Signalling, Nottingham, UK)

iii. Acknowledgments

"You can tell a lot about a place by how they treat their people"

-Amos, Leviathan Wakes.

I would like to start by thanking my PhD supervisors - Nicholas Holliday and Steven Charlton – for a fantastic four years of research and general fun in their lab groups. Their endless enthusiasm for the project and continued support – even when I tried to convince them that "it's not nothing" when I first got the TM-BRET working! I want to specifically thank Nick for dealing with the occasional moments of hysteria and for his patience when I decide that my work load should be a little bit more than is wise. Whilst I occasionally lose confidence in myself, I know I can count on you to tell me that I am where I'm supposed to be and to keep going.

The quote above symbolises how I feel about the cell signalling research group at the University Of Nottingham. I have always felt valued ever since coming into the group as an undergraduate student back in 2015 and have always felt welcome and part of the team. People who come and go through the research group comment on how special a place it is to work and I believe it is because there is a true culture of scientific passion, an excellent sense of humour, a well-placed lunch time crossword and complete respect for everyone in the lab. Whilst I could continue for a few more pages, this thesis is quite long enough, so I just want to specially thank: June McCulloch (come back June!) and Marleen Groenen for maintenance of the lab; Tim, Seema and the SLIM team, for helping me understand there is more to microscopy than calling the Ultra a "magic box"; and all the PI's who are always willing to give you time, whether it's to discuss your latest findings in the lab or to talk about the terrible central heating system. During my PhD I have had the privilege to train other students, with special thanks to Hannah Lockington, who at the time made me think I was an excellent teacher but now I have since learned she is simply just brilliant by nature! During my PhD I have made life-long friends and would like to thank every one of them, including: Chloe, Jack, Lydia, Clare, Charlie, Eddy, James, Sean, Joelle, Laura (both Kilpatrick and Humphrys), Rick, Leigh, Mark, Liz, (Call me) Al, Brad, Birgit, Noemi, George, Hannah, Marieke, Patrizia and everyone else who I may have missed! A special mention to Desi, with whom I completed my PhD in parallel

with in Nick and Steve's lab groups – I don't believe I would have made it without your cutting wit, laughter and incredible belief in me over the last four years!

I would like to thank Clare Harwood and the Dmitry Veprintsev lab for training and access to facilities to allow for expression and purification of HiBiT-mini Gαs protein.

I would also like to thank everyone at OMass Therapuetics for an excellent 3 month placement. In particular I would like to thank Jason and Paarth for their teachings, both in protein engineering and mass spectrometry. I also want to thank Paarth, Kiran and Fernando for the laughter and fun!

I would like to thank the BBSRC for the funding to complete my doctoral studies, as well as the Researcher Academy and Biochemical Society for awarding me travel grants to travel internationally to present my PhD findings.

I want to thank my loved ones. To my parents, you have provided me with nothing else other than loving support and encouragement throughout my education – even at the moment you realised I wasn't going to be an accountant! Even when I'm on my own, I have felt your support and through you I can always find a little bit of confidence tucked away somewhere. I dedicate my PhD and all my accomplishments to you both. I want to thank my sister, Ashleigh, who I can always rely on to vent and laugh with, as well as giving me a beautiful niece who, despite a rocky start, seems to finally quite like her Aunty "Ninni". I would lastly like to thank Ruud, who provided me with years of laughter and fun during our PhD's and I couldn't have imagined finishing without.

Hannah Lockington contributed replicates to the antagonist NanoBiT and TR-FRET assays in *Chapter 4*, through a summer studentship funded by the British Pharmacological Society.

iv. Abbreviations

AC	-	Adenylyl Cyclase
βAR	-	β Adrenoceptor
BRET	-	Bioluminescence Resonance Energy Transfer
BSA	-	Bovine Serum Albumin
cAMP	-	Adenosine-3',5' cyclic monophosphate
CHO	-	Chinese Hamster Ovary
DMEM	-	Dulbecco's modified Eagle's medium
DMSO	-	Dimethyl Sulphoxide
ECL	-	Extracellular Loop
ERK 1/2	-	Extracellular Regulated Kinase ½
FCS	-	Foetal Calf Serum
FRET	-	Förster (or Fluorescence) Resonance Energy Transfer
GDP	-	Guanosine 5'-diphosphate
GPCR	-	G Protein Coupled Receptor
GTP	-	Guanosine 5'-triphosphate
HanksBSS	-	Hank's Balanced Salt Solution
HEK	-	Human Embryonic Kidney
HepesBSS	-	Hepes Buffered Saline Solution
ICL	-	Intracellular Loop
kOM	-	Kinetic Operational Model
NSB	-	Non-Specific Binding
OM	-	Operational Model
PBS	-	Phosphate Buffered Saline
PCR	-	Polymerase Chain Reaction
PKA	-	Protein Kinase A
PKC	-	Protein Kinase C
RLU	-	Raw Luminescence Units
Rmax	-	Relative Maximal Response
Tb	-	Terbium
TCM	-	Ternary complex model
TM	-	Transmembrane Domain
TR-FRET	-	Time-Resolved FRET
TM-BRET	-	Transmembrane BRET

Contents

Chapter One:

General Introduction

1.1. Receptor Theory and G Protein-Coupled Receptors

1.1.1. Introduction to GPCRs and Ligand Pharmacology

Proteins spanning the plasma membrane of mammalian cells govern cellular communication from extracellular compartments and activate complex co-operating pathways within the cell, altering functions such as cyclic AMP production, calcium ion release and gene transcription (Pierce *et al.*, 2002; Ritter and Hall, 2009). A major family of such proteins is the G protein-coupled receptors (GPCRs).

GPCRs, also known as seven transmembrane (TM) proteins, transduce signalling from extracellular ligands including hormones, neurotransmitters and peptides (Ritter and Hall, 2009). GPCRs exist as several classes, categorised by their structural homology: class A, class B, class C, adhesion and frizzled receptors. The largest family is the class A GPCRs, which include rhodopsin receptors and adrenoceptors, each with binding sites formed within the transmembrane domains or at the extracellular surface, generated by the counter clockwise clustering of the transmembrane domain helices (Hilger *et al.*, 2018a).

At a basic level as receptors, GPCRs act as molecular switches, with the drug (D) and receptor (R) existing in a dynamic equilibrium, between unbound, inactive and active states (see below):

$$\underset{Unbound}{D + R} \leftrightharpoons \underset{Inactive}{DR} \leftrightharpoons \underset{Active}{DR^*}$$

Equation 1. 1

GPCR ligands may be defined by where they bind the receptor, either binding at the orthosteric site, which is typically the binding site for the native ligand, or the allosteric site, which is a site distinct from the orthosteric site. How well the drug can bind to a site of the receptor ($D + R \leftrightharpoons DR$) is known its "affinity", whilst the ability of the drug, once bound, to activate the receptor ($DR \leftrightharpoons DR^*$) is known as its (intrinsic) efficacy. The efficacy of a GPCR ligand is often described as how well it can activate secondary messenger effector proteins, including G proteins and arrestins.

Drug-receptor affinity is dependent upon the forward ($D + R \rightarrow DR$) and reverse ($DR \rightarrow D + R$) rates of interaction, which when described by the the law of mass action define association (k_{ON}) and dissociation (k_{OFF}) binding rate constants, respectively. At dynamic equilibrium, the forward and reverse rates of binding are equal and the affinity of the drug for the receptor can be represented by K_D, the equilibrium dissociation constant, which represents the ratio of rate constants (k_{OFF} / k_{ON}):

$$When\ k_{ON}\ ([DR]) = k_{OFF}\ ([D][R]),$$

$$K_D = \frac{k_{OFF}}{k_{ON}} = \frac{[D][R]}{[DR]}$$

Equation 1.2

K_D is related to the proportional receptor occupancy (alpha, α) and the drug concentration, as described by the Hill-Langmuir equation (Hill, 1909, 1910):

$$\alpha = \frac{[D]}{[D] + K_D}$$

Equation 1.3

When the K_D is equal to the concentration of the drug [D], the proportional receptor occupancy is 0.5, thus K_D may also be defined as the concentration of the drug to occupy 50% of receptors. K_D, is therefore the fundamental measure of how well a drug binds the receptor (affinity) within drug discovery. Its accurate measurement revolves around an assumption of equilibrium and for example, an understanding of the binding mode of action (e.g. competitive reversible interactions). Increasingly, the binding kinetic constants (i.e. k_{ON}, k_{OFF}) have also been recognised as important indicators of drug properties, for example slow dissociation rates can increase duration of action or change the observed mode of action (Vauquelin and Charlton, 2010; Sykes *et al.*, 2016). The importance of kinetics will be discussed further in *1. 5*, *Chapter 5* and *Chapter 6*.

As above, GPCR ligands can also be categorised by their ability to have an effect on the receptor – efficacy to either activate or inhibit signalling. Ligands binding at the orthosteric site to activate the receptor are known as agonists. Agonists can be described as full agonists when producing a maximal signalling response, whilst partial agonists produce a lower maximal response when compared to a full agonist, despite having full receptor occupancy

(*Figure 1. 1*). Ligands which bind the receptor but do not affect the receptor signalling may be antagonists, which block agonist signalling by directly competing for the same binding site or an allosteric location (discussed further in *Chapter 4*). Finally, inverse agonists stabilise the inactive conformation (R) of the receptor and so yield the opposite effect to agonists, typically by supressing spontaneous agonist-independent signalling by basal conversion of the receptor to R* (Figure 1. 1) (Norris *et al.*, 2013). Since they often compete for the same binding site as the agonist drug, they can also have antagonist properties.

Unlike affinity, the efficacy of a drug-receptor interaction is often more difficult to quantify. Whilst, the two state model set forward by del Castillo and Katz (1967) simply describes the activation of DR complexes, such discreet parameters are difficult to define experimentally and are often measured from functional downstream signalling events (del Castilo and Katz, 1957; Stott *et al.*, 2016). For example, the potency and relative maximal response of an agonist drug are both influenced by its intrinsic efficacy but are not direct measures of it. The functional response observed from drug-receptor activation ($DR \rightarrow DR^*$) may be amplified and not require full receptor occupancy to reach the maximal functional response. Under these circumstances the agonist potency (EC_{50}; the concentration of drug required for 50% maximal response), will be lower than the measured K_D in the same conditions (concentration of drug for 50 % receptor occupancy), and the system is said to have *receptor reserve* for that agonist (*Figure 1. 2*). This also means that agonists with lower intrinsic efficacy may not always be observed as partial agonists. Partial agonists may also appear as full agonists if there is sufficient signal amplification from the initial signal generated by an agonist, often by the activation of multiple downstream signalling proteins by a single activated receptor or intermediate effector protein.

1.2. Ligand Binding and Signalling Pathways at GPCRs

1.2.1. Structure of and Binding at GPCRs

Structurally, GPCRs consist of seven TM α-helical domains, spanning the plasma membrane, and are connected by intracellular and extracellular loops (ICL and ECL, respectively). The protein amino terminal (N-terminal) is located extracellularly and the carboxyl terminal (C-terminal) is located intracellularly, with the transmembrane helices collected in a cylindrical bundle in an anti-clockwise fashion (Lee *et al.*, 2015). Class A GPCRs

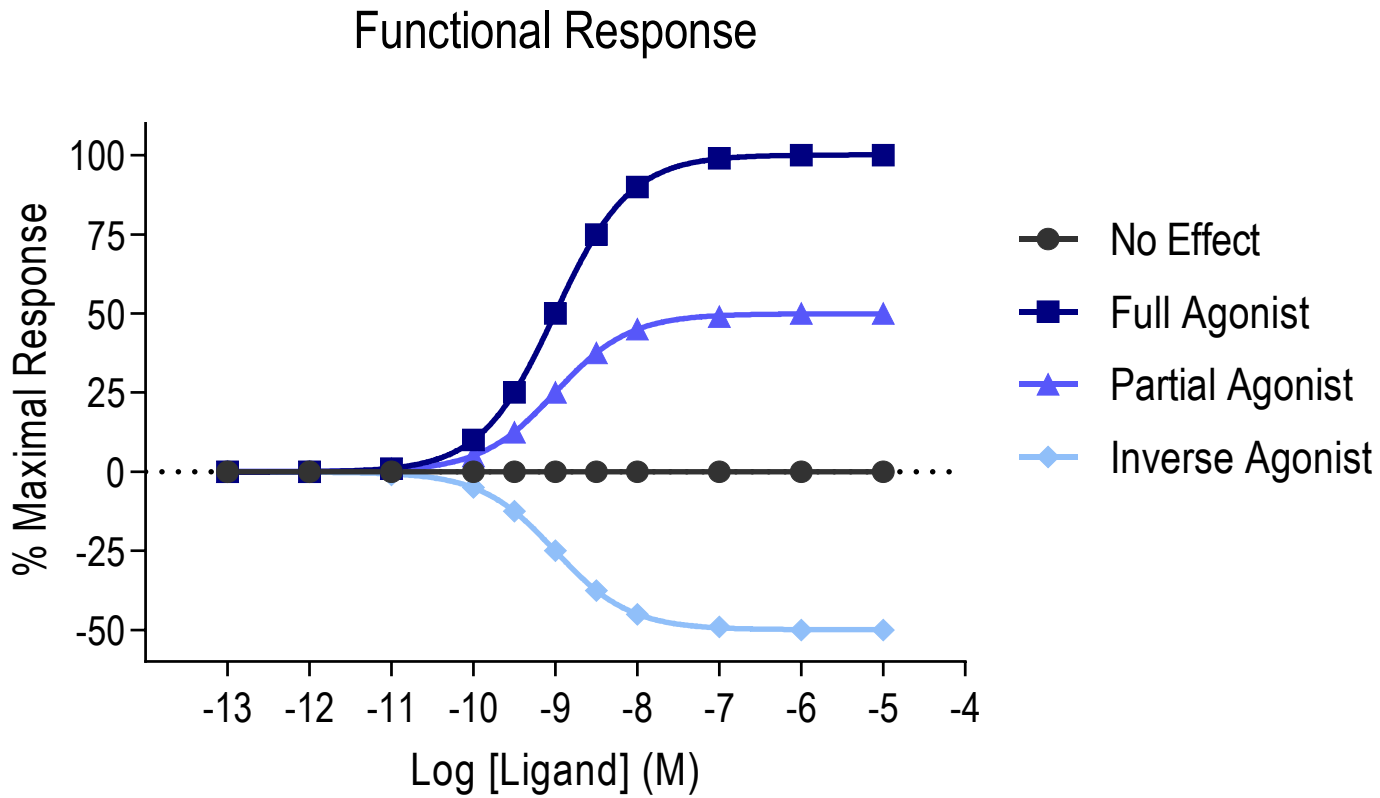

Figure 1. 1 Measures of Ligand Agonism. *Ligand dependent GPCR activation results in a functional response. The magnitude of response defines whether it is a full, partial or inverse agonist. As the concentration of ligand increases, as does the functional response, producing a dose response curve.*

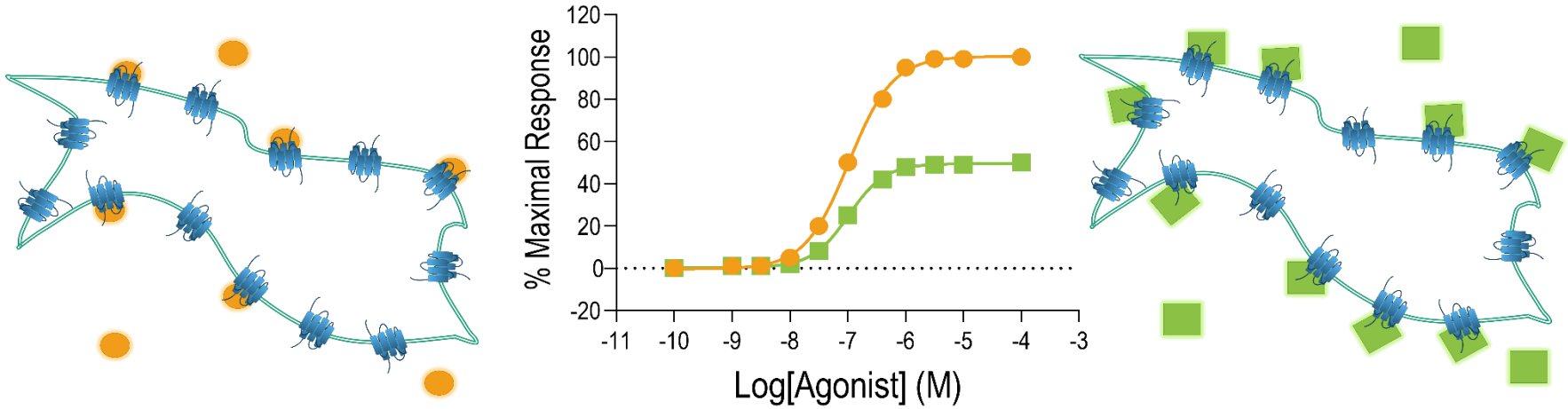

Figure 1. 2 Receptor reserve in GPCRs. *Receptor reserve describes when an agonist ligand (orange circles, above) only needs to bind and activate a small portion of receptors to produce the maximal response the system allows, whilst other agonists (green squares, above) require increased receptor occupancy to produce the maximal or a partial system response, i.e. there are no "spare receptors/receptor reserve".*

are often further characterised by an additional eighth helix which runs parallel to the plasma membrane and forms part of the C-terminus. The orthosteric binding site is generally found in the pore of the GPCR, within the extracellular half of the TM helices though the exact location is receptor-specific. The orthosteric ligand binding region and extracellular loops are the most structurally variable regions of the receptor, to allow for specificity of ligand interactions and receptor activation (Rosenbaum *et al.*, 2009). For example, whilst ECL2 of the rhodopsin receptor is formed of a short β-sheet secondary structure, ECL2 in β adrenoceptor subtypes consists of a short α-helix (Cherezov *et al.*, 2007; Rosenbaum *et al.*, 2007). To access the orthosteric binding site of class A GPCRs, ligands must traverse through ECLs and the extracellular vestibule and into the binding pocket (Dror *et al.*, 2011). Both the receptor and the ligands are required to dehydrate, displacing water molecules and allow contacts to occur between the ligand and the receptor (Dror *et al.*, 2011).

1.2.2. Ligand Activation of GPCRs

Orthosteric agonist binding at a class A GPCR commonly consists of ligand interactions with residues at the extracellular end of transmembrane helix (TM) 3, TM6 and TM7, with further receptor selective interactions with other TM residues (Lee *et al.*, 2015). Agonist engagement promotes the inward movement of extracellular regions of the TM domains, the rotation and outward movement of the intracellular ends and rearrangement of the intracellular G protein interface. Many Class A GPCRs have highly conserved regions and share common structural rearrangements during receptor activation (Venkatakrishnan *et al.*, 2016). The highly conserved TM6 proline residue (Pro^{6x50}) (Ballesteros–Weinstein numbering scheme; defining the amino acid, i.e. Pro=proline; transmembrane domain, i.e. ^{6}= TM6; and position, i.e. ^{x50}= position 50 of the TM6) is thought to act as a "toggle switch", as to allow for the inward movement of the extracellular end of TM6 and the outward movement of the intracellular region to allow access for G protein binding (Schwartz *et al.*, 2006). This has since been observed in active class A GPCR crystal structures (Rasmussen *et al.*, 2011; Carpenter *et al.*, 2016). The Pro^{6x50} forms part of the CWxP TM6 highly conserved motif, with Trp^{6x48} engaging with TM3 residues through inter-helical (π-π) bonds of the aromatic rings to stabilise the active conformation (Tehan *et al.*, 2014). A comprehensive comparison of inactive and active structures of 5 class A GPCRs by Venkatakrishnan *et al.* (2016)

identified common structural reorganisation of 3 residue contacts in TM3^{3x46}, TM6^{6x37} and TM7^{7x53}, all of which are close to the G protein binding interface and were consistently identified to be rearranged by receptor coupling to a range of receptor agonists. Activation and rearrangement of the receptor exposes previously inaccessible residues at the G protein binding interface and allow for G protein access. Ligand binding triggers the TM3^{3x46} residue to disengage from TM6^{6x37} and forms a new TM3-TM7 interaction with the highly conserved tyrosine residue at TM7^{7x53}, located in a highly conserved TM7 NPxxY motif. The movement of the TM6 outward allows for the 3x46/7x53 interaction by decreasing the distance between the residues compared to inactive state structures. The NPxxY motif is integral in maintaining a hydrophobic barrier around the E/DRY motif, the CWxP and the G protein – 'locking' the inactive receptor conformation. However, upon disruption, a hydrogen bond network may form and promote receptor activation and G protein binding (Trzaskowski *et al.*, 2012).

One of the most highly conserved motifs within peptide sequences of GPCRs is the E/DRY motif in the intracellular end of TM3 (Rovati *et al.*, 2017). Residue interactions of the motif were initially thought to stabilise the inactive conformation of the class A GPCRs, through intra-helical contacts with TM6 residues. Specifically, the salt bridge formed between Arg^{3x50} and Glu^{6x30} was thought to form an "ionic lock" between helices and was supported by mutation studies in GPCRs including the β_2 and the α_{1B} adrenoceptors (Scheer *et al.*, 1996; Rasmussen *et al.*, 1999; Ballesteros *et al.*, 2001). During activation, this lock is broken by TM3 movement with evidence that the acidic Glu/Asp^{3x49} is protonated (Sandova*l et al*, 2016). However the precise nature of the TM3 – TM6 ionic lock is not universal throughout class A GPCRs, with the lack of an acidic residue at the 6x30 residue and hydrogen bonding with alternative receptor regions (e.g. ICL2) in place of the TM6 salt bridge observed in some crystal structures (Rosenbaum *et al.*, 2007; Eddy *et al.*, 2016).

1.2.3. G protein Structure, Binding and Activation

As the activated agonist-GPCR complex undergoes this conformational change, heterotrimeric G proteins bind, existing as a complex of three subunits- α, β and γ. The Gα subunit consists of 2 domains: the Ras-like GTPase (GTPase) domain and the α-helical (αH) domain (Sprang, 1997; Oldham and Hamm, 2008). The GTPase domain is structurally composed of 5

α helices (α1- α5) and a 6-stranded β sheet, whilst the αH domain has 6 α-helices.

When bound to guanosine diphosphate (GDP), the Gα subunit binds the Gβγ dimer to form the inactive heterotrimeric complex which binds the receptor (*Figure 1. 3*) (Higashijima *et al.*, 1987; Hilger *et al.*, 2018). Our understanding of G protein binding has been advanced significantly by solving crystal structures of both inactive GPCRs and also some active GPCR structures bound to both ligands and G proteins or a G protein mimetic (Rasmussen, *et al*, 2011; Steyaert and Kobilka, 2011; Carpenter and Tate, 2017; García-Nafría, *et al*, 2018). Further analysis of active state GPCRs reveal the majority of G protein binding occurs through residues located in α5 of the GTPase domain of the Gαs subunit, specifically at the intracellular G protein interface of the GPCR at residues in intracellular loops and in TM3, TM5 and TM6. In early receptor mutagenesis studies, mutation of key residues in these TM and ICL regions, and the C-terminal, changed the specificity for Gα subtype coupling, highlighting the importance of residues (Blin, *et al*, 1995; Altenba*ch et al*, 1996; Wess, 1998). Moreover, Flock *et al.,* (2015) suggest that the residues of the GTPase's α5 form conserved interactions to bind their cognate receptor and form a universal mode of binding. Variable residues of the α5 domain of the GTPase subunit, as well as further Gα protein residues at receptor interface regions, are suggested to be important for selective coupling of different subtypes of the Gα subunits such as Gαs, Gαi/o and Gαq in mutagenesis studies (Flock *et al.*, 2015) and by using Gα chimera proteins were used to "swap in" the α5 (Conklin *et al.*, 1993; Mody *et al.*, 2000; Kostenis, *et al,* 2005; Okashah *et al.*, 2019).

Upon binding to the receptor, the Gα protein itself undergoes a rearrangement of conserved residues, with disengagement of intra-Gα residues contacts between residues in the α5 helix and the α1 helix in the GTPase domain; to allow formation with contacts with the receptor (Chung *et al*, 2011; Rasmussen *et al*, 2011). When engaged with α5, α1 is suggested to be key in stabilising the inactive Gα structure specifically the contacts made with the Gα hinge region and GDP to promote the GDP bound form. When disengaged from α5, the loss of α1 stabilisation decreases GDP contacts, and thus GDP affinity, and increases the likelihood of the opening of the hinge region (Flock *et al.*, 2015). Key residues involved in Gα rearrangement are

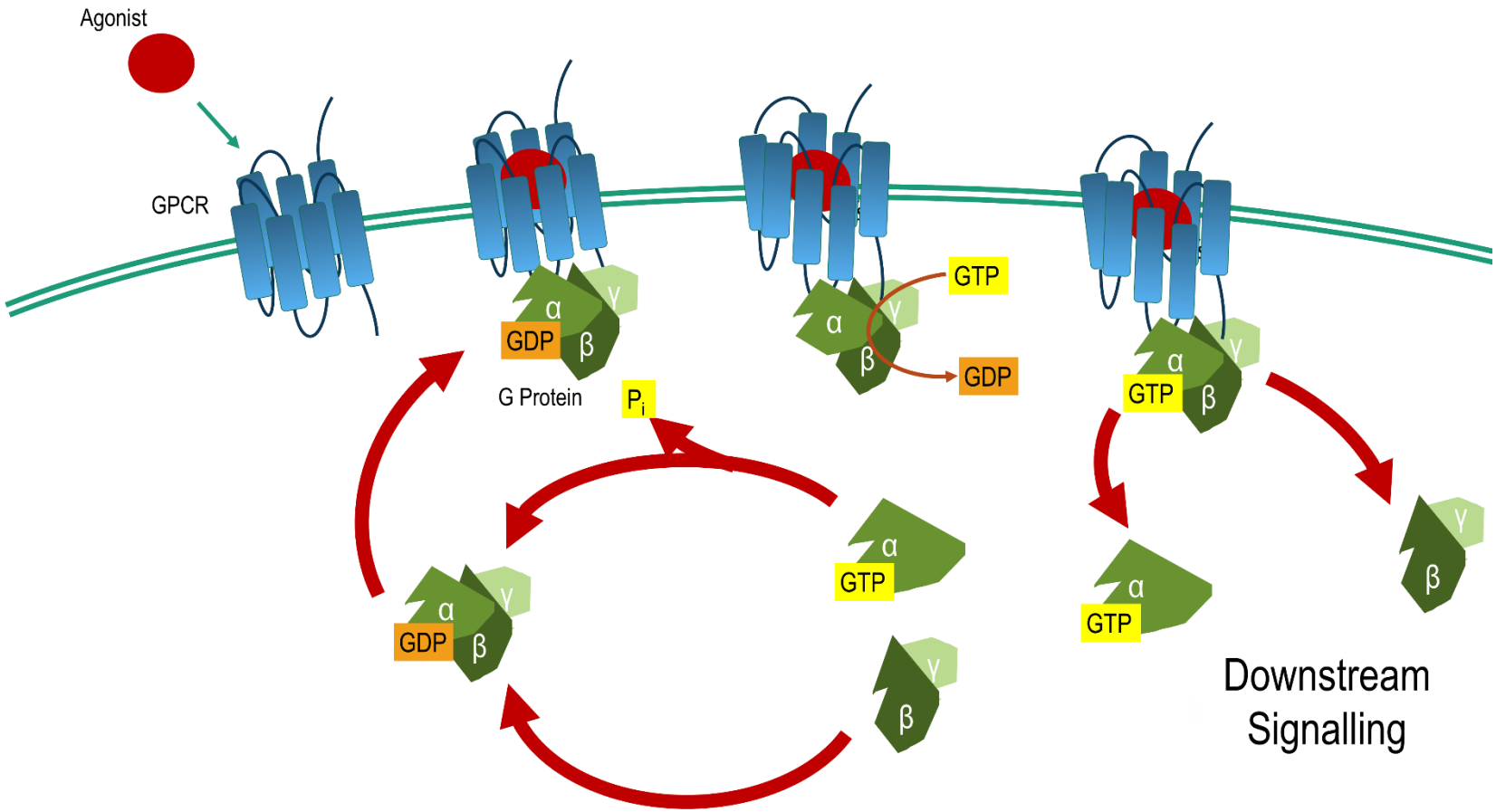

Figure 1. 3 Heterotrimeric G Protein Cycle. *G proteins exist as heterotrimeric complexes formed of α, β and γ gamma subunits, bound to GDP in their inactive conformation. When bound to a receptor, agonist binding initiates a conformational change to promote nucleotide exchange at the G protein interface – exchanging GDP for GTP. The GTP bound G protein then dissociates from the receptor, though still membrane bound though lipid modification, and initiates intracellular signalling pathways as either the Gβγ complex or the GTP-bound Gα subunit. Hydrolysis of GTP to GDP, releasing a phosphate, allows for the reformation of the GDP-bound Gαβγ complex, which can bind a GPCR and restart the cycle.*

highly conserved between Gα subtypes and thus likely to be a universal mechanism of Gα protein activation.

With the G protein coupled to the receptor, the Gα subunit acts as a site of nucleotide exchange, promoting the exchange of GDP for guanosine triphosphate (GTP) on the Gα subunit of the G protein, between the GTPase and αH domains (Noel *et al.*, 1990; Grishina and Berlot, 2000; Chung *et al.*, 2011; Eps *et al.,* 2011; Yao *et al.*, 2016; Gao *et al.*, 2017), and catalysing Gα dissociation from the receptor and Gβγ subunit. Several receptor-G protein residue contacts are thought to trigger GDP release from the G protein, including $TM6^{6x37}$ of the receptor which disengages from a hydrophobic residue at $TM3^{3x46}$ and forms a contact with the leucine residue in the H5 domain of the Gα protein, which is conserved across Gα subtypes (Flock *et al.*, 2015).

1.2.4. Canonical Signalling of Heterotrimeric G Proteins at GPCRs

Activated GTP-bound Gα and βγ subunits regulate downstream signalling molecules by interacting with secondary messengers such as adenylyl cyclase (AC) and phospholipase C (*Figure 1. 4*) (Ritter & Hall 2009; Capper & Wacker 2018).

The Gα subunit subtype dictates the signalling potential, with 21 different Gα subunits identified including Gαs, Gαi and Gαq families (Simon, *et al.,* 1991; Robishaw and Berlot, 2004; Oldham and Hamm, 2006; Khan *et al.*, 2013). The Gαs subtype, couples to such class A GPCRs, such as β_2 adrenoceptors and the EP2 prostanoid receptor, activating membrane bound AC to increase cellular cyclic adenosine monophosphate (cAMP), whilst the Gαi/o family, which couples to GPCRs such as the D2 dopamine receptor, inhibits AC to decrease cellular cAMP. An increase in cellular cAMP-dependent protein kinase A (PKA) by binding to the regulatory PKA domains of an inactive tetramer, freeing the catalytic PKA domains to act on downstream targets (Taylor *et al.*, 2012). These include modulating the activity of key intracellular signalling molecules in the mitogen-activated protein (MAP) kinase cascade pathway (Goldsmith and Dhanasekaran, 2007). Activated PKA also acts to: regulate L-type Ca^{2+} voltage channels, in cardiac for β_1 adrenoceptor mediated contraction (Budde, *et al*, 2002); and activate myosin light chain phosphatase, for β_2 adrenoceptor mediated smooth muscle relaxation (Aslam *et al.*, 2010). As a feedback mechanism, activated PKA can inactivate AC isoforms or activate cyclic nucleotide phosphodiesterase (PDE) to breakdown cAMP – regulating cellular cAMP

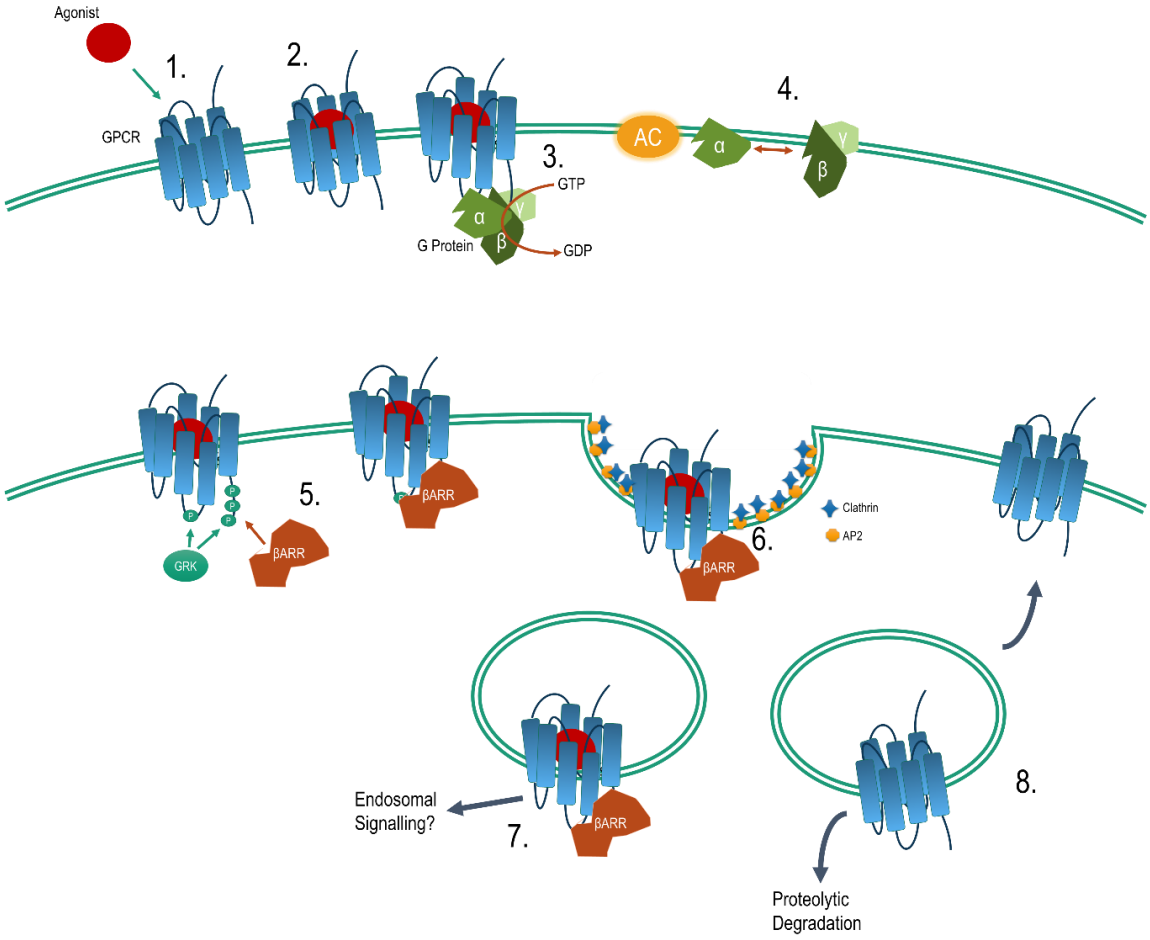

Figure 1. 4 Canonical GPCR Signalling and regulation through arrestin binding and intracellular trafficking. *GPCRs exist as membrane spanning proteins with binding domains accessible to extracellular ligands (1). Upon activation (2), GPCRs undergo a conformational change stabilising an active state to which heterotrimeric G proteins may bind and act as a site of guanine nucleotide exchange (GDP -> GTP) (3). Upon exchange, G protein subunits (αβγ) dissociate and activate other pathways via effectors such as adenylyl cyclase (AC) (4). Intracellular residues of the GPCR may be phosphorylated by G protein receptor kinases (GRKs), which then act as suitable substrates for beta arrestin (βARR) proteins (5). βARR association propagates clathrin and adaptor protein 2 (AP2) to be recruited and form clathrin coated pits to internalise the receptor (6). Once internalised, the ligand-GPCR-βARR has been proposed to continue to signal once in the endosome (7). Internalised ligand-GPCR-G protein complexes have also been suggested to have endosomal signalling (not illustrated above). Endosomal trafficking of the receptor will determine whether the receptor is recycled back to the plasma membrane or degraded by proteolytic enzymes (8).*

cAMP levels (Sassone-Corsi, 2012). In addition to PKA, cAMP may also signal through exchange proteins directly regulated by cAMP (EPAC) which binds cAMP and is associated with cellular functions including cell adhesion and formation of cell junctions (Cheng *et al.*, 2008). The Gαq subtype couples to phospholipase Cβ, increasing inositol 1,4,5-trisphosphate (IP3) generation and release of intracellular pools of calcium ($[Ca^{2+}]i$) (Campbell and Smrcka, 2018).

The Gβ and Gγ subunits each have 5 and 12 isoforms, respectively, and signal as a heterodimer, to modulate targets including phospholipase C and inwardly rectifying K^+ ion channels (Khan *et al.*, 2013). The Gβγ dimer interacts with effector proteins through a highly conserved sites located on the Gβ domain (Campbell and Smrcka, 2018). One such effector is G Protein-Coupled Receptor Kinase 2 (GRK2), which then selectively inhibits Gβγ signalling and acting as a negative feedback loop (Eckhart *et al.*, 2002; Bonacci *et al.*, 2006).

1.2.5. Mechanisms of Receptor Desensitisation

Following G protein activation and signalling, GPCRs may couple to further G proteins or to other intracellular effectors, such as GPCR phosphorylation by GPCR kinases (GRKs), arrestin proteins and subsequently recruit clathrin and clathrin adaptor proteins (AP2) (*Figure 1. 4*). Initially, GPCR phosphorylation was initially regarded to be conducted by second messenger dependent kinases, such as PKA and protein kinase C (PKC) (Benovic *et al.*, 1985), however observations of β_2 adrenoceptor phosphorylation in the absence of a functional PKA suggested that second messenger independent kinases may phosphorylate GPCRs (Benovic *et al.*, 1986; Strasser *et al*, 1986)– which resulted in the identification of GRKs.

Upon GPCR activation, GRKs are recruited to the receptor where phosphorylation of intracellular residues of the activated receptor occurs, most notably of C terminal and/or the third intracellular loop serine and threonine residues (Hilger, *et al*, 2018). There are 7 GRK subtypes (GRK1-7), which can be categorised further into: GRK1-like (GRK1 & GRK7), which are uniquely expressed in the rod and cone cells of the retina; GRK2-like (GRK2 & GRK3) which also bind Gβγ through a pleckstrin homology domain (Lodowski *et al*, 2006) and are ubiquitously expressed; and, GRK4-like (GRK,4, GRK5 & GRK6), which are located at the plasma membrane by lipid modification. Whilst the phosphorylation of receptor residues reduces GPCR signalling, it does not stop it entirely and requires recruitment of proteins known as arrestins to "switch off" the receptor (Irannejad & Von Zastrow 2014). The pattern and

extent of phosphoserine and phosphothreonine modifications by GRKs has been suggested to reflect the strength of the subsequent arrestin recruitment, with authors putting forward a 'barcoding' paradigm (Tobin, *et al,* 2008).

Arrestin proteins consist of 4 subtypes (arrestin 1-4), with the visual arrestins (arrestin1 and arrestin4) located in the retina (Black, *et al,* 2016). The non-visual arrestins (arrestin2 and arrestin3) also known as β-arrestin1 and β-arrestin2, respectively, are expressed ubiquitously and thought to not only block GPCR signalling but also facilitate receptor internalisation (Gurevich and Gurevich, 2019). The β-arrestin isoforms are thought to have some selectivity between different GPCRs and have different cellular localisations, with β-arrestin1 located in the nucleus and β-arrestin2 to the cytosol under basal conditions (Laporte and Scott, 2019). In addition, different receptors can produce different profiles of β-arrestin recruitment, i.e. transient, as seen in the β_2 adrenoceptor (Oakley *et al.*, 1999, 2000), or sustained, as seen at the histamine H1 receptor (Ma, *et al,* 2021). Arrestin proteins have been shown to require both active and phosphorylated GPCRs for high affinity binding (Gurevich and Gurevich, 2004), as demonstrated for both visual (Wilden, *et al,* 1986) and non-visual arrestins (Krasel *et al*, 2005).

Following recruitment to the receptor, β-arrestin isoforms bind clathrin and AP2, promoting targeting to clathrin coated pits and endocytic internalisation of the complex to endosomes (Tsvetanova, *et al,* 2015). The internalised clathrin coated pits are formed through a GTPase, dynamin, with the resultant vesicles directed to recycling or degradation pathways (Sorkin and Von Zastrow, 2009; Smith and Rajagopal, 2016). With desensitisation of receptors via arrestin binding and removal of the receptor from the membrane, continuing agonist presence no longer produces a functional response via G protein mechanisms (Williams, *et al*, 2013).

Relatively recent avenues of GPCR research have begun to focus on intracellular signalling from GPCR-arrestin associated endosomes. For some receptors, upon internalisation to early endosomes, ligand and arrestin dissociation occurs and receptors are sorted to determine either trafficking back to the membrane (resensitisation) or lysosomal facilitated proteolytic degradation (Jacobson, 2015). Under chronic administration, this leads to reductions in receptor expression and long-term drug tolerance. However, there are suggestions that some receptors, particularly Gαs coupled subtypes, exist in endosomes as both a ligand-receptor-arrestin complex (Wang, *et al*, 2018), as well as a postulated ligand-receptor-G protein-arrestin 'megaplex'

and may continue to signal from early endosomes (Thomsen, *et al,* 2016; Pavlos & Friedman 2017; Sposini & Hanyaloglu 2017).

1.2.6. β-arrestin Mediated Signalling at GPCRs

Whilst the role of arrestin proteins in the inactivation and desensitisation of receptors is well established, some studies have suggested that arrestin proteins themselves may be activated by the receptor and serve as cellular signalling proteins (Hanson *et al.*, 2006; Smith and Rajagopal, 2016; Peterson and Luttrell, 2017).

There is evidence that β-arrestin proteins may scaffold and signal through: extracellular signal-related kinases 1 and 2 (ERK1/2), as part of the MAP kinase pathway; and the c-Jun N-terminal kinase (JNK) (Smith and Rajagopal, 2016). Whilst the ERK1/2 signalling may also be driven by G protein activation, the spatiotemporal characteristics of β-arrestin mediated signalling are shown to be distinct. Moreover, G protein mediated ERK1/2 signalling has been shown to be transient and located at the nucleus, whilst β-arrestin mediated signalling generates a sustained response with a delayed initiation in the cytosol (Shenoy *et al.*, 2006). Binding to β-arrestin2 has also been observed at JNK3 as part of the signalling of MAP kinase kinase kinase and apoptosis signalling regulating kinase 1, demonstrating further involvement of arrestins as MAP kinase cascade scaffold (Zhan *et al.*, 2014).

However, whether β-arrestin signalling requires G protein activation is highly contested. Whilst many studies suggest that it is G protein independent (Luttrell *et al.*, 1999, 2018; Wei *et al.*, 2003; Charest *et al.*, 2007), O'Hayre *et al.*, (2017) and Grundmann *et al.*, (2018) both demonstrated that whilst arrestin proteins may be recruited to a receptor in the absence of G proteins, there was no activation of the ERK1/2 MAP kinase cascade. To add further complexity, the ERK1/2 MAP kinase cascade is a highly conserved sequence of signalling events and thus further consideration must be taken to understand signal initiation – whether this is G protein-dependent or G protein-independent is still not well understood (Gilbert, *et al,* 2021). Whilst the role of arrestin, more specifically β-arrestin, is not fully understood, the concept of G protein independent signalling provides a therapeutic opportunity to target specific cellular responses more selectively.

1.3. Biased Signalling at GPCRs

The concept that a single GPCR may activate G protein-independent pathways, or promiscuously activate more than one Gα subtype, provides an opportunity for ligands to activate one pathway to a greater extent than the other, in a way that is not solely explained by differences in agonist efficacy, or cellular / pathway context (for example signal amplification) – a phenomena known as biased signalling. Whilst the earliest papers identified bias between Gα subtypes (Mailman *et al*, 1998; Mottola *et al*, 2002), however the most common comparison, and the most experimental examples, come from biased signalling between G protein and β-arrestin signalling (Allen *et al*, 2011; Tschammer *et al*, 2011b; Liu *et al*, 2012; Soergel *et al*, 2014; Carr *et al*, 2016; Altarifi *et al*, 2017; Hayashi *et al*, 2018; McCorvy *et al*, 2018; Reyes-Alcaraz *et al*, 2018).

1.3.1. Theory of Biased Signalling and Therapeutic Potential

There has been considerable speculation on how biased signalling arises, with the general consensus that biased ligands form from specific functionally distinct activated receptor conformations which preferentially activate one pathway over another (*Figure 1. 5*). As described by the ternary complex theory (discussed below; *1. 4*), GPCR signalling is initiated by complexes formed of a ligand, a receptor and an intracellular transducer protein. Therefore both the ligand and the transducer can both bind the receptor and allosterically increase the affinity of the receptor for a specific transducer or ligand, respectively (De Lean, *et al,* 1980; Changeux and Edelstein, 2005; Kenakin, 2012; Smith, *et al,* 2018). Unlike the two-state "active and inactive" model put forward by del Castillo and Katz, (1957), conformational explanations of biased signalling suggest that distinct activated conformations of the ternary complex are stabilised to bias either ligand binding or transducer binding (Galandrin, *et al,* 2007; Kenakin, 2015). Beyond G protein vs β-arrestin bias, there are now further function responses in which ligand can be biased towards (Thompson *et al.*, 2015; Klein Herenbrink *et al.*, 2016), with further investigations of bias between different Gα subtypes (Mackenzie *et al.*, 2019).

Selectively controlling the signalling profile of drugs provides the potential to design drugs with reduced on-target side effects and increased efficacy at the required pathway in a clinical setting. However, there has been somewhat limited success in translation of ligand bias in *in vitro* and *in vivo*

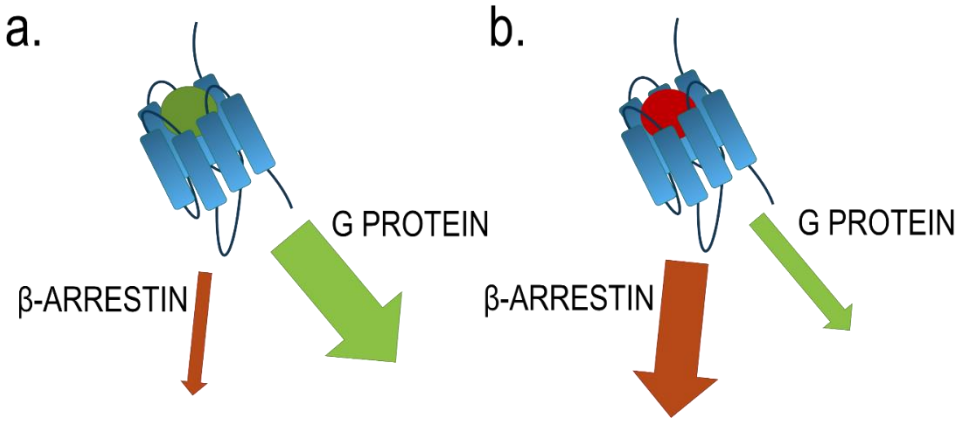

Figure 1. 5 GPCR Signalling Bias. *Activation of GPCRs may be bias toward different signalling pathways. Here, different ligands (green and red), preferentially activate either (a) G protein or (b) β arrestin mediated signalling pathways, respectively.*

studies and into clinical trials. For example, TRV-130 (oliceridine) was one of the first compounds to be suggested to show G protein bias at the mu opioid receptor, with high analgesic effects and reduced negative side effects (Chen *et al.*, 2013; DeWire *et al.*, 2013). However, in the repeated treatment of TRV-130 in mice, the adverse side effects, including respiratory depression and constipation, were still observed (Altarifi *et al.*, 2017). Further controversy of bias ligands at the mu opioid receptor has arisen from some suggesting that the side effects are not driven by β-arrestin dependent signalling (Gillis, *et al.*, 2020a), with Gillis, *et al.*, (2020b) suggesting the observed reductions in deleterious opioid side effects could be explained by partial agonism rather than signalling bias. However, such suggestions have been hotly contested by other studies, with Stahl and Bohn, (2021) suggesting poor cellular context and inappropriate analysis confounded finding from Gillis, *et al.*, (2020b) and Gillis, *et al.*, (2020a). It could be suggested that the recruitment of β-arrestin acts to shape the kinetics of the G protein signalling, through receptor desensitisation and receptor trafficking to the membrane or to cellular degradation. It is not still not fully understood if biased agonism results from true biased ligands or they simply reflect differences in agonist efficacy, which allow for different levels of pathway activation and thus place importance on using comparable cellular context when comparing activation of different signalling pathways.

1.3.2. Quantification of ligand bias using operational modelling

To estimate signalling from a receptor, a range of pharmacological models have been put forward, including Stephenson (Stephenson, 1956), Furchgott (Furchgott, 1966) and Black and Leff (Black and Leff, 1983; Black *et al.*, 1985), which all define a ligand by its affinity and its efficacy. Whilst affinity can be experimentally determined through the use of radioligand or fluorescent ligand binding assay, experimental estimation of efficacy is more difficult to quantify. Mechanistically, efficacy is the effect of a ligand to drive the inactive state to an active state, however in pharmacological models, due to limitations of what can be measured experimentally, efficacy parameters often try to the ligand's ability to produce an observed response (Stephenson, 1956; Smith, *et al,* 2018).

Whilst such models provide mathematical estimations of transducer signalling, there are important considerations when choosing the assays used to measure signalling and quantify ligand bias of each transducer protein. The first consideration is to use assays with similar levels of signal amplification, as

unbalanced assays may result in partial agonists appearing as full agonists in systems with high signal amplification. The second consideration is the use of a reference agonist, to correct for "system bias", generated by the efficiency of receptor-transducer coupling and stoichiometric hindrances, and "observational bias", generated by the individual experimenter and assay conditions (Kenakin and Christopoulos, 2012; Klein Herenbrink *et al.*, 2016; Rankovic, *et al*, 2016). Often the endogenous binding partner is used as the reference agonist, such as noradrenaline or adrenaline at β adrenoceptors. However, in some cases the native agonists may have reduced stability within the assay and a more chemically stable full agonist is used (Dijon, *et al,* 2021). For example, both adrenaline and noradrenaline oxidise quickly and thus isoprenaline is commonly used as the reference agonist at β adrenoceptors. By maintaining the same reference agonist between signalling assays, ligand bias is measured relative to the same agonist in different pathways. This correction aims to normalise for the effects of different coupling and amplification in each of the signalling cascades. A final consideration is whether there are kinetic effects significantly affecting measurements of ligand bias, which can be obscured based upon the ligand binding kinetics and the receptor signalling kinetics. Klein Herenbrink *et al.*, (2016) demonstrated that for dopamine D2 receptor assays, the direction and magnitude of bias for different ligands may change over time, because the system is not at equilibrium either for ligand binding at the receptor or signalling.

1.3.3. Black and Leff's Operational Model of Pharmacological Agonism

The original operational model of pharmacological agonism by Black and Leff, (1983), and then later extended by Black *et al.*, (1985), was generated from classical principles of pharmacology (*Figure 1. 6*) to analyse functional data and provide estimates of agonist affinity and an parameter describing agonist efficacy (τ). Unlike a concentration response curve defining agonist potency (EC50) and Rmax, the operational model relates an agonist response to its equilibrium dissociation constant for the receptor interaction (K_D but normally referred to as K_A in the model), and a transducer parameter (τ), with the latter reflecting both agonist efficacy at the receptor and the system coupling efficiency, for example governed by the extent of signal amplification and the receptor number (R_0). The maximum response of the system must also

$$(1) \qquad [AR] = \frac{[R_0][A]}{K_A + [A]}$$

$$(2) \qquad E = \frac{E_m\,[AR]}{K_E + [AR]}$$

$$(3) \qquad E = \frac{E_m\,\tau[A]}{K_A + [A](1 + \tau)}$$

Figure 1. 6 Derivation of the Black and Leff Operational Model from the Hill equation. *Equation (1) At equilibrium, when an agonist (A) binds to a receptor (R), the ratio of occupied receptors (AR) is based on agonist concertation ([A]), the total number of receptors (R0) and the agonist equilibrium constant (here described as K_A). Equation (2) To translate receptor occupancy by agonist (AR) to the pharmacological effect (E) a function was required, where the relationship between E and [AR] is assumed to be rectangular hyperbolic. With the K_E constant being [AR] when half of the maximal possible effect (Em). Equation (3). The Operational Model equation is a combination of equation (1) and equation (2) and the introduction of a transducer coefficient (τ, equal to R_0/K_E). (Black & Leff, 1983)*

be estimated in the fit (Emax), meaning that the operational model cannot be uniquely fitted to individual concentration response curves. A variety of approaches, including global fitting of multiple data sets have been used to address this (discussed further in *Chapter 3*; *3. 1. 5*. When considering bias between pathways, one option is to estimate transduction co-efficients (as the ratio Log τ/KA) for each agonist (within a pathway relative to a reference ligand (ΔLog τ/KA), with the aim to normalise the data for the system influences, as discussed above, – though this normalisation may be subject to discrepancies (Tschammer, *et al*, 2011; Szabo, *et al*, 2014; Klein Herenbrink, *et al*, 2016). Ligand bias is then reflected when there are pathway differences between these estimates (ΔΔLog τ/KA between pathways; either greater or less than 0).

The operational model utilises constants that assume equilibrium conditions (e.g. K_A) but have been widely applied in signalling bias investigations to assays conducted at often different time points where equilibrium has not been reached (Sengman*y et al*, 2017). As commented above, in their study on the D2 dopamine receptor, Klein Herenbrink et al (2016) demonstrated that measurements of bias via operational methods of change significantly based on the timepoint of the assay, particularly for ligands (such as aripiprazole) that have slow association kinetics.

1.3.4. Kinetic operational models

In recent years, there has been greater appreciation for how both binding and signalling kinetics can impact measures of affinity and efficacy. Mathematical models of GPCR activation and ligand bias have been proposed by both Woodroffe *et al* (2009) and Bridge *et al* (2018), which use simulations to determine kinetic influence on receptor signalling behaviour. However, such models require a thorough understanding of micro-parameters determining the complexities of GPCR signalling, feedback systems and the rates of each pathway that are difficult to determine experimentally (Gherbi *et al.*, 2020).

Applying a mathematical model to experimental data of GPCR signalling adds further complexities, as limited data is available to make estimates of required complex pathways or the sequence of activation steps between stimuli and functional response. One such model has been set forward by Hoare *et al.*, (2018), which uses the concept of Black and Leff's Operational Model as a basis to generate kinetic operational models to obtain equilibrium measures such as equilibrium dissociation constants (K_D) and a kinetic parameter of drug efficacy (discussed further in *Chapter 3* and *Chapter*

4). The kinetic operational models utilise kinetic signalling data to establish these parameters, though require assumptions of a rapidly equilibrating system and qualitatively choosing the model based on signalling profile, possibly introducing experimenter bias (discussed further: *Chapter 3* and *Chapter 4*).

1.4. The Ternary Complex Model

The activation of GPCRs and thus the conversion of the inactive "*DR*" complex to the "*DR**", is thought to rely on a conformational change of the complex (del Castillo and Katz, 1957). However, when receptor theory is applied to the GPCR superfamily, a further requirement is to incorporate the recruitment of intracellular effectors to the receptor by agonists. Whereby, agonist-bound GPCRs stabilise effector binding allosterically, while equally the presence of an effector bound to the receptor stabilises agonist binding and can increase its affinity. This three-way interaction, at equilibrium, is described by the 'ternary complex model' (De Lean et al. 1980) (*Figure 1. 7. a*), building on the classical two state model (del Castillo and Katz, 1957). Classical concepts of GPCR signalling (*Figure 1. 4*) begin with a ligand binding a receptor, as seen in traditional receptor theory. Upon agonist binding, the GPCR undergoes conformational changes which allow an active state to be stabilised and couple with an intracellular heterotrimeric G protein – forming the ternary complex. The ternary complex may also be formed with other secondary effectors, such as arrestin proteins.

However, upon identification that the receptor may adopt an active conformation in the absence of an agonist, known as constitutive activity, (Costa and Herz, 1989) prompted the model to be evolved further – producing the extended ternary complex model (*Figure 1. 7. b*) to incorporate this constitutive signalling (Samama *et al.*, 1993). The extended ternary complex model demonstrates that agonist binding promotes the stabilisation of the AR*G state, whilst the binding of an inverse agonist pushes the equilibrium toward the inactive receptor state.

This model was once again reformulated to incorporate the thermodynamic interactions between the receptor and G protein in the absence of the agonist – resulting in the cubic ternary complex model. (Weiss *et al.*, 1996) (*Figure 1. 7. c*). Whilst the cubic ternary complex model is the most complete theoretically, the increased complexity and introduction of finessed binding constants between states limits the practical application – making it unlikely to be able to obtain experimental representations. In addition, it has been observed that an activated receptor may exist in several active conformational states (Weis and Kobilka, 2018), the cubic ternary complex model itself

a.

$$A + R \rightleftharpoons AR + G \rightleftharpoons ARG$$

b.

$$\begin{array}{ccccc} AR + G & \rightleftharpoons & AR^* + G & \rightleftharpoons & AR^*G \\ \downuparrows & & \downuparrows & & \downuparrows \\ A + R + G & \rightleftharpoons & A + R^* + G & \rightleftharpoons & A + R^*G \end{array}$$

c.

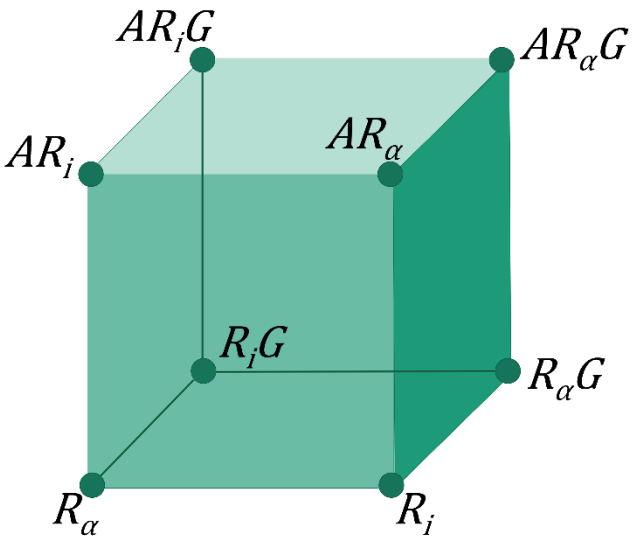

Figure 1. 7 Ternary complex models. *Ternary complex models describe interactions between receptors (R), agonists (A) and G proteins (G). (a.) The original ternary complex model evolved from the two-state model and incorporated G protein binding, where G protein binding promotes the stabilisation of the ARG complex (De Lean et al., 1980). (b.) The extended ternary complex model incorporated constitutively active receptors (R*) into the system, where a receptor can adopt the active conformation in the absence of an agonist (Costa et al., 1989; Samama et al., 1993) (c.) The cubic ternary complex model proses the receptor exists in eight different forms, either bound to a ligand (A) and/or a G protein (G) and existing in an active (R_α) or inactive (R_i) state. Adapted from Weiss et al., 1996.*

provides an incomplete model of agonist-receptor-G protein interactions, particularly when considering conformational origins of ligand bias.

Ternary complex models take into account conformational changes between active and inactive receptor states, as well as the influence of effector proteins and ligands on conformation. Such effects can be defined as “cooperativity” factors, describing how effector binding to the receptor influences ligand binding or visa versa. Cooperativity factors can be positive or negative, depending on whether the effector increases or decreases the affinity of the ligand for the receptor-effector complex, and provide a measure by the extent of the influence, i.e. high positive cooperativity would suggest a large increase in agonist affinity at the complex (Kenakin *et al.*, 2000).

1.5. Kinetics of Ligand Binding and Receptor Signalling at GPCRs

The temporal organisation of ligands binding and signalling from a target receptor are known as their binding and signalling kinetics, respectively, overall determining how experimental responses vary over time. Despite this, ligand affinity and signalling are often characterised by single time points, not always at equilibrium, and provide little insight into the binding or signalling kinetics of the ligand. In recent years, there has been greater appreciation of kinetics events which can allow for greater predictions of clinical drug efficacy.

1.5.1. Ligand-Receptor Binding Kinetics

1.5.1.1. Therapeutic importance of ligand binding kinetics

Ligand binding kinetics, specifically the ligand dissociation rate, have been shown to influence the duration of action in a clinical setting. Moreover, a slower dissociation rate and thus prolonged residence time is thought to be linked to an increased duration of action in in vivo studies (Núñez, *et al,* 2012; Sykes *et al.*, 2012). Drugs acting as receptor antagonists with slower dissociation rates can also provide insurmountable inhibition of the receptor under conditions where the competing agonist concentration varies dynamically, where even high levels of endogenous agonists are reached. This insurmountability could, for example, occur in synaptic clefts and cancerous microenvironments, in which transiently released high levels of ligands might normally out-compete antagonists with rapid

rates of dissociation (Scimemi and Beato, 2009; Ribrault, *et al*, 2011; Kumar, 2013; Murray, *et al,* 2014).

The association rate of a drug can also influence the effect in both *in vitro* and *in vivo* studies, specifically when considering drug rebinding (Gherbi *et al.*, 2020). Drug rebinding occurs when a drug dissociates from one receptor before associating with the same receptor or a receptor in the local membrane environment (Vauquelin and Charlton, 2010; Vauquelin, 2016). Rebinding is influenced by the tissue type and architecture, specifically where drug diffusion to and from the bulk compartment (e.g. the plasma). Under these circumstances, high rates of rebinding (fast association rate, high levels of target protein) increase the local drug concentrations in the restricted reservoir. The effect can be to increase receptor occupancy and clinically increase the duration of action in vivo (de Witte *et al.*, 2017). In such microenvironments, an increased association rate is suggested to act as the driving factor in promoting increased duration of action comparable or greater than the dissociation rate (Vauquelin, 2016b; Sykes *et al*, 2017; Gherbi *et al*, 2020).

Drug binding, specifically drug rebinding, can be highly influenced by the physiochemical properties of the drug. Highly lipophilic, non-polar drugs are likely to interact with the cell membrane and can be partitioned into the membrane, increasing the concentration of drug around the receptor at the membrane level and can increase the rate of association of the drug (Sykes *et al.*, 2017). This has been demonstrated experimentally by Gherbi *et al,* (2018), demonstrating that the local drug concentration at the level of the membrane in cell systems is greater than that of the bulk aqueous phase Such findings challenge fundamental pharmacological principles used to determine measures of ligand affinity and efficacy, which assume freely diffusing ligands.

1.5.1.2. Influence of pharmacokinetic profile of a ligand

In addition to ligand binding kinetics at the GPCR, clinical duration of drug action may be influenced by the pharmacokinetic profile of the drug. Pharmacokinetic properties, such as the rates of absorption, distribution, metabolism and elimination, can influence how much of the drug reaches the target receptor and how long it remains in the target tissue. Clinically the drug pharmacokinetic

elimination rate (k_{el}) may act to drive the duration of action a response, rather than the target dissociation rate (particularly if $k_{el} < k_{OFF}$) (Dahl and Akerud, 2013; de Witte *et al.*, 2016; Gherbi *et al.*, 2020). The relative importance of binding kinetics in determining in vivo target coverage therefore has a complex dependency on the balance between the pharmacodynamic and pharmacokinetic parameters of the drug, alongside the target distribution and tissue architecture (de Witte *et al.*, 2016)

1.5.1.3. Measuring ligand binding kinetics

To measure the kinetics of ligand binding, the common method is to use labelled ligands to monitor association and dissociation at a receptor, for example using fluorescently labelled or radiolabelled ligands. Other methods of measuring binding include using surface plasmon resonance (SPR), which is a label free detection method which monitors binding interactions between immobilised molecules and molecules in solution in real-time (Huber and Mueller, 2007). SPR may be applied to purified systems but it is more difficult to apply to membrane receptors in their native membrane environment (Gherbi *et al.*, 2020).

As will be discussed further in *Chapter 5*, the homogeneous, real time nature of some fluorescent ligand binding assays offers particular advantages over radiolabelled proteins for kinetic based assays. The kinetics of unlabelled ligands that bind competitively may also be determined by monitoring competition with the labelled ligand and applied to a range of models to estimate the association and dissociation rates of unlabelled ligands. For example, the Motulsky Mahan kinetic model of competitive binding (Motulsky and Mahan, 1984) is applied where the labelled and the unlabelled ligand simultaneously, whilst Hoare (2018) proposes multiple models where the receptors is pre-incubated with the unlabelled ligand with or without a washout step. In both models, the kinetic parameters of the labelled ligand are required (as discussed in *Chapter 5* and *Chapter 6*). Experimentally it is important to determine labelled ligands that are bound to the target receptor, unbound or bound to a non-specific site. To quantify unbound receptor, reactions may be filtered to isolate the bound fraction or in the case of fluorescently labelled ligands, the

fluorophore may be quenched when not interacting with the membrane or receptor, i.e. in the aqueous solution (Baker *et al.*, 2010). To identify the response generated from non-specific binding, i.e. to the plasma membrane due to lipophilic label, a ligand selective for the target receptor is used to displace the labelled ligand and isolate the non-specifically bound fraction.

To monitor ligand binding kinetics, receptors may be prepared in a purified manner or in within their native membrane, with the latter either in cells or as a membrane preparation. Receptors may be purified using detergents, nanodiscs and styrene maleic acid lipid particles (SMALPs) and can be applied in experimental assays such as SPR and mass spectrometry (Yen *et al.*, 2018; Warne *et al.*, 2019). Binding kinetics may also monitored in receptors in a membrane environment, either using intact cells or membrane preparations in which mechanisms such as receptor internalisation are removed. Binding kinetics have been monitored at membrane situated receptors in radioligand binding assays (Zeilinger *et al.*, 2017) and resonance energy transfer assays (Schiele, *et al*, 2015; Stoddart *et al.*, 2015; Klein Herenbrink *et al.*, 2016; Stoddart, *et al,* 2018), which will be discussed further in *Chapter 5*. Fluorescence imaging approaches may also be used, in which the fluorescence intensity of a fluorescently labelled ligand may be monitored as an indication of ligand binding (May *et al.*, 2011; Gherbi *et al.*, 2015) and can be applied to monitor ligand binding kinetics at a single cell level (Gherbi *et al.*, 2015). However, unlike some applications of radioligand and fluorescent ligand binding assays, fluorescence imaging techniques are relatively low throughput for monitoring ligand binding kinetics (Gherbi *et al.*, 2020). In addition, fluorescence imaging techniques are also less sensitive to low concentrations of fluorescent ligands (Stoddart *et al.*, 2016).

As there is now evidence to suggest that GPCRs exist in a range of conformations based on their activation profile (Weis and Kobilka, 2018) (see *Chapter 5* and *Chapter 6*), it can be suggested that agonist ligands may demonstrate different ligand binding kinetics at these different binding states. However, kinetic binding assays are often conducted at receptors thought to be in the inactive receptor conformation, due in part to difficulty in stabilising active

conformations of receptors in the absence of G proteins. This is often further ensured by the addition of Gpp(NH)p, a non-hydrolysable form of GTP, to ensure the removal of endogenous G proteins from a membrane preparation or purified receptor (Hubner *et al.*, 2016; Klein Herenbrink *et al.*, 2016; Sykes *et al.*, 2019). Ensuring a single population of an active receptor conformation may reveal greater insights into how ligands bind when a receptor is bound to an intracellular effector and in turn provide insight into the binding kinetics of drugs at wild type and constitutive activated or disease-related receptor subtypes.

1.5.2. Signalling kinetics following GPCR activation

Drug potency and efficacy are commonly estimated from concentration response data taken from a single timepoint monitoring receptor mediated signalling, i.e. cAMP levels or β-arrestin recruitment. The timepoint at which this is taken is often defined by the experimental window or methdology, i.e. transient peak in calcium release, or by experimental design, i.e. cells require lysis to assay cAMP. Whilst more and more studies have identified that drug pharmacology changes throughout a signalling timecourse, such snapshot estimates are still often implemented. The signalling profiles from GPCR activation can vary in onset and duration of action, for example: transient calcium signalling may occur between microsecond and seconds; ERK phosphorylation can takes minutes; and, gene transcription and phenotypic changes may take between hours to days (Gherbi *et al.*, 2020; Dijon, *et al,* 2021). This may confound measures of signalling and lead to incorrect estimations of signalling between pathways. For example, Sengmany *et al* (2017) demonstrate that a positive allosteric modulator of the metabotropic glutamate receptor 5 ($mGluR_5$) had a greater effect on inositol phosphate (IP_1) accumulation than on intracellular calcium signalling. However, this comparison was made using measurements of IP_1 at 1 hour following agonist addition and the peak calcium response at 20 seconds following agonist addition, with latter likely to taken from hemi-equilibrium conditions (Sengmany *et al.*, 2017). In addition, using single timepoints does not take into account transient or oscillatory signalling patterns, as seen in cAMP signalling (Peercy, *et al,* 2015) and protein kinase cascades (Garner *et al.*, 2017).

Spatially distinct signalling from endosomes and very early endosomes can produced sustained signalling, even after receptor

desensitisation and internalisation (Sposini and Hanyaloglu, 2017; Hanyaloglu, 2018; Wright *et al.*, 2021). Signalling from such endosomal compartments can range between 30 minutes to hours (Calebiro *et al*, 2009; Callander, *et al*, 2009; Ferrandon *et al*, 2009; Hothersall *et al*, 2015; Hothersall *et al*, 2016) and thus produce temporally distinct signalling profiles compared with receptors at the cell surface (Gherbi *et al.*, 2020).

When choosing the time at which to take concentration response data, it is also important to consider the effect the ligand binding kinetics may have (Bdioui *et al.*, 2018). For example, concentration response data from ligands with slow association rates may not be representative at early timepoints, due to delayed equilibration. The impact of binding kinetics on estimates of agonist affinity, efficacy and resultant measures of ligand bias was exemplified by Klein Herenbrink *et al* (2016). As discussed above, time dependent differences in ligand bias were attributed to different ligand binding kinetics and suggesting that observed biased properties were an artefact of slowly dissociating agonists. For example, the slowly dissociating partial agonist aripiprazole demonstrated an increase in agonist potency throughout the assay, which can be attributed to increased receptor occupancy over time (Klein Herenbrink *et al.*, 2016).

1.6. Adrenaline and the Adrenoceptors

1.6.1. Signalling, Synthesis and Distribution

The adrenoceptor (AR) family is a well-characterised collection of aminergic class A GPCRs, which can be further defined by receptor subtype: α_{1A}, α_{1B}, α_{1D}, α_{2A}, α_{2B}, α_{2C}, β_1, β_2 and β_3. Adrenoceptors respond to endogenous catecholamines such as adrenaline and noradrenaline and have widespread expression within the human body. Whilst α_1 and α_2 adrenoceptors couple to Gαq/11 and Gαi/o proteins, respectively, β adrenoceptors predominantly couple to Gαs proteins (Evans *et al.*, 2019). As a typical Gαs protein-coupled receptors, β adrenoceptor agonists activate the stimulatory G protein pathway to increase levels of cAMP, by activation of AC, and production of PKA (*Figure 1. 8*). PKA activity within the smooth muscle of the lungs acts to reduce $[Ca^{2+}]i$ and bronchodilation via muscle relaxation. In the cardiac muscle of the heart, PKA increases the heart rate and rate of relaxation. Whilst the β_1 adrenoceptor is thought to exclusively couple Gαs proteins, some have suggested that the

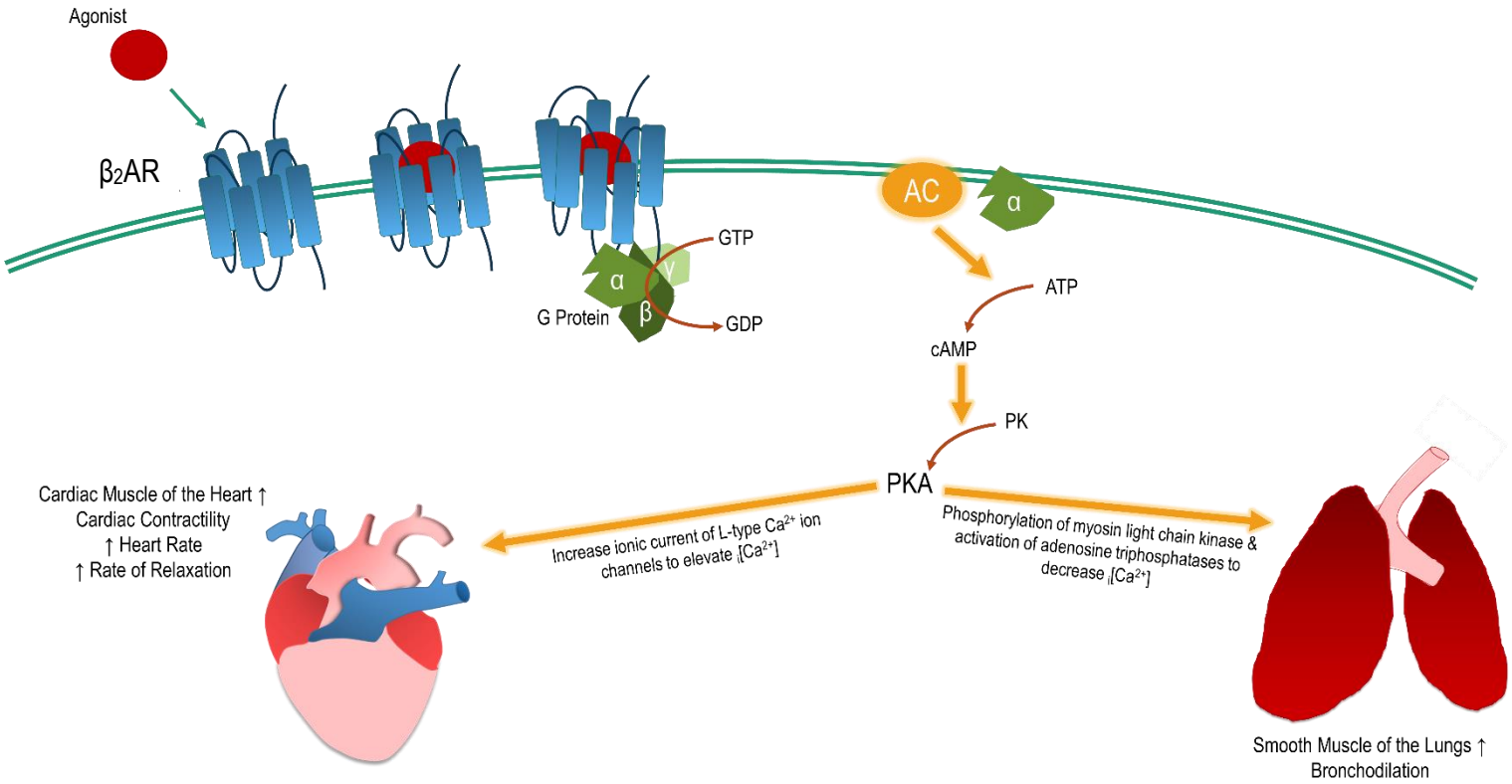

Figure 1. 8 β_2 adrenoceptor signalling. *Upon agonist-dependent activation of β2 adrenoceptors, stimulatory Gs proteins elevate downstream accumulation of cAMP, via membrane bound adenylyl cyclase (AC) and subsequently phosphorylates protein kinase A (PK to PKA). PKA activity within the smooth muscle of the lungs acts to decrease intracellular calcium ion concentration (i[Ca2+]) and bronchodilation via muscle relaxation. In the cardiac muscle of the heart, PKA increases the calcium channel current to increase i[Ca2+], leading to increase contractility heart rate and rate of relaxation.*

β_2 adrenoceptor may also recognise and activate Gαi proteins (Xiao *et al.*, 1999; Kilts *et al.*, 2000; Chakir, *et al.*, 2011; Chakir, *et al.*, 2011), though the extent to which this occurs in controversial. In addition to G proteins, βARs may couple to other intracellular effectors, forming alternative ternary complexes, such as GPCR phosphorylation by GRKs, arrestin proteins and subsequent recruitment of clathrin and clathrin adaptor proteins (AP2) (Miller and Lefkowitz, 2001; Milano *et al.*, 2002; Henry *et al.*, 2012). These receptor-effector interactions, initiate intracellular signalling cascades and receptor regulation, for example through internalisation (Mettlen *et al*., 2018).

The endogenous signalling molecules, adrenaline and noradrenaline, are part of a class of monoamine compound known as catecholamines – named from the presence of the catechol group in all the compounds in the family. Adrenaline and its precursor compound noradrenaline are both biologically active and are synthesised from L-tyrosine in the chromaffin cells of the adrenal gland, as well as adrenergic neurons in the medulla oblongata of the brain (Unsicker *et al.*, 2005). Adrenoceptors are found to be expressed through peripheral tissues, as well as on adrenergic neuronal populations in the central nervous system (Altosaar *et al.*, 2021). Specifically human β adrenoceptors subtypes β_1, β_2 and β_3 adrenoceptors are classically identified to be expressed in cardiac tissue, airway smooth muscle and adipose tissue, respectively (Johnson, 2006). Moreover, β_2 adrenoceptors are also expressed in the lung, not only in airway smooth muscle cells, but also in epithelial, endothelial and mast cells (Johnson, 2006). Radioligand binding studies and computed tomographic scanning identify that the expression of β_2 adrenoceptors is widely distributed in the respiratory tract (Johnson, 2006). A small population of β_2 adrenoceptors are also expressed in cardiac myocytes and fibroblasts and are thought to be pathophysiologically relevant in cardiac hypertrophy (Imaeda *et al.*, 2019). Whilst expressed at a low level compared to pulmonary β_2 adrenoceptors, cardiac β_2 adrenoceptors have been linked with cardiac failure. For example, Nikolaev *et al.*, (2010) identify β_2 adrenoceptor signalling changes the spatial localisation of cAMP production from isolated cAMP signalling at the transverse tubules in healthy cardiomyocytes to a much more diffuse cAMP in cardiomyocytes taken from models of chronic heart failure. This evidence suggested a change in the cAMP compartmentalisation might contribute to a failing cardiac phenotype.

1.6.2. The β_2 Adrenoceptor and Disease

The β_2 adrenoceptor is one of the well-characterised class A GPCRs, and with widespread expression, on-target as well as off-target side effects of β_2 adrenoceptor ligands are common and often need to be closely monitored, especially in cases of comorbidities (Baker 2010; Baker *et al*. 2017), such as seen in individuals with cardiovascular and respiratory diseases. One of the main clinical applications of the β_2 adrenoceptor is use of inhaled agonists, in obstructive airway diseases including asthma and chronic obstructive pulmonary disease (COPD). Within the smooth muscle cells of the lungs, β_2 adrenoceptor activation of Gαs increased levels of cAMP and leads to downstream bronchodilation, providing symptomatic relief (*Figure 1. 8*). The physiochemical properties of β_2 adrenoceptor agonists, such as their lipophilicity, also dictates receptor interactions. For example, hydrophilic agonists like salbutamol rapidly bind and dissociate from the receptor which is reflected in a short duration of action, whilst more lipophilic agonists such as salmeterol may be sequestered within the plasma membrane and gradually release to act on the receptor over a longer period of time (Matera, *et al*, 2018). There are more recently documented agonists, such as indacaterol and vilanterol, which provide a different mechanism action once again to provide fast onset and extended duration of action (Cazzola, *et al*, 2011). This is therapeutically advantageous as it allows for an increased duration between doses, increasing the likelihood of patient compliance. In these ultra-long acting agonists, it is suggested that high levels of membrane permeability and elevated partitioning of the ligand into the receptor microenvironment may allow for a long-term high efficacy effect (Lombardi, *et al,* 2009).

Whilst widely used, there are issues with clinical targeting of βARs. Firstly, chronic usage of β_2 adrenoceptor agonists in obstructive airway disease can lead to receptor desensitisation and downregulation and βAR agonist tolerance (Kersten, *et al,* 2017). With β-arrestin pathways responsible for receptor desensitisation, there has been significant interest in developing biased ligands which promote bronchodilator effects without affecting receptor expression at the membrane (Cazzola, *et al,* 2011).

As well as signalling bias, it is important to investigate βAR signalling to better understand subtype selectivity of ligands. Ligands of β adrenoceptors commonly lack sufficient selectivity between β_1 and β_2 adrenoceptors present in the heart and smooth muscle of lungs, respectively. Whilst activation of Gαs

coupled β_2 adrenoceptors allows for bronchodilation, a non-selective ligand also leads to activation of cardiac β_1 adrenoceptor to increase the force and rate of the contraction of the heart. Alternatively, beta blockers used to treat cardiovascular disease reduce the strength and rate of cardiac contraction, yet their action at β_2 adrenoceptors in the lungs can lead to smooth muscle contraction and airway obstruction. Clearly, clinical comorbidities in respiratory and cardiovascular disease therefore demonstrate how a lack of subtype selectivity can have potentially fatal effects.

As discussed above, the β_2 adrenoceptor has been suggested to activate Gαi proteins and this activation is thought to correlate with cardiac hypertrophy (Imaeda *et al.*, 2019), cardiac dysfunction and higher mortality (Nguyen *et al.*, 2015). However, there are studies to suggest cardiac β_2 adrenoceptor signalling may also be cardioprotective, with some suggesting β_2 adrenoceptor overexpression can ameliorate cardiac dysfunction in heart failure (Dorn Ii *et al.*, 1999; Tevaearai *et al.*, 2002; Rengo *et al.*, 2012) and improve cardiac contractility and maladaptive remodelling (Rengo *et al.*, 2012). Whilst the role of the β_2 adrenoceptor in heart failure is not fully understood, the β_2 adrenoceptor remains a steadfast target in asthma and COPD.

1.7. Protein Complementation Assays for Measuring GPCR Signalling

1.7.1. Protein complementation assays

Recent developments in imaging have provided opportunities to track dynamic changes in GPCR signalling, such as fluorescence and bioluminescence resonance energy transfer approaches (Hill and Watson, 2018), which are discussed further in *Chapter 3*. A further solution is the application of protein complementation assays (PCAs), which rely on the association of two split counterparts to indicate an interaction of the appended proteins (Luker and Luker, 2011). In imaging studies, the use of PCA methodology can be applied to fluorescent proteins and enzymes, with luciferase variants successfully used in vitro and in vivo studies (Remy and Michnick, 2006; Stefan *et al.*, 2007; Villalobos *et al.*, 2010). Luciferase enzyme complementation requires the addition of an appropriate substrate, such as coelenterazine or furimazine, to generate luminescence. Whilst luciferase PCAs are conceptually simple, the precise split to generate appropriate

fragments requires detailed consideration as it influences the size of luciferase fragments, to avoid stoichiometric hindrances, and the efficiency and reversibility of the complementation process (Dixon *et al*, 2016).

1.7.2. Generation of NanoLuc Binary Technology

The size of the luciferase is dependent on the variant used, with firefly luciferases (FLuc, derived from Photinus pyralis) and Renilla luciferases (RLuc, derived from Renilla reniformis) being relatively large at 61 and 38 kDa respectively (Stoddart, Kilpatrick and Hill, 2018) (*Figure 1. 9. a*). More recently, a luciferase derived from luminous deep-sea shrimp (Oplophorus gracilirostris) has been engineered to produce a stable 19 kDa protein which produces a bright (> 150-fold of RLuc), and long-lasting signal, with a half-life of greater than 2 hours (Hall *et al.*, 2012), and is known as nanoluciferase (NanoLuc) (*Figure 1. 9. b*). Unlike luciferases such as FLuc, NanoLuc does not require ATP for activity and may be used in extracellular positions or in membranes. Due to the small size and bright long-lasting luminescence, NanoLuc was shown to be a suitable candidate for PCAs (Dixon, *et al*, 2016).

Using NanoLuc, Dixon et al (2016) demonstrated effective methodology of splitting the luciferase and thus coining the term NanoLuc binary technology (NanoBiT, Promega). Protein complementation assays have also been established based on both FLuc (Paulmurugan, *et al*, 2002; Fujikawa and Kato, 2007; Ohmuro-Matsuyama, *et al*, 2013) and RLuc (Hattori and Ozawa, 2014; Wei *et al.*, 2018). By splitting the NanoLuc, and optimising fragment conformation using mutagenesis, Dixon et al (2015) demonstrated effective reversible complementation of a small 11 amino acid c-terminal fragment (Sm114) and the remaining 18kDa protein (LgBiT) (*Figure 1. 9. c*). Complementation of the LgBiT and Sm114 fragments was shown to produce a sustained robust luminescence signal upon furimazine treatment, with comparably unchanged spectrum compared to the original NanoLuc (emission peak = ~460nm). In addition, the LgBiT-Sm114 binding affinity (Kd = 19μM) was shown to be weak enough to not alter the binding kinetics of the fused proteins of interest and allowing for a representation of dynamic protein interactions (Dixon *et al.,* 2016). An alternate protein complementation assay

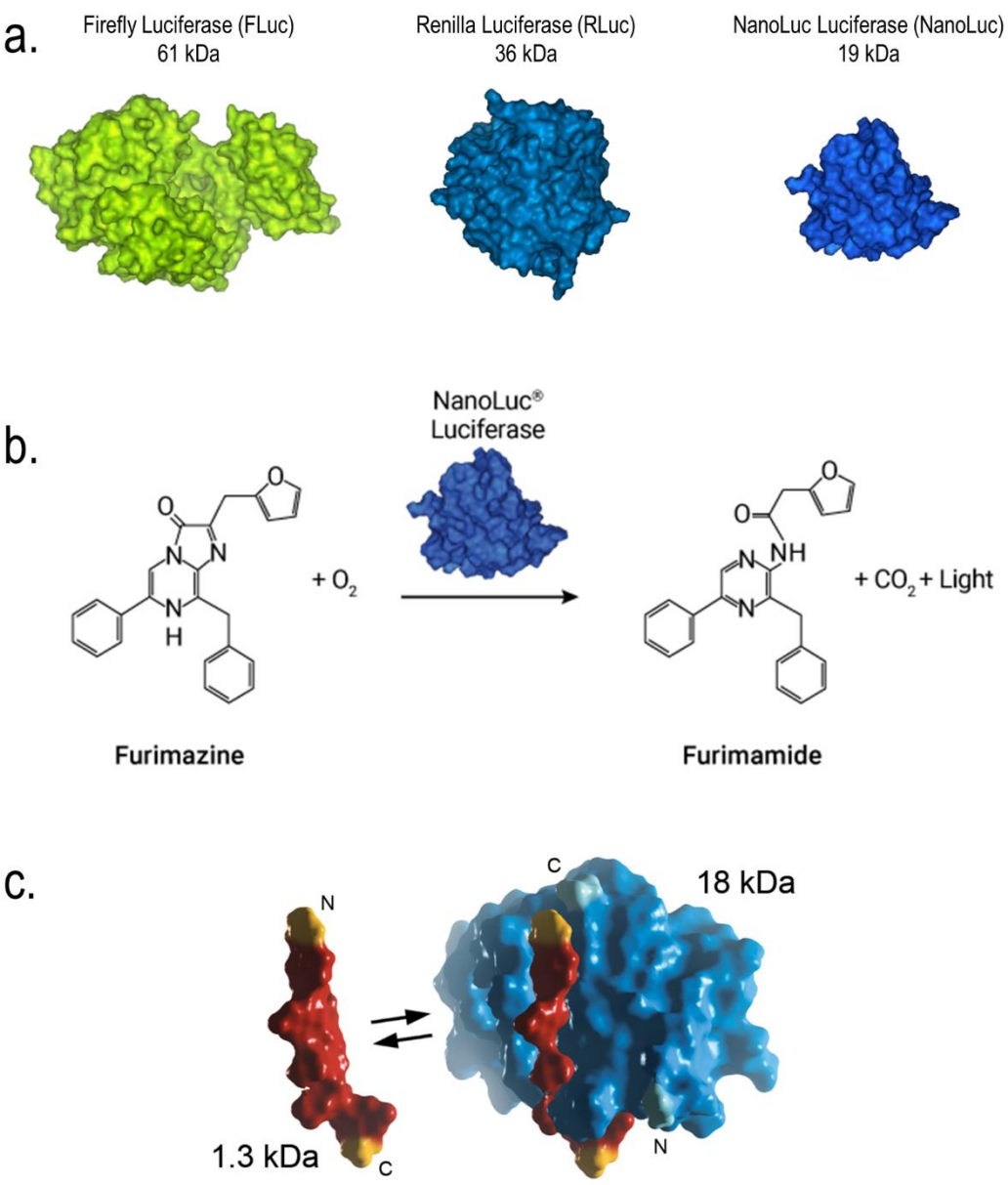

Figure 1. 9 Luciferase and split luciferase derivatives. *(a.) Luciferase enzymes exist in a range of sizes between 61 and 19 kDa. (b.) NanoLuc facilitates the conversion of furimazine substrate and oxygen to product and the product of visible photons. (Hall et al, 2012). (c.) Dixon et al., (2016) demonstrated split positioning of the NanoLuc enzyme to produce complementary fragments, applied in NanoLuc binary technology (NanoBiT). Images modified from Promega promotional material (Promega, Wisconsin) and Dixon et al., (2016).*

using the NLuc enzyme also been established, using alternate split variants to investigate protein:protein interactions at a range of GPCRs including the dopamine D1/D2, adenosine A2A and muscarinic M4 receptors (Yano *et al.*, 2018; Pedersen *et al.*, 2021)

In addition to the Sm114 weak binding fragment, a range of small complementary peptides (Sm-) were engineered with increasing the affinity for the LgBiT. Demonstrating a K_D of 700pM, the Sm86 fragment showed the greatest affinity for the LgBiT fragment and thus produces pseudo-irreversible binding to stabilise the protein-protein interaction (Dixon *et al.*, 2016). With the 11 amino acid fragments showing a range of binding affinities, the application of both the high and low affinity fragments may be utilised in analysing protein interactions, such as seen in GPCRs and intracellular effectors. Due to the original development of the NanoBiT technology being tested at adrenoceptors and vasopressin GPCRs (Dixon., *et al.*, 2016), it is unsurprising that the application within the GPCR research field has shown success and often cites the optimised split positioning of the LgBiT-Sm114 complementation.

1.7.3. Application of NanoLuc Binary Technology in signalling assays

The most common application of the LgBiT-Sm114 complementation is to monitor GPCR and β-arrestin2 interactions. In cannabinoid receptors, differential β-arrestin2 recruitment profiles can be observed at CB1 and CB2 receptors when treated with the same synthetic cannabinoid JWH-018 (Cannaert *et al.*, 2016). In other literature, activation of an orphan receptor (GPR27) with exogenous ligands was shown to successfully recruit β-arrestin2 to the receptor (Dupuis *et al*, 2017). Dupuis and colleagues (2017) state that the NanoBiT® assay demonstrates a reduction in luminescence signal compared to a FLuc PCA, again highlighting the significance of the weak LgBiT-Sm114 affinity in preserving reversible dynamic behaviour of the proteins interactions of interest. In addition, Qian *et al* (2018) demonstrated successful recruitment of Sm- (small fragment affinity not described) fused β-arrestin2 by LgBiT fused mu opioid receptor. The PCA was able to measure morphine induced β-arrestin2 recruitment elevation during GRK2 overexpression, agreeing with considerable literature (Groer *et al.*, 2011; Raehal *et al.*, 2011; Evron, *et al,* 2012; Williams *et al.*, 2013) and demonstrating how the complementation reflects well established pharmacology. In the

examples listed above and others (Cannaert *et al.*, 2016; Dupuis *et al.*, 2017; Qian *et al.*, 2018; Storme *et al.*, 2018a), the LgBiT fragment was fused to the intracellular C-terminus of the receptor and the Sm114 fragment fused to β-arrestin2 to monitor agonist dependent recruitment. However β-arrestin2 recruitment may also be monitored by reversing the configuration at chemokine receptors, with the small fragment fused to the GPCR C-terminal and the LgBiT fused to β-arrestin2 (Szpakowska *et al.*, 2018).

In 2018, Wan *et al* have also shown that the NanoBiT® methodology may be utilised to detect recruitment of a synthetic 'mini Gαs' protein, consisting of a thermostabilised form of the Ras-like GTPase domain of the Gα subunit. Whilst GPCR-mini Gαs complexes have previously been used in solving protein crystal structures (Carpenter and Tate, 2016; Carpenter *et al.*, 2016; Nehmé *et al.*, 2017), Wan *et al.,* (2018) established that mini Gαs protein recruitment to β_2 adrenoceptor is possible using a stimulatory Gαs variant of the mini G protein in human embryonic kidney (HEK293) cells.

The high affinity NanoBiT fragments have also been used to report GPCR signalling and binding behaviours. For example, Soave *et al* (2020) report use of the high affinity NanoBiT fragments to monitor GPCR-nanobody interaction at the chemokine CXCR4 receptor and nanobodies which binding the orthosteric site (Soave, *et al.*, 2020). The high affinity fragments have also been used to monitor receptor internalisation (Soave, *et al.*, 2020; White *et al.*, 2020), whereby GPCRs are N-terminally labelled with the HiBiT NanoBiT fragment and upon agonist treatment and internalisation are removed from the cell surface. The cells are then treated with a purified form of the LgBiT fragment and furimazine to identify the receptors remaining at the cell surface (Soave, *et al.*, 2020; White *et al.*, 2020).

Other studies have demonstrated alternative split points for NanoLuc based complementation. For example, novel complementary NanoLuc fragments have been used to monitor D1 or D2 dopamine receptor recruitment of Gαs or Gαi proteins, respectively (Yano *et al.*, 2018). The binding affinity between these complementary fragments were not published and so leaves open the effect on the dynamics of these protein-protein interaction.

1.7.4. Application of NanoLuc Binary Technology to stabilise GPCR conformations

Dixon *et al* (2016) first described the NanoBiT fragments, with significance placed on the Sm86 variant having the highest affinity for the LgBiT protein. Duan *et al* (2020) have utilised the high affinity fragments to tether the heterotrimeric protein to the vasoactive intestinal polypeptide receptor (VIP1R) bound to PACAP27 and solve the protein structure in cryo-electron microscopy studies (cryo-EM). By genetically encoding the LgBiT fragment at the C-terminal of the receptor and the Gβγ with the HiBiT fragment, the authors note increased stability of the complex when compared to the same complexes in the absence of NanoBiT fragments (Duan *et al.*, 2020).

1.8. Mini G Proteins

1.8.1. Mini G protein design

As mentioned above, mini G proteins are synthetic G protein mimetic tools which consist of the Ras-like GTPase domain of the Gα subunit with a truncated N terminus, removing the Gβγ binding interface and the membrane anchors, and deletion of the alpha helical domain (Carpenter and Tate, 2016) (*Figure 1. 10*). Removal of the membrane anchors allow the mini Gα protein to be located in the cytosol under basal conditions and recruited to the membrane upon GPCR activation *(Wan et al*, 2018). Several mutations were made to thermostablise the protein for expression and purification, including a mutation in the α5 helix of the mini Gα protein C terminal to uncouple nucleotide release upon mini Gαs protein-GPCR binding (Carpenter and Tate, 2016). Mutations in the mini Gαs protein gene sequence allow for variations of peptide expression on the GPCR interface and allow receptor specific binding and representing other Gαs protein families: Gαs, Gαi/o, Gαq/11 and Gα12/13 (Carpenter and Tate, 2016).

1.8.2. Mini Gαs Proteins in structural studies

Mini G proteins were initially engineered to provide insight into the active states of GPCR structures, with binding thought to promote a conformational change (Nehmé *et al.*, 2017; Warne *et al.*, 2019). Structural determination of GPCRs bound to agonists and/or effector proteins, such as G proteins, have primarily focused on using stabilising mutations and the inclusion of stabilising fragments such as T4 lysozyme – a protein that

crystallises under variable conditions (Rosenbaum *et al.*, 2007; Thorsen *et al.*, 2014). Many GPCR structures have been solved in complex with high affinity inverse agonists, which readily stabilise the inactive GPCR (Zhang, *et al.,* 2015). However, to solve GPCR structures in complex with agonists coupled to a heterotrimeric G protein is more difficult, requiring either NanoBiT tethering (Duan *et al.*, 2020) or the inclusion of both a stabilising nanobody and T4 lysozyme (Rasmussen, *et al*, 2011). Generation of mini Gα proteins provide structurally stable mimetics of the G protein interaction and has allowed for the determination of the crystal structures of multiple GPCR-mini Gα protein complexes, including: the adenosine A2A receptor in complex with mini Gαs protein (García-Nafría, e*t al.*, 2018); the visual rhodopsin receptor in complex with mini Gαi/o receptor (Tsai *et al.*, 2018); the $5HT_{1B}$ receptor in complex with mini Gαo/i protein (García-Nafría, *et al.*, 2018); and the β_1 adrenoceptor in complex with mini Gαs protein (Warne *et al.*, 2019).

Beyond solving protein crystal structures, GPCR-mini Gα protein complexes have been applied in nuclear magnetic resonance (NMR) spectroscopy studies to investigate receptor activation at an agonist bound β_1 adrenoceptor (Rößler *et al.*, 2020) and an agonist bound adenosine A2A receptor (Huang *et al.*, 2021), both in complex with the mini Gαs protein. Stabilised agonist bound complexes of both the β_1 adrenoceptor and the adenosine A2A receptor, bound to the mini Gαs protein, were also applied in native mass spectrometry studies to investigate the ability of phospholipid binding to modulate G protein binding (Yen *et al.*, 2018). The mini Gα proteins have also been used in pharmacological and functional readout assays (Wan *et al*, 2018; Höring *et al*, 2020), as discussed in *Chapter 3.*

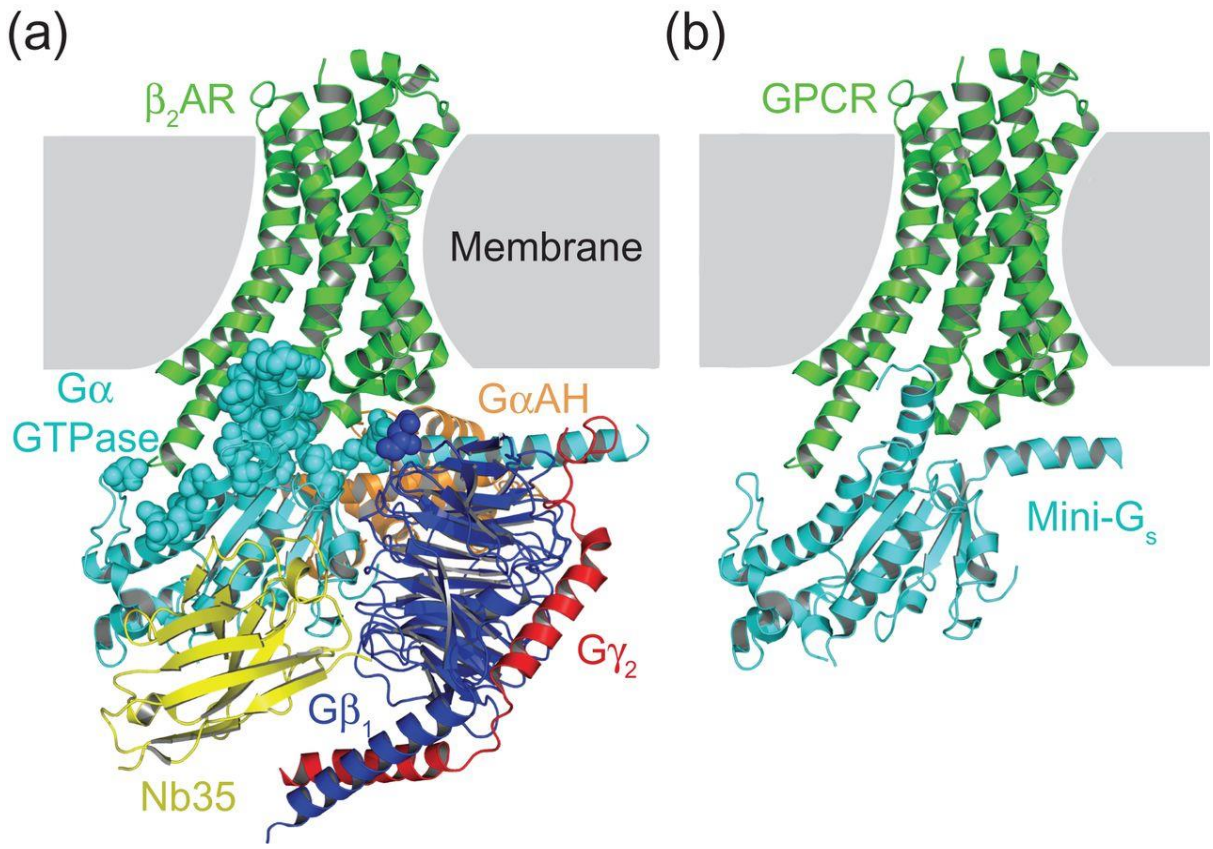

Figure 1. 10 Receptor bound structure of either a heterotrimeric G protein or the mini Gαs protein, from Carpenter and Tate (2016). *(a.) Crystal structure of β2 adrenoceptor (green) in complex with the heterotrimeric Gs protein (domains: Gα GTPase (cyan), GαAH (orange), $Gβ_1$ (dark blue) and $Gγ_2$ (red)), stabilised by nanobody 35 (Nb35) (yellow) (PDB code: 3SN6) (Rasmussen et al., 2011). (b.) Proposed structure of β2 adrenoceptor (green) in complex with the mini Gαs protein. (Figure prepared by Carpenter and Tate (2016), using PyMOL v1.7.4 (Schrödinger, LLC).*

1.9. Limitations of Pharmacological Measurements of Effector Dependent Signalling Kinetics and Ligand Binding Kinetics

As discussed above, it is clear that both signalling kinetics and ligand binding kinetics at GPCRs may alter estimations of ligand affinity, potency and efficacy, in both *in vivo* and *in vitro* pharmacological settings. Each kinetic parameter may influence the behaviour of a drug in a clinical setting, aided by the drug's pharmacokinetic profile.

Recently, dynamic biosensors, such as the NanoBiT complementation assay, have provided the tools to look at the signalling kinetics of dynamic protein:protein interactions over time and use concentration responses relationships to make estimations of ligand potency and efficacy across the timecourse. However, previous use of the NanoBiT complementation assay (Dupuis *et al.*, 2017; Qian *et al.*, 2018) has focused on taking concentration response relationships at single timepoints and not investigated how these relationships may change over time. Moreover, such concentration response data can be applied in estimations of ligand bias using operational models, which assume equilibrium of the experimental system. Whilst these models have been widely applied to investigate signalling at GPCRs, there are limited studies (Klein Herenbrink *et al.*, 2016) which incorporate the influence of time on estimations of ligand bias or incorporate hemi-equilibrium conditions. Kinetic operational models, outlined in Hoare *et al*., (2018), have been put forward as a method for analysing comprehensive concentration response timecourse data and take hemi-equilibrium conditions into account, but as of yet have not been robustly tested in their use to analyse either agonist or antagonist action at GPCRs.

Whilst there are examples of isolating conformational states of GPCRs for structural studies and estimations of ligand binding at equilibrium, there has not been published examples of how the ligand binding kinetics may be altered at the different receptor conformations. As described by the ternary complex model, binding of an agonist ligand and/or an effector protein can shift the equilibrium of the receptor conformation towards the active state, as seen in the crystal structure of the β_2 adrenoceptor in complex with the mini Gαs protein and isoprenaline (Warne, *et al,* 2019). Moreover, it has been suggested that the active conformation of the receptor may be different depending on the effector bound to the receptor. It could be suggested that the ligand binding kinetics at the orthosteric site may not only show differences between inactive and active receptor conformations, but also between effector dependent active receptor conformations.

1.10. Aims of thesis

Better understanding of ligand binding and signalling kinetics in principle provide greater insight into GPCR pharmacology, compared with equilibrium conditions which are unlikely to be fully replicated in an *in vivo* model or clinical studies.

It is clear that there is a lack of robust methods to measure receptor signalling kinetics in real-time, as well as a lack of pharmacological models available to analyse such kinetic responses. In addition, whilst the kinetics of ligand binding at GPCRs can be obtained routinely, there is a need to establish methods of stabilising active and inactive GPCR conformations and investigate the differences in ligand binding kinetics between these conformational states.

In this thesis, combinations of NanoBiT complementation assay and fluorescent ligand technologies will be applied to the study β adrenoceptor pharmacology and ligand binding and signalling kinetics, ultimately with the aim of quantifying kinetic parameters at identified receptor-effector complexes.

In *Chapter 3*, the low affinity LgBiT:SmBiT NanoBiT assay was implemented to monitor agonism at β adrenoceptor subtypes and demonstrate how potency and efficacy are impacted by the timepoints used to establish concentration response data. The assay monitored the recruitment of two effector proteins: β-arrestin2 and the synthetic mini Gαs protein. The signalling profiles of effector recruitment were applied in operational models, the Black and Leff Operation Model of Partial Agonism (Black and Leff, 1983) and a kinetic operational model to derive equilibrium agonist dissociation constants and parameters describing agonist efficacy.

The low affinity NanoBiT technology was further applied to monitor antagonist action at the β_2 adrenoceptor in *Chapter 4*, showing the effect of antagonists on effector recruitment over time in Schild based experiments. The relationship between antagonist binding kinetics and the appearance of antagonist insurmountability was explored, using time-resolved fluorescence resonance energy transfer (TR-FRET) assays to determine the binding kinetics of the antagonists. A kinetic operational model of antagonism was then applied to compare estimations of antagonist affinity between methods.

In *Chapter 5* high affinity NanoBiT fragments were applied in dual expression cell lines to establish NanoBiT stabilised complexes of the β_2 adrenoceptor with either β-arrestin2 or the mini Gαs protein. The affinity of a fluorescently labelled β_2

adrenoceptor ligand and unlabelled ligands were established using TR-FRET assays at each receptor condition: β_2 adrenoceptor alone or β_2 adrenoceptor stabilised by either β-arrestin2 or mini Gαs protein. To isolate binding measurements to the receptor population bound to an effector protein, the complemented NanoBiT luciferase fragments were used as the donor species in a novel transmembrane bioluminescence resonance energy transfer assay (TM-BRET), in which the luminescence from the intracellular complemented NanoBiT fragments is used to excite the bound fluorescently ligand. TM-BRET assays were successfully applied to establish affinities of fluorescently labelled and unlabelled ligands at different receptor conditions. This chapter finally explored the effectiveness in the use of the dual expression cell lines to produce sufficient receptor-effector complexes, both in cells and membranes.

The final results chapter, *Chapter 6*, explored the use of a purified HiBiT labelled mini Gαs protein in establishing NanoBiT stabilised complexes of the β_2 adrenoceptor. Equilibrium estimations of binding affinity of both fluorescently labelled and unlabelled ligands were established using TM-BRET and TR-FRET binding assays, in the presence and absence of the NanoBiT stabilised mini Gαs protein. TR-FRET assays were further applied to successfully measure ligand binding kinetics of a fluorescently labelled ligand and a panel of unlabelled β_2 adrenoceptor ligands with varied receptor efficacy, in the presence and absence of the purified mini Gαs protein. For the first time, the binding kinetics of an active conformation mini Gαs stabilised β_2 adrenoceptor could therefore be demonstrated, with implications for how the conformational change associated with GPCR activation slows agonist dissociation rates.

Chapter Two:

Materials and Methods

2.1. Materials

Noradrenaline and dopamine (Sigma Aldrich, UK) were made fresh on day of assay, while all other β adrenoceptor ligands (Tocris Bioscience, Bristol, UK) were pre-aliquoted in single-use aqueous aliquots at 10 mM concentration. Indacaterol and C26 (7-{(R)-2-[(1R,2R)-2-(benzyloxy)cyclopentyl]amino}-1-hydroxyethyl)-4-hydroxybenzo [d]thiazol-2(3H)-one) were synthesised at Novartis (UK). Mini Gαs protein sequence (Carpenter and Tate, 2016) was synthesised by GeneArt (Invitrogen; Paisley, UK), with SmBiT/HiBiT (Kozak (GCCACC)-SmBiT-5xSerGly linker / Kozak (GCCACC)-HiBiT-5xSerGly linker) and LgBiT (10xSerGly Linker-LgBiT) constructs obtained from Promega corporation (WI, USA). All mammalian expression vectors and lipofectamine/lipofectamine 3000 reagents were purchased from Invitrogen (Paisley, UK). pJ411 vector, BL21(DE3) NiCo competent cells and Gibson Assembly mix were gifted by the Veprintsev group (University of Nottingham, UK), originally obtained from New England BioLabs Inc. Purified HiBiT peptide was obtained from GenScript (New Jersey, US). Protein concentrators and Slide-A-Lyzer Dialysis Cassettes were obtained from Thermo Scientific™. HisTrap FF 5mL column was obtained from Cytiva Life Sciences. NanoGlo furimazine substrate was obtained from Promega Corporation (WI, USA). All cell culture reagents and additional buffer reagents were obtained from Sigma Aldrich (UK). For TR-FRET binding assays, BODIPY-FL-PEG8-(S)-Propranolol (CA200693) was purchased from HelloBio (UK), with Tag-lite labelling medium and SNAP-Lumi4-Tb obtained from Cisbio Bioassays (Bagnols-sur-Ce`ze, France). White 384 well Optiplates were purchased from PerkinElmer (Beaconsfield, UK), with 96 well white sided plated purchased from Greiner Bio-One (Stonehouse, UK).

2.2. Molecular Biology Methods

2.2.1. Mammalian Construct design

For transfection of mammalian DNA, pcDNA3.1(+) expression vectors were used to encode genes of interest. pcDNA3.1(+) vectors contained resistance genes for both ampicillin and either zeocin or G418/neomycin resistance, in pcDNA3.1(+) zeo and pcDNA3.1(+) neo constructs, respectively. Antibiotic resistance genes were used for selection in bacterial (ampicillin) and mammalian (zeocin or G418) expression. pcDNA3.1(+) vectors encoded the human cytomegalovirus immediate-early (CMV) promoter to induce high expression in mammalian cells and an ORI site to promote high copy number. Downstream of the gene of interest was a bovine growth hormone (BGH) polyadenylation signal for polyadenylation of mRNA and termination of gene transcription. T7 and BGH

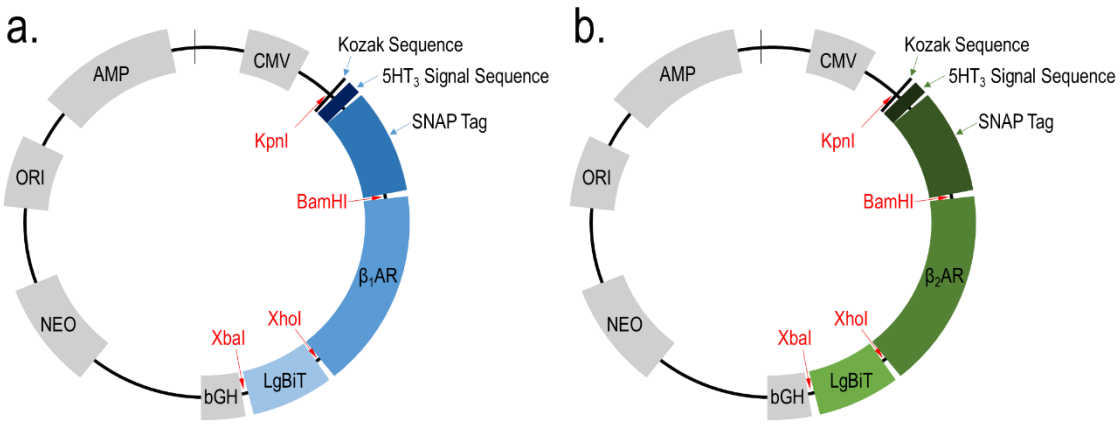

Figure 2.1 Mammalian vector maps of NanoBiT labelled receptors. *Vectors encoded modified adrenoceptors in pcDNA 3.1 (+) neo vectors. Each receptor, either (a.) β_1 or (b.) β_2 adrenoceptor was placed in the multiple cloning site between BamHI and XhoI restriction sites. A SNAP tag, with an N-terminal Kozak and $5HT_3$ signal sequence, was placed upstream of the receptor, between KpnI and BamHI. The LgBiT NanoBiT fragment was encoded at the C-terminal of the adrenoceptor, with a stop codon, between XhoI and XbaI.*

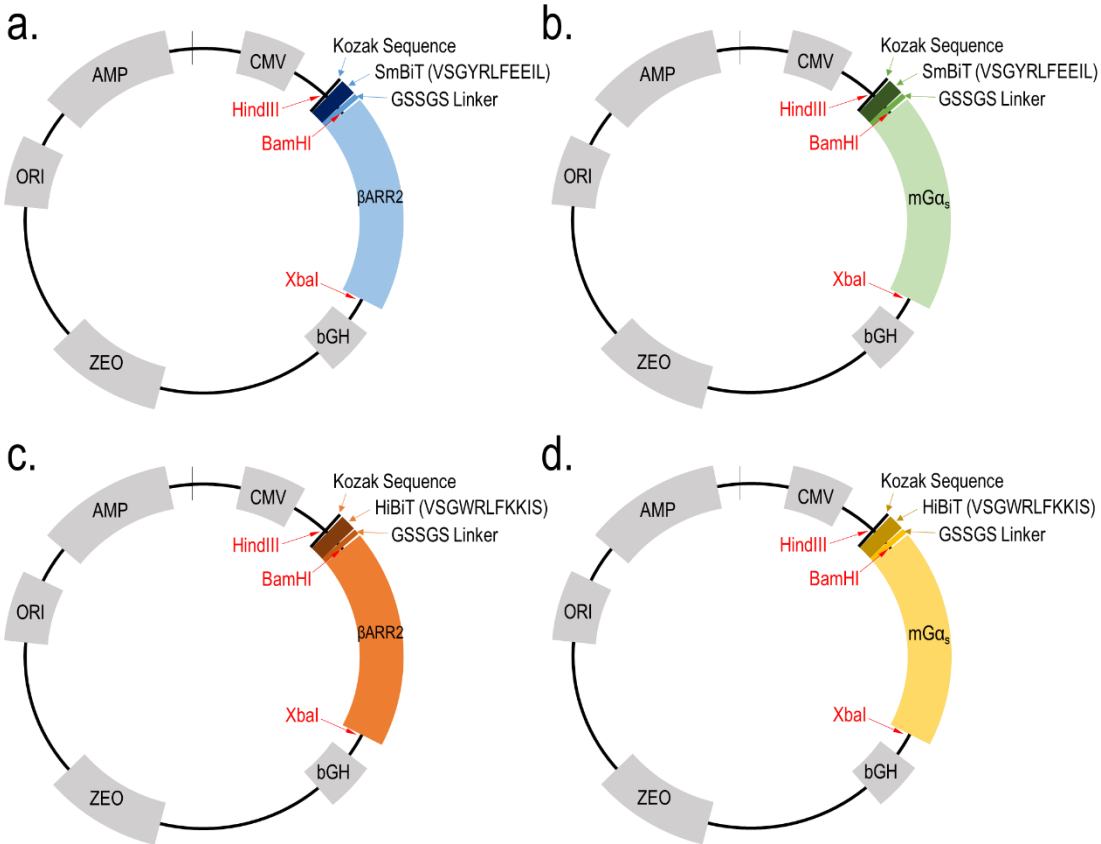

Figure 2.2 Mammalian vector maps of NanoBiT labelled effectors. *Vectors encoded modified effectors in pcDNA 3.1 (+) zeo vectors. Each effector, either (a. & c.) β-arrestin2 or (b. & d.) mini Gαs was placed in the multiple cloning site between BamHI and XbaI restriction sites. The HiBiT NanoBiT fragment was encoded at the N-terminal of the effector, with a 5 x serine glycine linker, between HindIII and BamHI.*

promotor regions bracket the multiple cloning site and were used for sequencing of DNA.

pcDNA3.1(+) neo expression vectors were used to encode GPCR constructs (*Figure 2.1*). The human β_2 adrenoceptor sequence (Genbank Ref: NM_000024.6) or human β_1AR sequence (Genbank Ref NM_000684.3), lacking start and stop codons, were cloned into the vector, between Bam*HI* and Xho*I* restriction sites. An N-terminal SNAP-tag (New England Biolabs; USA) sequence, preceded by a Kozak translation initiation site (GCC ACC ATG) and a murine serotonin 5-hydroxytryptamine 3A (5HT3R) signal sequence (Peptide sequence: MRLCIPQVLLALF LSMLTGPGEGSRK), was cloned upstream between Kpn*I* and Bam*HI* sites. The 5HT3R signal sequence was inserted to promote export of the receptor protein to the plasma membrane. The C-terminal LgBiT sequence (Dixon, *et al.*, (2016); Promega Coporation; WI, USA) was cloned following the receptor DNA between Xho*I* and Xba*I*. Due the length and flexibility of the C-termini of the β adrenoceptors, a peptide tag was not required between the receptor and the LgBiT tag.

pcDNA3.1(+) zeo expression vectors were used to encode effector constructs (*Figure 2.2*). Each effector, either human β-arrestin2 or mini Gαs was placed in the multiple cloning site between Bam*HI* and Xba*I* restriction sites. Effector DNA was preceded by a Kozak translation initiation site (GCC ACC ATG) and either SmBiT (VSGYRLFEEIL) or HiBiT (VSGWRLFKKIS) NanoBiT fragment, with a 5 x serine glycine linker, between Hind*III* and Bam*HI*. A serine-glycine peptide linker was used to attach the tag to allow flexibility of movement between the tag and the effector protein.

2.2.2. Polymerase Chain Reaction (PCR)

PCR was used to either (1) mutate nucleotides of existing DNA in site-directed mutagenesis or (2) amplify vector and insert fragments for Gibson assembly ligation reactions. Primers used in both protocols as described in *Table 2. 1*. In both protocols following PCR reaction, 20 µL of each PCR product was treated with 1 µL of the enzyme DpnI, which acts to selectively remove methylated template DNA, and incubated for 2 hours at 37°C.

2.2.2.1. Site-Directed Mutagenesis of SmBiT Fragment to Sm114

To mutate the SmBiT 11 amino acid fragment from V**S**GYRLFEEIL to Sm114 (V**T**GYRLFEEIL), a polymerase chain reaction (PCR) reaction was used. The complete vector was amplified using paired primers (*Table 2. 1*) to generate the serine>threonine

codon mutation, with the following experimental reaction: 50 ng of template DNA (pcDNA 3.1 zeo SmBiT β-arrestin2), 125 ng each of forward and reverse primers, 5 µL of accuzyme buffer (Final Concentrations: 60 mM Tris-Cl, 6m M $(NH_4)_2SO_4$, 10 mM KCl, 2 mM $MgSO_4$, pH 8.3) and 200 µM deoxynucleotide phosphates (dNTPs). A "Hotstart" protocol to initiate specific primer annealing prior to polymerase addition was used: an initial 2 minute DNA denaturing step (95°C), followed by 60°C at which point accuzyme polymerase was added. A negative control reaction was included without accuzyme addition. PCR reaction then continued with 16 cycles of denaturation (95°C, 30 seconds), annealing of primers (60°C, 1 minute) and extension of DNA via accuzyme polymerase (68°C, 11 minutes). Following DpnI treatment, the mutated vector was transformed into competent bacterial cells, with positive colonies cultured and DNA purified and screened for mutation (*Methods 2.2.5 — 2.2.6*).

2.2.2.2. PCR amplification of insert and vector DNA

PCR was used to isolate and amplify HiBiT insert from pcDNA3.1 HiBiT mini Gαs insert (*Figure 2. 2. d*) and pJ411 vector fragments from donor vectors, where appropriate restriction sites were not available for excision, using Q5® High-Fidelity DNA polymerase. For each vector and insert PCR, the following experimental reaction was used: 1 ng of template DNA (either donor vector or insert plasmid), forward and reverse primers at 10 µM each, 10 µL of Q5® reaction buffer and 200 µM dNTPs. A "Hotstart" protocol used an initial 2 minute DNA denaturing step (94°C) and holding at 55°C, at which point Q5® High-Fidelity DNA polymerase was added. Negative control reaction was prepared as described, with no Q5® High-Fidelity DNA polymerase added to the reaction. PCR reaction then continued with 25 cycles of denaturation(94°C, 2 minutes), annealing of primers (55°C, 1 minute) and extension of DNA via Q5® High-Fidelity DNA polymerase (72°C, 2 minutes), with a final elongation step of 7 minutes at 72°C. Following DpnI treatment, 5x loading dye was added to each PCR and DNA analysed using gel electrophoresis (*Methods 2.2.3.2.2*), isolated and purified using GenElute™ Gel Extraction Kit (Sigma-Aldrich)(*Methods 2.2.3.2.3*) and used in Gibson assembly reaction (*Methods 2.3.1*).

Reaction	*Oligonucleotide Primer*	*Sequence*
Site-directed Mutagenesis	Forward	5' CTTGCCACCATGGTGACCGGCTACCGGCTGTCC
	Reverse	5' GAACAGCCGGTAGCCGGTCACCATGGTGGCAAG
pJ411 Vector Amplification	Forward	5' ATCGAGAAACAATTGCAGAAAGACAAACAGGTC
	Reverse	5' GGATCCACCCTGGAAGTACAGGTTTTC
HiBiT Insert Amplification	Forward	5' TTCCAGGGTGGATCCGTTTCTGGATGGCGGCTGTTCAAGAAG
	Reverse	5' CAATTGTTTCTCGATTCCGCCGCTAGAGCCGCTGATC

Table 2.1 Summary of oligonucleotide primer sequences for site-directed mutagenesis and amplification PCR reactions. *Primers designed for site-directed mutagenesis, with highlighted mutations, complementary to pcDNA 3.1 zeo SmBiT β-arrestin vector. For amplification PCRs, primers anneal to donor pJ411 bacterial vector and HiBiT insert plasmids to produce fragments, with complementary overhanging Gibson fragments for Gibson assembly (Figure 2. 4). Primers were between 27-42 nucleotides in length and 3' ending in either C or G to help PCR polymerase priming.*

2.2.3. Restriction Enzyme Digestion and Purification

Restriction enzymes were used to isolate fragments from donor vectors and insert plasmids, using complementary restriction enzyme sites in the multiple cloning site of pcDNA3.1(+) templates.

2.2.3.1. Vector DNA Digestion & Purification

2.2.3.1.1. Vector Digestion

pcDNA3.1(+) vector DNA was prepared for subsequent ligations, using double digestion with multiple cloning sequence restriction enzymes, such as BamHI and XhoI. The following experimental reaction was set up in a 0.5 mL microcentrifuge tube: 2 µg DNA, 2 µL fast digest buffer made up to 20 µL with ddH_2O, prior to addition of 1 µL of each restriction enzyme. Digests were incubated for 1 hour at 37°C for enzyme digestion, and then 5 minutes at 80°C and 20 minutes 65°C to inactivate the restriction enzymes.

2.2.3.1.2. Alkaline Phosphatase Treatment & Vector Purification

To dephosphorylate sticky ends of digested vector DNA, fragments were treated with shrimp alkaline phosphatase. Removal of sticky ends of DNA fragments prevents re-ligation of vector DNA and thus reduces background colonies after transformation of ligation reactions. To the digested vector reaction, 2 µL of fast shrimp alkaline phosphatase and 2 µL fast shrimp alkaline phosphatase buffer (10 mM Tris-HCl, 5 mM $MgCl_2$, 100 mM KCl, 0.02% Triton X-100, 0.1 mg/mL bovine serum albumin (BSA); pH 8.0) was added and incubated for 90 minutes at 37°C, with a further 10 minutes at 75°C for enzyme inactivation.

Vector DNA was purified using GenElute™ PCR Clean-up kit (Sigma-Aldrich), in brief: a spin column was inserted into a 2 mL collection tube and prepared using 500 µL of column preparation solution, centrifuged (12,000 g, 30 seconds) and the elute discarded. 20 µL of the digested vector was mixed with 100 µL of (5x) binding solution, before being added to the prepared column. The column was centrifuged (12,000 g, 1 minute) and elute discarded. The column was washed with 500 µL of wash solution, centrifuged (12,000 g, 1 minute) and elute discarded before being further

centrifuged (12,000 g, 1 minutes). The column was removed to a clean 2 mL collection tube and 40 µL of ddH_2O was added directly onto the binding column membrane. The column was incubated at room temperature for 1 minute and centrifuged (12,000 g, 2 minutes) to elute purified vector DNA.

2.2.3.2. Insert DNA Digestion & Purification

2.2.3.2.1. Insert Digestion

Insert DNA was isolated from donor vectors by double digestion with restriction enzymes, such as BamHI and XhoI, using the following experimental reaction in a 0.5 mL microcentrifuge tube: 2 µg DNA, 2 µL fast digest (green) buffer and made up 20 µL with ddH_2O, before the addition of 1 µL of each restriction enzyme. The green fast digest buffer was used as it contained loading dye and glycerol, allowing for direct loading into agarose gels in gel electrophoresis. Digest was incubated for 1 hour at 37°C for enzyme digestion, 5 minutes at 80°C and 20 minutes 65°C to inactivate the restriction enzymes.

Insert DNA was isolated using gel electrophoresis, before being cut from the agarose gel and purified using GenElute™ Gel Extraction Kit (Sigma-Aldrich).

2.2.3.2.2. Gel Electrophoresis

DNA was separated by size using agarose gel electrophoresis, where an electric current causes negatively charged DNA to migrate towards the positive electrode. The migration is size dependent due to the pore size of the gel matrix, with smaller fragments migrating more rapidly towards the positive electrode. Agarose gels were generally prepared at 1%, though for the isolation of DNA fragments of less than 40 base pairs a 2% gel was prepared. For a 1% agargose gel, 400 mg of agarose solid dissolved in 40 mL TBE buffer (89mM Tris base, 89mM boric acid, 2mM EDTA; pH 7.6), using a microwave (2 minutes) to heat and aid solubilisation. Solution was cooled for ~5 minutes, before ethidium bromide (0.125 µg/mL) was added and the solution was poured into gel-casting mould to set for 30 minutes. Upon setting, the gel was removed from the cast and put into an electrophoresis tank, which was then filled with TBE buffer.

Digested DNA (or PCR product; see *Methods 2.2.2.2*) was loaded into agarose gel well in parallel with 1 kb DNA ladder (Promega, Madison, WI, USA). The gel was run at 80 volts for 40 minutes, and then illuminated with ultraviolet (UV) light to image ethidium bromide stained DNA bands on the gel. UV light exposure was kept at a minimum to avoid damage to the DNA.

2.2.3.2.3. Insert Purification

Inserts were identified by size compared to 1kb DNA ladder, for example predicted cDNA size of mini Gαs between BamHI and XbaI (*Figure 2.2. b & d*) is 699 base pairs. The band containing desired DNA was excised from the agarose gel, minimising the amount of extra agarose excised, and the gel weighed (~100 mg). 3 volumes of gel weight (~300 µL) of solubilisation solution was added to the gel and incubated at 50-60°C to dissolve, agitating using a vortex every 2-3 minutes. A silica binding column was prepared by placing column into 2 mL collection tube and adding 500 µL of column preparation buffer. Column and collection tube were centrifuged (12,000 g, 1 minutes) and elute was discarded. Once the gel had dissolved, 1 volume of gel weight (~100 µL) of isopropanol was added to the solubilised gel, mixed by inversion, added to the binding column and centrifuged (12,000 g, 1 minute). The elute was discarded and the column was washed with 700 µL of wash solution and centrifuged (12,000 g, 1 minute). The elute was discarded and column was further centrifuged (12,000 g, 1 minute). The binding column was transferred to a clean 2 mL collection tube and 50 µL ddH_2O was directly added onto the binding column membrane. The binding column was incubated at room temperature for 1 minute and centrifuged (12,000 g, 1 minute) to elute the DNA.

2.2.4. Ligation of Vector and Insert DNA

To ligate purified vector and insert DNA, a ligation reaction was set up typically using a molar ratio of vector:insert of 1:3 to increase ligation efficiency, using 50 ng of vector DNA. Experimental ligation reactions were set up using: appropriate volumes of purified vector and inert DNA, 1 µL T4 DNA ligase, 1 µL ligase buffer (40 mM Tris-HCl, 10 mM MgCl2, 10 mM dithiothreitol, 0.5 mM ATP; pH 7.8), with the volume made up to 10 µL with ddH_2O. Negative reaction was set

up with no insert added to the reaction. Reactions were incubated for 16 hours at 16°C.

2.2.5. Transformation of DNA into Chemically Competent Bacteria

Ligation reactions (*Methods 2.2.4*) or PCR products from site-directed mutagenesis (*Methods 2.2.2.1*) were stored on ice prior to bacterial transformation. One Shot™ TOP10 chemically competent E. coli cells (Invitrogen) were defrosted on ice, before adding 25 µL of cells into a 1.5 mL pre-chilled microcentrifuge tube. For transformation of pJ411 plasmids (*Figure 2. 3*) (*Methods 2.3.2.1*), E. coli strain BL21(DE3) NiCo cells (New England BioLabs Inc.) were used. Returning the tube to ice, 2.5 µL of DNA (ligation product or PCR reaction product) was added to cells and incubated on ice for 20 minutes. Cells were then 'heat-shocked' to promote cellular uptake of DNA by incubating tube at 42°C for 30 seconds and then returned to ice for 2 minutes. 500 µL of LB broth (20 g/L) was added to the tube and placed in a shaking incubator for 1 hour at 37°C, before 100 µL of the resultant culture was spread on LB agar plate (35 mg/mL) with either ampicillin (75 µg/mL) or kanamycin (30 µg/mL), dependent on the resistance gene of the vector. Plates were incubated at 37°C overnight (12-16 hours), with colonies used to identify E.coli cells which have taken up DNA plasmid containing antibiotic resistant gene. Negative controls of bacterial transformations were conducted as described, using ligation reactions without the addition of insert DNA.

2.2.6. DNA Purification from Miniprep Bacterial Culture

Positive colonies grown under antibiotic selection pressure were picked using a 200 µL sterile pipette tip, which was then expelled into 5 mL LB broth (20 g/L) containing ampicillin (100 µg/mL) or kanamycin (30 µg/mL) and placed in a shaking incubator overnight at 37°C.

To obtain DNA from overnight culture, the GenElute™ Plasmid Miniprep Kit (Sigma-Aldrich) was used according to manufacturer's guidelines. 3 mL of bacterial culture was pelleted using centrifugation (4000 g, 5 minutes), storing the remaining 2 mL of culture at 4°C. Removing the supernatant, the bacterial pellet was resuspended in 'resuspension solution', ensuring RNase was added to remove RNA. Cells were lysed using alkaline lysis solution containing sodium hydroxide and SDS, with neutralisation/binding solution then used to neutralise mixture and precipitate cell debris including denatured genomic DNA. Cell lysate was cleared via centrifugation (14,000 g, 10 minutes) with supernatant removed and added to silica binding column and centrifuged (12,000 g, 1 minute),

discarding the eluate. The column was washed with wash solution, containing ethanol (80 % v/v) and centrifuged (12,000 g, 30 seconds), discarding eluate, before further centrifugation (12,000 g, 2 minutes) to remove any further ethanol. The binding column was moved to a clean 2 mL microcentrifuge tube and 100 µL of ddH_2O was added to the binding column membrane. The binding column was incubated at room temperature for 1 minutes before the solubilised DNA was eluted by centrifugation (12,000 g, 1 minute). Following confirmation of mutation within insert DNA, desired insert DNA was cloned into a new pcDNA3.1 (+) vector (*Methods; 2.2.3 — 2.2.6*) to negate possible undesired mutations in vector sequence through the PCR process. For DNA produced from vector-insert ligation, a small sample was digested with restriction enzymes and imaged using gel electrophoresis (*Methods; 2.2.3.2.2*) to confirm ligation of DNA fragments.

2.2.7. DNA Purification from Maxiprep Bacterial Culture

Following the confirmation of insert-vector ligation, a larger bacterial preparation was set up for DNA purification, by adding 200 µL of stored working miniprep culture to 5 mL LB broth (20 g/L) and ampicillin (100 µg/mL) or kanamycin (30 µg/mL) and incubated in a shaking incubator for 37°C for ≥ 6 hours. Following incubation, 5 mL culture was added to 120mL LB broth (20 g/L) and ampicillin (100 µg/mL) or kanamycin (30 µg/mL) and placed in shaking incubator at 37°C for 12-16 hours.

To obtain DNA from overnight 120 mL culture, the commercial QIAGEN Plasmid Maxi Kit (Qiagen) was used adhering to manufacturer's guidelines. Cells were pelleted by centrifugation (4000 g, 20 minutes, 4°C), discarding the supernatant and resuspending pelleted cells in 10 mL of 'P1' buffer containing sucrose / TE and RNAse Cells were lysed with 10 mL of alkaline lysis 'P2' buffer and mix thoroughly by inversion 4-6 times, before incubating at room temperature for 5 minutes. The mixture was neutralised by adding 10 mL of 'P3' buffer, mixing by inversion and incubating in the filter column for 10 minutes. Mixture was then filtered to remove the precipitated cell debris, into a pre-equilibrated DNA binding column and allow to flow through via gravity. The binding column was washed twice with 'QC' solution, before eluting the bound plasmid DNA into a fresh 50 mL tube using 15 mL 'QF'. DNA was precipitated by addition of 0.7 volumes (10.5 mL) isopropanol, mixed by inversion and DNA was pelleted by centrifugation (4000 g, 60 minutes, 4°C). The supernatant was carefully removed and the pellet resuspended in 300 µL Tris EDTA (TE) buffer and transferred to a fresh 1.5 mL microcentrifuge tube. 0.1 volumes of 3M Sodium acetate (pH 5.2) and 2.2 volumes

of100 % ethanol were added and the mixture was centrifuged (14,000 g, 10 minutes). The DNA pellet was washed with 70 % ethanol and the mixture was centrifuged (14,000 g, 5 minutes). The wash supernatant was carefully removed and the pellet left to dry for 10 minutes before resuspension in 200 µL TE buffer and left to fully dissolve for 30 minutes.

2.2.8. Determination of DNA Concentration, Purity and Sequencing

All determination of DNA concentration and purity (as define by absorbance; 260nm/280nm between 1.7-1.9) was determined using NanoDrop™ spectrophotometer (Thermo Scientific™). For sequencing, a small sample was sent to the DNA sequencing facility at the University of Nottingham to confirm plasmid DNA sequence, using T7 and BGH sequencing primers for forward and reverse sequencing, respectively. Confirmed DNA sequences were then transfected into model cells, in either a single or dual expression cell line (See section *2. 4. 4*) and summarised in *Table 2. 3*.

2.3. Bacterial Expression & Purification of HiBiT-Mini Gαs Protein

2.3.1. Bacterial Vector Construction and Generation

For transfection and expression of DNA, in bacterial cells, a pJ411 expression vector was used to encode a HiBiT tagged mini Gαs (*Figure 2. 3*). The pJ411 vector contained resistance genes for kanamycin for selection in bacterial expression and an origin of replication (ORI) site to promote high copy number. A T7 promoter region was present upstream of the multiple cloning site, encoding the gene of interest, and was used for sequencing of HiBiT-mGαs DNA. An upstream lac operator was used to induce of gene expression, under the treatment of isopropylthio-β-galactoside (IPTG). A Tobacco Etch Virus (TEV) cleavage site was present between HiBiT DNA and the His10 sequence, with the latter used for protein purification. HiBiT DNA was inserted into pJ411 vector containing His10 tagged mini Gαs protein via Gibson assembly (*Figure 2. 4*), producing the bacterial vector illustrated in *Figure 2. 3*. In brief, vector and insert DNA fragments were generated by PCR amplification with template DNA digested with DpnI treatment, (*Methods 2.2.2.2*)), isolated using gel electrophoresis (*Methods 2.2.3.2.2*) and purified using GenElute™ Gel Extraction Kit (Sigma-Aldrich) (*Methods 2.2.3.2.3*). Fragments were ligated using Gibson reaction mix, using 50 ng of vector and insert fragments at 3:1 insert:vector molar ratio, incubating reaction at 50°C for 1 hour. Ligated DNA was transformed (*Methods 2.2.5*), cultures were grown from positive colonies and DNA was purified (*Methods 2.2.6*), and sequenced by the DNA sequencing facility at the University of Nottingham.

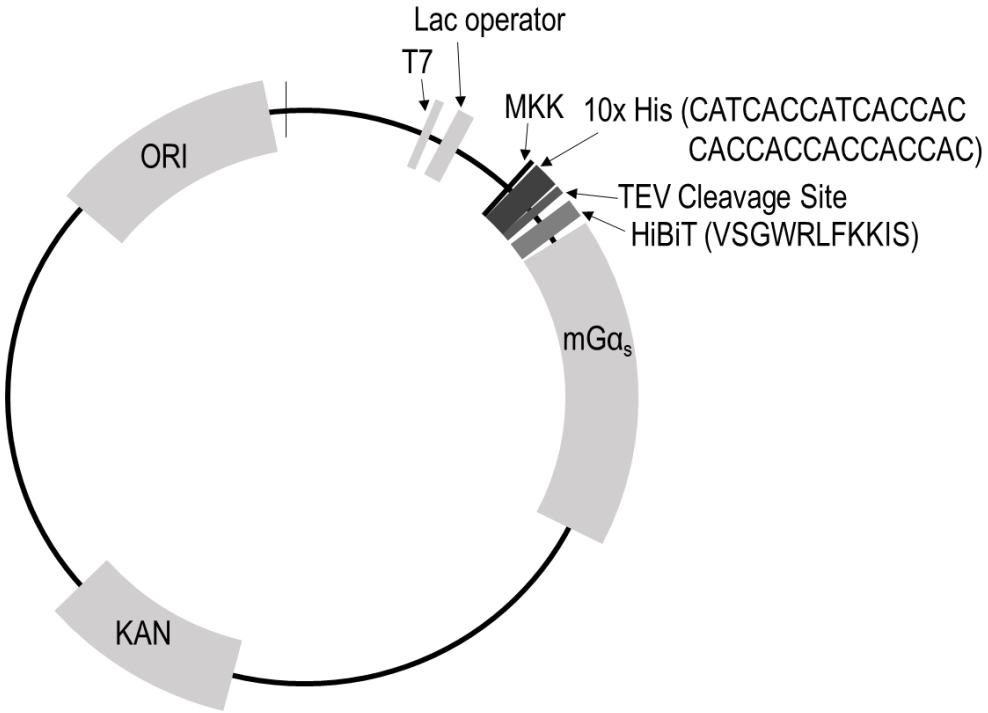

Figure 2. 3 Bacterial vector map of NanoBiT labelled mini Gα$_s$ protein. *pJ411 vectors encoded modified mini Gαs protein, N-terminally labelled Hisx10 tag followed by a Tobacco Etch Virus (TEV) cleavage site and 11 amino acid HiBiT sequence. The pJ411 vector contained resistance genes for kanamycin for selection in bacterial expression and an ORI site to promote high copy number. A T7 promoter region was present upstream of the multiple cloning site, encoding the gene of interest, and was used for sequencing of HiBiT-mGαs DNA. The lac operator was used for induction of bacterial gene expression, under the treatment of isopropylthio-ß-galactoside (IPTG).*

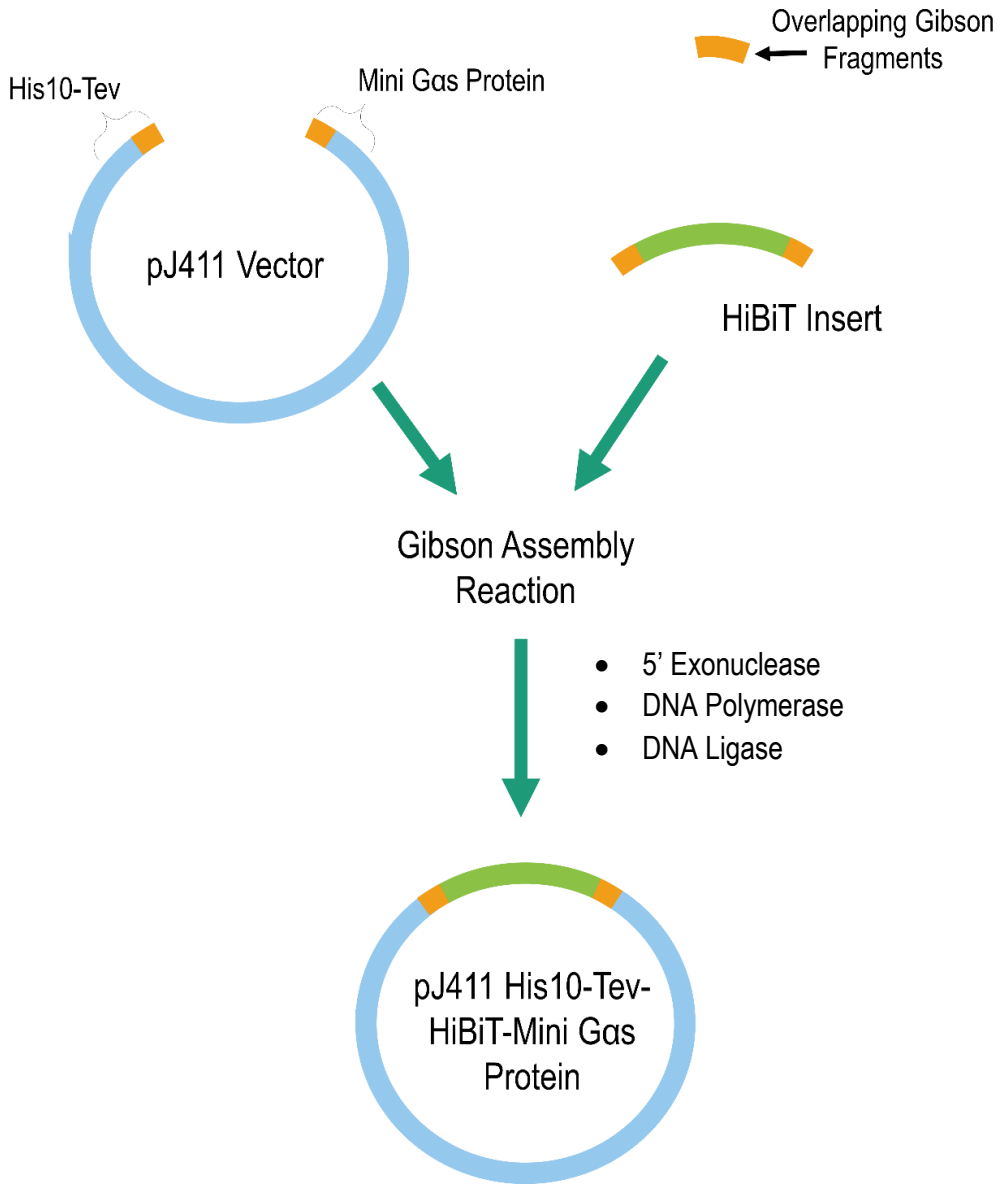

Figure 2. 4 Gibson assembly, for the construction of pJ411 His10-Tev-HiBiT-mini Gαs protein bacterial plasmid. *pJ411 vectors, encoding 10x histidine tag, followed by a TEV cleavage site and a mini Gαs protein, and HiBiT insert were produced via PCR amplification reaction using paired primers (2. 2. 2. 2; Table 2. 1) with overlapping 'Gibson fragments'. Gibson fragments are double stranded DNA, present in both the insert and vector DNA. The Gibson assembly reaction is isothermal, combing overlapping base pair fragments to combine DNA fragments. The Gibson assembly uses an exonuclease, which 'chews' the 5' end to generate long overhanging regions, DNA polymerase, to fill the gaps of the single strand regions, and DNA ligase, to seal the gaps between the fragments, to form the final plasmid.*

2.3.2. Bacterial Expression of pJ411 His10-Tev-HiBiT-mini Gαs Protein Bacterial Plasmid, Harvest and Purification

2.3.2.1. Protein Expression

The pJ411 construct encoding mini Gαs protein, with N-terminally tagged HiBiT (HiBiT-mini Gαs), was transformed into E. coli strain BL21(DE3) NiCo cells (*Methods 2.2.5*), and cultured in 5mL LB + 5 µg/mL kanamycin. The bacterial culture was propagated in 1L TB + 5 µg/mL kanamycin to an optical density (OD) of 0.6, before induction with IPTG (1 mM), for 24 h at 16 °C. Cells were harvested by centrifugation (3000 g, 20 minutes) and the pellet stored at -80°C until protein purification

2.3.2.2. Protein Purification

Cell pellets were thawed on ice and resuspended and lysed in lysis buffer (20mM HEPES, 500mM NaCl, 40mM Imidazole, 10% glycerol, 8mM β-mercaptoethanol, 1uM GDP, 40 µg/mL DNase I, 40 µg/mL lysozyme, supplemented with cOmplete™ Mini EDTA-free Protease Inhibitor Cocktail. pH7.5). Cells were lysed further via sonication on ice, with 5 bursts of 10 seconds at 30% power, followed by 30 second rest. The cell lysate was cleared by centrifugation (25,000 g, 45 minutes) and filtered through a 0.2 µm filter-tip. Filtered lysate was loaded onto a 5 mL HisTrap FF column. The column was washed with wash buffer (20mM HEPES, 500mM NaCl, 40mM Imidazole, 10% glycerol, 8mM β-mercaptoethanol, 1uM GDP. pH7.5) and then the bound His-tagged protein was eluted with elution buffer (20mM HEPES, 500mM NaCl, 400mM Imidazole, 10% glycerol, 8mM β-mercaptoethanol, 1uM GDP. pH7.5) on a 0-100% elution gradient (wash buffer to elution buffer) into 5 mL fractions. Protein presence in the fractions was indicated by UV illumination and confirmed using SDS-PAGE gel. Peak fractions were concentrated to ~4 mL using Pierce™ 10 kDa Protein Concentrators and dialysed into assay buffer (Hank's balanced salt solution (*Methods ; 2. 6. 3*), 10% glycerol, 8mM β-mercaptoethanol, 1uM GDP) for 18 hours using Slide-A-Lyzer™ 10 kDa Dialysis Cassettes (ThermoFisher Scientific). Dialysed protein was aliquoted, flash-frozen in liquid nitrogen, and stored at -80 °C, at a typical yield of 1 mg of HiBiT-mGαs per litre of bacterial culture.

2.4. Cell Culture and Transfection of HEK293T cells

2.4.1. Cell Maintenance and Passaging

Human embryonic kidney (HEK293T) cells were maintained in a humidified incubator at 37°C and 5 % CO_2, in sterile polystyrene flasks (25, 75 or 175 cm^2 growing surface; known as T25, T75 and T175, respectively),using Dulbecco's modified Eagle's medium (DMEM) based media (high glucose DMEM, supplemented with 10 % foetal calf serum (FCS); (DMEM/10%FCS). Cells were passaged at 70-90 % confluency, with a split ratio between 1:2 and 1:30. When splitting, DMEM/10%FCS was aspirated and cells were washed with sterile phosphate buffered saline (PBS). PBS was aspirated and either 0.5/1/3 mL of sterile trypsin solution was added to the T25/75/175 flask, respectively, and incubated for 5 minutes at 37°C. Flasks were physically agitated by knocking the side of the flask and, using 10 mL DMEM/10%FCS, cells were washed off the flask and collected in a 30 mL sterile universal tube. To remove trypsin and pellet cells, the universal was centrifuged (1000 g, 5 minutes) and the pellet resuspended in 10 mL of DMEM/10%FCS. Cells were split according to required ratio or a sample was counted for seeding plates.

2.4.2. Cell Counting and Plate Seeding

To ensure HEK293 cell adherence, 96 and 6 well plates were coated with poly-d-lysine on the day of cell seeding. 50 µL or 2.5 mL of 10 µg/mL poly-d-lysine was added to wells of 96 and 6 well plates, respectively, and incubated for 30 minutes. Poly-d-lysine was then aspirated and wells were washed with either 100µL or 3 mL of sterile DMEM/10%FCS in 96 and 6 well plates, respectively, before wells were seeded.

Cells were seeded 24 hours in advance of assays. Cells were removed from the flask and pelleted using centrifugation as described (*Methods 2.4.1*), then resuspended in 10 mL of DMEM/10%FCS. A sample of cell resuspension mix was added to a haemocytometer and cells were counted within the grid (1 mm^2, with a depth of 0.1 mm). To scale up to number of cells per mL of cell resuspension, cell count was multiplied by 10,000. Seeding densities and well volumes are detailed in Table 2.2, with the following equation used to determine volume of cell resuspension required for seeding solution:

$$\frac{Volume\ of\ Cell\ Suspension}{Required\ (mL)} = \frac{Number\ of\ Cells\ Required\ (per\ mL)\ x\ Required\ Seeding\ Volume\ (mL)}{Number\ of\ Counted\ Cells\ (per\ mL)}$$

The volume of cell resuspension required was then diluted up to seeding solution volume with DMEM/10%FCS and seeded into a poly-d-lysine coated plates using an Eppendorf Multipipette Combitip dispenser.

Plate Type	*Cell Density per Well*	*Seeding Volume per Well*	*Used in:*
96 Well, black flat-bottomed (655090, Greiner Bio-One)	25,000 - 30,000	100 µL	Receptor Internalisation Assay (*Methods; 2.6.1*)
96 Well, white flat-bottomed (655098, Greiner Bio-One)	35,000 – 40,000	100 µL	NanoBiT Complementation Assay (*Methods; 2.6.2*)
6 Well, clear flat-bottomed plates (3516; Corning Costar, Sigma-Aldrich)	200,000 - 250,000	3 mL	Transient Transfection (*Methods; 2.4.4.1*)

Table 2.2 Cell seeding densities and volumes for transfected HEK293T cells, in 6 and 96 well plates.

2.4.3. Freezing and Thawing Cells

To freeze, cells were grown to 90-100 % confluency in a T75 flask and pelleted using centrifugation (*Methods 2.4.1*). Following centrifugation, the cell pellet was resuspended in 2 mL of FCS/10%DMSO, with 1 mL added to two cryovials and placed in a room temperature freezing container (Nalgene Mr Frosty). The freezing container contained isopropyl to ensure cooling of cells by 1°C/min in -80°C freezer, thus preventing protein degradation through crystallisation. The freezing container was placed in -80°C freezer for 24 hours, before transferring cryovials to liquid nitrogen stores.

To thaw cells, a cryovial was removed from liquid nitrogen and warmed at room temperature until defrosted. Freezing media containing the cells was added to 10 mL of DMEM/10%FCS and centrifuged (1,000 g, 5 minutes). The pellet was resuspended in 1 mL of DMEM/10%FCS and all cells were added to a T75 flask containing DMEM/10%FCS. Cells were then incubated for 24 hours before replacing media and adding necessary antibiotics for selection maintenance.

2.4.4. Transfection and Antibiotic Selection of Cells

2.4.4.1. Transient Transfection

HEK293T cells were transiently transfected using Lipofectamine 3000 (Invitrogen, Paisley, UK) reagents, with the protocol adapted from manufacturer's guidelines. 24 hours prior to transfection, HEK293T cells were seeded into a poly-d-lysine coated 6 well plate (*Methods 2.4.2*) and grown to 60-70 % confluency on the day of transfection. 3.75 µL of Lipofectamine 3000 reagent was diluted in 125 µL of OptiMEM™ media and mixed by slowly aspirating and dispensing solution via a 1 ml pipette. 5 µg of cDNA was mixed with 125 µL of OptiMEM™ media and mixed by inversion, followed by the addition of 10 µL of P3000 reagent. The DNA/P3000 mix was mixed by inversion and added to dilute Lipofectamine 3000. The DNA/Lipofectamine mix was incubated at room temperature for 10-15 minutes. During incubation, HEK293T cells were washed with 2 mL/well of OptiMEM™ media and the media then replaced with a further 2.5 mL/well of OptiMEM™. Following 10-15 minute incubation, the DNA/lipofectamine 3000 mix was added directly onto HEK293T cells and incubated for 24 hours in a humidified incubator at 37°C and 5 % CO_2. Cells

were then split from 6 well plate and seeded onto 96 well assay plate (*Methods 2.4.1 - 2.4.2*).

2.4.4.2. Stable Transfection

For stable transfections, HEK293T cells were transfected once, with expression of plasmid DNA using antibiotic selection and maintenance.

HEK293T cells were stably transfected using Lipofectamine 3000 reagents, with protocol adapted from manufacturer's guidelines. HEK293T cells, cultured in a T25 flask were grown to 60-70 % confluency on the day of transfection. 7.5 µL of Lipofectamine 3000 reagent was diluted in 250 µL of OptiMEM™ media and mixed by slowly aspirating and dispensing solution via a 1 mL pipette. 10 µg of cDNA was mixed with 250 µL of OptiMEM™ media and mixed by inversion, followed by the addition of 20 µL of P3000 reagent. The DNA/P3000 mix was mixed by inversion and added to dilute Lipofectamine 3000. The DNA/Lipofectamine mix was incubated at room temperature for 10-15 minutes. During incubation, HEK293T cells were washed with 2 mL of OptiMEM™ media and the media replaced with a further 4 mL of OptiMEM™. Following 10-15 minute incubation, DNA/lipofectamine 3000 mix was added directly onto HEK293T cells and incubated for 24 hours in a humidified incubator at 37°C and 5 % CO_2. Cells were then split as described in 2.4.1, with a split ratio of 1:5 and further incubated for 24 hours. Media was then aspirated and replaced with fresh media containing appropriate antibiotic (500 µg/mL G418 and/or 5 µg/mL zeocin) for selection pressure for 7-10 days, with the flask passaged between 70-80 % confluency. During selection, antibiotic containing media was replaced every 3-5 days to remove any dead cells. After transfection, antibiotics were added to cell maintenance media: 100 µg/mL G418 and/or 2.5 µg/mL zeocin. A list of stable cell lines, with transfected DNA plasmids is provided in *Table 2. 3*.

2.5. Terbium Labelling of Receptors and Membrane Preparation

2.5.1. Terbium labelling of SNAP-β_2 adrenoceptor

Cells to be used for TR-FRET assays required labelling of receptors expressing the N-terminal SNAP-tag with terbium cryptate (*Figure 2. 5*). Using HTRF Tag-lite SNAP-Lumi4-Tb labelling reagent (Cisbio Bioassays, Bagnols-sur-Cèze, France) (SNAP-Lumi$_4$-Tb), a terbium cryptate fluorophore was covalently attached to the SNAP-tag of the receptor. Solid SNAP-Lumi$_4$-Tb was reconstituted in DMSO and LabMed reagent to 100 nM and stored at -20°C.

Cell Line	Transfected Constructs	Antibiotic Resistance
HEK β_2AR-LgBiT	pcDNA3.1 β_2AR-LgBiT	Neomycin
HEK β_2AR/SmBiT-β-arrestin2	pcDNA3.1 β_2AR-LgBiT	Neomycin
	pcDNA3.1 SmBiT-β-arrestin2	Zeocin
HEK β_2AR/SmBiT-Mini Gαs Protein	pcDNA3.1 β_2AR-LgBiT	Neomycin
	pcDNA3.1 SmBiT- Mini Gαs Protein	Zeocin
HEK β_2AR/HiBiT-β-arrestin2	pcDNA3.1 β_2AR-LgBiT	Neomycin
	pcDNA3.1 HiBiT-β-arrestin2	Zeocin
HEK β_2AR/HiBiT-Mini Gαs Protein	pcDNA3.1 β_2AR-LgBiT	Neomycin
	pcDNA3.1 HiBiT- Mini Gαs Protein	Zeocin
HEK β_1AR-LgBiT	pcDNA3.1 β_1AR-LgBiT	Neomycin
HEK β_1AR/SmBiT-β-arrestin2	pcDNA3.1 β_1AR-LgBiT	Neomycin
	pcDNA3.1 SmBiT-β-arrestin2	Zeocin
HEK β_1AR/SmBiT-Mini Gαs Protein	pcDNA3.1 β_1AR-LgBiT	Neomycin
	pcDNA3.1 SmBiT- Mini Gαs Protein	Zeocin

Table 2. 3 Summary of HEK cell lines, with transfected cDNA and antibiotic resistance.

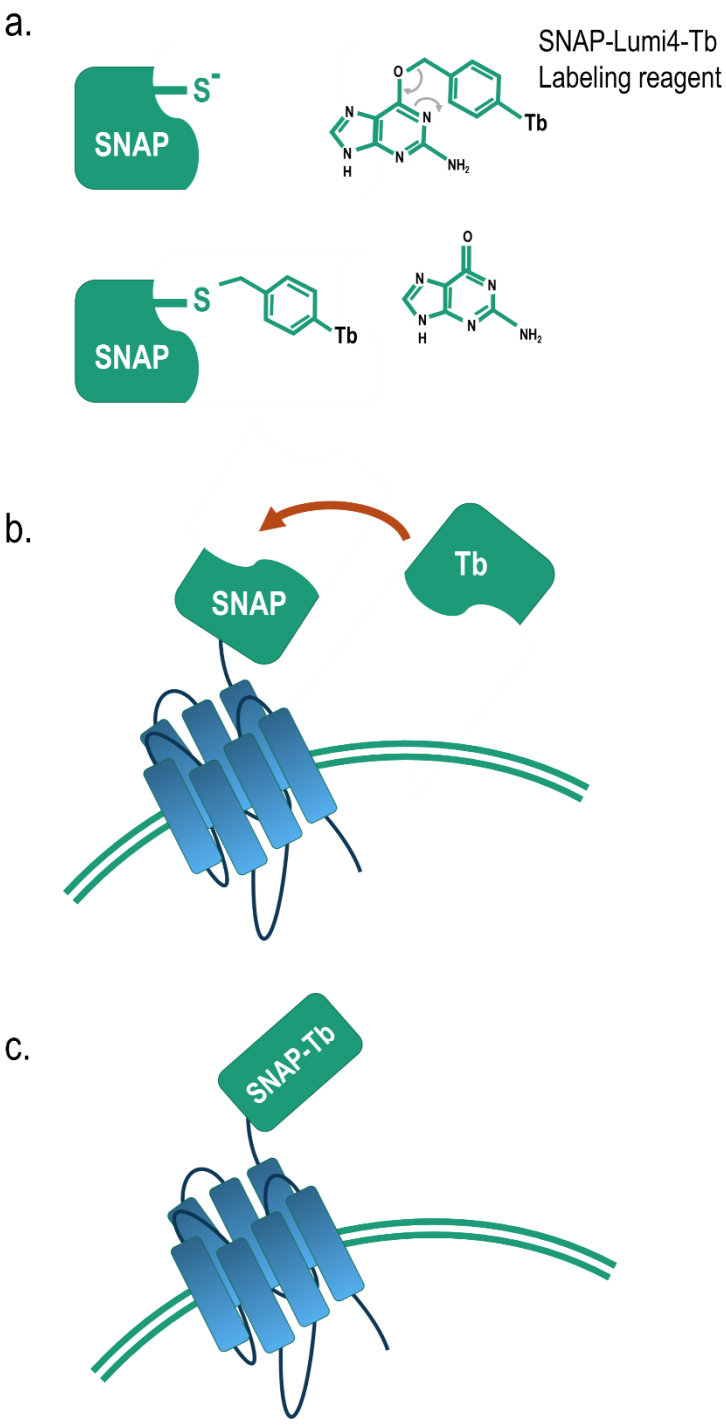

Figure 2. 5 Terbium labelled of N-terminal SNAP tag. *(a.)The SNAP-tag fusion protein is covalently labelled using the HTRF Tag-lite SNAP-Lumi4-Tb labelled reagent. (b.-c.) The genetically encoded SNAP-tag of receptor constructs are specifically labelled at cell-surface receptors.*

For labelling, HEK293 cells were grown to 90 % confluency in poly-d-lysine coated T175 flasks, in DMEM/10% FCS. Prior to terbium labelling, DMEM/10% FCS was removed and cells were washed with 2 x 15 mL PBS. Cells were incubated with 10 mL of 100 nM SNAP-Lumi$_4$-Tb at 37°C/5 % CO_2 for 1 hour. Following incubation, SNAP-Lumi$_4$-Tb was removed and cells were washed with 2 x 15 mL PBS. Cells were scraped into 10 mL DMEM/10% FCS and pelleted by centrifugation (2,000 g, 5 min). Pelleted cells were stored at -80 °C prior to membrane preparation.

2.5.2. Membrane preparation of HEK293T cell lines

Prior to membrane preparation, cells (± SNAP-Lumi$_4$-Tb labelling) were pelleted using centrifugation (2000 g, 5 minutes) and stored at -80 °C. All samples and reagents were kept at 4°C throughout preparation to avoid degrading of protein samples. Pelleted cell samples (containing 3-5 x T175 flasks) were resuspended in 20 mL of membrane wash buffer (10 mM HEPES, 10 mM EDTA pH 7.4) and homogenised using Ultra-Turrax (Ika-Werk GmbH & Co. KG, Staufen, Germany), at setting 4 for 8 x 1 second bursts. Homogenised samples were then centrifuged at (48,000 g, 30 minutes, 4°C) using a Beckman Avanti J-251 Ultracentrifuge and JA-25.50 Fixed-Angle Rotor (Beckman Coulter; CA, USA). Following centrifugation, the supernatant was discarded and pellet was resuspended in 20 mL membrane wash buffer. Samples were centrifuged again as described above, with the final membrane pellet resuspended in membrane storage buffer (10 mM HEPES, 0.1 mM EDTA; pH7.4). Protein concentration was determined by bicinchoninic acid protein assay (Smith et al., 1985), using bovine BSA as protein standard.

2.6. Functional Cellular Assays

2.6.1. Receptor Internalisation

2.6.1.1.1. Receptor Internalisation Assays

24 hours prior to the assay, cells were seeded into poly-d-lysine (10µg/mL) coated black, clear-bottomed, 96 well plates, at 25,000-30,000 cells per well, and incubated at 37°C/5% CO_2 for 24 hours prior to the assay. Cells were washed and replaced with pre-warmed 0.1 µM membrane-impermeant SNAP-surface AF488 in DMEM/10%FCS, and incubated for 30 minutes at 37°C/5% CO_2. Cells were washed with HEPES Balanced Salt Solution (HepesBSS;

10mM HEPES, 2mM sodium pyruvate, 146mM NaCl, 5mM KCl, 1mM MgSO4, 1.7mM CaCl2, 1.5mM NaHCO3, 5mM D-glucose; pH 7.45 with NaOH) with 0.1% BSA (HepesBSS/0.1% BSA) assay buffer and replaced with 50 µg/mL transferrin-AF546 in HepesBSS/0.1% BSA. Respective ligands were then diluted to 10x final assay concentrations in HepesBSS/0.1% BSA, as indicated in the results sections. Cells were incubated for 1 hour at 37°C/0% CO_2, before fixation. Cells were fixed with 3% paraformaldehyde, in PBS, for 15 minutes at room temperature before washing with PBS. Cells were stained with 2 µg/mL Hoechst 33342 nuclear stain (H33342), in PBS, and incubated at room temperature for 15 minutes, before being replaced with PBS and stored at 4°C. Cells were imaged using IX Ultra confocal plate reader (Molecular Devices, San Diego, CA, U.S.A.), using 4 sites per well and a Pan Fluor 40x NA0.6 extra-long working distance objective. Each site was excited using a DAPI, FITC and Texas Red laser filter for H33342, SNAP-AF488 and transferrinAF456 imaging, respectively

2.6.1.1.2. Translocation-Enhanced Module Analysis

Receptor internalisation was analysed using the Translocation Enhanced analysis Module (MetaXpress 5.01, Molecular Devices). The analysis uses an algorithm to identify translocation of AF488-SNAP-β_2AR-LgBiT (the translocation probe) to transferrinAF456 labelled endosomes (the compartment). The endosomal compartments were defined using based on a set approximate width (3 µm) and both minimum (3 μm^2) and maximum (100 μm^2) compartment areas. Compartments were defined for each individual experiment by setting a threshold brightness intensity above background.

As a measurement of receptor internalisation, the mean fluorescence intensity of the probe (SNAP-labelled receptor) within the identified transferrin compartments in each image was quantified by the algorithm. Intensity values from 4 sites per well, with assays run in duplicate wells, were normalised between vehicle (0 %) and 10 µM isoprenaline treated wells (100 %).

2.6.2. NanoBiT Complementation Assays

The NanoBiT complementation assay is based on the NanoLuc enzyme (Hall et al., 2012), which metabolises furimazine into furimamide and as a by-product produces a bright luminescent light. Dixon et al. (2016) were able to split the enzyme into two fragments: LgBiT and SmBiT. On their own, the fragments produce negligible luciferase activity but upon complementation, the enzyme regains function. The NanoBiT complementation assay was used to monitor the proximity of the complementary NanoBiT fragments appended to β adrenoceptors (also define by βAR) and either of two effectors: β-arrestin2 or mini Gαs protein (*Figure 2. 6*). In cells stably co-expressing both βAR-LgBiT and SmBiT tagged β-arrestin2 or mini Gαs protein, the NanoBiT complementation assay was used monitor agonist and antagonist responses.

In cell-based NanoBiT complementation assays, cells were seeded into poly-D lysine (10µg/mL) coated white, clear-bottomed, 96 well plates, at 35,000-40,000 cells per well, and incubated at 37°C/5% CO_2 for 24 hours prior to the assay. In membrane-based NanoBiT complementation assays, HEK293T membranes expressing either (1) β_2AR-LgBiT (2) β_2AR-LgBiT/HiBiT-β-arrsestin2 or (3) β_2AR-LgBiT/HiBiT-mini Gαs were prepared as described (*Methods; 2. 5. 2*) and thawed on ice prior to use.

All NanoBiT complementation assays were conducted in HepesBSS/0.1% BSA. All ligands and HiBiT peptide were prepared at 6x final assay concentration to account for experimental dilution when added to the assay plate, with the final assay concentrations denoted in the reults. Luminescence was measured using PHERAstarFS plate reader (BMG Labtech, Germany), pre-set at 37°C.

2.6.2.1. Measuring ligand responses in agonist mode.

Cells were washed and replaced with 40 µL pre-warmed assay buffer and pre-incubated with 10 µL NanoGlo furimazine substrate (1:943; final assay dilution from manufacturer's stock) for 5 minutes. The basal measure of luminescence was monitored for 5 minutes before the addition of 10 µL vehicle (assay buffer) or ligand to assay wells. Final assay volumes were 60 µL per well. Luminescence measurements were obtained from 1 min post ligand addition, for 30 minutes, at 120 second intervals, maintained at 37°C throughout assay.

2.6.2.2. Measuring antagonist action

Cells were washed and replaced with 40 µL antagonist diluted in pre-warmed assay buffer (HepesBSS/0.1% BSA). Cells were incubated for 10 minutes, before the addition of 10 µL NanoGlo furimazine substrate (1:943; final assay dilution from manufacturer's stock) for 5 minutes. The basal measure of luminescence was monitored for 5 minutes before the addition of 10 µL vehicle (assay buffer) or ligand to assay well. Luminescence measurements were obtained from 1 min post ligand addition, for 30 minutes, at 120 second intervals, maintained at 37°C throughout assay.

2.6.2.3. NanoBiT assay in detergent permeabilised cells

Cells were washed and replaced with 40 µL of either pre-warmed assay buffer (HepesBSS/0.1% BSA) or detergent dissolved in pre-warmed assay buffer (HepesBSS/0.1% BSA). Digitonin and saponin were diluted to 50 µg/mL and 1 mg/mL, respectively, in assay buffer, for ~10x critical micelle concentration, which is the concentration at which micelles spontaneously form, for each detergent. Cells were incubated for 15 minutes before the addition of 10 µL NanoGlo furimazine substrate (1:942; final assay dilution from manufacturer's stock) at 37°C for 5 minutes. 10 µL vehicle (assay buffer) or 10 µM HiBiT peptide was added to assay plate wells, which were then incubated for 5 minutes at 37°C before luminescence was measured.

2.6.2.4. NanoBiT assay in prepared membranes

Membranes expressing (1) β_2AR-LgBiT (2) β_2AR/HiBiT-β-arrestin2 or (3) β_2AR/HiBiT-mGαs were thawed on ice and diluted to 300 µg/mL in HepesBSS/0.1% BSA. 40 µL of membrane dilutions were added to wells of a 384 well Optiplate, followed by the addition of 10 µL NanoGlo furimazine substrate (1:943; final assay dilution from manufacturer's stock) and incubation at 37°C for 5 minutes. 10 µL of a range of concentrations of either SmBiT or HiBiT peptide were added to the assay plate as indicated in the results, the plate incubated at 37°C for 5 minutes before luminescence was measured.

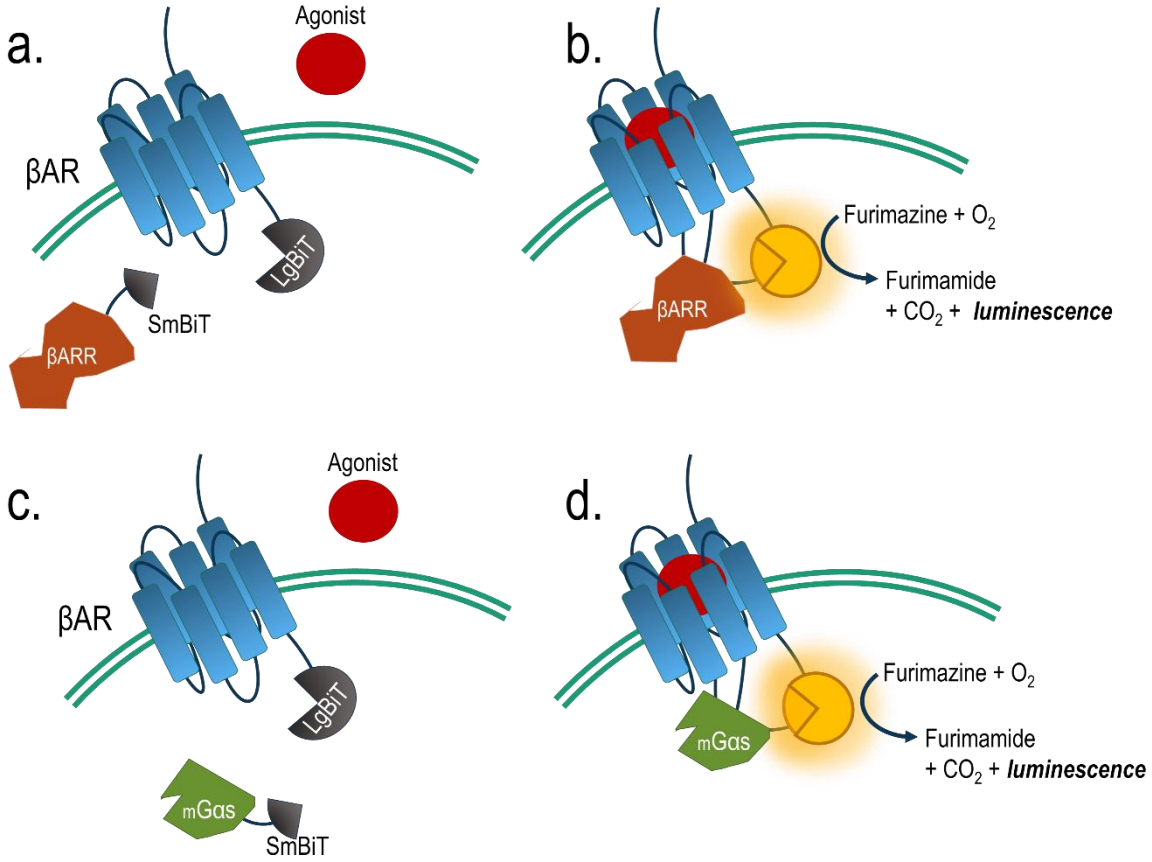

Figure 2. 6 NanoBiT complementation assay to monitor effector recruitment at βARs. *Schematic detailing recruitment of either β-arrestin2 (a.-b.) or a mini Gαs (c.-d.) protein at βARs. (a. & c.) In the absence of agonist activation there is limited recruitment of effector proteins by the βAR, NanoBiT fragments remain un-complemented and produce negligible luciferase activity. (b. & d.) Upon agonist activation, effectors are recruited to the receptor and NanoBiT fragments complement and gain luciferase action. This is indicated by the metabolism of the furimazine substrate to furimamide, producing a bright luminescent light as a by-product.*

2.7. Ligand Binding Assays

2.7.1. TR-FRET Assays of Ligand Binding

Time resolved fluorescence resonance energy transfer (TR-FRET) assays monitored the binding of BODIPY-FL-PEG8-(S)-Propranolol in membranes expressing βAR-LgBiT receptors, with an N-terminal genetically encoded SNAP-tag. Using SNAP-Lumi$_4$-Tb, the receptor construct was first labelled with an N-terminal terbium cryptate tag. As a lanthanide element, terbium cryptate's fluorescent emission has a long lifetime and measurements are made following a delay after excitation. During this period background auto-fluorescence decays, thus increasing signal:noise ratio for the specific FRET signal and assay sensitivity. When excited at a wavelength of 337 nm, terbium emits light at multiple longer wavelengths, including 490nm (see *Figure 2. 7* for energy transfer principles). For transfer of energy from the terbium emission to the BODIPY-FL-PEG8-(S)-Propranolol species, the fluorescent tracer ligand must within ~10 nm, most likely to occur when bound to the receptor. The fluorophore of BODIPY-FL-PEG8-(S)-Propranolol is then excited by the terbium emission of 490 nm and emits light at a wavelength of 520 nm (*Figure 2. 8. a*). A ratio of intensities at the acceptor / donor emission wavelengths was taken (520nm/490nm), with a greater FRET ratio demonstrating increased binding. A range of concentrations of BODIPY-FL-PEG8-(S)-Propranolol were incubated with membranes containing terbium labelled βAR-LgBiT receptors, to obtain binding properties of the fluorescent tracer, in an end point or kinetic format. Also, by obtaining binding parameters of the fluorescent tracer, the profiles of unlabelled ligands can be obtained when in competition with BODIPY-FL-PEG8-(S)-Propranolol (*Figure 2. 8. b*).

The binding assay buffer used for all TR-FRET binding experiments consisted of Hanks Balanced Salt solution (pH 7.4) (HanksBSS)(20 mM HEPES, 10% v/v glycerol, 10 μM GDP, 136 mM NaCl, 5.1 mM KCl, 0.44 mM KH_2PO_4, 4.17 mM $NaHCO_3$, 0.34 mM Na_2HPO_4), 20mM HEPES, 1% DMSO, 0.1mg/mL saponin and 0.02% pluronic acid. For all TR-FRET binding assays, BODIPY-FL-PEG8-(S)-Propranolol (HelloBio, CA200693, CellAura) was used as the tracer ligand. TR-FRET assays were conducted at 37°C, to replicate binding conditions during NanoBiT complementation assays.

As described above (*Methods*; *2. 5*), membranes expressing terbium labelled β_2AR receptor variants were first prepared. All membranes were thawed and kept on ice during experiments to avoid protein degradation. Membranes were prepared at 3 μg/well in assay

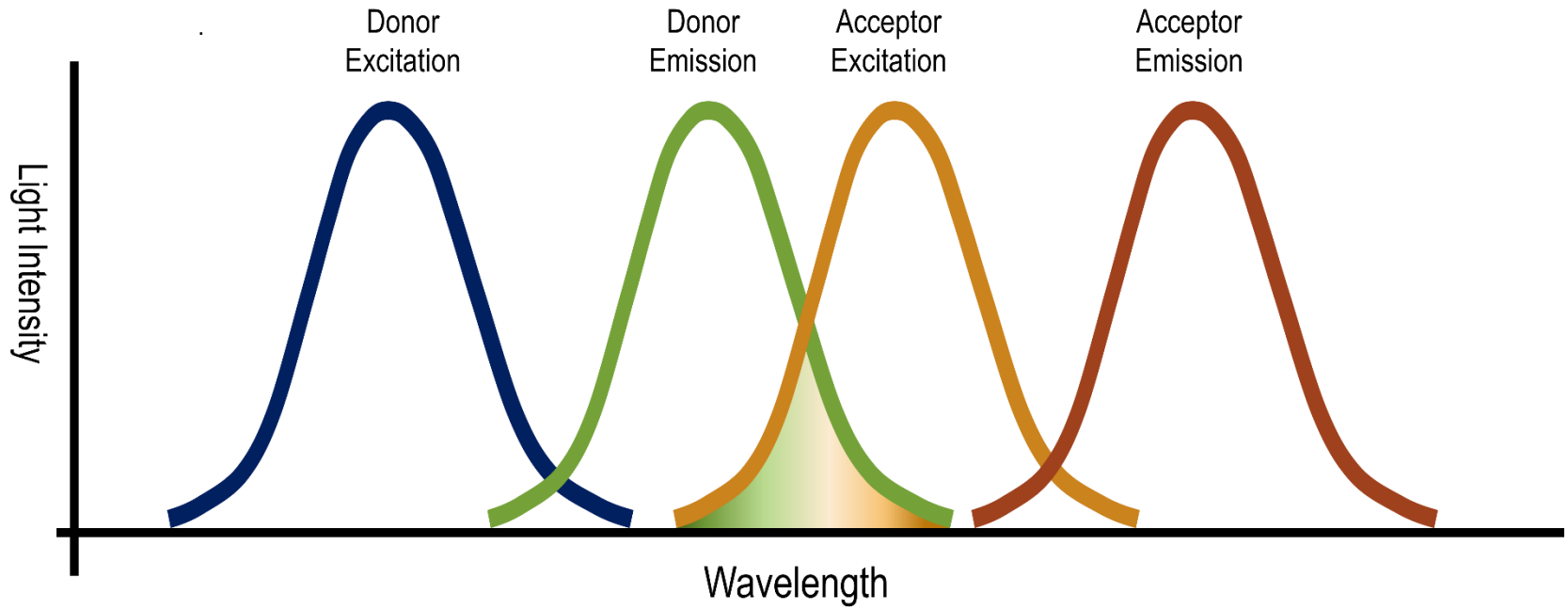

Figure 2. 7 Representation of Förster resonance energy transfer. *Spectrally overlapping of the donor species emission and acceptor species wavelengths, transfer of energy from the donor species to the acceptor species may occur.*

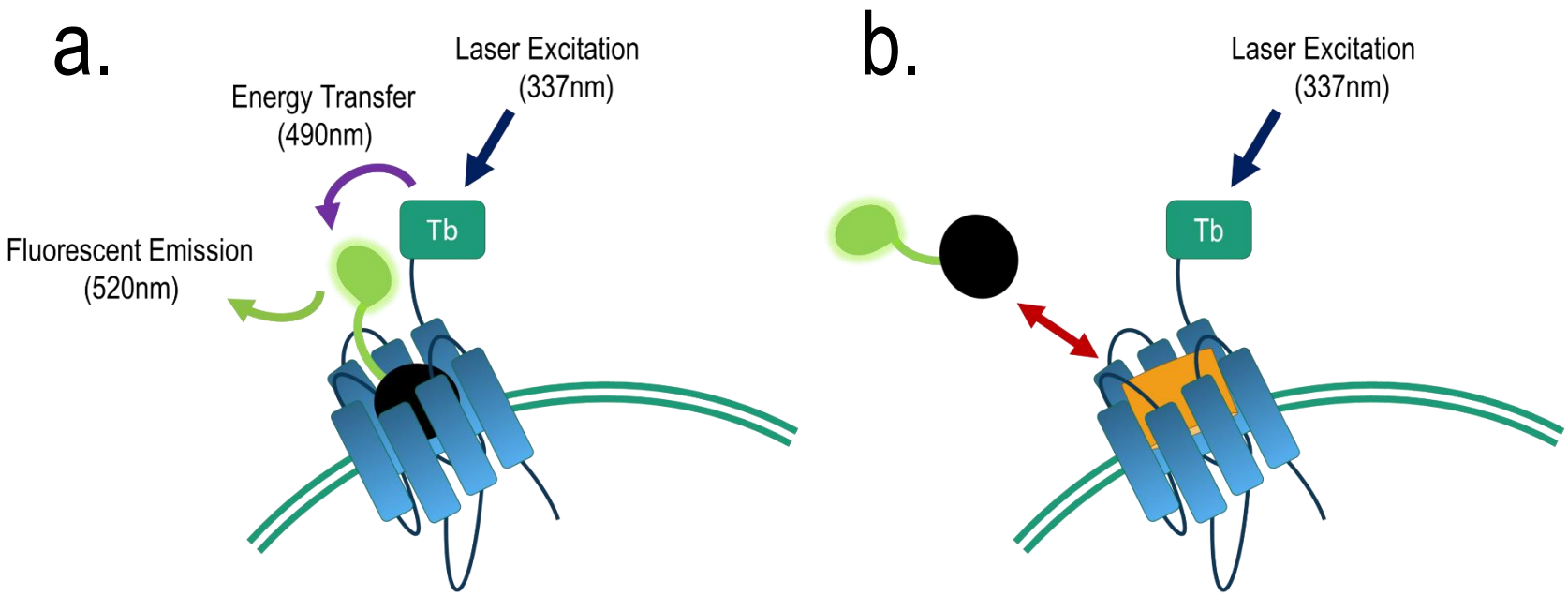

Figure 2. 8 TR-FRET Ligand Binding Assays. *Schematic detailing principles of time resolved fluorescence resonance energy transfer (TR-FRET) to monitor BODIPY-FL-PEG8-(S)-Propranolol binding at terbium labelled βARs. (a.) Terbium was excited at 337 nm, with an emission of 490nm. For Forster resonance energy transfer, known as FRET, to occur, the fluorescent tracer ligand must within ~10 nm. BODIPY-FL-PEG8-(S)-Propranolol is then excited by the 490 nm terbium emission and emits light at a wavelength of 520 nm. (b.)In the absence of BODIPY-FL-PEG8-(S)-Propranolol or when in competition with an unlabelled βAR ligand, the proximity between the terbium cryptate donor emission and the fluorophore of BODIPY-FL-PEG8-(S)-Propranolol is too great and no FRET occurs.*

buffer, unless otherwise stated. Immediately before the assay Gpp(NH)p was added to membrane dilution mix, for a final concentration of 100 µM in the assay. Gpp(NH)p acts as a non-hydrolysable form of GTP, and therefore binds without hydrolysis to endogenous heterotrimerics G proteins and cause them to dissociate into alpha and beta gamma subunits. This also destabilises the high affinity agonist – receptor – G protein transition state, effectively uncoupling membrane receptors from the G protein (Klein Herenbrink *et al.*, 2016). For binding assays, all compounds were prepared at 3x (*Methods; 2. 6. 3. 1 – 2. 6. 3. 3*) or 4x (*Methods; 2.7.1.4*) final assay concentration, to account for experimental dilutions when added to the assay plate. Final assay concentrations are reported in the results. All assays were conducted in 384-well Optiplates, with TR-FRET responses obtained using PHERAstarFS plate reader and HTRF module (laser excitation: 337 nm, emission readouts at 490 nm and 520 nm). FRET ratios were calculated as acceptor (520 nm) over donor (490 nm) emissions, x 10,000.

2.7.1.1. TR-FRET: Equilibrium Saturation Binding Assays

A range of concentrations of BODIPY-FL-PEG8-(S)-Propranolol were prepared in assay buffer, with total and non-specific binding quantified by incubating membranes and each concentration of BODIPY-FL-PEG8-(S)-Propranolol in the presence and absence of 10 µM ICI-118,551. 10 µL of each concentration of BODIPY-FL-PEG8-(S)-Propranolol and 10 µL vehicle/ICI-118,551 was added to the plate and centrifuged at 500 g for 30 seconds to spin small volumes to the base of the well. 10 µL of diluted membrane/Gpp(NH)p mix was added to assay wells using an electronic multi-channel pipette, for a final assay volume of 30 µL, and incubated at 37°C for 20 minutes. The assay plate was then directly placed into a pre-incubated (37°C) PHERAstarFS platereader and read for 1 cycle.

2.7.1.2. TR-FRET: Competition Equilibrium Binding Assays

10 µL of a range of concentrations of each unlabelled ligand, buffer only (for total binding) or 10 µM ICI-118,551 (for non-specific binding) were prepared in assay buffer, and added to Optiplate wells. 10uL of a set concentration of BODIPY-FL-PEG8-(S)-Propranolol was prepared, at a concentration indicated by figure legends, and added to all wells. As above, the plate was centrifuged at 500 g for 30 seconds to spin small volumes to the base of the well and the diluted membrane/Gpp(NH)p mix was added to assay wells using an electronic multi-channel pipette and incubated at

37°C for 20 minutes. The assay plate was then directly placed into a pre-incubated (37°C) PHERAstarFS platereader and read for 1 cycle.

2.7.1.3. TR-FRET: Kinetic Binding Assays

The for saturation and competition kinetic binding assays, assay plates was set up as described above (*Methods*; *2. 6. 3. 1* and *2. 6. 3. 2*, respectively). Diluted membrane/Gpp(NH)p mix was loaded into PHERAstarFS injector system and primed to equilibrate system and remove bubbles from injection lines. A PHERAstar injector protocol was used to inject 10 µL of membrane (3 µg membrane per well), for a final assay volume of 30 µL, and then read FRET responses over 20-25 minutes, at a read frequency indicated on individual figure legends.

2.7.1.4. TR-FRET: Influence of HiBiT/HiBiT-MiniGαs protein on BODIPY-FL-PEG8-(S)-Propranolol binding.

Assays investigating the influence of HiBiT peptide or HiBiT-mGαs protein on the binding of BODIPY-FL-PEG8-(S)-Propranolol and unlabelled βAR ligands were conducted as described above (*Methods; 2. 6. 3. 1* – *2. 6. 3. 1*), with the preparation of the membrane altered to incorporate either the co-incubation of HiBiT peptide or HiBiT-mGαs protein. For all assays, the final volume of the assay was increased from 30 µL to 40 µL and thus reagents were prepared at 4x final assay concentration. Final assay concentrations of membrane and either HiBiT or HiBiT-mini Gαs were 3 µg/well and 500 nM, respectively. Membranes (with Gpp(NH)p) and HiBiT or HiBiT-mGαs were diluted individually and then combined in equal volumes and incubated on ice for 20 minutes. Following 20 minute incubation, membrane/HiBiT and membrane/HiBiT-mGαs were applied to assay plate either using an electronic multi-channel pipette or PHERAstarFS injection system when conducting equilibrium or kinetic binding assays.

2.7.2. Transmembrane BRET Assays of Ligand Binding

To measure BODIPY-FL-PEG8-(S)-Propranolol binding at effector bound β_2AR complexes, transmembrane BRET (TM-BRET) assays were established and optimised to monitor energy transfer from intracellular complemented NanoBiT luciferase in β_2AR-LgBiT/HiBiT-effector membranes to extracellularly bound BODIPY-FL-PEG8-(S)-Propranolol. Using resonance energy transfer principles

(*Figure 2. 7*), TM-BRET uses the luminescence emitting from the luciferase activity of the complemented NanoBiT fragments as a donor emission (~460 nm) to excite the fluorescent tracer ligand bound to the extracellular surface of the receptor, which emits at a wavelength of 520 nm (*Figure 2. 9*). A ratio of each emission wavelength was taken (520 nm/460 nm), with a greater TM-BRET ratio demonstrating increased binding. BODIPY-FL-PEG8-(S)-Propranolol was incubated with membranes containing βAR-LgBiT/HiBiT-effector complexes to monitor the binding of BODIPY-FL-PEG8-(S)-Propranolol and unlabelled ligands, using an end point format.

The binding assay buffer used for TM-BRET binding experiments was identical to that used in TR-FRET assays, excluding an increase of saponin from 0.1 mg/mL to 1 mg/mL saponin. For all TM-BRET binding assays, BODIPY-FL-PEG8-(S)-Propranolol was used as the tracer ligand and TM-BRET assays were conducted at 37°C. TM-BRET assays were conducted on (1) membrane preparations from cells stably co-expressing β_2AR-LgBiT and HiBiT-effector proteins and (2) membrane preparations from cells stably expressing β_2AR-LgBiT and exogenously added HiBiT or HiBiT-mini Gαs protein.

Membrane preparations, not labelled with terbium, were generated as described (*Methods; 2. 5. 2*), and thawed and kept on ice during experiments to avoid protein degradation. Membranes prepared from cells co-expressing β_2AR-LgBiT and HiBiT appended to β-arrestin2 or mini Gαs, were diluted to 8 µg/well, final assay concentration, in assay buffer, unless otherwise stated. Membranes prepared from cells expressing β_2AR-LgBiT alone were diluted to 4 µg/well, final assay concentration in assay buffer, before mixing in equal volumes with HiBiT peptide or HiBiT-mini Gαs proteins prepared at 2.4 µM, for 300 nM final assay concentration. Membrane/peptide solutions were incubated on ice for 20 minutes on ice. Following membrane dilution, and prior to the addition of any HiBiT/HiBiT-mini Gαs peptides, Gpp(NH)p was added to membrane dilution mix, for a final concentration of 100 µM in the assay. All other compounds were prepared at 4x final assay concentration stated in the results, to account for experimental dilutions when added to the assay plate. All assays were conducted in 384-well Optiplates, with TM-BRET responses obtained using PHERAstarFS plate reader and dual emission module (Emission readouts at 535-30 nm and 475-30 nm). BRET ratios were calculated as acceptor (535-30 nm) over donor (475-30 nm) emissions.

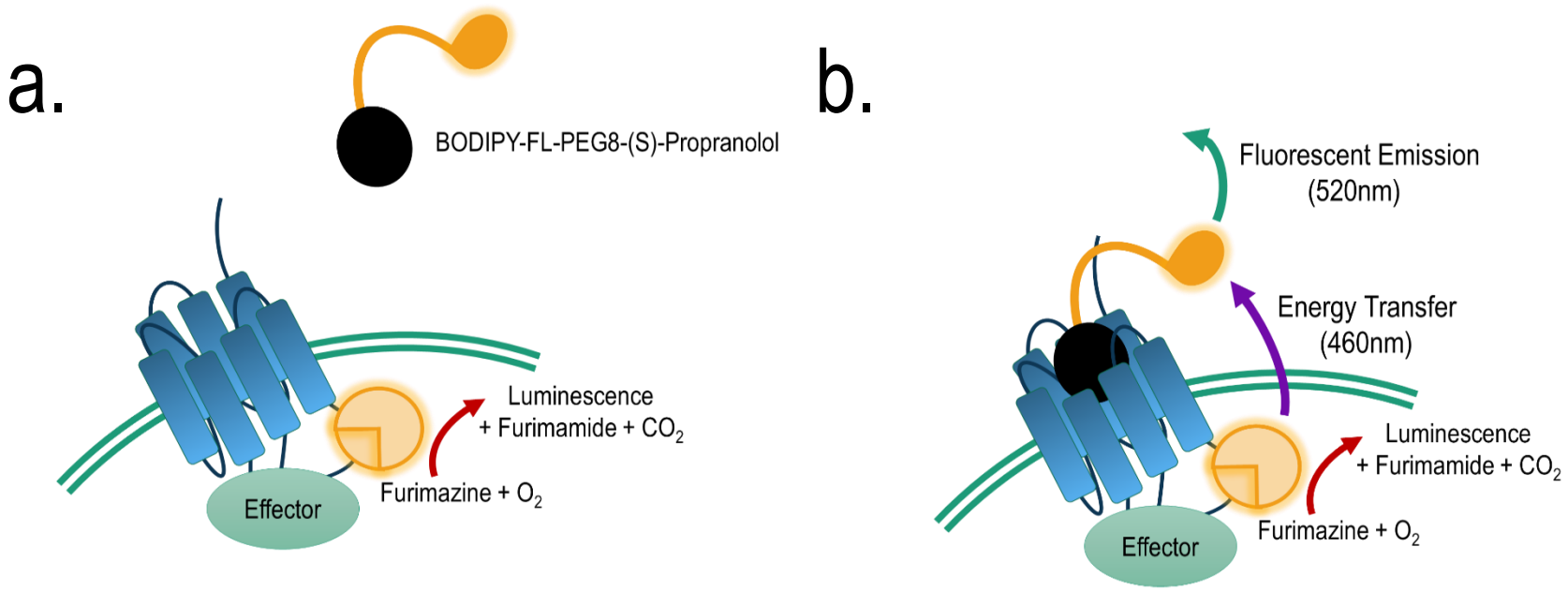

Figure 2. 9 TM-BRET Ligand Binding Assays. *Schematic detailing principles of transmembrane bioluminescence resonance energy transfer (TM-BRET) to monitor BODIPY-FL-PEG8-(S)-Propranolol binding at βARs with intracellularly complemented NanoBiT fragments, appended to βARs and effectors. TM-BRET used the luciferase activity of the complemented NanoBiT fragments as donor emission (~460 nm) (a.). For transfer of energy from the luminescent emission to the BODIPY-FL-PEG8-(S)-Propranolol species, the fluorescent tracer ligand needs to be within ~10 nm, most likely due to specific binding. BODIPY-FL-PEG8-(S)-Propranolol is then excited by the luminescent emission of 460 nm and emits light at a wavelength of 520 nm (b.).*

2.7.2.1. TM-BRET: Equilibrium Saturation Binding Assays

Assay plates were prepared as in *2. 6. 3. 1*, with the diluted membranes+HiBiT/HiBiT-mini Gαs/Gpp(NH)p mix added to assay wells using an electronic multi-channel pipette and incubated at 37°C for 20 minutes. Furimazine was prepared at 1:30 dilution, in assay buffer, and vortexed thoroughly. 10 µL of furimazine dilution was added to all assay wells and incubated at 37°C for 5 minutes. The assay plate was then directly placed into a pre-set (37°C) PHERAstarFS platereader and read for 1 cycle.

2.7.2.2. TM-BRET: Competition Equilibrium Binding Assays

Assay plates were prepared as in *2. 6. 3. 2*, with addition of membranes+HiBiT/HiBiT-mini Gαs/Gpp(NH)p mix and furimazine dilution, incubation and BRET reading as above *2. 6. 4. 1*.

2.8. Data Analysis

2.8.1. Data Collection and Software

All experiments were conducted in duplicate, excluding TR-FRET assays which were conducted in singlet for improved temporal resolution of readings. Estimates of ligand binding and signalling parameters, including EC_{50}, R_{max}, K_i, K_D, k_{ON} and k_{OFF}, were taken from individual experimental repeated and pooled. All pooled data are presented as mean ± standard error of the mean (s.e.m), unless otherwise stated, from at least 3 individual replicates. Ligand concentration response data from receptor internalisation and NanoBiT complementation assays were normalised to a reference ligand (either 10 µM isoprenaline or 1 µM formoterol) between assay repeats to allow for differences in cell seeding densities, between experimental replicates. Ligand binding responses were normalised between total and non-specific binding. Data were analysed and collated using GraphPad Prism 7.02 (GraphPad Software, La Jolla). Vector maps were viewed using SnapGene Viewer 4.2.11, with sequence alignments conducted using BLAST® (NCBI NIH, Bethesda, US). Confocal images from IX Ultra confocal plate reader (Molecular Devices, San Diego, CA, U.S.A.) were processed, collated and analysed using MetaXpress 2.0 software (Molecular Devices, USA).

2.8.2. Statistics

Statistical comparisons were conducted using GraphPad Prism 7.02, with significance defined as $P<0.05$, with greater significance denoted in individual figures and tables. Statistical tests used are denoted in figures and/or text. All statistical comparisons assumed normally distributed means and thus used parametric tests.

2.8.3. Functional Assays

2.8.3.1. Analysis of Agonist Concentration Responses

Results were analysed and presented using Prism 7.02 (GraphPad Software Inc., San Diego, CA). Normalised data (% 10μM isoprenaline response, with vehicle as 0%) were fitted using a model of non-linear regression, using the four parameter equation, Equation 2.1:

$$Response = Min + \frac{Max - Min}{1 + 10^{(LogEC_{50} - X) * Hill\ Slope}}$$

Equation 2.1

Where Min and Max represent the minimum and maximum plateau of each ligand response, the Hill Slope describes the steepness of the fit and the EC_{50} is the concentration of ligand to produce the response half way between Min and Max. The relative maximal response (Rmax) was defined as "Max – Min", with inverse agonism represented by a negative Rmax. EC_{50} and Rmax values from individual experiments were pooled, with averaged values denoted by the mean ± standard error of the mean (SEM). Normalised curve data for each ligand were also pooled and fitted to a nonlinear regression (Equation 2.1) analysis for representative figures.

2.8.3.2. Analysis of Antagonist Responses – Schild Analysis

Concentration response curves of isoprenaline were monitored in the absence and presence of a range of concentrations of competitive antagonists. Here, Schild analysis was used to quantify antagonist affinity at β_2ARs. At each concentration of antagonist, the shift of an isoprenaline concentration responficase curve was used to determine the concentration

ratio (CR), using the equi-effective concentrations of isoprenaline in the presence ([A']) and absence ([A]) of an antagonist:

$$CR = \frac{[A']}{[A]}$$

Equation 2.2

For Schild analysis (Arunlakshana and Schild, 1959), Log[CR-1] was plotted against the matching antagonist concentration (log [B]), with the affinity of the antagonist, in the form of $LogK_D$, described by the x-intercept (Equation 2.3).

$$Log\ K_D = Log\ (CR - 1) - Log[B]$$

Equation 2.3

2.8.4. Operational Models

2.8.4.1. Black and Leff Operational Model of Partial Agonism

The Operational Model of Partial Agonism (Black and Leff, 1983) (OM) was used to estimate the agonist dissociation equilibrium constant (K_A) and the transduction co-efficient of an agonist, reflecting agonist affinity and efficacy, respectively. The operational model derives a convolved measure of efficacy (tau or τ) from the total concentration of receptors (R_0) and the system coupling efficiency, with the latter defined by the concentration of agonist bound receptor to produce half the maximal effect. Therefore, τ is dependent on both the system coupling efficiency as well as the agonist efficacy. The OM is initially derived from the Hill equation; Equation 2.4, where Hill Slope was constrained to 1. At equilibrium, when an agonist (A) binds to a receptor (R), the concentration ofof occupied receptors (AR) is based on agonist concentration ([A]), the total number of receptors (R_0) and the agonist dissociation equilibrium constant (here described as K_A) - Equation 2.4:

$$[AR] = \frac{[R_0][A]}{K_A + [A]}$$

Equation 2.4

To translate receptor occupancy by agonist (AR) to the pharmacological effect (E) a function is required, where the relationship

between E and [AR] is assumed to be rectangular hyperbolic. Te K_E constant represents [AR] that produces half of the maximal possible effect (E_m) (Equation 2.5).

$$E = \frac{E_m[AR]}{K_E + [AR]}$$

Equation 2.5

The OM equation is a combination of Equation 2.4 and Equation 2.5, and the introduction of a transduction coefficient (τ or tau, equal to R_0/K_E) (Black and Leff, 1983) – Equation 2.6. The model was fit globally to all agonist concentration response data sets, with basal and E_{max} shared and determined by the reference agonist – isoprenaline. The equation shown assumes unit Hill slope for simplicity.

$$E = \frac{E_m\tau[A]}{K_A + [A](1 + \tau)}$$

Equation 2.6

To fit multiple agonists, including partial agonists, the OM was applied globally in Prism, sharing basal and E_m estimates across agonists. For partial agonists in the data set, tau can then be estimated uniquely, since the lower Rmax fitted is defined by the OM relationship:

$$R_{max} = \frac{E_{max}\tau}{1 + \tau}$$

Equation 2.7

With the Emax defined by the full agonists in the same data set.
By obtaining estimations of τ, K_A can then be estimated for partial agonists, from the definition of EC_{50} in the OM:

$$EC_{50} = \frac{K_A}{1 + \tau}$$

Equation 2.8

However, for full agonists in the assay (where R_{max} approaches E_{max}), τ and K_A cannot be uniquely deconvolved.

2.8.4.2. *Fitting tau / Ka in the adapted Black and Leff Operational Model* (Kenakin *et al.*, 2012; Van Der Westhuizen *et al.*, 2014)

An adaption of the OM was used to obtain single parameters to quantify bias between recruitment of β-arrestin2 and mini Gαs protein, for both full and partial agonists (Kenakin et al., 2012; Van Der Westhuizen et al., 2014). This model allows a transduction coefficient representing the ratio of τ/K_A (R) to be estimated from OM fitted data for all agonists, by adapting Equation 2.6 to give the simplified equation (Equation 2.9):

$$E = \frac{E_m R[A]}{1 + R[A]}$$

Equation 2.9

The R value for each agonist may be globally fitted unambiguously (Kenakin *et al.*, 2012; Van Der Westhuizen *et al.*, 2014; Reinartz *et al.*, 2015). Here, ligand responses, normalised to 10 μM isoprenaline and vehicle, for each individual experiment (n=5, performed in duplicate) was used to calculate LogR for each agonist. These transduction co-efficients were then subtracted from the same reference ligand in each assay (LogR isoprenaline) (ΔLogR), which has the effect of normalising the data and minimising the effect of system bias on the estimates (Stott, Hall and Holliday, 2015). These values were then compared by the difference between pathways to quantify LogBias values (ΔΔLogR), between recruitment of either β-arrestin2 or mini Gαs protein. Thus a ΔΔLogR = 0 indicates no pathway bias. This analysis was conducted at each of 15 time points across the assay window, at 120 second intervals.

2.8.4.3. *Kinetic Operational Models*

2.8.4.3.1. *"Rise and Fall" model of agonism*

To model the time-dependent recruitment of β-arrestin2 to βAR subtypes, a "Rise-and-Fall" kinetic operational model (kOM), as described by Hoare *et al.*, (2018), was used to quantify agonist dissociation equilibrium constants (K_A), a kinetic measure of agonist efficacy (ktau) and the signal decay rate (k_D) for each agonist. The model was applied to β-arrestin2 recruitment timecourse data for

each individual replicate at the β_1AR and β_2AR. The equation (Equation 2.8) was fitted globally to each experimental replicate of the timecourses of a concentration response experiment of an agonist over 16 timepoints between 1 and 31 minutes following agonist addition. The model was fit to data normalised as a percentage of the 3 minute luminescence response generated between 10 μM isoprenaline and vehicle.

The kOM is defined by Scheme 2.1, where Ep, the transduction potential, defines the total possible response. Activated agonist-receptor complexes (RA) convert the transduction potential to the response "E". The rate of this is governed by the response generation rate constant k_E. For the rise and fall variant of the model, response decay is included as a single phase exponential form with the response decay rate constant k_D:

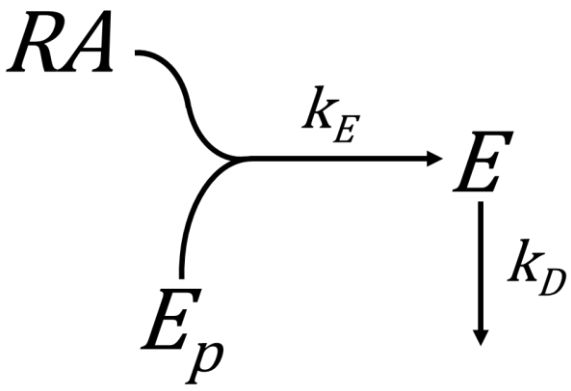

Scheme 2.1.

From this scheme, Equation 2.10 was defined:

$$E_t = \frac{S}{k_{obs-}\ k_D}\ (e^{-k_D t} - e^{-k_{obs} t}\ )$$

Equation 2.10

where,

$$S = k_\tau \frac{[A]}{K_A + [A]}$$

Equation 2.11

$$k_{obs} = \frac{[A]k_\tau / E_{P(TOT)}}{K_A + [A]}$$

Equation 2.12

$$k_\tau = E_{P(TOT)} R_{TOT}\, k_E$$

Equation 2.13

In Equation 2.10, over a set time (t) the response is measured (E_t), driven by both the signal response decay rate (k_D) and the observed rate of the response generation (k_{obs}). The observed rate of the response generation is influenced by the total transduction potential ($E_{P(TOT)}$), the agonist dissociation equilibrium constant (K_A), agonist concentration ([A]) and the transduction rate constant (kTau or kτ). Ktau itself being the rate at which the total receptor population ($R_{(TOT)}$) can convert the total transduction potential ($E_{P(TOT)}$), via the response generation rate (K_E). In this study, we have used the model to extract K_A, kTau and k_D.

2.8.4.3.2. Antagonist pre-treatment form of the rise and fall kOM

This extension of a kOM (Hoare et al., 2018) enabled timecourse data of isoprenaline driven recruitment of mini Gαs protein at β_2ARs, in the absence and presence of a competitive antagonist to be fitted (Hoare *et al.*, 2018). The intention was to estimate antagonist binding kinetic parameters, as well as agonist parameters from the data. As described by Scheme 2.2, the antagonist (B) is assumed to bind to the receptor in a single step interaction competing with the agonist.

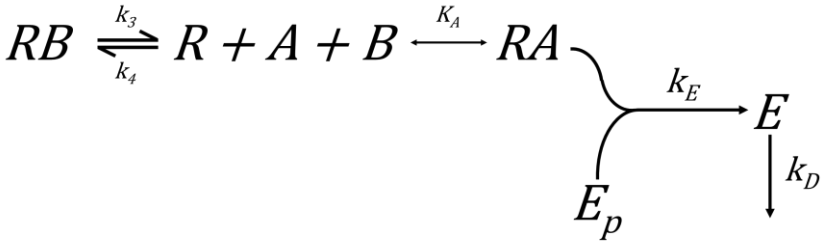

Scheme 2.2

The equation for fitting was derived based on an experimental schedule in which cells are pre-incubated with antagonist (B) to establish equilibrium binding. The modelled timecourse therefore incorporation hemi-equilibrium conditions after the addition of an agonist without washout of antagonist, in which the dissociation rate of the antagonist (k4) determines the kinetics of re-equilibration after addition of the second competitive receptor ligand (the agonist). Equation 2.14 is therefore derived from equation 2.10, but incorporates the time dependent changes in agonist-receptor occupancy predicted by the antagonist concentration present and its binding kinetics:

$$E_t = E_{[B]=0, t\to\infty} \frac{k_4}{k_{B(app)}} \left[1 + \frac{P - k_{B(app)}k_4}{N} e^{-k_D t} - \frac{P - k_4 k_D}{N} e^{-k_{B(app)} t}\right]$$

Equation 2.14

where,

$$N = k_4 (k_{B(app)} - k_D)$$

Equation 2.15

$$P = k_{B(app)} k_D (1 - \rho_{B(t=0)})$$

Equation 2.16

$$k_{B(app)} = [B]k_3(1 - \rho_A) + Kk_4$$

Equation 2.17

$$\rho_A = \frac{[A]}{K_A + [A]}$$

Equation 2.18

$$\rho_{B(t=0)} = \frac{[B]k_3}{[B]k_3 + k_4} (1 - e^{-([B]k_3 + k_4)t_{PI}})$$

Equation 2.19

With the new terms defined below:

Term	*Description*	*Units*
ρ_A	Fractional receptor occupancy by agonist in the absence of antagonist; $([A]/([A]+K_A))$	Unitless
B	Antagonist concentration	Molar
k_3	Antagonist association rate constant	$Molar^{-1}t^{-1}$
k_4	Antagonist dissociation rate constant	t^{-1}
K_B	Antagonist equilibrium dissociation constant = k4/k3	Molar
$k_{B(app)}$	Apparent (observed) antagonist association rate constant; $([B]k_3(1-\rho A)+k_4)$	t^{-1}
$\rho_{B(t=0)}$	Fractional receptor occupancy by antagonist at response initiation, in the absence of agonist	Unitless
$E_{[B]=0,\ t\to\infty}$	Response to agonist in absence of antagonist at steady-state	Response Unit
N	Macroscopic fitting parameter; $(k_4(k_{B(app)}-k_D)$	t^{-2}
P	Macroscopic fitting parameter; $(k_{B(app)}k_D(1-\rho_{B(t=0)})$	t^{-2}
t_{PI}	Time interval of the antagonist pre-incubation phase	Time unit

2.8.5. Binding Assays

To determine the affinity of the fluorescent tracer, BODIPY-FL-PEG8-(S)-Propranolol, ligand binding assays were conducted either when an assumed equilibrium end point had been reached or by quantifying the kinetic rates of binding in real-time. In a system with assumed equilibrium the forward (association; k_{ON}) and reverse (dissociation; k_{OFF}) rates of the reaction are equal. In all assays, non-specific binding was determined using 10 μM of ICI-118,551 and subtracted to correct for background signal.

2.8.5.1. Assumed Equilibrium Binding Assays

Saturation Binding Assays

Saturation binding assays were used to determine the affinity of BODIPY-FL-PEG8-(S)-Propranolol at βAR constructs, by using increasing concentrations of the fluorescently labelled ligand. Specific binding was quantified by subtracting the non-specific binding ratio from the total binding ratio at each concentration of BODIPY-FL-PEG8-(S)-Propranolol, from TR-FRET and TM-BRET binding assays.

Saturation binding data of total, non-specific and specific binding was plotted against increasing concentrations BODIPY-FL-PEG8-(S)-Propranolol on a linear x-axis, and fit to the following equations:

Total Binding:

$$y = \frac{B_{max}[A]}{[A] + K_D} + (mx + background)$$

Equation 2.20

Specific Binding:

$$y = \frac{B_{max}[A]}{[A] + K_D}$$

Equation 2.21

Non-Specific Binding:

$$y = mx + background$$

Equation 2.22

These equations were fit globally to multiple concentrations of BODIPY-FL-PEG8-(S)-Propranolol in GraphpadPrism. In the non-specific

binding linear equation, y is equal to the measured FRET or BRET ratio, m is the slope of the fit and background equal to the y-intercept. For non-linear fits for total and specific binding, B_{max} is equal to the maximum binding of BODIPY-FL-PEG8-(S)-Propranolol and K_D the equilibrium binding constant of BODIPY-FL-PEG8-(S)-Propranolol, when BODIPY-FL-PEG8-(S)-Propranolol occupies half of the receptors.

Competition End Point Binding Assays

To determine dissociation equilibrium constants of unlabelled βAR ligands, in the form of K_i values, increasing concentrations of at the unlabelled ligand were competed against a set concentration of BODIPY-FL-PEG8-(S)-Propranolol. From concentration inhibition curves, IC_{50} values of unlabelled ligands were converted to Ki values using the Cheng-Prusoff equation, assuming competitive reversible interactions (Equation 2.21):

$$K_i = \frac{IC_{50}}{1 + \frac{[L]}{K_D}}$$

Equation 2.23

where, [L] is the concentration of BODIPY-FL-PEG8-(S)-Propranolol and KD the dissociation equilibrium constant of BODIPY-FL-PEG8-(S)-Propranolol.

2.8.5.2. Kinetic Binding Assays

Association Kinetics of BODIPY-FL-PEG8-(S)-Propranolol

The binding of increasing concentrations of BODIPY-FL-PEG8-(S)-Propranolol was measured over time and globally fit to an exponential association function (Equation 2. 24):

$$y = B_{max}\,(1 - e^{-k_{obs}t})$$

Equation 2.24

where, t, time, is plotted on the x-axis against y, binding, on the y-axis. B_{max} is equal to the maximum binding of BODIPY-FL-PEG8-(S)-Propranolol and k_{obs} being observed association rate of each BODIPY-FL-PEG8-(S)-Propranolol concentration. A linear relationship between k_{obs} and [BODIPY-

FL-PEG8-(S)-Propranolol] was used determine a first order reaction and thus determine a single site of binding interaction. The k_{obs} plot may be used to estimate the k_{ON} and k_{OFF} from the Y intercept and the slope, respectively.

BODIPY-FL-PEG8-(S)-Propranolol association (k_{ON}) and dissociation (k_{OFF}) rates were determined concurrently, using a global single site model of association, according to Equation 2.25, by applying kobs values from Equation 2.24.

$$k_{obs} = k_{ON}[A] + k_{OFF}$$

Equation 2.25

With the reciprocal of the dissociation rate ($1/k_{OFF}$), equally the residence time of BODIPY-FL-PEG8-(S)-Propranolol. In addition to determining the affinity of BODIPY-FL-PEG8-(S)-Propranolol using assumed equilibrium binding assays, it can also be derived kinetically using Equation 2.24:

$$K_D = \frac{k_{OFF}}{k_{ON}}$$

Equation 2.26

Binding Kinetics of competitive unlabelled Ligands

Kinetic parameters (k_{ON}, k_{OFF} and kinetically derived K_D) of competitively binding ligands were determined using methodology from Motulsky and Mahan (1984). The Motulsky and Mahan method uses k_{ON} (k1) and k_{OFF} (k2) rates of a tracer ligand, such as BODIPY-FL-PEG8-(S)-Propranolol, that have been determined using association kinetic measurements described above in the same experiment. Tracer ligand association kinetics are then also measured in the presence of different concentrations of competing unlabelled ligands. These association kinetic timecourses adopt distinct time profiles dependent on the relative kinetics of tracer and unlabelled ligand.

The Motulsky Mahan Equations (2.27 - 2.30) allow fitting of these competitive association data (as specific binding) to estimate the kinetic constants for the unlabelled ligands. Global fitting was performed to data in the absence and presence of multiple concentrations of unlabelled ligand, fixing the fluorescent tracer kinetic parameters k1 and k2 to the separately estimated values as described above.

$$S = \sqrt{(K_A - K_B)^2 + 4k_1k_3[FL][UL]}$$

Equation 2.25

where,

$$K_A = k_1\,[FL] + k_2$$

Equation 2.26

$$K_B = k_3\,[UL] + k_4$$

Equation 2.27

$$RFL = Q\left(\frac{(k_4(K_F - K_S)}{K_F K_S} + \frac{k_4 - K_F}{K_F}e^{-K_F t} - \frac{k_4 - K_S}{K_S}e^{-K_S t}\right)$$

Equation 2.28

where,

$$K_F = \frac{K_A + K_B + S}{2}$$

Equation 2.29

$$K_S = \frac{K_A + K_B - S}{2}$$

Equation 2.30

$$Q = \frac{B_{max}[FL]k_1}{K_F - K_S}$$

Equation 2.31

Here, the concentration of the fluorescent and unlabelled ligands were defined by [FL] and [UL], respectively. RFL describes specific binding of the fluorescent ligand over time, and B_{max} is equal to the maximum binding of the fluorescent ligand. The fixed association and dissociation rates of the fluorescent ligand (estimated separately) were defined by k_1 and k_2, respectively, and the association and dissociation rates of the unlabelled ligand were defined by k_3 and k_4, respectively.

2.8.6. Confidence Intervals

Models fit to all data were applied using confidence intervals for each parameter fitting. In all model fits, confidence intervals were set to 95 % and reported the range between which the best-fit value is likely to be – with a 95% likelihood.

2.8.7. Correlation Plots

Linear regression analysis was used to determine correlation of data sets, using the following equation:

$$y = mx + c$$

Equation 2.32

where m is the gradient of the line and c is the y intercept, where x and y represent the respective data sets. The goodness of fit was determined by r^2 and P value describing whether the slope is significantly different from zero.

Chapter Three:

Monitoring agonist driven recruitment of β-arrestin2 and mini $G\alpha_s$ protein, in NanoBiT complementation assays at β_1 and β_2 adrenoceptors.

3.1. Introduction

3.1.1. GPCR Signalling Assays

As discussed in *Chapter 1*, GPCRs are dynamic seven transmembrane domain proteins activated by a range of chemical (i.e. hormones and small molecules) and physical (e.g. photons) stimuli. Upon activation, GPCRs signal through secondary messenger proteins to initiate signalling cascades within the cell. GPCR signalling can be monitored using a variety of methods, for example by directly monitoring activation of secondary messenger effectors, such as cAMP and the release of Ca^{2+} ions, gene transcription or monitoring downstream phenotypic outcomes, including cytokine release and proliferation. Whilst gene transcription and phenotypic responses provide a range of possible methods to monitor GPCR signalling, such downstream measurements of receptor activation can amplify the response, obscuring differences in agonist efficacy and confound "biased" effects of ligands between signalling pathways (Klein Herenbrink *et al.*, 2016). Outcomes of many standard assays are assessed using single "end point" measurements, and thus the kinetics of the signalling response are typically not considered. The kinetics of receptor signalling can provide critical information of the functional outcome (Krasel *et al.*, 2004; Klein Herenbrink *et al.*, 2016; Lane *et al.*, 2017), though this can prove challenging for many end point style assays that require cell lysis or fixation. Therefore assays that can provide direct measurements of receptor-effector interactions, and in real-time, are valuable indicators of how ligands can affect distinct signalling pathways and their signalling properties. A significant advance in GPCR biosensors was the development of resonance energy transfer (RET) assays (Scholes, 2003; Marullo and Bouvier, 2007), such as Förster or bioluminescence resonance energy transfer (FRET/BRET) assays, which measure the transfer of fluorescent or luminescent energy between a donor and an acceptor species to monitor the proximity of the species and the proteins of interest appended. Energy transfer assays can be monitored in real-time and are thought to more reliably monitor protein-protein interactions, due to a maximum distance of energy transfer of 10 nm between donor and acceptor species (Stryer and Haugland, 1967; Stryer, 1978). The bioluminescent donor known as NanoLuciferase (NanoLuc) (Hall et al., 2012) acts as an optimal donor in such assays due to its bright luminescence, wide emission spectrum and resultant wide range of possible acceptor species (Stoddart, *et al,* 2018). In contrast to end point style methods, energy transfer assays can be established to allow for monitoring protein-protein interactions in real-time and thus give

a greater insight into the dynamic interactions (Stoddart, *et al*, 2018; Wan et al., 2018; Soave, et al., 2020).

3.1.2. Non-Imaging Effector Recruitment Assays

A range of biosensors are available to directly monitor effector recruitment, with the most common assays monitoring the recruitment of G proteins and arrestin proteins, more specifically β-arrestins. Whilst some biosensors discussed use imaging-based methods, many are applied in non-imaging approaches which can increase throughput.

When investigating recruitment of β-arrestin proteins at GPCRs, direct interactions between the two proteins is often monitored using several non-imaging based approaches, with common assays including Tango™ (Invitrogen) (Van Der Lee et al., 2009) and PathHunter™ (DiscoveRx) (Mcguinness et al., 2009) assays, yet neither assay is able to report receptor-β-arrestin interactions in real-time. In the Tango™ assay (*Figure 3. 1. a*), the target receptor is labelled at the C-terminal with a transcription factor connected by a protease cleavage site. Upon receptor activation, β-arrestin proteins modified with a fused protease domain are recruited to the membrane and the protease cleaves the transcription factor from the receptor. The transcription factor is translocated to the nucleus, where a reporter gene is transcribed and used as a downstream indicator of β-arrestin recruitment. The PathHunter™ assay (*Figure 3. 1. b*) uses a complementation assay, where complementary fragments of the β-galactosidase enzyme are appended to the target receptor and β-arrestin protein. Upon receptor activation, β-arrestin is recruited to the receptor and the two enzyme fragments re-complement and regain function. The cells are then lysed and the β-galactosidase substrate is added and metabolised to produce a chemiluminescent signal, providing an indicator of receptor-β-arrestin complexes. A further β-arrestin recruitment complementation assay is the bimolecular fluorescence complementation (BiFC) assay (*Figure 3. 1. c*), which appends fragments of a fluorophore to the receptor and β-arrestin protein (Rose, *et al*, 2010). Upon receptor activation, β-arrestin is recruited to the target receptor where the fragmented fluorophore is re-complemented and used as an indicator of receptor-β-arrestin complexes. Whilst such assays are well established, all have disadvantages; the Tango™ assay relies on the transcription of reporter gene far downstream of receptor-β-arrestin recruitment, the PathHunter™ assay requires cell lysis, so only provides an endpoint measurement of signalling (Zhang and Xie, 2012)

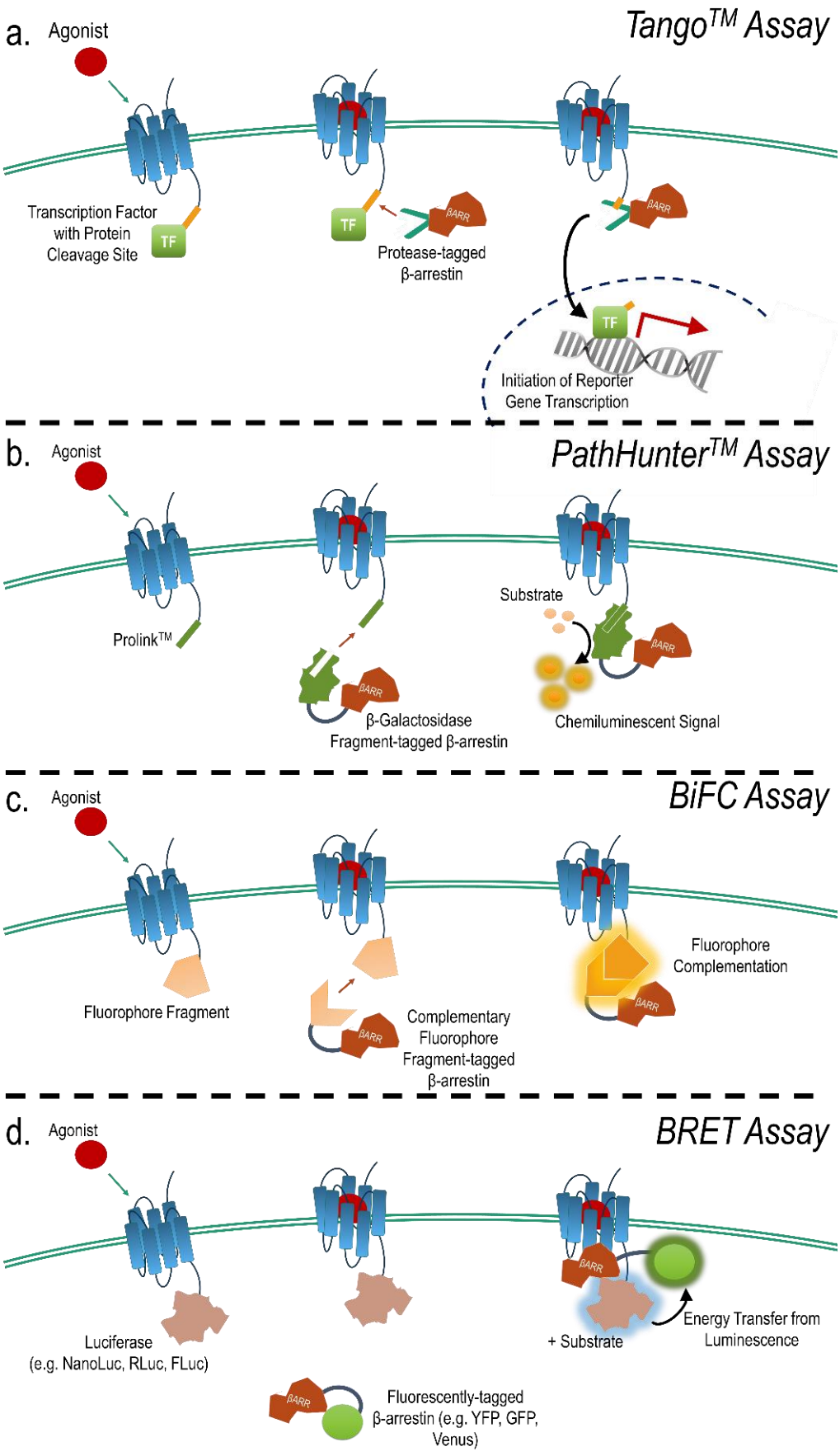
a.
Agonist
Tango™ Assay
Transcription Factor with Protein Cleavage Site
TF
TF
βARR
Protease-tagged β-arrestin
TF
Initiation of Reporter Gene Transcription
b.
Agonist
PathHunter™ Assay
Prolink™
βARR
β-Galactosidase Fragment-tagged β-arrestin
Substrate
βARR
Chemiluminescent Signal
c.
Agonist
BiFC Assay
Fluorophore Fragment
βARR
Complementary Fluorophore Fragment-tagged β-arrestin
Fluorophore Complementation
βARR
d.
Agonist
BRET Assay
Luciferase (e.g. NanoLuc, RLuc, FLuc)
βARR
+ Substrate
Energy Transfer from Luminescence
βARR
Fluorescently-tagged β-arrestin (e.g. YFP, GFP, Venus)

Figure 3. 1 Non-Imaging Biosensors of β-arrestin recruitment. *(a.) The Tango™ assay uses a receptor construct with C-terminal protease cleavage site and transcription factor (TF), whilst the β-arrestin is fused to a protease. Upon receptor activation and β-arrestin recruitment, the TF is cleaved and translocates to the nucleus to upregulate the transcription of a reporter gene. (b.) The PathHunter™ assay uses a receptor with a C-terminal Prolink™ fragment and β-arrestin is fused to an inactive form of β-galactosidase. Upon receptor activation and β-arrestin recruitment, the Prolink™ and β-galactosidase fragments complment to gain function, metablosing a substrate to produce a chemiluminescent signal. (c.)The biomolecular fluorescence complementation assay (BiFC) fuses complmentary fragments of a fluorophore to receptor and β-arrestin constructs. Upon receptor activation and β-arrestin recruitment, the fluorophore re-complements and emits light upon excitation. (d.) Bioluminescence resonance energy transfer (BRET) assays use a receptor with a C-terminla luciferase and a β-arrestin with a fluorescent tag. Upon receptor activation and β-arrestin recruitment, the two tags are close enough for the luminescence generated by the luciferase to excite the fluorescently tag, which then emits fluorescence at a longer wavelength.*

and finally the fluorophore complementation in the BiFC is irreversible and thus is not suitable to monitor the signalling kinetics of β-arrestin recruitment. RET based approaches have also been widely applied to monitor to monitor β-arrestin recruitment (*Figure 3. 1. d*) at a range of receptors including vasopressin V2, dopamine D2, histamine H1 and chemokine receptors (Kamal *et al.*, 2009; Donthamsetti *et al.*, 2015; Bonneterre *et al.*, 2016; Bosma *et al.*, 2016). In such BRET assays, the C –terminal of receptor and the β-arrestin are tagged with a fluorescent protein (e.g. GFP, YFP, Venus) or a luciferase protein, such as NanoLuc, with the arrangement of the tags and target proteins variable. Upon receptor activation and β-arrestin recruitment, the two tags are within close proximity (< 10 nm; (Stryer and Haugland, 1967; Stryer, 1978)) and the emission from the luciferase excites the fluorophore, which itself emits light at a longer wavelength. The BRET response is calculated as a ratio of the two emissions (fluorophore/luciferase) and allow for monitoring of dynamic protein-protein interactions in real-time. Further RET methods label subcellular locations, such as the plasma membrane or endosomes, with the donor or acceptor RET partner to avoid receptor modification and provide information of the localisation of intracellular receptor signalling *(Wan et al*, 2018). Such methods can be used in parallel with imaging techniques, where confocal microscopy approached can simultaneous detect labelled receptors and sub-cellular locations (Wright *et al.*, 2021).

G protein recruitment is often monitored from downstream indicators, resulting from activation of the G protein signalling cascade. Commonly, the level of cAMP is used as an indicator of the activation of Gα proteins (as discussed in *Chapter 1*; i.e. Gαs activation increases cellular cAMP; Gαi activation decreases cellular cAMP) as seen in such commercial assay systems as AlphaScreen™ (PerkinElmer) (Favara et al., 2021). The AlphaScreen™ assay (*Figure 3. 2. a*) monitors levels of cellular cAMP by competing endogenous cAMP with a fluorescent cAMP probe for antibody binding. The anti-cAMP antibody is tagged a fluorophore, which can be excited by FRET from the fluorescent cAMP probe. As levels of endogenous cAMP increase, the fluorescent cAMP probe is out-competed and the FRET signal decreases. A further assay monitoring G protein activation is the GloSensor™ assay (Promega) (Goulding, *et al*, 2018) (*Figure 3. 2. b*); the assay is an intramolecular sensor based upon the firefly luciferase, which upon cAMP binding undergoes a conformation change to restore luciferase activity and thus uses luminescence as a read-out of cAMP. Whilst the AlphaScreen methodology only reports cell signalling in an end-point manner, due to required cell lysis, the GloSensor™ assays allows for cAMP production to be reported

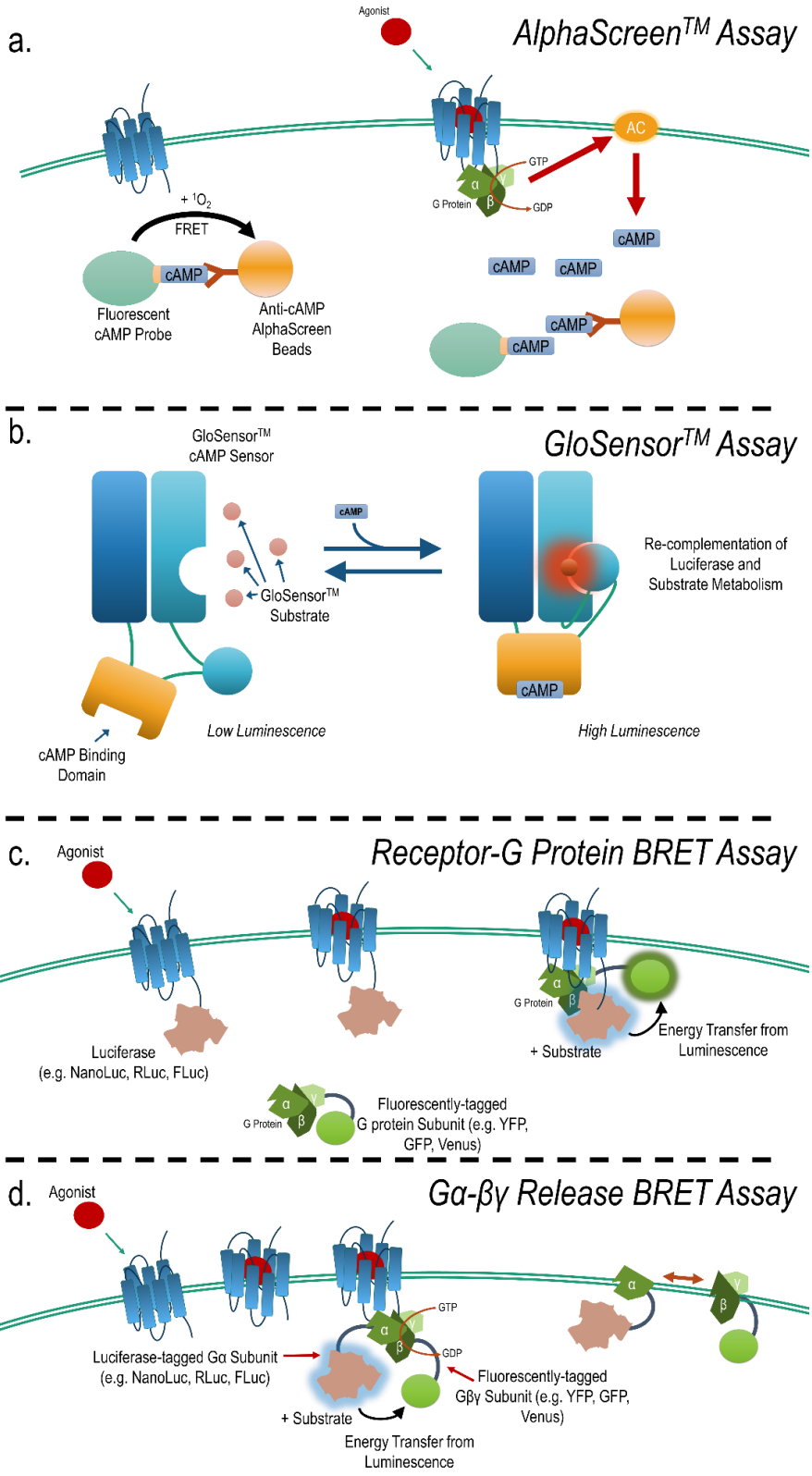
a.
AlphaScreen™ Assay
Agonist
AC
GTP
GDP
G Protein
+ $^1O_2$
FRET
cAMP
Fluorescent cAMP Probe
Anti-cAMP AlphaScreen Beads
b.
GloSensor™ Assay
GloSensor™ cAMP Sensor
GloSensor™ Substrate
Re-complementation of Luciferase and Substrate Metabolism
cAMP Binding Domain
Low Luminescence
High Luminescence
c.
Receptor-G Protein BRET Assay
Agonist
Luciferase (e.g. NanoLuc, RLuc, FLuc)
+ Substrate
Energy Transfer from Luminescence
Fluorescently-tagged G protein Subunit (e.g. YFP, GFP, Venus)
d.
Gα-βγ Release BRET Assay
Agonist
Luciferase-tagged Gα Subunit (e.g. NanoLuc, RLuc, FLuc)
Fluorescently-tagged Gβγ Subunit (e.g. YFP, GFP, Venus)
+ Substrate
Energy Transfer from Luminescence

Figure 3. 2 Non-Imaging Biosesnors of G protein activation/recruitment. *(a.) The AlphaScreen™ assay uses an anti-cAMP antibody tagged to a fluorophore and a fluorescent tracer cAMP probe. At low levels of endogenous cAMP, the cAMP probe binds the fluorescent antibody, which can be monitored by measuring the Förster resonance energy transfer (FRET) from the fluorescent cAMP probe to the antibody. As levels of endogenous cAMP increase, the fluorescent cAMP probe is out-competed and the FRET signal decreases. (b.) The GloSensor™ assay (Promega) is an intramolecular sensor based upon the firefly luciferase, which upon cAMP binding undergoes a conformation change to restore luciferase activity and thus uses luminescence as a read-out of cAMP. (c. and d.) Bioluminescence resonance energy transfer (BRET) assays tag partners of either (c.) the receptor and the G protein or (d.) the Gα and the Gβγ subunits with a luciferase and a fluorescent tag. Upon proximity of the two partners, the two tags are close enough for the luminescence generated by the luciferase to excite the fluorescently tag, which then emits fluorescence at a longer wavelength.*

in real-time and allows imaging of luminescence using imaging based measurements. G protein activation can also be monitored using GTPγS assays, in which a non-hydrolysable radiolabelled form of GTP (i.e. [^{35}S]-GTPγS) is incubated with membranes expressing the target receptor. Upon receptor and subsequent G protein activation, GDP is exchanged for GTP to initiate G protein dissociation and G protein mediated signalling. In the endogenous pathway GTP is hydrolysed back to GDP and can then re-associate with the receptor. In GTPγS assays, GDP is exchanged for [^{35}S]-GTPγS irreversibly at Gα subunits, which can then be detected by filtration and scintillation to quantify radioactivity. Whilst a direct measure of G protein activation, the [^{35}S]-GTPγS assay once again does not monitor G protein activation in real-time and requires the use of radiolabelled GTP, which itself requires careful handling and waste management. RET assays have been employed to monitor receptor-G protein interactions in real-time (*Figure 3. 2. c*), with fluorescent and luminescent species used to label the receptor of interest and a subunit of the G protein heterotrimer. Whilst this assay provides real-time measurements of receptor-G protein interactions, it does not provide information on the activation state of the G protein or nucleotide exchange. To monitor the process of G protein subunit dissociation, and thus the initiation of G protein signalling, Gα-βγ BRET release assays use fluorescent and luminescent tags used to label the Gα and Gβγ subunits (*Figure 3. 2. d*). A structurally simplified version of Gα proteins, known as mini Gα proteins (*Chapter 1*; *1. 8*), have been engineered from the GαGTPase domain of the Gα subunit and was first applied in structural studies monitoring GPCR-G protein interactions (Carpenter and Tate, 2016; Nehmé *et al.*, 2017). Under basal conditions, the mini Gα protein is located in the cytosol, due to a lack of membrane anchors and thus provide very low signal to noise ratios when applied in recruitment assays. Mini Gα proteins have been applied in BRET and split luciferase complementation assays to measure the initial recruitment of a G protein-like interface at a GPCR (Wan *et al*, 2018b; Höring *et al*, 2020).

3. 1. 3 NanoLuc® Binary Technology (NanoBiT)

The use of luciferase proteins in BRET assays allows for dynamic measurements of receptor-effector interactions, with the NanoLuc protein as an optimal donor in such assays due to its bright luminescence, wide emission spectrum and resultant wide range of possible acceptor species (Stoddart, *et al*, 2018). As discussed

in *Chapter 1*, dynamic biosensors monitoring GPCR signalling have been further developed by applying NanoLuc in a luciferase complementation assay known as NanoLuc Binary Technology (NanoBiT®, Promega) which is becoming more prominent (Dixon *et al.*, 2017; Reyes-Alcaraz *et al.*, 2018; Storme *et al.,* 2018; Soave *et al.*, 2020; Soave *et al*., 2020). Using NanoLuc, Dixon *et al*., (2016) optimised NanoLuc fragments to obtain effective reversible complementation of a small 11 amino acid C-terminal fragment (SmBiT) and the remaining 18kDa protein (LgBiT), known as NanoLuc binary technology (NanoBiT). Complementation of the LgBiT and SmBiT fragments was shown to produce a sustained robust luminescence signal upon furimazine treatment, with comparably unchanged spectrum compared to original NanoLuc (emission peak = ~460nm). The first advantage of development of NanoBiT is that the sequence of the 11 amino acid fragment can altered to tailor the affinity at the LgBiT complementation partner. The low affinity LgBiT-SmBiT binding partners (K_D = 190 μM; (Dixon, *et al.*, 2016)) was shown to be weak enough to not alter the binding kinetics of the fused proteins of interest and allow for an accurate representation of dynamic protein-protein interactions (Dixon *et al.*, 2016). High affinity "HiBiT" fragments, with a K_D as low 700 pM, showed the greatest affinity for the LgBiT fragment and thus produces pseudo-irreversible binding to stabilise protein-protein complexes (Dixon, *et al.*, 2016; Duan *et al.*, 2020). The second advantage of the NanoBiT assay is the small size of 11 amino acid, compared to that of other luciferases or fluorophores, which allows the protein of interest to be labelled without disrupting the function or used to modify the endogenous protein with ease using CRISPR (White *et al.*, 2020).

3. 1. 4 Describing GPCR Ligand Pharmacology

The availability of signalling measurements from multiple timepoints has enhanced the capacity to study GPCR signalling using full timecourse data, with multiple end point readouts made to look at responses over time. However, a single endpoint measurement is still often used to describe ligand pharmacology, assuming system equilibrium. Typically, the subsequent concentration response relationships are used to define ligand potency and maximal response and are analysed through the use of mathematical models, which aim to extract fundamental GPCR pharmacology, such as ligand affinity, efficacy or bias from functional data. These models assume system equilibrium and so can be affected by the kinetic context in which endpoint measurements are taken, where equilibrium may not in fact have been established (Klein Herenbrink *et al.*, 2016).

This can be exemplified when calculating ligand bias, a phenomenon in which an agonist activates a GPCR to preferentially activate one intracellular pathway over another, relative to a reference ligand (*Chapter 1*; *1. 3*). Bias is often explained in terms of the stabilisation of functionally distinct active drug-receptor (DR*) conformations (*Chapter 1*) (Urban *et al.*, 2007). Commonly, measures of ligand bias are obtained by comparing ligand activation of G protein and β-arrestin signalling pathways using pharmacology obtained from separate functional responses (Nijmeijer *et al.*, 2012). However, analysis of signalling bias originating from ligand driven receptor conformations is often difficult to separate from "system" effects (e.g. cellular context and amplification) or non-equilibrium influences (e.g. binding kinetics). To able to produce valid conclusions of the links between biased ligands and inform structure activity relationships, a robust measure of ligand efficacy is necessary in which a 'like for like' comparison of different pathways may be made.

3. 1. 5 The Operational Model of Agonism

The operational model of agonism put forward by Black and Leff (1983) (*Chapter 1*; *1. 3. 3*) is the most commonly used method to analyse functional data (Black and Leff, 1983; Black *et al.*, 1985). The operational model derives estimates for the equilibrium dissociation constant for the agonist receptor interaction (K_A) and a transducer parameter (τ or tau), with the latter reflecting both agonist efficacy at the receptor and the system coupling efficiency, for example governed by the extent of signal amplification and the receptor number (R_0). When considering bias between pathways, transduction co-efficients are used to ratio the effects of each agonist (described asΔLog τ/K_A) within a pathway relative to a reference ligand (Stott, Hall and Holliday, 2015). This relative comparison has the important aim to normalise the data for the system influences (Kenakin *et al.*, 2012; Stott, *et al*, 2015; Thompson *et al.*, 2016). Measurements of bias are then constructed as the differences between transduction co-efficients between pathways, $\Delta\Delta$LogTau/K_A, with the interpretation that bias is detected when $\Delta\Delta$Log Tau/K_A differs from 0.

The operational model utilises constants that assume equilibrium conditions (e.g. K_A) but have been widely applied in signalling bias investigations to assays conducted at often different time points where equilibrium has not been reached and/or the response is highly dynamic. For example, there is now a growing appreciation for the confounding effects of GPCR signalling kinetics and the influence of binding kinetics

on signalling responses. When investigating the bias properties of aripiprazole, a partial agonist at the dopamine D2 receptor, Tschammer *et al*., (2011) reported aripiprazole to have no bias between the inhibition of cAMP production and ERK1/2 phosphorylation. However, Capuano *et al*., (2014) describe aripiprazole as a biased ligand towards cAMP production when compared with ERK1/2 phosphorylation. In these and other such publications (Urb*an et al*, 2007; Masri *et al*, 2008; McPherson *et al*, 2010; Molinari *et al*, 2010; Allen *et al*, 2011; Tschammer *et al*, 2011a; Szabo *et al*, 2014), discrepancies in drug bias have been observed, with the explanation that these result from a lack of correction for experimental or system bias. In particular, the endpoint time for assay measurement of different responses is often chosen for the characteristics of the assay (signal window, robust and reproducible measurement) and not always to ensure appropriate pharmacological comparison and modelling of the data to evaluate bias. This was systematically investigated by Klein Herenbrink et al., (2016), who demonstrated that both ligand-binding kinetics and the intrinsic signalling kinetics of different intracellular pathways (e.g. activation, desensitisation) had a profound influence on the observations of biased agonism. Aripiprazole, and other example ligands such as bifuprenox, were particularly noted to have slow ligand-binding kinetics which was reflected as an increase in functional potency over time, as its dopamine D2 receptor occupancy approached equilibrium (Charlton and Vauquelin, 2010). Thus, to better understand ligand affinity, efficacy and bias measurements, modelled from functional data, there needs to be a greater appreciation of both binding and signalling kinetics, aided by methods which routinely map timecourse measurements of receptor signalling pathways. However due the complexities of GPCR signalling cascades, there are still few models which extract fundamental pharmacological parameters, such as affinity and efficacy, from experimental signalling kinetic data.

3. 1. 6 A Kinetic Operational Model

In recent years, a kinetic operational model has been put forward (Hoare *et al.*, 2018; Hoare, *et al.*, 2020) which can be used to obtain agonist equilibrium dissociation constants, as well as empirical descriptors of ligand efficacy and desensitisation rates, from data taken from timecourse-based experiments. The kinetic operational model (defined by equations in *Methods*; *Equations 2. 4- 2. 9*) was derived from Black and Leff's original 1983 operational model where the maximal activity of the system is defined by a single term (Emax) (Black and Leff, 1983). However, these new kinetic

operational models temporally distinguish the maximal system effect into two terms: the transduction potential (Ep), which is the maximum possible effect from the system, such as the total amount of cytosolic β-arrestin2 available for recruitment; and the actual response (E), generated by agonist occupied receptors converting Ep to E. The initial rate at which Ep is converted to E is governed by the transduction rate constant kTau, and thought to be a descriptor of efficacy. As much as it is a descriptor of ligand efficacy, as for the operational model, kTau not only represents the agonist efficacy but it also encapsulates the system-dependent kinetic efficacy.

The kinetic operational model, described in Hoare et al (2018), covers a range of eventualities, both for the rates of ligand binding and a variety of kinetic behaviours for the receptor signalling stimulated. In most of the described models it is assumed there is instantaneous binding equilibrium established and thus would be most suitable for systems with fast ligand-receptor binding kinetics. In the "rise-and-fall" kinetic model considered in this chapter, depletion of signal as a decay of Ep is incorporated through inclusion of a response decay rate constant – k_D. In GPCR signalling pathways this accounts for transient responses that may be generated from many different inactivation processes, for example termination of G protein signalling by β-arrestin binding to the receptor or the transient signalling response of β-arrestin2 recruitment at the β_2AR (Oakley *et al.*, 1999). As there are a range of available kinetic operational models, selection has to be based on the available experimental data, which can introduce experimenter bias. However, these models are beneficial in their ability to use timecourse data from single agonist concentration response curves to estimate affinity and kTau. In the standard operational model, tau and K_A cannot be resolved unambiguously by fitting a single agonist concentration response relationship, and multiple data sets are usually required using agonists of differing efficacy (Black and Leff, 1983; Black *et al.*, 1985; Stott, *et al,* 2015), or before and after receptor depletion (Furchgott, 1966). Potentially, such models may also prove more valuable when comparing ligand signalling in different systems and pathways, as the pharmacology is derived from timecourse reports of receptor signalling and not a single timepoint of assumed equilibrium.

3.2 Chapter Aims

The work completed in Chapter Three: Results I, aimed to:

(1) Establish NanoBiT complementation assays to monitor real-time recruitment of β-arrestin2 and a mini $G\alpha_s$ protein at β-adrenoceptors (ARs).

(2) Using these assays, identify kinetic influences on measurements of agonist pharmacology at βARs.

(3) Apply Black and Leff's operational model of partial agonism to determine agonist affinity and efficacy parameters, from concentration response data at single timepoints.

(4) Determine whether application of a kinetic operational model provided valid estimates of βAR agonist affinity and efficacy, demonstrating its utility in analysing NanoBiT timecourse data.

3.3 Results

3.3.1 Construct design and comparison of 11 amino acid fragments

In all constructs, the 158 amino acid LgBiT sequence (Dixon et al 2016) was appended to the C-terminal of either the β_1 or β_2 adrenoceptor (*Methods; Figure 2. 1*). As the LgBiT partner, we used the following SmBiT sequence: VSGYRLFEEIL. This sequence was equivalent in LgBiT affinity to the low affinity fragment "Sm114" (amino acid sequence: VTGYRLFEEIL) from Dixon et al., (2016), as described in the Promega patent (Dixon *et al.,* 2018). NanoBiT responses using both Sm114 and SmBiT, located at the N or C terminus of the arrestin protein, was compared to confirm similar agonist pharmacology and β-arrestin2 recruitment profiles at the β_2AR (*Figure 3. 3*).

In HEK239T cells stably expressing SNAP-β_2AR-LgBiT, 10μM isoprenaline produced a window of 2.43-fold and 2.49-fold luminescence over vehicle, in cells transiently transfected with SmBiT-β-arrestin2 and Sm114-β-arrestin2, respectively (*Figure 3. 3. a*). N-terminal SmBiT labelling of β-arrestin2 produced a greater signal window in comparison to C-terminal labelling, with 10μM isoprenaline producing 2.43-fold and 1.36-fold luminescence over vehicle, respectively (*Figure 3. 3. a*). Agonist stimulated recruitment of SmBiT-β-arrestin1 to the β_2AR was also detected in this system, but the response was smaller than observed after transfection of SmBiT-β-arrestin2 (*Figure 3. 3. a*).

Using both SmBiT and Sm114 N-terminal arrestin labelling, the NanoBiT assay reported a transient recruitment of β-arrestin2 at the β_2AR. In each case, a rapid recruitment of β-arrestin2 between 0-3 minutes was observed, with the signal decaying between 3-31 minutes (*Figure 3. 3. b*). Isoprenaline concentration response curves constructed at the 31 minutes timepoint between the two NanoBiT systems, using SmBiT- or Sm114- β-arrestin2, were indistinguishable from each other (*Figure 3. 3. c*).

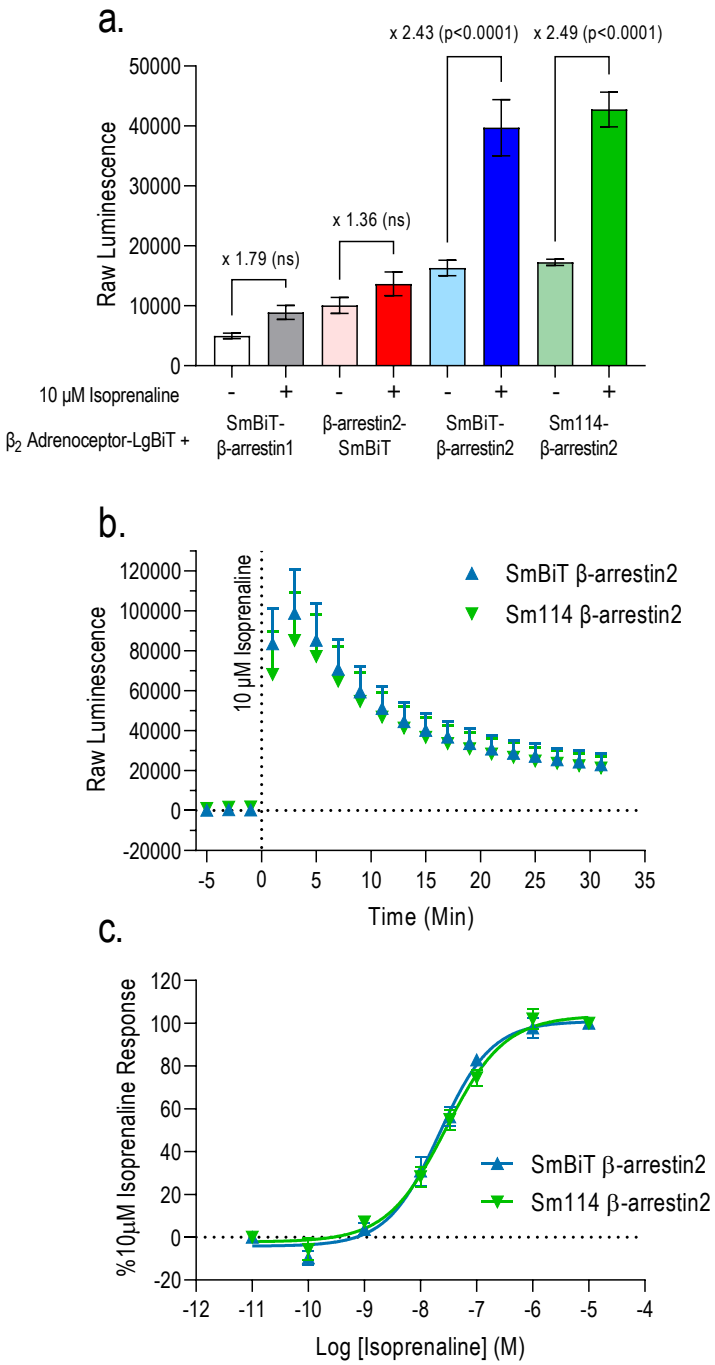

Figure 3. 3 SmBiT and Sm114 NanoBiT fragments report comparable recruitment of β-arrestin proteins at the β_2AR. HEK293T cells, stably transfected with SNAP-β_2AR-LgBiT, were transiently transfected with β-arrestin tagged with either SmBiT (VSGYRLFEEIL) or Sm114 (VTGYRLFEEIL) DNA. *(a.) NanoBiT luciferase activity in the presence and absence of 10µM isoprenaline, in cells expressing SNAP-β2AR-LgBiT and: β-arrestin1 with N-terminal SmBiT tag; β-arrestin2 with C-terminal SmBiT tag; β-arrestin2 with N-terminal SmBiT tag; and β-arrestin2 with N-terminal Sm114 tag. P<0001; Student's t-test. Cells expressing SNAP-β2AR-LgBiT and either β-arrestin2 with N-terminal SmBiT tag, or β-arrestin2 with N-terminal Sm114 tag, were (b.) treated with 10 µM isoprenaline and monitored over 31 minutes and (c.) titrated with increasing concentrations of isoprenaline to give pEC_{50} values of 7.69±0.08 and 7.55±0.07 for SmBiT β-arrestin2 and Sm114 β-arrestin2 expressing cells, respectively. All data represented as mean ± s.e.m. (n=4). Concentration response data taken from 31 minutes post-isoprenaline addition and normalised to 10 µM isoprenaline response.*

3.3.2 Characterisation of β_2AR/effector NanoBiT cell lines

To establish NanoBiT assays for mini Gαs and β-arrestin2 recruitment, mixed population stable HEK293T cells were established by consecutive stable transfection of either (1) SmBiT-βarrestin2 or (2) SmBiT-Mini Gαs protein, and SNAP-β_2AR-LgBiT construct cDNAs, with cell lines referred to as β_2AR/SmBiT-β-arrestin2 and β_2AR/SmBiT-Mini Gαs, respectively. Initially these cell lines were evaluated for cell surface expression of SNAP-β_2AR-LgBiT and receptor localisation following either vehicle or 10 μM isoprenaline treatment.

Cells expressing SNAP-β_2AR-LgBiT at the plasma membrane were labelled with a membrane impermanent fluorophore (SNAP-surface AF488) for 30 minutes, following which the cells were then incubated with either vehicle or 10 μM isoprenaline in buffer containing transferrinAF546. The transferrinAF546 reagent labelled the clathrin mediated endosomal and recycling pathway defined by the transferrin receptor (Hols*t et al*, 2004; Watson, *et al,* 2012). Cells were then fixed and imaged with an IX Ultra imaging plate-reader. Under vehicle conditions, both cells lines displayed labelled SNAP-β_2AR-LgBiT largely localised to the plasma membrane, whilst cells incubated with 10 μM isoprenaline for 1 hour internalised (*Figure 3. 4* and *Figure 3. 5* for β_2AR/SmBiT-β-arrestin2 and β_2AR/SmBiT-Mini Gαs cell lines, respectively).

Isoprenaline, salbutamol and salmeterol were then compared in their abilities to internalise the SNAP-β_2AR or SNAP-β_2AR-LgBiT receptors (*Figure 3. 6*; *Table 3. 1*). Figure 3. 6 displays that each of the three ligands internalised the SNAP-labelled receptor in all HEK293T cell lines: (1) SNAP-β_2AR, (2) β_2AR/SmBiT-β-arrestin2 and (3) β_2AR/SmBiT-Mini Gαs. Isoprenaline was used as the reference agonist, with salbutamol and salmeterol acting as partial agonists in all cell lines. However, the relative maximal response of salbutamol and salmeterol were comparable between cells expressing SNAP-β_2AR (Rmax % 10 μM isoprenaline = 60.08 ± 8.12 and 33.15 ± 6.27, for salbutamol and salmeterol respectively), β_2AR/SmBiT-βarrestin2 (Rmax % 10 μM isoprenaline = 55.32 ± 6.45 and 42.13 ± 7.50, for salbutamol and salmeterol respectively) and β_2AR/SmBiT-Mini Gαs cell lines (Rmax % 10 μM isoprenaline = 24.46 ± 15.84 and 17.39 ± 2.01, for salbutamol and salmeterol respectively). Moreover, agonist potencies, as indicated by pEC_{50} values, were also not significantly different between cell lines (*Table 3. 1*).

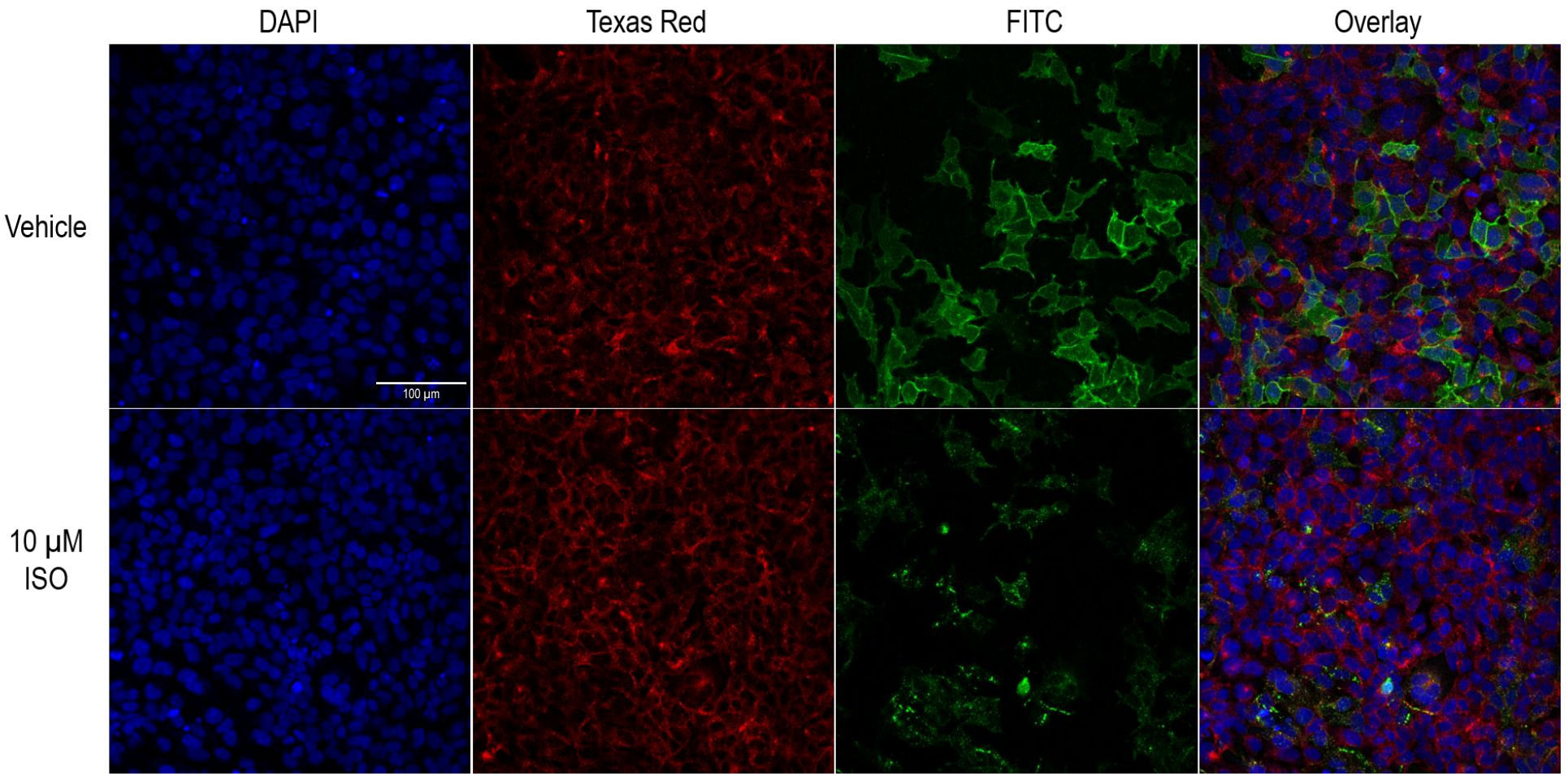

Figure 3. 4 Internalisation of the SNAP-tagged β_2AR, with C-terminal LgBiT, in cells expressing β_2AR/SmBiT-βarrestin2 DNA, in response to 10 µM isoprenaline stimulation. *Cells were labelled with cell-impermeable AF488-SNAP reagent for 30 minutes, with a subsequent 1 hour treatment of TrasnferrinAF546 and 10 µM isoprenaline. Cells nuclei were labelled with Hoechst stain (33342), before cell fixation. Representative images of each treatment show cell nuclei, imaged using DAPI filter (blue), transferrin labelled endosomes, imaged using Texas Red filter (red), and AF488-SNAP-β2AR-LgBiT receptors, imaged using FITC filter (green), with an overlay of each image shown.*

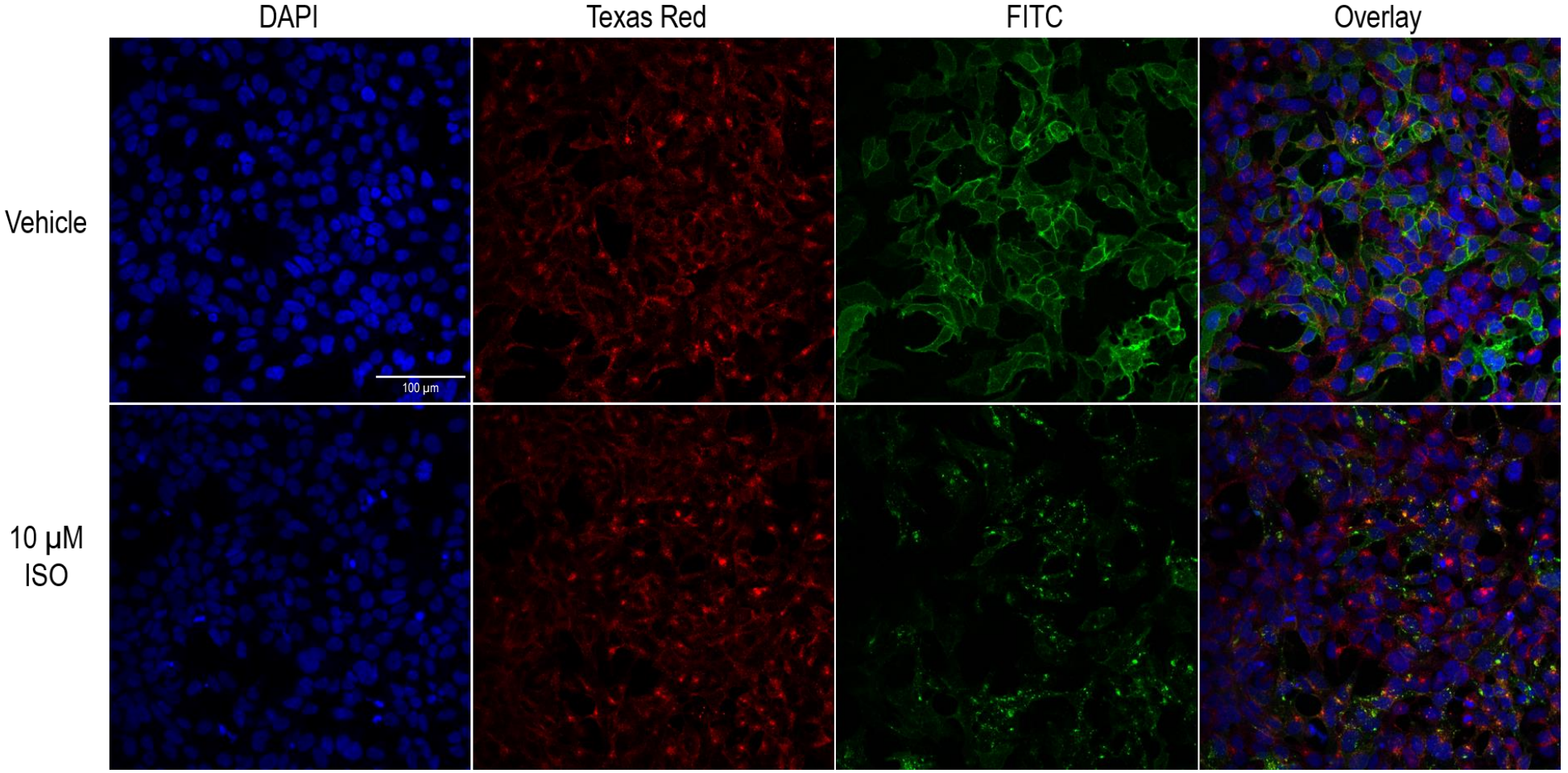

Figure 3. 5 Internalisation of the SNAP-tagged β_2AR, with C-terminal LgBiT in, in cells expressing β_2AR/SmBiT-Mini Gαs DNA, in response to 10 µM isoprenaline stimulation. *Cells were labelled with cell-impermeable AF488-SNAP reagent for 30 minutes, with a subsequent 1 hour treatment of TrasnferrinAF546 and 10 µM isoprenaline. Cells nuclei were labelled with Hoechst stain (33342), before cell fixation. Representative images of each treatment show cell nuclei, imaged using DAPI filter (blue), transferrin labelled endosomes, imaged using Texas Red filter (red), and AF488-SNAP-β2AR-LgBiT receptors, imaged using FITC filter (green), with an overlay of each image shown.*

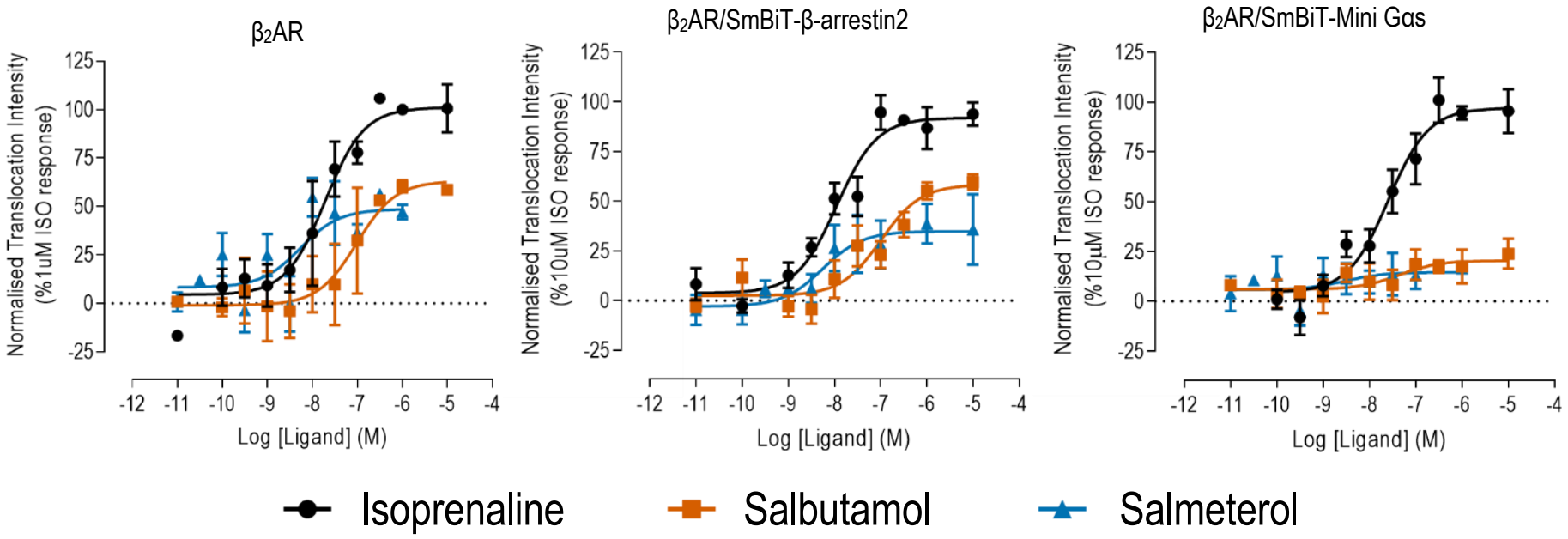

Figure 3. 6 Quantification of agonist driven internalisation responses, of AF488-SNAP-tagged β_2AR in WT and NanoBiT cell lines. *Receptor internalisation was evaluated for the SNAP-β_2AR ±LgBiT, in response to 1 hour treated of increasing concentrations of isoprenaline, salbutamol and salmeterol. Translocation Enhanced analysis quantified translocation of AF488-SNAP-tagged β_2ARs to TransferrinAF546 labelled endosomes. Data points represent 3-5 individual experiments conducted in duplicate, normalised to 10 μM isoprenaline (100%) and vehicle (0%) controls. Agonist potencies and maximal responses are summarised Table 3.1*

Cell Line	*Ligand*	*pEC_{50} (M)*	*R_{max} (% 10 μM Iso)*
β_2AR	*Isoprenaline*	*7.85 ± 0.28*	*109.70 ± 11.49*
	Salbutamol	*7.56 ± 0.03*	*60.08 ± 8.12*
	Salmeterol	*8.25 ± 0.25*	*33.15 ± 6.27*
β_2AR/ SmBiT-βarrestin2	*Isoprenaline*	*7.92 ± 0.22*	*94.84 ± 4.04*
	Salbutamol	*6.51 ± 0.86*	*55.32 ± 6.45*
	Salmeterol	*7.80 ± 0.38*	*42.13 ± 7.50*
β_2AR/ SmBiT-Mini $G\alpha_s$	*Isoprenaline*	*7.52 ± 0.26*	*98.97 ± 12.09*
	Salbutamol	*7.86 ± 1.71*	*24.46 ± 15.84*
	Salmeterol	*8.35 ± 0.27*	*17.39 ± 2.01*

Table 3. 1 Summary of maximal responses and pEC_{50}s from internalisation assays of SNAP-tagged β_2AR in WT and NanoBiT cell lines. *Data are derived from the concentration response curves shown in Figure 3.* **6** *6. Data represented as mean ± s.e.m., from 3-5 individual experiment conducted in duplicate. Rmax represents % 10 μM isoprenaline response. No significant differences in pEC50 or Rmax were observed between cell lines.*

3.3.3 Effect of furimazine concentration on agonist pharmacology, as determined in the β_2AR NanoBiT complementation assays.

Once cell lines were established, a protocol was determined to measure NanoBiT complementation in both β_2AR/SmBiT-βarrestin2 and β_2AR/SmBiT-Mini Gαs protein cells in response to a panel of ligands (*Methods; 2.6.2*). In the conventional protocol, furimazine was added to cells and given 5 minutes to equilibrate. A ligand was then added to the cells and immediately placed in the BMG PHERAstar FS platereader to be read in 120 second cycles, with the first cycle described as the 1 minute response for all wells. To investigate the concentration of furimazine to be used in subsequent NanoBiT assays, a range of dilution ratios were applied to β_2AR/SmBiT-βarrestin2 and β_2AR/SmBiT-Mini $G\alpha_s$ cells and the agonist response of isoprenaline was monitored over 31 minutes (*Figure 3. 7*). The final assay concentration represented a range between 1:300 and 1:2640 from the manufacturer's furimazine stock.

In β_2AR/SmBiT-βarrestin2 cells, as the dilution ratio increased the luminescence response decreased yet still maintained a transient profile of β-arrestin2 recruitment upon 10 μM isoprenaline treatment (*Figure 3. 7. a*). In cells expressing β_2AR/SmBiT-Mini $G\alpha_s$, there was also a negative correlation between dilution ratio and luminescence response (*Figure 3. 7. e*). In both cell lines, when luminescence was normalised to 10μM isoprenaline at the 3 minute timepoint, the timecourse profiles at different furimazine concentrations were shown to be indistinguishable (*Figure 3. 7. b & f*). In both β_2AR/SmBiT-βarrestin2 and β_2AR/SmBiT-Mini Gαs protein cells, isoprenaline concentration response curves were also constructed using the range of furimazine dilution ratios. In both cell lines, the luminescence window of response increased in as the dilution ratio decreased (*Figure 3. 5. c & g)*. When normalised, the isoprenaline concentration response curves were shown to be superimposable (*Figure 3. 5. d & h*). The final dilution ratio of 1:192 was used in subsequent NanoBiT assays.

3.3.4 Reverse timecourse experiments demonstrate furimazine depletion does not account for the transient β_2AR/β-arrestin2 recruitment profile

To further investigate the robustness of the established NanoBiT complementation assays, a reverse timecourse assay was run to determine if the transient recruitment profile seen in β_2AR/SmBiT-βarrestin2 cells was due to substrate depletion. At a range of timepoints between 5 and 65 minutes, either vehicle or a saturating concentration (10 μM) of isoprenaline or salbutamol was added to cells incubating at 37°C. At the final addition, the furimazine substrate was added and left for 5 minutes before luminescence measurement on PHERAstar FS. When compared to the conventional mode measuring NanoBiT activity where furimazine is first added to the cells and agonist action is monitored in real-time, the reverse timecourse experiment showed a comparable transient profile of β-arrestin2 recruitment to the receptor (*Figure 3. 8).* In addition, relative to 10 μM isoprenaline a partial agonist response to salbutamol was observed. In the conventional NanoBiT assay, the peak isoprenaline luciferase activity was observed at 3 minutes. Due to the time needed for substrate equilibration, a timepoint of earlier than 5 minutes was not taken in the reverse timecourse assay. Thus, in the reverse timecourse, when treated with 10 μM isoprenaline the peak response was observed at 5 minutes with a smaller plateauing luminescence response in the timepoints between 35 and 65 minutes post-ligand addition (*Figure 3. 8*).

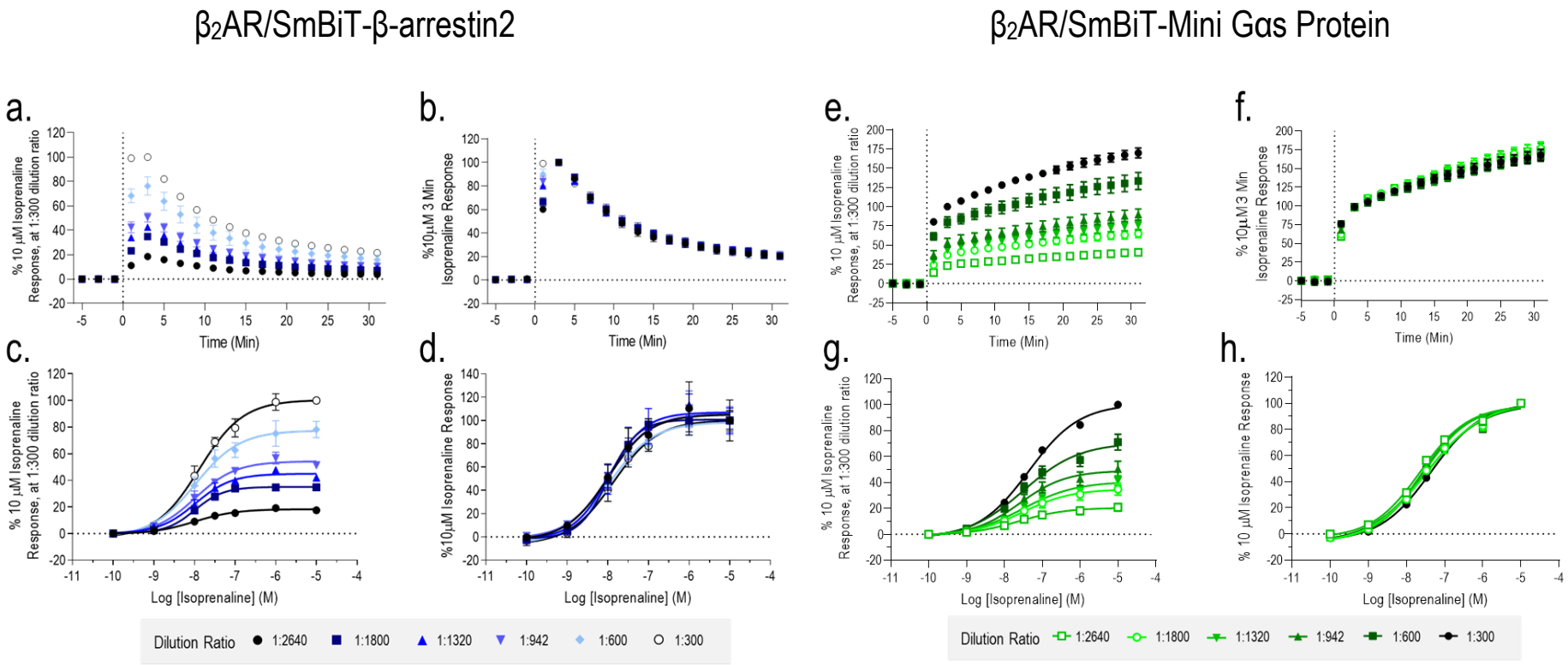

Figure 3. 7 Comparison of isoprenaline response, using increasing concentrations of furimazine substrate. *Timecourse profiles of β_2AR recruitment of (a.-b.) β-arrestin2 and (c.-d.) mini Gα_s recruitment, stimulated by 10µM isoprenaline, with increasing dilutions (from stock concentration from manufacturer) of furimazine substrate. Responses were normalised as a percentage of 10µM isoprenaline response at 3 minutes of (a. & e.) the 1:300 dilution condition and (b. & f.) each dilution condition. Isoprenaline concentration response curves were generated for (c.-d.) β-arrestin2 and (g.-h.) mini Gα_s recruitment, at the 31 minute timepoint, using the furimazine concentration range. (c. & g.) Data normalised to 10 µM response of 1:300 dilution condition for each cell line produced concentration response curves with increasing luciferase activity, which overlapped when normalised as a % of 10µM isoprenaline response of each concentration (e. & h.).*

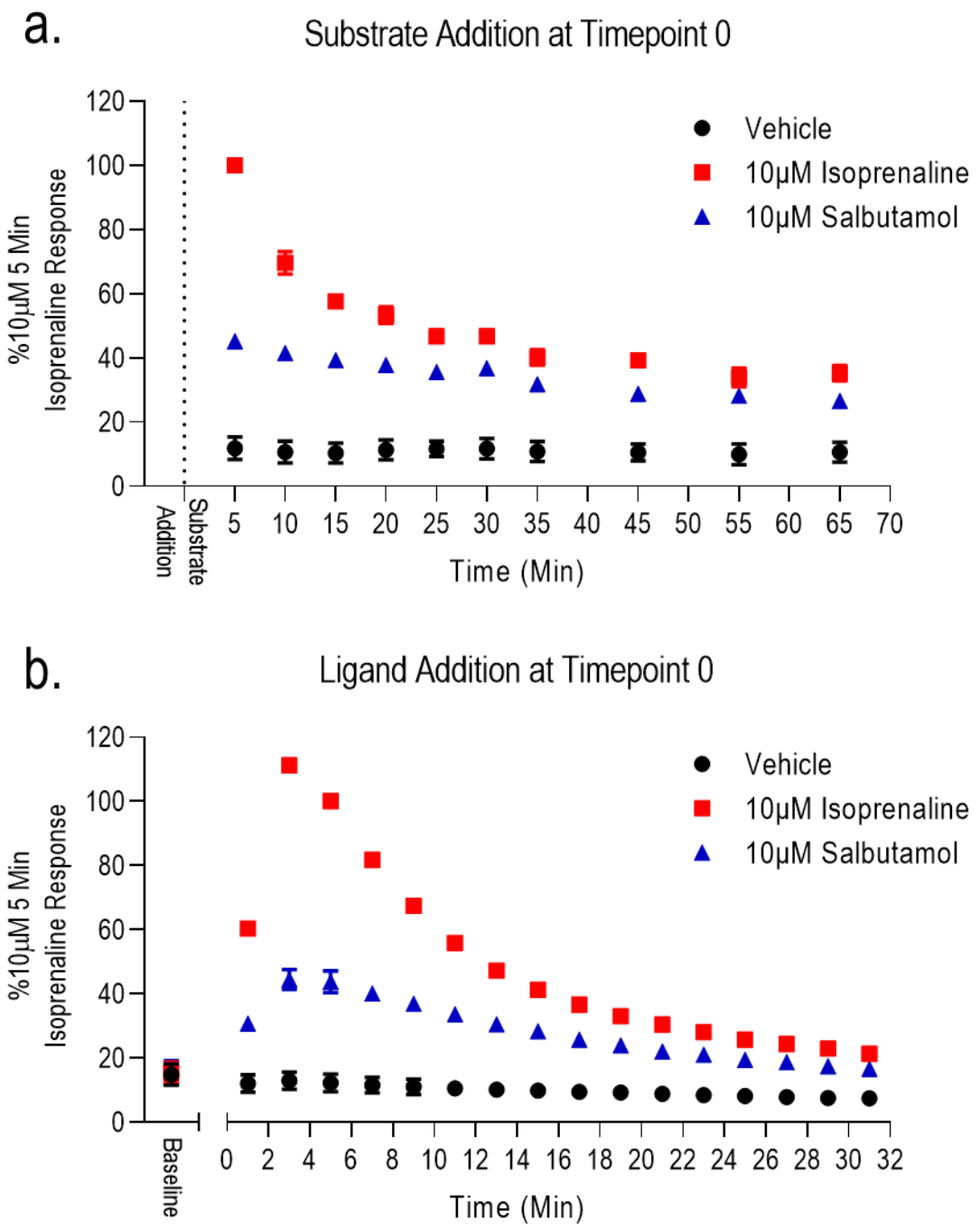

Figure 3. 8 Reverse timecourse experiments demonstrate substrate depletion does not affect β-arrestin2 recruitment profile to the β_2AR. *Recruitment of β-arrestin2 to β_2ARs was monitored using (a.) a reverse timecourse, where vehicle/10 µM isoprenaline/10 µM salbutamol were added over the course of 70 minutes, before furimazine was added for 5 min and the response read in an end-point manner. Data was normalised as a % of 10 µM isoprenaline response from the final timepoint addition (5 minutes). (b.) In the typical NanoBiT assay, furimazine was added to the cells for 5 minutes, after which each of vehicle/10 µM isoprenaline/10 µM salbutamol was added and monitored over 31 minute timecourse. Data was normalised as a % of 10 µM isoprenaline response 5 minute response.*

3.3.5 NanoBiT complementation assay reflects distinct profiles of β-arrestin2 and mini $G\alpha_s$ protein recruitment in response to full agonist isoprenaline, at β_2ARs.

NanoBiT complementation of LgBiT and SmBiT fragments was shown to have a basal level of complementation prior to the addition of β_2AR ligands, in both SmBiT-β-arrestin2 and SmBiT-mini Gαs cell lines. In response to a saturating concentration of isoprenaline (10μM), a β_2AR full agonist, recruitment of β-arrestin2 produced a transient response. β-arrestin2 was rapidly recruited to the receptor between 0 and 3 minutes, where the response peaked, before luminescence dropped significantly to leave a reduced sustained luciferase activity at 31 minutes (*Figure 3. 9*). When treated with 10μM isoprenaline, the mini Gαs protein was shown to be rapidly recruited to the β_2AR between 0 and 5 minutes, with a second phase of steady increase in luciferase activity between 5 and 31 minutes (*Figure 3. 9*). In both cell lines, the potency of isoprenaline significantly increased between the 3 and 31 minute timepoints, increasing 9 and 4 fold in β-arrestin2 and mini Gαs protein recruitment assays, respectively (pEC_{50} values: β-arrestin2: 7.11±0.06 vs 8.07±0.09, at 3 and 31 minutes, respectively; mini Gαs: 7.45±0.13 vs 8.01±0.13, at 3 and 31 minutes, each $p<0.05$, Student's t-test) (*Figure 3. 12*; *Table 3. 2*).

3.3.6 Comparison of β_2AR agonist pharmacology between mini $G\alpha_s$ protein and β-arrestin2 recruitment

The effects of an agonist panel, reported to vary agonist efficacy and affinity (Hanania *et al.*, 2002), were examined in both mini Gαs protein and β-arrestin2 recruitment assays. Concentration response data were taken from the 3 minute and 31 minute time points of each signalling assay, where ligand responses (R_{max}) were normalised between the vehicle and the reference agonist isoprenaline (10μM) (*Figure 3. 12*; *Table 3. 2*).

Concentration dependent recruitment of β-arrestin2 to β_2ARs by β_2AR agonists was monitored over 31 minutes (*Figure 3. 10*). All β_2AR agonists, excluding salbutamol and dopamine, demonstrated a significant increase in potency between time points seen in the concentration response curves (*Figure 3. 12. a – d)* and pEC50 values (*Table 3. 2*). Despite the increase in potency, the overall rank order of potency saw little change: C26=salmeterol=formoterol>

indacaterol=isoprenaline>salbutamol>noradrenaline>dopamine vs C26= formoterol=salmeterol>isoprenaline=indacaterol>salbutamol>noradrenaline>dop amine, at 3 and 31 minutes respectively (*Table 3. 2*). The rank order of relative maximal response of β-arrestin2 recruitment (%10μM isoprenaline) changed between 3 and 31 minutes: noradrenaline=isoprenaline=C26>formoterol> indacaterol>salbutamol>dopamine=salmeterol vs isoprenaline=noradrenaline= formoterol=C26>salbutamol=indacaterol>salmeterol>dopamine, at 3 and 31 minutes respectively (*Table 3. 2*). By 31 minutes, the relative maximal response of formoterol increased to within 10% of isoprenaline and noradrenaline responses, whilst the maximal response of salbutamol and salmeterol was shown to increase between 3 and 31 minutes (salbutamol: 38.3±4.4% vs 70.5±9.0%; salmeterol: 17.6±1.7% vs 48.2±5.6%; $p<0.05$,Student's t-test). Overall, an increase in potency and relative maximal response of β-arrestin2 recruitment was observed between 3 and 31 minutes, with the effect more pronounced in certain ligands (salbutamol, salmeterol and formoterol) over others (dopamine).

Unlike the transient recruitment of β-arrestin2, ligand stimulated recruitment of the engineered 'mini' Gαs protein was shown to be much more stable once reaching the peak luminescence response (*Figure 3. 11*). However, the potency of isoprenaline, salbutamol and formoterol was observed to increase between 3 and 31 minutes (pEC_{50} values: isoprenaline 7.45±0.13 vs 8.01±0.13; salbutamol 6.88±0.09 vs 7.24±0.10; salmeterol 7.63±0.09 vs 8.39±0.03; at 3 and 31 minutes, respectively $p<0.05$, Student's t-test) (*Table 3. 2*).

The rank order of agonist potencies demonstrated few changes between 3 and 31 minutes: C26>indacaterol=formoterol=isoprenaline>salbutamol= salmeterol>noradrenaline>dopamine and C26>formoterol=indacaterol= isoprenaline>salmeterol=salbutamol>noradrenaline>dopamine, at 3 and 31 minutes respectively (*Figure 3. 12*; *Table 3. 2*). The relative maximal response of C26 increased between 3 and 31 minutes (117.1±6.4% vs 138.4±6.2%; $p<0.05$, Student's t-test) and became the first in relative maximal response rank order. Noradrenaline and salmeterol showed higher rank order of relative maximal response between 3 and 31 minutes: formoterol>indacaterol=C26>isoprenaline= noradrenaline=salbutamol>salmeterol>dopamine vs C26>formoterol> noradrenaline=indacaterol=isoprenaline>salbutamol>dopamine> salmeterol, at 3 and 31 minutes respectively (*Figure 3. 12*; *Table 3. 2*).

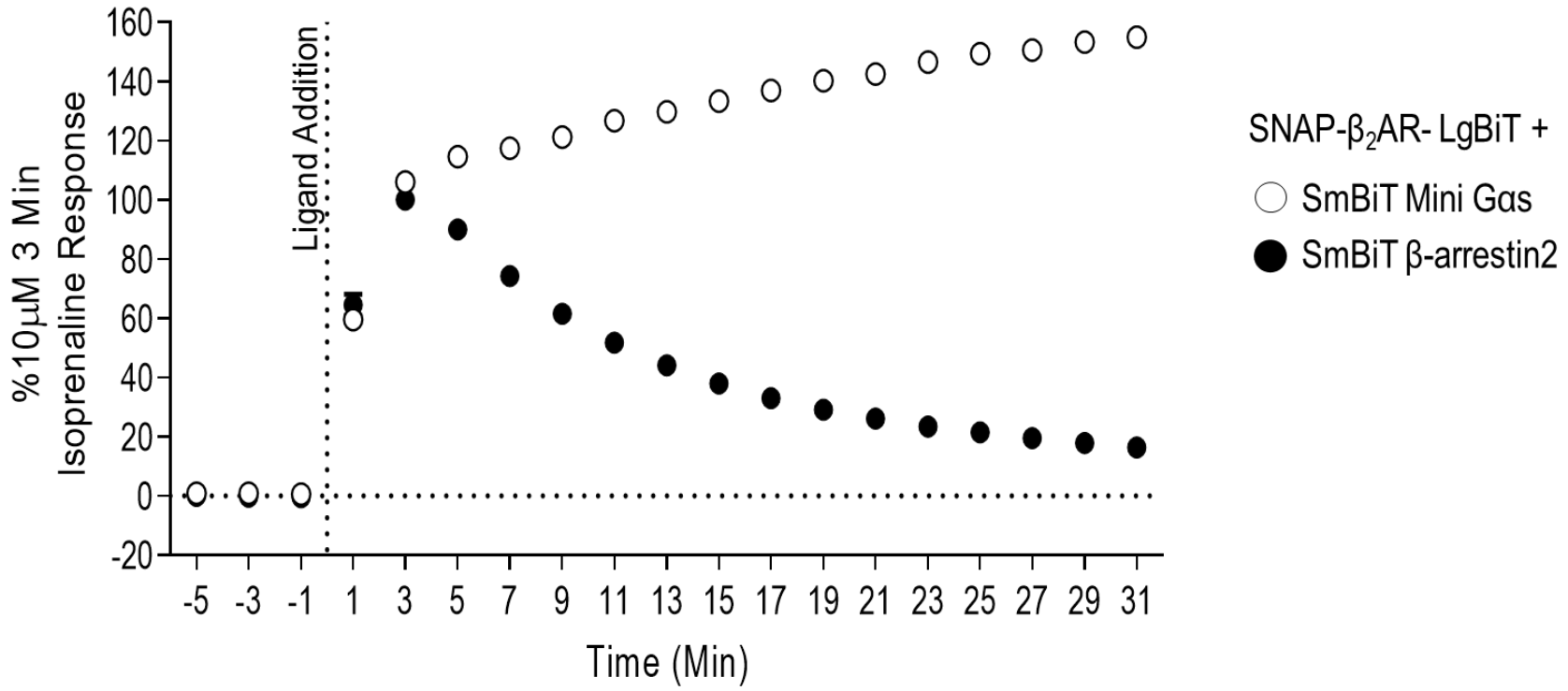

Figure 3. 9 NanoBiT assay reflects distinct profiles of effector recruitment to β_2AR in response to 10 μM isoprenaline. *10 μM isoprenaline stimulation (timepoint 0) initiated recruitment of β-arrestin2 and mini Gαs to β_2AR. Pooled timecourse data represent mean ± s.e.m. of 5 individual experiments, conducted in duplicate. Recruitment responses were normalised as a % of 10 μM isoprenaline response at 3 minutes for each cell line.*

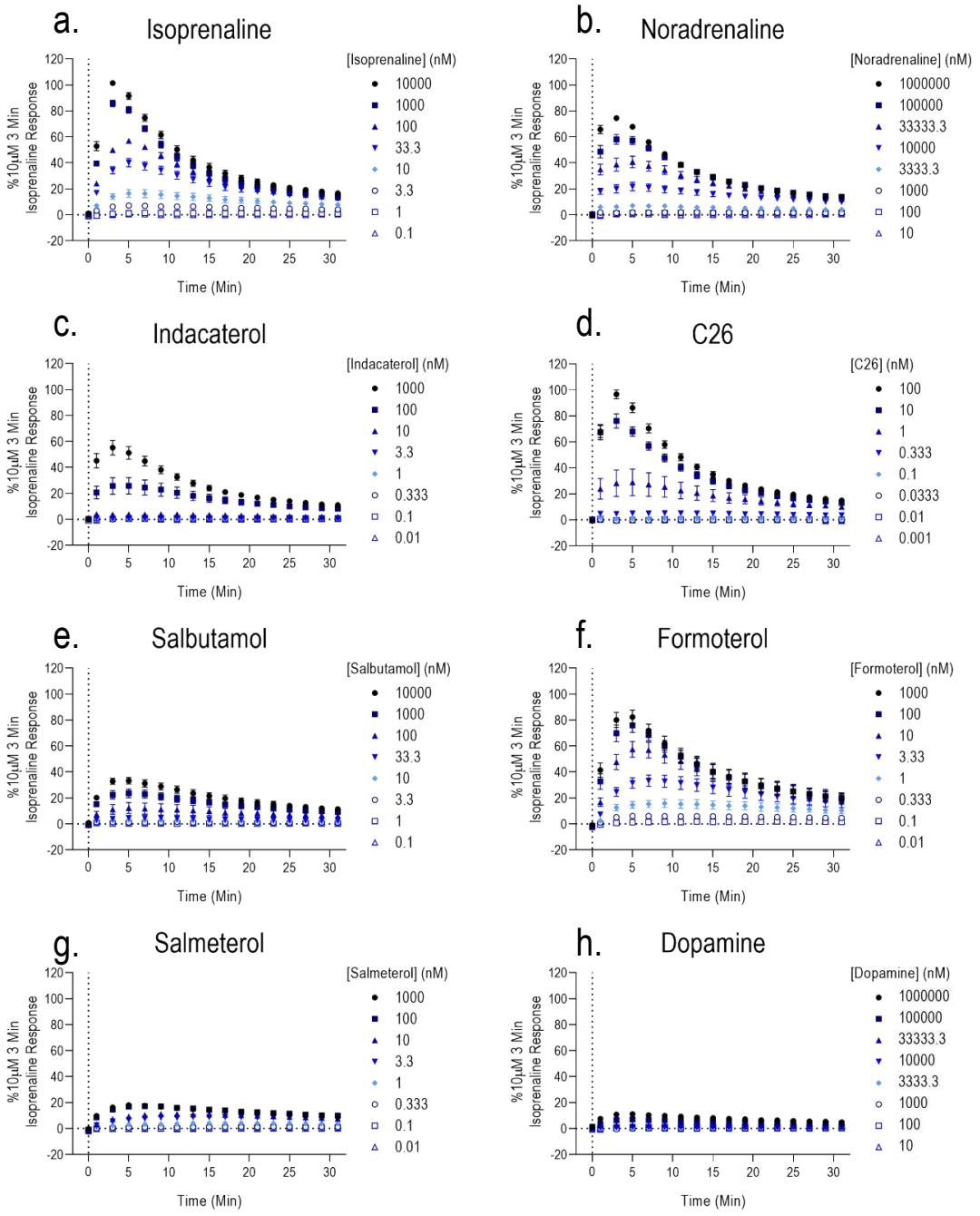

Figure 3. 10 NanoBiT complementation assay reports real-time measurement of agonist stimulated β-arrestin2 recruitment, at the β_2AR. *Agonist stimulation (time 0; indicated by dotted line) using a range of agonist concentrations, initiated recruitment of β-arrestin2. Pooled timecourse data represent mean ± s.e.m., from 5 independent experiments, conducted in duplicate. Relative maximal responses quantified as % 10μM isoprenaline response at 3 min.*

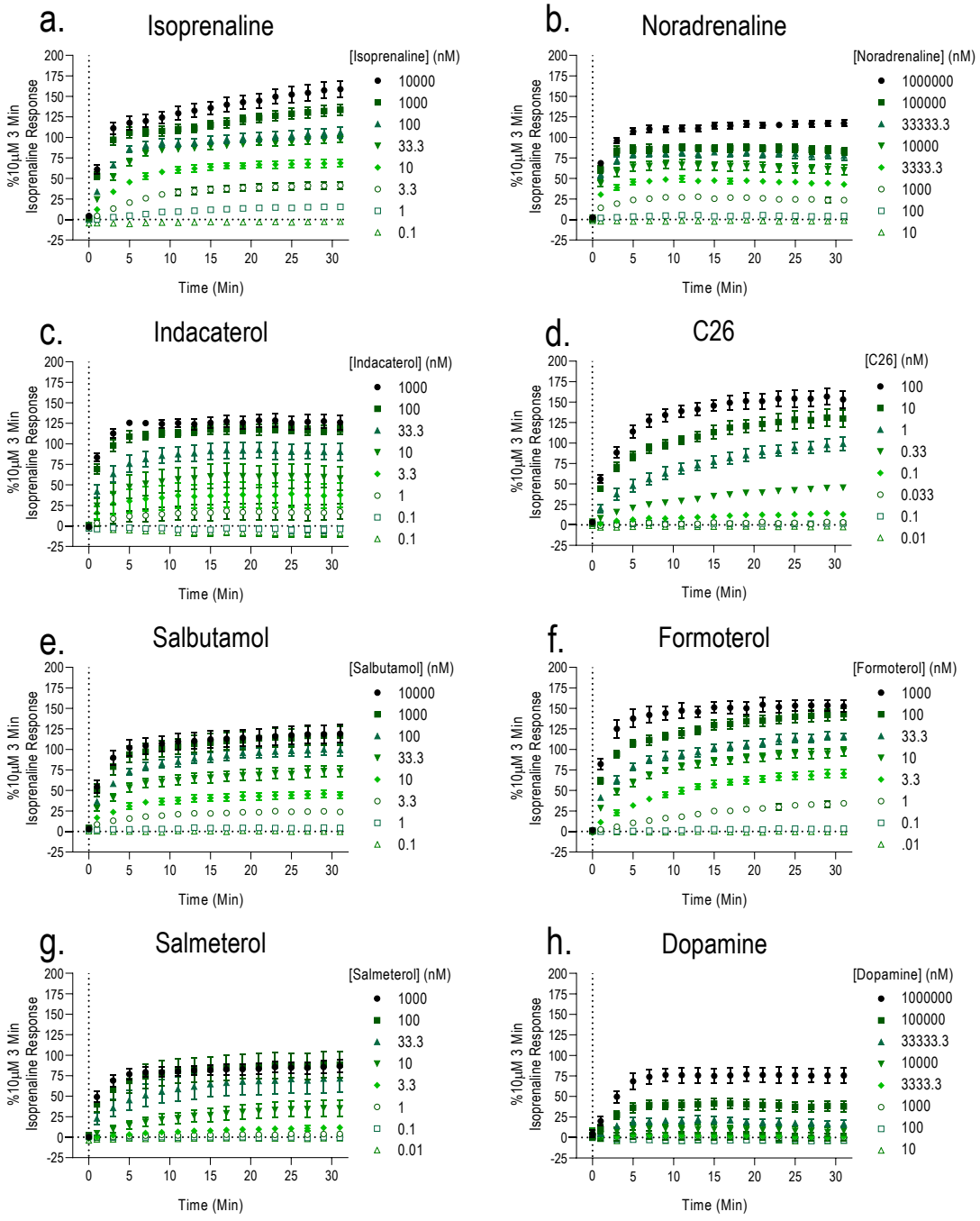

Figure 3. 11 NanoBiT complementation assay reports real-time measurement of agonist stimulated mini Gαs protein recruitment, at the β_2AR. *Agonist stimulation (time 0; indicated by dotted line) using a range of agonist concentrations, initiated recruitment of mini $G\alpha_s$ proteinβ-arrestin2. Pooled timecourse data represent mean ± s.e.m., from 5 independent experiments, conducted in duplicate. Relative maximal responses quantified as % 10μM isoprenaline response at 3 min.*

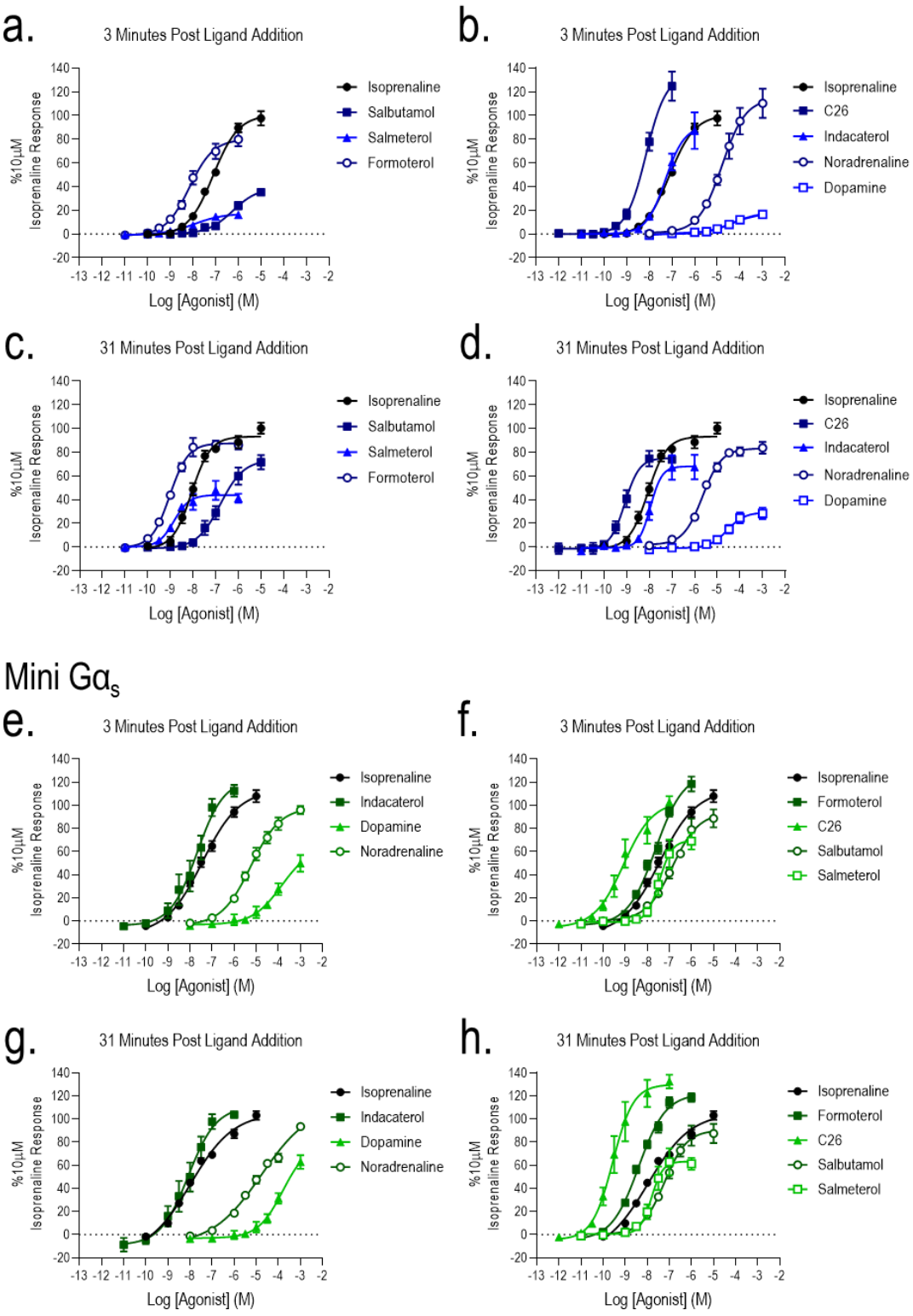

Figure 3. 12 Concentration response curves of β-arrestin2 (a.-d.) and mini Gαs (e.-h.) recruitment, at β_2AR. *Concentration response curves of ligand panel demonstrated full and partial agonism for the luciferase complementation response at 3 (a., b., e. & f.) and 31 minutes (c., d., g. & h.). Data represent pooled values (mean ± s.e.m., n=5), with maximal response relative to 10μM isoprenaline at each respective time point. For clarity, ligand data was spread across multiple concentration response panels, with isoprenaline response present for each panel as a reference agonist.*

	β-arrestin2				Mini Gα Protein			
	pEC_{50} (M)		Rmax (% 10 µM Isoprenaline)		pEC_{50} (M)		Rmax (% 10 µM Isoprenaline)	
	3 Minutes	31 Minutes	3 Minutes	31 Minutes	3 Minutes	31 Minutes	3 Minutes	31 Minutes
Isoprenaline	7.11 ± 0.06	8.07 ± 0.09*	102.7 ± 6.8	94.8 ± 4.8	7.45 ± 0.13	8.01 ± 0.13*	109.0 ± 7.7	109.9 ± 11.7
Salbutamol	6.25 ± 0.14	6.69 ± 0.27	38.3 ± 4.4	70.5 ± 9.0*	6.88 ± 0.09	7.24 ± 0.10*	95.0 ± 6.6	90.2 ± 7.4
Formoterol	8.01 ± 0.19	9.02 ± 0.05*	83.8 ± 5.6	88.3 ± 4.5	7.63 ± 0.09	8.39 ± 0.03*	132.8 ± 8.3	127.1 ± 6.2
Noradrenaline	4.81 ± 0.04	5.63 ± 0.04*	109.8 ± 9.3	88.3 ± 6.1	5.24 ± 0.11	4.51 ± 0.36	103.4 ± 3.4	118.3 ± 11.5
Dopamine	3.67 ± 0.63	4.54 ± 0.09	19.6 ± 3.1	30.4 ± 4.0	3.80 ± 0.20	3.78 ± 0.09	73.61 ± 12.6	84.0 ± 9.1
Salmeterol	8.05 ± 0.09	8.77 ± 0.10*	17.6 ± 1.7	48.2 ± 5.6*	6.67 ± 0.87	7.53 ± 0.32	76.0 ± 6.4	71.2 ± 3.8
Indacaterol	7.37 ± 0.19	8.03 ± 0.14*	60.5 ± 3.9	68.5 ± 8.8	7.82 ± 0.30	8.14 ± 0.31	123.1 ± 5.8	117.3 ± 8.9
C26	8.30 ± 0.15	9.11 ± 0.08*	94.0 ± 9.6	82.7 ± 7.8	8.84 ± 0.37	9.43 ± 0.30	117.1 ± 6.4	138.4 ± 6.2*

Table 3. 2 Summary of effector recruitment pharmacology at β_2AR. Pooled pEC_{50} and R_{max} (% 10 µM isoprenaline at the same timepoint) for agonist-dependent protein β-arrestin2 and mini Gαs recruitment. **P<0.05; 3 minutes vs 31 minutes for each agonist (Student's t-test). Data represent averaged values (mean±s.e.m.) of 5 individual experiments, performed in duplicate. Coloured boxes indicate significant differences.*

3.3.7 NanoBiT complementation assay reports appropriate agonist selectivity between β adrenoceptor subtypes.

The NanoBiT complementation assay was then applied to monitor effector recruitment at β_1AR. As conducted in the β_2AR NanoBiT cell lines, HEK293T cells were consecutively stably transfected with either (1) SmBiT-βarrestin2 or (2) SmBiT-Mini Gαs and SNAP-β_1AR-LgBiT cDNA, to produce mixed population cell lines, referred to as β_1AR/SmBiT-βarrestin2 and β_1AR/SmBiT-Mini Gαs protein cell lines, respectively.

As seen in β_2AR NanoBiT assays, 10 μM isoprenaline treatment stimulated transient β-arrestin2 recruitment to the β_1AR, with peak luciferase activity observed at 3 minutes and a smaller sustained response by 31 minutes (*Figure 3. 13*). Whilst the background luminescence responses of β_1AR NanoBiT cell lines were comparable to β_2AR NanoBiT cell, the overall increase in luminescence from β_1AR stimulation was less than that of β_1AR cells. A panel of βAR agonists was studied in the NanoBiT β_1AR/β-arrestin2 recruitment assay, demonstrating full agonism for noradrenaline, and partial agonism for formoterol, salbutamol and dopamine, relative to isoprenaline (*Figure 3. 13*; *Figure 3. 15. a – b*; *Table 3. 3*). The rank order of potency remained the same between 3 and 31 minutes: isoprenaline>formoterol>noradrenaline> salbutamol>dopamine. As seen with the β_2AR NanoBiT assays, an increase in potency was observed between 3 and 31 minutes for isoprenaline (pEC_{50} values: 7.58±0.15 vs 8.47±0.22, at 3 and 31 minutes, respectively $p<0.05$, Student's t-test) and salbutamol (pEC_{50} values: 5.56±0.01 vs 5.76±0.05, at 3 and 31 minutes, respectively $p<0.05$, Student's t-test).

At the β_1AR, the mini Gαs protein was rapidly recruited to the receptor between 0-5 minutes (*Figure 3. 14*). However, high concentrations of isoprenaline (1-10 μM) produced a recruitment response which failed to a plateau. All β_1AR agonists demonstrated a concentration dependent recruitment of the mini Gαs protein, though the noradrenaline driven recruitment response did not reach a defined maximum and a concentration response curve was not able to be fully defined in any individual experiment. From the remaining βAR agonist panel, isoprenaline demonstrated the highest potency at 3 minutes, but was surpassed by formoterol at 31 minutes: isoprenaline>formoterol>salbutamol>dopamine vs

formoterol>isoprenaline> salbutamol>dopamine, at 3 and 31 minutes respectively (*Figure 3. 14*; *Figure 3. 15. c - d*; *Table 3. 3*).

The selectivity of the βAR ligands between β_1 and β_2 adrenoceptors is presented in *Table 3. 4*, as defined by relative activity values ($Rmax/EC_{50}$), between receptor subtypes. The magnitude of subtype selectivity was overall greater in β-arrestin2 recruitment assays, compared with assays monitoring the recruitment of the mini Gαs protein. Across both recruitment assays, noradrenaline and formoterol demonstrated consistent β_2AR selectivity whilst dopamine was selective for the β_1AR. Isoprenaline demonstrated β_1AR selectivity in β-arrestin2 recruitment assays, compared β_2AR selectivity of a greater magnitude in assays monitoring the recruitment of the mini Gαs protein (*Table 3. 4*)

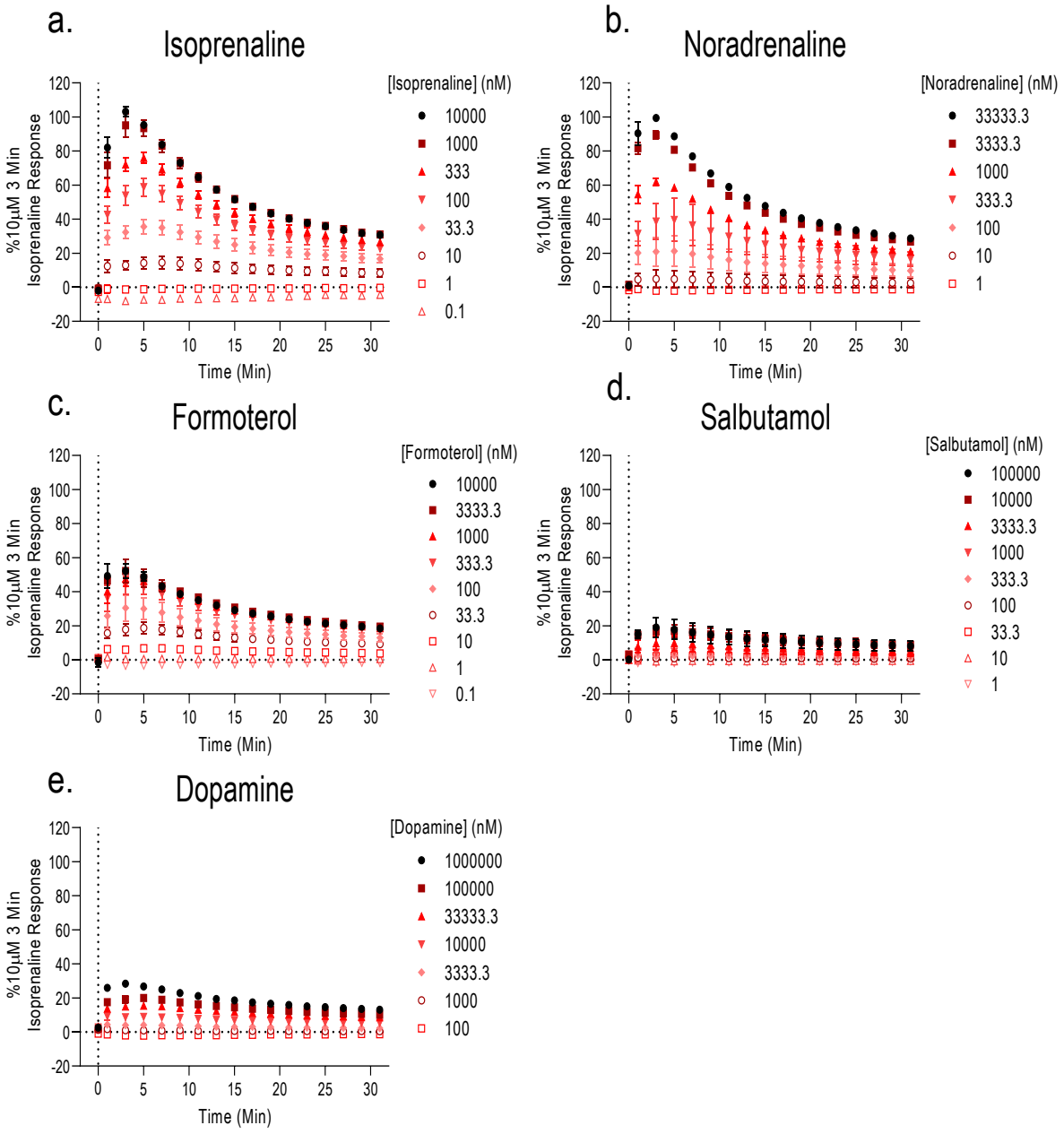

Figure 3. 13 NanoBiT complementation assay reports real-time measurement of agonist stimulated β-arrestin2 recruitment, at the β_1AR. *Agonist stimulation (time 0; indicated by dotted line) using a range of agonist concentrations, initiated recruitment of β-arrestin2. Pooled timecourse data represent mean ± s.e.m., from 3 independent experiments, conducted in duplicate. Relative maximal responses quantified as % 10μM isoprenaline response at 3 min.*

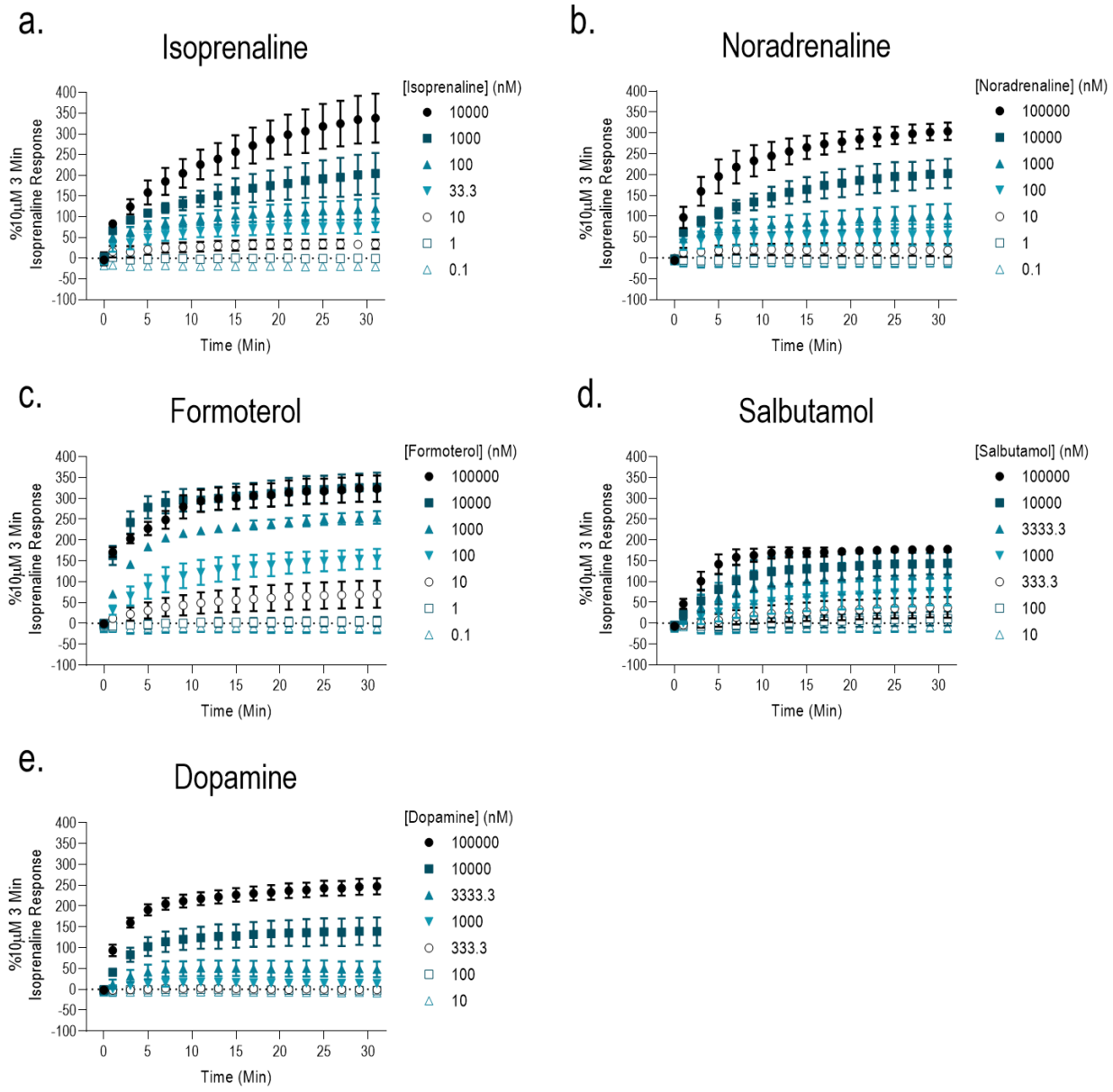

Figure 3. 14 NanoBiT complementation assay reports real-time measurement of agonist stimulated mini $G\alpha_s$ recruitment, at the β_1AR. *Agonist stimulation (time 0; indicated by dotted line) using a range of agonist concentrations, initiated recruitment of mini $G\alpha_s$. Pooled timecourse data represent mean ± s.e.m., from 3 independent experiments, conducted in duplicate. Relative maximal responses quantified as % 10μM isoprenaline response at 3 min.*

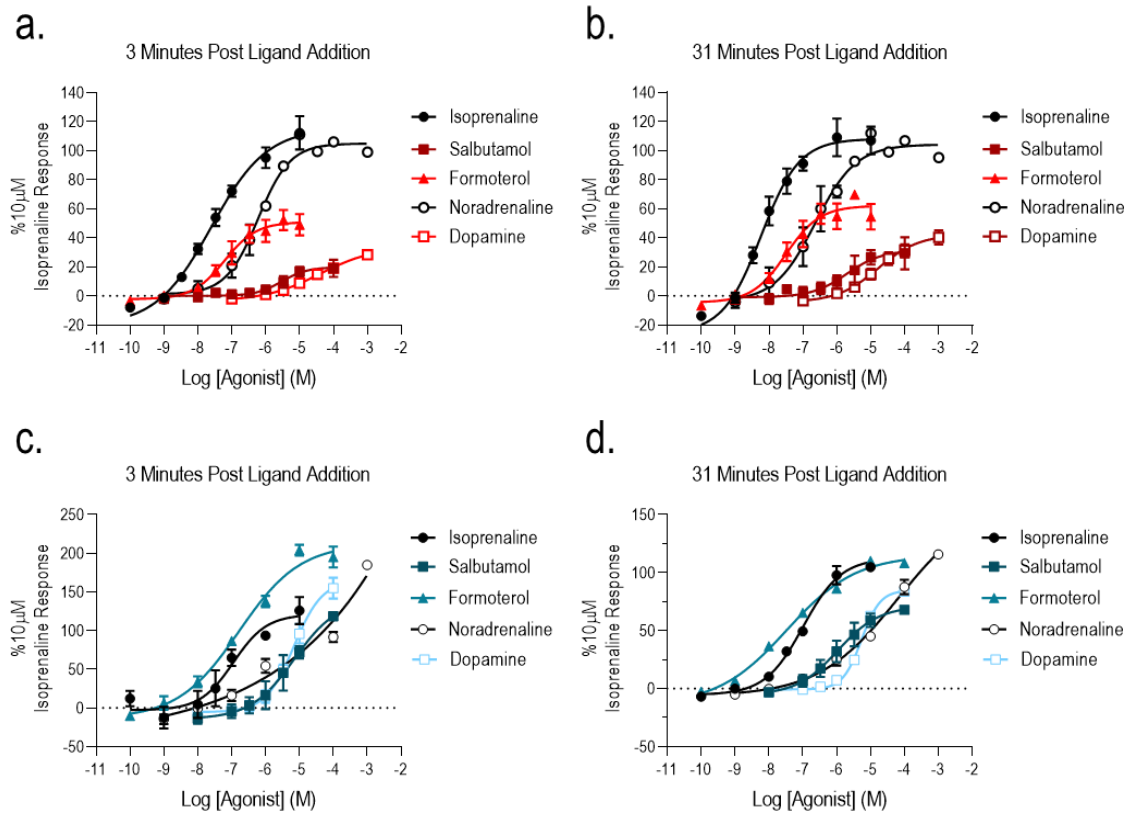

Figure 3. 15 Concentration response curves of (a. & b.) β-arrestin2 and (c. & d.) mini Gαs recruitment, at β_1ARs. *Concentration response curves of ligand panel demonstrated full and partial agonism of luciferase complementation at (a.& c.) 3 and (b. & d.) 31 minutes. Data represents pooled values (mean ± s.e.m., n=3), with maximal response relative to 10μM isoprenaline at each respective time point.*

	β-arrestin2				Mini $G\alpha_s$ Protein			
	pEC_{50} (M)		Rmax (% 10 µM Isoprenaline)		pEC_{50} (M)		Rmax (% 10 µM Isoprenaline)	
	3 Minutes	31 Minutes	3 Minutes	31 Minutes	3 Minutes	31 Minutes	3 Minutes	31 Minutes
Isoprenaline	7.58 ± 0.15	8.47 ± 0.22*	112.2 ± 5.3	113.5 ± 9.4	7.06 ± 0.05	6.78 ± 0.06*	108.3 ± 3.4	119.5 ± 18.1
Salbutamol	5.56 ± 0.01	5.76 ± 0.05*	20.9 ± 4.3	34.9 ± 6.9	5.50 ± 0.13	6.24 ± 0.02*	143.5 ± 12.2	72.7 ± 2.8*
Formoterol	6.97 ± 0.19	7.36 ± 0.10	61.1 ± 8.6	73.6 ± 9.0	6.73 ± 0.15	7.43 ± 0.12*	225.7 ± 18.8	130.9 ± 6.2*
Noradrenaline	6.19 ± 0.13	6.67 ± 0.40	100.1 ± 7.8	102.1 ± 15.4	-	-	-	-
Dopamine	4.27 ± 0.30	4.75 ± 0.13	40.4 ± 5.1	54.3 ± 4.3	5.23 ± 0.03	5.23 ± 0.02	166.3 ± 13.7	86.6 ± 2.0*

Table 3. 3 Summary of effector recruitment pharmacology, at the β_1AR. *Pooled pEC50 and Rmax (% 10 µM isoprenaline at the same timepoint) for agonist-dependent protein β-arrestin2 and mini Gαs recruitment. *P<0.05; 3 minutes vs 31 minutes (Student's t-test). Data represent averaged values (mean±s.e.m.) of 3 individual experiments, performed in duplicate. Coloured boxes indicate significant differences.*

	β-arrestin2 Recruitment	*Mini Gαs Protein Recruitment*
	β_2/β_1	β_2/β_1
Isoprenaline	0.33	15.62
Noradrenaline	17.19	12.41
Formoterol	54.84	8.86
Salbutamol	0.08	-
Dopamine	0.34	0.03

Table 3. 4 NanoBiT complementation assays can be used to observe receptor selectivity from relative activity estimaes of ligands for β_1 and β_2 adrenoceptors. *Selectivity ratios were taken from quantified relative activity values for each agonist (Rmax//EC50, at 31 minutes post ligand addition; Table 3.3), in both β-arrestin2 and mini Gαs protein recruitment assays. Whilst a ratio of 1 demonstrates no selectivity, values of more than or less than 1 demonstrates selectively for β_2ARs and β_1ARs, respectively.*

3.3.8 Detection of inverse agonism using NanoBiT effector recruitment assays at β_2ARs.

Upon treatment of saturating concentrations of ICI-118,551 or alprenolol (1 μM) inverse agonism was observed in the β_2AR/β-arrestin2 recruitment assay, as demonstrated by a reduction in the luminescence signals below vehicle throughout the assay timecourse (*Figure 3. 16. a*). These decreases occurred in a concentration dependent manner, allowing estimates of inverse agonist potency (*Figure 3. 17. a & b*; *Table 3. 5*).

ICI-118,551 inhibition of β_2AR mediated β-arrestin2 recruitment underwent changes over longer incubation times between 3 and 31 minutes, with increased potency ($P<0.05$, Student's t-test; *Table 3. 5*) and increased inverse agonism response, relative to isoprenaline ($P<0.05$, Student's t-test; *Table 3. 5*). Whilst, the potency and the inverse agonism response, relative to isoprenaline, of alprenolol was not significantly different between timepoints ($P>0.05$, Student's t-test; *Table 3. 5*).

In the β_2AR/SmBiT mini Gαs protein NanoBiT assays, ICI-118,551 treatment did not statistically alter the luminescence signal in comparison with background luminescence at either timepoint. Alprenolol produced an agonist response in β_2AR/SmBiT mini Gαs protein cells at micro-molar concentrations at 3 minutes (*Figure 3.6. b*; *Figure 3. 17. c & d*; *Table 3. 5*), which was shown to be negligible by 31 minutes (*Figure 3.7. d*; *Table 3. 5*).

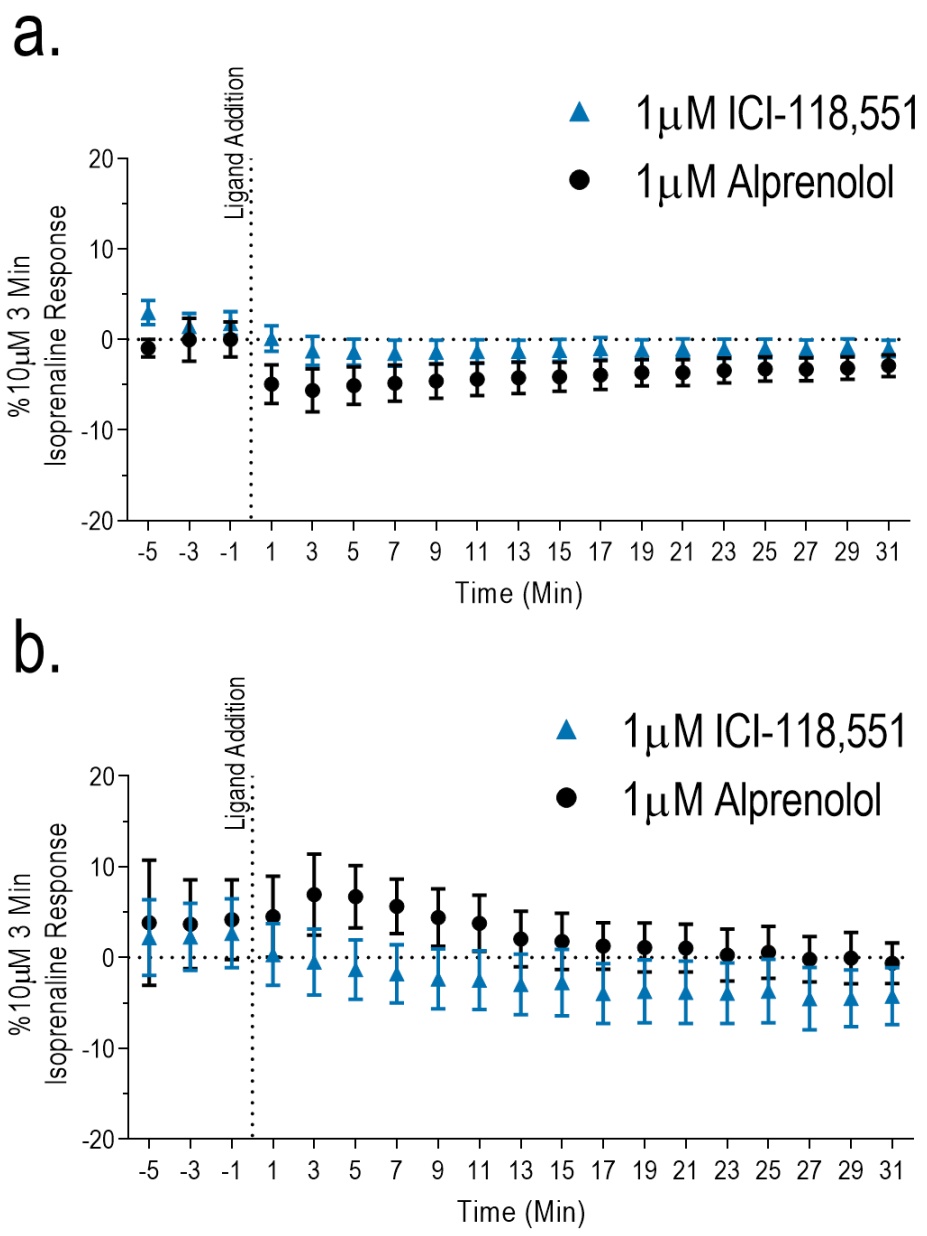

Figure 3. 16 The effect of ICI-118,551 and alprenolol on (a.) β-arrestin2 and (b.) mini $G\alpha_s$ recruitment, at β_2AR. *ICI-118551 or alprenolol was added at 0 minutes (indicated by dotted line), iwht the recruitment of (a.) β-arrestin2 and (b.) mini Gαs monitored over 31 minutes. Pooled timecourse data (mean ± s.e.m.), represent 5 independent experiments, conducted in duplicate. Relative maximal responses quantified as % 10μM isoprenaline response at 3 min.*

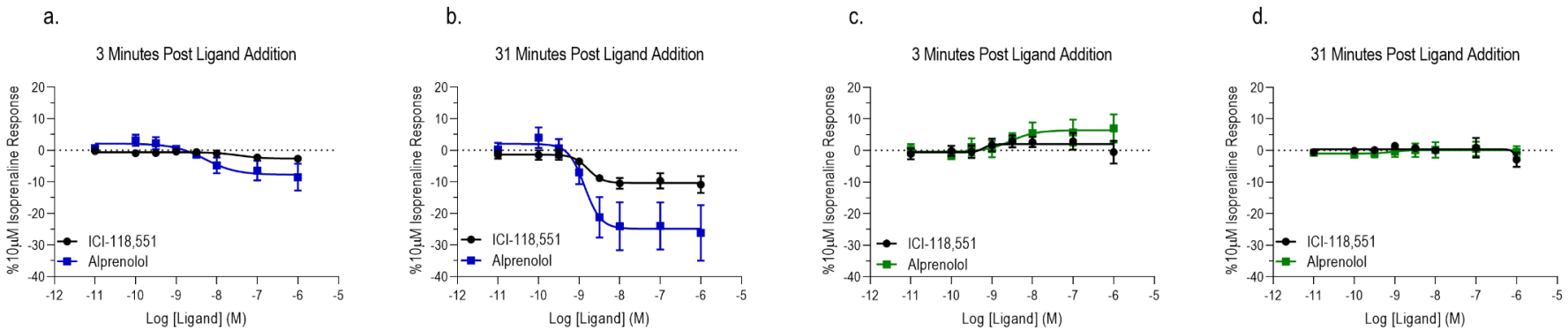

Figure 3. 17 Pharmacology of inverse agonism in NanoBiT complementation assay. *Concentration response curves of ICI-118,551 and alprenolol, describing their effects on recruitment β-arrestin2 (a. & b.) and mini Gαs (c. & d.) at 3 (a. & c.) and 31 (b. & d.) minutes, at the β_2AR. Pooled normalised data (mean ± s.e.m.), represent 5 independent experiments, conducted in duplicate. Relative maximal responses quantified as % 10μM isoprenaline response, at respective timepoints.*

	β-arrestin2				Mini Gαs Protein			
	pEC_{50} (M)		Rmax (% 10 μM Isoprenaline)		pEC_{50} (M)		Rmax (% 10 μM Isoprenaline)	
	3 Minutes	31 Minutes	3 Minutes	31 Minutes	3 Minutes	31 Minutes	3 Minutes	31 Minutes
ICI-118,551	7.90 ± 0.10	8.76 ± 0.16*	-2.9 ± 0.1	-11.2 ± 0.9*	8.77 ± 0.13	AMB	4.8 ± 0.6	-2.9 ± 2.3†
Alprenolol	8.16 ± 0.44	8.89 ± 0.01	-10.5 ± 4.2	-27.2 ± 8.8	8.49 ± 0.15#	AMB	10.3 ± 5.1	-0.4 ± 1.8†

Table 3. 5 Summary of inverse agonist pharmacology in the NanoBiT assays. *Pooled pEC_{50} & Rmax (% 10μM Isoprenaline at same timepoint) for agonist-dependent β-arrestin2/mini Gαs recruitment. *P <0.05; 3 minutes vs 31 minutes (Student's t-test). Data represent averaged values (mean ± s.e.m.) of 5 independent experiments performed in duplicate. AMB of individual experiments, indicate ambiguous fit, with Rmax given as the average (mean ± s.e.m.) response (% 10 μM Isoprenaline) at 1 μM ICI-118,551 or alprenolol, indicated by †.*

3.3.9 Kinetic analysis of ligand bias in the β_2AR NanoBiT assay, using the Black and Leff operational model of agonism.

From the agonist concentration response data obtained at 120 second intervals for 31 minutes for both β_2AR-effector recruitment assays (*Figure 3. 10*; *Figure 3. 11*; *Figure 3. 12*), a modified operational model of bias (*Methods; 2. 7. 4. 2*) (Black and Leff, 1983; Van Der Westhuizen et al., 2014) was used to estimate LogR values (equivalent to Log(tau/K_A)) for each ligand, which were normalised to a reference ligand, isoprenaline, to produce ΔLogR values. The ΔLogR values were compared between pathways to produce LogBias values (ΔΔLog(tau/K_A)) for each ligand at each timepoint (*Figure 3. 18*). In these estimates, no pathway bias is indicated by ΔΔLog(tau/K_A) = 0.

No agonist studied demonstrated bias between mini Gs and β-arrestin2 assays of more than 10 fold (ΔΔLog(tau/K_A) > 1 or < -1), nor were the bias measurements observed significantly different from 0 ($P>0.05$; Student's t-test at each timepoint). Limited biased agonism (< 10x fold) for either pathway was observed for the panel of agonists employed, relative to isoprenaline. At 31 minutes the most positive LogBias values, indicating a preference for mini Gαs recruitment, were obtained from C26, whilst the most negative, indicating a preference for β-arrestin2 recruitment, were obtained from salmeterol (*Figure 3. 18*). However, noradrenaline and formoterol demonstrated a weak trend in changing bias ("drift") over the 31 min assay window, but these changes were not significantly different between 3 and 31 minutes.

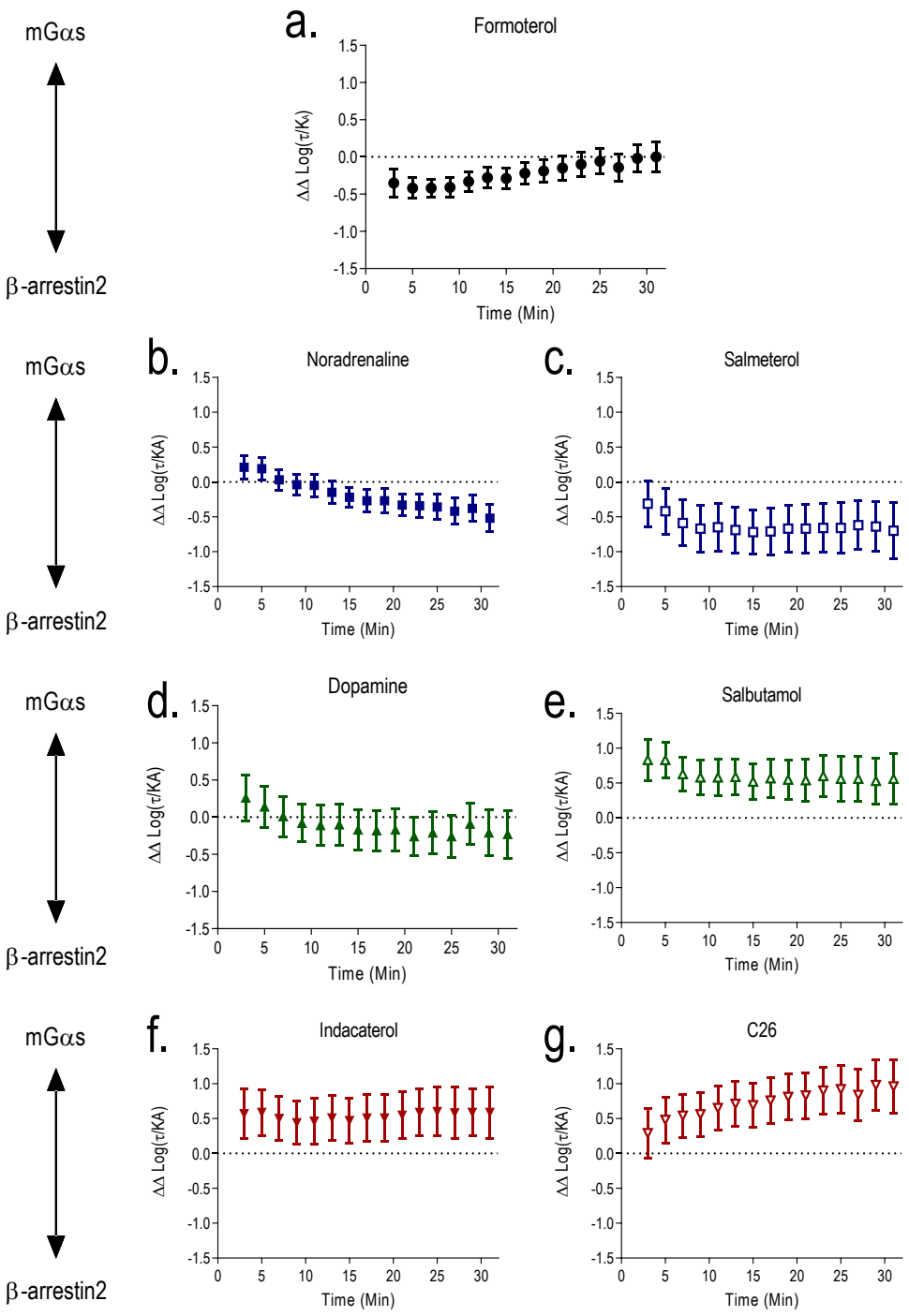

Figure 3. 18 Real-time measure of pathway bias over time, using a modified operational model of bias. *Pooled timecourse bias data (mean ± s.e.m.), represent 5 independent experiments, conducted in duplicate. Normalised ligand pharmacology for each of individual experiments (n=5) for each pathway was performed in duplicate was used to calculate transduction co-efficients (Equation 5; LogR), which were normalised to a reference ligand (isoprenaline) (ΔLogR), to remove system bias (Stott et al., 2016). These values are compared between pathways to quantify LogBias values (ΔΔLogR), between recruitment of either β-arresin2 or mini Gαs protein (ΔLogR mini Gαs-ΔLogRβ-arrestin2). Here, this has been conducted at 15 time points across the assay window, at 120 second intervals.*

3.3.10 Use of a kinetic Operational Model predicts agonist affinities, efficacies and desensitisation rate, from effector driven functional assays.

The use of an operational model was shown to be influenced by the timepoint at which measures of receptor signalling were obtained (*Figure 3. 18*). Its application was also limited in estimating an overall Log(Tau/K_A) parameter for each agonist (including full agonists), rather than deconvolution of the functional agonist affinity (K_A) estimate from agonist / system efficacy (Tau). To test alternative forms of analysis for the timecourse data, we therefore applied a kinetic operational model from Hoare *et al.*, (2018) to β-arrestin2 recruitment signalling data, at both the β_1 and β_2 adrenoceptors (*Figure 3. 10; Figure 3. 13*). Due to the lack of saturable mini Gαs recruitment observed at the both the β_1 and β_2 adrenoceptors (e.g. to isoprenaline), we were unable to fit the timecourse data for this assay to any of the kinetic operational models.

From the Hoare *et al*., (2018) paper, we chose to apply the "rise-and-fall" kinetic operational model to the β-arrestin2 recruitment responses from the β_1 and β_2 adrenoceptors. The model is defined by *Equation 2. 10 - 13* (*Methods; 2.7.4.3*). Here, the transduction potential, Ep, which is the maximal possible response available, acts as the pre-cursor to the response 'E', with the conversion facilitated by activated agonist-receptor complexes. The rate of this conversion is governed by the response generation rate constant k_E. Importantly, this model also incorporated response decay, which itself is governed by the response decay rate constant k_D. The equation is fit globally to each individual agonist concentration response experiment, from luminescence responses at 16 timepoints between 0 and 31 minutes.

The model was fitted to each experimental repeat of β-arrestin2 recruitment at the β_1 and β_2 adrenoceptors (*Figure 3. 19*; *Figure 3.* **14***20*), with kinetically derived pharmacology pooled for (1) agonist equilibrium dissociation constants (K_A), (2) kinetic efficacy parameters (kTau) and (3) the signal decay rate (k_D).

The agonist dissociation equilibrium constants for both βAR subtypes obtained from the "rise-and-fall" kinetic operational model correlated strongly with agonist binding affinity values obtained from published radioligand binding assays (Baker, 2010; Beattie *et al.*, 2012; Rosethorne *et al.*, 2016) ($P<0.0001$; *Figure 3. 22. a & b*), with the absolute measures of agonist affinity agreeing more at the

β_2AR than at the β_1AR. To confirm using an experimental measure of binding affinity at the β_2AR in a similar system, TR-FRET binding assays were conducted using membranes prepared from HEK293T cells expressing terbium labelled SNAP-β_2AR-LgBiT receptors (*Figure 3. 21*). The binding affinity of a fluorescently labelled β_2AR tracer, BODIPY-FL-PEG8-(S)-propranolol, was determined as 2.53 ± 0.29 nM by an equilibrium saturation binding assay (*Figure 3. 21. a*). Increasing concentrations of unlabelled βAR agonists were used to compete against a fixed concentration of BODIPY-FL-PEG8-(S)-propranolol (5nM), from which competition binding curves were generated (*Figure 3. 21. b*). Agonist dissociation equilibrium constants in the form of Ki values, were obtained by correction from the binding IC_{50} values (*Table 3. 7*). When comparing the agonist dissociation equilibrium constants from the kinetic operational model to the Ki values obtained the TR-FRET assays, a very strong correlation was observed (Slope=0.9100; P<0.0001; r^2= 0.8866; *Figure 3. 22. c*). Moreover, there was strong agreement between the actual measurements of agonist binding affinities, with the slope of the trend line being close to the line of unity (*Figure 3. 22. c*).

The kinetic measures of efficacy (kTau) and decay rate (k_D) of each agonist (*Table 3. 6*) were correlated at the β_2AR (*Figure 3. 23. a*) and β_1AR (*Figure 3. 24. a*). At the β_2AR, there was a strong positive correlation between kTau and k_D (r^2=0.7462), with individual ligands strongly adhering to the trend line (Slope=117.8; r^2 = 0.7462; P<0.0001). Generally, agonists with increased kTau demonstrated a greater k_D, specifically C26, noradrenaline and indacaterol. However, salbutamol was an outlier in this relationship, adhering to the trend the least, and demonstrated a low kTau value (30.91±0.94 min^{-1}) compared to isoprenaline and formoterol (78.37±3.75 & 55.70±8.42 min^{-1}, respectively), and yet a greater k_D (salbutamol: 0.75±0.02 min^{-1}; isoprenaline: 0.64±0.02 min^{-1}: formoterol: 0.51±0.05 min^{-1}). In contrast at the β_1AR, there was no discernible correlation between agonist kTau and kD values (r^2<0.0001). The rank order of agonist kTau values were: noradrenaline>isoprenaline>formoterol>dopamine> salbutamol.

In concentration response data from β-arrestin2 recruitment at 3 and 31 minutes, the Black and Leff's operational model can be globally fitted to a set of agonists containing partial agonist data to obtain individual Tau and K_A values for each agonist, at the β_1AR and β_2AR. As isoprenaline was used as the reference agonist, from which the Emax (the maximal effect of the system) was defined, it does not appear in the correlations.

At the β_2AR, a stronger positive correlation was observed between LogTau and kTau at 3 (Slope=0.09; P<0.0001; r^2=0.5311; *Figure 3. 23. b*) relative to 31 (Slope = 0.03; P<0.0001; r^2=0.1454; *Figure 3. 23. c*) minutes. Moreover, the relationship between LogTau and kD at 3 minutes was positively correlated at 3 minutes (Slope = 9.90; P<0.0001; r^2=0.4310; *Figure 3. 23. d*), but not at 31 minutes (Slope=3.48; P=0.081; r^2=0.0896; *Figure 3. 23. e*).

At the β_1AR, strong correlations were observed between LogTau and kTau, at both 3 (Slope= 0.07; P=0.002; r^2=0.7585; *Figure 3. 24. b*) and 31 (Slope=0.01; P<0.0001; r^2=0.9024; *Figure 3. 24. c*) minutes. However, when comparing LogTau and kD, poorer fits were observed with the linear regression with either a weak or no correlation observed at 3 (Slope= 38.84; P=0.004; r^2=0.5727; *Figure 3. 24. d*) and 31 (Slope= 2.37; P=0.1128; r^2=0.2125; *Figure 3. 24. e*) minutes, respectively.

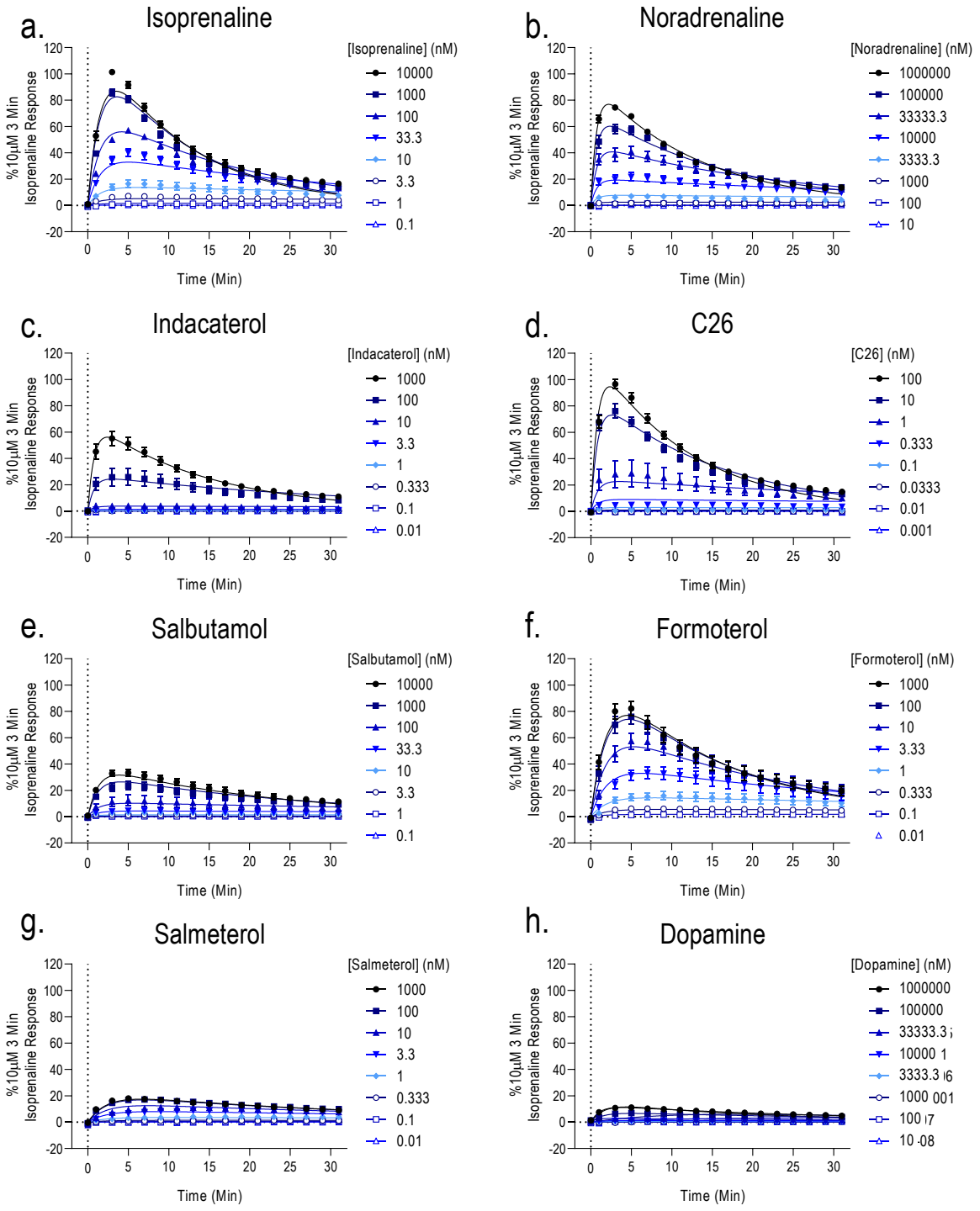

Figure 3. 19 Curve fitting of "Rise-and-fall" kinetic operational model to NanoBiT monitored recruitment of β-arrestin2 at β_2ARs. *Timecourse data, see Figure 3.10, from NanoBiT monitoring β-arrestin2 recruitment at β_2ARs. "Rise-and-fall" kinetic operational model fit to pooled data, with pharmacology in Table 3. 6 showing mean from 5 individual fittings of the kinetic operational model to experimental replicates. Data points represents pooled timecourse data, as mean ± s.e.m., from 5 independent experiments, conducted in duplicate. Relative maximal responses quantified as % 10μM isoprenaline response at 3 min.*

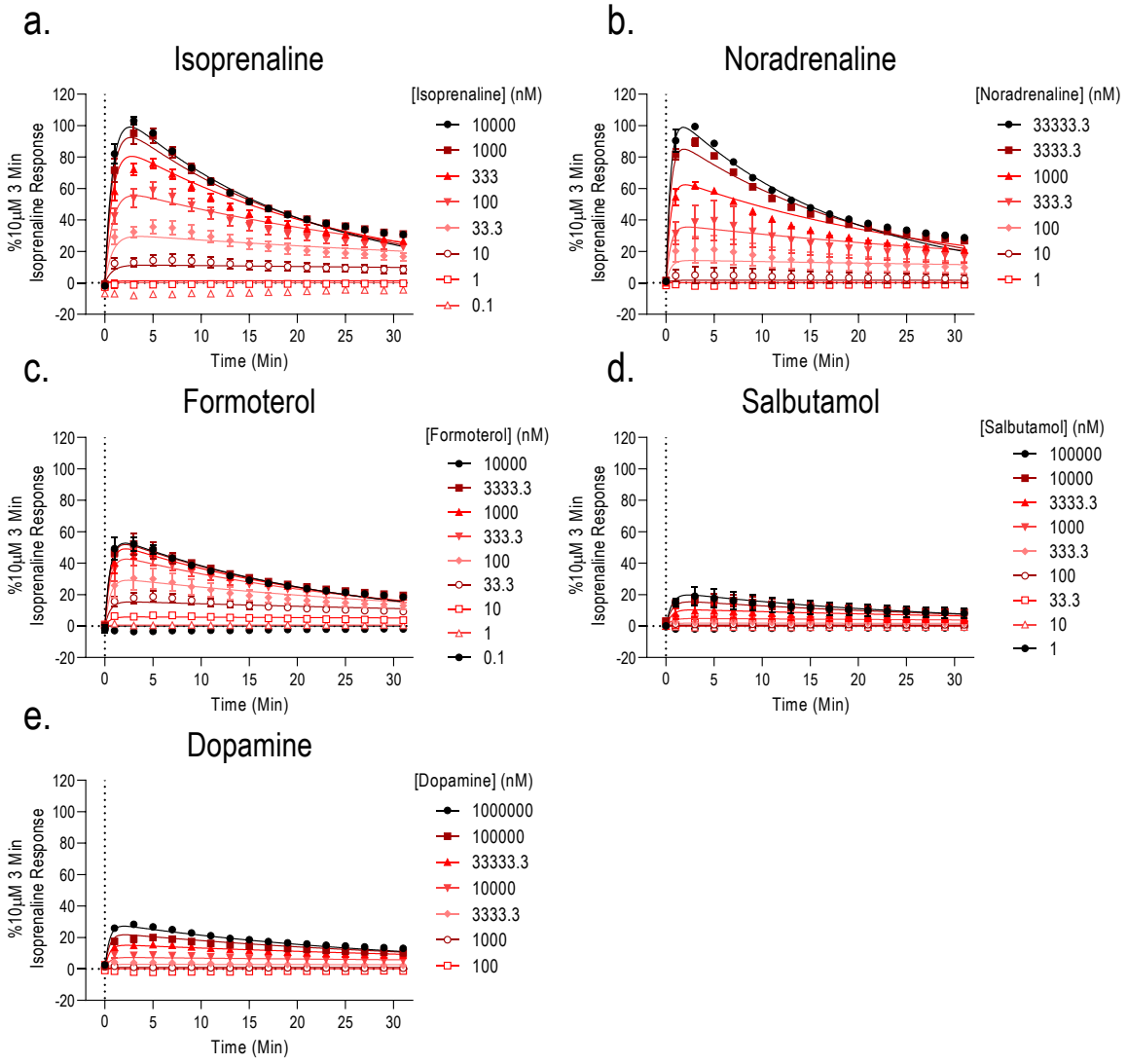

Figure 3. 20 Curve fitting of "Rise-and-fall" kinetic operational model to NanoBiT monitored recruitment of β-arrestin2 at β_1ARs. *Timecourse data, see Figure 3. 13, from NanoBiT monitoring β-arrestin2 recruitment at β_2ARs. "Rise-and-fall" kinetic operational model fit to pooled data, with pharmacology in Table 3. 6 showing mean from 3/4 individual fittings of the kinetic operational model to experimental replicates. Data points represents pooled timecourse data, as mean ± s.e.m., from 3/4 independent experiments, conducted in duplicate. Relative maximal responses quantified as % 10μM isoprenaline response at 3 min.*

	Agonist Equilibrium Dissociation Constant: LogK_A (M)		Kinetic Efficacy: kTau (Luminescence Min^{-1})		Signal Decay Rate: k_D (Min^{-1})	
	β_1AR (n=3/4)	β_2AR (n=5)	β_1AR (n=3/4)	β_2AR (n=5)	β_1AR (n=3/4)	β_2AR (n=5)
Isoprenaline	-7.04 ± 0.11	-7.14 ± 0.09	149.65 ± 16.35	78.37 ± 3.75	1.29 ± 0.16	0.64 ± 0.02
Salbutamol	-5.45 ± 0.19	-6.46 ± 0.21	42.54 ± 2.68	30.91 ± 0.94	2.04 ± 0.35	0.75 ± 0.02
Formoterol	-6.92 ± 0.08	-8.22 ± 0.10	130.42 ± 31.87	55.70 ± 8.42	1.90 ± 0.31	0.51 ± 0.05
Dopamine	-4.47 ± 0.17	-3.54 ± 0.30	60.86 ± 2.35	18.39 ± 4.51	2.06 ± 0.07	0.29 ± 0.15
Noradrenaline	-6.23 ± 0.19	-4.42 ± 0.07	251.83 ± 54.50	132.86 ± 10.80	2.24 ± 0.39	1.39 ± 0.07
Salmeterol		-8.38 ± 0.13		9.67 ± 1.58		0.44 ± 0.04
Indacaterol		-6.58 ± 0.19		108.49 ± 9.06		1.21 ± 0.07
C26		-8.40 ± 0.14		151.96 ± 11.18		1.24 ± 0.08

Table 3. 6 Kinetically modelled agonist pharmacology, from a NanoBiT complementation assay monitoring β-arrestin2 recruitment at βAR subtypes. *A "rise-and-fall" kinetic operational model was fit to individual experiments monitoring β-arrestin2 recruitment at β_1AR and β_2AR. From each replicate agonist equilibrium dissociation constants (K_A), kinetic descriptor of efficacy (kTau) and signal decay rate (k_D). Quoted pharmacology represents mean ± s.e.m., from 3-5 individual replicates.*

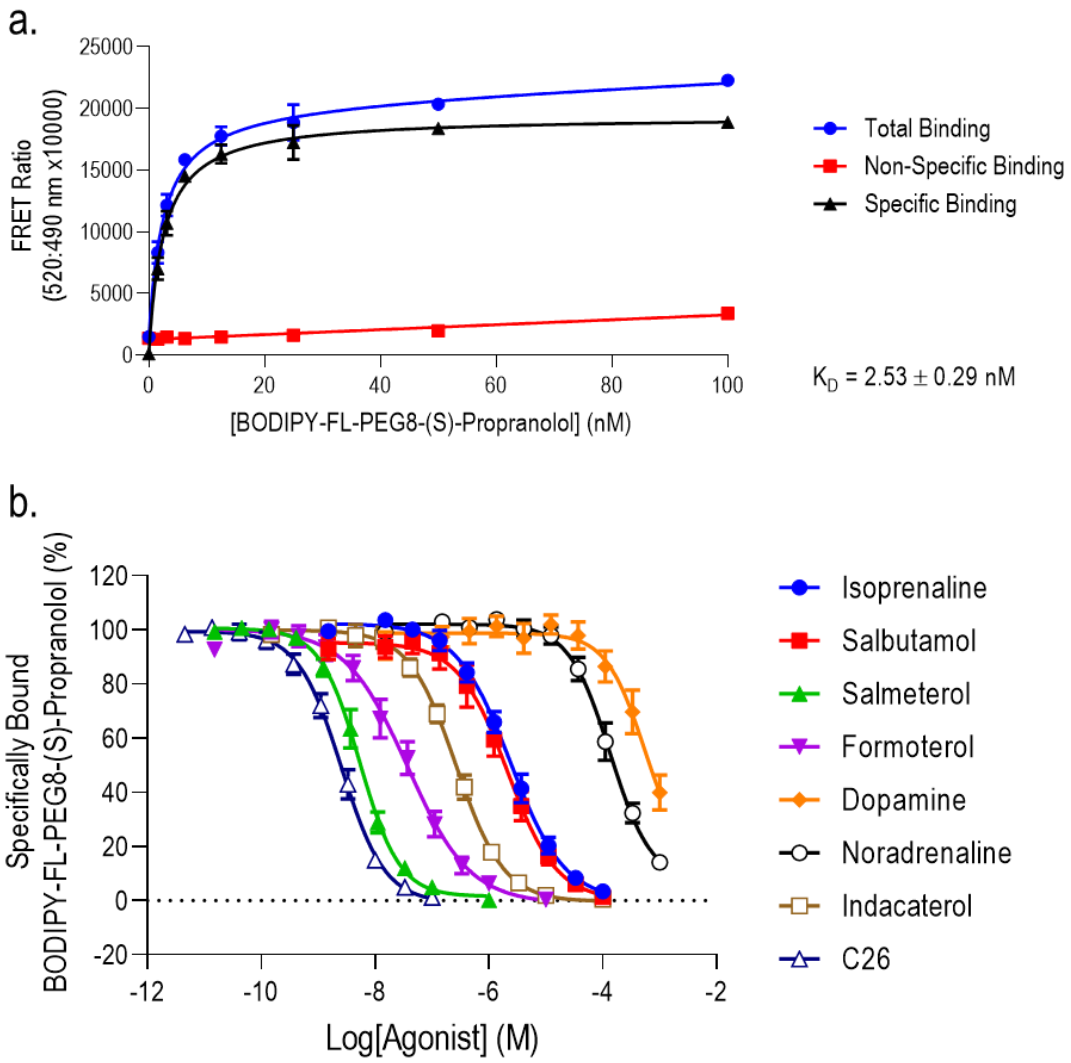

Figure 3. 21 Use of TR-FRET binding assay to establish agonist equilibrium binding constants of fluorescent or unlabelled ligands, at β_2AR-LgBiT constructs. *(a) Determination of BODIPY-FL-PEG8-propranolol affinity at β_2AR-LgBiT, using a TR-FRET saturation binding experiment. (b.) Competition binding between BODIPY-FL-PEG8-propranolol and β_2AR ligands for β_2AR –LgBiT construct expressed in HEK293T membranes, in the presence of 100 µM GppNHp. Competition for 5 nM BODIPY-FL-PEG8-propranolol by increasing concentrations of unlabelled β_2AR agonists. End point data taken after 18 minute incubation at 37°C. Non-specific binding was quantified using 10µM ICI-118,551. Data points represent mean ± S.E.M., performed in duplicate (n=5).*

	pIC_{50} (M)	Corrected to pK_i (M)
Isoprenaline	5.58 ± 0.09	5.96 ± 0.08
Salbutamol	5.70 ± 0.11	6.05 ± 0.11
Salmeterol	8.23 ± 0.08	8.61 ± 0.09
Formoterol	7.47 ± 0.14	7.83 ± 0.14
Dopamine	3.13 ± 0.13	3.58 ± 0.03
Noradrenaline	3.88 ± 0.09	4.14 ± 0.11
Indacaterol	6.57 ± 0.06	6.93 ± 0.06
C26	8.59 ± 0.07	8.94 ± 0.07

Table 3. 7 Summary of agonist equilibrium dissociation constants of BODIPY-FL-PEG8(S)-propranolol and unlabelled β_2AR agonists, using TR-FRET binding assays. *pIC50 values were obtained from competition TR-FRET assays (Figure 3. 21). In conjunction with the affinity of BODIPY-FL-PEG8(S)-propranolol at β_2AR-LgBiT receptors (2.53 nM) and its concentration (5 nM), Ki values we obtained for each agonist by the Cheng-Prusoff correction. Data represent mean ± s.e.m. for pIC50 obtained and converted Ki values in 5 individual experiments, conducted in duplicate.*

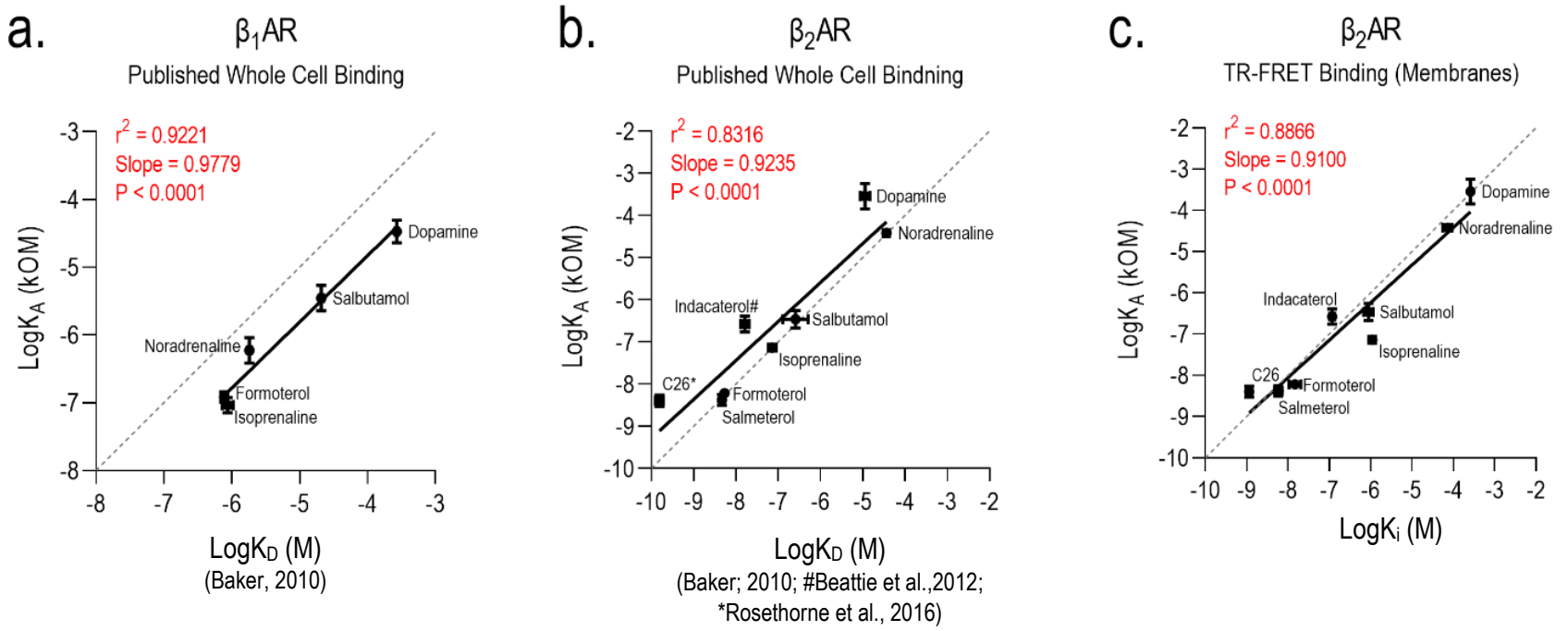

Figure 3. 22 Correlating agonist equilibrium dissociation constants obtained from a kinetic operational model and experimental binding assays, at βARs. *Correlations between kinetically derived LogK_A and agonist affinity values (Table 3. 6) obtained from published radioligand binding data (a.) Baker (2010), (b.) (Baker; 2010; #Beattie et al.,2012; *Rosethorne et al., 2016) and (c.) TR-FRET binding assays (Table 3. 7), for the (a.) β_1AR and (b.-c.) β_2AR. Data represent mean ± s.e.m., from data point from n = 3-5. Goodness of fit reported by r^2, with slope reported and significantly sloped data reported by P value.*

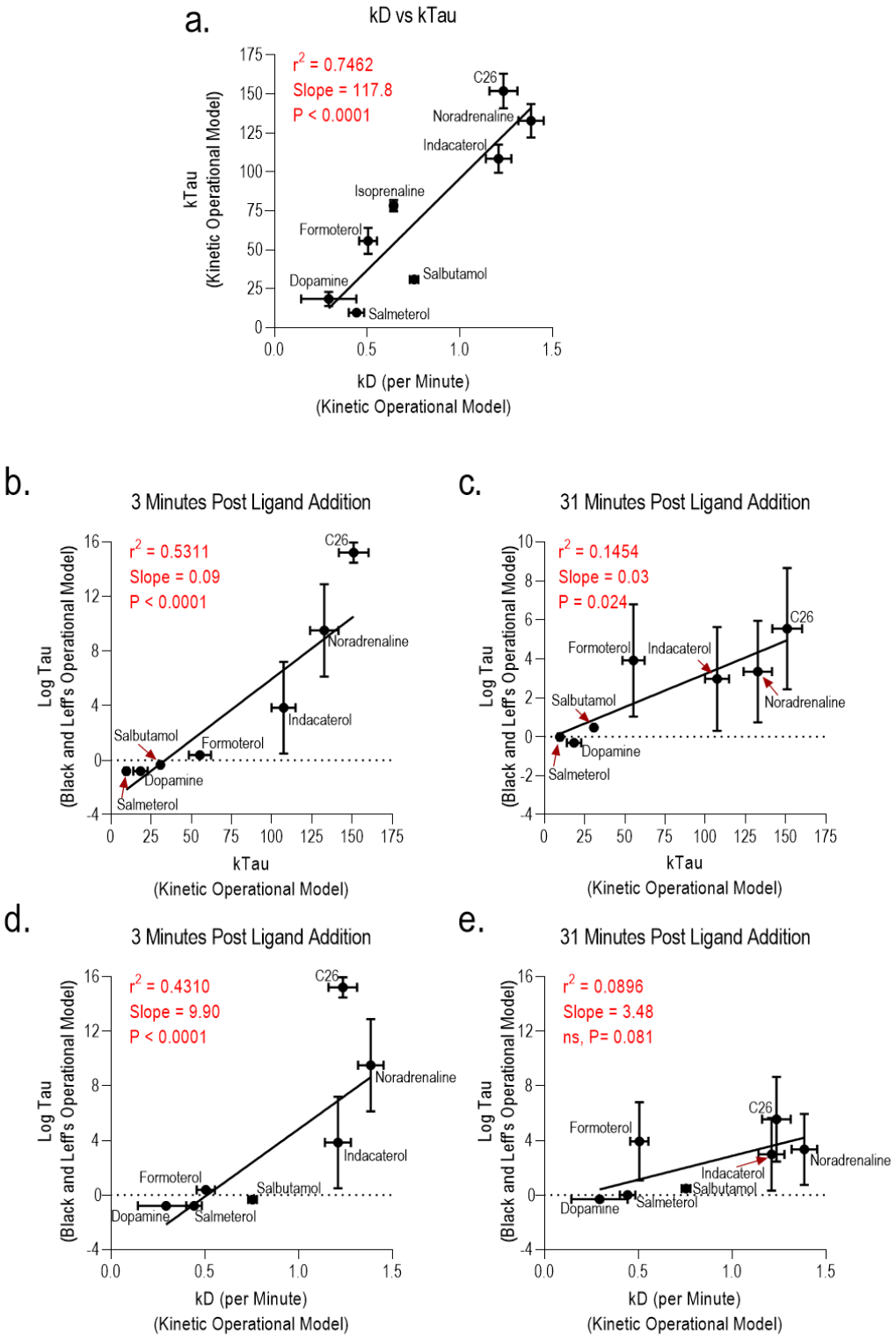

Figure 3. 23 Correlations of efficacy and signal decay rate, as described by a kinetic operational model and Black and Leff's Operational Model of partial agonism, at β_2ARs. *(a) Correlations between kinetically derived agonist efficacy (kTau) and signal decay rate (k_D) as quoted in Table 3. 6, obtained from "rise-and-fall" kinetic operational model. Correlations between LogTau values of agonist efficacy at (b. & d.) 3 and (c. & e.) 31 minutes, and (b.-c.) kTau and (d.-e.) kD. Data represent mean ± s.e.m., from data point from n = 3-5. Goodness of fit reported by r^2, with slope reported and significantly sloped data reported by P value.*

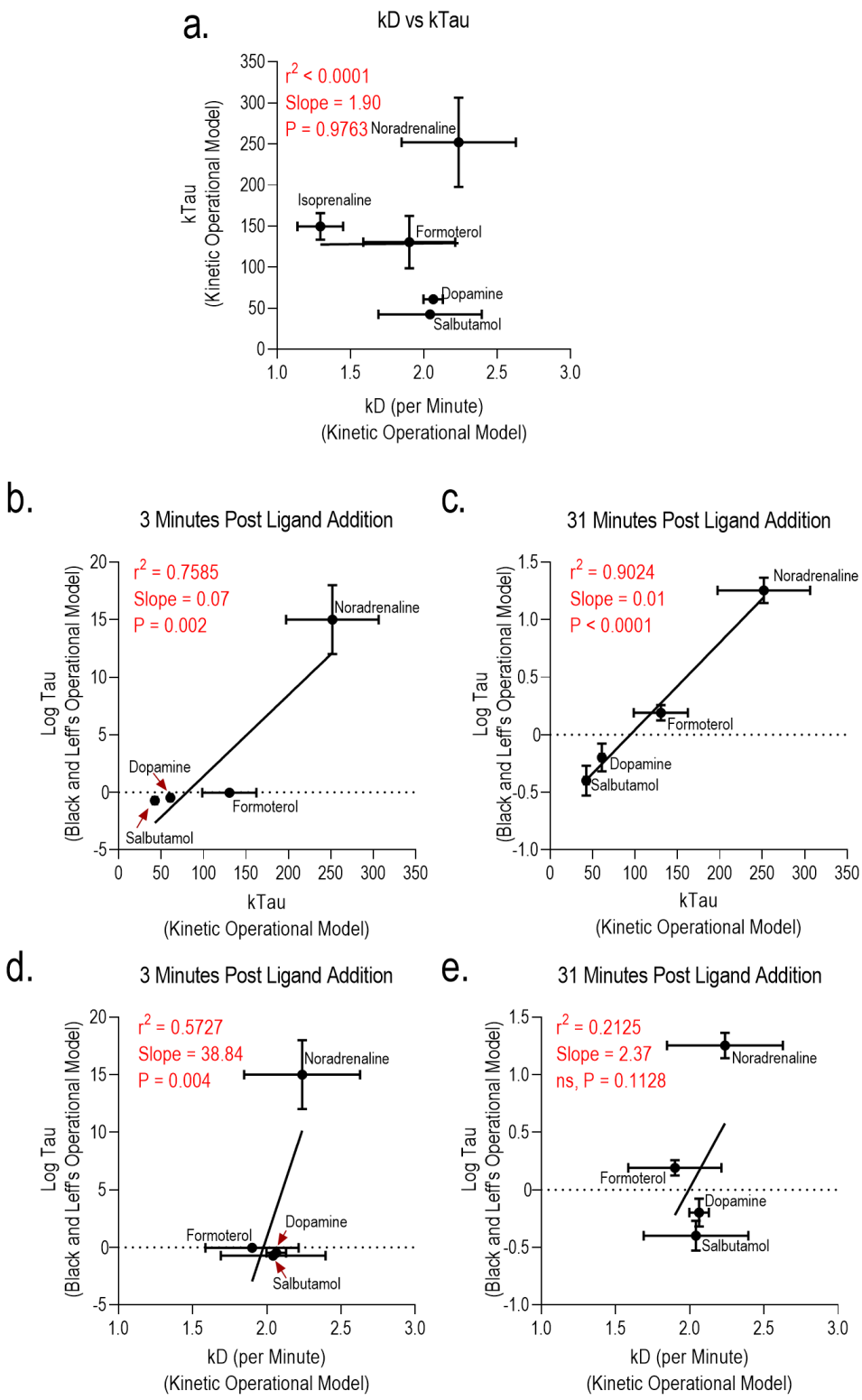

Figure 3. 24 Correlations of efficacy and signal decay rate, as described by a kinetic operational model and Black and Leff's Operational Model of partial agonism, at β_1ARs. *(a) Correlations between kinetically derived agonist efficacy (kTau) and signal decay rate (k_D) as quoted in Table 3. 6, obtained from "rise-and-fall" kinetic operational model. Correlations between LogTau values of agonist efficacy at (b. & d.) 3 and (c. & e.) 31 minutes, and (b.-c.) kTau and (d.-e.) kD. Data represent mean ± s.e.m., from data point from n = 3-5. Goodness of fit reported by r^2, with slope reported and significantly sloped data reported by P value.*

3.4 Discussion

In this chapter, NanoBiT complementation assays were established and used to monitor the real-time recruitment of two effector proteins (β-arrestin2 and mini $G\alpha_s$ protein; the latter synthetically derived from the GTPase domain of the $G\alpha_s$ subunit) primarily at the human β_2AR. A panel of 8 ligands were applied to each assay to produce recruitment profiles in a timecourse manner, producing responses from full, partial and inverse agonists. A smaller panel was applied to β_1AR based NanoBiT complementation assay, again monitoring the recruitment of β-arrestin2 and the mini $G\alpha_s$ protein to the receptor in real-time. Operational models were then employed to estimate fundamental GPCR pharmacological parameters, such as affinity and efficacy constants. This was conducted either at single timepoints, using Black and Leff's operational model of partial agonism, or from multiple timepoints of a signalling response, using a kinetic operational model. Furthermore, the predicted measures of agonist affinity, in the form of the agonist equilibrium dissociation constant, was shown to strongly correlate with estimated agonist equilibrium dissociation constants obtained in published radioligand binding assays and TR-FRET ligand binding assays. The experimental data presented demonstrate the utility of NanoBiT complementation assays, allowing for the characterisation of agonists pharmacology of specific receptor-effector interactions. Moreover, kinetic analysis of NanoBiT timecourse assays from a single agonist, with no reference agonist, allowed for generation of estimate agonist affinity and efficacy.

3.4.1 NanoBiT complementation assay reported accurate agonist pharmacology at the βAR subtypes.

NanoBiT cell lines were used to investigate recruitment of β-arrestin2 proteins and min Gαs protein at βAR subtypes, with initial studies identified increased recruitment of β-arrestin2 over β-arrestin1 at β_2ARs, agreeing with published literature (Kohout *et al*, 2001; Violin, *et al,* 2006). Moreover, despite similar basal luminescence in β_1AR/SmBiT-β-arrestin2 and β_2AR/SmBiT-β-arrestin2 a saturating concentration of isoprenaline produced a greater increase in luminescence in β_2AR cells, which was consistent with literature (Suzuki *et al.*, 1992; Green and Liggett, 1994; Shiina *et al.*, 2000; Liang *et al.*, 2003) and suggested β-arrestin2 recruitment is greater at β_2AR than β_1AR subtypes. The use of the NanoBiT assays provides timecourse data for recruitment of effector at multiple receptors, yet it is difficult to confidently compare pharmacology between

cell lines as it is difficult to control for absolute levels of effector proteins (i.e. β-arrestin1, β-arrestin2, mini Gαs protein).

Low affinity NanoBiT fragments (LgBiT-SmBiT) were used to report recruitment of β-arrestin2 and an engineered mini Gαs protein, in response to an agonist panel of a range of well-established potencies and efficacies (Hanania *et al*., 2002; Carter and Hill, 2005; Scola *et al*., 2009; Brunskole Hummel *et al*., 2013; Warne and Tate, 2013; Chan, *et al,* 2016). Recruitment of β-arrestin2 to the β_2AR presented as a transient 'rise and fall' recruitment profile, as previously described for the β_2AR (Oakley *et al*., 2000; Dixon, *et al*., 2016; Cahill *et al*., 2017). NanoBiT monitoring of β_2AR recruitment of β-arrestin2 separated ligand responses between full (isoprenaline, noradrenaline, formoterol and C26) and partial agonists (salbutamol, salmeterol, dopamine and indacaterol), with a range of potencies, which reflected data obtained through assays including bimolecular fluorescence complementation (BiFC) (Rose, Briddon and Holliday, 2010), bioluminescence resonance energy transfer (BRET) (Charest, *et al*, 2005) and high content imaging analysis of receptor internalisation (Valentin-Hansen et al., 2012). Between 3 and 31 minutes, an increase in agonist potency was observed across the agonist panel. Moreover, it is suggested that agonist pharmacology at early timepoints may be influenced by the kinetic differences between agonists, such as delayed onset of system equilibrium arising from "slow" agonists (i.e. agonists with slow dissociation rates). Delayed equilibrium may also arise from subsequent signalling kinetics of the receptor, with the kinetic profile influenced by: rates of receptor internalisation and recycling; the rate and extent of receptor phosphorylation and dephosphorylation; and the persistence of NanoBiT complexes upon receptor internalisation.

In contrast to previous complementation methods, such as BiFC (Rose, et al, 2010), the detection of inverse agonism, in conjunction with the transient timecourse data of β_2AR/SmBiT-β-arrestin2 cells and further antagonist studies in *Chapter 4*, supports the reversibility of NanoBiT fragments, correlating with the initial development of the NanoBiT methodology by Dixon, *et al*., (2016).

Treatment of 10 μM isoprenaline produced a sustained recruitment of mini $G\alpha_s$ to β_2ARs, suggesting persistent stable agonist-receptor-effector complexes. Correlating with previously reported in cAMP accumulation and reporter gene studies as an indicator of G protein signalling (January *et al*., 1997; Baker, *et al*, 2002; Hanania *et al*., 2002; Baker, *et al*, 2003; Rosethorne *et al*., 2016), full agonism of mini Gαs recruitment was observed for isoprenaline, noradrenaline,

formoterol, C26 and salbutamol with partial agonism observed for salmeterol and dopamine. The orders of potency was similar to previously reported comparisons, with greatest potency observed for C26 (Rosethorne *et al*, 2016) and least potent compounds being the endogenous catecholamines noradrenaline and dopamine. Wan *et al.*, (2018) also note the sustained interaction at the β_2AR with the mini $G\alpha_s$, using BRET studies and by application of NanoBiT in the reverse conformation of fragments as shown in the data here (i.e. β_2AR with C-terminal fused SmBiT and mini $G\alpha_s$ fused to LgBiT) (Wan *et al*, 2018). In the development of the mini Gαs protein for structural studies, several mutations were made for increased thermostability and to avoid stoichiometric clashes, including the I372A mutation in the α5 helix (Carpenter et al., 2016). It has been suggested that the mutation of this residue interrupts communication between the nucleotide binding pocket and the GPCR interface, slowing the dissociation of the mini G protein from the activated receptor. This would agree with data presented here and in literature (Wan *et al.*, 2018).

The inability of the mini Gαs protein to dissociate from the receptor may also be a possible explanation (other than ligand pathway bias) for the lack of inverse agonist activity detected in this assay (for example, to ICI118551). Overall, the mini Gas protein NanoBiT assay appears to provide reliable estimates of agonist potency and efficacy at the β_2AR, and may reflect the ability of these agonists to promote agonist confirmation which engage with a G protein interface. The assay window for receptor-mini Gαs protein association may also be enhanced because of its recruitment from the cytoplasm to the plasma membrane. However, key thermostabilising mutations were shown to alter the protein function, including the insensitivity of the mini Gαs protein to guanine nucleotides (Carpenter et al., 2016), as well as the lack of membrane anchor and the mini Gαs protein does not require Gβγ binding for stabilisation of the active receptor conformation (Nehmé *et al.*, 2017). Moreover, it is unlikely that assays using engineered mini G protein structures will represent the dynamic protein interactions present between endogenous GPCRs and G proteins. To provide a more physiologically relevant application on the NanoBiT methodology to monitor G protein activation, split fragments could be applied to monitor Gα - Gβγ subunit dissociation, as seen in BRET studies described in *Figure 3. 2. d*.

NanoBiT complementation assays report real-time recruitment of β-arrestin2 and mini Gα protein, at both the β_1AR and β_2AR. Transient β-arrestin2 recruitment was reported at both receptor subtypes, with responses distinguishing between

full and partial agonists, as reported in previous literature (Baker, 2010). As seen in β_2AR NanoBiT assays, we noted that over the period of the assay mini Gαs protein recruitment responses did not saturate, suggesting an ongoing recruitment of the effector. This might occur as the result of rearrangement of existing complexes, with the recruitment of mini Gαs protein to newly stimulated βARs being delivered to the plasma membrane, or recruitment of mini Gαs protein to endosomal pools of mini Gαs protein that are only slowly accessible to ligand. However it is not clear why this behaviour was evident for some agonists, such as isoprenaline, and not to others of equivalent efficacy

3.4.2 The application of the Black and Leff operational model to explore β_2AR ligand bias, between mini Gαs and β-arrestin2 recruitment assays over different timepoints.

The NanoBiT assays allowed for real-time reporting of effector recruitment and thus allowed for direct comparisons between pathways, following ligand-stimulation, and application of Black and Leff's operational model of agonism (Black and Leff, 1983; Kenakin *et al.*, 2012; Van Der Westhuizen *et al.*, 2014) to investigate bias in effector recruitment at different timepoints. Black and Leff's operational model (1983) and subsequent adaptations act as the standard methods of analysis of agonist efficacy, moving beyond parameters such as previously proposed pharmacological descriptors: EC_{50} and R_{max} (Clark, 1933). To remove system-dependent efficacy a reference ligand is used and thus measures of efficacy taken from the model are relative to the reference ligand. Due to the many parameters fit in the operational model, a single agonist concentration response curve cannot be used to provide unambiguous estimations of Tau and K_A. To overcome this issue, here the operational model is globally fit to multiple agonist concentration response data including partial agonists. As partial agonists do not have receptor reserve in the assay, their maximal responses define Tau unambiguously and thus Tau and K_A can be individually fit for partial agonists only. When the Rmax of an agonist approaches the Rmax of the reference full agonist, Tau and K_A become ambiguous. A further approach, not applied here, is to globally fit the operational model to the same agonist concentration response data in the presence of an irreversible antagonist which decreases the number of receptors. This decrease in the total number of receptors, alters Tau whilst other parameters, such as K_A, remain shared. A final approach simplifies the operational model as to define LogTau/K_A as LogR, rather than fit the parameters individually. Such

adapted forms of the operational model were applied in data in published literature (Kenakin *et al.*, 2012; Van Der Westhuizen *et al.*, 2014) and in data presented here (3.3.9. Kinetic analysis of ligand bias, using an adapted form of Black and Leff's operational model of agonist). Whilst measures of affinity cannot be measured directly, the transduction coefficient (Tau/K_A or R) can be used to calculate bias.

Whilst the data presented here showed limited bias for either pathway across the agonist panel, a modest drift in bias was observed over time for agonists such as noradrenaline. This corroborates findings made by Klein Herenbrink et al., (2016) and commentary from Lane *et al*, (2017) that there are confounding factors, such as different ligand-receptor binding and signalling kinetics, which can change measures of bias over time. In addition, the application of the model to our established NanoBiT systems also have limitations. Here both the receptor and effector proteins have been over-expressed and, although the structural engagement of the mini G protein at the receptor is likely to representative of endogenous behaviour, the association of the two proteins may observe different kinetics. Furthermore, when comparing bias between pathways, it is important to keep the cell context the same. For example, ensuring total receptor number in both β-arrestin2 and mini Gαs protein NanoBiT cell lines – which was not quantified in these studies. Due to the constitutive level of effector recruitment reported by the NanoBiT assay, models such as the Slack and Hall model of inverse agonism may be applied here. Unlike Black and Leff's operational model of bias (Black and Leff, 1983), Slack and Hall's model can be used to define the system contribution to ligand-effector coupling and thus provide the intrinsic ligand efficacy (Slack, Hall and Hall, 2012).

Overall, in principle the data shows that the kinetic data generated by a single NanoBiT assay, which could be expanded to other effectors, can be used for pharmacological analysis of bias across kinetic timepoints.

3.5 The value of a kinetic operational model to provide accurate estimations of agonist affinities and efficacies.

The use of traditional versions and adaptions of Black and Leff's operational model (Black and Leff, 1983; Black *et al*, 1985; Kenakin *et al*, 2012; Slack, *et al*, 2012; Van Der Westhuizen *et al*, 2014) are wide-spread within GPCR research and yet, as discussed above, they require multiple agonist data sets, or manipulations (e.g. receptor number) to estimate individual affinity K_A and Tau

values. More and more biosensors, such as the NanoBiT complementation assay, are now being used to provide a greater insight and monitor GPCR signalling in real-time, giving kinetic data sets (Marullo and Bouvier, 2007; Lohse, *et al,* 2012; Tewson *et al*., 2012; Dixon *et al*., 2016). Yet, the method of analysis of agonist pharmacology is generally limited to single time point measures and ignores information that can be extracted from a wider kinetic timecourse.

Here, we applied and assessed the value of a kinetic operational model, proposed by Hoare *et al*, (2018) as a method of determining agonist affinity and efficacy at from effector recruitment data at βARs. Application of "rise-and-fall" kinetic operational model using β-arrestin2 recruitment data produced highly accurate estimates of affinity for a range of βAR agonists, with the explicit measures of agonist affinity very similar compared to published (Baker, 2010; Beattie *et al*, 2012; Rosethorne *et al*., 2016) and obtained TR-FRET measures of binding. Unlike the Black and Leff operational mode, single agonist concentration response curve, collected as a timecourse measurement, can be fit to the kinetic operational model to provide fundamental estimates of agonist affinity, rather than using EC_{50} values which can differ between experimental assays. Multiple agonists, of varying efficacies are not required, nor does the model require manipulation of receptor number using irreversible antagonists.

It is important to consider that the model assumes instantaneous binding equilibrium and the accuracy of the K_A estimates obtained here suggest this is a valid assumption for the β_2AR agonists. However, this method may not be suitable for slow-equilibrating agonists and receptors where ligands slowly bind or in a multi-step process. In future studies, it would be interesting to apply the kinetic operational model to a range of "slower" receptor systems (i.e. peptide receptors) to assess the accuracy of affinity measurements.

In addition to K_A, descriptors of agonist efficacy were generated for each agonist in the form of: kTau, a kinetic descriptor of efficacy used to describe the initial generation rate of β-arrestin2 recruitment; and k_D, the decay rate of the signal. Unlike receptor desensitisation, which describe when receptors decrease their response to a stimuli, here the decay rate describes the decrease in βAR-β-arrestin2 NanoBiT complexes. In this system, βAR-β-arrestin2 recruitment is likely to peak at the plasma membrane, leading to internalisation of in βAR-β-arrestin2 NanoBiT complexes, dephosphorylation of βARs and thus endosomal dissociation of the complexes. β adrenoceptor can then be rapidly recycled to the plasma

membrane for re-stimulation and allow NanoBiT recruitment profile to relax into a steady state – as reflected by the transient luminescence recruitment profile. It is reasonable to expect his dynamic process, with a peak/steady state, would be driven by efficacy and the extent of β-arrestin2 recruitment, and thus k_D and kTau values correlated well in β_2ARs. Whilst the "rise-and-fall" kinetic operational model describes agonist properties, specifically affinity K_A values, accurately, it is important to emphasize that the data suggests that the β-arrestin2 recruitment plateaus at steady state but the model predicts full inactivation- thus some inaccuracy may arise, particularly when estimating kTau and k_D.

Compared to K_A correlations, estimations of the kinetic efficacy (kTau) were well correlated for both βAR subtypes, with β_1AR showing increased variability and weaker correlations with measures of agonist efficacy generated by Black and Leff's operational model. The decay rate (k_D) was well correlated with Black and Leff derived measure of agonist efficacy at the β_2AR at 3 minutes, but not by 31 minutes or at the β_1AR. In addition, methods adapted from Black and Leff's operational model provide convolved measures of agonist action in the form of Log(Tau/K_A), which required external estimates of agonist affinity from either published radioligand binding studies (Baker, 2010; Beattie *et al*, 2012; Rosethorne *et al*, 2016) and TR-FRET assays (*Figure 3. 21*) to de-convolve. Overall, more convincing correlations were observed at the β_2AR, compared to the β_1AR, though this is in part due to the increase number of agonists and thus more reliable fitting of a trendline.

There are a range of kinetic operational models, and yet they each share the output parameters, e.g. kTau, K_A, k_D. Thus, direct comparisons of individual parameters can be made across models fit to different signalling profiles (Hoare et al, 2018, 2020). However, to choose an appropriate model the experimenter is required to qualitatively assess the form the experimental data, which may introduce experimenter bias. Unlike correlations between measures of modelled and experimental affinity, it is difficult to assess the value of the kinetic operational model's predictions of efficacy (kTau) and decay rate (k_D), as there is little existing comparable data. Moreover, while kTau may have a basis in biology (i.e. the formation of an active receptor complex), k_D is much more difficult to define from a complex signalling process in different assays.

3.6 Chapter Conclusions

This chapter explored the use of a NanoBiT complementation assay to characterise agonist pharmacology and obtain real-time signalling profiles of effector recruitment at βARs. The distinct signalling profiles identified transient recruitment of β-arrestin2, whilst the mini Gαs protein recruitment was sustained throughout the assay. The sustained nature of the receptor-mini Gαs interaction was consistent with the GTP insensitivity of the mini Gαs protein. Real-time measurements of signalling revealed the kinetic influence of signalling on determining agonist pharmacology from concentration response data, demonstrated with increased potency of βAR agonists.

Mathematical modelling of functional data was applied to obtain estimates of agonist affinities, efficacies and bias. It was shown Black and Leff's operational model can be used to determine kinetic influence on measured agonist bias (using transduction co-efficients) between β-arrestin2 and mini Gαs protein recruitment. To incorporate receptor signalling profiles over time, a kinetic operational model was applied. This demonstrated (in contrast to the Black and Leff's operational model fitting) that for the β_1AR and β_2AR fundamental estimates of agonist affinity (K_A) could be obtained from single agonist concentration response curve data sets over time. These estimates were in very good agreement with binding and literature data, in addition to the provision of estimates of efficacy (kTau) as well as a decay parameter (k_D). Future studies should determine whether the kOM can be applied more broadly to receptor and systems with distinct signalling profiles and slower binding kinetics.

Chapter Four:

Estimation of antagonist pharmacology from cell-based NanoBiT complementation assay, monitoring recruitment of β-arrestin2 and mini Gαs protein at the β_2AR.

4.1. Introduction

4.1.1. Antagonist Action at GPCRs

Canonically, agonists activate GPCRs by promoting the recruitment and downstream signalling of intracellular effectors, such as heterotrimeric G proteins and β-arrestin proteins (*Figure 4. 1*). An antagonist may bind the receptor at the orthosteric or an allosteric site to inhibit agonist action, receptor activation and thus downstream signalling (*Figure 4. 1*). Cell-based measures of antagonist action are often obtained by either monitoring effects on agonist-stimulated second messenger accumulation, such as cAMP (Hansen *et al.*, 2016; Sparre-Ulrich *et al.*, 2016; Walker *et al.*, 2017) and inositol phosphates (Sergeev *et al.*, 2017), or by taking the peak signal from a transient response, such as intracellular Ca^{2+} ion release (Liu *et al.*, 2010; Suen *et al.*, 2014) or β-arrestin2 recruitment at β_2ARs (Vauquelin, *et al*, 2002).

Structurally, the binding of true competitive antagonists at the human β_2AR is suggested to be independent of the state of the receptor (inactive: R or active: R*) (Emtage *et al.*, 2016), though many "antagonists" in fact have inverse agonist properties arising from a higher affinity for the inactive R conformation (such as ICI-118,551, Chapter 3; (Hanania, *et al*, 2010)). In common with agonist molecules, β_2AR structures obtained in X-Ray crystallography studies described the importance of the ethanolamine core of an antagonist for affinity, present in such antagonists as propranolol, ICI-118,551 and CGP-12177, which forms hydrogen and salt-bridge bonds with $Asn^{7.39}$ and $Asp^{3.32}$ (Ballesteros-Weinstein (BW) numbering scheme), respectively (Rasmussen *et al*, 2007; Wacker *et al*, 2010; Rasmussen, *et al*, 2011; Zou, *et al*, 2012; Emtage *et al* , 2016). Whilst the ethanolamine tail of the antagonist occupies the region nearest the extracellular surface, the larger aromatic pharmacophore head group resides in the hydrophobic binding pocket of the receptor, interacting with $Phe^{5.32}$ and $Phe^{6.52}$ residues through the formation of π-π stacking bonds (Chelikani *et al.*, 2007; Cherezov *et al.*, 2007; Rasmussen *et al.*, 2007; Hanson *et al.*, 2008; Bokoch *et al.*, 2010; Wacker *et al.*, 2010; Rasmussen, *et al.*, 2011; Rasmussen, *et al.*, 2011; Zou, *et al*, 2012; Emtage *et al.*, 2016). The chemical moieties present on this head group are thought to contribute to whether the ligand is an agonist or an antagonist (Emtage *et al.*, 2016), with antagonists typically having a methyleneoxy space between the ethanolamine and aromatic groups. X-Ray crystallography studies suggest this spacer propels the aromatic head group further into the binding pocket and reduce

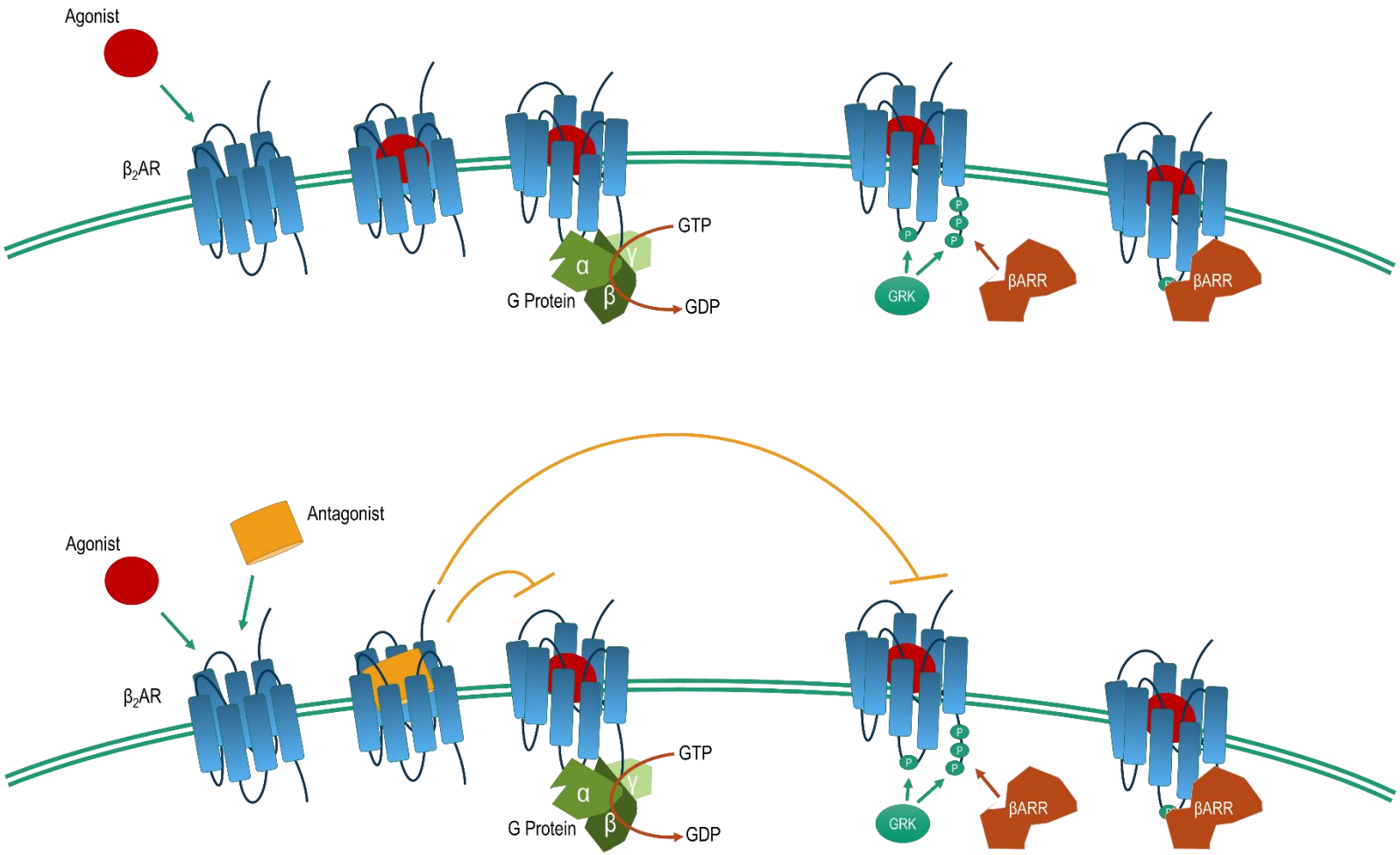

Figure 4. 1 Canonical GPCR Signal Transduction. *GPCRs exist as membrane spanning proteins with binding domains accessible to extracellular ligands. Upon agonist activation, GPCRs form active states to which recruit heterotrimeric G proteins which act as a site of guanine nucleotide exchange. Intracellular residues of the GPCR may be phosphorylated by G protein receptor kinases (GRKs), which then act as suitable substrates for beta arrestin (βARR) proteins. Antagonist ligands bind at orthosteric or allosteric binding sites to inhibit agonist signalling, including G protein activation, GRK phosphorylation activity and βARR recruitment.*

interactions with serine residues in transmembrane helix 5 ($Ser^{5.42}$ and $Ser^{5.46}$), unlike agonist interactions (discussed in *Chapter 1*), thus conferring antagonist action (Cherezov *et al.*, 2007; Rasmussen *et al.*, 2007; Hanson *et al.*, 2008; Bokoch *et al.*, 2010; Wacker *et al.*, 2010; Zou, *et al,* 2012; Emtage *et al.*, 2016).

4.1.2. Classification of Receptor Antagonism

Antagonist action can be described by whether the antagonism is surmountable, meaning that the effect of the antagonist can be overcome by increasing the agonist concentration. In a Schild based experiment (Arunlakshana and Schild, 1959), increasing concentrations of an antagonist will shift the EC_{50} and concentration response curve of an agonist to the right, reducing agonist potency, but produce the same maximal response at higher agonist concentrations (*Figure 4. 2. a*) (Vauquelin and Szczuka, 2007). If the antagonist inhibition is insurmountable, then the maximal response decreases as the antagonist concentration increases (*Figure 4. 2. b*) (Vauquelin and Szczuka, 2007). Insurmountable antagonism can be caused by non-equilibrium conditions, due to slow receptor binding kinetics of an orthosteric antagonist (Kenakin, *et al*, 2006; Vauquelin and Szczuka, 2007), or by allosteric binding, at a site distinct from the orthosteric binding pocket (Kenakin, *et al*, 2006). Determining the mechanism of antagonist action can be a valuable stage in the drug discovery pipeline as subsequent studies may differ depending on the nature of antagonism, with orthosteric and allosteric binding compounds having different binding properties (Kenakin, 2004; Kenakin, *et al*, 2006).

The insurmountable effect of competitive antagonists with slow-receptor binding rates, and thus extended receptor occupancy and antagonism, has been suggested to translate to long-lasting effects in *in vivo* and clinical studies, especially where high agonist concentrations fluctuate (Vauquelin and Van Liefde, 2006; Vauquelin and Charlton, 2010; Sykes *et al.*, 2016). For example, long lasting CB1 antagonism of the AM6538 compound in *in vivo* rodent and primate studies (Paronis *et al.*, 2018) correlated with AM6538 slow dissociation rates as determined by Laprairie *et al.*, (2019) in kinetic cAMP Schild analysis experiments. Similar correlations between slow dissociation rates of GPCR antagonists and long lasting *in vivo* effects have been observed at the CC chemokine receptor 2 (Bot *et al.*, 2017), the muscarinic M3 receptor (Noord *et al.*, 2002), the urotensin 2 receptor (Behm *et al.*, 2010) and the neurokinin 1 receptor (Lindström *et al.*, 2007).

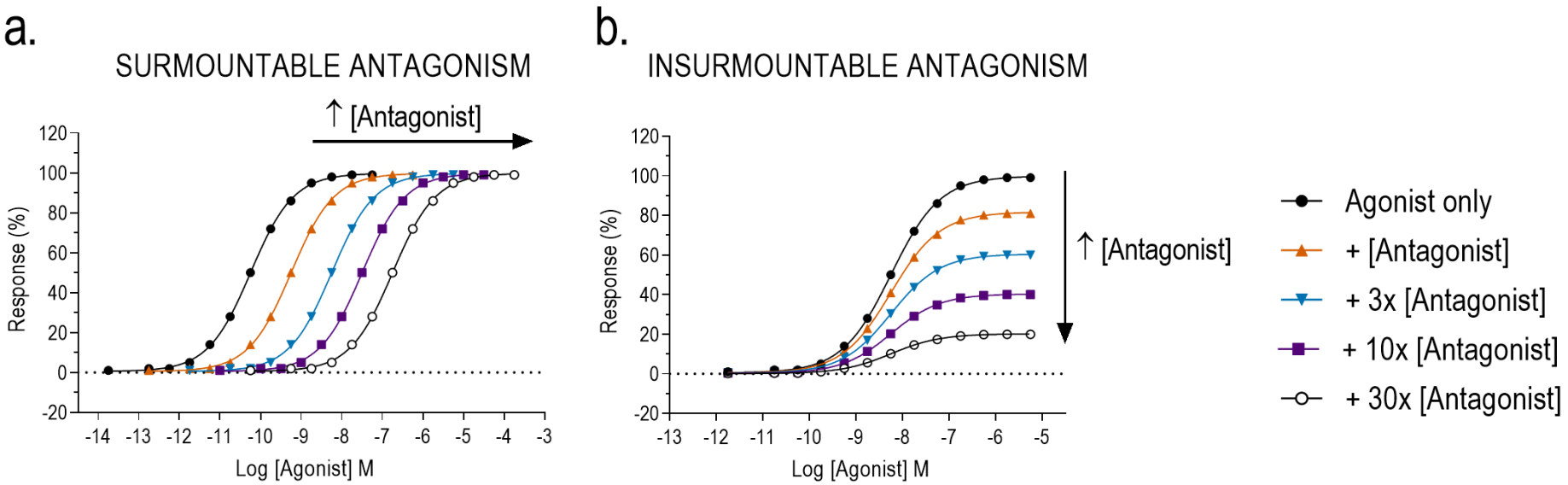

Figure 4. 2 Surmountable and insurmountable antagonist actions of concentration response curves. *Antagonist action can be described by whether the antagonism is surmountable, meaning that the effect of the antagonist can be overcome by increasing the agonist concentration. In a Schild based experiments (Arunlakshana and Schild, 1959), increasing concentrations of an antagonist will shift the EC50 and concentration response curve of an agonist to the right, reducing agonist potency, but produce the same maximal response at higher agonist concentrations (a.). An insurmountable antagonist cannot be overcome by increasing agonist concentration where there is no receptor reserve, resulting in reduced relative maximal response (b.).*

4.1.3. Pharmacological Models of GPCR Antagonism

As described above, antagonism action is often quantified by competing an antagonist with an agonist driven response to derive concentration response inhibition curves of an antagonist, using the IC_{50} as a descriptor of antagonist potency. IC_{50} values derived from single inhibition curves are affected by agonist/antagonist properties, as well as system agonist concentration. Thus, pharmacological models are often applied to provide insights into antagonist action, independent of the agonist, with one of the most common methods being Gaddum (Gaddum, 1937) and Schild analysis (Arunlakshana and Schild, 1959). Gaddum/Schild analysis is used to predict antagonist action, within a receptor system by monitoring the effect of increasing concentrations of an antagonist on an agonist concentration response curve. A concentration ratio between EC_{50} values of the agonist concentration response curve is plotted against antagonist concentration to give a Schild plot, which, if linear (with a slope of 1), indicates antagonist is both competitive and reversible, with the system at equilibrium. Provided the Schild plot is linear, the x-intercept defines the antagonist equilibrium dissociation constant (K_D or pA_2) which acts as a fundamental measure of antagonist affinity at the receptor, independent of agonist actions. Moreover, the antagonist equilibrium dissociation constants obtained should align with equivalent values obtained by other methods such as binding assays. The Gaddum/Schild approach is derived from an assumption that agonist/antagonist proportional receptor occupancy is driven by the law of mass action, with the derivation of the relationship requiring dynamic equilibrium. Other methods have been considered for interpreting antagonist effects when the system is not at equilibrium, as it is often the case for transient GPCR signalling events (such as calcium mobilisation, or transient arrestin recruitment). For example, assays that measure peak agonist response may be run under hemi-equilibrium conditions. In these circumstances antagonist pre-treatment allows receptor binding to reach equilibrium, prior to the addition of agonist. The peak response (for example a rapid calcium transient) may be measured before re-equilibration of agonist/antagonist binding – and if the antagonist has slow binding kinetics (slow k_{off}), this may lead to a suppression of the maximum response. The hemi-equilibrium model (Kenakin, *et al*, 2006; Mould *et al.*, 2014; Riddy *et al.*, 2015) has been developed to account for insurmountability driven by slow antagonist binding kinetics and thus a lack of system equilibrium under these conditions, and can be used to obtain system independent estimations of antagonist k_{OFF} as well as K_D for timecourse data. In this model, antagonists with slow binding kinetics are

described to irreversibly bind to a portion of the receptors and thus presenting a depression of the agonist maximal response (Kenakin, 2009). Mould *et al.*, (2014) applied the hemi-equilibrium model estimate antagonist dissociation constants of slowly dissociating antagonists, suvorexant and almorexant, at the orexin 2 receptor. More recently, Hoare *et al.*, (2018) describes a kinetic operational model of antagonism to extract kinetic binding parameters from timecourse signalling assays at GPCRs, incorporating agonist or antagonist pre-incubation, simultaneous addition and wash out experimental settings (Hoare *et al.*, 2018). Whilst the proposed methods require caveats, such as rapid equilibration of agonist-receptor binding and the assumption of competitive inhibition of the antagonist, this provides a further, but relatively untested method to obtain association and dissociation rates of an antagonist, and the resultant kinetic K_D, from functional signalling data. In comparison, standard antagonist IC_{50} values, quantified from an inhibition of an agonist response, may be related to the K_D of the antagonist but are not equivalent, as they may be altered by agonist concentration and properties. Moreover unlike Schild analysis, the kinetic operational model based analysis requires an antagonist concentration inhibition data for only a single concentration of agonist, though collecting a full timecourse for each response.

As established in *Chapter 3*, NanoBiT complementation assays can be used to monitor signalling at β adrenoceptors in real-time and discern between signalling profiles of a range of β adrenoceptor agonists. NanoBiT complementation methodology has previously been used to determine binding of GPCR antagonists, specifically at the chemokine receptor 4 (CXCR4) (Soave, *et al.*, 2020) and relaxin receptor 3 (Li *et al.*, 2020). From published literature, the only use of NanoBiT methodology to monitor real-time GPCR antagonism in cell-based assays is from a recently published methodology article, published by our group (Dijon, *et al*, 2021).

Here, NanoBiT complementation assays were applied to observe antagonism at the β_2AR, monitoring the recruitment of β-arrestin2 and a mini Gαs protein, using SmBiT NanoBiT cell lines established in *Chapter 3*. Moreover the timecourse assay data was then analysed by pharmacological models: firstly, Schild analysis of antagonist action from multiple timepoints to determine measures of antagonist affinity; and secondly the kinetic operational model, as proposed by Hoare *et al.*, (2018), to assess its ability to obtain estimates of antagonist association and dissociation rates from signalling data.

4.2. Chapter Aims

The work completed in Chapter Four: Results II, aimed to:

(1) Use NanoBiT complementation assays to monitor antagonism of β-arrestin2 and a mini Gαs protein at the β_2AR.

(2) Identify the kinetic influence on measurements of antagonist pharmacology, from Schild analysis, at the β_2AR.

(3) Apply the kinetic operational model to determine antagonist kinetic binding parameters, using functional data from timecourse measurements of effector recruitment at the β_2AR.

4.3. Results

4.3.1. Monitoring antagonism of β-arrestin2 recruitment, using a NanoBiT complementation assay at the β_2AR.

The agonist NanoBiT responses in live HEK293T β_2AR/SmBiT- β-arrestin2 stable cell lines were previously described in *Chapter 3.*, in the absence of an antagonist and in response to 1 μM formoterol, β-arrestin2 was rapidly recruited to β_2ARs, between 0 and 3 minutes where the luminescent signal peaked (*Figure 4. 3, see also Figure 3. 10*). Between 3 and 61 minutes, the signal decreased and formed a steady response, approaching zero. Pre-treatment with 3 antagonists for 20 minutes, either (S)-propranolol (known as propranolol; *Figure 4. 3. a*), ICI-118,551 (*Figure 4. 3. b*) or CGP-12177 (*Figure 4. 3. c*) (10 minute antagonist followed by 10 minute furimazine addition), in a range of concentrations between 0 and 30 nM were shown to reduce the transient peak and sustained formoterol response in a concentration dependent manner.

In Schild analysis experiments, the time dependent effects on the formoterol concentration response relationships were probed in the presence of increasing concentrations of propranolol (*Figure 4. 4. a, d & g*), ICI-118,551 (*Figure 4. 4. b, e & h*) and CGP-12177 (*Figure 4. 4. c, f & i*). At 3 minutes post-formoterol addition, antagonism looked insurmountable, whether in the presence of propranolol (*Figure 4. 4. a*), ICI-118,551 (*Figure 4. 4. b*) or CGP-12177 (*Figure 4. 4. c*), with ≥1.1 nM of all antagonist concentrations reducing the maximal formoterol response compared to control ($P<0.01$; one-way ANOVA, with Dunnett's multiple comparison).

At later timepoints, 31 and 61 minutes, the effect of propranolol became more surmountable, with a more parallel concentration response curve shift to the right. However, inverse agonism was also apparent in this assay, reducing the basal luminescence observed compared to the absence of antagonist (*Figure 4. 4. d & g*). A similar profile was observed in Schild analysis experiments investigating antagonist action of ICI-118,551 (*Figure 4. 4. e & h*). CGP-12177 antagonism as appeared more insurmountable at all timepoints, at 3 (*Figure 4. 4. c*), 31 (*Figure 4. 4. f*) and 61 (*Figure 4. 4. i*) minutes. At 31 minutes, insurmountable antagonism of ICI-118,551 and CGP-12177, as demonstrated by significantly depressed response of 1 μM formoterol, concentrations of ≥3.3 nM and ≥1.1 nM, respectively ($P<0.01$; one-way ANOVA, with Dunnett's multiple comparison). By 61 minutes, insurmountable antagonism of ICI-118,551 and CGP-12177, as

demonstrated by significantly depressed response of 1 μM formoterol, was still observed for concentrations of ≥10 nM ($P<0.01$; one-way ANOVA, with Dunnett's multiple comparison). In addition, in the presence of CGP-12177, inverse agonism was not observed in comparison to propranolol and ICI-118,551.

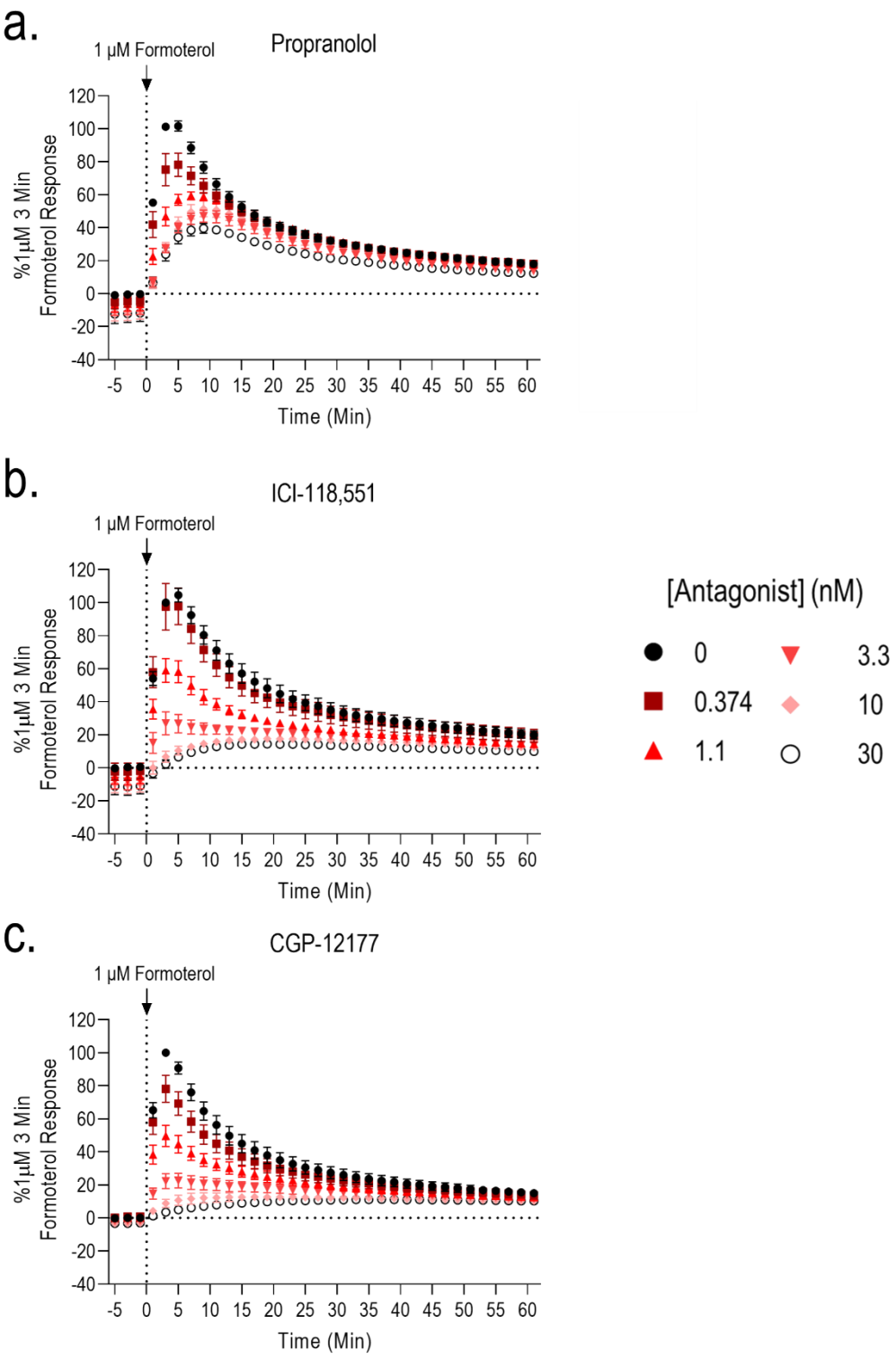

Figure 4. 3 Concentration dependent antagonism of β-arrestin2 recruitment at the β_2AR. *β_2AR/SmBiT β-arrestin2 cells were pre-incubated (20 minutes) with a range of concentrations between 0-3 0 nM of either propranolol (a.), ICI-118,551 (b.), or CGP-12177 (c.), before 1 µM formoterol addition (time 0; indicated by dotted line) initiated recruitment of β-arrestin2. Pooled timecourse data represent mean ± s.e.m., from 5 independent experiments, conducted in duplicate. Relative maximal responses quantified as % 10µM isoprenaline response at 3 min.*

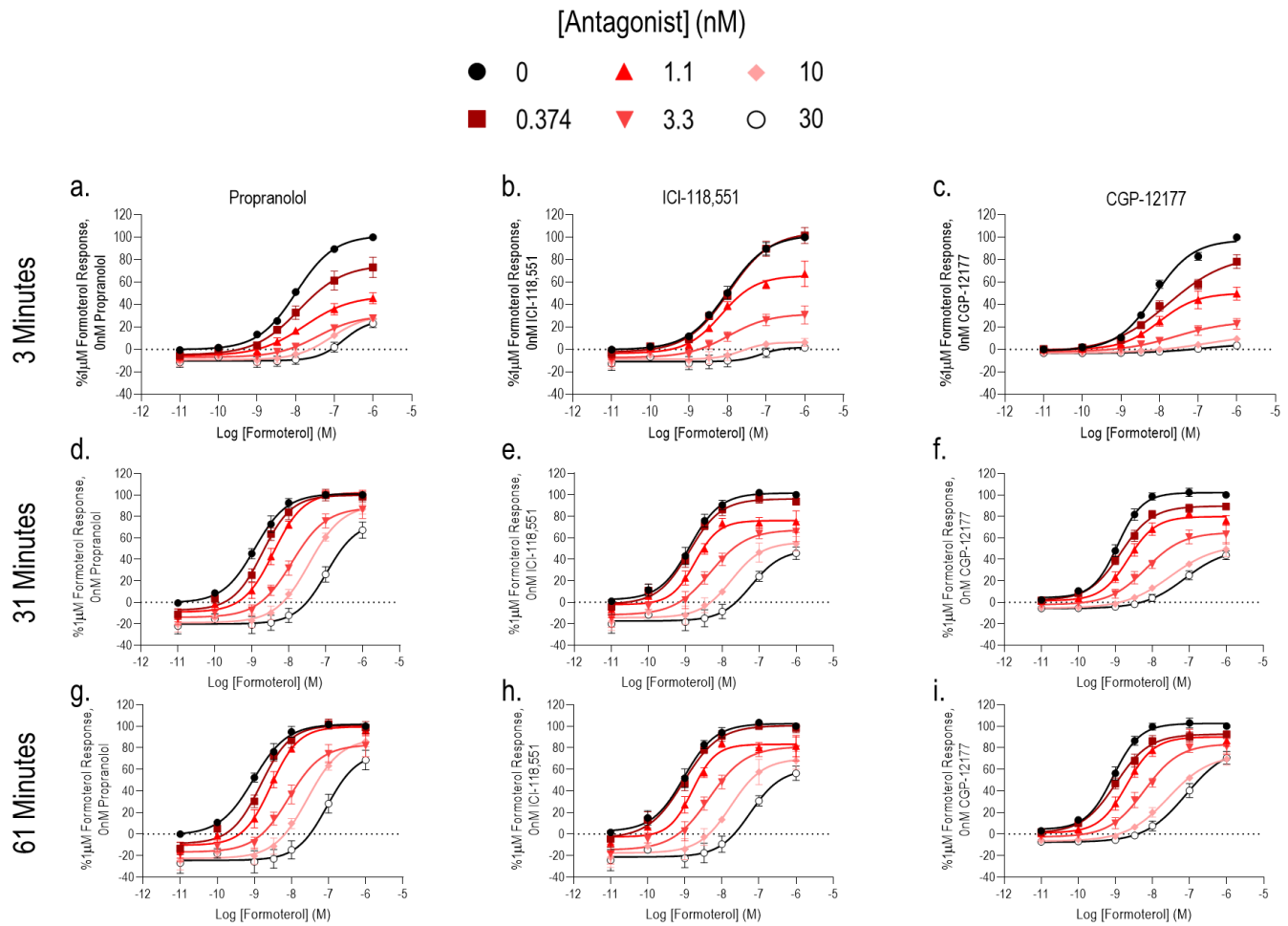

Figure 4. 4 Schild analysis of propranolol (a, d & g), ICI-118,551 (b, e & h) and CGP-12177 (c, f & i) in NanoBiT complementation assay monitoring β-arrestin2 recruitment at β_2ARs, at 3 (a – c), 31 (d – f) and 61 (g – i) minutes following formoterol addition. *HEK β2AR/SmBiT β-arrestin2 cells were pre-treated with increasing concentrations of antagonists for 20 minutes prior to formoterol addition at time 0 minutes. Data represents pooled data, as mean ± S.E.M. from 5 independent replicates, performed in duplicate. Luminescence responses were normalised between NanoBiT luminescence responses of 0nM formoterol/ 0nM antagonist (0%) and 1 μM formoterol/0 nM antagonist (100%).*

4.3.2. Monitoring antagonism of mini Gαs recruitment, using a NanoBiT complementation assay at the β_2AR.

In the HEK293T cells β_2AR/SmBiT-mini Gαs protein NanoBiT cell line, in the absence of an antagonist and in response to 1 μM formoterol, mini Gαs protein was rapidly recruited to β_2ARs, between 0 and 5 minutes (*Figure 4. 5. See also Figure 3. 11*). Between 5 and 61 minutes, the signal steadily increased. Antagonist pre-treatment (0 – 30 nM) for 20 minutes, selecting either propranolol (*Figure 4. 5. a*), ICI-118,551 (*Figure 4. 5. b*) or CGP-12177 (*Figure 4. 5. c*) reduced both peak and sustained 1 μM formoterol responses in a concentration dependent manner.

As before, Schild analysis experiments then examined the effects on a formoterol concentration response curves of increasing concentrations of propranolol (*Figure 4. 6. a, d & g*), ICI-118,551 (*Figure 4. 6. b, e & h*) and CGP-12177 (*Figure 4. 6. c, f & i*). At 3 minutes following formoterol addition, antagonism appeared insurmountable with reduced relative maximal response when treated with ≥3.3 nM of propranolol (*Figure 4. 6. a*), ICI-118,551 (*Figure 4. 6. b*) and CGP-12177 (*Figure 4. 6. c*). In addition, at 3 minutes inverse agonism was observed upon treatment of each antagonist (*Figure 4. 6. a. – c.*), and not at the later timepoints of 31 (*Figure 4. 6. d. – f.*) and 61 (*Figure 4. 6. g. – i.*) minutes.

At later timepoints of 31 and 61 minutes, all antagonist treatments of ≥1.1 nM shifted the formoterol concentration response curve significantly to the right decreasing the potency of formoterol (from EC_{25} values; one-way ANOVA; Dunnett's multiple comparison's test) (*Figure 4. 6. d. – i.*). However, antagonism again appeared insurmountable, with decreased relative maximal responses at ≥ 10nM propranolol or ICI-118,551 and ≥ 3.3 nM CGP-12177, compared to 1 μM formoterol response in the absence of an antagonist (one-way ANOVA; Dunnett's multiple comparison's test).

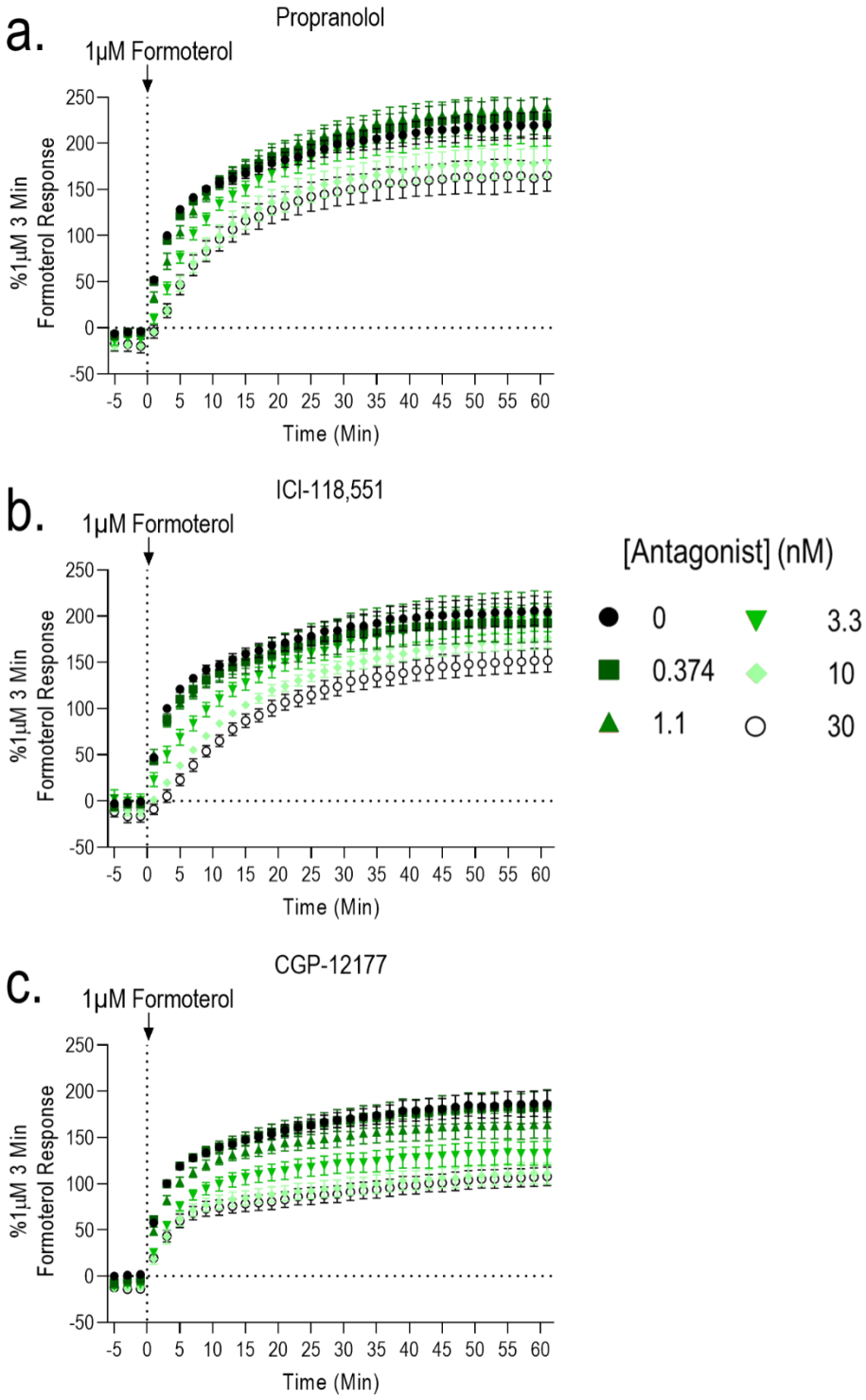

Figure 4. 5 Concentration dependent antagonism of mini Gαs protein recruitment at the β_2AR. *HEK β_2AR/SmBiT mini Gαs protein cells were pre-incubated (20 minutes) with a range of concentrations between 0-30 nM of either propranolol (a.), ICI-118,551 (b.), or CGP-12177 (c.), before 1 μM formoterol addition (time 0; indicated by dotted line) initiated recruitment of mini Gαs protein. Pooled timecourse data represent mean ± s.e.m., from 5 independent experiments, conducted in duplicate. Relative maximal responses quantified as % 10μM isoprenaline response at 3 min.*

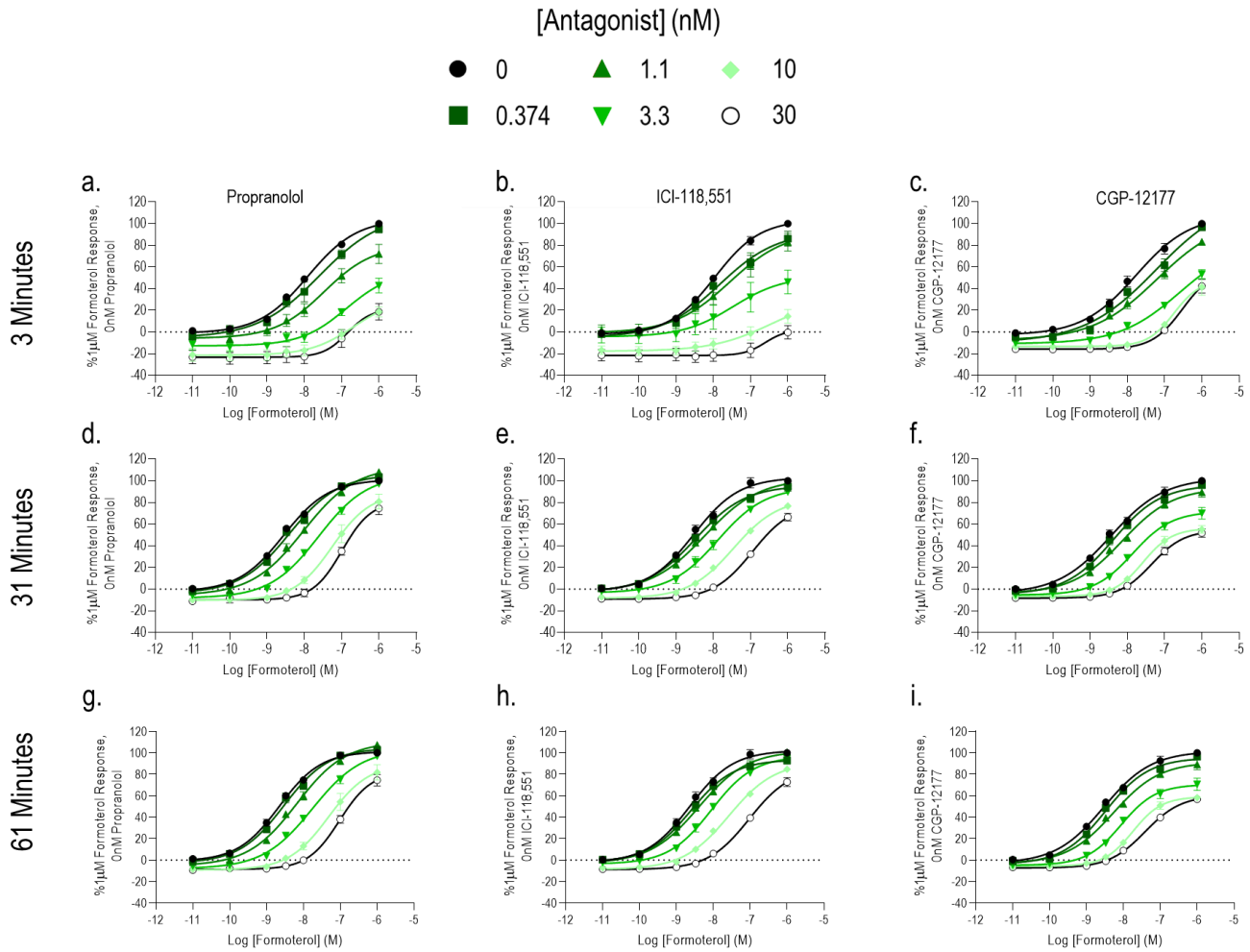

Figure 4. 6 Schild analysis of propranolol (a., d. & g.), ICI-118,551 (b., e. & h.) and CGP-12177 (c., f. & i.) in NanoBiT complementation assay monitoring mini Gαs recruitment at β_2ARs, at 3 (a. – c.), 31 (d. – f.) and 61 (g. – i.) minutes following formoterol addition.

HEK β2AR/SmBiT mini Gαs protein cells were pre-treated with increasing concentrations of antagonists for 20 minutes prior to formoterol addition at time 0 minutes. Data represents pooled data, as mean ± S.E.M. from 5 independent replicates, performed in duplicate. Luminescence responses were normalised between NanoBiT luminescence responses of 0nM formoterol/ 0nM antagonist (0%) and 1 µM formoterol/0 nM antagonist (100%).

4.3.3. Prediction of antagonist affinities using Schild analysis of β_2AR NanoBiT complementation responses.

Due to the inverse agonist properties of the antagonists, the baseline of formoterol concentration response curves was reduced as antagonist concentration increased (F*igure 4. 4*; *Figure 4. 6*). Thus to determine equilibrium dissociation constants of antagonist in the form of pA_2 values (= pK_D), Schild analysis was performed using concentration ratios taken at agonist equi-effective concentrations, as described by Kenakin (2009). Rather than use the agonist EC_{50} for each concentration response curve, concentration ratios were estimated from the concentration of formoterol, at each antagonist condition, which produced the same response as the half maximal (50 %) formoterol effect in the absence of an antagonist. Schild analyses was conducted at 31 and 61 minute timepoints (*Figure 4. 7*; *Figure 4. 8*; *Table 4. 1*).

All recruitment assays of each antagonists produced linear Schild plots at both 31 and 61 minutes (*Figure 4. 7*; *Figure 4. 8*). A slope of greater than 1 indicated that the system was not equilibrium. The slope of the propranolol Schild plot in the β_2AR/SmBiT-mini Gαs recruitment assay was significantly steeper than CGP-12177 at both 31 and 61 minutes ($P<0.05$; Student's t-test), reflecting a reduced association rate of CGP-12177 in comparison to propranolol.

Predicted affinity estimates (pA_2) for all antagonists were shown to be consistent between 31 min and 61 min, in both the β_2AR/SmBiT-β-arrestin2 and β_2AR/SmBiT-mini Gαs recruitment assays (*Table 4. 1*) ($P>0.05$; Student's t-test). Whilst predicted antagonist affinity values were consistent between timepoints, estimated propranolol affinities were 6-fold and 7-fold lower at 31 and 61 minute timepoints from Schild analysis of mini Gαs protein recruitment compared to β-arrstin2 recruitment assays ($P<0.01$, Student's t-test) (*Table 4. 1*). Unlike propranolol, estimates of pA_2 values for ICI-118,551 and CGP-12177 were not reduced when compared between mini Gαs protein recruitment and β-aresstin2 recruitment assays, from Schild analysis at either 31 or 61 minutes (*Table 4. 1*).

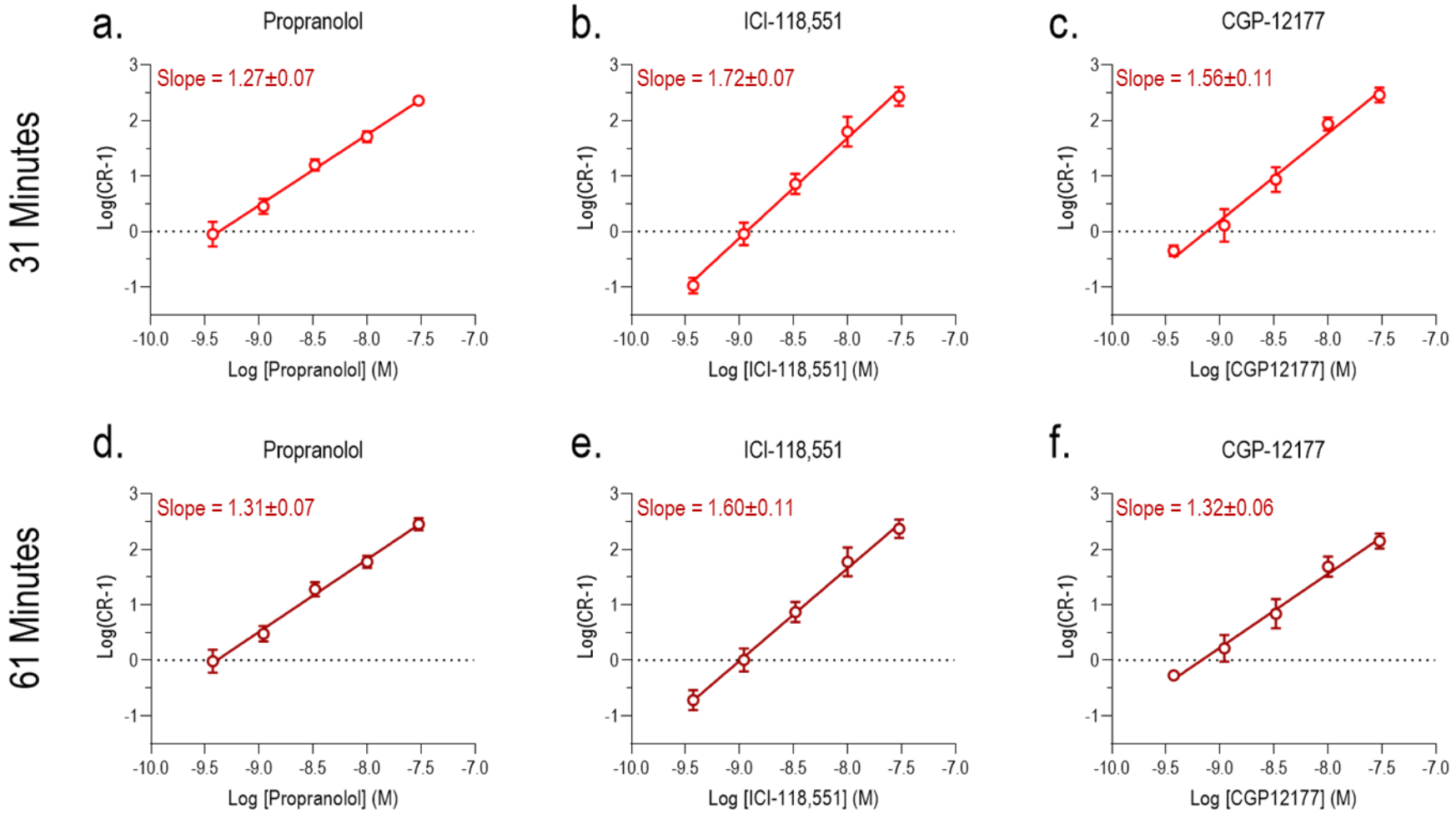

Figure 4. 7 Estimation of antagonist affinities using Schild plots of propranolol (a. & d.), ICI-118,551 (b. & e.) and CGP-12177 (c. & f.) in NanoBiT complementation assay monitoring β-arrestin2 recruitment at β_2ARs, at 31 (a. – c.) and 61 (d. – f.) minutes following formoterol addition. *From Schild analysis, as shown in Figure 4. 4, concentration ratios (CR) were quantified at equi-effective agonist concentrayions and Log(CR-1) was plotted against antagonist concentration. Data represent pooled data, as mean ± S.E.M. from 5 independent replicates, performed in duplicate. For the estimated pA2 values extracted for propranolol, ICI-118,551 and CGP-12177 at 31 and 61 minutes (Table 4.1), Schild plots for each experiment data set were used and the individual pA2 values pooled.*

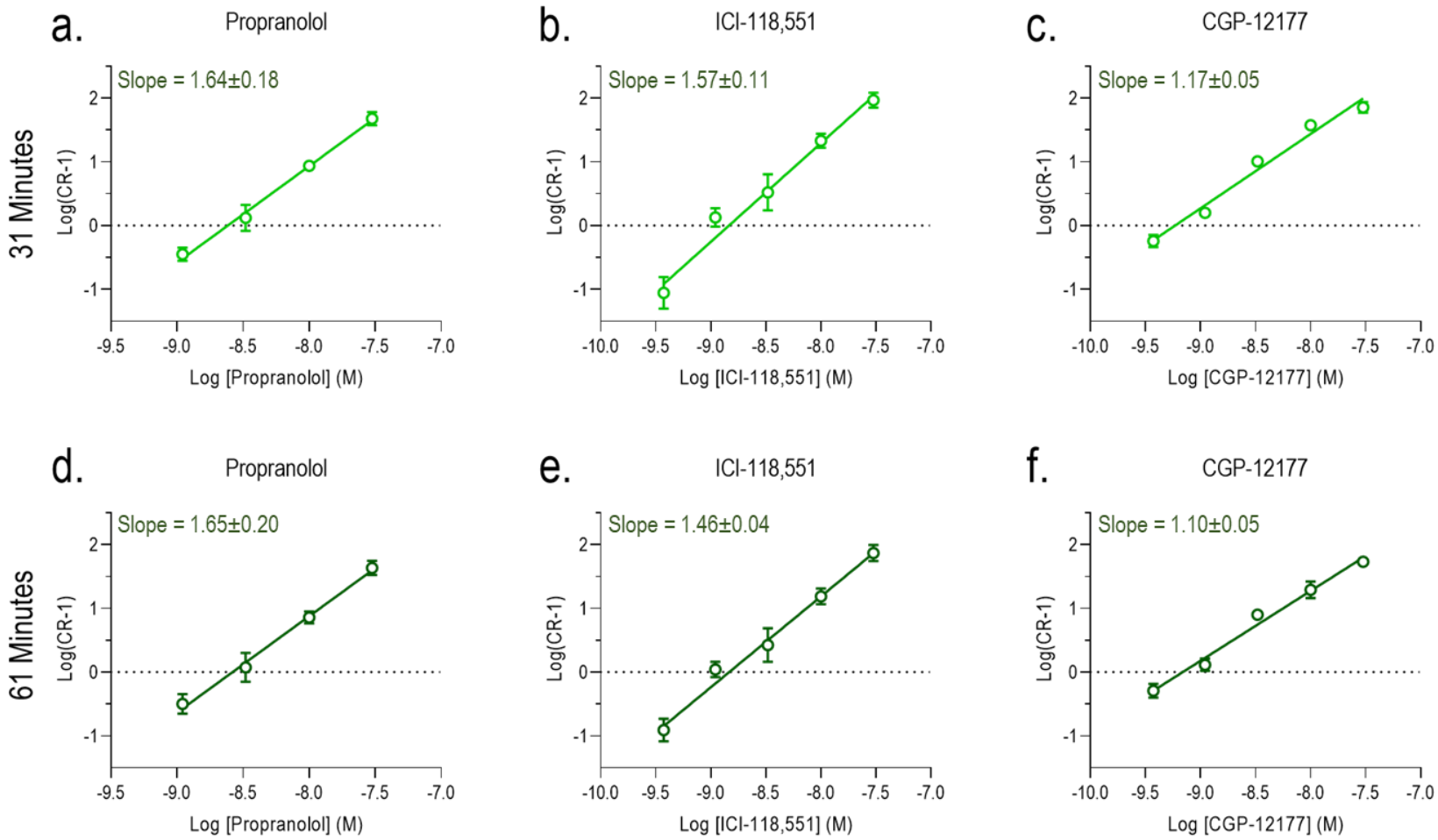

Figure 4. 8 Estimation of antagonist affinities using Schild plots of propranolol (a. & d.), ICI-118,551 (b. & e.) and CGP-12177 (c. & f.) in the NanoBiT complementation assay monitoring mini Gαs recruitment at β_2ARs, at 31 (a. – c.) and 61 (d. – f.) minutes following formoterol addition. *From Schild analysis, as shown in Figure 4. 4, concentration ratios (CR) were quantified at equi-effective agonist concentrations and Log(CR-1) was plotted against antagonist concentration. Data represent pooled data, as mean ± S.E.M. from 5 independent replicates, performed in duplicate. The pA2 estimates for propranolol, ICI-118,551 and CGP-12177 at 31 and 61 minutes (Table 4.1) were obtained by pooling Schild plot data for each individual experiment.*

	pA_2 (- log M)			
	31 Minutes		61 Minutes	
	β-arrestin2 Recruitment	Mini Gαs Recruitment	β-arrestin2 Recruitment	Mini Gαs Recruitment
Propranolol	9.40 ± 0.15	8.62 ± 0.07*	9.42 ± 0.14	8.56 ± 0.10*
ICI-118,551	8.98 ± 0.10	8.82 ± 0.10	9.04 ± 0.10	8.81 ± 0.12
CGP 12177	9.16 ± 0.12	9.24 ± 0.06	9.19 ± 0.13	9.18 ± 0.08

Table 4. 1 Summary of calculated antagonist affinities (pA_2) at the β_2AR, at 31 and 61 minutes following formoterol addition. *Affinities calculated from Schild analysis of individual NanoBiT complementation assay experiments, monitoring β-arrestin2 and mini Gαs recruitment at β_2ARs. Data represent pooled data, as mean ± S.E.M. from 5 independent experiments. *P<0.05, Student's t-test between mini G protein and b-arrestin2 data sets, unpaired, two-tailed.*

4.3.4. The degree of insurmountability of β_2AR antagonists in the NanoBiT assays is correlated with slower antagonist dissociation kinetics

Antagonist insurmountability observed in formoterol stimulated β-arrestin2 and mini Gαs protein recruitment assays was shown to be more pronounced after CGP-12177 and ICI-118,551 treatment, when compared to the effects of propranolol (*Figure 4. 4*; *Figure 4. 6*). To investigate the involvement of antagonist kinetics on the observed insurmountability, the association and dissociation rates of propranolol, ICI-118,551 and CGP-12177 were determined using a TR-FRET kinetic competition binding assay. Whilst the TR-FRET competition binding assay, as seen in *Chapter 3* (*Figure 3. 19*), can be used to determine the ligand dissociation equilibrium constants of fluorescently labelled and unlabelled ligands, a kinetic competition binding assay was required determine the association and dissociation rates of the antagonist panel.

The kinetic parameters of the tracer ligand, BODIPY-FL-PEG8-(S)-Propranolol, were determined by applying multiple concentrations of BODIPY-FL-PEG8-(S)-Propranolol to membranes expressing SNAP-β_2AR-LgBiT receptors, labelled with terbium on the N-terminal SNAP tag (*Figure 4. 9*). Energy transfer between the laser-excited terbium label and the fluorescent ligand was monitored over time to generate a set of BODIPY-FL-PEG8-(S)-Propranolol association curves (plotted as the specific TR-FRET ratio). Global fitting of these data to a one site association model enabled calculation of the BODIPY-FL-PEG8-(S)-Propranolol k_{ON}= 2.94 ± 1.26 x10^7 $M^{-1}min^{-1}$ and k_{OFF}= 0.394 ± 0.031 min^{-1} (mean± s.e.m.; n=4) (*Figure 4. 9. a*; *Table 4. 2*). From this, a kinetic K_D was calculated as 13.92±4.86 nM (K_D= k_{OFF}/k_{ON}; mean± s.e.m.; n=4), equivalent to the endpoint saturation K_D previously estimated in *Figure 3. 21. a*. A plot of observed association rate at each BODIPY-FL-PEG8-(S)-Propranolol concentration (k_{Obs}) against BODIPY-FL-PEG8-(S)-Propranolol concentration was linear (*Figure 4. 9. b*), consistent with a single affinity site receptor population. A homogenous population of receptor binding sites supported subsequent application of the Motulsky Mahan model to competition kinetic experiments

The association of 10 nM BODIPY-FL-PEG8-(S)-Propranolol was then measured in the absence and presence of a range of concentrations of the different unlabelled antagonists. Competitive association was initiated by addition of terbium labelled HEK SNAP-β_2AR-LgBiT membranes, and monitored over a 25

minute timecourse. The Motulsky-Mahan kinetic model was applied to determine the association and dissociation rates of propranolol, ICI-118,551 and CGP-12177 (*Figure 4. 10*; *Table 4. 2*). In each experiment the kinetic parameters of the fluorescent ligand were independently estimated using association kinetic curves at different concentrations (*Figure 4. 9*). These experimental k_{ON} and k_{OFF} estimates were used to fix the fluorescent ligand parameters in the Motulsky Mahan model, so that the unlabelled antagonist kinetics could be determined. The goodness of fit for the model in individual experiments was considered by monitoring the 95 % confidence intervals for the kinetic rate constants. For example, in a typical experiment. the best-fit estimate for propanolol k_{OFF} was 0.3404 Min^{-1}, with lower and upper confidence intervals of 0.3124 and 0.3723 Min^{-1}, respectively, and thus the confidence intervals were within 9% of the best-fit estimation. The best-fit estimate of propranolol k_{ON} was $2.30x10^8$ $M^{-1}Min^{-1}$, with lower and upper confidence intervals of $2.12x10^8$ and $2.50x10^8$ $M^{-1}Min^{-1}$, respectively. Thus the confidence intervals were also within 9% of the best-fit estimation. When a mean was taken from all of the individual experimental fits of the model, the confidence intervals of the kinetic operational modelling of antagonist dissociation rates were within 8% of the modelled best-fit values, whilst the confidence intervals of the antagonist association rates were within 11%, demonstrating that the best fit measurements provided reliable estimates

The order of association rate constants (k_{ON}) was propranolol>ICI-118,551>CGP-12177, representing overall a 12 fold change (*Table 4. 2*) Equally the same order of dissociation rate constants (k_{OFF}) was observed, with propranolol k_{OFF} 8 fold faster than those of CGP-12177 (*Table 4. 2*).

Kinetically derived K_D values, obtained from the ratio of dissociation and association rates (k_{OFF}/k_{ON}) were 1.27±0.16, 2.32±0.59 and 1.76±0.40 nM for propranolol, ICI-118,551 and CGP-12177, respectively (*Table 4. 2*).

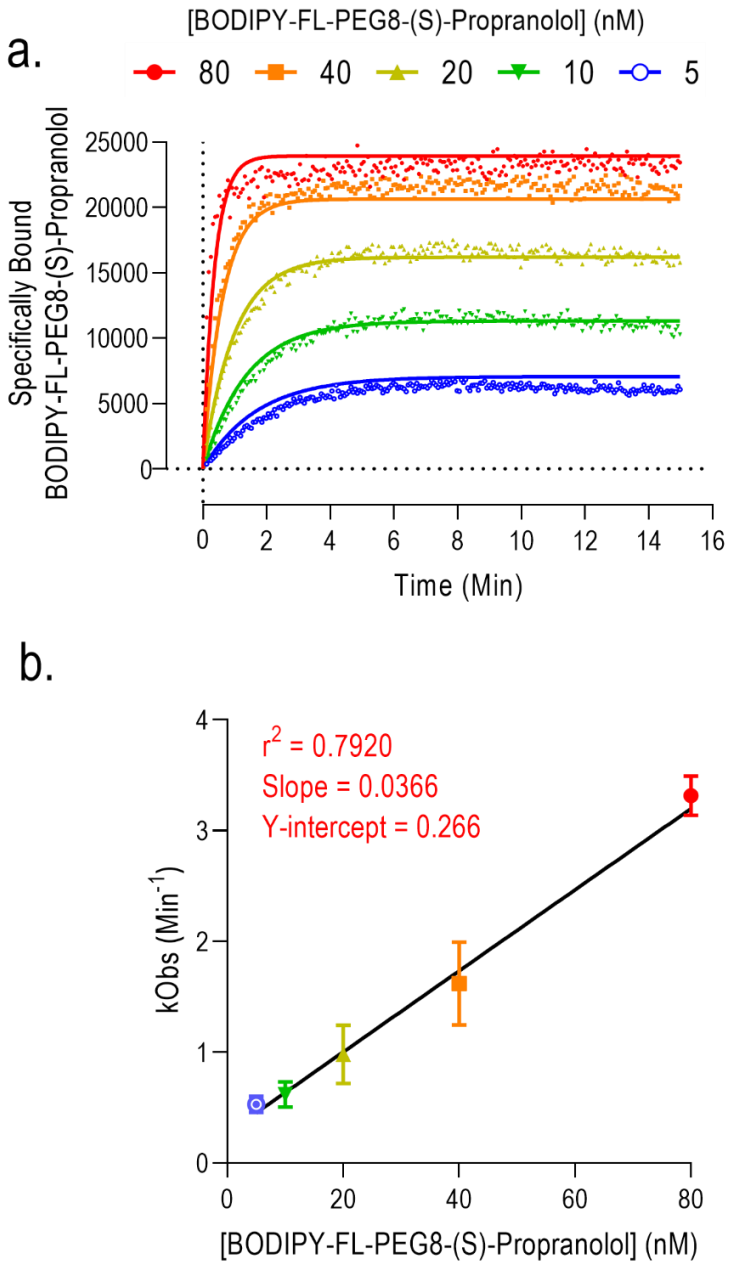

Figure 4. 9 Association binding kinetics of BODIPY-FL-PEG8-(S)-Propranolol at membrane prepared from HEK293T cells stably expressed terbium-labelled SNAP-β_2AR-LgBiT. *(a.) Membranes were prepared from HEK293T cells stably expressing SNAP-β_2AR-LgBiT receptors, which had been terbium-labelled using SNAP-Lumi4-Tb labelling reagent. Membranes were incubated with increasing concentrations of BODIPY-FL-PEG8-(S)-Propranolol, with 10 μM ICI-118,551 used to determine non-specific binding. Dual emission wavelengths (490nm & 520nm) were monitored for 15 minutes and binding was represented by a ratio of TR-FRET binding (520/490 *10,000). Data points show the specific binding (total – non specific) for a representative experiment fitted to a global model of association kinetics for single site binding. (b.) The observed association rate at each BODIPY-FL-PEG8-(S)-Propranolol concentration (k_{Obs}) was plot against BODIPY-FL-PEG8-(S)-Propranolol concentration, producing a linear relationship (r^2=0.7920).*

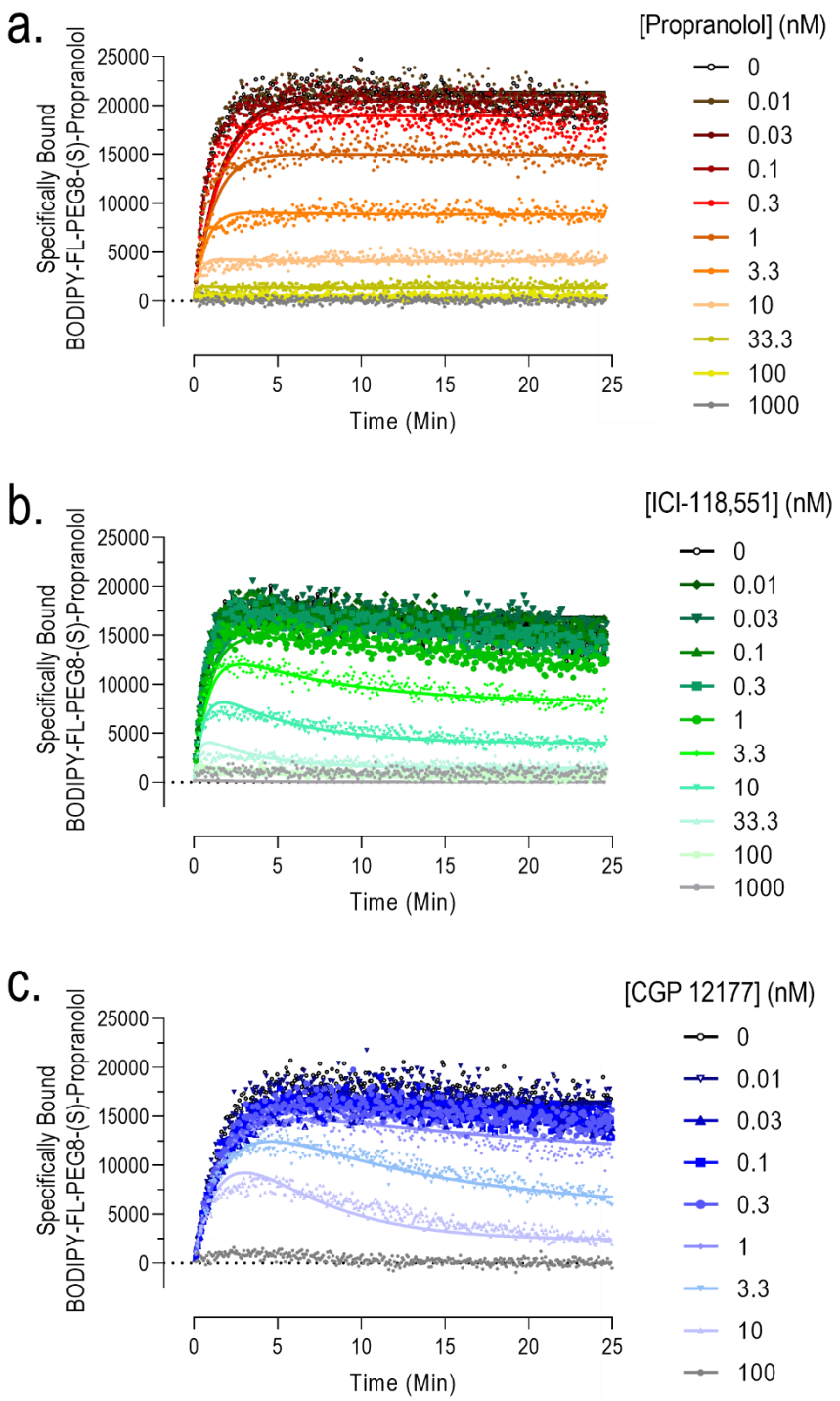

Figure 4. 10 Competition binding kinetics of unlabelled βAR antagonists against BODIPY-FL-PEG8-(S)-Propranolol at β_2AR-LgBiT constructs. *Membranes were prepared from HEK293T cells stably expressing SNAP-β_2AR-LgBiT, which had been terbium-labelled using SNAP-Lumi4-Tb reagent. Membranes were incubated with increasing concentrations of antagonist and a fixed concentration (10 nM) of BODIPY-FL-PEG8-(S)-Propranolol, with 10 μM ICI-118,551 used to determine non-specific binding. Dual emission wavelengths (490nm & 520nm) were monitored for 15 minutes and specific binding was plotted as the TR-FRET ratio (520/490 *10,000). Data points show a representative experiment fit to the Motulsky-Mahan global model of competitive binding kinetics.*

	k_{ON} ($M^{-1}min^{-1}$)	k_{OFF} (min^{-1})	Kinetic K_D (nM)
Labelled Ligand			
BODIPY-FL-PEG8-(S)-Propranolol	2.94 ± 1.26 x 10^7	0.394 ± 0.031	13.92 ± 4.86
Unlabelled Ligands			
Propranolol	2.58 ± 0.15 x10^8	0.324 ± 0.039	1.27 ± 0.16
ICI-118,551	6.51 ± 1.50 x10^7	0.125 ± 0.012	2.32 ± 0.59
CGP 12177	2.21 ± 0.08 x10^7	0.038 ± 0.008	1.76 ± 0.40

Table 4. 2 Summary of ligand binding pharmacology of BODIPY-FL-PEG8-(S)-Propranolol (Figure 4. 9) and unlabelled βAR antagonists (Figure 4. 10). *Kinetic binding parameters of BODIPY-FL-PEG8-(S)-Propranolol and unlabelled antagonists from global association fits and the Motulsky-Mahan model of competitive binding. Kinetically derived K_D values were derived from a ratio of dissociation and association rates (K_D= k_{OFF}/k_{ON}). Data represent pooled data, as mean ± S.E.M. from 4 independent experiments.*

4.3.5. Estimation of β_2AR antagonist kinetic binding parameters from timecourse NanoBiT recruitment data, using a kinetic operational model of antagonism.

As seen in *Chapter 3*, mathematical models can be fitted to timecourse experimental data to obtain kinetically derived pharmacological parameters. Here, we applied a kinetic operational model of antagonism from Hoare *et al*, (2018) (*Methods 2.7.4.3.2.*) to the mini Gαs protein recruitment data at β_2ARs. (*Figure 4. 11*; *Table 4. 3*). Due to the transient recruitment profile of β-arrestin2 at β_2ARs, the kinetic operational model of antagonism could not be fitted to the antagonist data sets from the β-arrestin2 assay. From Hoare *et al*, (2018), we chose to apply "Model 14", which assumes antagonist pre-incubation, to determine the association (k_{ON}) and dissociation (k_{OFF}) rates of each antagonist (Hoare *et al.*, 2018) (*Figure 4. 12*; *Table 4. 3*). The model was fitted to timecourse recruitment data 0-61 minutes post 100 nM formoterol addition.

The association rates of ICI-118,551 and CGP-12177 estimated by the kinetic operational model were similar to those determined by TR-FRET binding assay ($p>0.05$; Student's t-test; Two-tailed). However the association rate of propranolol was 45-fold faster when estimated by TR-FRET binding studies than in the kinetic operational model (. $P<0.0001$, Student's t-test; Two-tailed) (*Figure 4. 12. a; Table 4. 3*). Predicted dissociation rates between estimates obtained in the TR-FRET binding assay were shown to be comparable for CGP-12177 ($p>0.05$; Student's t-test; Two-tailed), but the TR-FRET dissociation rate estimates were 10-fold and 3-fold faster compared to the kinetic operational model, for propranolol ($P<0.0001$, Student's t-test; Two-tailed) and ICI-118,551 ($P=0.0004$, Student's t-test; Two-tailed), respectively (*Figure 4. 12. b.*; *Table 4. 3*). These differences also led to a different rank order for the antagonists when association and dissociation rates were compared via the kinetic operational model (*Figure 4. 11*; *Figure 4. 12. a.*; *Table 4. 3*) and the TR-FRET kinetic binding assay (*Figure 4. 10*;*table 4. 2*) (fastest to slowest; kinetic operational model: CGP-12177>ICI-118,551>propranolol; TR-FRET: propranolol>ICI-118,551>CGP-12177).

As with the Motulsky-Mahan model applied to TR-FRET binding assay data, the kinetic operational model is fitted globally and as such the accuracy of the estimations association and dissociation rates can be reflected in the parameter confidence intervals of individual experiment fits. For example, the kinetic operational model was applied to a mini Gas protein NanoBiT assay

timecourse monitoring ICI-118,551 antagonism of a 100 nM formoterol response. The best-fit estimate of k_{OFF} was 0.0460 Min^{-1}, with lower and upper confidence intervals of 0.0388 and 0.0548 Min^{-1}, respectively, and thus the confidence intervals were within 20% of the best-fit estimation. The best-fit estimate of k_{ON} was $4.96x10^7$ $M^{-1}Min^{-1}$, with lower and upper confidence intervals of $3.50x10^7$ and $6.68x10^7$ $M^{-1}Min^{-1}$, respectively. Thus the confidence interval was within 35% of the best-fit estimation. When a mean was taken from all individual experimental fits of the model, the confidence intervals of the kinetic operational modelling of antagonist dissociation rates were within 25% of the modelled best-fit values, whilst the confidence intervals of the antagonist association rates were within 39%. Between antagonists, the average confidence limit range for model fitting of both k_{ON} and k_{OFF}, was within 27, 32 and 31 % of the best-fit estimations, for propranolol, ICI-118,551 and CGP-12177.

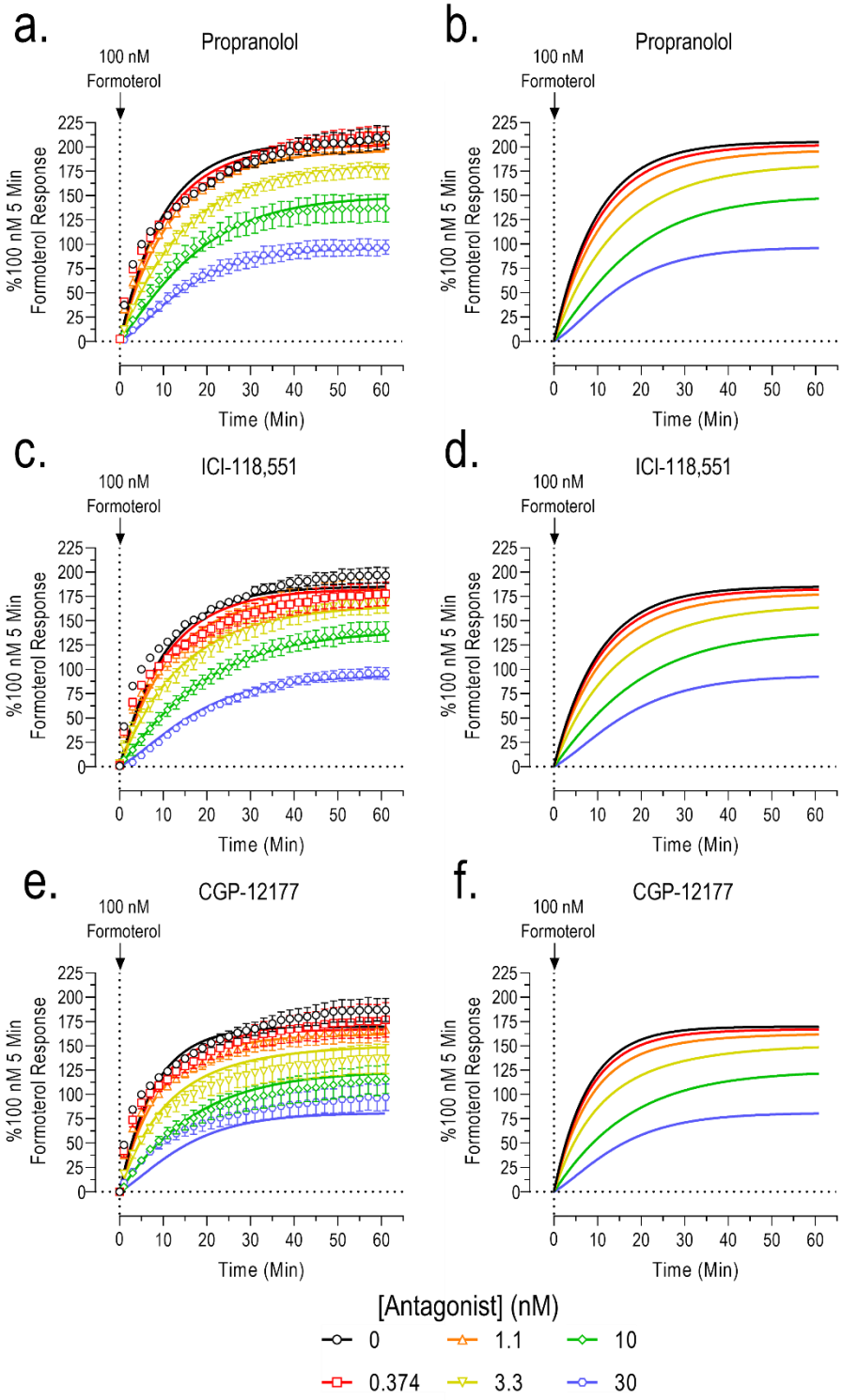

Figure 4. 11 Curve fitting of the "Antagonist Pre-Incubation" kinetic operational model to NanoBiT monitored recruitment of mini Gαs protein at β_2ARs. *Timecourse data from NanoBiT monitoring antagonism of 100 nM formoterol stimulated mini Gαs protein recruitment at β_2ARs, following propranolol (a.– b.), ICI-118,551 (c.– d.) and CGP-12177 (e.– f.) pre-treatment (20 min). "Antagonist Pre-Incubation" kinetic operational model was fitted to the representative data, with pooled parameters given in Table 4. 3. For clarity, raw data points have been removed in the duplicate figure panels (b., d. & f.). Data points represent mean ± s.e.m., from an independent representative experiment, conducted in duplicate. Responses were quantified as % 100 nM formoterol response at 5 minutes.*

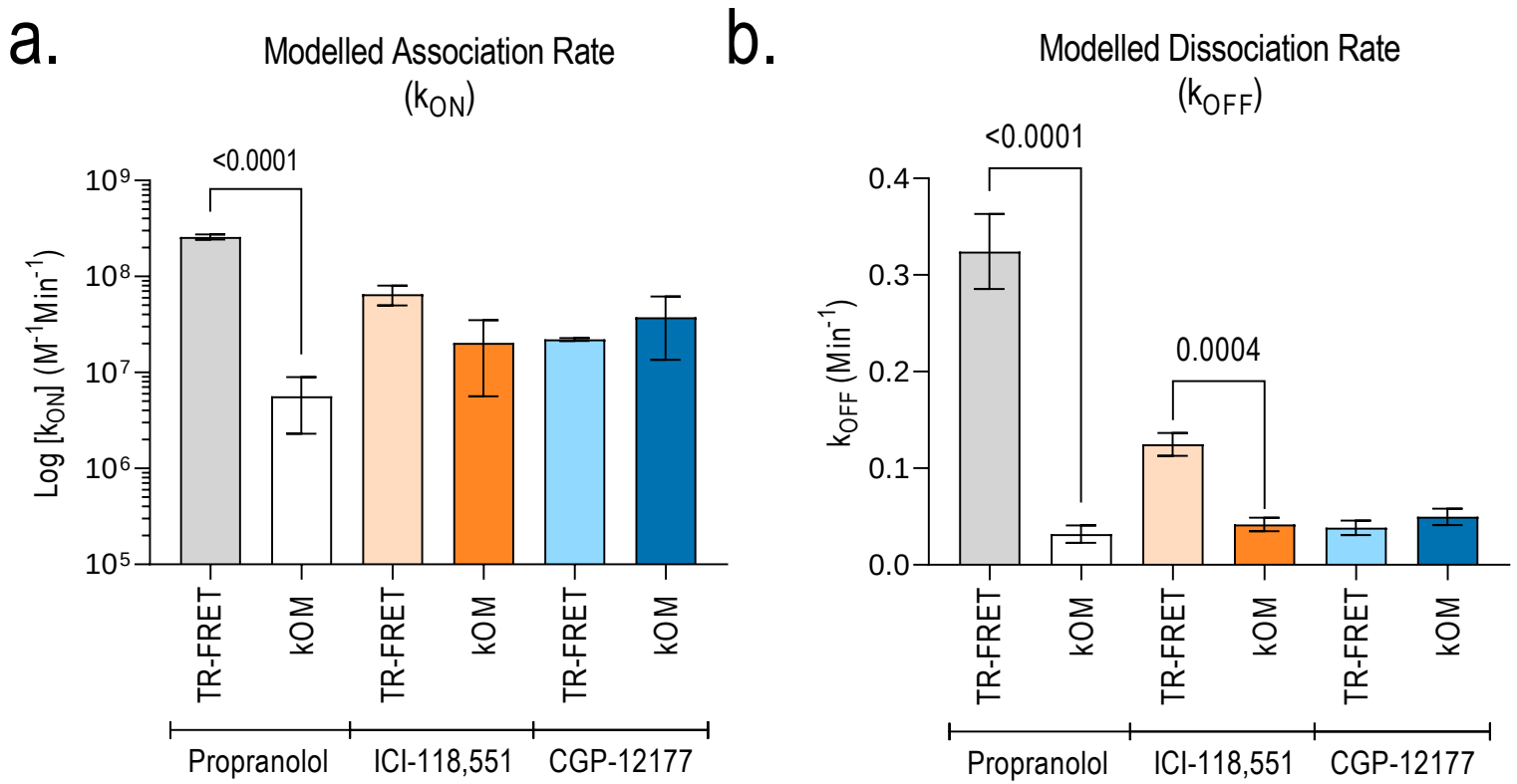

Figure 4. 12 Predicted antagonist association (a.) and dissociation (b.) rate constants from TR-FRET binding studies and kinetic operational modelling of β_2AR - mini Gαs NanoBiT complementation assay data. *Global models were used to fit association and dissociation rates from the Motulsky-Mahan model applied toTR-FRET binding studies and a kinetic operational model (kOM) of antagonism of mini Gαs recruitment from a NanoBiT complementation assay. Pooled antagonist association (k_{ON}; $M^{-1}min^{-1}$) and dissociation (k_{OFF}; min^{-1}) rate constants are represented as mean ± S.E.M., from 4 or 5 individual replicates, for TR-FRET and kOM data, respectively.*

	k_{ON} ($M^{-1}min^{-1}$)	k_{OFF} (min^{-1})	Kinetic pK_D (M)
Antagonist			
Propranolol	5.64 ± 3.33 x10^6	0.032 ± 0.009	8.37 ± 0.17
ICI-118,551	2.04 ± 1.47 x10^7	0.042 ± 0.007	8.42 ± 0.26
CGP 12177	3.76 ± 2.41 x10^7	0.050 ± 0.009	8.66 ± 0.32

Table 4. 3 Kinetically modelled antagonist pharmacology, from a NanoBiT complementation assay monitoring antagonism of formoterol stimulated mini Gαs protein recruitment at β_2ARs. *A kinetic operational model of antagonism was fitted to individual experiments monitoring antagonism of formoterol stimulated mini Gαs recruitment at β_2ARs to derive antagonist association (k_{ON}; $M^{-1}min^{-1}$) and dissociation (k_{OFF}; min^{-1}) rates. Kinetic pK_D values were derived from a ratio of dissociation and association rates (pK_D = -Log(k_{OFF}/k_{ON})). Quoted pharmacology represents mean ± s.e.m., from 5 individual replicates, conducted in duplicate.*

4.3.6. Comparison of β_2AR antagonist affinity estimates using Schild analysis, TR-FRET binding assays and a kinetic operational model of antagonism.

Estimates of antagonist affinity as the equilibrium dissociation constant were compared between TR-FRET binding assays and affinity values derived from modelling of NanoBiT recruitment assay data, either through Schild analysis (61 minute data) or through the kinetic operational model of antagonism, using the timecourse signalling of 61 minutes following 100 nM formoterol addition (*Figure 4. 13*). The affinity of propranolol for the β_2AR-LgBiT construct was estimated to be 7-fold and 11-fold lower when estimated by Schild analysis in the β-arrestin2 recruitment assays, than compared to Schild analysis in the mini Gαs recruitment assays ($P=0.001$, one-way ANOVA, Tukey's multiple comparisons post-hoc test) and kinetic operational modelling of mini Gαs recruitment assay timecourse data ($P=0.0004$, one-way ANOVA, Tukey's multiple comparisons post-hoc test). ICI-118,551 and CGP-12177 affinity estimates were shown to be comparable between all methodologies (*Figure 4. 13*) ($P>0.05$; one-way ANOVA, Tukey's multiple comparisons post-hoc test).

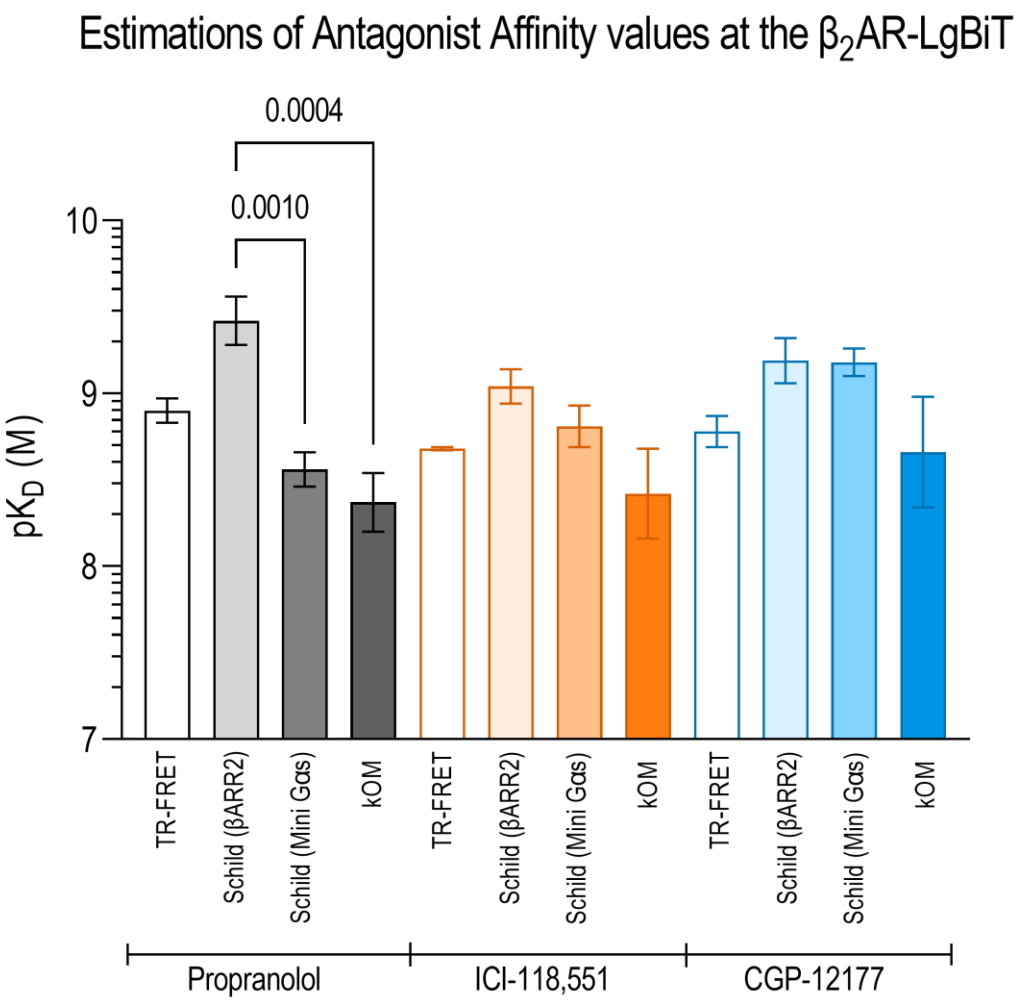

Figure 4. 13 Summary of antagonist equilibrium dissociation constants predicted by different methodologies. *Estimations of propranolol, ICI-118,551 and CGP-12177 affinity, described by pK_D values, at the β_2AR-LgBiT from TR-FRET binding studies, Schild analysis of NanoBiT complementation assays monitoring recruitment of β-arrestin2 (βARR2) and a mini Gαs protein (Mini Gαs) and kinetic operational modelling of NanoBiT complementation assay, monitoring mini Gαs recruitment. Bars represent mean ± S.E.M., from 4- 5 individual replicates, respectively. Statistical differences between pK_Ds derived for the same antagonist were determined using a one-way ANOVA, with Tukey's multiple comparison post-hoc test, with P values reported on the figure.*

4.4. Discussion

In this chapter, NanoBiT complementation assays (established in *Chapter 3*) were used to investigate antagonism at β_2ARs, by measuring recruitment of β-arrestin2 and a mini Gαs protein. A panel of three antagonists (propranolol, ICI-118,551 and CGP-12177) were applied in Schild based assays, where a concentration response relationship of formoterol was monitored in the presence of increasing concentrations of each antagonist. Antagonism of recruitment of either β-arrestin2 or the mini Gαs protein was monitored in real time, allowing for multiple sets of concentrations response curves from multiple time points. This allowed for the kinetic context of antagonism to be compared between timepoints, mapping the time dependent transition between insurmountable and surmountable antagonism. To correlate the degree of functional insurmountability with binding kinetics, antagonist kinetic binding parameters were derived from HEK293T membranes expressing terbium labelled SNAP-β_2AR-LgBiT constructs, in TR-FRET binding assays. This demonstrated a correlation between slow off rates of the antagonist and the persistence of non-surmountable antagonism at later time points in the functional assay. Measures of antagonism are often determined from single timepoints, and using a single concentration of agonist to derive an IC_{50} value. This has the disadvantage in that the IC_{50}s obtained (unlike Schild pA_2 values) depend on both the antagonist affinity and mode of action, and the agonist effects. As an alternative, a kinetic operational model was implemented to estimate association and dissociation rate constants, and K_D of antagonists from the 61 minute signalling timecourses for a single agonist concentration and different antagonist concentrations. Notably, measures of each antagonist's equilibrium dissociation constant at the β_2AR through the kinetic operational model of antagonism, TR-FRET binding assays and Schild analysis were highly correlated – suggesting the kinetic operational model of antagonism has some benefit in estimating antagonist affinity from these data. However, individual association and dissociation rate constants estimated by the kinetic operational model were poorly correlated with the TR-FRET binding data, and unable to be fitted with a high degree of confidence. This suggests that the kinetic operation model of antagonism has potential benefits in extracting antagonist parameters from functional timecourse data, but further refinements to incorporate agonist binding kinetics and signalling time profiles may be required.

4.4.1. Mapping the time-dependent changes in antagonist mode of action using the real time NanoBiT complementation assays for the β_2AR.

Low affinity NanoBiT fragments (LgBiT-SmBiT) were used to report antagonist action on the recruitment of β-arrestin2 and a mini Gαs protein, at the β_2AR, pre-treating using a panel of 3 well-characterised β_2AR antagonist ligands: propranolol, ICI-118,551 and CGP-12177 (Baker, *et al*, 2002; Baker, 2005; Carter and Hill, 2005). As seen in *Chapter 3*, formoterol stimulation in the absence of an antagonist produces a transient "rise-and-fall" recruitment of β-arrestin2 to the β_2AR (*Figure 4. 3*), whilst the mini Gαs protein was rapidly recruited between 0-5 minutes before a sustained complementation response was observed suggested sustained complementation (*figure 4. 5*). Whilst the effects of antagonists are often measured in signalling assays by considering peak signal responses to agonists, such as intracellular Ca^{2+} ion release (Liu *et al.*, 2010; Suen *et al.*, 2014) or β-arrestin2 recruitment at β_2ARs (Vauquelin, *et al*, 2002). The disadvantage of such an approach is that the measurements can then reflect non-equilibrium or hemi-equilibrium conditions. For example, assays may pre-incubate with a competitive antagonist to allow a sufficient time for binding equilibrium to be established; however on addition of agonist a new dynamic equilibrium must be generated for agonist / antagonist occupancy at the receptor. If the dissociation kinetics (k_{OFF}) for the antagonist is slow, the time for this to be achieved is extended and the effects of the antagonist (though competitive and reversible) appear insurmountable at early time points (1 – 2 min) that often represent the peak for initial GPCR signalling events. The advantage of the NanoBiT assays used here is that β_2AR recruitment of β-arrestin2 or mini Gαs protein can be followed in real time to monitor the time dependent changes in antagonist dependent behaviour. We demonstrated this applicability by using a using a panel of 3 well-characterised β_2AR antagonist ligands: propranolol, ICI-118,551 and CGP-12177 (Baker, *et al*, 2002; Baker, 2005; Carter and Hill, 2005). We showed insurmountable effects were observed at the early peak time point for all antagonists, even for the most rapidly equilibrating antagonist (propranolol). However the transition to surmountable behaviour for propranolol, and to a less degree ICI-118,551 and CGP-12177, could be followed in the same experiment through Schild analysis at later timepoints. These data reinforce the well-recognised contribution of slowly reversible kinetics to generating insurmountable properties under non-equilibrium conditions (Kenakin, *et al*, 2006; Vauquelin and Szczuka, 2007). It is therefore

important when investigating insurmountable antagonism to first investigate the possibility of competitive but long-lasting receptor occupancy, before any conclusions are made regarding the site of binding, e.g. non-competitive action (Vauquelin and Szczuka, 2007). Assays such as NanoBiT, as described in published methodology (Dijon, *et al*, 2021), which deliver full timecourse data across a meaningful period within a single experiment, provide a useful practical approach to monitor this in routine GPCR compound profiling.

4.4.2. Insurmountable antagonism in β_2AR NanoBiT complementation assays is correlated with antagonist binding kinetics.

Schild analysis experiments observed at early timepoints of propranolol and ICI-118,551 antagonism and all timepoints monitoring CGP-12177 antagonism reveal insurmountable antagonism, indicated by reduced relative maximal response in the absence of a reduced basal signalling.

To demonstrate the correlation between functional insurmountability and binding kinetics, the competition association method combined with TR-FRET binding assays was used to derive the antagonist k_{ON} and k_{OFF} parameters at the β_2AR. The dissociation rate constant for CGP-12177 was 10-fold slower than propranolol, supporting its prolonged insurmountable action compared to propranolol in the functional assays, with the k_{ON} and k_{OFF} measurements were in general agreement with the published kinetic properties of each antagonist (Sykes, *et al*, 2014). Unlike homogenous TR-FRET binding assays presented here, Sykes *et al* (2014) used radioligand binding assay to establish kinetic properties of ligands which requires separate wells to establish binding at multiple timepoints. Moreover, TR-FRET binding assays have the advantage over traditional radioligand binding assays as they can be conducted in medium-high throughput format, enabling kinetics for multiple concentrations of antagonists and improve fitting of models such as the Motulsky Mahan. However, the use of the Motulsky Mahan also requires the unlabelled ligand to be competitive with the probe ligand. The Motulsky Mahan model was successfully applied here due to the considerations made to ensure a single relevant “pharmacological” receptor site was isolating. For example, the isolation of the receptors within membranes provided a system where receptors were not internalised, as well as the addition of Gpp(NH)p to the buffer to ensure the dissociation of endogenous G proteins

from the receptor and promote the inactive receptor conformation. Whilst this is easier to achieve for antagonists that do not discriminate between inactive (R) and active (R*) conformations or prefer the R conformation, it is more difficult at receptors influenced by further bound proteins (see *Chapter 5 & 6*) or agonist ligands which are thought to have higher affinity at active receptor conformations (Warne *et al.*, 2019).

Slow rates of receptor dissociation have been suggested to be due to increased engagement of the antagonist aromatic head group with increased close contact residues with key amino acids in the 7th transmembrane domain helix deep within the hydrophobic binding pocket (Tyr$^{7.35}$, Ile$^{7.36}$ and Tyr$^{7.43}$) (Audet and Bouvier, 2008; Sykes, *et al*, 2014). It has also been suggested that antagonist binding affinities at GPCRs can either be driven by a slow dissociation rate or an increased membrane partition coefficient, the latter indicating the antagonist drug can be partitioned within lipid pockets of the membrane and increasing the apparent antagonist association rate (Syk*es et al*, 2014). Moreover, increased membrane partition coefficients can alter micro-pharmacokinetic environment to increase local drug concentration at the membrane (Vauquelin and Packeu, 2009; S*ykes et al*, 2014; Gherbi, *et al*, 2018) to increase the duration of antagonist action (Charlton and Vauquelin, 2010) and potential antagonist rebinding (Charlton and Vauquelin, 2010; Vauquelin and Charlton, 2010; Vauquelin, 2016a). There may be disadvantages to increasing membrane ligand residence and local concentration in this manner, since non-specific drug interactions may also be promoted leading to increased incidence of side effects and a less optimal drug profile (Hughes *et al.*, 2008). However, for the three test antagonists however, we observed that both k_{ON} and k_{OFF} were highest for propranolol and lowest for CGP. Therefore it is most likely that the slow dissociation rate, rather than fast association and rebinding, accounts for the degree of insurmountability observed for each antagonist in the functional assays.

4.4.3. Modelling kinetic data and hemi-equilibrium conditions to derive antagonist binding parameters from NanoBiT data.

The availability of global timecourse functional data should allow an estimation of antagonist binding kinetics, assuming antagonists binding in a competitive and reversible manner, as well as establishing equilibrium parameters.

One method of approaching this is the use of the hemi-equilibrium model (Kenakin, *et al*, 2006; Mould *et al.*, 2014) which can obtain antagonist k_{OFF} as well

as K_D from Schild analysis (Arunlakshana and Schild, 1959) data sets at different timepoints. However, this model was not successfully applied to the current data set (data not shown) to provide parameter estimates with a sufficient degree of fitting accuracy. Moreover, as established in *Chapter 3*, the NanoBiT assay revealed inverse agonism in β_2AR/SmBiT-β-arrestin2 cell lines, and thus lowering the basal signal of concentration response curves (*Figure 4. 4* & *Figure 4. 6*) which is not accounted for in the hemi-equilibrium model.

An alternative approach is the kinetic operational mode of antagonism (Hoare *et al*, 2018), which are applied to timecourse data which monitor antagonist action in functional assays. One attractive feature of this model is its ability to take standard IC_{50} data sets as timecourses (single agonist concentration & multiple antagonist concentrations) and estimate the antagonist affinity as an antagonist K_D. Antagonist IC_{50} measurements (as estimated by endpoints) are still widely used for compound profiling, but suffer from the fact the IC_{50} measured is also dependent on the assay and agonist used – therefore, unlike antagonist K_D, IC_{50}'s are not comparable across different assays. In support, we showed that the kOM provided reasonably good estimates of antagonist affinity from the data, comparable to both Schild and binding estimates. This suggests it may be a useful tool to analyse IC_{50} style assays where kinetic data can be routinely collected.

However, the kinetic operational mode of antagonism provided only poorly defined k_{ON} and k_{OFF} estimates for the antagonists, that were not well correlated with the more robust binding measurements in our TR-FRET study, or earlier binding data (Sykes et al 2014). Moreover, the models do assume equilibrium of the agonist ligand to be reached rapidly, which may not be suitable for GPCRs with slower canonical binding rate such as peptide and class-B GPCRs. In addition, Hoare *et al.*, (2018) only provides antagonist models for experimental systems where the response vs time relationship does not decay and thus is unsuitable for the β-arrestin2 recruitment assay, at the β_2AR. Like the hemi-equilibrium model, the kinetic operational model of antagonist does not consider inverse agonist activity. In contrast, in Schild analysis conducted here the concentration ratio (CR) calculation was adjusted to take this into account by using equi-effective agonist concentrations. Finally, the kinetic operational model of antagonism accounts for differences in antagonist binding kinetics in analysing functional data, but assumes a competitive mode of action. If this is not the case in compound profiling (i.e. non-competitive/allosteric), then erroneous estimates would be obtained, and like basic IC_{50} determinations, this is not easy to check. In

Schild analysis, which also assumes a competitive and reversible mode of action at equilibrium, there is the means to check validity by considering the linearity and slope of the Schild plot.

It would be useful to develop model fitting to consider global fitting of the full Schild analysis data set (i.e. multiple agonist concentrations, as well as multiple antagonist concentration time courses) to establish whether parameter accuracy can be improved.

4.4.4. Correlations of β_2AR antagonist affinity across binding and functional assay.

For antagonists with a competitive and reversible mechanism of action, the antagonist K_D is a valuable measurement because it is a fundamental measure of antagonist affinity, unlike a functional or a binding IC_{50} value. For a true competitive antagonist at a given receptor subtype, the K_D estimate should be the same, regardless of the methodology provided temperature and buffer conditions are the same (binding, function at different signalling pathways, types of analysis). With the exception of a modest difference for propranolol in one assay format, the K_D estimates of each antagonist was shown to be consistent between estimates established in the binding and functional analysis performed

In published literature, there are estimates of an antagonist K_D which have been shown to be different between different functional and binding readouts. The most common explanation for such results is that equilibrium conditions were not reached in an assay as required, thus increasing the value of timecourse data to monitor this for both binding/functional technologies, as shown in this chapter. In addition to non-equilibrium conditions, dissimilar K_D estimations may result from multiple receptor subtypes being measured from, rather than the desired subtype, or that antagonist ligands have functional activity at the receptor themselves, rather than acting by simply competing for the agonist ligand. Moreover functional activity, such as inverse agonism and biased agonism, may lead to pathway specific effects. For example, Azzi *et al* (2003) were one of the first publications to report on biased β_2AR ligand, including ICI-118,551 which was suggested to act as an inverse agonist of cAMP and yet active ERK. Other known β_2AR antagonists, including carvedilol, propranolol and atenolol, have also been suggested to active ERK (Wisler *et al.*, 2007; Brunskole *et al.*, 2013), though results are difficult to reproduce in nuclear compartments (Cleveland *et al.*, 2018). Whilst equilibrium

conditions are required for estimations of antagonist K_D, binding equilibrium may be unable to be reached due to the signalling behaviour of the receptor complexes. For example, receptor trafficking and internalisation may limit the exposure of receptors to membrane impairment ligands over the time of the assay. Lastly, the ligand-receptor interaction could be more complex than a direct competitive relationship, for example, a study investigating antagonism at the β_1AR noted a number of ligands appear to bind the β_1AR at 2 sites rather than the simple orthosteric site model (Baker, *et al*, 2003)

4.4.5. Pre-clinical and clinical relevance for understanding antagonist binding kinetics.

As discussed above, antagonist K_D constants require an assumption of system equilibrium and, thus when not at equilibrium, estimates of antagonist affinity can be confounded, lacking translation into pre-clinical studies. A key example can be seen in the development of corticotropin-releasing factor 1 antagonists, where non-equilibrium conditions were used to determine affinity (Hoare, *et al.*, 2020). Hoare *et al.*, (2020) describe how such calculated affinities were shown to be overestimations and resulted in a lack of successful translation to *in vivo* studies – issues resolved through true estimates of antagonist binding affinities through the use of binding kinetics. Therefore, when system equilibrium is not determined, it is important to consider antagonist binding kinetics when determining valid estimations of GPCR antagonists. In addition to equilibrium dissociation constants, kinetic descriptors of antagonist binding are becoming more common within drug discovery settings where antagonist binding kinetics have been shown to be important in assessment of side-effect profiles (Kapur and Seeman, 2001), onset and duration of action (Dowling and Charlton, 2006; Mould *et al.*, 2014) and drug efficacy (Dorr *et al.*, 2005; Jacqmin, *et al*, 2008).

While the duration of action of a ligand has historically been the target in the design of clinically successful drugs (Kume, 2005; Vauquelin, 2010), the optimisation of antagonist kinetic binding parameters have provided improved inhibitory efficacy and may be more useful in generating compounds with a desired therapeutic profile (Dowling and Charlton, 2006; Behm *et al.*, 2010; Gatfield *et al.*, 2012; Sykes *et al.*, 2012, 2016). In many biological systems, an equilibrium between the antagonist, agonist and receptor may never reached – for example because of changes in stimulating ligand concentration (a synaptic neurotransmitter, or a cytokine burst during inflammation) are rapid and dynamic. These dynamics pose the risk that the effects of rapidly equilibrating antagonists

may be surmounted by bursts in stimulating messenger concentration during the disease process, limiting their inhibition. Developing ligands with slow off rates may preserve antagonism through insurmountability under these conditions, and thereby offer a route to improved therapeutic effect. The ability to functionally map the degree of insurmountable antagonism, in a single assay timecourse, indicates the potential benefit for inhibitor screening using GPCR NanoBiT assays in future.

4.5. Chapter Conclusions

Chapter 4 used NanoBiT complementation assays, established in *Chapter 3* to monitor the antagonist action of propranolol, ICI-118,551 and CGP12177 on the recruitment of effector proteins at β_2ARs. Each antagonist pre-treatment produced concentration dependent reductions in effector recruitment, and a Schild analysis style shift in a formoterol concentration response curve. A transition from insurmountable to surmountable mode of action was observed in the real time timecourse data as this system approached equilibrium for propranolol, whilst insurmountability was observed for ICI-118,551 and, to a greater extent, CGP-12177 at all timepoints. TR-FRET binding assays supported the correlation between slow off rate and insurmountability – for example CGP-12177, which presented as the most insurmountable antagonist, was shown to have a 9-fold and 3-fold slower dissociation rate constant, in comparison to propranolol and ICI-118,551, respectively. A kinetic operational model was applied to NanoBiT timecourse data of antagonism, to determine kinetic binding properties of each antagonist as well as a further estimate of affinity. The utility of this model was demonstrated in providing reasonable antagonist K_D estimates compared to binding and Schild analysis – from single agonist concentration data, which at endpoint, would yield only an IC_{50} value. However, k_{ON} and k_{OFF} rate constants were not estimated with a high degree of accuracy and differed from both TR-FRET binding and literature measurements. This suggests further developments of the kinetic operational model of antagonism are required to incorporate agonist binding kinetics and different signalling behaviours. A complete kinetic operational model, with a global fitting of full Schild analysis data sets, would be useful to improve functional kinetic measurements for the β_2AR and other GPCRs.

Chapter Five:

Determination of ligand binding kinetics at mini G or arrestin driven conformations of β_2ARs, using HiBiT trapped receptor-effector complexes.

5.1. Introduction

GPCR activation is typically a balance between two interfaces: ligand binding at the extracellular or transmembrane surface of the receptor and the intracellular binding of the receptor to a secondary effector protein, initiating intracellular signalling cascades. The data presented so far has used NanoBiT methodology to monitor the action of a range of βAR ligands to stimulate (*Chapter 3*) or inhibit (*Chapter 4*) receptor communication with example effectors, measuring the recruitment of β-arrestin2 or a mini Gαs protein. However ultimately this process is driven by agonist binding and the stabilisation of particular active conformations of the receptor that then engage signalling partners. Here we show how we can not only measure how a ligand binds a receptor population and the rate at which it binds and dissociates, but also investigate the influence on ligand affinity and binding kinetics in specific pre-coupled receptor-effector complexes.

5.1.1. Ligand Affinity and Efficacy

As described in *Chapter 1*, receptor signalling can be viewed a combination of drug and receptor binding (affinity) (D+R→DR) and activation (or intrinsic efficacy) (DR→DR*), as defined by Stephenson (1956). The affinity of a drug or ligand is defined by its ability to bind to a receptor and it's reciprocal, the equilibrium dissociation constant (K_D) is used to describe the concentration of drug or ligand required to occupy 50% of the receptor population. The manner in which a drug binds can provide structural information on how receptors can be activated and thus inform structure-activity relationships (SAR). Not only do binding affinity measurements provide information on target engagement, but can lead to improved safety profiles *in vivo* as selective compounds may be identified and thus few off target side effects (Baker, 2005, 2010). Once bound, an agonist drug can be described by its efficacy – the ability of the agonist-receptor complex to activate and produce a response through effector proteins such as G proteins.

5.1.2. The (Extended) Ternary Complex Model

The ternary complex model describes the interactions between GPCRs, their associated G protein and ligands (as discussed in *Chapter 1*). As extracellular signals, in the form of agonists, bind a GPCR, cognate heterotrimeric G proteins are recruited to the receptor and act as a site for nucleotide exchange, initiating a cascade of cellular signalling. The original ternary complex model (*Chapter 1*; *Figure 1. 7*) used a two-site model, based upon radioligand binding studies (De Lean, *et al*, 1980), which demonstrated shallow binding curves, i.e. with Hill

coefficients less than 1, which represented a heterogeneous receptor population (Park, *et al*, 2008). In both experimental radioligand binding data (Manglik, *et al*, 2017) and modelled binding data from the β_2AR (Kent, *et al*, 1980), it was demonstrated that upon the addition of Gαs protein or the removal of GTP, respectively, a biphasic binding curve was observed. The shallow biphasic binding curve revealed multiple states of the receptor conformations with a high or low affinity for agonists, demonstrating that G proteins of different activation states interact with GPCRs to induce conformational changes. In addition, agonist ligands may also shift the equilibrium in favour of the "high affinity" active state of the receptor, canonically to initiate GPCR activation and signalling, as they have a higher affinity (e.g. K_D high) for the active state of the G protein coupled conformation than the uncoupled receptor (e.g. K_D low). Moreover, inverse agonists shift the equilibrium toward, and have higher affinity for, the uncoupled inactive receptor state and thus reduce constitutive receptor activation. One way to consider efficacy is to compare the ratio between the high and low affinity states – with the higher the ratio, the higher efficacy agonist, as described by del Castillo and Katz, (1957). In addition, the active state of receptor may be adopted in the absence of G proteins (Sum, *et al*, 2002), suggesting the existence of the active state is an intrinsic property of the receptor (Rovati *et al.*, 2017) which can be promoted by agonist or effector binding. A number of studies provided evidence for the high and low agonist affinity states of the GPCRs. For example, in GPCR radioligand binding assays, agonist binding can be observed as two site under some assay conditions. Seifert *et al.*, (1999) demonstrate increased agonist affinity at the β_2 adrenoceptor in the presence of GDP, which can be disrupted by high GTP. The GTP disrupts the active RG* complex by promoting dissociation of the G protein heterotrimer. In addition, the high affinity conformation can be promoted by low sodium ion (Na^+) concentration, as Na+ is a negative allosteric modulator for several GPCRs (Pihlavisto *et al.*, 1998; Katritch *et al.*, 2014; Schiffmann and Gimpl, 2018).

As discussed in *Chapter 1*, the ternary complex model originally supported a two-state activation process for GPCRs (R→R*)(Ghanouni *et al.*, 2001; Vilardaga *et al.*, 2003, 2005; Banères *et al.*, 2005), yet further investigations suggested that the activation process may be more complex in some GPCRs, with receptor activation occurring through and stabilising multiple conformational states (Swaminath *et al.*, 2004, 2005; Yao *et al.*, 2006; Deupi and Kobilka, 2010; Manglik and Kobilka, 2014; Latorraca, *et al*, 2016) resulting in "extended" ternary complex models. The ability to switch between these multiple conformations may be

modulated by agonist efficacy, which at a molecular level can be defined as the agonist's ability to form active receptor conformation and engage G proteins (Hilger, *et al*, 2018b). Moreover, decreased agonist efficacy, as observed in partial agonists, is thought to increase the affinity of GDP at receptor-G protein complexes (Selley *et al.*, 1997; Seifert *et al.*, 1999; Roberts, *et al*, 2004; Zhang *et al.*, 2004; Gregorio *et al.*, 2017), which decreases rates of nucleotide exchange and subsequent cellular signalling.

There are good examples of isolating specific ternary complexes, supporting the idea that the agonist, receptor and effector act as a ternary complex model (see below; *5. 1. 5*), including isolating ligand high/low affinities for different conformations and co-operatively factors governing the allosteric interaction. Typically an "affinity" is measured for an agonist (a "macroscopic" affinity, which are quantified in *Chapter 3* and *Chapter 4*) which reflects contributions from the "individual" affinities of the receptor conformations present in the assay, which can depend on the assay conditions, including: the degree of coupling, expression of receptors and various other influencers. Similar considerations apply when measuring individual kinetic binding constants (k_{ON}, k_{OFF}) which typify the properties of the overall receptor population. A system to identify conformation specific binding constants would therefore be useful for deeper understanding of agonist mechanisms at GPCRs, as well as considering the nature of agonist selection between different receptor-effector complexes that might underlie some observations of ligand bias.

5.1.3. Relevance of Ligand Binding Kinetics

As discussed, equilibrium measurements of ligand affinities are used to describe the binding of a ligand at a receptor when the system is at equilibrium. The rates at which the ligand associates and dissociates from the receptor are known as the ligand binding kinetics (see *Chapter 1*) and provide important information beyond equilibrium measurements. For example, target residence time (reciprocal; k_{OFF}) is correlated with increased duration of action as increased receptor occupancy and activation promotes prolonged signalling (Copeland, 2010; J. Hothersall *et al.*, 2016). In addition, ligands of similar affinity but different k_{OFF} can provide different target engagement, due to prolonged receptor occupancy (Sykes *et al.*, 2012). It is also important to understand the kinetics of ligand binding when investigating receptor signalling, as equilibrium measurements of receptor signalling are directly driven by binding kinetics and can

provide hemi-equilibrium estimations of ligand potency and efficacy if taken too early (Klein Herenbrink *et al.*, 2016).

The equilibrium dissociation constant (K_D) is the ratio of the dissociation and association rates ($K_D = k_{ON}/k_{OFF}$; *Chapter 1*) and so variation in either rate can directly influence measured ligand affinity. Historically, it has been assumed that the k_{OFF} is the primary determinant of K_D and that slower dissociation rates are primarily determined by the strength of the ligand-receptor interactions (as described in *Chapter 1*; *1. 2. 1*). Pan *et al.*, (2013) highlight that the electrostatic interactions between a charged ligand a charged receptor impact both the association and dissociation rates. It is suggested that whilst k_{ON} is more sensitive to electrostatic attractions or repulsions, whilst the k_{OFF} is more greatly affected by short-range interactions, including hydrogen bonds, salt bridges and van der Waals contacts (Schreiber and Fersht, 1996; Fedosova, *et al,* 2002; Pan *et al.*, 2013). Moreover, the presence of water molecules at the extracellular surface of the receptor can further influence the binding kinetics, as water molecules can interrupt ligand-receptor hydrogen bonds and thus ligand-receptor hydrogen bonds shielded from the extracellular surface result in a more kinetically stable contact (Schmidtke *et al.*, 2011). The association rate has received less attention as a determined of K_D and it is often assumed that little difference in the rate of diffusion into the binding pocket for molecules of a similar molecular weight. However, there is now increasingly more evidence that the k_{ON} is just as, if not more, important than the k_{OFF}. Changes in the chemical structures of β_2 adrenoceptor ligands have been observed to alter ligand association rates and subsequent ligand affinity (Guo *et al.*, 2012; Sykes *et al.*, 2014b) and the ligand association rate is thought to be governed by diffusion, desolvation and rotational orientation of the ligand (Copeland, *et al*, 2006; Núñez, *et al*, 2012; Pan *et al.*, 2013). As suggested for the dissociation rate, physiochemical properties of the ligand are thought to influence the association rate. This is exemplified at the β_2AR, where Sykes *et al.*, (2014) concluded that drug association rates are enhanced by the membrane micro-environments. In theory, highly lipophilic drugs are thought to more easily displace energetically unstable water molecules from the binding site and thus increase the association rate (Sykes *et al.*, 2014b) at both GPCRs (Dror *et al.*, 2011) and other proteins (Schuetz *et al.*, 2018). Molecular weight has also been suggested to correlate with association rate, though this is thought to be receptor specific (Unett *et al.*, 2013; Wacker, *et al*, 2017). For receptor association Dror *et al.*, (2011) demonstrate that a key mechanism of drug entry and receptor association is dehydrations of both the receptor and the ligand – removing water

molecules to ensure formation of hydrogen bond contacts. The pathway of orthosteric ligands to the binding site is canonically through the extracellular vestibule of the GPCR (Dror *et al.*, 2011), however depending on the lipophilicity of the ligand other pathways may be available. For example, high lipophilicity of both muscarinic receptors and adrenoceptor ligands have been suggested to correlate with routes of binding site access through the membrane (Sykes *et al.*, 2012). This is more clear for some lipid GPCRs, such as free fatty acid (Lu *et al.*, 2017), purinergic (Zhang *et al.*, 2015) and cannabinoid (Shao *et al.*, 2016) receptors. Emtage *et al.*, (2016) discuss this method of membrane access to the canonical binding site at β adrenoceptors, identifying a possible "keyhole" between TM4 and TM5

5.1.4. Monitoring Ligand Binding

Traditional methods used to monitor ligand binding affinities and binding kinetics at GPCRs were conducted using radiolabelled ligands, based on pharmacophores with affinity for the receptor of interest (Insel and Stoolman, 1978; Bürgisser, *et al*, 1981; García-Sevilla, *et al*, 1981). In such assays, membranes on whole cells expressing the receptor of interest are prepared and incubated with a radioligand. Once the binding parameters of the radioligand have been established, the radioligand is competed against unlabelled ligands to obtain binding information about the latter. Radioligand binding assays have been used to identify high/low affinity states of GPCRs, isolated by the addition of G proteins or a G protein mimetic (Manglik, *et al*, 2017; Warne *et al.*, 2019) or the addition of GTP (DeVree *et al.*, 2016). Whilst radioligand binding studies are well established (Leifert *et al.*, 2009; Maguire, *et al*, 2012; Flanagan, 2016) and have been applied to study a range of GPCRs (Baker, 2010; Teitler *et al.*, 2010; Niessen *et al.*, 2012), there are disadvantages to the methodology including safety issues associated with the use of radioactive materials. Secondly, due to experimental limitations early timepoints cannot be obtained – which are vital when estimating binding kinetics of both labelled and, to a greater extent, unlabelled compounds. Moreover temporal resolution is further impacted by the need to separate out radioligand bound to the receptor and free radioligand, which requires filtration of each assay well – decreasing the ability to determine binding at early timepoints. There are further kinetic assays such as scintillation proximity assay (SPA) assays, which does not require filtration of bound/free radioligand (Xia *et al.*, 2016). Whilst this increases the temporal resolution and ability to obtain early timepoints, SPA are

less sensitive in acquiring real-time measurements compared to fluorescent ligand approaches.

In more recent years, fluorescently labelled molecules have been employed as the tracer ligand and used to monitor the interactions binding kinetics of unlabelled ligands at GPCRs. Fluorescent ligands are safer, both in handling and waste management, and have been designed to target a wide range of receptors (Ciruela, *et al*, 2014; Vernall, *et al*, 2014). Measurements of fluorescent ligand binding can be determined by using confocal microscopy (May *et al.*, 2010; Gherbi *et al.*, 2015), however temporal resolution to monitor binding of the fluorescent ligand is low and it is a low throughput method. To overcome such issues, resonance energy transfer (RET) methods have been developed whereby a donor energy source tagged to the receptor is used to excite the fluorescently labelled tracer ligand. Bioluminescence and fluorescence (also known as Förster) RET (BRET and FRET assays, respectively) assays have been applied to monitor binding of fluorescent and unlabelled ligands at both GPCRs (Ilien *et al.*, 2003; Leyris *et al.*, 2011; Fernández-Dueñas *et al.*, 2012; Schiele, *et al*, 2015; Stoddart *et al.*, 2015; Christiansen *et al.*, 2016; Klein Herenbrink *et al.*, 2016; Stoddart, *et al*, 2018) and receptor tyrosine kinases (Peach *et al.*, 2018). Whilst FRET assays utilise fluorescently labelled receptors, which are activated by an external light source such as a laser, BRET assays use receptors tagged with luciferase proteins, such as the small, bright luciferase NanoLuc (Hall *et al.*, 2012). In addition to improved safety and increased throughput, FRET and BRET assays are dependent upon the proximity between donor and acceptor species being less than 10 nm (100 Å) for energy transfer and thus provides a highly specific report of ligand binding.

5.1.5. Isolating Effector Driven GPCR Conformations

Whilst the technology by which ligand-receptor binding is monitored has progressed significantly, measurements of drug binding at GPCRs are generally taken from a mixed population of receptors, existing in multiple conformations (i.e. low/high affinity conformation) due to the dynamic nature of GPCRs. GPCRs are known to signal through multiple intracellular effectors, such as G proteins and β-arrestins, which have been suggested to pre-couple to the receptor (Tian, *et al.,* (1994); Shea and Linderman, 1997; Nobles, *et al*, 2005; Oldham and Hamm, 2008) and influence drug binding (Warne *et al.*, 2019; Lee *et al.*, 2020). At equilibrium, an increase in agonist affinity at the “high affinity” has been observed (as previously above; further discussed in *Chapter 1*), in the presence of G proteins,

a G protein mimetic, GDP and GTPγS (Seife*rt et al*, 1999; Rasmussen, *et al*, 2011a; Steyaert and Kobilka, 2011; Nehmé *et al*, 2017; Warne *et al*, 2019). For example, Warne *et al.*, (2019) have demonstrated that binding of the synthetically derived mini Gαs protein at the β_1AR can increase the affinity for β_1AR agonists, such as isoprenaline and salbutamol. This is thought to result from the receptor-mini Gαs complex adopting the alternative "active" high affinity conformation. Active and inactive conformations of the β_2AR have also been identified through crystal studies stabilised by agonist, antagonists and nanobodies 80 (Nb80) and 6B9 (Nb6B9), with Nb80 and Nb6B9 designed to stabilise the active conformation of the receptor (Rasmussen, C*hoi, et al*, 2011b; Rasmussen, DeVree, *et al*, 2011; Rosenbaum *et al*, 2011; Ring *et al*, 2013), though it is likely that receptors exist in a range of conformations. Whilst such studies are beginning to provide snap-shot information on the relationship between high affinity GPCR conformations and ligand binding there is limited information on how this high affinity conformation can affect the kinetics of ligand binding. To investigate the influence of effector binding on ligand-receptor interactions, single populations of receptor conformations must be isolated.

As demonstrated in *Chapter 3* and *Chapter 4*, NanoBiT complementation assays use low affinity fragments of the NanoLuc luciferase enzyme to determine cellular signalling at βARs. The low affinity NanoBiT fragments were required, to avoid interfering with the natural dynamics of the appended proteins. However, when the NanoBiT split-luciferase assay was developed further, variants of the 11 amino acid fragment were synthesised and demonstrated increased affinity for the LgBiT fragment compared to the SmBiT fragment and even the native peptide. The fragment which demonstrated the greatest affinity is known as "HiBiT" (amino acid sequence: VSGWRLFKKIS), which demonstrated an affinity of 700 pM for the complementary LgBiT fragment (Dixon *et al.*, 2016). The LgBiT-HiBiT system has been used in literature to study protein expression (Oh-hashi *et al.*, 2017) and GPCR receptor internalisation (Boursier *et al.*, 2020; Soave, *et al.*, 2020) on the basis that it stabilises the protein complexes under study. The high affinity of the LgBiT and HiBiT fragments for each other has also been used in structural biology, whereby Duan *et al.*, (2020) used the fragments to tether the Gβγ subunit to the C-terminal of the vasoactive intestinal polypeptide receptor and image the complex using cryo-electron microscopy – highlighting its ability to stabilise complexes.

Here, we used high affinity luciferase fragment complementation technology (HiBiT) to stabilise conformations of the β_2AR, bound to β-arrestin2, a

synthetic ‘mini’ Gαs protein or unbound to an effector. This was conducted by co-expressing (1) β_2AR-LgBiT and (2) either β-arrestin2 or Mini Gαs with an N-terminal HiBiT tag. Apparent binding affinities of a fluorescently labelled propranolol (BODIPY-FL-PEG8-(S)-Propranolol) were then obtained for these complexes, via time-resolved fluorescence energy transfer (TR-FRET) assays. To further isolate receptor populations bound to either β-arrestin2, mini Gαs protein or unbound to an effector, the luminescence from the complemented NanoBiT fragment luciferase activity was used as a transmembrane donor in novel transmembrane saturation bioluminescence resonance energy transfer (TM-BRET) assays.

5.2. Chapter Aims

The work completed in Chapter Five: Results III, aimed to:

(1) Produce HEK293T cell lines, co-expressing (1) β_2AR-LgBiT and (2) either β-arrestin2 or mini Gαs protein with an N-terminal HiBiT tag.

(2) Describe kinetic and equilibrium agonist binding properties in membranes where receptor-effector complexes stabilised by HiBiT, using time-resolved fluorescence resonance energy transfer (TR-FRET) assays.

(3) Develop and optimise novel transmembrane bioluminescence resonance energy transfer assays (TM-BRET).

(4) Use TM-BRET to quantify ligand binding at ligand-receptor-effector bound complexes, in which the binding signal is directly attributed to the molecular receptor-effector complex.

5.3. Results

5.3.1. Dual receptor-HiBiT effector expression cell line development.

Following consecutive transfection of either (1) HiBiT-βarrestin2 or HiBiT-Mini Gαs and (2) SNAP-β_2AR-LgBiT construct cDNA in HEK293T cells (which will be referred to as β_2AR/HiBiT-βarrestin2 and β_2AR/HiBiT-mini Gαs protein), cells were selected for dual DNA expression using antibiotics and these "mixed population cell lines" were then examined for cell surface receptor expression. In addition, for initial assessment of receptor function and localisation, cells were treated with either vehicle or 10 μM isoprenaline to monitor receptor internalisation. Cells expressing SNAP-β_2AR-LgBiT at the plasma membrane were labelled with a membrane impermanent fluorophore (SNAP-surface AF488) for 30 minutes, following which the cells were incubated with either vehicle or 10 μM isoprenaline for 1 hour before fixation with paraformaldehyde and imaging with an IX Ultra imaging plate-reader. Under vehicle conditions, both cell lines displayed labelled SNAP-β_2AR-LgBiT, localised to both the plasma membrane as well as accumulated in intracellular compartments (*Figure 5. 1*). β_2AR/HiBiT-βarrestin2 cells incubated with 10 μM isoprenaline for 1 hour internalised, translocating from the plasma membrane, whilst isoprenaline stimulated β_2AR/HiBiT-Mini Gαs protein cells showed a receptor distribution comparable to vehicle (*Figure 5. 1*).

The high affinity "HiBiT" cell lines (β_2AR/HiBiT-βarrestin2 and β_2AR/SmBiT-Mini Gαs), as well as low affinity "SmBiT" cell lines established in *Chapter 3* (β_2AR/SmBiT-βarrestin2 and β_2AR/SmBiT-Mini Gαs), were treated with 10 μM isoprenaline, 10 μM ICI-118,551 or vehicle for 31 minutes to determine cell-based interactions of NanoBiT labelled proteins by monitoring complemented luciferase activity (*Figure 5. 2*). Basal luminescence of HiBiT cell lines were 166-fold and 196-fold greater ($P<0.01$, Student's t-test) than comparable SmBiT cell lines, for β-arrestin2 and mini Gαs protein cell lines, respectively. As previously observed (*Chapter 3*), isoprenaline treatment of SmBiT cell lines increased luminescence response by 11.3-fold and 4.2-fold compared to vehicle, in β_2AR/SmBiT-βarrestin2 or β_2AR/SmBiT-Mini Gαs cells, respectively ($P=0.0019$; one way ANOVA; Tukey's multiple comparison's post-hoc test). ICI-118,551 produced a concentration dependent reduction in luminescence in β_2AR/SmBiT-βarrestin2, but not β_2AR/SmBiT-Mini Gαs cells (*Chapter 3*) (*Figure 3. 14; Figure 3. 15; Table 3. 5*). However, treatment of either HiBiT cell line with either 10 μM isoprenaline or 10 μM ICI-118,551 stimulated no increase or decrease in luminescence, respectively, compared to vehicle (*Figure 5. 2*).

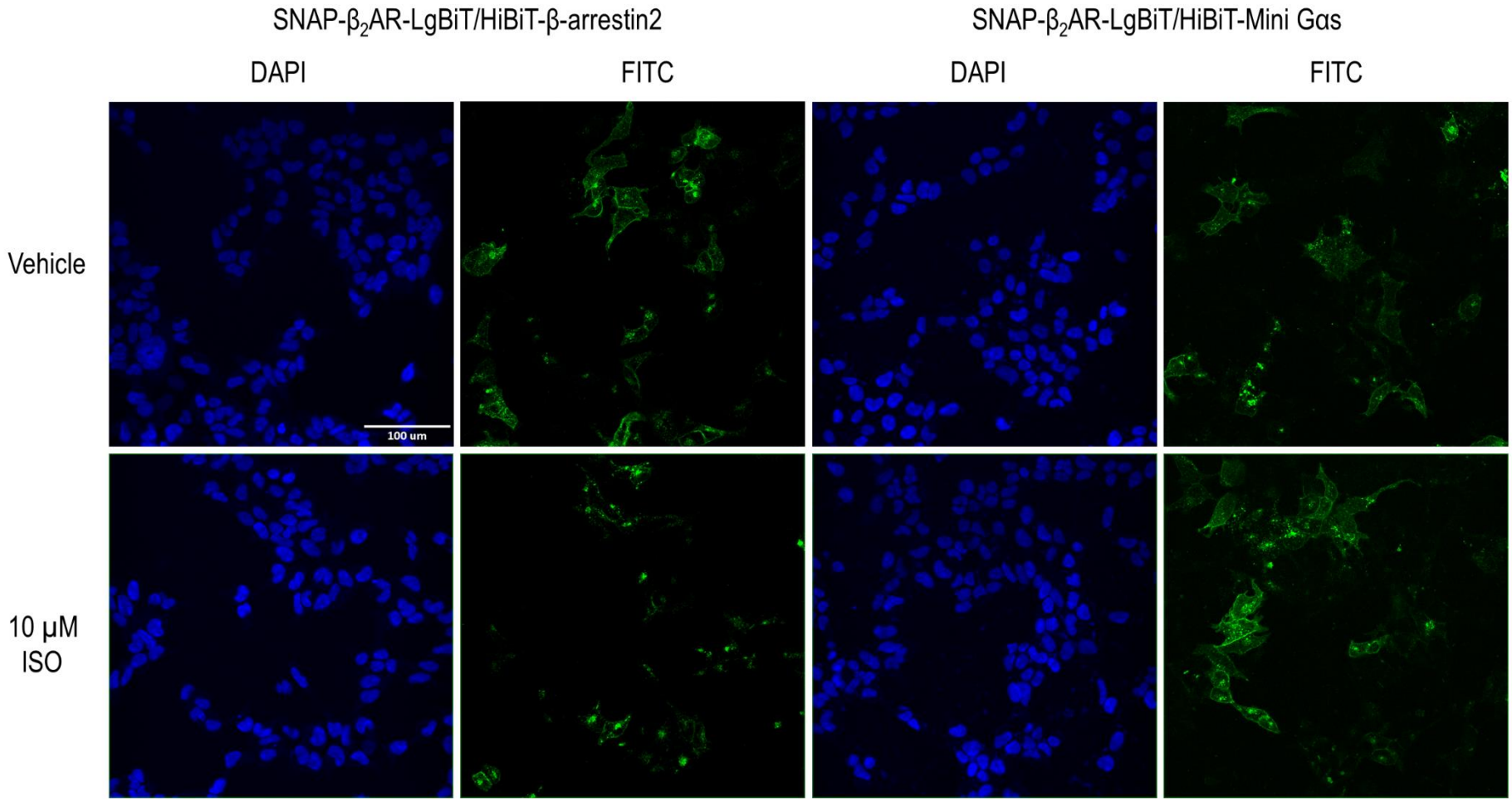

Figure 5. 1 Internalisation of the SNAP-tagged β_2AR-LgBiT, in cells expressing SNAP-β_2AR-LgBiT/HiBiT-βarrestin2 and SNAP-β_2AR-LgBiT/HiBiT-Mini Gαs protein DNAs, in response to 1 hour vehicle or 10 µM isoprenaline stimulation. *Cells were first pre-labelled with cell-impermeable AF488-SNAP reagent for 30 minutes.,. Cell nuclei were labelled with Hoechst stain (H33342), before cell fixation. Representative images of each treatment show cell nuclei, imaged using DAPI filter (blue) and AF488-SNAP-β_2AR-LgBiT receptors, imaged using FITC filter (green), with an overlay of each imaged shown.*

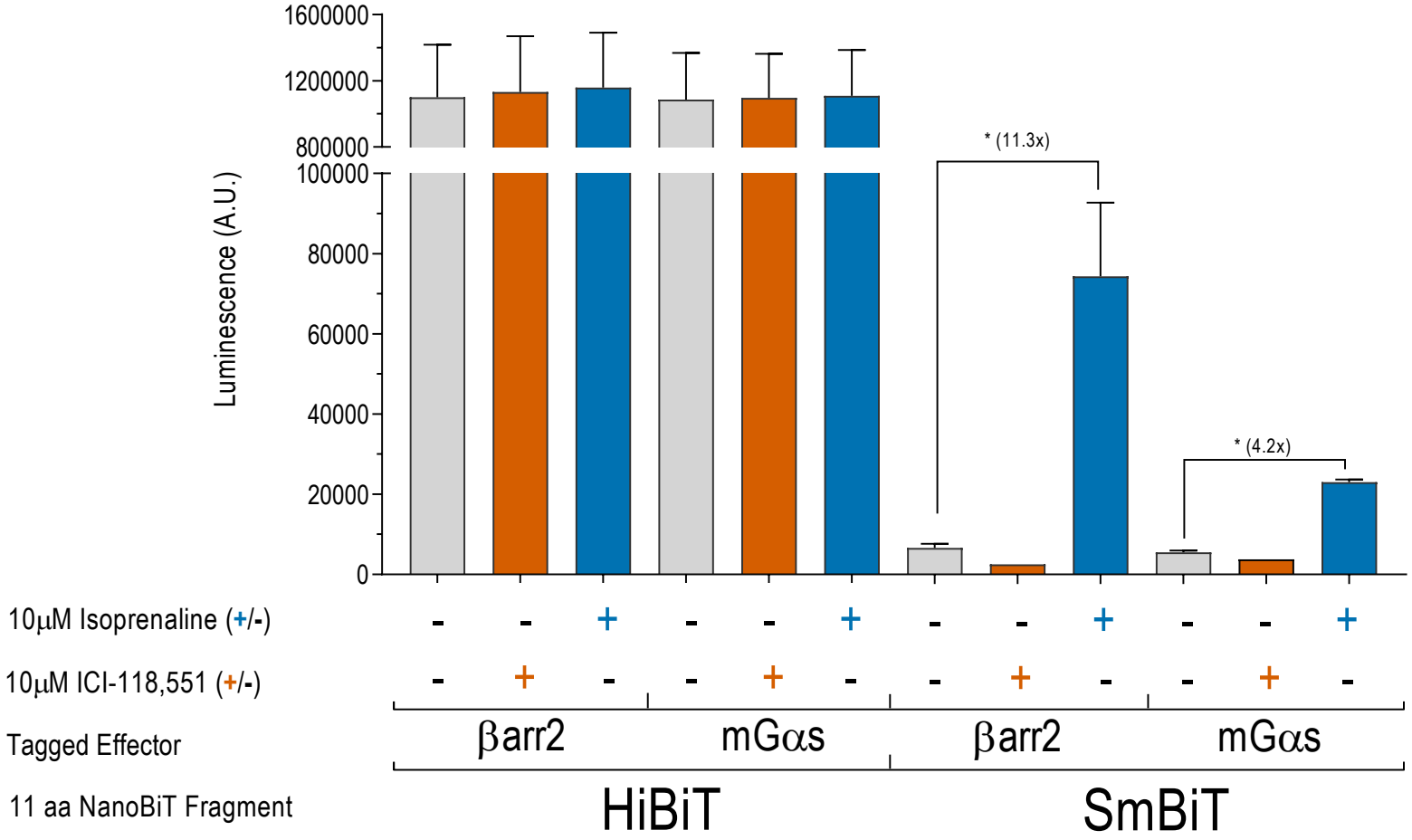

Figure 5. 2 Basal and ligand stimulated luciferase activity from complemented NanoBiT fragments in cells co-expressing SNAP-β$_2$AR-LgBiT and βarrestin2 and Mini Gαs N-terminally tagged with either HiBiT or SmBiT. *Cellular luciferase responses of HiBiT or SmBiT complementation systems upon treatment with vehicle, 10 μM isoprenaline or 10 μM ICI-118,551. Fold change of luminescence shown between vehicle and isoprenaline treated cells in the SmBiT system. Column data pooled from raw luminescence counts in individual experiments (n=3-5), each conducted in duplicate. * P<0.01 vehicle versus isoprenaline data groups, one way ANOVA, Tukey's multiple comparison's post-hoc test.*

5.3.2. Determination of the association kinetics of BODIPY-FL-PEG8-(S)-Propranolol using TR-FRET in HiBiT β_2AR / effector membranes

Cells expressing either (1) SNAP-β_2AR-LgBiT alone, β_2AR/HiBiT-β-arrestin2 or (3) β_2AR/HiBiT-mini Gαs protein were labelled with terbium and membranes prepared and used in TR-FRET assays to determine the association kinetics of BODIPY-FL-PEG8-(S)-Propranolol and unlabelled ligands (as previously described; *Chapter 4*)(*Figure 5. 3*).

In both β_2AR/HiBiT-β-arrestin2 and β_2AR/HiBiT-mini Gαs protein membrane preparations, specific BODIPY-FL-PEG8-(S)-Propranolol association was observed (*Figure 5. 3. a - c*), with a linear relationship between the observed association rate constant (k_{obs}) and tracer concentration (*Figure 5. 4*). As previously discussed (*Chapter 2* and *Chapter 3*), this relationship is expected for tracer binding to a single site homogeneous receptor population.

A global model of single site association kinetics was therefore applied to the data at different tracer concentrations to derive the k_{ON} and k_{OFF} of BODIPY-FL-PEG8-(S)-Propranolol (*Methods 2.8.5.2*), and resultant equilibrium dissociation constant quantified by k_{OFF}/k_{ON} (*Figure 5. 5*; *Table 5. 1*). Each kinetic binding parameter (k_{ON}, k_{OFF} and the resultant kinetically derived K_D) was shown to be comparable between SNAP-β_2AR-LgBiT, β_2AR/HiBiT-β-arrestin2 and β_2AR/HiBiT-mini Gαs cell lines, as determined by One-way ANOVA, with Tukey's multiple comparisons test ($P>0.05$) (*Figure 5. 5*; *Table 5. 1*) and comparable with previously established kinetic parameters of BODIPY-FL-PEG8-(S)-Propranolol (*Chapter 4*; *Figure 4.9*; *Table 4.2*) as determined by One-way ANOVA, with Tukey's multiple comparisons test ($P>0.05$).

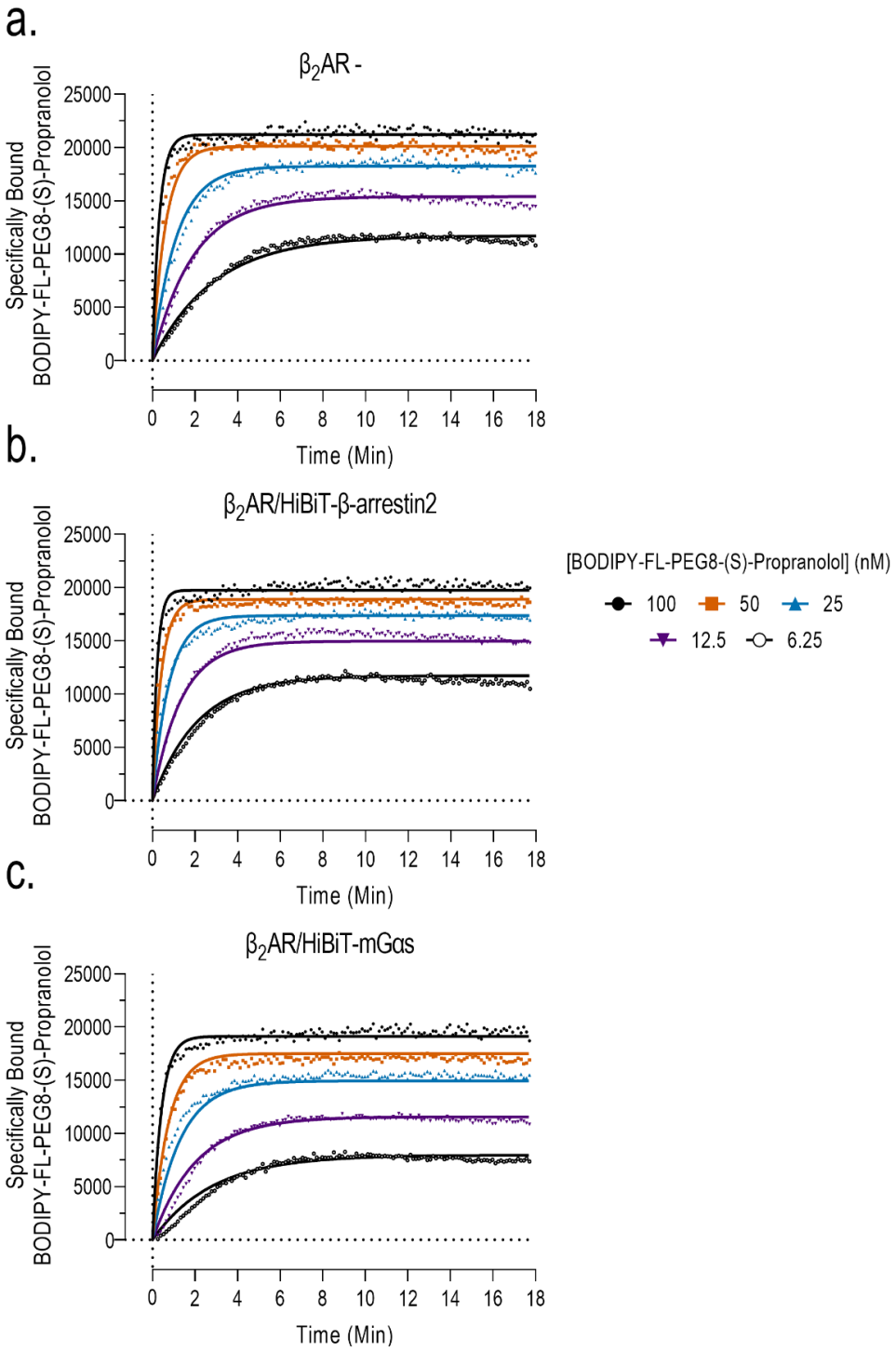

Figure 5. 3 Association binding kinetics of BODIPY-FL-PEG8-(S)-Propranolol at membranes prepared from HEK293T cells, stably expressing terbium-labelled SNAP-β2AR-LgBiT ± HiBiT labelled β-arrestin2 or mini Gαs DNA.*. Membranes were incubated with increasing concentrations of BODIPY-FL-PEG8-(S)-Propranolol, with 10 μM ICI-118,551 used to determine non-specific binding at each concentration of BODIPY-FL-PEG8-(S)-Propranolol. Dual emission wavelengths (490nm & 520nm) were monitored for 18 minutes and binding was represented by a ratio of TR-FRET binding (520/490*10,000). Data are from representative experiment, fitted to a global model of association kinetics.*

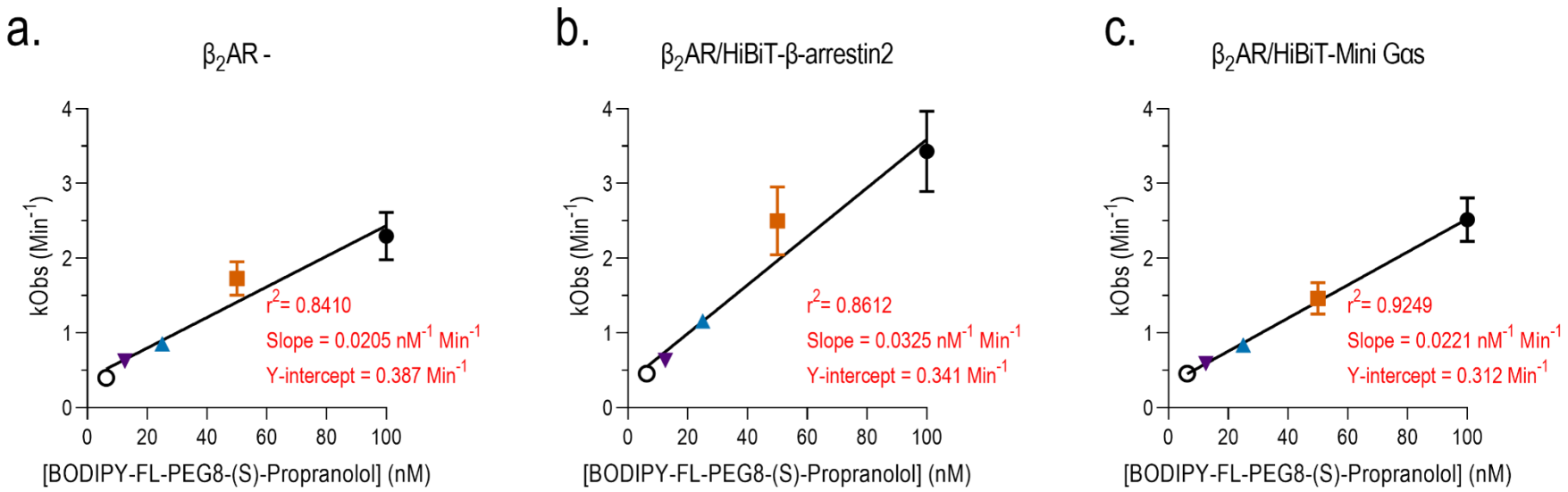

Figure 5. 4 The linear relationship between observed association rate constant (kobs) and tracer concentration, in TR-FRET binding assays using membranes expressing SNAP-β_2AR-LgBiT alone (a.) ± co-expression HiBiT labelled β-arrestin2 (b.) or mini Gαs DNA (c.). *The association rate constant (k_{obs}; Min^{-1}) at each concentration of BODIPY-FL-PEG8-(S)-Propranolol was calculated by individual one phase association fits to the data, and plotted against concentration of BODIPY-FL-PEG8-(S)-Propranolol, with the linear regression determined and goodness of fit defined by r^2 statistic, with slope and y-intercept quoted. Data points represent pooled kObs rates from 3 independent experiments, conducted in singlet.*

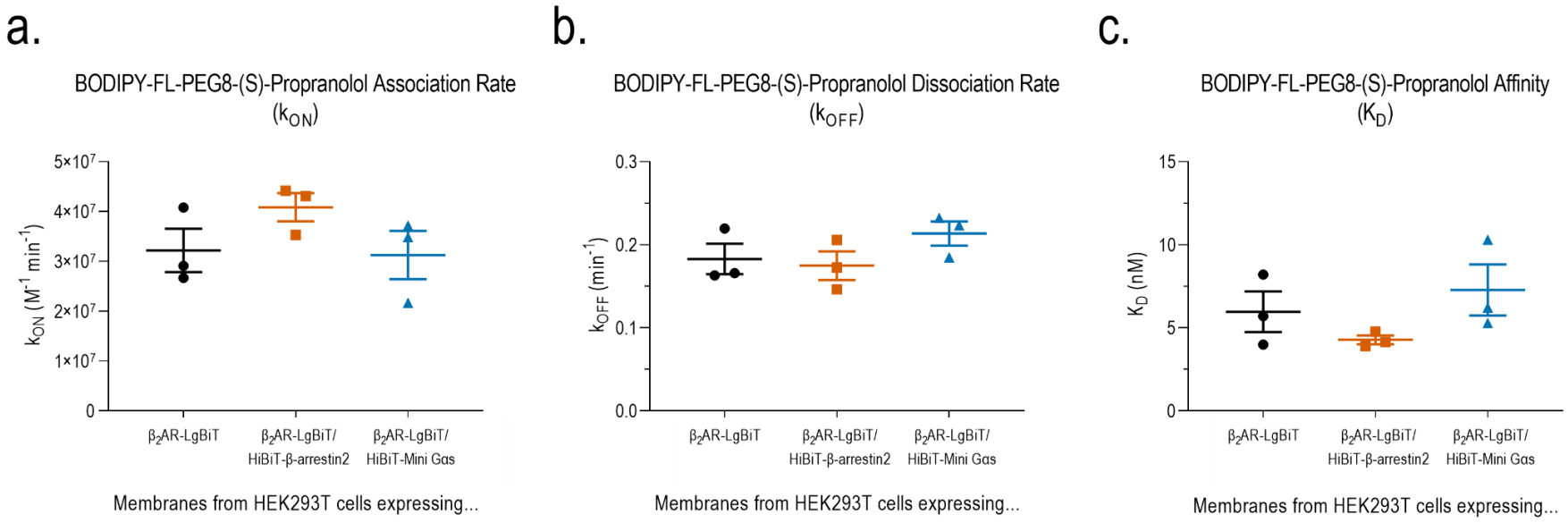

Figure 5. 5 Pooled association rate (k_{ON}) (a.), dissociation rate constants (k_{OFF}) (b.) and kinetically described equilibrium constants (K_D) (c.) of BODIPY-FL-PEG8- (S)-Propranolol derived in TR-FRET binding assays using membranes expressing SNAP-β_2AR-LgBiT alone ± co-expressed HiBiT labelled β-arrestin2 (b.) or mini Gαs DNA (c.). *Pooled rate and equilibrium constants for BODIPY-FL-PEG8-(S)-Propranolol were from 3 independent experiments, conducted in singlet. Data points represent mean ± S.E.M., with each replicate displayed.*

	k_{ON} ($M^{-1}min^{-1}$)	k_{OFF} (min^{-1})	K_D (nM)	n
β_2AR-LgBiT	*3.22 ± 0.44 x10^7*	*0.183 ± 0.018*	*5.97 ± 1.22*	*3*
β_2AR-LgBiT/HiBiT-β-arrestin2	*4.09 ± 0.28 x10^7*	*0.175 ± 0.017*	*4.28 ± 0.26*	*3*
β_2AR-LgBiT/HiBiT-Mini Gαs	*3.13 ± 0.49 x10^7*	*0.214 ± 0.015*	*7.28 ± 1.54*	*3*

Table 5. 1 Summary of BODIPY-FL-PEG8-(S)-Propranolol binding properties from membranes prepared from HEK293T cells stably expressing terbium-labelled SNAP-β_2AR-LgBiT ± HiBiT labelled β-arrestin2 or mini Gαs DNA. *Kinetic binding parameters, and kinetically derived K_D values of BODIPY-FL-PEG8-(S)-Propranolol were estimated from global models of association (Figure 5. 3) and summarised in Figure 5. 5. Pooled data are mean ± S.E.M. from 3 independent experimental replicates.*

5.3.3. Estimation of the equilibrium binding constants for the unlabelled β_2AR ligands in membranes derived from the HiBiT stabilised receptor-effector cell lines

To determine the binding affinities of unlabelled βAR ligands, competition binding assays were conducted using each membrane preparation. Here, increasing concentrations of each unlabelled ligand were competed against a fixed concentration of BODIPY-FL-PEG8-(S)-Propranolol (10 nM) for 20 minutes 37°C to complement cell-based NanoBiT signalling assays (*Chapter 3* & *Chapter 4*) and human physiological temperature.

All unlabelled ligands fully inhibited binding of BODIPY-FL-PEG8-(S)-Propranolol in a concentration dependent manner, producing IC_{50} competition binding curves (*Figure 5. 6*). Using the BODIPY-FL-PEG8-(S)-Propranolol affinity constants (K_D), obtained in kinetic association binding TR-FRET assays (*Figure 5. 3*; *Figure 5. 5. c*; *Table 5. 1*), the IC50 of each unlabelled ligand was converted to pKi values, using the Cheng-Prusoff equation which assumes competitive binding to a single site (*Methods*; *Equation 2. 23*).

The order of affinity was consistent between membranes from HEK293T β_2AR-LgiBiT cells and β_2AR/HiBiT-β-arrestin2 and β_2AR/HiBiT-Mini Gαs protein cells, as described by pK_i values: propranolol>ICI-118,551=salmeterol> formoterol>isoprenaline=salbutamol (*Table 5. 2*). Hill slopes of competition binding curves ranged between 0.75 and 1.28, with no Hill slope significantly less than 1 (*Table 5. 2*).

Equilibrium binding constants of unlabelled ligands were not significantly different between the β_2AR/HiBiT-effector cell lines and control β_2AR-LgBiT membrane preparations, with the greatest mean difference in affinity being 1.7-fold increase in the pK_i of propranolol in β_2AR-LgBiT membranes, compared with that of β_2AR/HiBiT-mini Gαs protein membranes (*Table 5. 2*).

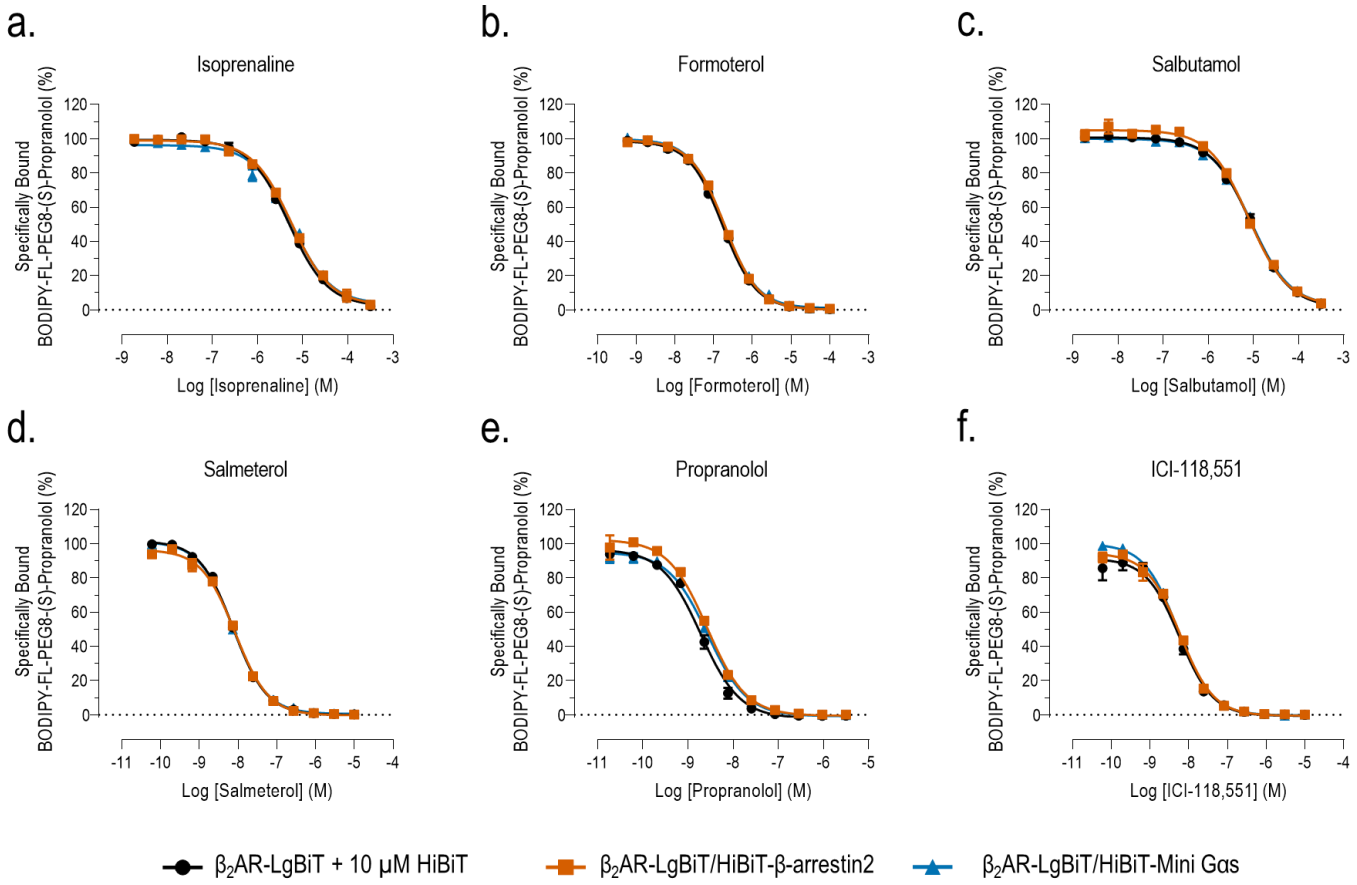

Figure 5. 6 TR-FRET competition binding assays for unlabelled β_2AR ligands, from membranes prepared from HEK293T cells stably expressed terbium-labelled SNAP-β_2AR-LgBiT alone (black) ± co-expressed HiBiT labelled β-arrestin2 (orange) or mini Gαs (blue) DNA. *Competition binding between 10 nM BODIPY-FL-PEG8-propranolol and increasing concentrations of β_2AR ligands ((a.) isoprenaline; (b.) formoterol; (c.) salbutamol; (d.) salmeterol; (e.) propranolol and (f.) ICI-118,551), supplemented with 100 μM GppNHp. Control SNAP-β_2AR-LgBiT membranes were supplemented with 10 μM HiBiT peptide. End point data taken after 18 minute incubation at 37°C. NSB quantified using 10μM ICI-118,551. Data points represent mean ± S.E.M., performed in duplicate (n=3).*

Ligand	Cell Line	pK_i (M)	Hill Slope	n
Isoprenaline	β_2AR -	5.68 ± 0.06	0.90 ± 0.04	4
	β_2AR/HiBiT-β-arrestin2	5.72 ± 0.05	0.87 ± 0.02	4
	β_2AR/HiBiT-Mini Gαs Protein	5.53 ± 0.09	0.75 ± 0.06	4
Formoterol	β_2AR -	7.25 ± 0.05	0.96 ± 0.02	4
	β_2AR/HiBiT-β-arrestin2	7.30 ± 0.06	1.04 ± 0.03	4
	β_2AR/HiBiT-Mini Gαs Protein	7.15 ± 0.04	0.94 ± 0.04	4
Salmeterol	β_2AR -	8.56 ± 0.01	1.09 ± 0.03	4
	β_2AR/HiBiT-β-arrestin2	8.63 ± 0.03	1.09 ± 0.03	4
	β_2AR/HiBiT-Mini Gαs Protein	8.47 ± 0.04	1.08 ± 0.03	4
Salbutamol	β_2AR -	5.50 ± 0.02	0.93 ± 0.01	4
	β_2AR/HiBiT-β-arrestin2	5.64 ± 0.04	1.00 ± 0.05	4
	β_2AR/HiBiT-Mini Gαs Protein	5.48 ± 0.06	0.90 ± 0.04	4
Propranolol	β_2AR -	9.18 ± 0.03	1.28 ± 0.07	4
	β_2AR/HiBiT-β-arrestin2	9.12 ± 0.06	1.17 ± 0.05	4
	β_2AR/HiBiT-Mini Gαs Protein	8.95 ± 0.04	1.18 ± 0.08	4
ICI-118,551	β_2AR -	8.74 ± 0.09	1.28 ± 0.13	4
	β_2AR/HiBiT-β-arrestin2	8.81 ± 0.06	1.11 ± 0.03	4
	β_2AR/HiBiT-Mini Gαs Protein	8.69 ± 0.03	1.01 ± 0.02	4

Table 5. 2 Summary of ligand equilibrium dissociation constants of unlabelled β_2AR agonists, using TR-FRET binding assays from membranes prepared from HEK293T cells stably expressing terbium-labelled SNAP-β_2AR-LgBiT ± co-expressed HiBiT labelled β-arrestin2 or mini Gαs DNA. pIC50 values obtained from competition TR-FRET assays (*Figure 5.6*) were converted to pKi values, describing the affinities of unlabelled ligands at β_2AR-LgBiT receptors, ± co-expression HiBiT labelled β-arrestin2 or mini Gαs DNA. Data represent pooled pKi values, as mean ± S.E.M., from 4 individual experiments, conducted in duplicate.

5.3.4. Use of novel TM-BRET assays to monitor the binding of a fluorescent propranolol

To isolate measures of ligand binding from the individual receptor-effector populations, membranes were prepared from SNAP-β_2AR-LgBiT/HiBiT-effector cell lines, or membranes prepared from SNAP-β_2AR-LgBiT cell lines were supplemented with 10 μM exogenously added HiBiT peptide for 25 minutes prior to the assay. For TM-BRET assays, terbium labelling was not required as donor luminescence resulted from complemented NanoBiT fragments. Membrane or membrane/peptide preparations were then applied in a fluorescent ligand binding BRET assay, where the luminescence from the complemented NanoBiT luciferase enzyme acted as the transmembrane donor emission (rather than in TR-FRET, the Terbium labelled N terminal SNAP tag), as illustrated in schematic representations of transmembrane BRET (*Figure 5. 7. a.– c.*).

Saturation binding assays measured the BRET response when incubating each membrane or membrane/peptide preparation at increasing concentrations of BODIPY-FL-PEG8-(S)-Propranolol, in the presence and absence of the unlabelled competitor (10 μM ICI-118,551) to determine total and non-specific binding, respectively (*Figure 5. 7. a.– c.*).

Following a 25 minute incubation, total binding of BODIPY-FL-PEG8-(S)-Propranolol was saturable when using SNAP-β_2AR-LgBiT+10 μM HiBiT, β_2AR/HiBiT-β-arrestin2 and SNAP-β_2AR-LgBiT/HiBiT-mini Gαs membrane preparations (*Figure 5. 7. a.– c.*). Whilst levels of non-specific binding were linear in relation to BODIPY-FL-PEG8-(S)-Propranolol concentration, the level of non-specific binding at each tracer concentration was relatively high when compared to measures of BODIPY-FL-PEG8-(S)-Propranolol binding in TR-FRET saturation assays at SNAP-β_2AR-LgBiT constructs (*Chapter 3*; *Figure 3. 19. a.*).

Equilibrium dissociation constants of BODIPY-FL-PEG8-(S)-Propranolol derived from TM-BRET assays, demonstrated BODIPY-FL-PEG8-(S)-Propranolol bound with nanomolar affinity at each membrane preparation (*Figure 5. 8*; *Table 5. 3)*.

The K_D values of BODIPY-FL-PEG8-(S)-Propranolol was shown to be greater in SNAP-β_2AR-LgBiT/HiBiT-β-arrestin2 (2.21-fold; $P<0.05$, One-way ANOVA, with post-hoc Tukey's multiple comparisons test) and SNAP-β_2AR-LgBiT/HiBiT-mini Gαs (2.75-fold; $P<0.01$, One-way ANOVA, with post-hoc Tukey's

multiple comparisons test), compared with SNAP-β_2AR-LgBiT membranes + 10 µM HiBiT peptide (*Figure 5. 8*). The K_D values of BODIPY-FL-PEG8-(S)-Propranolol obtained in TR-FRET assays (*Table 5. 1*), were most similar to values obtained in TM-BRET assays from β_2AR-LgBiT membranes + 10 µM HiBiT peptide (*Table 5. 3*).

To confirm the selectivity of TM-BRET, saturation binding assays were repeated using a non-β_2AR selective fluorescent ligand with similar excitation/emission properties, known as "Green-CXCL12". Green-CXCL12 was shown to bind at the human chemokine receptor 4 (CXCR4) previously (Caspar., 2019). In each saturation binding assay, in either β_2AR-LgBiT+10 µM HiBiT or β_2AR/HiBiT-effector membrane preparations, similar levels of total and non-specific binding were observed at all Green-CXCL12 concentrations and linear correlation was observed between Green-CXCL12 and BRET ratio, in both total and non-specific binding (*Figure 5. 9*).

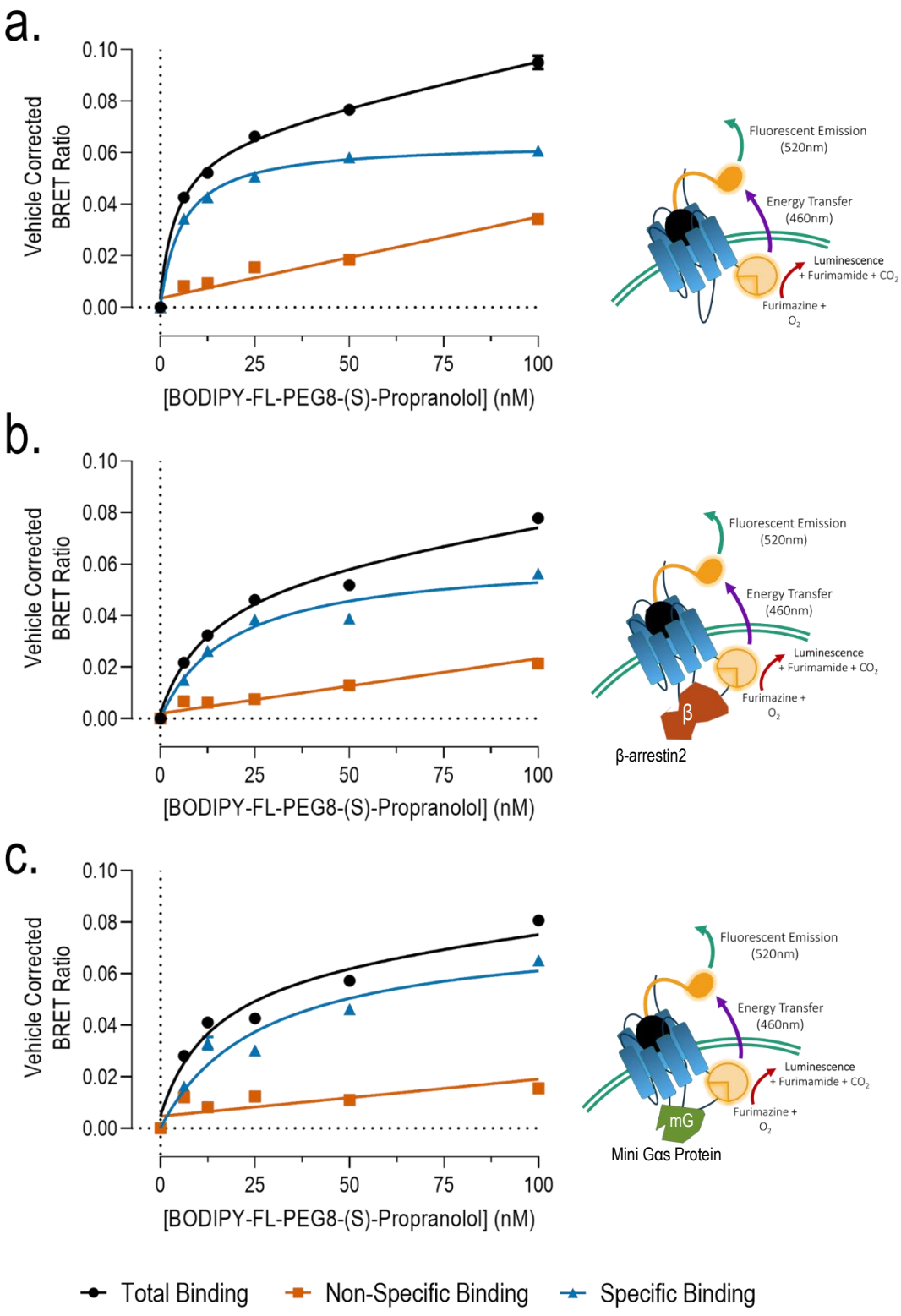

Figure 5. 7 TM-BRET saturation binding assays for BODIPY-FL-PEG8-(S)-Propranolol, from membranes prepared from cells expressing SNAP-β2AR-LgBiT, with either 10 μM HiBiT peptide (a.) or ± co-expressed HiBiT labelled β-arrestin2 (b.) or mini Gαs (c.) DNA. *Total, non-specifc and specific binding of BODIPY-FL-PEG8-(S)-Propranolol was pooled from 4-5 independent experiments, conducted in duplicate. Data points represent mean ± S.E.M..*

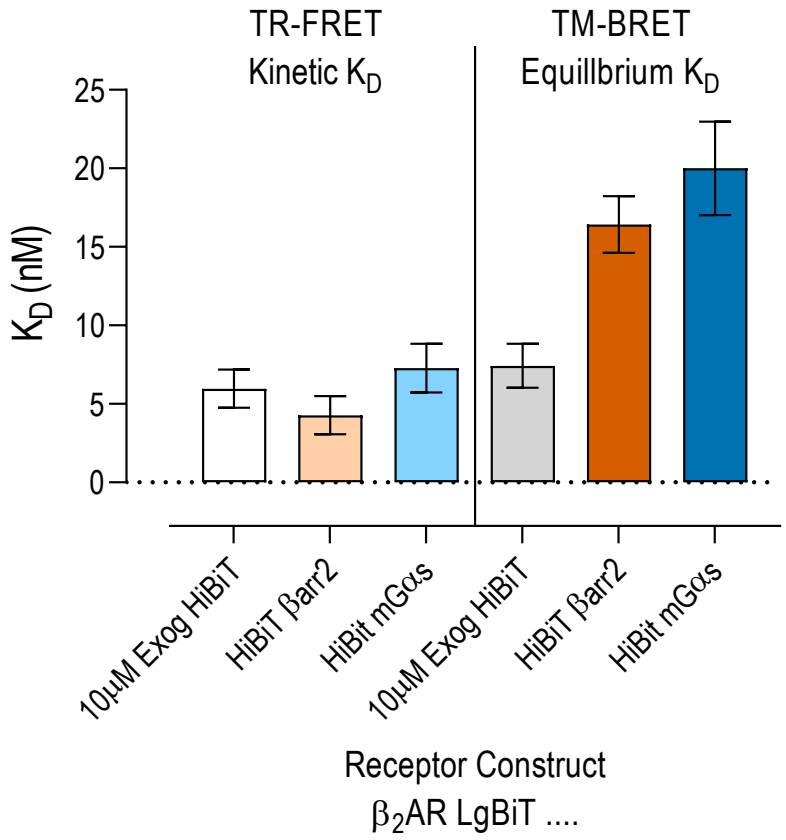

Figure 5. 8 Pooled equilibrium dissociation constants (K_D) of BODIPY-FL-PEG8-(S)-Propranolol at different effector-receptor complexes, in TR-FRET (left) and TM-BRET (right) binding assays, from membranes prepared from cells expressing SNAP-β_2AR-LgBiT, with either 10 µM HiBiT peptide or ± co-expressed HiBiT labelled β-arrestin2 or mini Gαs DNA. *Pooled kinetically derived K_D values for BODIPY-FL-PEG8-(S)-Propranolol from kinetic TR-FRET association assays (Figure 5. 3; summarised in Table 5. 1), with bars representing 3 independent experiments, conducted in singlet. Pooled equilibrium constants of BODIPY-FL-PEG8-(S)-Propranolol from TM-BRET assays (Figure 5. 7; summarised in Table 5. 3), with bars representing 4-5 independent experiments, conducted in duplicate. All bars represent mean ± S.E.M..*

SNAP-β_2AR-LgBiT	*+ 10µM HiBiT*	*HiBiT β-arrestin2*	*HiBiT mGαs*
K_D (nM)	7.43 ± 1.40	16.42 ± 1.80*	20.44 ± 2.96*

Table 5. 3 Pooled equilibrium dissociation constants (K_D) of BODIPY-FL-PEG8-(S)-Propranolol at different effector-receptor complexes, in TM-BRET binding assays. *Values obtained from membranes prepared from cells expressing SNAP-β_2AR-LgBiT, with either 10 µM HiBiT peptide or ± co-expressed with HiBiT labelled β-arrestin2 or mini Gαs DNA (Figure 5. 7). BODIPY-FL-PEG8-(S)-Propranolol equilibrium constants given as mean ± S.E.M, pooled from 4-5 independent experiments. *=P<0.05; Compared to "+ 10 µM HiBiT" condition; One-way ANOVA, with Tukey's multiple comparisons test.*

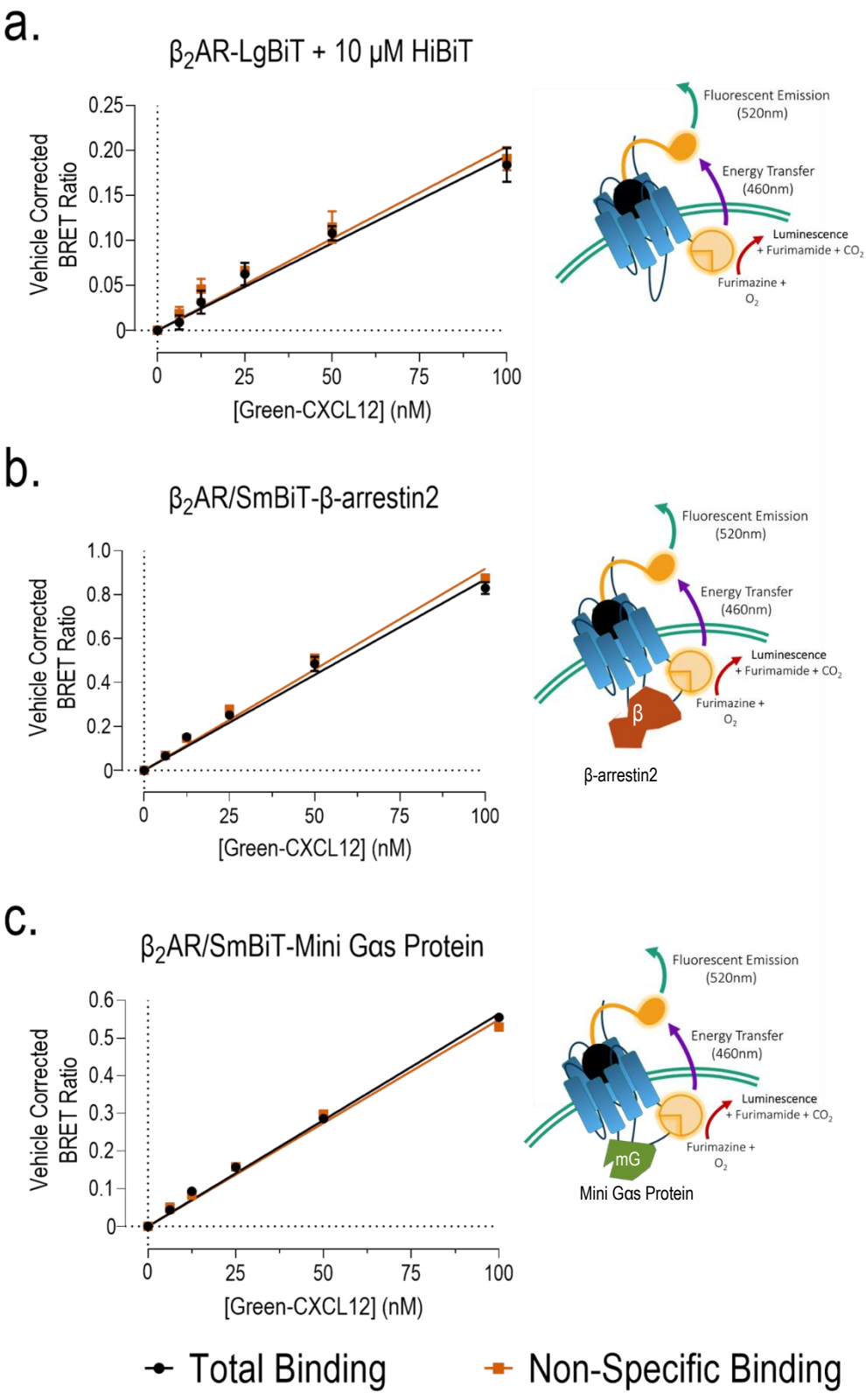

Figure 5. 9 TM-BRET saturation binding assays for Green-CXCL12, from membranes prepared from cells expressing β_2AR-LgBiT, with either 10 μM HiBiT peptide (a.) or ± co-expressed HiBiT labelled β-arrestin2 (b.) or mini Gαs (c.) DNA. *Non-specific binding was quantified in the presence of 10 μM ICI-118,551. Vehicle-corrected total and non-specific binding of Green-CXCL12 were pooled from 3 independent experiments, conducted in duplicate. Data points represent mean ± S.E.M..*

5.3.5. Use of novel TM-BRET assays to quantify equilibrium binding constants of unlabelled β_2AR ligands at effector-driven β_2AR conformations.

TR-FRET competition binding assays did not identify changes binding affinities of either BODIPY-FL-PEG8-(S)-Propranolol or unlabelled ligands after HiBiT complementation of the receptor-effector complexes (*Figure 5. 6*; *Table 5. 2*). To attempt to measure ligand binding at effector bound complexes, competition binding studies using the novel TM-BRET assay were conducted against the same ligand panel as used in TR-FRET competition binding assays.

TM-BRET assays were able to discern the binding affinities of a range of unlabelled ligands with binding affinities between micromolar and near picomolar affinity (*Figure 5. 10*; *Table 5. 4*), comparable to values derived in TR-FRET binding assays (*Figure 5. 6*; *Table 5. 2*) and published pKi values (Baker, 2005, 2010; Sykes *et al*, 2014).

As described by TR-FRET binding assays (*Figure 5. 6*; *Table 5. 2*), the order of affinity was consistent between membranes, as described by pK_i values: propranolol>ICI-118,551=salmeterol>formoterol>isoprenaline=salbutamol (*Table 5. 4*).

Complementing TR-FRET binding assays (*Figure 5. 6*; *Table 5. 2*), the equilibrium binding constants of unlabelled ligands obtained in TM-BRET assays were again unchanged between the different HiBiT and control membrane preparations (*Figure 5. 10*; *Table 5. 4*), with the greatest non-significant difference in affinity being 1.8-fold increase in the of pK_i of formoterol in SNAP-β_2AR-LgBiT/HiBiT-mini Gαs membranes, compared with that of SNAP-β_2AR-LgBiT membranes supplemented with 10 μM exogenous HiBiT peptide (*Table 5. 4*). Hill slopes of all competition binding curves were shown to not significantly differ from 1 (one-way ANOVA; Dunnet's multiple comparison's test; P>0.05) (*Table 5. 4*).

In comparison to TR-FRET competition binding assays, there was an overall increase in variability observed between experimental repeats in TM-BRET competition binding assays (*Table 5. 2*; *Table 5. 4*).

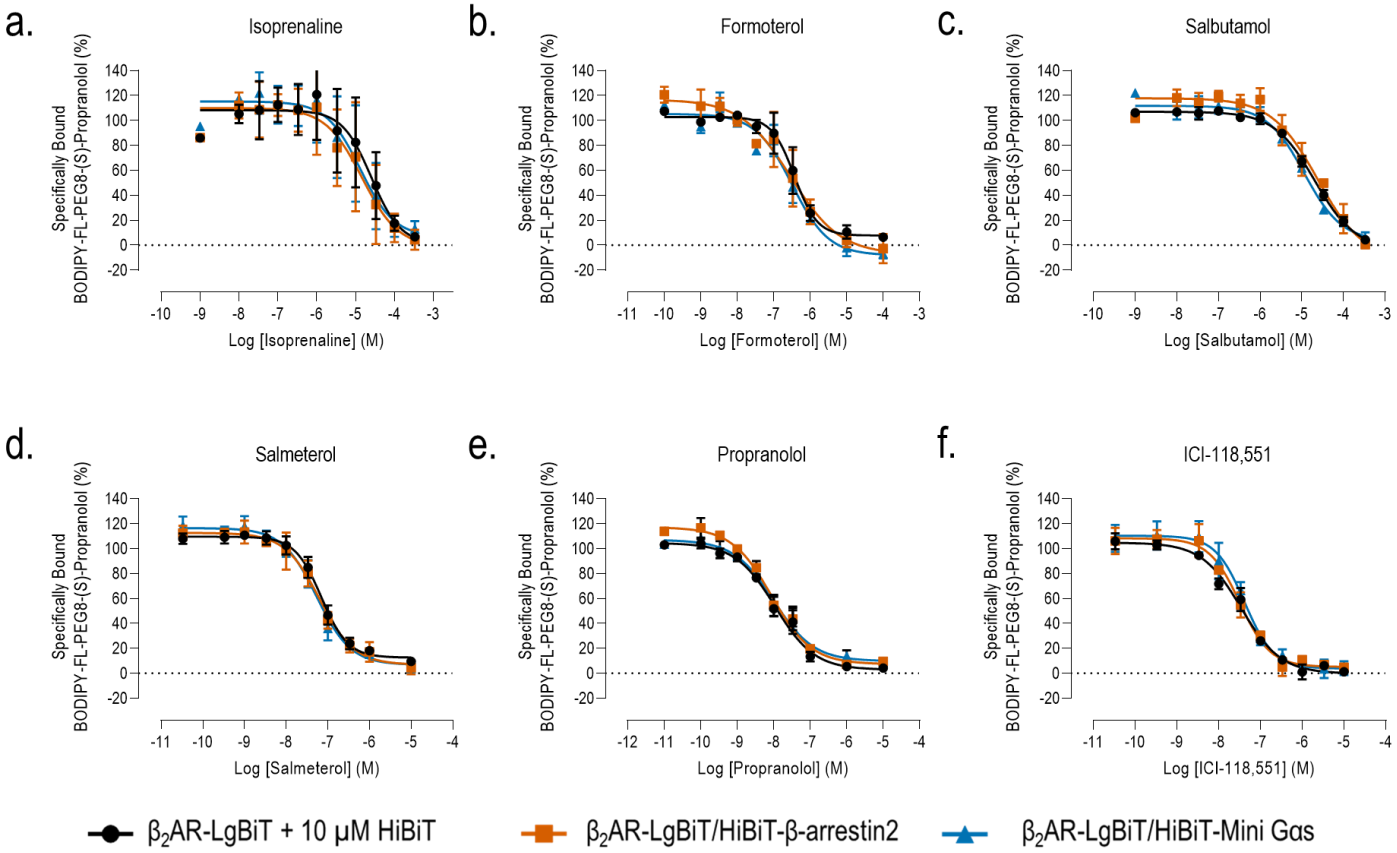

Figure 5. 10 TM-BRET competition binding assays evaluating unlabelled β_2AR ligands, from membranes prepared from HEK293T cells stably expressing terbium-labelled SNAP-β_2AR-LgBiT, with either 10 μM HiBiT peptide (black) or co-expressed HiBiT labelled β-arrestin2 (orange) or mini Gαs (blue) DNA. *Competition binding between 10 nM BODIPY-FL-PEG8-propranolol and increasing concentrations of β_2AR ligands ((a.) isoprenaline; (b.) formoterol; (c.) salbutamol; (d.) salmeterol; (e.) propranolol and (f.) ICI-118,551), supplemented with 100 μM GppNHp. End point data taken after 18 minute incubation at 37°C. NSB quantified using 10μM ICI-118,551. Data points represent mean ± S.E.M., performed in duplicate (n=3).*

Ligand	Cell Line	pK_i (M)	Hill Slope	n
Isoprenaline	β_2AR + 10 µM HiBiT	5.86 ± 0.38	1.14 ± 0.30	3
	β_2AR/HiBiT-β-arrestin2	5.78 ± 0.41	1.23 ± 0.27	3
	β_2AR/HiBiT-Mini Gαs Protein	5.76 ± 0.40	1.21 ± 0.29	3
Formoterol	β_2AR + 10 µM HiBiT	7.36 ± 0.21	1.81 ± 0.55	3
	β_2AR/HiBiT-β-arrestin2	7.22 ± 0.26	1.22 ± 0.55	3
	β_2AR/HiBiT-Mini Gαs Protein	7.09 ± 0.18	1.15 ± 0.39	3
Salmeterol	β_2AR + 10 µM HiBiT	7.97 ± 0.14	1.44 ± 0.23	3
	β_2AR/HiBiT-β-arrestin2	7.77 ± 0.18	1.01 ± 0.06	3
	β_2AR/HiBiT-Mini Gαs Protein	7.76 ± 0.20	1.20 ± 0.20	3
Salbutamol	β_2AR + 10 µM HiBiT	5.62 ± 0.11	1.00 ± 0.08	3
	β_2AR/HiBiT-β-arrestin2	5.41 ± 0.15	0.93 ± 0.14	3
	β_2AR/HiBiT-Mini Gαs Protein	5.47 ± 0.11	1.00 ± 0.09	3
Propranolol	β_2AR + 10 µM HiBiT	8.87 ± 0.12	0.81 ± 0.05	3
	β_2AR/HiBiT-β-arrestin2	8.72 ± 0.12	0.90 ± 0.08	3
	β_2AR/HiBiT-Mini Gαs Protein	8.61 ± 0.10	0.91 ± 0.11	3
ICI-118,551	β_2AR + 10 µM HiBiT	8.30 ± 0.08	1.24 ± 0.46	3
	β_2AR/HiBiT-β-arrestin2	7.96 ± 0.12	1.56 ± 0.54	3
	β_2AR/HiBiT-Mini Gαs Protein	7.96 ± 0.10	1.51 ± 0.44	3

Table 5. 4 Summary of ligand equilibrium dissociation constants of unlabelled β_2AR agonists, using TM-BRET binding assays from membranes prepared from HEK293T cells stably expressing terbium-labelled SNAP-β_2AR-LgBiT, with either 10 µM HiBiT peptide or co-expression HiBiT labelled β-arrestin2 or mini Gαs DNA. *pIC50 values obtained from competition TM-BRET assays (Figure 5. 9) were converted to pKi values, describing the affinities of unlabelled ligands. Pooled pKi values are, mean ± S.E.M., from 3 individual experiments, conducted in duplicate.*

5.3.6. The addition of exogenous HiBiT peptide reveals that many SNAP-β_2AR-LgBiT receptors are uncoupled from the labelled effector proteins in the HiBiT membrane preparations.

TR-FRET and TM-BRET studies could discern no significant differences in the binding of BODIPY-FL-PEG8-(S)-Propranolol or unlabelled ligands at the β_2AR in the presence or absence of HiBiT-tagged effectors (*Figure 5. 6*; *Table 5. 2*; *Figure 5. 10*; *Table 5. 4*).

To establish whether the level of complementation provided sufficient NanoBiT complexes for efficient energy transfer and signal, membranes prepared from cells stably expressing (1) β_2AR-LgBiT, (2) β_2AR-LgBiT/HiBiT-β-arrestin2 and (3) β_2AR-LgBiT/HiBiT-mini Gαs protein were incubated with increasing concentrations of exogenous HiBiT peptide to identify non-complemented LgBiT fragments (*Figure 5. 11*).

Initial treatment of furimazine in the different membrane preparations demonstrated basal luciferase activity of LgBiT fragments, with some background in SNAP-B2AR-LgBiT membranes alone, but with membranes containing β_2AR-LgBiT/HiBiT-β-arrestin2 and β_2AR-LgBiT/HiBiT-mini Gαs complexes demonstrating much greater luminescence of 8.1-fold and 7.9-fold, respectively (*Figure 5. 11. a.*). When treated with 10 μM HiBiT peptide, luminescence from β_2AR-LgBiT membranes increased 107-fold (*Figure 5. 11. a.*) and thus represents the donor signal used in previous TM-BRET assays (*Chapter 5*; *5. 3. 4* – *5. 3. 5*).

When treated with 10 μM HiBiT peptide, membranes expressing β_2AR-LgBiT/HiBiT-β-arrestin2 and β_2AR-LgBiT/HiBiT-mini Gαs complexes had increased luminescence of 17-fold and 10-fold greater than in the absence of 10 μM HiBiT, respectively (*Figure 5. 11*). From the fraction of luciferase activity in the absence and presence of 10 μM HiBiT, donor emission in TM-BRET assays were quantified as 5.9 % and 10 % of the total possible donor emission, in β_2AR-LgBiT/HiBiT-β-arrestin2 and β_2AR-LgBiT/HiBiT-mini Gαs membranes, respectively.

Titration of the HiBiT against membranes expressing β_2AR-LgBiT ± co-expressed HiBiT labelled effectors provided luminescence response curves to indicate the approximate affinity of the HiBiT peptide (*Figure 5. 11. b*). Measures of HiBiT peptide affinity at β_2AR constructs was shown to be consistent between cell lines: with K_D values of 16.7±2.4, 11.3±5.9 and 19.0±2.9 nM (n=3) at β_2AR-LgBiT, β_2AR-LgBiT/HiBiT-β-arrestin2 and β_2AR-LgBiT/HiBiT-Mini Gαs protein membranes respectively.

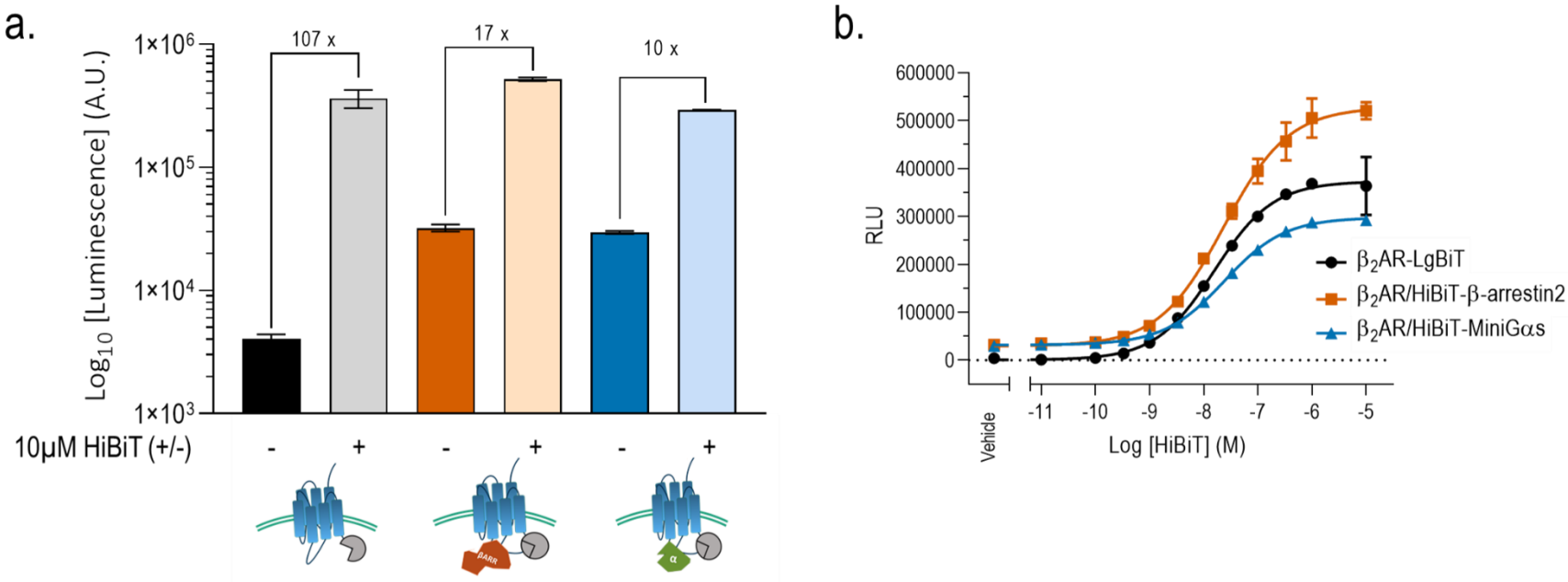

Figure 5. 91 HiBiT complementation of NanoBiT fragments in membranes prepared from cells expressing either SNAP-β2AR-LgBiT alone (β2AR-LgBiT), or co-expressed with HiBiT tagged β-arrestin2 (β2AR/HiBiT-β-arrestin2) and mini Gαs (β2AR/HiBiT-Mini Gαs). *(a.) Luciferase responses of complemented NanoBiT fragments ± 10 μM HiBiT; fold change of luminescence shown between vehicle and 10 μM HiBiT treated membranes. Note that the luminescence response (Y axis) is plotted on a logarithmic scale (b.) Concentration-luminescence response of HiBiT peptide when added to membranes expressing either SNAP-β2AR-LgBiT alone, or co-expressed with HiBiT tagged βarrestin2 and mini Gαs. Column data and concentration response data pooled (mean±S.D.) from raw luminescence counts in individual experiments (n=2), each conducted in duplicate.*

5.3.7. Unbalanced expression of LgBiT and HiBiT present in cells.

From *Figure 5. 11*, it was observed that the majority of β_2AR-LgBiT receptors were not occupied with HiBiT-effectors in dual-expression membrane preparations (β_2AR-LgBiT/HiBiT-β-arrestin2 and β_2AR-LgBiT/HiBiT-Mini Gαs). To determine whether HiBiT-effector proteins could have been lost during membrane preparation (*Methods*; *2. 5. 2*), β_2AR-LgBiT/HiBiT-β-arrestin2 and β_2AR-LgBiT/HiBiT-mini Gαs cell lines were treated with 10 μM HiBiT in the presence of the furimazine substrate (*Figure 5. 12*). To allow access of the membrane impermanent HiBiT peptide, β_2AR-LgBiT/HiBiT-β-arrestin2 and β_2AR-LgBiT/HiBiT-mini Gαs cells were first treated with either vehicle, digitonin or saponin, before the addition of furimazine and 10 μM HiBiT (*Figure 5. 12*).

In the absence of a detergent, luciferase activity in both cell lines did not increase significantly between vehicle and 10 μM HiBiT peptide treated wells ($P=0.6442$ and $P=0.9986$, Students t-test at β_2AR-LgBiT/HiBiT-β-arrestin2 and β_2AR-LgBiT/HiBiT-mini Gαs cells, respectively) (*Figure 5. 13*). When treated with detergent, there was a greater increase in luminescence between vehicle and 10 μM HiBiT peptide treated cells in both cell lines ($P<0.001$, Students t-test).

In cells co-expressing β_2AR-LgBiT and HiBiT-β-arrestin2, when treated with 10 μM HiBiT an increase in luminescence was observed ($P<0.0001$ in both detergent conditions, Students t-test) compared to vehicle. Moreover, measures of luminescence increased 6.9-fold and 9.8-fold over vehicle in digitonin and saponin treated cells, respectively (*Figure 5. 13*).

Similarly, cells co-expressing β_2AR-LgBiT and HiBiT-Mini Gαs DNA also demonstrated increased luminescence when treated with 10 μM HiBiT, when compared to vehicle ($P<0.001$ in both detergent conditions, Student's t-test). Moreover, measures of luminescence increased 3.0-fold and 13.2-fold over vehicle in digitonin and saponin treated cells, respectively (*Figure 5. 13*).

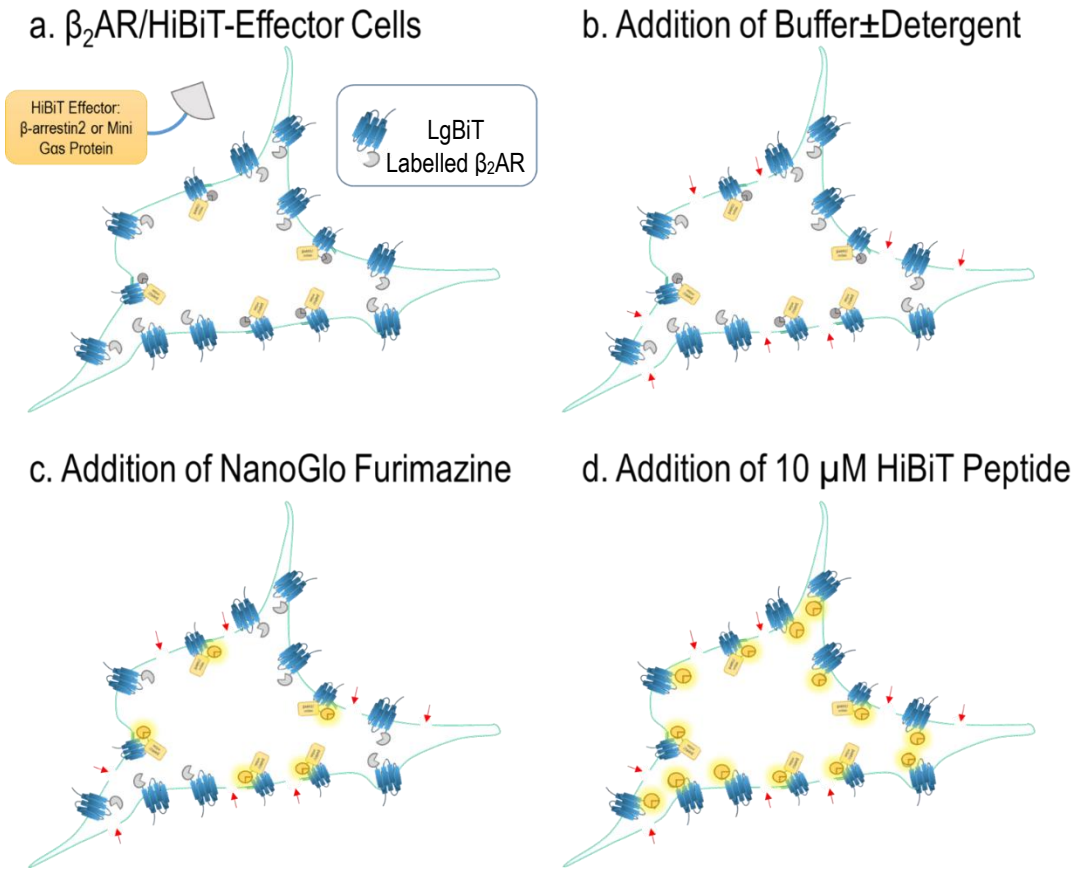

Figure 5. 10 Schematic of HiBiT complementation assay, in detergent permeablised HEK293T cells co-expressing SNAP-β2AR-LgBiT and HiBiT-tagged β-arrestin2 or mini Gαs. *Cells were pre-treated with buffer ± detergent for 15 minutes before the addition of NanoGlo furimazine substrate. Cells were then incubated for 5 minutes before the addition of 10 µM HiBiT.*

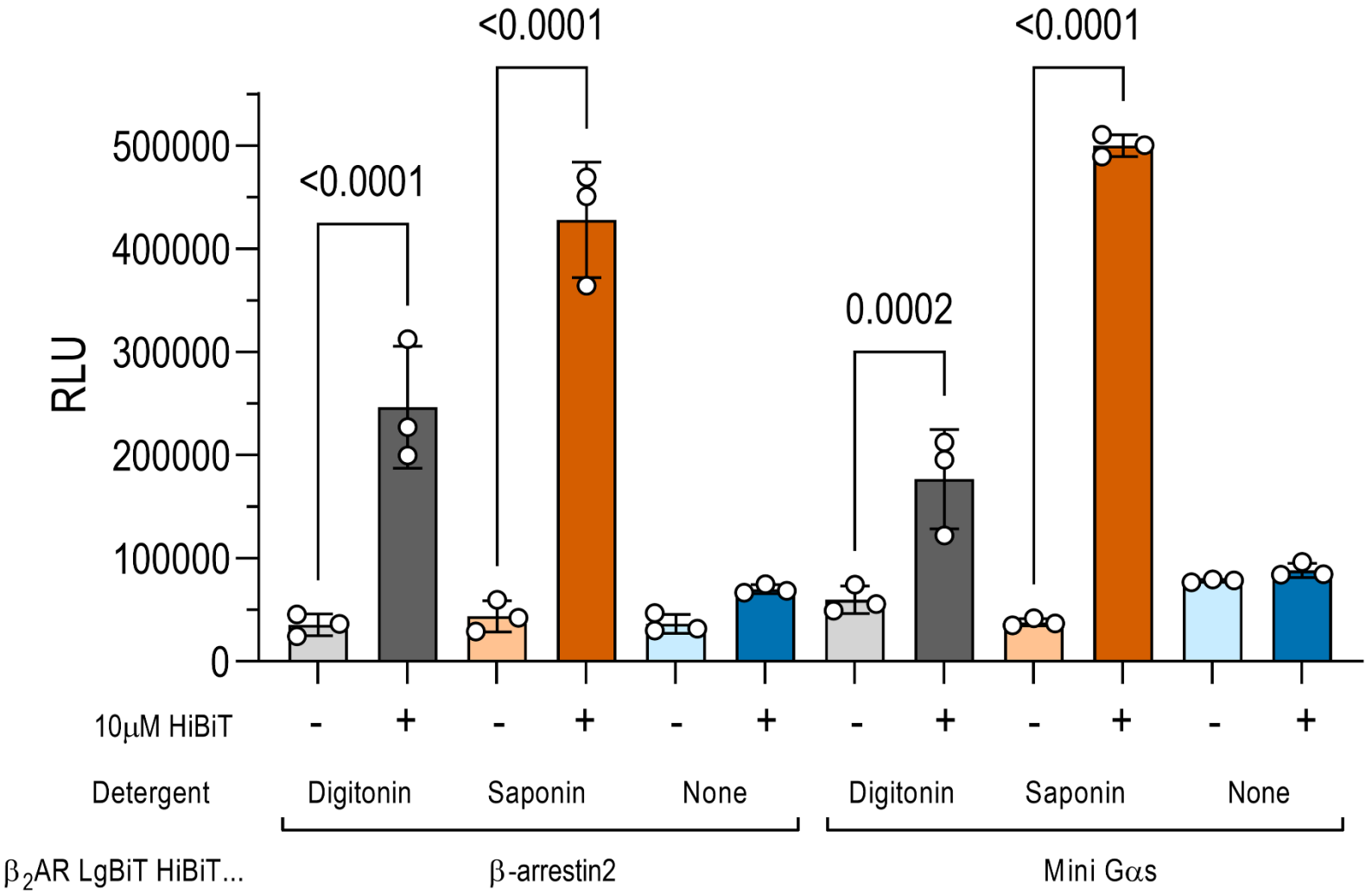

Figure 5. 113 HiBiT complementation in detergent permeablised HEK293T cells co-expressing SNAP-β$_2$AR-LgBiT and HiBiT-tagged β-arrestin2 or mini Gαs. *HEK293T cells co-expressing SNAP-β$_2$AR-LgBiT and HiBiT-tagged βarrestin2 or mini Gαs, were pre-incubated with buffer, digitonin and saponin and treated with furimazine. After the addition of buffer or 10 μM HiBiT peptide, raw luminescence values were pooled from 3 independent experiments, conducted in duplicate. Data points represent mean ± S.E.M., with each replicate displayed. Significant differences between vehicle and HiBiT treated cells denoted by P value, Student's t-test.*

5.4. Discussion

In this chapter, in cell NanoBiT complementation, using high affinity HiBiT fragments, was applied to stabilise β_2AR receptor-effector complexes. The ambition of this approach was to develop a methodology whereby the binding parameters of particular agonist-receptor-effector ternary complexes could be studied in isolation. HEK293T cells stably expressing SNAP-β_2AR-LgBiT and HiBiT-tagged β-arrestin2 or mini Gαs produced luminescence which was unaffected when treated with 10 μM isoprenaline and ICI-118,551, suggesting stable interactions of NanoBiT tagged proteins. Membranes prepared from dual-expression cells lines were used in TR-FRET binding assays to determine the kinetic binding pharmacology of BODIPY-FL-PEG8-(S)-Propranolol and binding affinity values of unlabelled β_2AR ligands, though no changes were observed between (1) SNAP-β_2AR-LgBiT +10 μM HiBiT, (2) SNAP-β_2AR-LgBiT/HiBiT-β-arrestin2 and (3) SNAP-β_2AR-LgBiT/HiBiT mini Gαs membrane preparations. Second, we demonstrated for the first time that the intracellular NanoBiT complemented luciferase could be used as a donor for the fluorescently labelled propranolol acceptor, establishing the principle of transmembrane TM-BRET. We then used TM-BRET successfully to measure the specific binding of the tracer and unlabelled β_2AR agonists and antagonists at the labelled – receptor-mGαs protein/β-arrestin complexes. However, no difference in the binding affinities of β_2AR agonists was again observed in TM-BRET competition binding assays. Addition of exogenous HiBiT peptide revealed most SNAP-β_2AR-LgBiT proteins in membranes prepared from dual-expression SNAP-β_2AR-LgBiT/HiBiT-effector cells lines were largely unoccupied, and that this arose from an excess of receptor compared to effector expression in the stable cell lines. Future studies could develop the TM-BRET methodology further in cell lines where the stoichiometry of receptor: effector expression is equalised, and in using isolated purified effector proteins (Chapter 6).

5.4.1. High affinity NanoBiT fragments generate stable complemented β_2AR/effector complexes.

As previously discussed, the high affinity NanoBiT fragment partners (LgBiT-HiBiT) have previously been used to study protein expression (Oh-hashi *et al.*, 2017) and GPCR receptor internalisation (Boursier *et al.*, 2020; Soave, *et al.*, 2020). The use of these fragments to tether the Gβγ subunit to the C-terminal of the vasoactive intestinal polypeptide receptor for cryo-electron microscopy studies (Duan *et al.*, 2020), suggests the high affinity of the fragments can be used to form stable protein-protein complexes during purification and analysis. The high affinity

NanoBiT fragments were applied here in an attempt to stabilise complexes of β_2AR with either β-arrestin2 or the mini Gαs protein. Imaging of NanoBiT cell lines, either β_2AR/HiBiT-β-arrestin2 or β_2AR/HiBiT-Mini Gαs, revealed receptors to be located at cell surface and intracellular locations under both vehicle and isoprenaline conditions, with further internalisation stimulated by isoprenaline only in the HiBiT β-arrestin2 line. Although this was not investigated in detail in this study, the lack of further agonist promoted internalisation in the mini Gαs HiBiT line might suggest that mini Gαs impedes interaction with arrestin and reduces arrestin-dependent endocytosis.

Agonist stimulation did not increase the constitutive level of HiBiT luminescence further in the β_2AR-effector lines, indicating that all available HiBiT effector complexes had been recruited. Similarly, treatment of ICI-118,551 did not reduce luciferase activity, further suggesting that HiBiT complexes once formed were stable and not reversed by a β_2AR inverse agonist. Previously, methods of receptor stabilisation, in both active and inactive states, have been applied at the β_2AR to stabilise the receptor, primarily for structural studies. For example fusion of the soluble protein T4-lysozyme has been used to produce crystal structure of the β_2AR (Cherezov *et al.*, 2007; Rosenbaum *et al.*, 2007; Hanson *et al.*, 2008; Wacker *et al.*, 2010), with the T4-lysozyme interaction being suggested to shift the receptor conformation to the active state (Eddy *et al.*, 2016). Other methods utilise nanobodies to replicate the G protein interface to form active conformations of the receptor (Rasmussen, *et al*, 2011a; Rasmussen, *et al*, 2011b; Rosenbaum *et al*, 2011; Ring *et al*, 2013). As discussed above, Warne *et al.*, (2019) used the mini Gαs protein to stabilise the active conformations of the β_1AR and β_2AR, where mini Gαs receptor interactions were shown to increase the affinity of adrenaline and noradrenaline both by >100-fold at the β_2AR, by using radioligand binding studies. Such studies supported our hypothesis that co-expression of the mini Gαs protein or β-arrestin2 stabilised by the HiBiT NanoBiT fragments would form stable β_2AR receptor-effector complexes, whose binding properties might then be studied selectively.

5.4.2. TR-FRET binding assays did not reveal differences binding of either BODIPY-FL-PEG8-(S)-Propranolol or unlabelled ligands at effector driven conformations of the β_2AR.

Initially, TR-FRET assays were implemented to monitor changes in BODIPY-FL-PEG8-(S)-Propranolol binding kinetics in membranes prepared from

HEK293T cells expressing SNAP-β_2AR-LgBiT supplemented with 10 μM HiBiT or from HiBiT cells co-expressing SNAP-β_2AR-LgBiT and HiBiT tagged β-arrestin2 or mini Gαs protein. In this method, the TR-FRET readout therefore arises from all the terbium / SNAP-labelled receptors within the preparations, which provide the donor excitation. As the pharmacophore of the fluorescent tracer was based on the β_2AR neutral antagonist propranolol, which is thought to show no preference for the coupled or uncoupled receptor conformations (Samama *et al.*, 1994), it was unsurprising that the kinetic binding pharmacology of BODIPY-FL-PEG8-(S)-Propranolol was unchanged in membranes prepared from cells expressing either of HiBiT tagged β-arrestin2 and mini Gαs protein. This correlates with findings from (Warne *et al.*, 2019), which show the affinity of the β_1AR antagonist cyanopindolol to be unchanged at the β_1AR in presence and absence of the mini Gαs protein. However, in competition binding assays, the presence of both β-arrestin2 and the mini Gαs protein also did not affect the binding affinity values of any of a range of unlabelled ligands, which correlated previously published affinities (Baker, 2010; Sykes *et al.*, 2014; Baker *et al.*, 2017). This was surprising, especially when investigating high efficacy β_2AR agonists such as isoprenaline and formoterol. As there was no significant difference in Hill slope from 1, there was no indication of the presence of additional binding sites. The binding buffer included the non-hydrolysable GTP derivative Gpp(NH)p in the assay buffer, to dissociate native G protein coupling, and thus it was intended to ensure receptors associated with native G proteins did not contribute to the binding results. In the future, it may be possible to increase the likelihood of observing the high affinity ternary complex binding by changing the buffer constituents, for example by reducing the concentration of sodium ions (Shearer *et al.*, 1973; Katritch *et al.*, 2014). The disadvantage of this approach is that as the sodium ion concentration is reduced, the experimental environment becomes less like a whole cell and thus reducing the value of the function measurements.

It was concluded that the TR-FRET binding assay was still monitoring all receptors within the population and thus a more selective method was required to ensure binding measurements were being made from receptors occupied by either β-arrestin2 or a mini Gαs protein.

5.4.3. Establishment of a novel transmembrane BRET biosensor, to monitor binding of BODIPY-FL-PEG8-(S)-Propranolol and unlabelled ligands.

Here, we successfully engineered and developed a novel TM-BRET assay to monitor ligand binding at the β_2AR, using the luminescence generated from the complemented NanoBiT fragments at the C-terminal of the receptor as a donor emission. The concept of a transmembrane energy transfer assay is thought to be limited by the energy transfer through the lipid bilayer, which is thought to be too great a distance for efficient and detectable energy transfer. However, we demonstrated that this barrier can be overcome. Firstly, the lipid bilayer is thought to be approximately 30 Å in thickness (Jaud *et al.*, 2009; Regan *et al.*, 2019), which is within the 100 Å distance thought to be the maximum distance for energy transfer assays (Stryer and Haugland, 1967; Stryer, 1978). In addition, the fluorescent dipyrrometheneboron (BODIPY-FL) dye that was applied in the TM-BRET studies here (BODIPY-FL-PEG8-(S)-Propranolol) is known to be highly lipophilic (Makrigiorgos, 1997). Thus, the fluorophore is likely to have an affinity for the lipid membrane (Baker *et al.*, 2010), instead of being extended into the extracellular space. It is likely that the combination of TM binding pharmacophore, linker and fluorophore, enables the insertion of the fluorophore within the membrane environment reducing the distance of energy transfer further. The specificity of the TM-BRET measurements were further supported by the lack of specific binding observed by Green-CXCL12, which has a pharmacophore non-selective at the β_2 adrenoceptor but with a fluorophore of similar excitation/emission wavelengths. Known applications of transmembrane energy transfer assays to our knowledge, limited to a single publication monitoring glycoforms of transmembrane proteins using FRET based biosensors (Haga *et al.*, 2012). In this case, FRET responses between an intracellular labelled GFP and extracellular tetramethylrhodamine fluorophore were monitored using microscopic imaging and individual fluorescence intensities of each wavelength performed on filtered images. Whilst this method demonstrated proof of concept, the application of transmembrane energy transfer assays was limited to single timepoints and conditions.

Here, TM-BRET assays were developed and used to determine the binding affinity of BODIPY-FL-PEG8-(S)-Propranolol at the β_2AR at each condition: SNAP-β_2AR-LgBiT supplemented with 10 μM HiBiT or from cells co-expressing SNAP-β_2AR-LgBiT and HiBiT tagged β-arrestin2 or mini Gαs protein. The affinity of BODIPY-FL-PEG8-(S)-Propranolol was within 4-fold of estimates made by TR-FRET binding assays but overall increased variability between experimental replicates. Interestingly, the affinity of BODIPY-FL-PEG8-(S)-Propranolol was

significantly lower at HiBiT-mini Gαs stabilised β_2AR constructs. The ternary complex model suggests G protein binding shifts the equilibrium towards the high affinity conformation for agonists, though should not affect antagonist binding. There is some evidence that propranolol may act as an inverse agonist (Chidiac *et al.*, 1994; Baker, *et al*, 2003; Anderson *et al.*, 2014) and thus would have the highest affinity for the uncoupled receptor state and lower affinity at the receptor coupled to the mini Gαs protein or β-arrestin2, agreeing with data presented here.

Whilst a decrease in BODIPY-FL-PEG8-(S)-Propranolol affinity at HiBiT-mini Gαs stabilised receptors suggested the β_2AR conformation may be influenced by an effector, competition binding assays saw no differences in binding affinity of all unlabelled ligands, whether agonists or antagonists. It was hypothesised that high efficacy agonists, such as isoprenaline and formoterol, would have the greatest increase in affinity – due to HiBiT stabilisation of the agonist – receptor – effector ternary complex - followed by partial agonists, such as salmeterol, yet no changes in affinity were observed. Despite a decrease in BODIPY-FL-PEG8-(S)-Propranolol binding affinity in the presence of HiBiT-mini Gαs protein, the affinity of each unlabelled antagonist tested was not observed to decrease.

5.4.4. Exogenous HiBiT peptide reveals unequal expression of NanoBiT labelled β_2AR and effector proteins in the recombinant system.

The donor signal, and subsequent TM-BRET interaction, was dependent on the complementation of NanoBiT fragments and thus the interaction of the receptor - effector protein partners. However, this specific signal might be reduced due to an excess of SNAP-β_2AR-LgBiT fragments within the membrane preparations, either indirectly, or because LgBiT alone can contribute a low level of donor luminescence (Dixon et al 2016). The presence of a large excess of SNAP-β_2AR-LgBiT in the membranes was confirmed by the addition of 10 μM HiBiT to each membrane preparation, which saw >10-fold increase in luminescence in both membranes prepared from cells co-expressing SNAP-β_2AR-LgBiT/HiBiT-effector cDNA. This suggests that the majority of receptors were not effector bound. Membranes prepared from cells expressing SNAP-β_2AR-LgBiT alone, and in the absence of 10 μM HiBiT peptide, were shown to produce >1000 units of detectable luminescence (as described in Dixon et al 2016). In a large

excess, otherwise uncoupled SNAP-β_2AR-LgBiT binding to tracer might still contribute significantly to the TM-BRET data and obscure the specific binding for the agonist-receptor-effector complex that was the objective for isolation. It is also possible that some HiBiT tethered receptor-complexes may not associate in a manner that stabilises the active ternary complex conformation. For example, being linked by HiBiT interactions, but not with an appropriate receptor/mini Gαs or receptor/βarrestin2 interface forming. These are the current limitations of the TM-BRET studies presented in this chapter.

It is clear that the dual-expression cell lines prepared as described were not optimised sufficiently to ensure a stoichiometry of receptor – effector expression that generated a high proportion of HiBiT complexes. Our experiments demonstrated that it was the initial formation of HiBiT complexes, rather than their subsequent stability during membrane preparation that limited their number in membrane binding experiments. Moving forward in cell systems, methodology needs to be altered to ensure the saturation of SNAP-β_2AR-LgBiT proteins with HiBiT effector interactions. One method is employ techniques to ensure equivalent expression levels, such as the use of a polycistronic plasmid to ensure expression of both proteins from the same mRNA instead of multiple plasmids (Bouabe, *et al*, 2008). An alternative method would be use a purified version of the HiBiT-effector and thus ensure the saturation of all SNAP-β_2AR-LgBiT proteins. The advantage of using a purified system is that the mini Gαs protein was first synthesised as a purified protein, to aid crystallisation studies, and thus well-established protocols are available (Carpenter and Tate, 2016, 2017; Carpenter *et al.*, 2016; Nehmé *et al.*, 2017).

5.5. Conclusions

This chapter aimed to obtain ligand binding parameters for fluorescently labelled and unlabelled β_2AR ligands, from identified receptor complexes with β-arrestin2 and mini Gαs proteins, stabilised by high affinity NanoBiT fragments. In particular we demonstrated the potential of a novel TM-BRET binding assay, which used the specific complemented NanoBiT fragments from SNAP-β_2AR-LgBiT and HiBiT-effector proteins for donor emission to monitor the binding of BODIPY-FL-PEG8-(S)-Propranolol and unlabelled ligands. However, no changes in binding affinity of a range of full agonists, partial agonists and antagonists were observed in TR-FRET or novel TM-BRET assays, which led to investigations into the proportion of β_2AR/effector coupling in the cell systems. Addition of exogenous HiBiT peptide to both dual-expression cell lines and membrane preparation demonstrated a large excess of SNAP-β_2AR- LgBiT, which by itself produced some luminescence – this could contribute to the TM-BRET signal and so obscure the desired analysis of binding to specific HiBiT complexes. Future studies could optimise cell expression of receptors and effectors to obtain an improved stoichiometry and a greater proportion of HiBiT complexes within the total receptor population. Alternatively, Chapter 6 pursued an alternative approach to combine the NanoBiT / HiBiT approach with titratable, labelled and purified effector proteins.

Chapter Six:

Isolating ligand binding at “active” conformations of β_2ARs, using HiBiT stabilised mini Gαs proteins.

6.1. Introduction

6.1.1. Obtaining Specific Ternary Complexes to Study GPCR pharmacology

As discussed in *Chapter 1* and *Chapter 5*, the ternary complex model describes interactions between a ligand, receptor and its associated G protein. The ternary complex model represents a complex set of allosteric molecular interactions and switches between agonist binding, GPCR conformational changes and G protein activation. As seen in *Chapter 5*, isolating known conformations of this heterotrimeric complex for pharmacological study provides challenges. Recent advances in our understanding of agonist-GPCR-G protein complex interactions have originated from X-ray crystallography and cryo-EM structural studies using purified GPCRs, as well as purified G proteins and G protein mimetics.

6.1.2. GPCR Protein Purification and the use of Mini Gαs Proteins

Studies investigating the structural influence of GPCR-G protein binding have utilised the availability of purified recombinant proteins and mimetic proteins. The full length Gαs protein was the first G protein to be purified (Harris *et al.*, 1985; Gilman, 1987; Neer and Clapham, 1988) and has been applied to the β_2AR in X-ray crystallography studies to provide structural insights into ligand binding and β_2AR activation (Manglik *et al.*, 2015). Expression of recombinant G proteins used in crystallography studies were initially conducted in *e.coli* (Lee, *et al*, 1994), though due to the lack of bacterial post-translational modifications, purified G proteins lacked prenylation sites involved in assembly and trafficking of heterotrimeric G proteins. To rectify this, G proteins were then purified from insect expression systems, such as *sf9* cells, and thus improved the capability of functional interactions with GPCRs (Seifert *et al.*, 1998; Lee *et al.*, 1999).

Whilst methods of purification of Gα subunits has been further improved and applied to study β_2ARs (Chu*ng et al*, 2011; Rasmussen, *et al*, 2011b), more thermostable G protein surrogates have been developed to mimic the interactions of the G protein, and in particular stabilise an active conformation of a GPCR. One approach was to use conformation specific nanobodies, which are recombinant camelid single-domain antibody fragments (Manglik, *et al*, 2017), designed to stabilise the active state of a GPCR (Steyaert and Kobilka, 2011). For example

Nanobody80 (Nb80) was identified from initial studies (Rasmussen, *et al.*, 2011a), which induced changes in receptor conformation of the β_2AR comparable with activated β_2AR-Gαs complexes (Yao *et al.*, 2009). Therefore it was concluded that the allosteric interactions of Gαs proteins, as described by the ternary complex model above, could be recapitulated by Nb80. Subsequently, nanobodies have also been applied to mimic Gαi interactions at both the muscarinic M2 (Kruse *et al.*, 2013) and the μ opioid (Huang *et al.*, 2015) receptors. Whilst not behaving directly as a G protein mimetic, nanobody 35 (Nb35) was also engineered to help stabilise Gαs bound GPCR complexes, at which an increase in agonist affinity at the β_2AR was observed (Westfield *et al.*, 2011).

In addition to nanobodies, mini Gαs proteins have been engineered to mimic Gα protein actions at GPCRs in crystallisation studies, with improved thermostability, and moreover adopt the active GPCR binding conformation of the G protein (Carpenter and Tate, 2016). As discussed in *Chapter 1*, the mini Gα protein consists of the GTPase domain of the Gα protein (GαGTPase domain), with 3 deletions and 7 mutations to improve the thermostability of the protein (Carpenter and Tate, 2016). Some thermostabilising mutations were thought to have functional consequences, with the L272D mutation removing the necessity of the mini Gαs protein to form a heterotrimer with the Gβγ subunits for receptor coupling, and the I372A mutation conferring GTP insensitivity. Ile 372, in the native Gα subunit, is suggested to act a relay between the GPCR binding pocket and the regions associated with nucleotide binding (α1 helix and P-loop), by sterically clashing with Met 60 on the α1 helix of the Gαs protein (Carpenter and Tate, 2016). The first engineered mini G protein was designed to mimic the stimulatory Gαs protein (Carpenter and Tate, 2016), and was shown to increase agonist affinity at both the β_1AR and the adenosine A_{2A} receptor (Carpenter and Tate, 2016; Carpenter *et al.*, 2016). Carpenter and Tate (2016) suggest that the mini Gαs protein stabilises the active conformation of Gαs coupled GPCR to a greater extent compared with Nb80; as an β_1AR-mini Gαs complexes provided increased affinity for isoprenaline and thermostability compared to β_1AR-Nb80 and β_1AR-Gαs complexes. This suggests that binding of mini Gα proteins are able to produce the most stable form of a GPCR in an active conformation and provide a suitable complex from which to obtain ligand binding information, both in structural studies, and potentially in pharmacological measures of binding affinity and kinetics.

6.1.3. Use of mini Gαs Proteins to Isolate Ligand Binding Affinities at Active GPCR Conformations

The identification of G protein mimicking proteins and Gαs-GPCR stabilising nanobodies have provided structural insights into the multiple conformational states of GPCRs, using agonist affinities and crystal structures to describe changes in receptor conformation. As discussed, the mini Gαs protein binds and stabilises active GPCR conformations, as described by shifts in agonist affinity and increased thermostability (Carpenter and Tate, 2016).

As attempted in *Chapter 5*, one method to form active complexes of GPCR is to co-express the individual target GPCR and mini Gα proteins, enhancing the probability that active complexes form, and monitor the associated effects on ligand binding. Höring *et al.* (2020) conducted similar methodology, co-expressing the histamine H2 receptor and increasing DNA amounts of mini Gαs protein to determine changes in histamine affinity. Increased transfections of mini Gαs protein DNA resulted in biphasic competition binding curves and suggested mini Gαs stabilised a population of receptors within the assay, whilst not saturating nor fully stabilising all histamine H_2 receptors expressed (Höring *et al.*, 2020). Thus, findings from *Chapter 5* and Höring *et al.*, (2020) suggest co-expression of the individual components of the GPCR/mini Gαs protein may not be sufficient to ensure full saturation of the target GPCR as the desired complex. Moreover, such conclusions highlighted the advantages of using a purified mini Gαs protein, which have been used to fully-reveal active state binding affinities for ligands of adenosine A2A receptors (Carpenter *et al.*, 2016), β_1ARs (Warne *et al.*, 2019; Lee *et al.*, 2020) and β_2AR (Warne *et al.*, 2019). Whilst such studies have demonstrated how mini Gαs protein may stabilise active conformations of GPCRs, resulting in increased agonist affinity, as of yet no information has been obtained on mini Gαs binding may influence the kinetics of ligand binding at the specific GPCR-mGs complex.

6.1.4. Binding Kinetics in Drug Discovery

The kinetics of ligand binding at GPCRs (as discussed in *Chapter 1*; *1. 8. 1* and *Chapter 5*; *5. 1. 3*) has become a useful consideration for compound profiling in early phases of the drug discovery process, having been identified as a key factor in improving translation between *in vitro*, *in vivo* and clinical studies (Swinney *et al*, 2015; Guo, *et al*, 2016b; Vauquelin, 2016; Guo *et al*, 2018). Better understanding of ligand-receptor binding provides information into both how the

ligand recognises and binds the target receptor (association rate; k_{ON}) and how long lasting the ligand-receptor interaction (dissociation rate; k_{OFF}) (Guo *et al.*, 2014; Guo, *et al*, 2016a, 2016b) (see *Chapter 1*). For example, an antagonist with a slower k_{OFF}, compared to the competing agonist, may produce insurmountable inhibition of a receptor, even at high agonist concentrations (as discussed in *Chapter* 1 and demonstrated in *Chapter 4*).

Kinetic parameters have particular influence on compound properties *in vivo* when biological systems are not at equilibrium – as is commonly the case under conditions where the free drug concentration at the site of action, or that of the competing native messenger (e.g. a neurotransmitter), vary dynamically. Slow ligand dissociation rates (reciprocal, receptor residence time) can impact on duration of action (Lu and Tonge, 2010; Dahl and Akerud, 2013; Guo *et al.*, 2014; J. D. Hothersall *et al.*, 2016; Rosethorne *et al.*, 2016) (Further discussed in *Chapter 1*; *1. 8. 1*) if the compound pharmacokinetic properties (specifically rapid elimination rate) are unfavourable (Lindström *et al.,* 2007b; Guo, *et al*, 2016a). Equally application of drugs with rapid dissociation rates at the relevant receptors may be used to offset toxicity issues arising from on or off target side effects, (Vauquelin *et al.*, 2012). Moreover, a more comprehensive understanding of drug-receptor interactions allows for improved target engagement and safety profiles (Copeland, 2010; Swinney *et al.*, 2015; J. D. Hothersall *et al.*, 2016; Hoare, *et al.*, 2020).

As discussed in *Chapter 5* there are a range of factors which govern the speed of drug association and dissociation at the target receptor, including allosteric interactions of intracellular proteins, such as G proteins. As described above, agonist equilibrium dissociation constants have been shown to increase in affinity in more “active” conformations, i.e. in the presence of G proteins or mimetics, and as of yet agonist binding kinetics have yet to have been determined at such conformations. It could be suggested that the increased affinity is due to slower association or dissociation rate, however the extent each is influenced by G protein binding is unknown.

6.1.5. Isolating Active Conformations of the β_2 Adrenoceptors.

As seen in *Chapter 5*, attempts were made to isolate populations of the β_2AR, stabilised by either β-arrestin2 and or Gαs protein using both dual-expression systems, using complementary high affinity NanoBiT fragments, and the development of a novel TM-BRET assay. However, unbalanced expression of

receptors and effector proteins suggested that only a fraction of the receptor population was coupled to effector proteins in these systems. In this chapter, to saturate β_2AR-LgBiT receptor constructs, HiBiT-mini Gαs protein was purified and coupled to the receptor in pre-coupling reactions before being used to determine the affinity of β_2AR ligands in TM-BRET and TR-FRET assays. Whilst the affinities of β_2AR ligands at 'active' conformations have been obtained, primarily at in radioligand binding assay, here we aimed to obtain both binding equilibrium and kinetic information at active conformations of β_2AR, using the mini Gαs and high affinity NanoBiT fragments for complex stabilisation.

6.2. Chapter Aims

The work completed in Chapter Six: Results IV, aimed to:

(1) Engineer and purify mini Gαs protein, N-terminally tagged with HiBiT peptide tag.

(2) Use novel transmembrane TM-BRET assays to isolate ligand binding affinities at the β_2AR stabilised by purified mini Gαs protein.

(3) Use TR-FRET assays to isolate ligand binding affinities and kinetic binding properties, at β_2AR stabilised by mini Gαs proteins.

6.3. Results

6.3.1. Purification of a functional HiBiT tagged mini Gαs protein

Whilst HiBiT peptide was synthesised commercially, HiBiT-mini Gαs constructs were engineered and purified in-house. Mini Gαs protein DNA, N-terminally tagged with HiBiT sequence and an upstream 10x HisTag and Tobacco Etch Virus (TEV) cleavage site (*Figure 6. 1. a*), was encoded in IPTG inducible pJ411 bacterial plasmids (*Methods; Figure 2. 2*) to ensure high copy number. The bacterial mini Gαs plasmid was transformed into BL21(DE3) chemically competent E. coli cells, cultured and protein expression induced with IPTG. Cells were harvested and purified using immobilized metal affinity chromatography and a HisTrap FF column, eluting the protein a gradient of imidazole (40-400 mM imidazole), with a further 8 column volumes of 100% imidazole (400 mM imidazole) (*Figure 6. 1. b*). Purified protein was concentrated and buffer exchanged from elution buffer to storage buffer (see *Methods* for buffer constituents) to remove excess imidazole salt. Protein was concentrated to a maximum concentration of 35 μM, with protein observed to be insoluble at higher concentrations.

Increasing concentrations of purified HiBiT peptide or HiBiT-mini Gα protein were incubated with membranes prepared from HEK293T cells expressing SNAP-β_2AR-LgBiT DNA (*Methods; 2.6.2.4.*) and furimazine, producing concentration dependent increase in luminescence which was monitored over 12 minutes (*Figure 6. 2*). A global model of association kinetics (*Methods; 2.8.5.2*) was applied to luminescence responses for each SNAP-β_2AR-LgBiT/HiBiT and SNAP-β_2AR-LgBiT/HiBiT-mini Gαs protein membrane preparation, to derive association, dissociation and kinetically derived affinity values for HiBiT and HiBiT-mini Gαs protein (*Table 6. 1*). Confidence intervals were used to determine the range in which the true estimated parameter (i.e. k_{ON} or k_{OFF}) lies, here at 95% certainty, and this can be compared to the 'best-fit' value. However, confidence intervals of association and dissociation rates of the global association model were shown to be as great as 45% around the best fit mean value.

To further investigate the affinity of HiBiT±mini Gαs protein at SNAP-β_2AR-LgBiT membrane preparations, increasing concentrations of HiBiT or HiBiT-mini Gαs protein were incubated with SNAP-β_2AR-LgBiT membranes for 20 minutes. Furimazine was then added and a concentration dependent increase in luminescence was measured for both HiBiT and HiBiT-mini Gαs protein reactions

(*Figure 6. 3*). Binding curves of HiBiT±mini Gαs protein were used to determine endpoint equilibrium dissociation constants of both HiBiT (22.5±2.9 nM) and HiBiT-mini Gαs protein (147.9±29.3 nM) at SNAP-β_2AR-LgBiT receptor constructs (*Table 6.2*).

In all subsequent binding assays, 500 nM HiBiT±mini Gαs protein was incubated with SNAP-β_2AR-LgBiT membrane preparations in a pre-coupling reaction (20 minutes on ice). As the HiBiT-mini Gαs protein stock concentration was limited by solubility issues, the concentration of 500 nM was chosen for maximum saturation of SNAP-β_2AR-LgBiT receptor constructs, with the lowest appropriate dilution of HiBiT-mini Gαs protein into assay buffer.

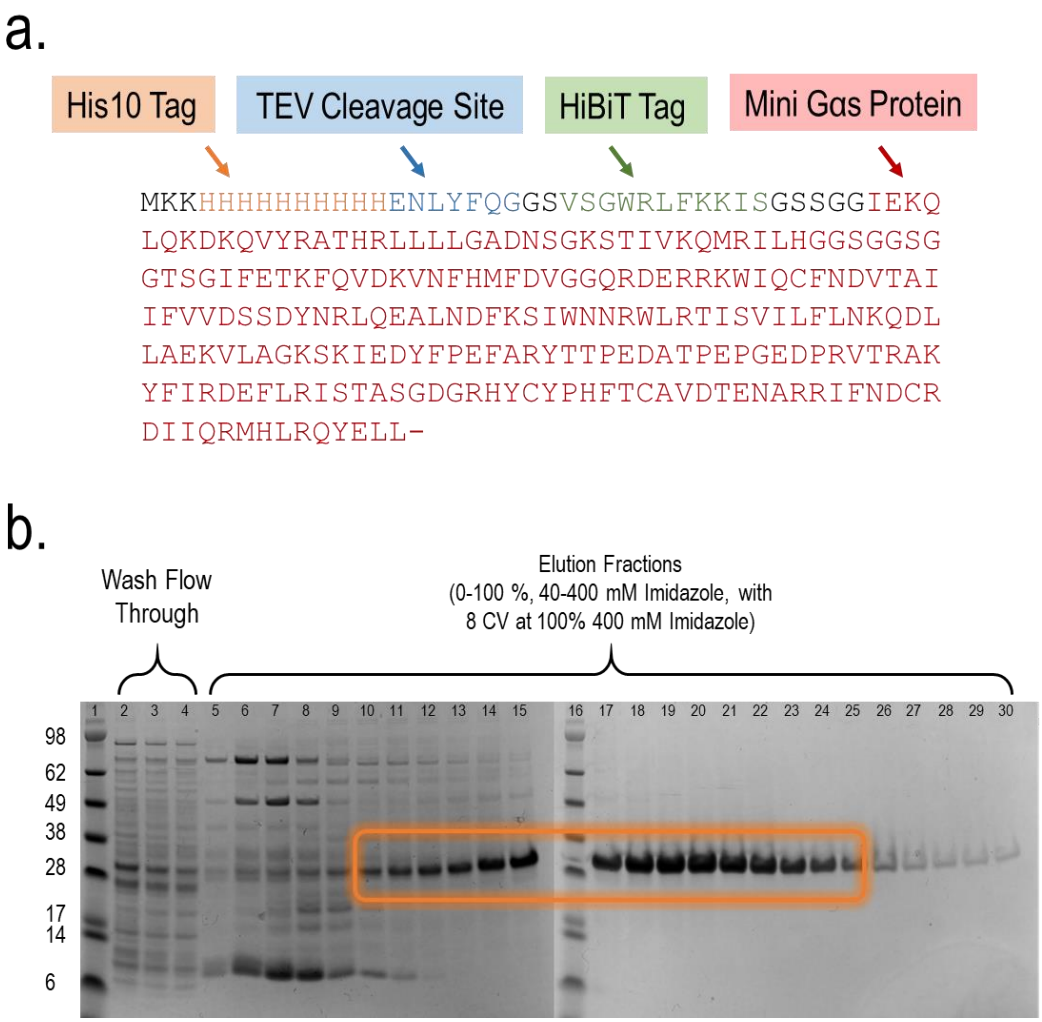

Figure 6. 1 Engineering and Purification of HiBiT-tagged mini Gαs. *(a.) Amino acid sequence of modified mini Gαs protein, N-terminally labelled Hisx10 tag followed by a TEV-cleavage site and 11 amino acid HiBiT sequence. (b.) SDS-PAGE protein purification gel from immobilized metal affinity chromatography column purification. Column 1 & 16: SeeBlue™ Plus2 Pre-stained Protein Standard. Column 2-4: fractions from washing of HisTrap column. Column 5-15 & 17-30: Elution fractions, with fractions selected for protein concentration highlighted by orange box overlay.*

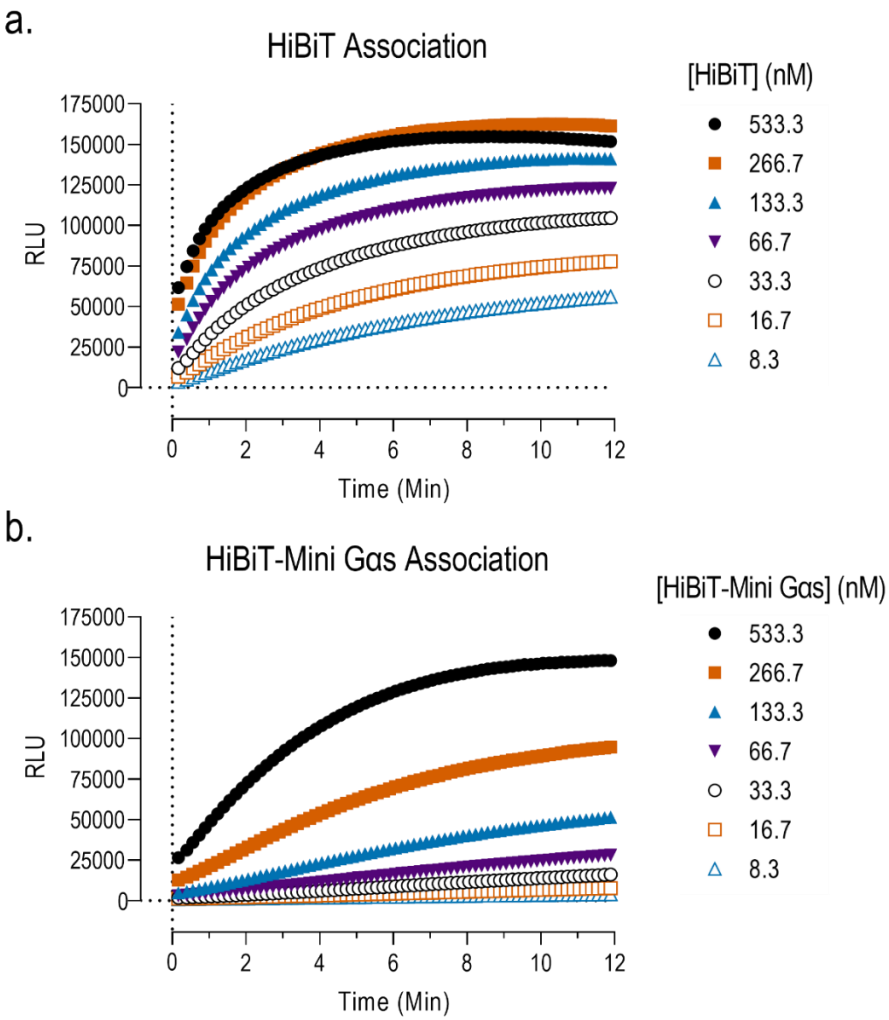

Figure 6. 2 Kinetic NanoBiT complementation assays at membranes prepared from HEK293 cells expressing SNAP-β$_2$AR-LgBiT, with the addition of increasing concentrations of purified HiBiT peptide and purified HiBiT-mini Gαs protein at timepoint 0. *Representative trace of HiBiT±Mini Gαs protein binding kinetics in NanoBiT complementation assay reported as raw luminescence units (RLU). Data are from an individual experiment, conducted in singlet, representative of n=3.*

	k_{ON} ($M^{-1}Min^{-1}$)	k_{OFF} (Min^{-1})	K_D (nM)	N
HiBiT	*$3.77x10^6 \pm 8.00x10^5$*	*0.037 ± 0.011*	*11.3 ± 5.3*	*3*
HiBiT-Mini Gα$_s$	*$1.97x10^5 \pm 2.98x10^4$*	*0.128 ± 0.015*	*688.8 ± 147.9*	*3*

Table 6. 1 Pooled kinetic binding parameters of purified HiBiT peptide and purified HiBiT-mini Gαs protein at membranes prepared from cells expressing SNAP-β$_2$AR-LgBiT, in kinetic NanoBiT complementation assays. *Pooled association (k_{ON}), dissociation (k_{OFF}) and resultant kinetic derived equilibrium dissociation constant (kinetic K_D= k_{OFF}/k_{ON}) obtained from a global model of association kinetics were pooled from 3 independent experiments, conducted in singlet, with each binding property represented as mean ± S.E.M..*

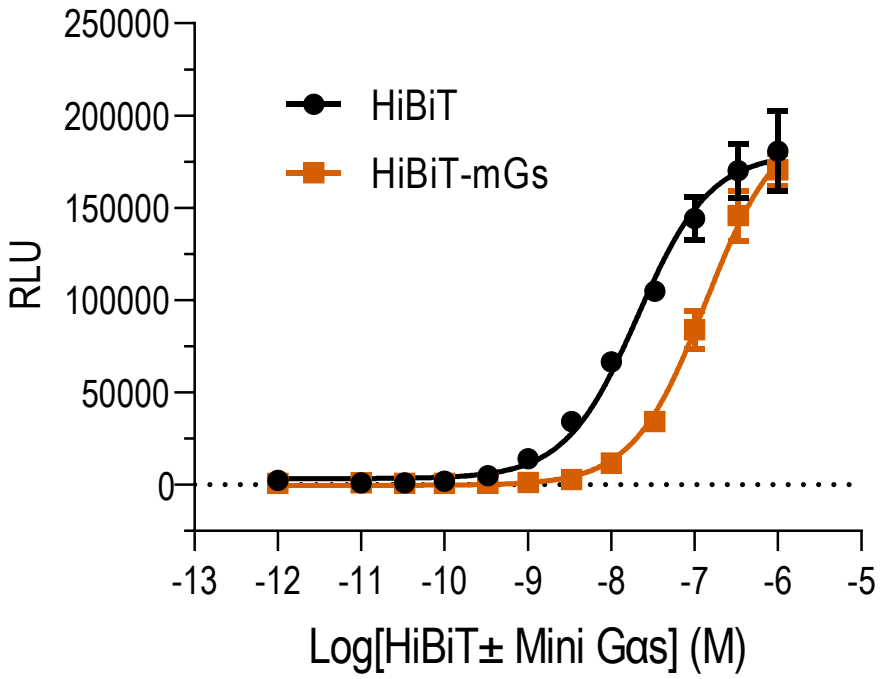

Figure 6. 3 Concentration dependent luminescence from NanoBiT complementation assays at membranes prepared from cells expressing SNAP-β$_2$AR-LgBiT, following 20 minute incubation with increasing concentrations of purified HiBiT peptide and purified HiBiT-mini Gαs protein. *Data points represent pooled raw luminescence units (RLU), as mean ± S.E.M., from 3 independent experiments, conducted in duplicate.*

	pK_D (M)	K_D (nM)	n
HiBiT	7.66 ± 0.06	22.5 ± 2.9	3
HiBiT-Mini Gαs	6.85 ± 0.09	147.9 ± 29.3	3

Table 6.2 Pooled equilibrium dissociation constants (K_D) of purified HiBiT peptide and purified HiBiT-mini Gαs protein, from membranes prepared from cells expressing SNAP-β$_2$AR-LgBiT, in end-point NanoBiT complementation assays. *Equilibrium dissociation constant were pooled from 3 independent experiments, conducted in duplicate. pK_D and K_D values represented as mean ± S.E.M.*

6.3.2. Use of TM-BRET in the presence and absence of a mini Gαs protein to determine BODIPY-FL-PEG8-(S)-Propranolol affinity at the SNAP-β_2AR-LgBiT.

To isolate measures of ligand binding from selected receptor populations, membranes were prepared from SNAP-β_2AR-LgBiT cell lines were supplemented with 500 nM of purified HiBiT peptide or HiBiT-mini Gαs protein, and incubated on ice for 20 minutes prior to the assay. As in *Chapter 5*, for all TM-BRET assays no terbium labelling was required as donor luminescence resulted from complemented NanoBiT fragments. Membrane/peptide preparations were then applied in the fluorescent ligand binding BRET assay, in which the luminescence from the complemented NanoBiT luciferase enzyme acted as the transmembrane donor emission, as illustrated in schematic representations of TM-BRET (*Figure 6. 4*) (also demonstrated in *Chapter 5*).

Saturation binding assays measured the TM-BRET response when incubating each SNAP-β_2AR-LgBiT/HiBiT peptide or SNAP-β_2AR-LgBiT/HiBiT-mini Gαs preparation with increasing concentrations of BODIPY-FL-PEG8-(S)-Propranolol, in the presence and absence of the unlabelled competitor (10 µM ICI-118,551) to determine total and non-specific binding, respectively (*Figure 6. 4*). Following a 20 minute incubation, total binding of BODIPY-FL-PEG8-(S)-Propranolol was saturable in SNAP-β_2AR-LgBiT/HiBiT (*Figure 6. 4. a*) and SNAP-β_2AR-LgBiT/HiBiT-mini Gαs (*Figure 6. 4. b*) preparations, whilst levels of non-specific binding were linear in relation to BODIPY-FL-PEG8-(S)-Propranolol concentration.

Equilibrium dissociation constants of BODIPY-FL-PEG8-(S)-Propranolol derived from TM-BRET assays, demonstrated BODIPY-FL-PEG8-(S)-Propranolol bound with nanomolar affinity at both SNAP-β_2AR-LgBiT/HiBiT (K_D=7.08±1.08 nM, n=4) and SNAP-β_2AR-LgBiT/HiBiT-mini Gαs (K_D=9.44±0.85 nM, n=5) preparations. These values were similar to those obtained in in *Chapter 5* transmembrane BRET assays from β_2AR-LgBiT membranes + 10 µM HiBiT peptide (*Chapter 5*; *Table 5.3*).

The emission wavelengths of both the NanoBiT luminescence and BODIPY-FL-PEG8-(S)-Propranolol fluorescence were also compared between wells, to ensure binding observed in the BRET ratio was not an artefact of changes in the donor signal (*Figure 6. 5*). In both SNAP-β_2AR-LgBiT/peptide membrane preparations, NanoBiT luminescence emissions (475-30 nm) were consistent

between treatment conditions, with increasing concentrations of BODIPY-FL-PEG8-(S)-Propranolol and in the presence and absence of 10 μM ICI-118,551 (*Figure 6. 5. a.-b.*). BODIPY-FL-PEG8-(S)-Propranolol fluorescent emissions (535-30 nm) were positively correlated with BODIPY-FL-PEG8-(S)-Propranolol concentration, which was reduced in the treatment of 10 μM ICI-118,551, in both SNAP-β_2AR-LgBiT/HiBiT (*Figure 6. 5. c.*) and SNAP-β_2AR-LgBiT/HiBiT-mini Gαs (*Figure 6. 5. d.*) preparations.

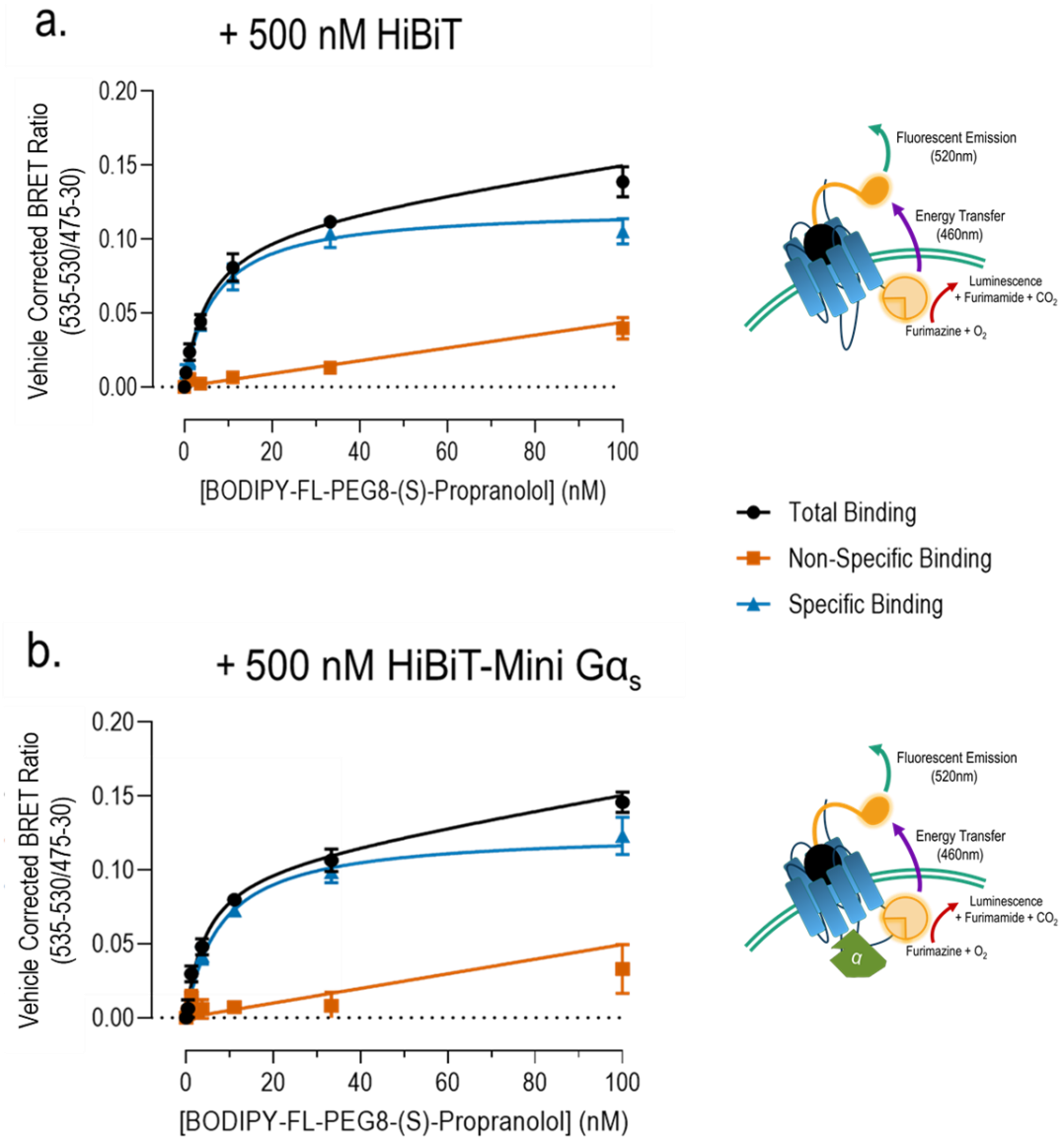

Figure 6. 4 TM-BRET saturation binding assays for BODIPY-FL-PEG8-(S)-Propranolol, at membranes prepared from cells expressing SNAP-β2AR-LgBiT, supplemented with either 500 nM purified HiBiT peptide (a.) or 500 nM purified HiBiT-mini Gαs protein (b.). *Total, non-specific and specific binding of BODIPY-FL-PEG8-(S)-Propranolol was pooled from 4-5 independent experiments, conducted in duplicate. Data points represent mean ± S.E.M..*

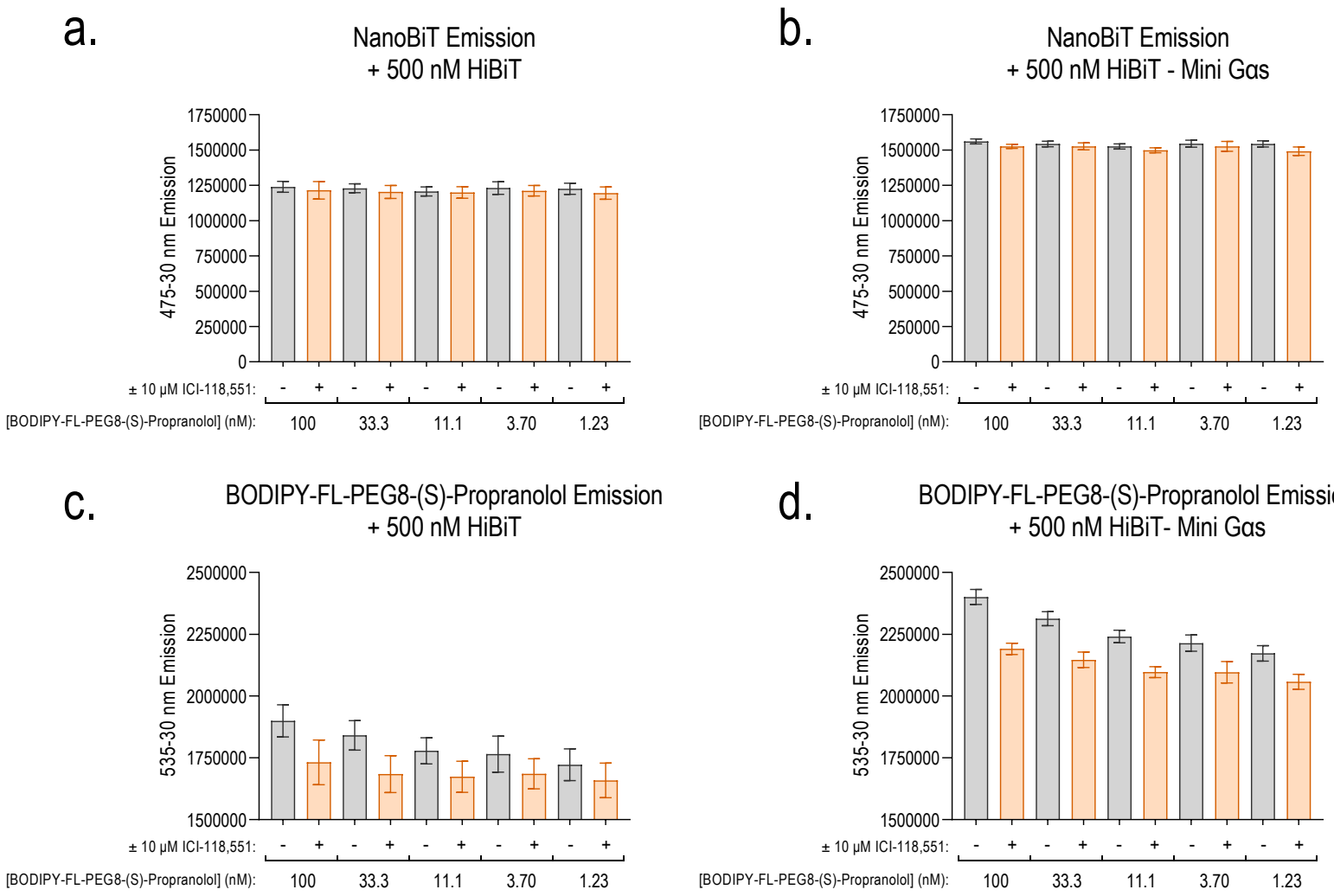

Figure 6. 5 NanoBiT and BODIPY-FL-PEG8-(S)-Propranolol emission wavelengths from saturation TM-BRET binding assays. *NanoBiT (475-30 nm) (a. – b.) and BODIPY-FL-PEG8-(S)-Propranolol (535-30 nm) (c. – d.) emissions from TM-BRET saturation binding assays (Figure 6. 4), at SNAP-β_2AR-LgBiT receptors, supplemented with purified HiBiT peptide (a. & c.) and HiBiT-mini Gαs protin (b. & d.). Bars represent pooled emissions as mean ± S.E.M, averaged from 4-5 independent experimental replicates, in TR-FRET assays with increasing concentrations of BODIPY-FL-PEG8-(S)-Propranolol and in the presence and absence of 10 µM ICI-118-551.*

6.3.3. The purified HiBiT-mini Gαs protein increases agonist affinities at β_2ARs, using the TM-BRET assay.

In *Chapter 5*, novel TM-BRET assays were used to try and identify changes in ligand affinity in membranes prepared from dual-expression cells of SNAP-β_2AR-LgBiT and HiBiT labelled effectors. Here, SNAP-β_2AR-LgBiT membranes supplemented with purified HiBiT± mini Gαs protein were applied in the established TM-BRET assay to determine the effect of the mini Gαs protein on β_2AR ligand binding affinities, following a 20 minute pre-coupling reaction on ice.

Increasing concentrations of each β_2AR ligand (isoprenaline, formoterol, salmeterol and ICI-118,551) were able to compete with BODIPY-FL-PEG8-(S)-Propranolol binding in a concentration dependent manner (*Figure 6. 6*). IC_{50} values for each ligand were converted to K_i values, using the Cheng Prusoff equation (*Methods; Equation 2.23*) in each membrane/peptide preparation (*Table 6. 3*), using equilibrium dissociation constants for BODIPY-FL-PEG8-(S)-Propranolol obtained in saturation TM-BRET assays under the same conditions (*Figure 6. 4*).

In SNAP-β_2AR-LgBiT membranes supplemented with HiBiT-mini Gαs protein, the affinity of isoprenaline increased 240-fold compared with the same membrane supplemented with HiBiT peptide (Student's t-test, $P<0.0001$) (*Figure 6. 7*; *Table 6. 3*). Moreover, the affinity of formoterol and salmeterol were shown to increase 5-fold and 4-fold, respectively, in SNAP-β_2AR-LgBiT membranes supplemented with HiBiT-mini Gαs protein in comparison with HiBiT peptide (Student's t-test, $P<0.05$) (*Figure 6. 7*; *Table 6. 3*). However, the affinity of ICI-118,551 was unchanged between HiBiT and HiBiT-mini Gαs protein supplemented membrane preparations (Student's t-test, $P>0.05$) (*Figure 6. 7*; *Table 6. 3*).

The Hill slopes of each competition binding curve were pooled between replicates, with the shallowest Hill Slope averaged from isoprenaline binding curves in SNAP-β_2AR-LgBiT/HiBiT membranes (0.54±0.09) (*Table 6. 3*). Overall, Hill Slopes obtained from competition binding assays were below unity ($P<0.01$; Student's t-test), excluding the Hill Slope from formoterol binding curves in SNAP-β_2AR-LgBiT/HiBiT-mini Gαs membranes (1.13±0.34) (*Table 6. 3*).

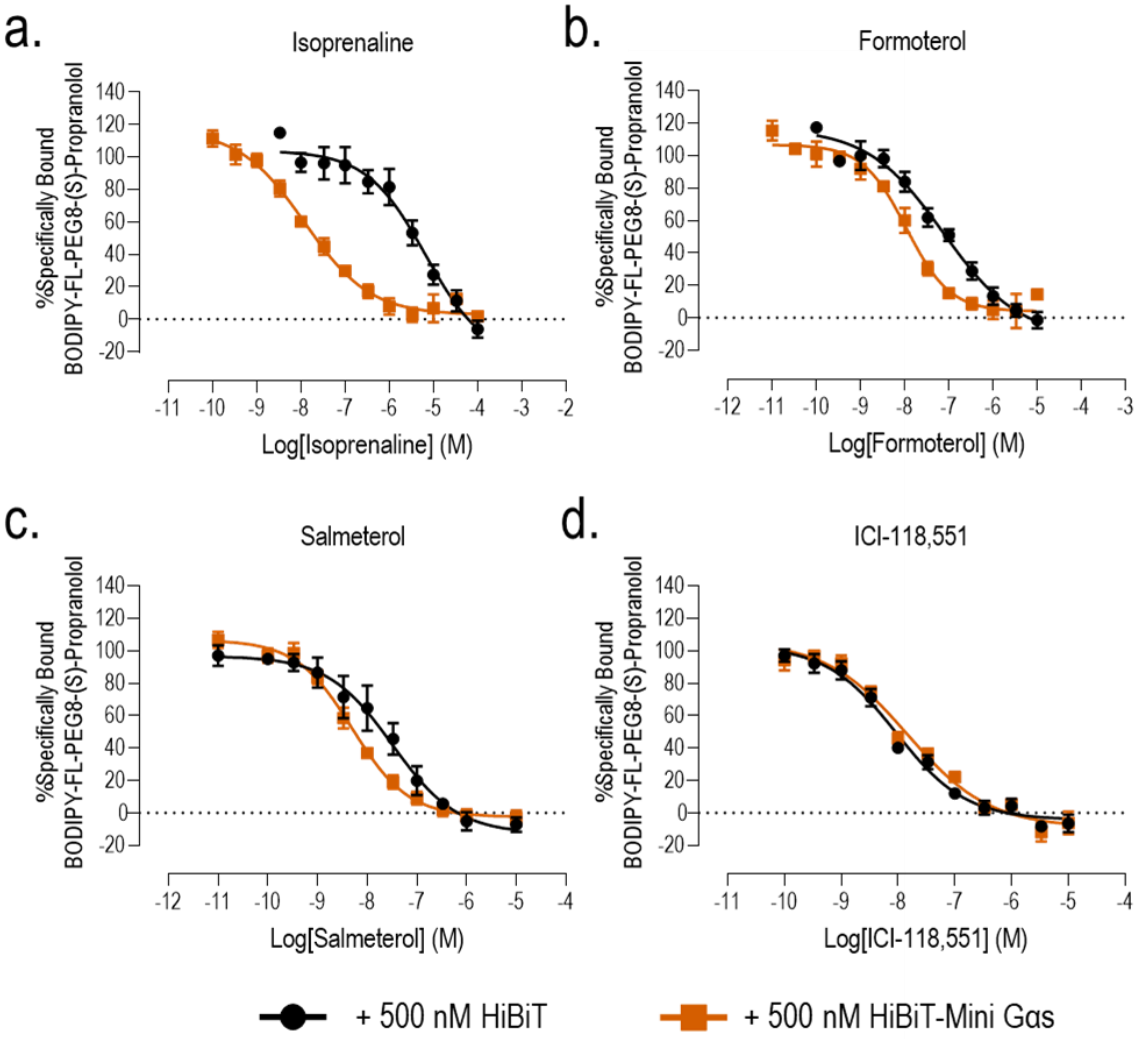

Figure 6. 6 TM-BRET competition binding assays establish agonist equilibrium binding constants of unlabelled β_2AR ligands, from membranes prepared from cells expressing SNAP-β_2AR-LgBiT, supplemented with 500 nM purified HiBiT peptide (black) or 500 nM purified HiBiT-mini Gαs protein (orange). *Competition binding between 10 nM BODIPY-FL-PEG8-propranolol and increasing concentrations of β_2AR ligands ((a.) isoprenaline; (b.) formoterol; (c.) salmeterol; and (d.) ICI-118,551) at membranes prepared from HEK293T cells stably expressing terbium-labelled SNAP-β_2AR-LgBiT, supplemented with 500 nM purified HiBiT peptide or 500 nM purified HiBiT-mini Gαs protein, supplemented with 100 μM GppNHp. End point data taken after 20 minute incubation at 37°C. Non-specific binding quantified using 10μM ICI-118,551. Data points represent TM-BRET response as a % of specific BODIPY-FL-PEG8-(S)-Propranolol binding, mean ± S.E.M., performed in duplicate (n=4).*

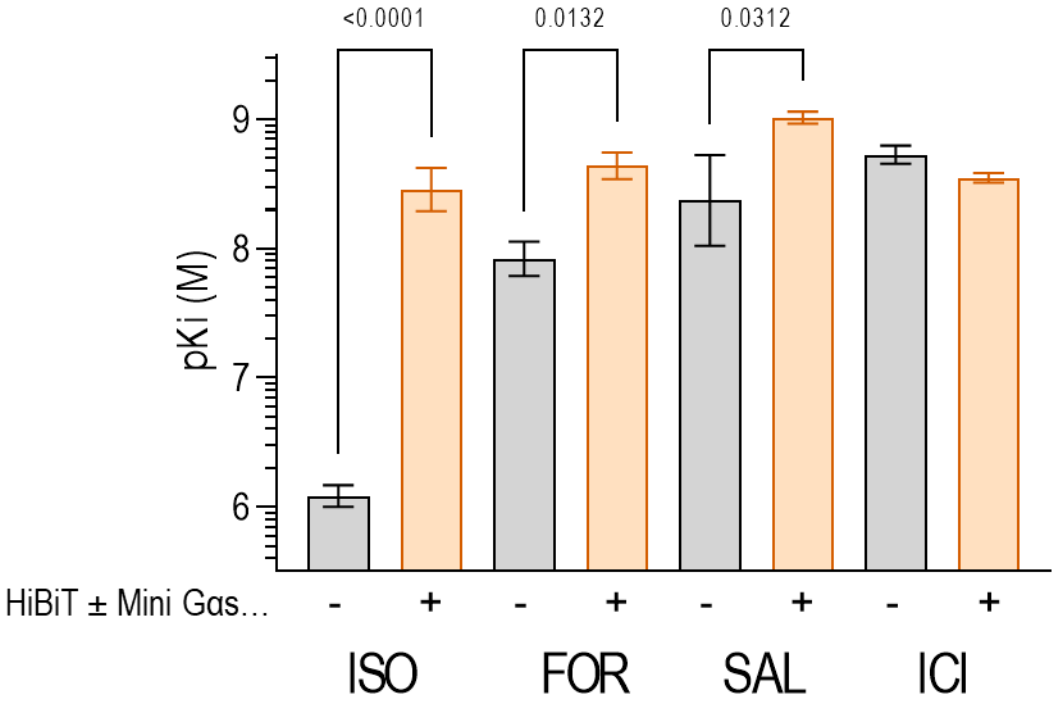

Figure 6. 7 Pooled ligand equilibrium dissociation constants of unlabelled β_2AR agonists, using TM-BRET binding assays from membranes prepared from HEK293T cells stably expressing SNAP-β_2AR-LgBiT, supplemented with 500 nM purified HiBiT peptide (grey bars) or 500 nM purified HiBiT-mini Gαs protein (orange bars). *pIC_{50} values obtained from competition TM-BRET assays (Figure 6. 6) were converted to pKi values, describing the affinities of unlabelled ligands. Bars represent pooled pKi values, as mean ± S.E.M., from 4 individual experiments, conducted in duplicate.*

	pKi (M)		*Hill Slope*	
	HiBiT	HiBiT – Mini Gαs	HiBiT	HiBiT – Mini Gαs
Isoprenaline	6.08 ± 0.08	8.46 ± 0.17*	0.63 ± 0.17	0.54 ± 0.09
Formoterol	7.92 ± 0.13	8.64 ± 0.10*	0.57 ± 0.07	1.13 ± 0.34
Salmeterol	8.37 ± 0.35	9.01 ± 0.05*	0.82 ± 0.12	0.81 ± 0.04
ICI-118,551	8.73 ± 0.07	8.55 ± 0.04	0.67 ± 0.08	0.61 ± 0.07

Table 6. 3 Summary of ligand equilibrium dissociation constants and Hill slopes of unlabelled β_2AR agonists, using TM-BRET binding assays from membranes prepared from HEK293T cells stably expressing SNAP-β_2AR-LgBiT, supplemented with 500 nM purified HiBiT peptide or 500 nM purified HiBiT-mini Gαs protein. *pIC_{50} values obtained from competition TM-BRET assays (Figure 6. 6) were converted to pKi values, describing the affinities of unlabelled ligands. Pooled data are shown as mean ± S.E.M., from 4 individual experiments, conducted in duplicate.*

6.3.4. Determination of BODIPY-FL-PEG8-(S)-Propranolol affinity at the SNAP-β_2AR-LgBiT, in the presence and absence of mini Gαs, in TR-FRET binding assays.

To complement TM-BRET studies (*Figure 6. 4*), TR-FRET assays were applied to monitor binding of BODIPY-FL-PEG8-(S)-Propranolol in SNAP-β_2AR-LgBiT membrane preparations supplemented with HiBiT peptide and HiBiT-tagged mini Gαs protein.

As conducted in TM-BRET assays (*Chapter 6*; *6. 3. 2*), membranes prepared from terbium labelled SNAP-β_2AR-LgBiT cell lines were supplemented with 500 nM of purified HiBiT peptide or HiBiT-mini Gαs protein, and incubated on ice for 20 minutes prior to the assay. Membrane/peptide preparations were then applied in the fluorescent ligand binding TR-FRET assay (Chapter 5). Saturation binding assays measured the TR-FRET response when incubating each SNAP-β_2AR-LgBiT/HiBiT±mini Gαs preparation with increasing concentrations of BODIPY-FL-PEG8-(S)-Propranolol, in the presence and absence of the unlabelled competitor (10 μM ICI-118,551) to determine total and non-specific binding, respectively (*Figure 6. 8*).

Following a 20 minute incubation, total binding of BODIPY-FL-PEG8-(S)-Propranolol was saturable in SNAP-β_2AR-LgBiT/HiBiT (*Figure 6. 8. a*) and SNAP-β_2AR-LgBiT/HiBiT-mini Gαs (*Figure 6. 8. b*) preparations, whilst levels of non-specific binding were negligible and linear in relation to BODIPY-FL-PEG8-(S)-Propranolol concentration.

Equilibrium dissociation constants of BODIPY-FL-PEG8-(S)-Propranolol derived from TR-FRET assays, demonstrated BODIPY-FL-PEG8-(S)-Propranolol bound with nanomolar affinity in both SNAP-β_2AR-LgBiT/peptide preparations (*Figure 6. 8*). Moreover, The affinity of BODIPY-FL-PEG8-(S)-Propranolol was observed to be significantly less in SNAP-β_2AR-LgBiT /HiBiT preparations (K_D=7.48±0.56 nM, n=3), compared with SNAP-β_2AR-LgBiT/HiBiT-mini Gαs (K_D=10.63±0.34 nM, n=3) preparations (Student's t-test; $P<0.01$), though the magnitude of this difference was very small.

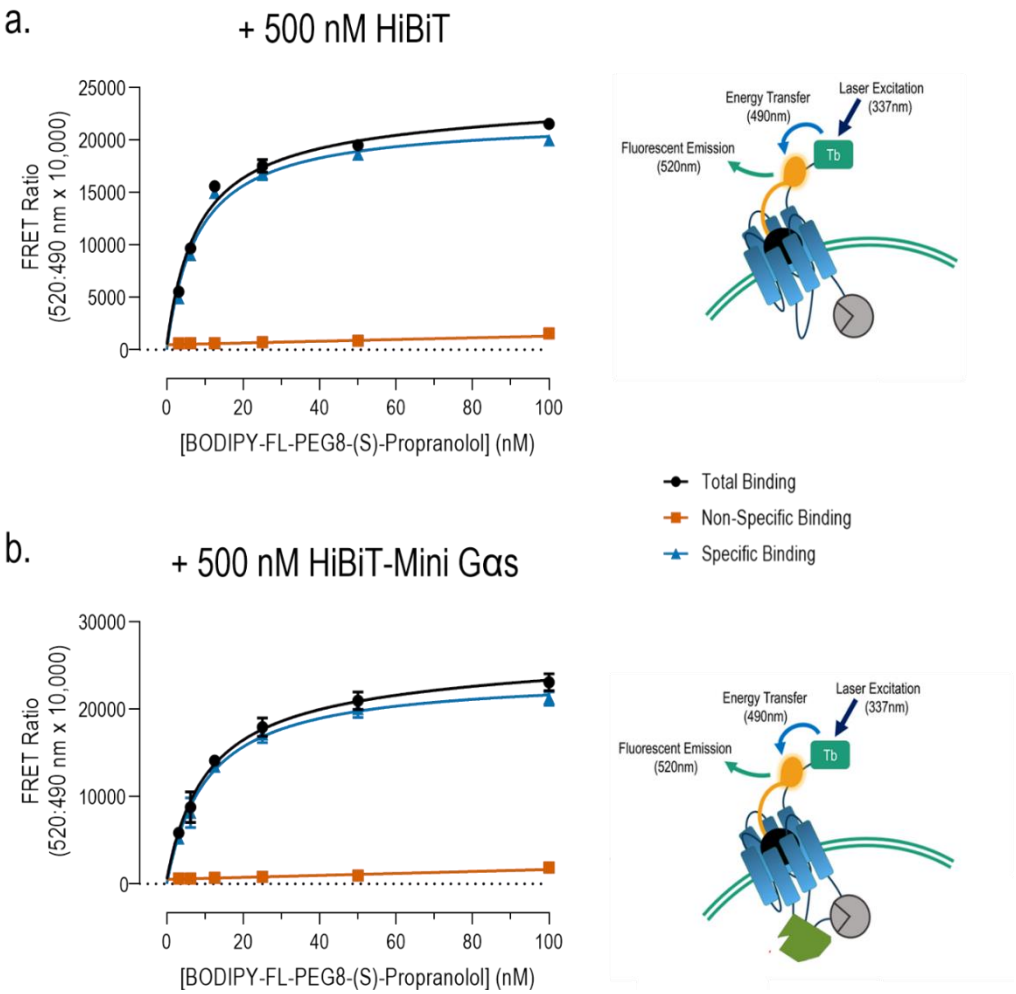

Figure 6. 8 TR-FRET saturation binding assays of BODIPY-FL-PEG8-(S)-Propranolol, from membranes prepared from cells expressing SNAP-β_2AR-LgBiT, supplemented with either 500 nM purified HiBiT peptide (a.) or 500 nM purified HiBiT-mini Gαs protein (b.). *Total, non-specific and specific binding of BODIPY-FL-PEG8-(S)-Propranolol were pooled from 3 independent experiments, conducted in duplicate. Data points represent mean ± S.E.M..*

6.3.5. The presence of purified HiBiT-mini Gαs protein increases agonist affinities at β_2ARs, measured by TR-FRET competition binding assays.

To complement TM-BRET competition binding studies (*Figure 6. 6*; *Figure 6. 7*; *Table 6. 3*), TR-FRET competition assays were used to compete unlabelled β_2AR ligands against BODIPY-FL-PEG8-(S)-Propranolol in SNAP-β_2AR-LgBiT membrane preparations supplemented with HiBiT peptide and HiBiT-tagged mini Gαs protein.

All β_2AR ligands (isoprenaline, formoterol, salmeterol and ICI-118,551) reduced BODIPY-FL-PEG8-(S)-Propranolol binding in a concentration dependent manner (*Figure 6. 9*). IC_{50} values were converted to K_i values for each ligand, using the Cheng Prusoff equation (*Methods*; *Equation 2.23*) in each membrane/peptide preparation (*Table 6. 5*), using equilibrium dissociation constants for BODIPY-FL-PEG8-(S)-Propranolol obtained in saturation TR-FRET assays (*Figure 6. 8*).

Following a 20 minute TR-FRET binding reaction, the affinity of isoprenaline increased 282-fold in SNAP-β_2AR-LgBiT membranes supplemented with HiBiT-mini Gαs protein in comparison with HiBiT peptide (Student's t-test, $P<0.0001$) (*Figure 6. 9*; *Figure 6. 10*; *Table 6. 5*). In addition, in SNAP-β_2AR-LgBiT membranes supplemented with HiBiT-mini Gαs protein the affinity of formoterol and salmeterol were shown to increase 38-fold and 10-fold, respectively, compared with SNAP-β_2AR-LgBiT membranes supplemented with HiBiT peptide (Student's t-test, $P<0.0001$) (*Figure 6. 9*; *Figure 6. 10*; *Table 6. 5*). As seen in TM-BRET binding assays, the affinity of ICI-118,551 obtained in the TR-FRET assay was not significantly different between HiBiT and HiBiT-mini Gαs protein supplemented SNAP-β_2AR-LgBiT membrane preparations (Student's t-test, $P>0.05$) (*Figure 6. 9*; *Figure 6. 10*; *Table 6. 5*).

As before, the Hill Slope of each competition binding curve was averaged, with the shallowest Hill Slope averaged from isoprenaline binding curves in SNAP-β_2AR-LgBiT/HiBiT membranes (0.80±0.06) (*Table 6. 5*). Overall, Hill Slopes obtained from competition binding assays were within 0.11 of the unit Hill slopes (1.00), excluding the average Hill Slope from isoprenaline curves in SNAP-β_2AR-LgBiT/HiBiT-mini Gαs membranes (*Table 6. *), and no Hill slope was significantly different from 1.00 ($P>0.05$; Student's t-test). In comparison to TM-

BRET competition studies, Hill slopes obtained from competition binding curves in TR-FRET assays were steeper (P=0.009, Student's t-test) and demonstrated Hill Slopes closer to 1.00 (0.95±0.03), which is expected for one-site binding interactions at equilibrium.

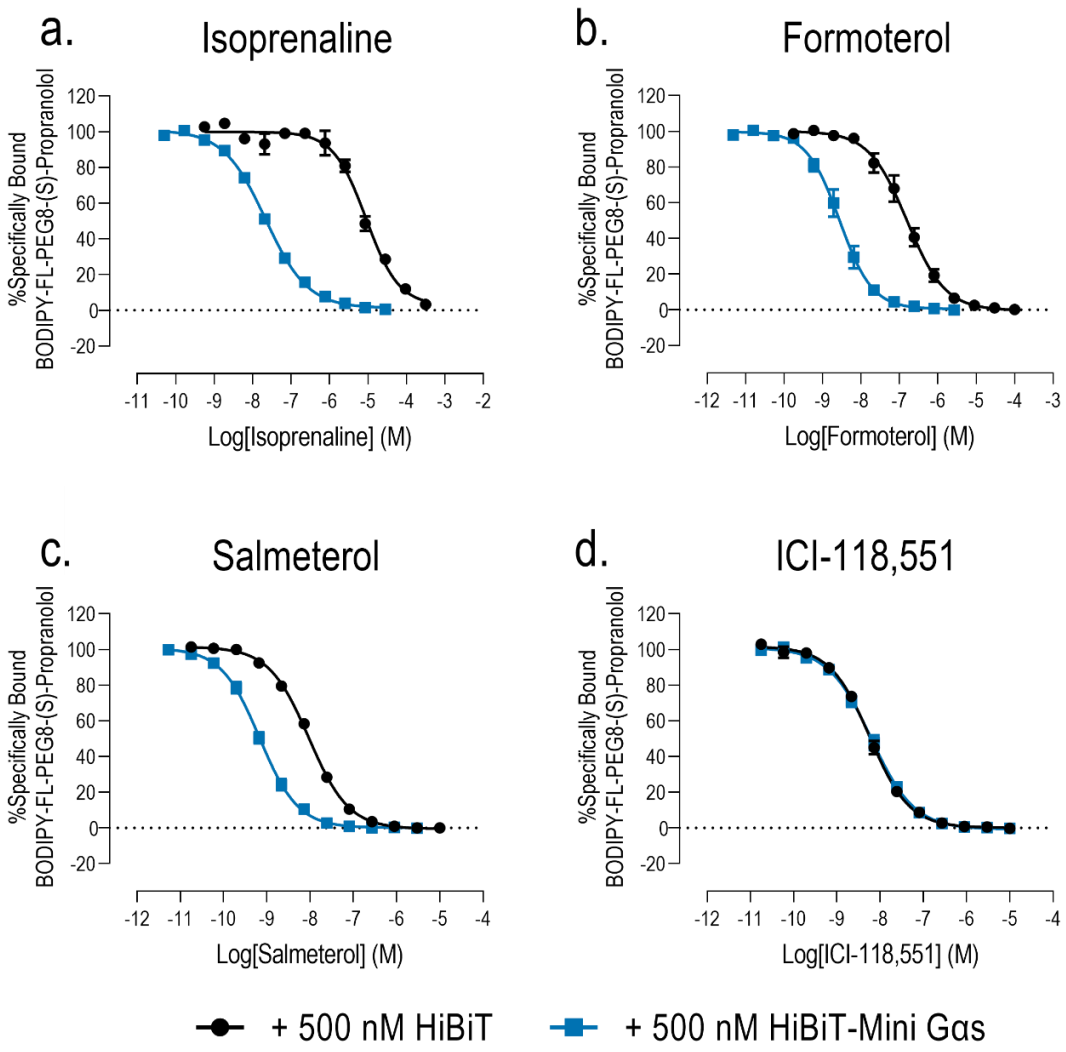

Figure 6. 9 TR-FRET competition binding assays establish ligand competition binding curves for unlabelled β_2AR ligands, from membranes prepared from cells expressing terbium labelled SNAP-β_2AR-LgBiT, supplemented with 500 nM purified HiBiT peptide (black) or 500 nM purified HiBiT-mini Gαs protein (blue). *Competition binding between 10 nM BODIPY-FL-PEG8-propranolol and increasing concentrations of β_2AR ligands ((a.) isoprenaline; (b.) formoterol; (c.) salmeterol; and (d.) ICI-118,551), with assays performed in the additional presence of supplemented with 100 µM GppNHp. End point data taken after 20 minute incubation at 37°C. Non-specific binding quantified using 10µM ICI-118,551. Data points represent TR-FRET response as a % of specific BODIPY-FL-PEG8-(S)-Propranolol binding, mean ± S.E.M., performed in duplicate (n=3).*

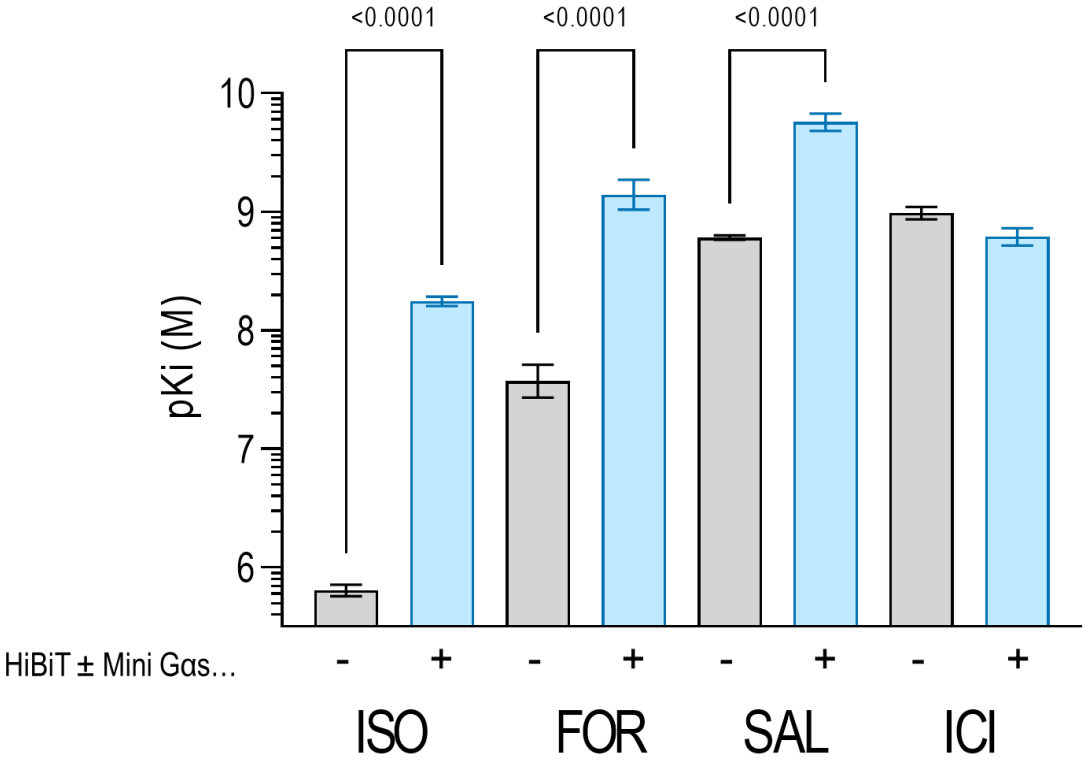

Figure 6. 10 Pooled ligand equilibrium dissociation constants of unlabelled β_2AR agonists, using TR-FRET binding assays from membranes prepared from HEK293T cells stably expressing terbium-labelled SNAP-β_2AR-LgBiT, supplemented with 500 nM purified HiBiT peptide (grey bars) or 500 nM purified HiBiT-mini Gαs protein (blue bars). *pIC_{50} values obtained from competition TR-FRET assays (Figure 6. 9) were converted to pKi values, describing the affinities of unlabelled ligands. Bars represent pooled pKi values, as mean ± S.E.M., from 3 individual experiments, conducted in duplicate.*

	pKi (M)		*Hill Slope*	
	HiBiT	HiBiT – Mini Gαs	HiBiT	HiBiT – Mini Gαs
Isoprenaline	5.80 ± 0.05	8.25 ± 0.04*	1.02 ± 0.18	0.80 ± 0.06
Formoterol	7.57 ± 0.14	9.15 ± 0.13*	0.91 ± 0.07	1.08 ± 0.05
Salmeterol	8.78 ± 0.02	9.76 ± 0.07*	0.94 ± 0.01	1.00 ± 0.07
ICI-118,551	8.99 ± 0.05	8.79 ± 0.07	0.96 ± 0.04	0.89 ± 0.01

Table 6. 5 Summary of ligand equilibrium dissociation constants and Hill slopes of unlabelled β_2AR agonists, using TR-FRET binding assays from membranes prepared from HEK293T cells stably expressing terbium-labelled SNAP-β_2AR-LgBiT, supplemented with 500 nM purified HiBiT peptide or 500 nM purified HiBiT-mini Gαs protein. *pIC_{50} values obtained from competition TR-FRET assays (Figure 6. 9) were converted to pKi values via the Cheng-Prusoff correction. Pooled pKi values and Hill Slopes are mean ± S.E.M., from 3 individual experiments, conducted in duplicate.*

6.3.6. Ligand binding kinetics measured at β_2ARs stabilised by HiBiT-mini Gαs proteins, in TR-FRET kinetic binding assays.

To further interrogate the influence of mini Gαs interaction on ligand binding at the β_2AR, kinetic TR-FRET binding assays were conducted from membranes prepared from HEK293T cells expressing SNAP-β_2AR-LgBiT receptor constructs and supplemented in the 20 min pre-coupling incubation with purified HiBiT± mini Gαs protein. SNAP-β_2AR-LgBiT/HiBiT peptide or SNAP-β_2AR-LgBiT/HiBiT-mini Gαs preparations were then added to increasing concentrations of BODIPY-FL-PEG8-(S)-Propranolol in the presence and absence of 10 μM ICI-118,551, with the specific TR-FRET association kinetics monitored over 18 minutes (*Figure 6. 11*).

BODIPY-FL-PEG8-(S)-Propranolol binding at both terbium labelled β_2AR preparations was concentration dependent, with increased FRET ratio responses observed at higher BODIPY-FL-PEG8-(S)-Propranolol concentrations (*Figure 6. 11*). The observed association rate (kObs) at each concentration of BODIPY-FL-PEG8-(S)-Propranolol was positively correlated with BODIPY-FL-PEG8-(S)-Propranolol concentration, and a linear regression was fitted to the data points for both SNAP-β_2AR-LgBiT/HiBiT (*Figure 6. 11. a*; *Figure. 6. 12 a*) and SNAP-β_2AR-LgBiT/HiBiT-mini Gαs (*Figure 6. 11. b*; *Figure 6. 12. b*). Linear fits suggested the interaction between receptors and BODIPY-FL-PEG8-(S)-Propranolol was defined by a first order interaction as expected for a single site receptor population.

As conducted in *Chapter 4*, a global single site model of association kinetics to BODIPY-FL-PEG8-(S)-Propranolol binding across different concentrations to derive kinetic binding properties (*Methods 2.8.5.2*), in each SNAP-β_2AR-LgBiT/HiBiT±mini Gαs preparation. Each kinetic binding parameter for the antagonist (k_{ON}, k_{OFF} and the resultant residence time and kinetic K_D; *Table 6. 6*) was shown to be comparable between SNAP-β_2AR-LgBiT/HiBiT and SNAP-β_2AR-LgBiT/HiBiT-mini Gαs preparations, determined by Student's t-test, unpaired.

To obtain association and dissociation rates of unlabelled ligands, pre-coupled SNAP-β_2AR-LgBiT/HiBiT±mini Gαs preparations were added to increasing concentrations of an unlabelled ligand and a set concentration of BODIPY-FL-PEG8-(S)-Propranolol (25 nM, approximately 3 x K_D) (*Figure 6. 13*; *Figure 6. 14*). The binding was monitored for 18 minutes and fitted to a Motulsky-

Mahan model of competitive binding (Motulsky and Mahan, 1984) to determine association and dissociation rates of the unlabelled ligands: two full β_2AR agonists (isoprenaline and formoterol), one partial β_2AR agonist (salmeterol) and one β_2AR antagonist (ICI-118,551) (ligand efficacies as described by NanoBiT assays; *Chapter 3 & 4*).

The association rate constants (k_{ON}) for all β_2AR ligands were shown to be unchanged between rates obtained in SNAP-β_2AR-LgBiT/HiBiT and SNAP-β_2AR-LgBiT/HiBiT-mini Gαs preparations ($P>0.05$; Student's t-test, unpaired), with the same order of association rate, slowest to fastest: isoprenaline<salmeterol=formoterol<ICI-118,551 (*Figure 6. 15. a*; *Table 6. 7*).

However, estimated dissociation rate constants of isoprenaline, formoterol and salmeterol were 104-fold, 107-fold and 15-fold slow slower in SNAP-β_2AR-LgBiT/HiBiT-mini Gαs membrane preparations, respectively, compared with SNAP-β_2AR-LgBiT/HiBiT ($P<0.05$; Student's t-test) (*Figure 6. 15. b*; and *Figure 6. 15. c* (as residence time); *Table 6. 8*). The ligand dissociation rate constant of the β_2AR antagonist ICI-118,551 did not significantly change between SNAP-β_2AR-LgBiT/HiBiT and SNAP-β_2AR-LgBiT/HiBiT-mini Gαs TR-FRET assays (*Figure 6. 15. b.-c.*; *Table 6. 7*).

As observed in end-point derived equilibrium dissociation constants in both TM-BRET (*Figure 6. 6*; *Figure 6. 7*; *Table 6.*) and TR-FRET (*Figure 6.* **6***9*; *Figure 6. 10*; *Table 6. 5*) assays, kinetically derived K_D values of all β_2AR agonists significantly increased in SNAP-β_2AR-LgBiT/HiBiT-mini Gαs membrane preparations, compared with SNAP-β_2AR-LgBiT/HiBiT ($P<0.001$; Student's t-test), whilst the affinity of ICI-118,551 was unchanged ($P>05$; Student's t-test) (*Table 6. 6*).

Confidence intervals from individual fits of the Motulsky-Mahan model of competitive binding provided a guide to how well the model fitted the experimental data and thus the reliability of estimated kinetic binding parameters. The overall confidence intervals from modelled association rates were within 8% of the 'best fit' value, whilst the confidence intervals of the β_2AR ligand dissociation rates were within 14% of the 'best fit' value. Between β_2AR ligands, the 'best fit' estimates of both k_{ON} and k_{OFF} rates were within 11, 18 and 9 % of the best-fit estimations, for isoprenaline, formoterol and ICI-118,551, respectively. Whilst the fit of the model to the salmeterol kinetic binding data in SNAP-β_2AR-LgBiT/HiBiT-mini Gαs membrane preparations appears to fit the

model poorly, the ‘best fit’ estimates of both k_{ON} and k_{OFF} rates were within 12 % of the best-fit values.

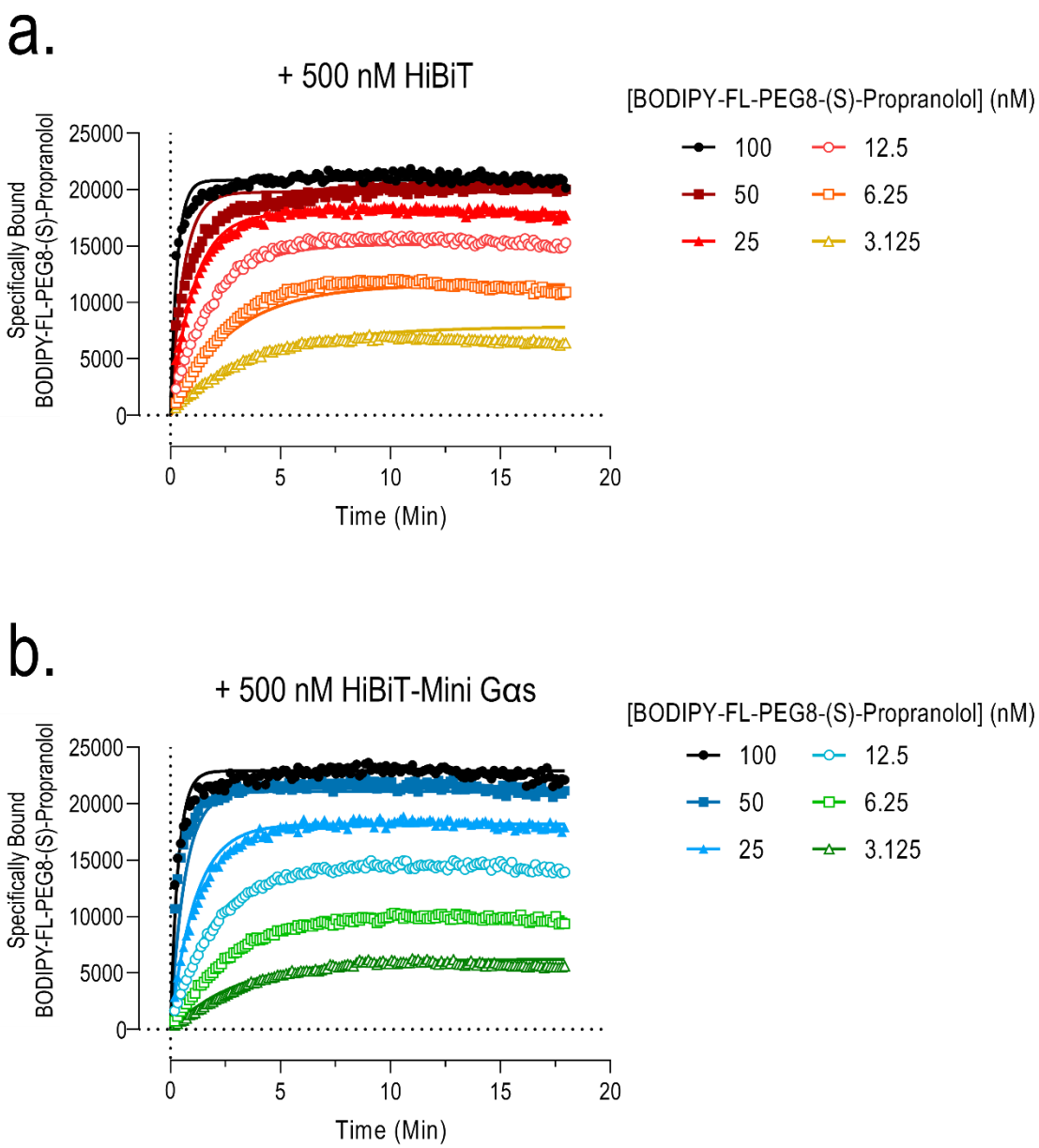

Figure 6. 11 Association binding kinetics of BODIPY-FL-PEG8-(S)-Propranolol from membranes prepared from HEK293T cells stably expressing terbium-labelled SNAP-β_2AR-LgBiT, supplemented with 500 nM purified HiBiT peptide (a.) or 500 nM purified HiBiT-mini Gαs protein (b.). *Membranes were incubated with increasing concentrations of BODIPY-FL-PEG8-(S)-Propranolol, with 10 µM ICI-118,551 used to determine non-specific binding at each concentration of BODIPY-FL-PEG8-(S)-Propranolol. Dual emission wavelengths (490nm & 520nm) were monitored for 18 minutes and binding was represented by a ratio of TR-FRET binding (520nm/490nm*10,000). Data from a representative experiment, fitted to a global model of association kinetics.*

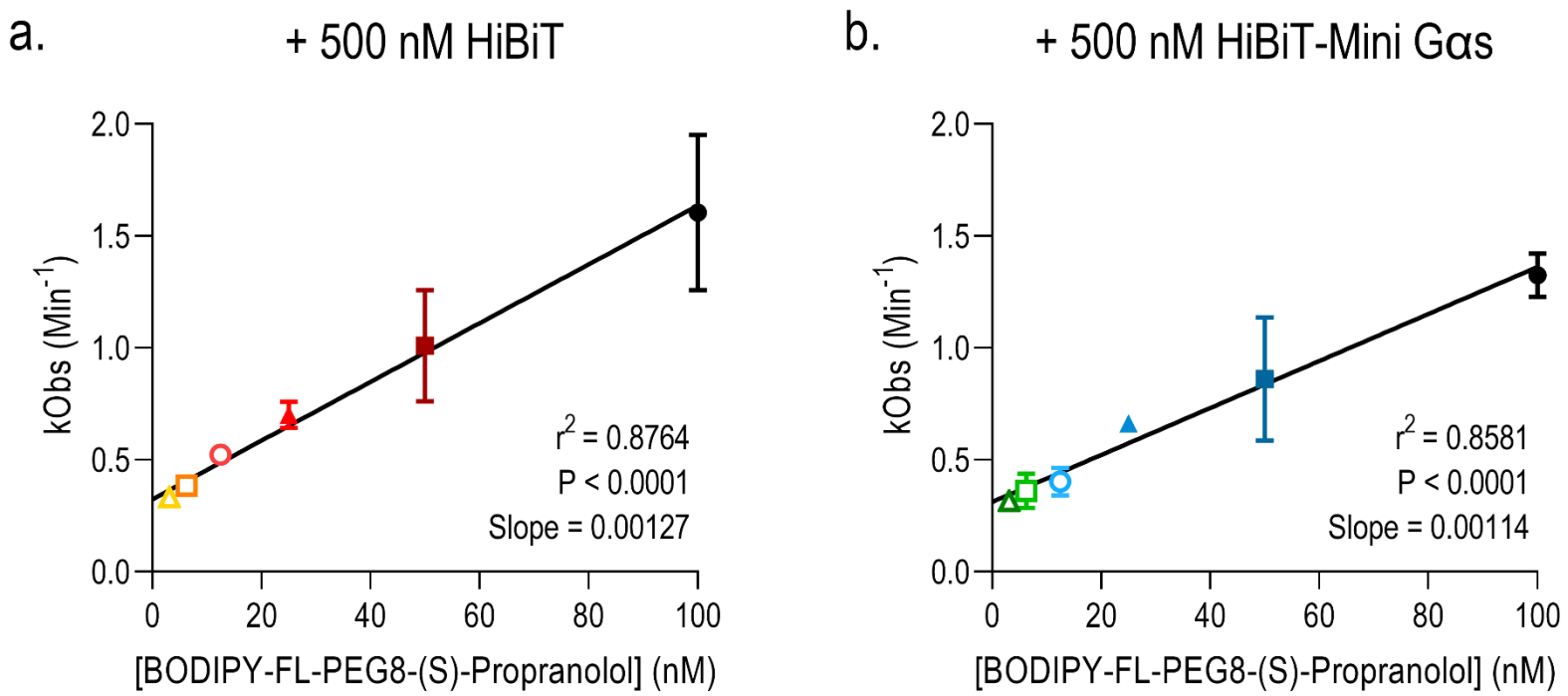

Figure 6. 12 The linear relationship between the observed kinetics association rate constant of BODIPY-FL-PEG8-(S)-Propranolol and fluorescent ligand concentration, in TR-FRET binding assays using HEK293Tmembranes stably expressing terbium-labelled SNAP-β_2AR-LgBiT, supplemented with 500 nM purified HiBiT peptide (a.) or 500 nM purified HiBiT-mini Gαs protein (b.). Observed association rates (kObs; Min^{-1}) of each concentration of BODIPY-FL-PEG8-(S)-Propranolol were pooled and plotted against concentration of BODIPY-FL-PEG8-(S)-Propranolol, with the linear regression goodness of fit defined by r^2 statistic, slope (this is kon), and significance of the linear slope described by P value. Data points represent pooled kObs rates from 3 independent experiments, conducted in singlet.

	k_{ON} (M^{-1} min^{-1})	k_{OFF} (min^{-1})	Residence Time (Min)	Kinetic K_D (nM)
+ 500 nM HiBiT	3.14 ± 0.47 x10^7	0.153 ± 0.011	6.62 ± 0.45	5.28 ± 0.94
+ 500 nM HiBiT-Mini Gαs	2.54 ± 0.64 x10^7	0.191 ± 0.017	5.39 ± 0.53	8.61 ± 1.46

Table 6. 6 Summary of kinetic binding properties of BODIPY-FL-PEG8-(S)-Propranolol, from membranes prepared from HEK293T cells stably expressing terbium-labelled SNAP-β_2AR-LgBiT, supplemented with 500 nM purified HiBiT peptide or 500 nM purified HiBiT-mini Gαs protein. *Kinetic binding parameters of BODIPY-FL-PEG8-(S)-Propranolol were estimated from global fitting a single site binding model to the association kinetic data. Residence time is derived as the reciprocal of k_{OFF} and kinetically derived K_D values were derived from a ratio of dissociation and association rates (K_D= k_{OFF}/k_{ON}). Data represents pooled data, as mean ± S.E.M. from 3 independent experimental replicates.*

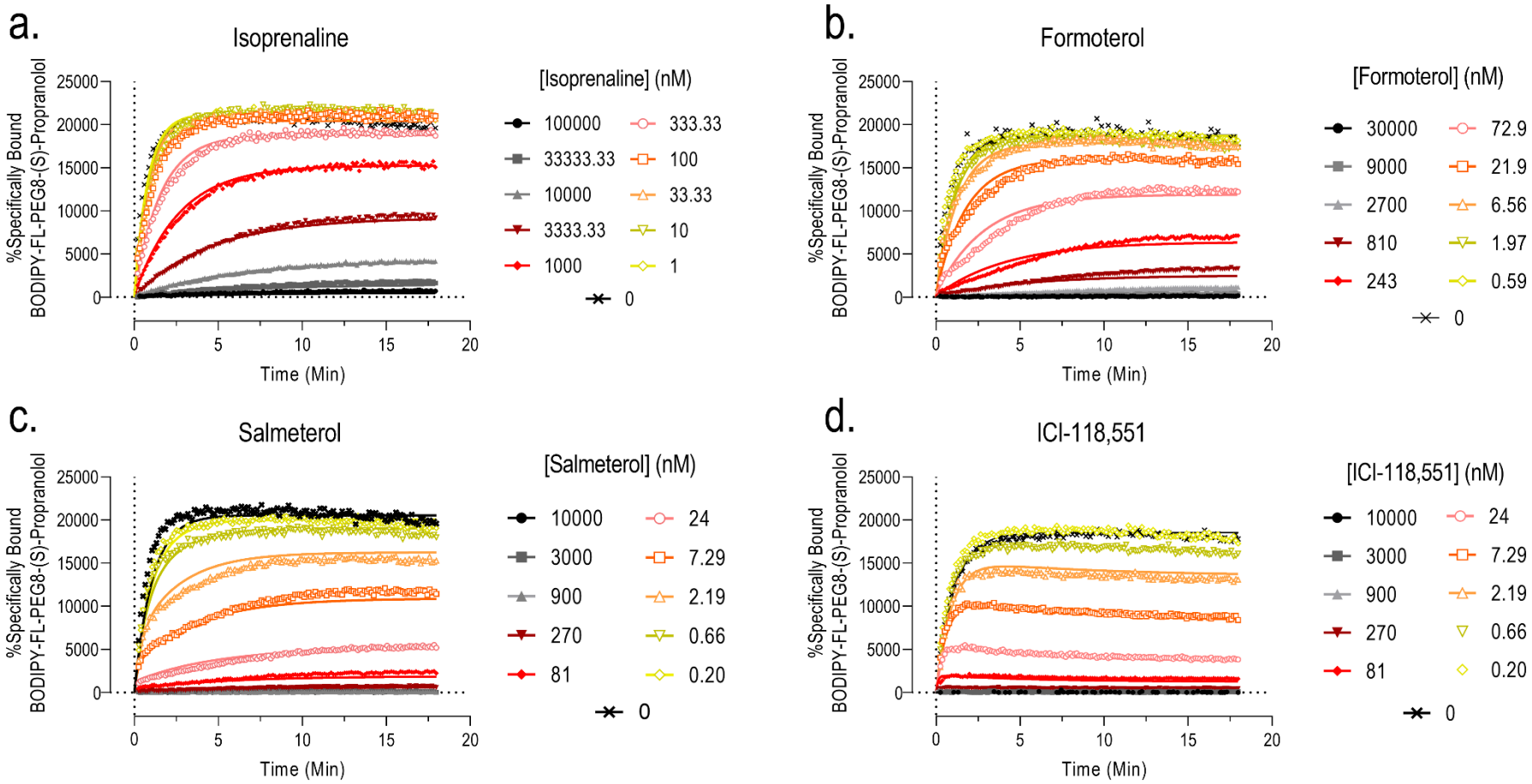

***Figure 6. 13 Competition association kinetics in the TR-FRET assay for unlabelled β_2AR ligands against BODIPY-FL-PEG8-(S)-Propranolol, at* membranes prepared from HEK293T cells stably expressing terbium-labelled SNAP-β_2AR-LgBiT, supplemented with 500 nM purified HiBiT peptide.** *Membranes were incubated with increasing concentrations of unlabelled ligands ((a.) isoprenaline; (b.) formoterol; (c.) salmeterol; and (d.) ICI-118-551) and a fixed concentration (25 nM) of BODIPY-FL-PEG8-(S)-Propranolol, with 10 µM ICI-118,551 used to determine non-specific binding. Dual emission wavelengths (490nm & 520nm) were monitored for 18 minutes and binding was represented by a ratio of TR-FRET binding (520nm/490nm *10,000). Data points show a representative experiment fitted to a Motulsky-Mahan global model of competitive binding kinetics.*

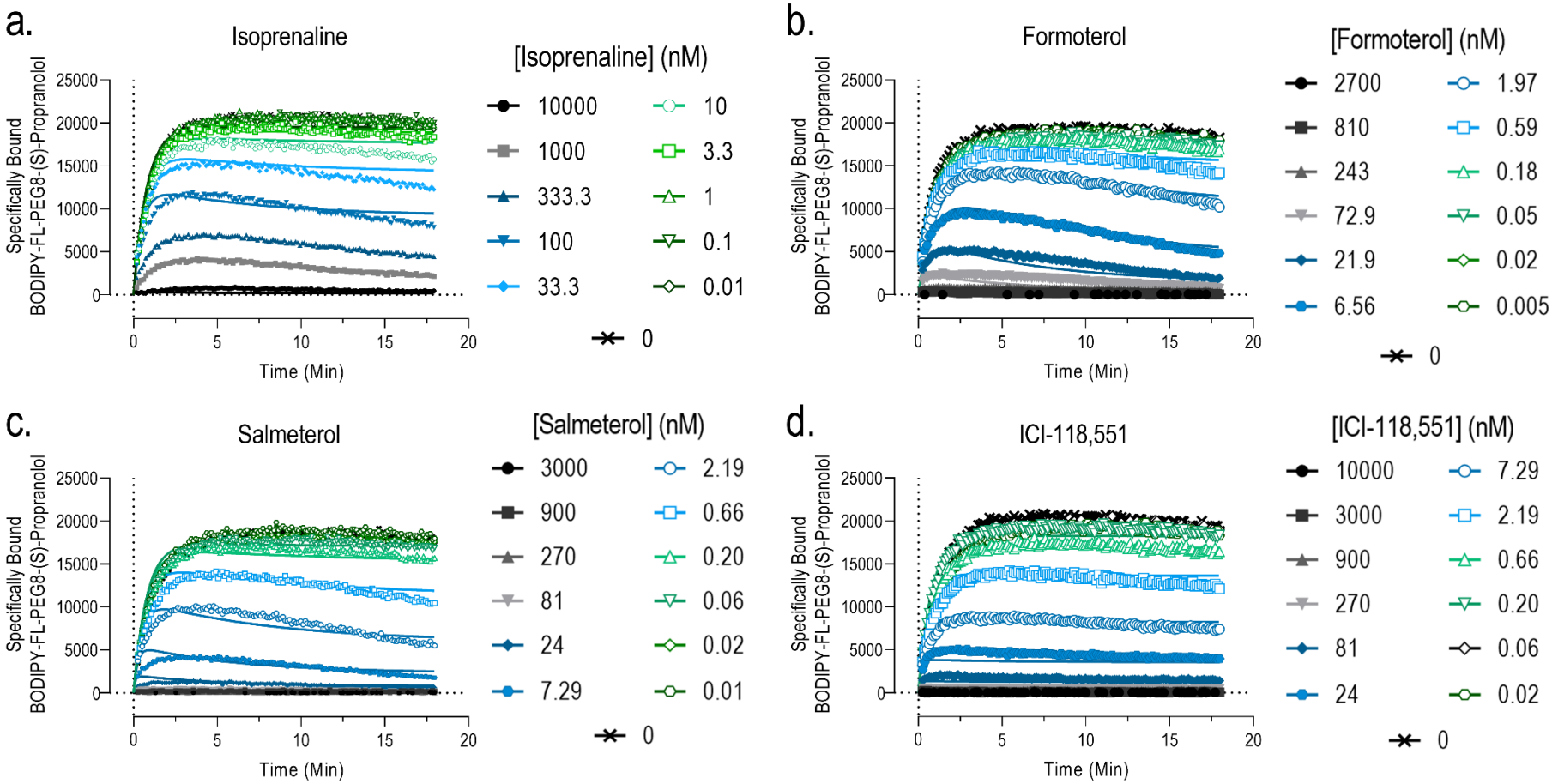

Figure 6. 14 Competition association experiments in the TR-FRET assay for unlabelled β_2AR ligands against BODIPY-FL-PEG8-(S)-Propranolol, at membranes prepared from HEK293T cells stably expressing terbium-labelled SNAP-β_2AR-LgBiT, supplemented with 500 nM purified HiBiT-mini Gαs protein. *Membranes were incubated with increasing concentrations of unlabelled ligands ((a.) isoprenaline; (b.) formoterol; (c.) salmeterol; and (d.) ICI-118-551) and a fixed concentration (25 nM) of BODIPY-FL-PEG8-(S)-Propranolol, with 10 μM ICI-118,551 used to determine non-specific binding. Dual emission wavelengths (490nm & 520nm) were monitored for 18 minutes and binding was represented by a ratio of TR-FRET binding (520nm/490nm *10,000). Data points are for a representative experiment fit to a Motulsky-Mahan global model of competitive binding kinetics.*

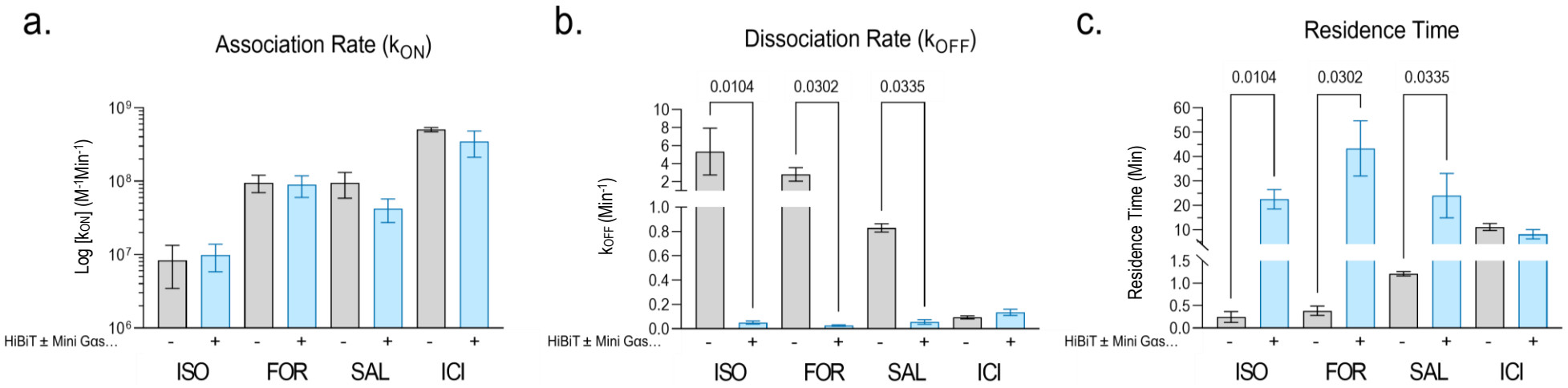

Figure 6. 15 Pooled kinetic binding properties of unlabelled β_2AR ligands, from membranes prepared from HEK293T cells stably expressing terbium-labelled SNAP-β_2AR-LgBiT, supplemented with 500 nM purified HiBiT peptide or 500 nM purified HiBiT-mini Gαs protein. *Association rate constants (k_{ON}) (a.), dissociation rate constants (k_{OFF}) (b.) and residence time of (ISO: isoprenaline; FOR: formoterol; SAL:salmeterol; and ICI:ICI-118-551) from Motulsky-Mahan models of competitive binding, fit globally. Residence time derived as the reciprocal of k_{OFF}. Data represent pooled data, as mean ± S.E.M. from 3 independent experimental replicates.*

	k_{ON} (M^{-1} min^{-1})			k_{OFF} (min^{-1})			Kinetic pK_D (M)			Residence Time (Min)	
	HiBiT	HiBiT – Mini Gαs	HB/HB-mG Ratio	HiBiT	HiBiT – Mini Gαs	HB/HB-mG Ratio	HiBiT	HiBiT – Mini Gαs	HB/HB-mG Ratio	HiBiT	HiBiT – Mini Gαs
Isoprenaline	8.40 ± 4.94 x10^6	9.86 ± 4.02 x10^6	<1	5.324 ± 2.591	0.051 ± 0.012*	105	5.68 ± 0.05	8.18 ± 0.04***	316	*0.25 ± 0.12*	*22.47 ± 4.00**
Formoterol	9.54 ± 2.54 x10^7	8.94 ± 2.93 x10^7	1	2.798 ± 0.751	0.026 ± 0.006*	108	7.45 ± 0.14	9.08 ± 0.13***	43	*0.39 ± 0.10*	43.35 ± 11.31*
Salmeterol	9.49 ± 3.62 x10^7	4.24 ± 1.50 x10^7	2	0.829 ± 0.034	0.055 ± 0.019*	15	8.66 ± 0.02	9.69 ± 0.07***	11	*1.21 ± 0.05*	23.96 ± 9.11*
ICI-118,551	5.05 ± 0.33 x10^8	3.47 ± 1.35 x10^8	1	0.093 ± 0.013	0.135 ± 0.026	<1	8.87 ± 0.05	8.72 ± 0.07	<1	*11.12 ± 1.45*	8.14 ± 1.90

Table 6. 7 Summary of kinetic binding properties of unlabelled β_2AR ligands, from membranes prepared from HEK293T cells stably expressing terbium-labelled SNAP-β_2AR-LgBiT, supplemented with 500 nM purified HiBiT peptide or 500 nM purified HiBiT-mini Gαs protein. *Association (k_{ON}) and dissociation k_{OFF}) rates derived from Motulsky-Mahan models of competitive binding, fit globally. Residence time was derived as the reciprocal of k_{OFF} and kinetically derived K_D values were derived from a ratio of dissociation and association rates (K_D= k_{OFF}/k_{ON}). Ratio of k_{ON}, k_{OFF} and kinetic pK_D are given as values from HiBiT/HiBiT-Mini Gαs (HB/HB-mG.)Data represents pooled data, as mean ± S.E.M. from 3 independent experimental replicates. *=P<0.05,***=P<0.001; Student's t-test, unpaired.*

6.4. Discussion

In this chapter, bacterial constructs encoding HiBiT-tagged mini Gαs protein were expressed in bacterial cultures and the mini Gαs purified using immobilized His tag - nickel affinity chromatography. The function of purified mini Gαs was confirmed by its titration against membranes prepared from HEK293T cells stably expressing SNAP-β_2AR-LgBiT receptor constructs. Increased luminescence was positively correlated with HiBiT-mini Gαs concentration and equilibrium dissociation constants for HiBiT peptide and HiBiT-mini Gαs were determined. In transmembrane TM-BRET and TR-FRET binding assays, established in *Chapter 5*, similar equilibrium dissociation constants of BODIPY-FL-PEG8-(S)-Propranolol were determined at SNAP-β_2AR-LgBiT membranes, supplemented with HiBiT±mini Gαs, but a marked effect of mini Gαs in increasing agonist (isoprenaline, formoterol and salmeterol) but not antagonist (ICI118551) affinity was observed. Whilst previous studies have obtained equilibrium binding affinity values at mini Gαs stabilised GPCR conformations (Carpenter *et al.*, 2016; Warne *et al.*, 2019; Lee *et al.*, 2020), kinetic binding assays have yet to applied to obtain kinetic information of ligand binding at GPCRs stabilised by mini G proteins. Here, we applied kinetic TR-FRET competition binding assays and a Motulsky-Mahan model of competitive bringing to determine the kinetics of unlabelled β_2AR ligands. Using this method we demonstrated for the first time that the selective high affinity agonist conformation represented by the "active" β2AR- mGs complex is generated principally through a slowed dissociation rate of agonists from the receptor, with the association rate constant unaffected.

6.4.1. Stabilisation of high affinity GPCR conformational states using the mini Gαs protein.

"High affinity" conformations of GPCRs are thought to arise from receptors in complex with nucleotide-free Gα proteins, with multiple approaches used to isolate such complexes at both the β_2AR (Yao *et al.*, 2009; Rasmussen, *et al.*, 2011a; Rasmussen, *et al.*, 2011b; Ring *et al.*, 2013; Warne *et al.*, 2019) and other GPCRs including β_1AR (Warne *et al.*, 2019), muscarinic M2 (Kruse *et al.*, 2013) and μ opioid (Huang *et al.*, 2015) receptors. When choosing a method of active state receptor stabilisation, the value of each method was considered. Whilst using a full-length Gαs protein may best represent the most physiological representation of the active complex, the full-length protein is the least thermostable and requires *sf9* insect expression to ensure for post-translational modifications. Moreover, nanobody stabilisation of active GPCR conformations

provide tools with increased thermostability but may not provide information of key GPCR/Gαs interactions. The use of the mini Gαs protein has both increased thermostability and replicates the receptor interface of a full length Gαs protein, thus, despite reduced solubility, it was chosen to be applied here in TM-BRET and TR-FRET assays. Moreover, the extensive literature available on the expression and purification of the mini Gα protein (Carpenter and Tate, 2016, 2017; Carpenter *et al*, 2016; Nehmé *et al*, 2017; Wan *et al*, 2018a) suggested the protein would be functional upon purification. The absence of guanine nucleotide regulation in mini Gαs also simplifies the system in providing a stable complex for the desired binding study, compared to a transient formation of the receptor-Gαs nucleotide free transition state, prior to G protein activation via GTP binding.

Due to limited resources, purification of HiBiT-β-arrestin2 was reserved for future studies, with the application potentially providing information on how β-arrestin2 and other effector proteins may alter the conformation of GPCRs.

The use of the NanoBiT high affinity fragments was thought to add further GPCR/G protein complex stability and has been supported by a recent study (Duan *et al.*, 2020), which stabilised GPCR/G protein complexes for cryo-EM studies using high affinity NanoBiT tethering. A further benefit of using the high affinity NanoBiT fragments is that upon stable complementation and substrate addition, the resultant luminescence may act as a donor in BRET based assays. The luciferase activity acted as a key indicator of function of the purified HiBiT-mini Gαs protein and provided information on the appropriate mGs concentration required for receptor saturation. Recently this approach has been used to study ligand binding at both GPCRs (Kozielewicz *et al.*, 2021) and receptor tyrosine kinases (Peach *et al.*, 2021) using extracellular located NanoBiT tags, though here we demonstrated the first use of NanoBiT luminescence across the membrane in a TM-BRET assay. The applicability of this approach is significant, since many GPCR regulatory proteins that might modulate ligand binding affinity exert their effects on the intracellular domains of the receptors concerned.

6.4.2. Purified mini Gαs proteins selectively stabilise β_2AR conformations with increased agonist affinity.

Stabilisation of the β_2AR in the active "high affinity" conformation is often identified by monitoring the affinity of an agonist, as conducted here in the presence or absence of the mini Gαs protein. This can be seen in published findings which observed increased agonist affinity, as seen in reduced equilibrium dissociation constants, at the β_2AR stabilised by full-length Gαs proteins (Yao *et*

al., 2009; Rasmussen, *et al.*, 2011a; Rasmussen, *et al.*, 2011b), Nb80 (Rasmussen, *et al.*, 2011a), nanobody 6B9 (Ring *et al.*, 2013) and the mini Gαs protein (Warne *et al.*, 2019). Here, both TM-BRET and TR-FRET studies demonstrated an increase in agonist affinity in the presence of the mini Gαs protein, with the majority of TM-BRET and FR-FRET Ki estimations within 3-fold of each other for each ligand.

In competition binding assays, a Hill slope of 1 would be expected from a single site homogeneous population, whilst shallower curves may suggest multiple competition binding relationships from pharmacologically distinct receptor populations with differing affinity are being monitored. The observed Hill slopes of the competition binding curves were shallower in TM-BRET assays, in comparison to TR-FRET assays. Shallow curves in TM-BRET assays were not thought to be due to incomplete saturation of β_2AR receptor constructs by HiBiT/HiBiT-mini Gαs protein, and thus multiple conformations, as TR-FRET assays from the same pre-coupled β_2AR/HiBiT±mini Gαs protein preparations presented competition binding curves with Hill slopes comparable to 1.00. Potentially, the shallow curves may be due to a lower assay window in the TM-BRET studies compared to TR-FRET, as well as additional complexity resulting from the transmembrane nature of the energy transfer. Whilst the width of the lipid bilayer, approximately 3 nm (Jaud *et al.*, 2009; Regan *et al.*, 2019), is less than 10 nm, the distance thought to be the maximum distance for energy transfer assays (Stryer and Haugland, 1967; Stryer, 1978), dynamic movement of the complemented NanoBiT away from the membrane may reduce the efficiency of the energy transfer. This may lower the assay window and result in low signal to noise ratio. In future studies, artificial prenylation of the receptor C-terminus may secure the adjacent LgBiT and subsequent completed NanoBiT closer to the membrane and stabilise energy transfer. Whilst nearly all class A GPCRs have a C-terminal closely associated with the membrane through post-translational modifications, such as palmitoylation (Ng *et al.*, 1994; Grünewald *et al.*, 1996), the length of the C terminal varies between receptors. For example, some GPCRs, such as dopamine D2 receptor isoforms, have a shorter C terminus. It would be interesting to extend the TM-BRET assays to these natural receptor examples, where the LgBiT is positioned close to the membrane, and determine whether the signal is enhanced-assays.

6.4.3. The effect on agonist affinity in mini Gαs protein stabilised β_2ARs is principally derived from slowed agonist dissociation kinetics

We showed for the first time that the TR-FRET methodology could be extended to obtain binding kinetics of both fluorescently labelled and unlabelled ligands at "active" conformations of the β_2AR, stabilised by the mini Gαs protein. The choice of the β_2AR as model provided published comparisons of kinetic binding properties (Sykes *et al.*, 2014), which were shown to broadly agree to association rates and the "inactive" β_2AR/HiBiT conformation dissociation rates, obtained in TR-FRET kinetic binding assays (as previously discussed in *Chapter 5*).

Our key finding was that agonists were shown to dissociate slower at "active" β_2AR/HiBiT-mini Gαs protein conformations, compared to "uncoupled" β_2AR/HiBiT peptide receptor complexes, whilst no significant differences were observed in agonist association rate. We also found that the measured k_{off} for the active β_2 adrenoceptor-mGs complex was equivalent for a representative agonist of lower intrinsic efficacy (salmeterol) compared to formoterol or isoprenaline. Differences in efficacy were instead predicted by extent of the reduction in dissociation rate, with the k_{OFF} ratio, and kinetically derived K_D ratio, for the uncoupled/mGs complex measurements correlating with agonist efficacy (as predicted by the ternary complex model; see *Chapter 1*; *1. 4*). Such observations provide insight into the structural basis of agonist residence time and ligand efficacy, with the molecular interactions of agonist and G protein binding thought to translate to cellular signalling and phenotypic responses. It would be useful to extend these studies to a broader range of β_2 adrenoceptor agonists of differing efficacy, to confirm its correlation with uncoupled / active conformation k_{OFF} ratios.

Structural studies of GPCRs bound to nucleotide free G proteins suggest the receptor adopts the "active" conformation with increased affinity for agonist ligands, compared to the uncoupled state, and this difference in affinity is the basis of agonism in the ternary complex model (Chung *et al.*, 2011; Rasmussen, *et al.*, 2011b; Westfield *et al.*, 2011). However, whilst correlations between dissociation rate and functional efficacy at a single receptor preparation have been suggested before (Sykes *et al.*, 2012), no published observations have been directly made on the effect of receptor conformation on binding kinetics. Whilst it is logical to assume the binding kinetics of agonist ligands would dissociate slower based on a closed binding pocket in "active" conformations (DeVree *et al.*, 2016), unchanged association rates could suggest that the full "active" receptor conformation is driven

by binding of both agonists and mini Gαs proteins, and the extracellular path to the binding pocket governing association is not affected in the unoccupied receptor-Gαs complex This is further supported by the unchanged equilibrium dissociation constants and dissociation rate constants of the β_2AR antagonist ICI-118,551 as well as the fluorescent antagonist BODIPY-propranolol used in our study. The pharmacological evidence is that these antagonist ligands do not discriminate the uncoupled or mini Gαs bound receptors. Such conclusions are supported by "active" β_2AR/Gαs and β_2AR/Nb80 crystal structures, which form closed binding pockets by the inward movement of Phe193^{ECL2} and Tyr308$^{7.35}$ in the presence of the agonist BI-167107 not but the antagonist carazolol (DeVree *et al.*, 2016).

6.4.4. Potential applications of TM-BRET and monitoring the kinetics of effector stabilised GPCRs.

Whilst established in *Chapter 5*, data presented in this chapter helped identify ligand equilibrium dissociation constants at "active" and "inactive" conformations of the β_2AR, stabilised by mini Gαs proteins and high affinity NanoBiT fragments. Whilst there is further optimisation required to improve consistency of transmembrane luminescent emissions such pilot studies provide successful proof of concept for application of TM-BRET methodology to monitor binding at defined GPCR complexes. There are many BRET based biosensors used to monitor ligand binding kinetics at membrane proteins, whereby NanoLuc or complemented NanoBiT fragments are used to label the receptor at the extracellular surface and act as donor species in BRET assays. Such assays have been used to monitor ligand binding at both GPCRs (Bouzo-Lorenzo *et al.*, 2019; Hoare *et al.*, 2019; Grätz *et al.*, 2020; Rosier *et al.*, 2021) and receptor tyrosine kinases (Kilpatrick *et al.*, 2017; Peach *et al.*, 2019, 2021), and provide potential to further optimise and develop the TM-BRET assay platform for kinetic binding assays.

Kinetic TR-FRET competition assays present the opportunity to identify ligand binding kinetics at effector-bound receptor conformations. Biased signalling theories (See *Chapter 1*) suggest GPCRs may preferentially engage different effectors dependent on agonist driven receptor conformations, but also that the kinetics of agonist-receptor binding may influence spatiotemporal signalling patterns through different pathways in a ligand selective manner. The methodologies in this study in principle show a route to deconvolve both "kinetic" and conformational aspects of ligand bias, through a greater understanding of how

agonist binding kinetics is influenced by the conformational repertoire of receptor signalling complexes in cells. A key challenge remains to apply the HiBiT systems in future to purified relevant native effector proteins (e.g. G proteins, arrestins, kinases), beyond engineered mG proteins and nanobodies.

6.5. Chapter Conclusions

This chapter explored the use of a purified mini Gαs to stabilise "active" conformations of the β_2AR, which was then stably labelled using high affinity NanoBiT fragments. The mini Gαs protein, N-terminally tagged with the HiBiT label, was successfully expressed and purified using a bacterial expression system and immobilized metal affinity chromatography, respectively. The purified protein was shown to successfully complement LgBiT labelled β_2ARs in HEK293 membranes, producing a concentration dependent increase in luciferase activity. Addition of the mini Gαs protein was shown to increase the affinity of agonist ligands, but not antagonist ligands, in both a novel TM-BRET ligand binding assay as well as a TR-FRET binding assay. A kinetic TR-FRET binding assay monitored the kinetic binding properties of β_2AR ligands in the presence and absence of mini Gαs protein to provide measurements of ligand binding at active and uncoupled conformations of the β_2AR for the first time. The kinetic binding assay demonstrated that the increase in agonist efficacy is driven by a decrease in dissociation rate in the presence of the mini Gαs protein, with the association rate unchanged. The extent to which the affinity of the agonist increased was shown to correlate with agonist efficacy, in line with the ternary complex model, and correlation was also evident for the ratios of the uncoupled / mini Gαs protein complex k_{OFF} measurements. Such observations suggest structural interactions between agonist residence time, mini G protein engagement and ligand efficacy. In future, these studies provide proof of concept methodology and data to explore the relationship between conformational specific GPCR binding kinetics and its translation to cellular signalling and phenotypic responses.

Chapter Seven:

General Discussion and Conclusions

7.1. General Discussion

GPCRs signal through a complex cascade of signalling pathways, with GPCR activation eliciting responses that show large variation in temporal patterns between microseconds to hours or even days. The pattern of signalling is key to functional outcomes, and is determined by multiple factors including the kinetics of receptor activation and deactivation, the downstream signalling pathway as well as ligand binding kinetics to the receptor. Despite this, single timepoints are typically used to obtain concentration response data and applied to models to derive estimations of affinity, potency and efficacy for potential therapeutic ligands. Many of these pharmacological models require the experimental system to be at equilibrium; a condition which is unlikely to represent *in vivo* conditions. More recently, the influence of signalling kinetics and ligand binding kinetics on functional responses and resultant estimations of drug affinity and efficacy have been investigated (Klein Herenbrink *et al.*, 2016; Lane *et al.*, 2017). Moreover, kinetic pharmacological models are now being devised to use drug concentration response data from multiple timepoints to better represent the dynamic nature of GPCR activation and signalling (Bridge *et al.*, 2018; Hoare *et al.*, 2018; Zhu *et al.*, 2019; Finlay, *et al*, 2020).

GPCR activation can be described by ternary complex models, illustrating the interactions with both ligands and intracellular effectors (De Lean, et al, 1980; Samama *et al.*, 1993; Weiss *et al.*, 1996), advancing our understanding of receptor activation beyond the two-state "active and inactive" model (Del Castillo and Katz, 1957) (*Introduction*; *1. 4*). Ternary complex models suggest the binding of an agonist may induce a conformational change to an active state and increase the affinity of the receptor for an intracellular signalling protein. It has been suggested that there are multiple conformationally distinct populations of active agonist bound receptors and this has been suggested to be responsible for biased signalling, where an agonist may induce a conformational change to preferentially activate one signalling pathway to a greater extent than another (*Introduction*; *1. 3*). Similarly, both the extended and the cubic ternary complex model propose the existence of active conformations of receptors in the absence of an agonist and are thought to be stabilised by the binding of an intracellular signalling protein such as a G protein. The active GPCR-G protein conformation has been shown to have increase affinity for agonists, compared to the GPCR alone (Warne *et al.*, 2019), though the effect on ligand binding kinetics has not been explored in literature previous to the novel studies in this thesis (*Chapter 6*; *6. 3. 6*).

This thesis explored how both low and high affinity NanoBiT complementation technologies could be applied to investigate both signalling and ligand binding kinetics at βARs, interrogating how ligand and effector binding can allosterically influence receptor interactions within the ternary complex.

Chapter 3 & 4 established effector recruitment assays using low affinity NanoBiT fragments to monitor βAR interactions with β-arrestin2 and a novel mini Gαs protein. In *Chapter 3*, measures of agonist potency and efficacy derived from concentration response relationships taken from early timepoints were shown to be significantly altered when compared with later timepoints and are likely to represent non-equilibrium or hemi-equilibrium conditions (*Chapter 1*; *1. 8. 2*). Full kinetic agonist signalling profiles of β-arrestin2 recruitment applied in a kinetic operational model were used to derive measures of agonist affinity and efficacy, with the modelled equilibrium dissociation constants aligning strongly with equilibrium TR-FRET binding assays. This chapter highlighted the importance of assessing the signalling kinetics for different GPCR intracellular effectors and that this non-equilibrium or hemi-equilibrium conditions may confound estimations of agonist potency, efficacy and results measures of bias. *Chapter 4* demonstrated how the binding kinetics of different β_2 adrenoceptor antagonists may affect the agonist stimulated recruitment profiles of β-arrestin2 and the mini Gαs protein in NanoBiT complementation assays. Schild based assays demonstrated the importance of hemi-equilibrium conditions in influencing antagonism, transitioning from insurmountable to surmountable antagonism over the timecourse. The extent of insurmountability at later timepoints was shown to correlate with slow dissociation rates of the antagonist. Insurmountable antagonism can also be observed for inhibitors binding at an allosteric site - thus slow antagonist binding kinetics, and the resultant non-equilibrium conditions, can confound conclusions on mechanism of action for novel antagonists without the ability to collect kinetic assay data as illustrated in this chapter. An antagonist derivation of the kinetic operational model, which accounts for non-equilibrium ligand binding conditions, was applied to timecourses monitoring recruitment of the mini Gαs protein, at the β_2AR after antagonist pre-treatment. Antagonist equilibrium dissociation constants from Schild analysis, TR-FRET binding assays and the kinetic operational showed overall comparable estimations, whilst the antagonist dissociation rates were poorly correlated between TR-FRET binding data and the kinetic operational mode. The findings highlighted the potential value of the kinetic operational model as a tool to model non-equilibrium data, though further refinements are required.

Chapter 5 and *Chapter 6* investigated the effect of receptor-mini Gαs protein binding on equilibrium measurements of agonist binding affinities, as well as binding kinetics. Due to the dynamic nature of GPCR conformations, drug binding affinities are commonly estimated from a mixed populations of receptor conformations or the inactive receptor conformation, by removal of the endogenous G protein using Gpp(NH)p. Here we used high affinity NanoBiT fragments to tether the β_2 adrenoceptor and effector proteins, promoting engagement of the proteins and the formation of the effector dependent conformation, e.g. the high affinity "active" receptor conformation.

Two approaches were used to produce NanoBiT stabilised receptor-effector complexes. In *Chapter 5*, the first approach used dual expression HEK293T cells, expressing both β_2 adrenoceptors C-terminally tagged with the LgBiT tag and HiBiT-tagged effector proteins, either β-arrestin2 or mini Gαs protein. This approach, used in *Chapter 5*, was not an efficient method in producing a homogenous population of receptors bound to either the β-arrestin2 or the mini Gαs protein, as there was unbalanced expression which resulted in receptors unoccupied with an effector protein. To correct this, receptor and effector DNA could have been encoded using a poly-cistronic vector and thus result in 1:1 protein expression (Hsiao *et al.*, 2011). Whilst a poly-cistronic vector ensures 1:1 mRNA transcription, differences in the post-translational trafficking of the receptor and effector proteins to the membrane and cytosol, respectively, (Michaelson *et al.*, 2002; Duvernay, *et al*, 2005; Dong *et al.*, 2007; Marrari *et al.*, 2007) and may have still resulted in unbalanced protein concentration within the cell. In *Chapter 6* HiBiT-tagged mini Gα proteins were expressed and purified from bacterial cultures and added exogenously to membranes prepared from HEK293T cells stably expressing β_2 adrenoceptors. This method allowed for β_2 adrenoceptor binding kinetics to be investigated while ensuring the receptors were applied with a saturating concentration of the purified mini Gαs protein (*Chapter 6; 6. 3. 1*).

In both *Chapter 5* and *Chapter 6*, the formation of the reconstituted NanoBiT allowed for the resulting luciferase activity and luminescence to be used as the donor species in a novel transmembrane BRET assay. In Chapter *6*, we used the NanoBiT stabilised β_2 adrenoceptor-mini Gαs protein complexes to, for the first time, measure the binding kinetics of labelled and unlabelled ligands at both the inactive and active receptor conformations in TR-FRET kinetic binding assays. Study of the active receptor states demonstrated increased affinity of agonists as expected, but also showed that this was principally driven by a slower ligand dissociation rate, which correlated with agonist efficacy. To further investigate whether the extent of the increase in affinity and

reduction in dissociation rate is correlated with efficacy, a larger ligand panel of a variety of efficacies should be applied in ligand binding assays in future.

The establishment of TM-BRET in *Chapter 5* and *Chapter 6* provided the opportunity to directly monitor ligand binding at GPCRs in complex with an effector protein. Although the width of the membrane (~ 7 nm) places inherent limitations on the detections of transmembrane interactions by resonance energy transfer, we not only demonstrated that TM-BRET is possible but also that it can be used to monitor selected populations of receptors. In *Chapter 5* and *Chapter 6*, the equilibrium dissociation constants of BODIPY-FL-PEG8-(S)-Propranolol obtained in TM-BRET studies were similar to each other and TR-FRET assays in *Chapter 3*, demonstrating the accuracy of TM-BRET measurements. However, the competition ligand binding curves observed in TM-BRET studies in *Chapter 6* were shallow and suggested more than one site of binding or multiple receptor conformations. It could be suggested that the efficiency of the energy transfer between the donor/acceptor species may alter depending on the flexibility of the position of the reconstituted NanoLuc enzyme on an extended C-terminus of the receptor. Further development of the approach is required to identify if the shallow binding curves result from differences in NanoLuc position, and the resultant distance from the ligand, and whether this might be assisted by membrane tethering of the luciferase, for example by using a consensus sequence for fatty acid modification (e.g. prenylation CAAX motif, palmitoylation) (Zhang *et al.*, 2022). The Hill slopes of TR-FRET competition binding curves at the β_2 adrenoceptor were not significantly different from 1, suggesting a single site of binding, and thus the shallow curves seen in the TM-BRET studies are unlikely to result from receptors not fully complemented by mini G protein. The G protein mimetic has been previously used to measure changes in agonist binding affinity at βARs at equilibrium (Warne *et al.*, 2019), yet the effect on the binding kinetics has not been investigated. This is likely to be due to a lack of sufficient stabilisation of the receptor-G protein complexes to ensure a single population for a kinetic measurement, which as we have demonstrated may be aided by the HiBiT complementation.

Overall, the data presented in thesis focused on answering two main questions. Firstly, what is the value of signalling kinetics and kinetic operational models in understanding GPCR signalling? Secondly, how do conformationally distinct binding kinetics provide insight into GPCR pharmacology?

What is the value of measuring real-time GPCR timecourse data and how kinetic operational models tell about GPCR activation and how valuable are such models in compound profiling?

The data presented in *Chapter 3* and *Chapter 4* highlight the importance of both signalling kinetics and binding kinetics, and how both can confound estimations of drug potency and efficacy, as well as misrepresent the mechanism of action. Whilst there is now greater appreciation for understanding kinetics as a central part of drug discovery, often peak responses are still used to characterise both agonist and antagonist responses. Therefore the generation of timecourse profiling of GPCR activation produces powerful datasets, which can be tailored to investigate specific effector recruitment. Here, we have demonstrated the function of the NanoBiT complementation assays at monitoring recruitment of multiple effectors and adrenoceptor subtypes, to report dynamic changes in receptor signalling. Traditionally, concentration response data is taken from single timepoints and applied to pharmacological models which require system equilibrium. The kinetic operational models (Hoare *et al.*, 2018), which take hemi-equilibrium conditions into account, applied here provide powerful tools, especially to estimate drug effects through transient signalling pathways. Development of kinetic models is highly challenging, as GPCRs signal through interconnected signalling pathways and thus the framework required is highly complex. Approaches have been used to develop kinetic models to estimate agonist bias (Bridge *et al.*, 2018), agonist internalisation (Zhu *et al.*, 2019) and kinetic parameters of drug affinity and efficacy (Hoare *et al.*, 2018), avoiding the need for system equilibrium. As discussed by Finlay, *et al,* (2020), such kinetic models require agonist dose response data from multiple timepoints to fully assess their value in comparison to traditional equilibrium models of receptor activation, highlighting the value of the timecourse data provided by our NanoBiT complementation assays (*Chapter 3* & *Chapter 4*). The methods outlined here present a method for increasing throughput, as separate ligand binding assays are not required for early estimations of agonist affinity.

However, kinetic operational models are limited as they require suitable assay systems to record kinetic data (i.e. biosensor labelled proteins, over expression of target proteins) but still maintain physiological system behaviours. For example, the application of NanoBiT technology in over-expressing cell lines was required to study GPCR signalling in this thesis, for the expression of NanoBiT tagged proteins. However, protein overexpression can disrupt cellular behaviours, poorly representing

physiological interactions. CRISPR/Cas9 technology has previously been used to insert NanoBiT fragment DNA within the genome sequence and thus express at endogenous levels. White *et al (*2020) demonstrated that the signalling profiles of β-arrestin2 recruitment at the human chemokine receptor 4 produced at endogenous expression levels were different than overexpressed. Considering the accuracy of the kinetic operational model used to predict agonist affinities from kinetic signalling data in *Chapter 3*, kinetic operational models should be applied to comparable data under endogenous expression system to test the robustness of the model.

In addition, the kinetic operational models used in this thesis are empirical, with the results based on the data sets provided - rather than the actual mechanism. For example, the model applied to the transient NanoBiT recruitment profile is a model of signal desensitisation (*Chapter 3*; "model 4"), rather than specifically of transient β-arrestin2 recruitment which could lead to discrepancies between what the model is actually predicting based on the protein:protein interactions. In the case of the β_2 adrenoceptor, the recruitment of β-arrestin2 and receptor desensitisation/internalisation is thought to be transient and followed by the recycling of the receptor back to the membrane (Oakley *et al*, 1999). However, "model 4" describes the transduction potential as depleting, rather than recycling, providing differences in the empirical model and what the data mechanistically represents. To improve the model, additional terms may be incorporated into the model to better represent the cellular system. For example, recycling the receptor to membrane may be represented by further parameters with rates governing the rate of recycling. A further modification may be made to add a time-limiting recycling, to delay the recycling of the effect 'E' to allow for receptors with slowly recycling receptors.

Lastly, the β adrenoceptor/β-arrestin2 recruitment signalling profiles applied to a kinetic operational model of agonist signalling (*Chapter 3*; *3. 3. 10*) provided estimates of agonist affinity which strongly aligned with those established in equilibrium ligand binding assays. However, a caveat of this model is that it assumes instantaneous binding equilibrium and it would be interesting to investigate the value of the model at receptors with slowly dissociating agonists or using signalling profiles with a delayed onset of response. To further validate the ability of the kinetic operational model as a method for determine agonist affinities from functional data, signalling profiles from other GPCRs and recruitment of other effectors (such as β-arrestin1, GRKs and full length Gα proteins) should be applied to investigate how universal this model is as a tool for predicting agonist affinities from functional data.

Overall, timecourse datasets of receptor signalling and kinetic operational models provide powerful tools to understand dynamic GPCR. However, further exploration into the robustness of kinetic operational models is still required before routine use in compound profiling, specifically in antagonist kinetic operational models.

How can we obtain binding affinities and kinetics from conformationally distinct GPCRs, how do they drive specific signalling and how can this insight be used to improve drug discovery?

Chapter 5 and *Chapter 6* of this thesis outlined a framework for studying GPCRs stabilised by mini Gαs proteins, allowing for ligand binding affinities of both labelled and unlabelled ligands in equilibrium TM-BRET and TR-FRET assays and ligand binding kinetics in kinetic TR-FRET binding assays. To advance this approach, we need to apply "real" effectors to improve correlations with signalling and functional effects. For example, whilst the mini Gαs protein are valuable tools for structural understanding of G proteins, stabilised receptors in complex with heterotrimeric G proteins would improve the physiological relevance, as well as other effectors including β-arrestins and kinases. This study focused on the conformational changes observed upon binding of a minetic of the Gαs protein, however more Gα proteins should be applied to investigate conformational effects of non-canonical G proteins. For example, as discussed in *Chapter 1*, it has been suggested that the β_2 adrenoceptor may couple to the Gαi protein to produce distinct signalling profiles compared to Gαs, thus it could be suggested that the receptor in complex with each Gα protein may have a different conformation and may affect agonist binding. In addition, conformationally distinct complexes of receptors with physiological relevant effector proteins are difficult to isolate due to their dynamic movement and modification by other processes. For example, receptors in complex with G proteins are influenced by: GDP and GTP association/dissociation, and dissociation of the G protein; as well as, receptor phosphorylation and dephosphylation of both the G protein and the receptor.

From the kinetic TR-FRET assays, we concluded that the increase in agonist affinity at active "high affinity" receptor conformations is driven by the conformationally specific k_{OFF}, from a ligand panel of 4 ligands at a single receptor. Therefore, further investigation of a wider ligand panel at multiple receptor subtypes should be conducted to explore the ability to apply the methodology. Whilst we have used a classical class A GPCR activated by small neurotransmitters, it would be interesting to see how the NanoBiT tethering and active conformation stabilisation affects receptor binding of different classes For example, Class B receptors, which are endogenously activated by

peptides – especially those with slower binding kinetics such as the glucagon-like peptide (GLP-1) (Van Der Velden *et al.*, 2021) and the parathyroid hormone (PT) (Emami-Nemini *et al.*, 2013) receptors. In addition to slow binding kinetics, it would be interesting to investigate the conformationally selective binding kinetics of receptors with mutli-step binding, such as the H2 relaxin receptor (Hoare *et al.*, 2019) and the chemokine receptor CXCR3 (Xanthou, Williams and Pease, 2003). However, the experimental approaches outlined in this thesis require both tagging the receptor with an extracellular SNAP-tag and/or an intracellular LgBiT tag. The fused tags are genetically encoded and expressed in cell based systems, however the addition of the tag may affect both receptor expression and/or trafficking to the plasma membrane (Stoddart *et al.*, 2016). In addition to tagged receptor, fluorescently labelled ligands are also needed, which require a suitable high affinity pharmacophore to be tagged by a fluorophore with suitable excitation and emission properties to allow resonance energy transfer. In some cases, a suitable fluorescent ligands may be derived from the endogenous agonist, though an antagonist pharmacophore is often preferred as an agonist can initiate conformational changes at the receptor or receptor internalisation in binding assays are conducted in whole cell systems. This would require purification of multiple full length and/or mini Gα protein subtypes, though not all of the 21 different subtypes have been successfully expressed in the mini G format.

In addition to receptors of further classes, NanoBiT stabilised active state structures may also be used to investigate how ligand binding is altered at constitutively active mutant proteins, which are frequently associated in disease states in both GPCRs (Kallio *et al.*, 2018; Dustin, *et al*, 2019) and other intracellular scaffolding proteins (Wang *et al.*, 2018). For example, the R1465W mutation of the C-terminal of the adhesion GPCR, BAI2, increases constitutive activity and is identified in patients of neuromuscular disease (Purcell *et al.*, 2017). Understanding ligand binding kinetics of the active conformation of such constitutively active mutants may allow for improved drug design, providing better onset and duration of drug action.

This thesis suggests that the increase in agonist affinity at the “active” conformation of the receptor is driven by slower dissociation from the receptor, which was highly correlated with ligand efficacy. Measurements of conformational kinetics provide the framework to gain a kinetic understanding of GPCR activation of multiple pathways and provide a kinetic understand of observed ligand bias. Whilst current explanations of ligand bias arise from both conformational (Shukla, *et al*, 2014; Latorraca, *et al*, 2017; Wingler and Lefkowitz, 2020) and kinetic (Klein Herenbrink *et al.*,

2016; Lane *et al.*, 2017) explanations, here we propose a bridge to a combined theory where bias may be explained by the change in dissociation rate at selected receptor/effector conformations. For example, it would be expected that a G protein bias ligand would have a greater ratio of dissociation rates between high/low receptor confirmations at a receptor in complex with a G protein (or mimetic), in comparison to a receptor in complex with another effector, such as β-arrestin. This approach bridges idea of conformational and kinetic explanations of observed bias and may be used to predict ligand efficacy and bias in future studies.

As the prediction of pathway efficacy is shown to be correlated with the reduction in dissociation rate, the approaches outlined here present a new method for screening for efficacious ligands. A high throughput approach with the NanoBiT stabilisation of the target receptor and effector protein applied to a screening program, with hit identification based upon increased affinity and reduced dissociation rate in the presence of the effector protein. Moreover, this may be used to identify lead compounds with specific pathway activation in a 'clean-cut' system by removing confounding factors arising from a cellular environment, such as signal amplification or negative feedback interactions. This is specifically applicable to quantifying biased signalling, as the methods currently available using widely different cellular approaches and often have conflicting results.

Existing ternary complex models assume equilibrium conditions of binding between agonist, receptor and G protein, and do not consider the differences in kinetics between conformational states. A recent study from Culhane *et al*, (2022) established a kinetic ternary complex model incorporating "rate-limiting transitions" between the agonist/receptor/G protein conformations, incorporating non-equilibrium conditions. In addition, this model incorporated the competition of a secondary effector protein of much weaker affinity to better represent cellular conditions (Culhane *et al.*, 2022). This kinetic point of view would also allow for the population of active receptor conformations to change over time and be reflected in GPCR activation and signalling.

Lastly, TM-BRET provides a tool to look at transmembrane interactions within cellular environments such as endosomes. For example, fluorescently labelled ligands may induce internalisation of a receptor, however whether the ligand is internalised with the receptor is often difficult to observe due to membrane markers often expressed on the cytosol surface of the endosome. Therefore, use of TM-BRET, with complementary NanoBiT fragments on the endosomal marker and C-terminal of the receptor may be used to identify if the fluorescent ligand has been internalised with the receptor.

7.2. Final Conclusions

The data presented in this thesis demonstrates the importance of signalling and binding kinetics when investigating GPCR signalling and activation – establishing and validating methodology to identify more efficacious drugs.

In the first two results chapters, we applied NanoBiT binding partners to monitor the recruitment timecourse of effector proteins and highlight how the kinetic context may alter the concentration response data, in both agonist and antagonist modes of the assay. When timecourse data of β-arrestin2 and mini Gαs protein recruitment were applied to a kinetic operational model, generally reliable estimations of agonist equilibrium dissociation constants were obtained and highlighted the value of the model. Whilst the investigations were limited to 2 receptor subtypes, they provide potential methods to obtain both signalling and binding information from a single functional assay. The removal of the need for a binding assay improves throughput at the early stages of the drug discovery pipeline, i.e. “hit identification”.

In the final two results chapters, we used high affinity NanoBiT fragments to stabilise receptor-effector complexes, enabling us to discriminate both equilibrium measurements of ligand binding affinities and binding kinetics between active and inactive receptor conformations. For the first time were able demonstrate transmembrane transfer of energy in TM-BRET assays, measuring binding from selected populations of receptor, which had complemented intracellular NanoBiT fragments. These approaches revealed that increased agonist affinities at active receptor conformations are driven by a slower dissociation rate. These findings provide novel methods to interrogate agonist efficacies at selected receptor-effector complexes and design drugs to selectively target signalling through specific effector pathways.

Chapter VIII: Bibliography

Allen, J. A., Yost, J. M., Setola, V., Chen, X., Sassano, M. F., Chen, M., ... & Jin, J. (2011). Discovery of β-arrestin–biased dopamine D2 ligands for probing signal transduction pathways essential for antipsychotic efficacy. *Proceedings of the National Academy of Sciences*, *108*(45), 18488-18493.

Altarifi, A. A., David, B., Muchhala, K. H., Blough, B. E., Akbarali, H., & Negus, S. S. (2017). Effects of acute and repeated treatment with the biased mu opioid receptor agonist TRV130 (oliceridine) on measures of antinociception, gastrointestinal function, and abuse liability in rodents. *Journal of Psychopharmacology*, *31*(6), 730-739.

Altenbach, C., Yang, K., Farrens, D. L., Farahbakhsh, Z. T., Khorana, H. G., & Hubbell, W. L. (1996). Structural features and light-dependent changes in the cytoplasmic interhelical E− F loop region of rhodopsin: a site-directed spin-labeling study. *Biochemistry*, *35*(38), 12470-12478.

Altosaar, K., Balaji, P., Bond, R. A., Bylund, D. B., Cotecchia, S., Devost, D., ... & Zylbergold, P. (2021). Adrenoceptors in GtoPdb v. 2021.3. *IUPHAR/BPS Guide to Pharmacology CITE*, *2021*(3).

Anderson, W. J., Short, P. M., Williamson, P. A., Manoharan, A., & Lipworth, B. J. (2014). The inverse agonist propranolol confers no corticosteroid-sparing activity in mild-to-moderate persistent asthma. *Clinical science*, *127*(11), 635-643.

Arunlakshana, O. T., & Schild, H. O. (1959). Some quantitative uses of drug antagonists. *British journal of pharmacology and chemotherapy*, *14*(1), 48-58.

Aslam, M., Härtel, F. V., Arshad, M., Gündüz, D., Abdallah, Y., Sauer, H., ... & Noll, T. (2010). cAMP/PKA antagonizes thrombin-induced inactivation of endothelial myosin light chain phosphatase: role of CPI-17. *Cardiovascular research*, *87*(2), 375-384.

Audet, M., & Bouvier, M. (2008). Insights into signaling from the β 2-adrenergic receptor structure. *Nature chemical biology*, *4*(7), 397-403.

Azzi, M., Charest, P. G., Angers, S., Rousseau, G., Kohout, T., Bouvier, M., & Piñeyro, G. (2003). β-Arrestin-mediated activation of MAPK by inverse agonists reveals distinct active conformations for G protein-coupled receptors. *Proceedings of the National Academy of Sciences*, *100*(20), 11406-11411.

Baker, J. G. (2005). The selectivity of β-adrenoceptor antagonists at the human β1, β2 and β3 adrenoceptors. *British journal of pharmacology*, *144*(3), 317-322.

Baker, J. G., Middleton, R., Adams, L., May, L. T., Briddon, S. J., Kellam, B., & Hill, S. J. (2010). Influence of fluorophore and linker composition on the pharmacology of fluorescent adenosine A1 receptor ligands. *British journal of pharmacology*, *159*(4), 772-786.

Baker, J. G. (2010). The selectivity of β-adrenoceptor agonists at human β1-, β2-and β3-adrenoceptors. *British journal of pharmacology*, *160*(5), 1048-1061.

Baker, J. G., Gardiner, S. M., Woolard, J., Fromont, C., Jadhav, G. P., Mistry, S. N., ... & Fischer, P. M. (2017). Novel selective β1-adrenoceptor antagonists for concomitant cardiovascular and respiratory disease. *The FASEB Journal*, *31*(7), 3150-3166.

Baker, J. G., Hall, I. P., & Hill, S. J. (2002). Pharmacological characterization of CGP 12177 at the human β2-adrenoceptor. *British journal of pharmacology*, *137*(3), 400-408.

Baker, J. G., Hall, I. P., & Hill, S. J. (2003). Agonist actions of "β-blockers" provide evidence for two agonist activation sites or conformations of the human β1-adrenoceptor. *Molecular pharmacology*, *63*(6), 1312-1321.

Baker, J. G., Hall, I. P., & Hill, S. J. (2003). Influence of agonist efficacy and receptor phosphorylation on antagonist affinity measurements: differences between second messenger and reporter gene responses. *Molecular pharmacology*, *64*(3), 679-688.

Ballesteros, J. A., Jensen, A. D., Liapakis, G., Rasmussen, S. G., Shi, L., Gether, U., & Javitch, J. A. (2001). Activation of the β2-adrenergic receptor involves disruption of an ionic lock between the cytoplasmic ends of transmembrane segments 3 and 6. *Journal of Biological Chemistry*, *276*(31), 29171-29177.

Baneres, J. L., Mesnier, D., Martin, A., Joubert, L., Dumuis, A., & Bockaert, J. (2005). Molecular characterization of a purified 5-HT4 receptor: a structural basis for drug efficacy. *Journal of Biological Chemistry*, *280*(21), 20253-20260.

Bdioui, S., Verdi, J., Pierre, N., Trinquet, E., Roux, T., & Kenakin, T. (2018). Equilibrium assays are required to accurately characterize the activity profiles of drugs modulating Gq-protein-coupled receptors. *Molecular Pharmacology*, *94*(3), 992-1006.

Beattie, D., Beer, D., Bradley, M. E., Bruce, I., Charlton, S. J., Cuenoud, B. M., ... & Wissler, E. (2012). An investigation into the structure–activity relationships associated with the systematic modification of the β2-adrenoceptor agonist indacaterol. *Bioorganic & medicinal chemistry letters*, *22*(19), 6280-6285.

Behm, D. J., Aiyar, N. V., Olzinski, A. R., McAtee, J. J., Hilfiker, M. A., Dodson, J. W., ... & Douglas, S. A. (2010). GSK1562590, a slowly dissociating urotensin-II receptor antagonist, exhibits prolonged pharmacodynamic activity ex vivo. *British journal of pharmacology*, *161*(1), 207-228.

Benovic, J. L., Pike, L. J., Cerione, R. A., Staniszewski, C., Yoshimasa, T., Codina, J., ... & Lefkowitz, R. J. (1985). Phosphorylation of the mammalian beta-adrenergic receptor by cyclic AMP-dependent protein kinase. Regulation of the rate of receptor phosphorylation and dephosphorylation by agonist occupancy and effects on coupling of the receptor to the stimulatory guanine nucleotide regulatory protein. *Journal of Biological Chemistry*, *260*(11), 7094-7101.

Benovic, J. L., Strasser, R. H., Caron, M. G., & Lefkowitz, R. J. (1986). Beta-adrenergic receptor kinase: identification of a novel protein kinase that phosphorylates the agonist-occupied form of the receptor. *Proceedings of the National Academy of Sciences*, *83*(9), 2797-2801.

Black, J. B., Premont, R. T., & Daaka, Y. (2016, February). Feedback regulation of G protein-coupled receptor signaling by GRKs and arrestins. In *Seminars in cell & developmental biology* (Vol. 50, pp. 95-104). Academic Press.

Black, J. W., Leff, P., Shankley, N. P., & Wood, J. (1985). An operational model of pharmacological agonism: the effect of E/[A] curve shape on agonist dissociation constant estimation. *British journal of pharmacology*, *84*(2), 561.

Black, J. W., & Leff, P. (1983). Operational models of pharmacological agonism. *Proceedings of the Royal society of London. Series B. Biological sciences*, *220*(1219), 141-162.

Blin, N., Yun, J., & Wess, J. (1995). Mapping of Single Amino Acid Residues Required for Selective Activation of Gq/11 by the m3 Muscarinic Acetylcholine Receptor (∗). *Journal of Biological Chemistry*, *270*(30), 17741-17748.

Bokoch, M. P., Zou, Y., Rasmussen, S. G., Liu, C. W., Nygaard, R., Rosenbaum, D. M., ... & Kobilka, B. K. (2010). Ligand-specific regulation of the extracellular surface of a G-protein-coupled receptor. *Nature*, *463*(7277), 108-112.

Bonacci, T. M., Mathews, J. L., Yuan, C., Lehmann, D. M., Malik, S., Wu, D., ... & Smrcka, A. V. (2006). Differential targeting of Gßγ-subunit signaling with small molecules. *Science*, *312*(5772), 443-446.

Bonneterre, J., Montpas, N., Boularan, C., Gales, C., & Heveker, N. (2016). Analysis of arrestin recruitment to chemokine receptors by bioluminescence resonance energy transfer. In *Methods in enzymology* (Vol. 570, pp. 131-153). Academic Press.

Bosma, R., Moritani, R., Leurs, R., & Vischer, H. F. (2016). BRET-based β-arrestin2 recruitment to the histamine H1 receptor for investigating antihistamine binding kinetics. *Pharmacological Research*, *111*, 679-687.

Bot, I., Ortiz Zacarías, N. V., de Witte, W. E., de Vries, H., van Santbrink, P. J., van der Velden, D., ... & Heitman, L. H. (2017). A novel CCR2 antagonist inhibits atherogenesis in apoE deficient mice by achieving high receptor occupancy. *Scientific reports*, *7*(1), 1-12.

Bouabe, H., Fässler, R., & Heesemann, J. (2008). Improvement of reporter activity by IRES-mediated polycistronic reporter system. *Nucleic acids research*, *36*(5), e28.

Boursier, M. E., Levin, S., Zimmerman, K., Machleidt, T., Hurst, R., Butler, B. L., ... & Ohana, R. F. (2020). The luminescent HiBiT peptide enables selective quantitation of G protein–coupled receptor ligand engagement and internalization in living cells. *Journal of Biological Chemistry*, *295*(15), 5124-5135.

Bouzo-Lorenzo, M., Stoddart, L. A., Xia, L., IJzerman, A. P., Heitman, L. H., Briddon, S. J., & Hill, S. J. (2019). A live cell NanoBRET binding assay allows the study of ligand-binding kinetics to the adenosine A3 receptor. *Purinergic Signalling*, *15*(2), 139-153.

Bridge, L. J., Mead, J., Frattini, E., Winfield, I., & Ladds, G. (2018). Modelling and simulation of biased agonism dynamics at a G protein-coupled receptor. *Journal of theoretical biology*, *442*, 44-65.

Brunskole Hummel, I., Reinartz, M. T., Kälble, S., Burhenne, H., Schwede, F., Buschauer, A., & Seifert, R. (2013). Dissociations in the effects of β2-adrenergic receptor agonists on cAMP formation and superoxide production in human neutrophils: support for the concept of functional selectivity. *PLoS One*, *8*(5), e64556.

Budde, T., Meuth, S., & Pape, H. C. (2002). Calcium-dependent inactivation of neuronal calcium channels. *Nature Reviews Neuroscience*, *3*(11), 873-883.

Burgisser, E., Lefkowitz, R. J., & Delean, A. (1981). Alternative explanation for the apparent" two-step" binding kinetics of high-affinity racemic antagonist radioligands. *Molecular Pharmacology*, *19*(3), 509-512.

Cahill, T. J., Thomsen, A. R., Tarrasch, J. T., Plouffe, B., Nguyen, A. H., Yang, F., ... & Lefkowitz, R. J. (2017). Distinct conformations of GPCR–β-arrestin complexes mediate desensitization, signaling, and endocytosis. *Proceedings of the National Academy of Sciences*, *114*(10), 2562-2567.

Calebiro, D., Nikolaev, V. O., Gagliani, M. C., De Filippis, T., Dees, C., Tacchetti, C., ... & Lohse, M. J. (2009). Persistent cAMP-signals triggered by internalized G-protein–coupled receptors. *PLoS biology*, *7*(8), e1000172.

Callander, G. E., Thomas, W. G., & Bathgate, R. A. (2009). Prolonged RXFP1 and RXFP2 signaling can be explained by poor internalization and a lack of β-arrestin recruitment. *American Journal of Physiology-Cell Physiology*, *296*(5), C1058-C1066.

Campbell, A. P., & Smrcka, A. V. (2018). Targeting G protein-coupled receptor signalling by blocking G proteins. *Nature reviews Drug discovery*, *17*(11), 789-803.

Cannaert, A., Storme, J., Franz, F., Auwärter, V., & Stove, C. P. (2016). Detection and activity profiling of synthetic cannabinoids and their metabolites with a newly developed bioassay. *Analytical chemistry*, *88*(23), 11476-11485.

Carpenter, B., Nehmé, R., Warne, T., Leslie, A. G., & Tate, C. G. (2016). Structure of the adenosine A2A receptor bound to an engineered G protein. *Nature*, *536*(7614), 104-107.

Carpenter, B., & Tate, C. G. (2016). Engineering a minimal G protein to facilitate crystallisation of G protein-coupled receptors in their active conformation. *Protein Engineering, Design and Selection*, *29*(12), 583-594.

Carpenter, B., & Tate, C. G. (2017). Expression, purification and crystallisation of the adenosine A2A receptor bound to an engineered mini G protein. *Bio-protocol*, *7*(8).

Carr, R., Schilling, J., Song, J., Carter, R. L., Du, Y., Yoo, S. M., ... & Benovic, J. L. (2016). β-arrestin–biased signaling through the β2-adrenergic receptor promotes cardiomyocyte contraction. *Proceedings of the National Academy of Sciences*, *113*(28), E4107-E4116.

Carter, A. A., & Hill, S. J. (2005). Characterization of isoprenaline-and salmeterol-stimulated interactions between β2-adrenoceptors and β-arrestin 2 using β-galactosidase complementation in C2C12 cells. *Journal of Pharmacology and experimental therapeutics*, *315*(2), 839-848.

Caspar, B (2019), 'Investigating the mode of action of intracellular loop 1 pepducins at the CXCR4 receptor', PhD Thesis, University Of Nottingham, Nottingham, UK.

Castillo, J. D., & Katz, B. (1957). Interaction at end-plate receptors between different choline derivatives. *Proceedings of the Royal Society of London. Series B-Biological Sciences*, *146*(924), 369-381.

Cazzola, M., Calzetta, L., & Matera, M. G. (2011). β2-adrenoceptor agonists: current and future direction. *British journal of pharmacology*, *163*(1), 4-17.

Chakir, K., Depry, C., Dimaano, V. L., Zhu, W. Z., Vanderheyden, M., Bartunek, J., ... & Kass, D. A. (2011). Gαs-biased β2-adrenergic receptor signaling from restoring synchronous contraction in the failing heart. *Science translational medicine*, *3*(100), 100ra88-100ra88.

Chakir, K., Zhu, W., Tsang, S., Woo, A. Y. H., Yang, D., Wang, X., ... & Xiao, R. P. (2011). RGS2 is a primary terminator of β2-adrenergic receptor-mediated Gi signaling. *Journal of molecular and cellular cardiology*, *50*(6), 1000-1007.

Chan, H. C., Filipek, S., & Yuan, S. (2016). The Principles of Ligand Specificity on beta-2-adrenergic receptor. *Scientific reports*, *6*(1), 1-11.

Changeux, J. P., & Edelstein, S. J. (2005). Allosteric mechanisms of signal transduction. *Science*, *308*(5727), 1424-1428.

Charest, P. G., Oligny-Longpré, G., Bonin, H., Azzi, M., & Bouvier, M. (2007). The V2 vasopressin receptor stimulates ERK1/2 activity independently of heterotrimeric G protein signalling. *Cellular signalling*, *19*(1), 32-41.

Charest, P. G., Terrillon, S., & Bouvier, M. (2005). Monitoring agonist-promoted conformational changes of β-arrestin in living cells by intramolecular BRET. *EMBO reports*, *6*(4), 334-340.

Charlton, S. J., & Vauquelin, G. (2010). Elusive equilibrium: the challenge of interpreting receptor pharmacology using calcium assays. *British journal of pharmacology*, *161*(6), 1250-1265.

Chelikani, P., Hornak, V., Eilers, M., Reeves, P. J., Smith, S. O., RajBhandary, U. L., & Khorana, H. G. (2007). Role of group-conserved residues in the helical core of β2-adrenergic receptor. *Proceedings of the National Academy of Sciences*, *104*(17), 7027-7032.

Chen, X. T., Pitis, P., Liu, G., Yuan, C., Gotchev, D., Cowan, C. L., ... & Yamashita, D. S. (2013). Structure–Activity Relationships and Discovery of a G Protein Biased μ Opioid Receptor Ligand,[(3-Methoxythiophen-2-yl) methyl]({2-[(9 R)-9-(pyridin-2-yl)-6-oxaspiro-[4.5] decan-9-yl] ethyl}) amine (TRV130), for the Treatment of Acute Severe Pain. *Journal of medicinal chemistry*, *56*(20), 8019-8031.

Cheng, X., Ji, Z., Tsalkova, T., & Mei, F. (2008). Epac and PKA: a tale of two intracellular cAMP receptors. *Acta biochimica et biophysica Sinica*, *40*(7), 651-662.

Cherezov, V., Rosenbaum, D. M., Hanson, M. A., Rasmussen, S. G., Thian, F. S., Kobilka, T. S., ... & Stevens, R. C. (2007). High-resolution crystal structure of an engineered human β2-adrenergic G protein–coupled receptor. *science*, *318*(5854), 1258-1265.

Chidiac, P., Hebert, T. E., Valiquette, M., Dennis, M., & Bouvier, M. (1994). Inverse agonist activity of beta-adrenergic antagonists. *Molecular pharmacology*, *45*(3), 490-499.

Christiansen, E., Hudson, B. D., Hansen, A. H., Milligan, G., & Ulven, T. (2016). Development and characterization of a potent free fatty acid receptor 1 (FFA1) fluorescent tracer. *Journal of medicinal chemistry*, *59*(10), 4849-4858.

Chung, K. Y., Rasmussen, S. G., Liu, T., Li, S., DeVree, B. T., Chae, P. S., ... & Sunahara, R. K. (2011). Conformational changes in the G protein Gs induced by the β2 adrenergic receptor. *Nature*, *477*(7366), 611-615.

Ciruela, F., Jacobson, K. A., & Fernández-Dueñas, V. (2014). Portraying G protein-coupled receptors with fluorescent ligands. *ACS chemical biology*, *9*(9), 1918-1928.

Clark, A. J. (1933). The mode of action of drugs on cells.

Cleveland, K. H., Yeung, S., Huang, K. M., Liang, S., Andresen, B. T., & Huang, Y. (2018). Phosphoproteome profiling provides insight into the mechanism of action for carvedilol-mediated cancer prevention. *Molecular carcinogenesis*, *57*(8), 997-1007.

Conklin, B. R., Farfel, Z., Lustig, K. D., Julius, D., & Bourne, H. R. (1993). Substitution of three amino acids switches receptor specificity of Gqα to that of Giα. *Nature*, *363*(6426), 274-276.

Copeland, R. A. (2010). The dynamics of drug-target interactions: drug-target residence time and its impact on efficacy and safety. *Expert opinion on drug discovery*, *5*(4), 305-310.

Copeland, R. A., Pompliano, D. L., & Meek, T. D. (2006). Drug–target residence time and its implications for lead optimization. *Nature reviews Drug discovery*, *5*(9), 730-739.

Costa, T., & Herz, A. (1989). Antagonists with negative intrinsic activity at delta opioid receptors coupled to GTP-binding proteins. *Proceedings of the National Academy of Sciences*, *86*(19), 7321-7325.

Culhane, K. J., Gupte, T. M., Madhugiri, I., Gadgil, C. J., & Sivaramakrishnan, S. (2022). Kinetic model of GPCR-G protein interactions reveals allokairic modulation of signaling. *Nature communications*, *13*(1), 1-9.

Dahl, G., & Akerud, T. (2013). Pharmacokinetics and the drug–target residence time concept. *Drug discovery today*, *18*(15-16), 697-707.

Deupi, X., & Kobilka, B. K. (2010). Energy landscapes as a tool to integrate GPCR structure, dynamics, and function. *Physiology*, *25*(5), 293-303.

DeVree, B. T., Mahoney, J. P., Vélez-Ruiz, G. A., Rasmussen, S. G., Kuszak, A. J., Edwald, E., ... & Sunahara, R. K. (2016). Allosteric coupling from G protein to the agonist-binding pocket in GPCRs. *Nature*, *535*(7610), 182-186.

DeWire, S. M., Yamashita, D. S., Rominger, D. H., Liu, G., Cowan, C. L., Graczyk, T. M., ... & Violin, J. D. (2013). AG protein-biased ligand at the μ-opioid receptor is potently analgesic with reduced gastrointestinal and respiratory dysfunction compared with morphine. *Journal of Pharmacology and Experimental Therapeutics*, *344*(3), 708-717.

Dijon, N. C., Nesheva, D. N., & Holliday, N. D. (2021). Luciferase Complementation Approaches to Measure GPCR Signaling Kinetics and Bias. In *G Protein-Coupled Receptor Screening Assays* (pp. 249-274). Humana, New York, NY.

Dixon, A. S., Schwinn, M. K., Hall, M. P., Zimmerman, K., Otto, P., Lubben, T. H., ... & Wood, K. V. (2016). NanoLuc complementation reporter optimized for accurate measurement of protein interactions in cells. *ACS chemical biology*, *11*(2), 400-408.

Dixon, A. S., Encell, L., Hall, M., Wood, K., Wood, M., Schwinn, M., ... & Machleidt, T. (2018). *U.S. Patent No. 9,869,670*. Washington, DC: U.S. Patent and Trademark Office.

Dong, C., Filipeanu, C. M., Duvernay, M. T., & Wu, G. (2007). Regulation of G protein-coupled receptor export trafficking. *Biochimica et Biophysica Acta (BBA)-Biomembranes*, *1768*(4), 853-870.

Donthamsetti, P., Quejada, J. R., Javitch, J. A., Gurevich, V. V., & Lambert, N. A. (2015). Using Bioluminescence Resonance Energy Transfer (BRET) to characterize agonist-induced arrestin recruitment to modified and unmodified G protein-coupled receptors. *Current protocols in pharmacology*, *70*(1), 2-14.

Dorn, G. W., Tepe, N. M., Lorenz, J. N., Koch, W. J., & Liggett, S. B. (1999). Low-and high-level transgenic expression of β2-adrenergic receptors differentially affect cardiac hypertrophy and function in Gαq-overexpressing mice. *Proceedings of the National Academy of Sciences*, *96*(11), 6400-6405.

Dorr, P., Westby, M., Dobbs, S., Griffin, P., Irvine, B., Macartney, M., ... & Perros, M. (2005). Maraviroc (UK-427,857), a potent, orally bioavailable, and selective small-molecule inhibitor of chemokine receptor CCR5 with broad-spectrum anti-human immunodeficiency virus type 1 activity. *Antimicrobial agents and chemotherapy*, *49*(11), 4721-4732.

Dowling, M. R., & Charlton, S. J. (2006). Quantifying the association and dissociation rates of unlabelled antagonists at the muscarinic M3 receptor. *British journal of pharmacology*, *148*(7), 927-937.

Dror, R. O., Pan, A. C., Arlow, D. H., Borhani, D. W., Maragakis, P., Shan, Y., ... & Shaw, D. E. (2011). Pathway and mechanism of drug binding to G-protein-coupled receptors. *Proceedings of the National Academy of Sciences*, *108*(32), 13118-13123.

Duan, J., Shen, D. D., Zhou, X. E., Bi, P., Liu, Q. F., Tan, Y. X., ... & Jiang, Y. (2020). Cryo-EM structure of an activated VIP1 receptor-G protein complex revealed by a NanoBiT tethering strategy. *Nature communications*, *11*(1), 1-10.

Dupuis, N., Laschet, C., Franssen, D., Szpakowska, M., Gilissen, J., Geubelle, P., ... & Hanson, J. (2017). Activation of the orphan G protein–coupled receptor GPR27 by surrogate ligands promotes β-arrestin 2 recruitment. *Molecular Pharmacology*, *91*(6), 595-608.

Dustin, D., Gu, G., & Fuqua, S. A. (2019). ESR1 mutations in breast cancer. *Cancer*, *125*(21), 3714-3728.

Duvernay, M. T., Filipeanu, C. M., & Wu, G. (2005). The regulatory mechanisms of export trafficking of G protein-coupled receptors. *Cellular signalling*, *17*(12), 1457-1465.

Eckhart, A. D., Ozaki, T., Tevaearai, H., Rockman, H. A., & Koch, W. J. (2002). Vascular-targeted overexpression of G protein-coupled receptor kinase-2 in transgenic mice attenuates β-adrenergic receptor signaling and increases resting blood pressure. *Molecular pharmacology*, *61*(4), 749-758.

Eddy, M. T., Didenko, T., Stevens, R. C., & Wüthrich, K. (2016). β2-adrenergic receptor conformational response to fusion protein in the third intracellular loop. *Structure*, *24*(12), 2190-2197.

Emami-Nemini, A., Roux, T., Leblay, M., Bourrier, E., Lamarque, L., Trinquet, E., & Lohse, M. J. (2013). Time-resolved fluorescence ligand binding for G protein–coupled receptors. *Nature protocols*, *8*(7), 1307-1320.

Emtage, A. L., Mistry, S. N., Fischer, P. M., Kellam, B., & Laughton, C. A. (2017). GPCRs through the keyhole: the role of protein flexibility in ligand binding to β-adrenoceptors. *Journal of Biomolecular Structure and Dynamics*, *35*(12), 2604-2619.

Van Eps, N., Preininger, A. M., Alexander, N., Kaya, A. I., Meier, S., Meiler, J., ... & Hubbell, W. L. (2011). Interaction of a G protein with an activated receptor opens the interdomain interface in the alpha subunit. *Proceedings of the National Academy of Sciences*, *108*(23), 9420-9424.

Evans, B. A., Merlin, J., Bengtsson, T., & Hutchinson, D. S. (2019). Adrenoceptors in white, brown, and brite adipocytes. *British journal of pharmacology*, *176*(14), 2416-2432.

Evron, T., Daigle, T. L., & Caron, M. G. (2012). GRK2: multiple roles beyond G protein-coupled receptor desensitization. *Trends in pharmacological sciences*, *33*(3), 154-164.

Favara, D. M., Liebscher, I., Jazayeri, A., Nambiar, M., Sheldon, H., Banham, A. H., & Harris, A. L. (2021). Elevated expression of the adhesion GPCR ADGRL4/ELTD1 promotes endothelial sprouting angiogenesis without activating canonical GPCR signalling. *Scientific reports*, *11*(1), 1-13.

Fedosova, N. U., Champeil, P., & Esmann, M. (2002). Nucleotide binding to Na, K-ATPase: the role of electrostatic interactions. *Biochemistry*, *41*(4), 1267-1273.

Fernández-Dueñas, V., Gómez-Soler, M., Jacobson, K. A., Kumar, S. T., Fuxe, K., Borroto-Escuela, D. O., & Ciruela, F. (2012). Molecular determinants of A2AR–D2R allosterism: role of the intracellular loop 3 of the D2R. *Journal of neurochemistry*, *123*(3), 373-384.

Ferrandon, S., Feinstein, T. N., Castro, M., Wang, B., Bouley, R., Potts, J. T., ... & Vilardaga, J. P. (2009). Sustained cyclic AMP production by parathyroid hormone receptor endocytosis. *Nature chemical biology*, *5*(10), 734-742.

Finlay, D. B., Duffull, S. B., & Glass, M. (2020). 100 years of modelling ligand–receptor binding and response: A focus on GPCRs. *British journal of pharmacology*, *177*(7), 1472-1484.

Flanagan, C. A. (2016). GPCR-radioligand binding assays. In *Methods in cell biology* (Vol. 132, pp. 191-215). Academic Press.

Flock, T., Ravarani, C. N., Sun, D., Venkatakrishnan, A. J., Kayikci, M., Tate, C. G., ... & Babu, M. M. (2015). Universal allosteric mechanism for Gα activation by GPCRs. *Nature*, *524*(7564), 173-179.

Fujikawa, Y., & Kato, N. (2007). Technical Advance: Split luciferase complementation assay to study protein–protein interactions in Arabidopsis protoplasts. *The Plant Journal*, *52*(1), 185-195.

Furchgott, R. F. (1966). The use of β-haloalkylamines in the differentiation of receptors and in the determination of dissociation constants of receptor-agonist complexes. *Adv. Drug Res.*, *3*, 21-55.

Gaddum, J. H. (1937). The quantitative effects of antagonistic drugs. *J. physiol*, *89*, 7P-9P.

Galandrin, S., Oligny-Longpré, G., & Bouvier, M. (2007). The evasive nature of drug efficacy: implications for drug discovery. *Trends in pharmacological sciences*, *28*(8), 423-430.

Gao, Y., Westfield, G., Erickson, J. W., Cerione, R. A., Skiniotis, G., & Ramachandran, S. (2017). Isolation and structure–function characterization of a signaling-active rhodopsin–G protein complex. *Journal of Biological Chemistry*, *292*(34), 14280-14289.

García-Nafría, J., Lee, Y., Bai, X., Carpenter, B., & Tate, C. G. (2018a). Cryo-EM structure of the adenosine A2A receptor coupled to an engineered heterotrimeric G protein. *Elife*, *7*, e35946.

García-Nafría, J., Nehme, R., Edwards, P. C., & Tate, C. G. (2018b). Cryo-EM structure of the serotonin 5-HT1B receptor coupled to heterotrimeric Go. *Nature*, *558*(7711), 620-623.

García-Sevilla, J. A., Hollingsworth, P. J., & Smith, C. B. (1981). α2-adrenoreceptors on human platelets: selective labelling by [3H] clonidine and [3H] yohimbine and competetive inhibition by antidepressant drugs. *European Journal of Pharmacology*, *74*(4), 329-341.

Garner, K. L., Voliotis, M., Alobaid, H., Perrett, R. M., Pham, T., Tsaneva-Atanasova, K., & McArdle, C. A. (2017). Information transfer via gonadotropin-releasing hormone receptors to ERK and NFAT: sensing GnRH and sensing dynamics. *Journal of the Endocrine Society*, *1*(4), 260-277.

Gatfield, J., Mueller Grandjean, C., Sasse, T., Clozel, M., & Nayler, O. (2012). Slow receptor dissociation kinetics differentiate macitentan from other endothelin receptor antagonists in pulmonary arterial smooth muscle cells.

Ghanouni, P., Steenhuis, J. J., Farrens, D. L., & Kobilka, B. K. (2001). Agonist-induced conformational changes in the G-protein-coupling domain of the β2 adrenergic receptor. *Proceedings of the National Academy of Sciences*, *98*(11), 5997-6002.

Gherbi, K., May, L. T., Baker, J. G., Briddon, S. J., & Hill, S. J. (2015). Negative cooperativity across β1-adrenoceptor homodimers provides insights into the nature of the secondary low-affinity CGP 12177 β1-adrenoceptor binding conformation. *The FASEB Journal*, *29*(7), 2859-2871.

Gherbi, K., Groenewoud, N. J., Holliday, N. D., Sengmany, K., & Charlton, S. J. (2020). Kinetics of ligand binding and signaling. In *GPCRs* (pp. 171-194). Academic Press.

Gherbi, K., Briddon, S. J., & Charlton, S. J. (2018). Micro-pharmacokinetics: Quantifying local drug concentration at live cell membranes. *Scientific reports*, *8*(1), 1-8.

Gilbert, C. J., Longenecker, J. Z., & Accornero, F. (2021). ERK1/2: an integrator of signals that alters cardiac homeostasis and growth. *Biology*, *10*(4), 346.

Gillis, A., Kliewer, A., Kelly, E., Henderson, G., Christie, M. J., Schulz, S., & Canals, M. (2020a). Critical assessment of G protein-biased agonism at the μ-opioid receptor. *Trends in Pharmacological Sciences*, *41*(12), 947-959.

Gillis, A., Gondin, A. B., Kliewer, A., Sanchez, J., Lim, H. D., Alamein, C., ... & Canals, M. (2020). Low intrinsic efficacy for G protein activation can explain the improved side effect profiles of new opioid agonists. *Science Signaling*, *13*(625), eaaz3140.

Gilman, A. G. (1987). G proteins: transducers of receptor-generated signals. *Annual review of biochemistry*, *56*(1), 615-649.

Goldsmith, Z. G., & Dhanasekaran, D. N. (2007). G protein regulation of MAPK networks. *Oncogene*, *26*(22), 3122-3142.

Goulding, J., May, L. T., & Hill, S. J. (2018). Characterisation of endogenous A2A and A2B receptor-mediated cyclic AMP responses in HEK 293 cells using the GloSensor™ biosensor: Evidence for an allosteric mechanism of action for the A2B-selective antagonist PSB 603. *Biochemical Pharmacology*, *147*, 55-66.

Grätz, L., Tropmann, K., Bresinsky, M., Müller, C., Bernhardt, G., & Pockes, S. (2020). NanoBRET binding assay for histamine H2 receptor ligands using live recombinant HEK293T cells. *Scientific reports*, *10*(1), 1-10.

Green, S. A., & Liggett, S. B. (1994). A proline-rich region of the third intracellular loop imparts phenotypic beta 1-versus beta 2-adrenergic receptor coupling and sequestration. *Journal of Biological Chemistry*, *269*(42), 26215-26219.

Gregorio, G. G., Masureel, M., Hilger, D., Terry, D. S., Juette, M., Zhao, H., ... & Blanchard, S. C. (2017). Single-molecule analysis of ligand efficacy in β2AR–G-protein activation. *Nature*, *547*(7661), 68-73.

Grishina, G., & Berlot, C. H. (2000). A surface-exposed region of Gsα in which substitutions decrease receptor-mediated activation and increase receptor affinity. *Molecular pharmacology*, *57*(6), 1081-1092.

Groer, C. E., Schmid, C. L., Jaeger, A. M., & Bohn, L. M. (2011). Agonist-directed interactions with specific β-arrestins determine μ-opioid receptor trafficking, ubiquitination, and dephosphorylation. *Journal of Biological Chemistry*, *286*(36), 31731-31741.

Grundmann, M., Merten, N., Malfacini, D., Inoue, A., Preis, P., Simon, K., ... & Kostenis, E. (2018). Lack of beta-arrestin signaling in the absence of active G proteins. *Nature communications*, *9*(1), 1-16.

Guo, D., Mulder-Krieger, T., IJzerman, A. P., & Heitman, L. H. (2012). Functional efficacy of adenosine A2A receptor agonists is positively correlated to their receptor residence time. *British journal of pharmacology*, *166*(6), 1846-1859.

Guo, D., Hillger, J. M., IJzerman, A. P., & Heitman, L. H. (2014). Drug-target residence time—a case for G protein-coupled receptors. *Medicinal research reviews*, *34*(4), 856-892.

Guo, D., Peletier, L. A., Bridge, L., Keur, W., de Vries, H., Zweemer, A., ... & IJzerman, A. P. (2018). A two-state model for the kinetics of competitive radioligand binding. *British Journal of Pharmacology*, *175*(10), 1719-1730.

Guo, D., Heitman, L. H., & IJzerman, A. P. (2016a). Kinetic aspects of the interaction between ligand and G protein-coupled receptor: the case of the adenosine receptors. *Chemical Reviews*, *117*(1), 38-66.

Guo, D., Heitman, L. H., & IJzerman, A. P. (2016b). The added value of assessing ligand–receptor binding kinetics in drug discovery. *ACS Medicinal Chemistry Letters*, *7*(9), 819-821.

Gurevich, V. V., & Gurevich, E. V. (2004). The molecular acrobatics of arrestin activation. *Trends in pharmacological sciences*, *25*(2), 105-111.

Gurevich, V. V., & Gurevich, E. V. (2019). GPCR signaling regulation: the role of GRKs and arrestins. *Frontiers in pharmacology*, *10*, 125.

Haga, Y., Ishii, K., Hibino, K., Sako, Y., Ito, Y., Taniguchi, N., & Suzuki, T. (2012). Visualizing specific protein glycoforms by transmembrane fluorescence resonance energy transfer. *Nature communications*, *3*(1), 1-7.

Hall, M. P., Unch, J., Binkowski, B. F., Valley, M. P., Butler, B. L., Wood, M. G., ... & Wood, K. V. (2012). Engineered luciferase reporter from a deep sea shrimp utilizing a novel imidazopyrazinone substrate. *ACS chemical biology*, *7*(11), 1848-1857.

Hanania, N. A., Sharafkhaneh, A., Barber, R., & Dickey, B. F. (2002). β-agonist intrinsic efficacy: measurement and clinical significance. *American journal of respiratory and critical care medicine*, *165*(10), 1353-1358.

Hanania, N. A., Dickey, B. F., & Bond, R. A. (2010). Clinical implications of the intrinsic efficacy of beta-adrenoceptor drugs in asthma: full, partial and inverse agonism. *Current opinion in pulmonary medicine*, *16*(1), 1.

Hansen, L. S., Sparre-Ulrich, A. H., Christensen, M., Knop, F. K., Hartmann, B., Holst, J. J., & Rosenkilde, M. M. (2016). N-terminally and C-terminally truncated forms of glucose-dependent insulinotropic polypeptide are high-affinity competitive antagonists of the human GIP receptor. *British journal of pharmacology*, *173*(5), 826-838.

Hanson, M. A., Cherezov, V., Griffith, M. T., Roth, C. B., Jaakola, V. P., Chien, E. Y., ... & Stevens, R. C. (2008). A specific cholesterol binding site is established by the 2.8 Å structure of the human β2-adrenergic receptor. *Structure*, *16*(6), 897-905.

Hanson, S. M., Francis, D. J., Vishnivetskiy, S. A., Kolobova, E. A., Hubbell, W. L., Klug, C. S., & Gurevich, V. V. (2006). Differential interaction of spin-labeled arrestin with inactive and active phosphorhodopsin. *Proceedings of the National Academy of Sciences*, *103*(13), 4900-4905.

Hanyaloglu, A. C. (2018). Advances in membrane trafficking and endosomal signaling of G protein-coupled receptors. *International review of cell and molecular biology*, *339*, 93-131.

Harris, B. A., Robishaw, J. D., Mumby, S. M., & Gilman, A. G. (1985). Molecular cloning of complementary DNA for the alpha subunit of the G protein that stimulates adenylate cyclase. *Science*, *229*(4719), 1274-1277.

Hattori, M., & Ozawa, T. (2014). Split luciferase complementation for analysis of intracellular signaling. *Analytical Sciences*, *30*(5), 539-544.

Hayashi, H., Hess, D. T., Zhang, R., Sugi, K., Gao, H., Tan, B. L., ... & Stamler, J. S. (2018). S-nitrosylation of β-arrestins biases receptor signaling and confers ligand independence. *Molecular cell*, *70*(3), 473-487.

Henry, A. G., Hislop, J. N., Grove, J., Thorn, K., Marsh, M., & von Zastrow, M. (2012). Regulation of endocytic clathrin dynamics by cargo ubiquitination. *Developmental cell*, *23*(3), 519-532.

Higashijima, T., Ferguson, K. M., Sternweis, P. C., Smigel, M. D., & Gilman, A. G. (1987). Effects of Mg2+ and the beta gamma-subunit complex on the interactions of guanine nucleotides with G proteins. *Journal of Biological Chemistry*, *262*(2), 762-766.

Hilger, D., Masureel, M., & Kobilka, B. K. (2018). Structure and dynamics of GPCR signaling complexes. *Nature structural & molecular biology*, *25*(1), 4-12.

Hill, A. V. (1910). The possible effects of the aggregation of the molecules of haemoglobin on its dissociation curves. *j. physiol.*, *40*, 4-7.

Hill, A. V. (1909). The mode of action of nicotine and curari, determined by the form of the contraction curve and the method of temperature coefficients. *The Journal of physiology*, *39*(5), 361.

Hill, S. J., & Watson, S. P. (2018). Fluorescence approaches unravel spatial and temporal aspects of GPCR organisation, location, and intracellular signalling. *Trends in Pharmacological Sciences*, *39*(2), 91-92.

Hoare, B. L., Bruell, S., Sethi, A., Gooley, P. R., Lew, M. J., Hossain, M. A., ... & Bathgate, R. A. (2019). Multi-component mechanism of H2 Relaxin binding to RXFP1 through NanoBRET kinetic analysis. *IScience*, *11*, 93-113.

Hoare, S. R., Pierre, N., Moya, A. G., & Larson, B. (2018). Kinetic operational models of agonism for G-protein-coupled receptors. *Journal of Theoretical Biology*, *446*, 168-204.

Hoare, S. R. (2018). Receptor binding kinetics equations: Derivation using the Laplace transform method. *Journal of Pharmacological and Toxicological Methods*, *89*, 26-38.

Hoare, S. R., Tewson, P. H., Quinn, A. M., Hughes, T. E., & Bridge, L. J. (2020). Analyzing kinetic signaling data for G-protein-coupled receptors. *Scientific reports*, *10*(1), 1-23.

Hoare, S. R., Fleck, B. A., Williams, J. P., & Grigoriadis, D. E. (2020). The importance of target binding kinetics for measuring target binding affinity in drug discovery: a case study from a CRF1 receptor antagonist program. *Drug Discovery Today*, *25*(1), 7-14.

Holst, B., Holliday, N. D., Bach, A., Elling, C. E., Cox, H. M., & Schwartz, T. W. (2004). Common structural basis for constitutive activity of the ghrelin receptor family. *Journal of Biological Chemistry*, *279*(51), 53806-53817.

Höring, C., Seibel, U., Tropmann, K., Grätz, L., Mönnich, D., Pitzl, S., ... & Strasser, A. (2020). A dynamic, split-luciferase-based mini-G protein sensor to functionally characterize ligands at all four histamine receptor subtypes. *International journal of molecular sciences*, *21*(22), 8440.

Hothersall, J. D., Brown, A. J., Dale, I., & Rawlins, P. (2016). Can residence time offer a useful strategy to target agonist drugs for sustained GPCR responses?. *Drug discovery today*, *21*(1), 90-96.

Hothersall, J. D., Bussey, C. E., Brown, A. J., Scott, J. S., Dale, I., & Rawlins, P. (2015). Sustained wash-resistant receptor activation responses of GPR119 agonists. *European journal of pharmacology*, *762*, 430-442.

Hothersall, J. D., Brown, A. J., Dale, I., & Rawlins, P. (2016). Can residence time offer a useful strategy to target agonist drugs for sustained GPCR responses?. *Drug discovery today*, *21*(1), 90-96.

Hsiao, E. C., Nguyen, T. D., Ng, J. K., Scott, M. J., Chang, W. C., Zahed, H., & Conklin, B. R. (2011). Constitutive Gs activation using a single-construct tetracycline-inducible expression system in embryonic stem cells and mice. *Stem cell research & therapy*, *2*(2), 1-12.

Huang, S. K., Pandey, A., Tran, D. P., Villanueva, N. L., Kitao, A., Sunahara, R. K., ... & Prosser, R. S. (2021). Delineating the conformational landscape of the adenosine A2A receptor during G protein coupling. *Cell*, *184*(7), 1884-1894.

Huang, W., Manglik, A., Venkatakrishnan, A. J., Laeremans, T., Feinberg, E. N., Sanborn, A. L., ... & Kobilka, B. K. (2015). Structural insights into μ-opioid receptor activation. *Nature*, *524*(7565), 315-321.

Huber, W., & Mueller, F. (2006). Biomolecular interaction analysis in drug discovery using surface plasmon resonance technology. *Current pharmaceutical design*, *12*(31), 3999-4021.

Hübner, H., Schellhorn, T., Gienger, M., Schaab, C., Kaindl, J., Leeb, L., ... & Gmeiner, P. (2016). Structure-guided development of heterodimer-selective GPCR ligands. *Nature communications*, *7*(1), 1-12.

Hughes, J. D., Blagg, J., Price, D. A., Bailey, S., DeCrescenzo, G. A., Devraj, R. V., ... & Zhang, Y. (2008). Physiochemical drug properties associated with in vivo toxicological outcomes. *Bioorganic & medicinal chemistry letters*, *18*(17), 4872-4875.

Ilien, B., Franchet, C., Bernard, P., Morisset, S., Odile Weill, C., Bourguignon, J. J., ... & Galzi, J. L. (2003). Fluorescence resonance energy transfer to probe human M1 muscarinic receptor structure and drug binding properties. *Journal of neurochemistry*, *85*(3), 768-778.

Imaeda, A., Tanaka, S., Tonegawa, K., Fuchigami, S., Obana, M., Maeda, M., ... & Nakayama, H. (2019). Myofibroblast β2 adrenergic signaling amplifies cardiac hypertrophy in mice. *Biochemical and biophysical research communications*, *510*(1), 149-155.

Insel, P. A., & Stoolman, L. M. (1978). Radioligand binding to beta adrenergic receptors of intact cultured S49 cells. *Molecular Pharmacology*, *14*(4), 549-561.

Jacobson, K. A. (2015). New paradigms in GPCR drug discovery. *Biochemical pharmacology*, *98*(4), 541-555.

Jacqmin, P., McFadyen, L., & Wade, J. R. (2008). A receptor theory-based semimechanistic PD model for the CCR5 noncompetitive antagonist maraviroc. *British journal of clinical pharmacology*, *65*, 95-106.

January, B., Seibold, A., Whaley, B., Hipkin, R. W., Lin, D., Schonbrunn, A., ... & Clark, R. B. (1997). β2-Adrenergic receptor desensitization, internalization, and phosphorylation in response to full and partial agonists. *Journal of Biological Chemistry*, *272*(38), 23871-23879.

Jaud, S., Fernández-Vidal, M., Nilsson, I., Meindl-Beinker, N. M., Hübner, N. C., Tobias, D. J., ... & White, S. H. (2009). Insertion of short transmembrane helices by the Sec61 translocon. *Proceedings of the National Academy of Sciences*, *106*(28), 11588-11593.

Johnson, M. (2006). Molecular mechanisms of β2-adrenergic receptor function, response, and regulation. *Journal of Allergy and Clinical Immunology*, *117*(1), 18-24.

Kallio, H. M., Hieta, R., Latonen, L., Brofeldt, A., Annala, M., Kivinummi, K., ... & Visakorpi, T. (2018). Constitutively active androgen receptor splice variants AR-V3, AR-V7 and AR-V9 are co-expressed in castration-resistant prostate cancer metastases. *British journal of cancer*, *119*(3), 347-356.

Kamal, M., Marquez, M., Vauthier, V., Leloire, A., Froguel, P., Jockers, R., & Couturier, C. (2009). Improved donor/acceptor BRET couples for monitoring β-arrestin recruitment to G protein-coupled receptors. *Biotechnology journal*, *4*(9), 1337-1344.

Kapur, S., & Seeman, P. (2001). Does fast dissociation from the dopamine D2 receptor explain the action of atypical antipsychotics?: A new hypothesis. *American Journal of Psychiatry*, *158*(3), 360-369.

Katritch, V., Fenalti, G., Abola, E. E., Roth, B. L., Cherezov, V., & Stevens, R. C. (2014). Allosteric sodium in class A GPCR signaling. *Trends in biochemical sciences*, *39*(5), 233-244.

Kenakin, T., Morgan, P., Lutz, M., & Weiss, J. (2000). The evolution of drug-receptor models: The cubic ternary complex model for G protein-coupled receptors. In *The pharmacology of functional, biochemical, and recombinant receptor systems* (pp. 147-165). Springer, Berlin, Heidelberg.

Kenakin, T. (2004). G-protein coupled receptors as allosteric machines. *Receptors and Channels*, *10*(2), 51-60.

Kenakin, T. (2009). *A pharmacology primer: theory, application and methods*. Academic Press.

Kenakin, T., Watson, C., Muniz-Medina, V., Christopoulos, A., & Novick, S. (2012). A simple method for quantifying functional selectivity and agonist bias. *ACS chemical neuroscience*, *3*(3), 193-203.

Kenakin, T. (2015). G addum M emorial L ecture 2014: receptors as an evolving concept: from switches to biased microprocessors. *British journal of pharmacology*, *172*(17), 4238-4253.

Kenakin, T. (2015). The effective application of biased signaling to new drug discovery. *Molecular pharmacology*, *88*(6), 1055-1061.

Kenakin, T., Jenkinson, S., & Watson, C. (2006). Determining the potency and molecular mechanism of action of insurmountable antagonists. *Journal of Pharmacology and Experimental Therapeutics*, *319*(2), 710-723.

Kenakin, T. P. (2012). Biased signalling and allosteric machines: new vistas and challenges for drug discovery. *British journal of pharmacology*, *165*(6), 1659-1669.

Kent, R. S., De Lean, A. N. D. R. E., & Lefkowitz, R. J. (1980). A quantitative analysis of beta-adrenergic receptor interactions: resolution of high and low affinity states of the receptor by computer modeling of ligand binding data. *Molecular Pharmacology*, *17*(1), 14-23.

Kersten, E. T., Koppelman, G. H., & Thio, B. J. (2017). Concerns with beta2-agonists in pediatric asthma-a clinical perspective. *Paediatric respiratory reviews*, *21*, 80-85.

Khan, S. M., Sleno, R., Gora, S., Zylbergold, P., Laverdure, J. P., Labbé, J. C., ... & Hébert, T. E. (2013). The expanding roles of Gβγ subunits in G protein–coupled receptor signaling and drug action. *Pharmacological reviews*, *65*(2), 545-577.

Kilpatrick, L. E., Friedman-Ohana, R., Alcobia, D. C., Riching, K., Peach, C. J., Wheal, A. J., ... & Hill, S. J. (2017). Real-time analysis of the binding of fluorescent VEGF165a to VEGFR2 in living cells: effect of receptor tyrosine kinase inhibitors and fate of internalized agonist-receptor complexes. *Biochemical pharmacology*, *136*, 62-75.

Kilts, J. D., Gerhardt, M. A., Richardson, M. D., Sreeram, G., Mackensen, G. B., Grocott, H. P., ... & Kwatra, M. M. (2000). β2-adrenergic and several other G protein–coupled receptors in human atrial membranes activate both Gs and Gi. *Circulation research*, *87*(8), 705-709.

Klein Herenbrink, C., Sykes, D. A., Donthamsetti, P., Canals, M., Coudrat, T., Shonberg, J., ... & Lane, J. R. (2016). The role of kinetic context in apparent biased agonism at GPCRs. *Nature communications*, *7*(1), 1-14.

Kohout, T. A., Lin, F. T., Perry, S. J., Conner, D. A., & Lefkowitz, R. J. (2001). β-Arrestin 1 and 2 differentially regulate heptahelical receptor signaling and trafficking. *Proceedings of the National Academy of Sciences*, *98*(4), 1601-1606.

Kostenis, E., Waelbroeck, M., & Milligan, G. (2005). Techniques: promiscuous Gα proteins in basic research and drug discovery. *Trends in pharmacological sciences*, *26*(11), 595-602.

Kozielewicz, P., Shekhani, R., Moser, S., Bowin, C. F., Wesslowski, J., Davidson, G., & Schulte, G. (2021). Quantitative profiling of WNT-3A binding to all human frizzled paralogues in HEK293 cells by NanoBiT/BRET assessments. ACS Pharmacology & Translational Science, 4(3), 1235-1245.

Krasel, C., Vilardaga, J. P., Bünemann, M., & Lohse, M. J. (2004). Kinetics of G-protein-coupled receptor signalling and desensitization.

Krasel, C., Bünemann, M., Lorenz, K., & Lohse, M. J. (2005). β-Arrestin binding to the β2-adrenergic receptor requires both receptor phosphorylation and receptor activation. *Journal of biological chemistry*, *280*(10), 9528-9535.

Kruse, A. C., Ring, A. M., Manglik, A., Hu, J., Hu, K., Eitel, K., ... & Kobilka, B. K. (2013). Activation and allosteric modulation of a muscarinic acetylcholine receptor. *Nature*, *504*(7478), 101-106.

Kumar, V. (2013). Adenosine as an endogenous immunoregulator in cancer pathogenesis: where to go?. *Purinergic signalling*, *9*(2), 145-165.

Kume, H. (2005). Clinical use of β2-adrenergic receptor agonists based on their intrinsic efficacy. *Allergology International*, *54*(1), 89-97.

Lane, J. R., May, L. T., Parton, R. G., Sexton, P. M., & Christopoulos, A. (2017). A kinetic view of GPCR allostery and biased agonism. *Nature chemical biology*, *13*(9), 929-937.

Laporte, S. A., & Scott, M. G. (2019). β-Arrestins: multitask scaffolds orchestrating the where and when in cell signalling. *Beta-Arrestins*, 9-55.

Laprairie, R. B., Vemuri, K., Stahl, E. L., Korde, A., Ho, J. H., Grim, T. W., ... & Bohn, L. M. (2019). Probing the CB1 cannabinoid receptor binding pocket with AM6538, a high-affinity irreversible antagonist. *Molecular Pharmacology*, *96*(5), 619-628.

Latorraca, N. R., Venkatakrishnan, A. J., & Dror, R. O. (2017). GPCR dynamics: structures in motion. *Chemical reviews*, *117*(1), 139-155.

De Lean, A., Stadel, J., & Lefkowitz, R. J. (1980). A ternary complex model explains the agonist-specific binding properties of the adenylate cyclase-coupled beta-adrenergic receptor. *Journal of Biological Chemistry*, *255*(15), 7108-7117.

Lee, E., Linder, M. E., & Gilman, A. G. (1994). [12] Expression of G-protein a subunits in Escherichia coli. In *Methods in enzymology* (Vol. 237, pp. 146-164). Academic Press.

van der Lee, M. M., Blomenröhr, M., van der Doelen, A. A., Wat, J. W., Smits, N., Hanson, B. J., ... & Zaman, G. J. (2009). Pharmacological characterization of receptor redistribution and β-arrestin recruitment assays for the cannabinoid receptor 1. *Journal of biomolecular screening*, *14*(7), 811-823.

Lee, S. M., Booe, J. M., & Pioszak, A. A. (2015). Structural insights into ligand recognition and selectivity for classes A, B, and C GPCRs. *European journal of pharmacology*, *763*, 196-205.

Pulliainen, J., Luojus, K., Derksen, C., Mudryk, L., Lemmetyinen, J., Salminen, M., ... & Norberg, J. (2020). Molecular basis of beta-arrestin coupling to formoterol-bound beta (1)-adrenoceptor.

Lee, Y., Warne, T., Nehmé, R., Pandey, S., Dwivedi-Agnihotri, H., Chaturvedi, M., ... & Tate, C. G. (2020). Molecular basis of β-arrestin coupling to formoterol-bound β1-adrenoceptor. *Nature*, *583*(7818), 862-866.

Leifert, W. R., Bucco, O., Abeywardena, M. Y., & Patten, G. S. (2009). Radioligand binding assays: Application of [125 I] angiotensin II receptor binding. In *G Protein-Coupled Receptors in Drug Discovery* (pp. 131-141). Humana Press, Totowa, NJ.

Leyris, J. P., Roux, T., Trinquet, E., Verdié, P., Fehrentz, J. A., Oueslati, N., ... & Marie, J. (2011). Homogeneous time-resolved fluorescence-based assay to screen for ligands targeting the growth hormone secretagogue receptor type 1a. *Analytical biochemistry*, *408*(2), 253-262.

Li, H. Z., Li, N., Shao, X. X., Liu, Y. L., Xu, Z. G., & Guo, Z. Y. (2020). Hydrophobic interactions of relaxin family peptide receptor 3 with ligands identified using a NanoBiT-based binding assay. *Biochimie*, *177*, 117-126.

Liang, W., Austin, S., Hoang, Q., & Fishman, P. H. (2003). Resistance of the human β1-Adrenergic receptor to agonist-mediated down-regulation: Role of the C terminus in determining β-subtype degradation. *Journal of Biological Chemistry*, *278*(41), 39773-39781.

Lindström, E., Von Mentzer, B., Påhlman, I., Ahlstedt, I., Uvebrant, A., Kristensson, E., ... & Vauquelin, G. (2007). Neurokinin 1 receptor antagonists: correlation between in vitro receptor interaction and in vivo efficacy. *Journal of Pharmacology and Experimental Therapeutics*, *322*(3), 1286-1293.

Liu, J. J., Horst, R., Katritch, V., Stevens, R. C., & Wüthrich, K. (2012). Biased signaling pathways in β2-adrenergic receptor characterized by 19F-NMR. *Science*, *335*(6072), 1106-1110.

Liu, K., Southall, N., Titus, S. A., Inglese, J., Eskay, R. L., Shinn, P., ... & Zheng, W. (2010). A multiplex calcium assay for identification of GPCR agonists and antagonists. *Assay and drug development technologies*, *8*(3), 362-374.

Lodowski, D. T., Tesmer, V. M., Benovic, J. L., & Tesmer, J. J. (2006). The structure of G protein-coupled receptor kinase (GRK)-6 defines a second lineage of GRKs. *Journal of Biological Chemistry*, *281*(24), 16785-16793.

Lohse, M. J., Nuber, S., & Hoffmann, C. (2012). Fluorescence/bioluminescence resonance energy transfer techniques to study G-protein-coupled receptor activation and signaling. *Pharmacological reviews*, *64*(2), 299-336.

Lombardi, D., Cuenoud, B., & Krämer, S. D. (2009). Lipid membrane interactions of indacaterol and salmeterol: do they influence their pharmacological properties?. *European Journal of Pharmaceutical Sciences*, *38*(5), 533-547.

Lu, H., & Tonge, P. J. (2010). Drug–target residence time: critical information for lead optimization. *Current opinion in chemical biology*, *14*(4), 467-474.

Lu, J., Byrne, N., Wang, J., Bricogne, G., Brown, F. K., Chobanian, H. R., ... & Soisson, S. M. (2017). Structural basis for the cooperative allosteric activation of the free fatty acid receptor GPR40. *Nature structural & molecular biology*, *24*(7), 570-577.

Luker, G. D., & Luker, K. E. (2011). Luciferase protein complementation assays for bioluminescence imaging of cells and mice. In *Molecular Imaging* (pp. 29-43). Humana Press, Totowa, NJ.

Luttrell, L. M., Ferguson, S. S. N. G., Daaka, Y., Miller, W. E., Maudsley, S., Della Rocca, G. J., ... & Lefkowitz, R. J. (1999). β-Arrestin-dependent formation of β2 adrenergic receptor-Src protein kinase complexes. *Science*, *283*(5402), 655-661.

Luttrell, L. M., Wang, J., Plouffe, B., Smith, J. S., Yamani, L., Kaur, S., ... & Lefkowitz, R. J. (2018). Manifold roles of β-arrestins in GPCR signaling elucidated with siRNA and CRISPR/Cas9. *Science Signaling*, *11*(549), eaat7650.

Ma, X., Leurs, R., & Vischer, H. F. (2021). NanoLuc-Based Methods to Measure β-Arrestin2 Recruitment to G Protein-Coupled Receptors. In *G Protein-Coupled Receptor Screening Assays* (pp. 233-248). Humana, New York, NY.

Mackenzie, A. E., Quon, T., Lin, L. C., Hauser, A. S., Jenkins, L., Inoue, A., ... & Milligan, G. (2019). Receptor selectivity between the G proteins Gα12 and Gα13 is defined by a single leucine-to-isoleucine variation. *The FASEB Journal*, *33*(4), 5005-5017.

Maguire, J. J., Kuc, R. E., & Davenport, A. P. (2012). Radioligand binding assays and their analysis. In *Receptor binding techniques* (pp. 31-77). Humana Press, Totowa, NJ.

Mailman, R. B., Nichols, D. E., Lewis, M. M., Blake, B. L., & Lawler, C. P. (1998). Functional effects of novel dopamine ligands: dihydrexidine and Parkinson's disease as a first step. *Dopamine Receptor Subtypes: From Basic Science to Clinical Application*, 64-83.

Makrigiorgos, G. M. (1997). Detection of lipid peroxidation on erythrocytes using the excimer-forming property of a lipophilic BODIPY fluorescent dye. *Journal of biochemical and biophysical methods*, *35*(1), 23-35.

Manglik, A., Kim, T. H., Masureel, M., Altenbach, C., Yang, Z., Hilger, D., ... & Kobilka, B. K. (2015). Structural insights into the dynamic process of β2-adrenergic receptor signaling. *Cell*, *161*(5), 1101-1111.

Manglik, A., & Kobilka, B. (2014). The role of protein dynamics in GPCR function: insights from the β2AR and rhodopsin. *Current opinion in cell biology*, *27*, 136-143.

Manglik, A., Kobilka, B. K., & Steyaert, J. (2017). Nanobodies to study G protein–coupled receptor structure and function. *Annual review of pharmacology and toxicology*, *57*, 19-37.

Marrari, Y., Crouthamel, M., Irannejad, R., & Wedegaertner, P. B. (2007). Assembly and trafficking of heterotrimeric G proteins. *Biochemistry*, *46*(26), 7665-7677.

Marullo, S., & Bouvier, M. (2007). Resonance energy transfer approaches in molecular pharmacology and beyond. *Trends in pharmacological sciences*, *28*(8), 362-365.

Masri, B., Salahpour, A., Didriksen, M., Ghisi, V., Beaulieu, J. M., Gainetdinov, R. R., & Caron, M. G. (2008). Antagonism of dopamine D2 receptor/β-arrestin 2 interaction is a common property

of clinically effective antipsychotics. *Proceedings of the National Academy of Sciences*, *105*(36), 13656-13661.

Matera, M. G., Page, C., & Rinaldi, B. (2018). β2-Adrenoceptor signalling bias in asthma and COPD and the potential impact on the comorbidities associated with these diseases. *Current opinion in pharmacology*, *40*, 142-146.

May, L. T., Self, T. J., Briddon, S. J., & Hill, S. J. (2010). The effect of allosteric modulators on the kinetics of agonist-G protein-coupled receptor interactions in single living cells. *Molecular pharmacology*, *78*(3), 511-523.

May, L. T., Bridge, L. J., Stoddart, L. A., Briddon, S. J., & Hill, S. J. (2011). Allosteric interactions across native adenosine-A3 receptor homodimers: quantification using single-cell ligand-binding kinetics. *The FASEB Journal*, *25*(10), 3465-3476.

McCorvy, J. D., Wacker, D., Wang, S., Agegnehu, B., Liu, J., Lansu, K., ... & Roth, B. L. (2018). Structural determinants of 5-HT2B receptor activation and biased agonism. *Nature structural & molecular biology*, *25*(9), 787-796.

Mcguinness, D., Malikzay, A., Visconti, R., Lin, K., Bayne, M., Monsma, F., & Lunn, C. A. (2009). Characterizing cannabinoid CB2 receptor ligands using DiscoveRx PathHunter™ β-arrestin assay. *Journal of biomolecular screening*, *14*(1), 49-58.

McPherson, J., Rivero, G., Baptist, M., Llorente, J., Al-Sabah, S., Krasel, C., ... & Kelly, E. (2010). μ-opioid receptors: correlation of agonist efficacy for signalling with ability to activate internalization. *Molecular pharmacology*, *78*(4), 756-766.

Mettlen, M., Chen, P. H., Srinivasan, S., Danuser, G., & Schmid, S. L. (2018). Regulation of clathrin-mediated endocytosis. *Annual review of biochemistry*, *87*, 871-896.

Michaelson, D., Ahearn, I., Bergo, M., Young, S., & Philips, M. (2002). Membrane trafficking of heterotrimeric G proteins via the endoplasmic reticulum and Golgi. *Molecular biology of the cell*, *13*(9), 3294-3302.

Milano, S. K., Pace, H. C., Kim, Y. M., Brenner, C., & Benovic, J. L. (2002). Scaffolding functions of arrestin-2 revealed by crystal structure and mutagenesis. *Biochemistry*, *41*(10), 3321-3328.

Miller, W. E., & Lefkowitz, R. J. (2001). Expanding roles for β-arrestins as scaffolds and adapters in GPCR signaling and trafficking. *Current opinion in cell biology*, *13*(2), 139-145.

Mody, S. M., Ho, M. K., Joshi, S. A., & Wong, Y. H. (2000). Incorporation of Gαz-Specific Sequence at the Carboxyl Terminus Increases the Promiscuity of Gα16toward Gi-Coupled Receptors. *Molecular pharmacology*, *57*(1), 13-23.

Molinari, P., Vezzi, V., Sbraccia, M., Grò, C., Riitano, D., Ambrosio, C., ... & Costa, T. (2010). Morphine-like opiates selectively antagonize receptor-arrestin interactions. *Journal of biological chemistry*, *285*(17), 12522-12535.

Mottola, D. M., Kilts, J. D., Lewis, M. M., Connery, H. S., Walker, Q. D., Jones, S. R., ... & Mailman, R. B. (2002). Functional selectivity of dopamine receptor agonists. I. Selective activation of postsynaptic dopamine D2 receptors linked to adenylate cyclase. *Journal of Pharmacology and Experimental Therapeutics*, *301*(3), 1166-1178.

Motulsky, H. J., & Mahan, L. C. (1984). The kinetics of competitive radioligand binding predicted by the law of mass action. *Molecular pharmacology*, *25*(1), 1-9.

Mould, R., Brown, J., Marshall, F. H., & Langmead, C. J. (2014). Binding kinetics differentiates functional antagonism of orexin-2 receptor ligands. *British journal of pharmacology*, *171*(2), 351-363.

Murray, I. A., Patterson, A. D., & Perdew, G. H. (2014). Aryl hydrocarbon receptor ligands in cancer: friend and foe. *Nature Reviews Cancer*, *14*(12), 801-814.

Neer, E. J., & Clapham, D. E. (1988). Roles of G protein subunits in transmembrane signalling. *Nature*, *333*(6169), 129-134.

Nehmé, R., Carpenter, B., Singhal, A., Strege, A., Edwards, P. C., White, C. F., ... & Tate, C. G. (2017). Mini-G proteins: Novel tools for studying GPCRs in their active conformation. *PloS one*, *12*(4), e0175642.

Ng, G. Y., O'Dowd, B. F., Caron, M., Dennis, M., Brann, M. R., & George, S. R. (1994). Phosphorylation and palmitoylation of the human D2L dopamine receptor in Sf9 cells. *Journal of neurochemistry*, *63*(5), 1589-1595.

Nguyen, M. N., Kiriazis, H., Ruggiero, D., Gao, X. M., Su, Y., Jian, A., ... & Du, X. J. (2015). Spontaneous ventricular tachyarrhythmias in β2-adrenoceptor transgenic mice in relation to cardiac interstitial fibrosis. *American Journal of Physiology-Heart and Circulatory Physiology*, *309*(5), H946-H957.

Niessen, K. V., Tattersall, J. E. H., Timperley, C. M., Bird, M., Green, C., Thiermann, H., & Worek, F. (2012). Competition radioligand binding assays for the investigation of bispyridinium compound affinities to the human muscarinic acetylcholine receptor subtype 5 (hM5). *Drug Testing and Analysis*, *4*(3-4), 292-297.

Nijmeijer, S., Vischer, H. F., Rosethorne, E. M., Charlton, S. J., & Leurs, R. (2012). Analysis of multiple histamine H4 receptor compound classes uncovers Gαi protein-and β-arrestin2-biased ligands. *Molecular pharmacology*, *82*(6), 1174-1182.

Nikolaev, V. O., Moshkov, A., Lyon, A. R., Miragoli, M., Novak, P., Paur, H., ... & Gorelik, J. (2010). β2-adrenergic receptor redistribution in heart failure changes cAMP compartmentation. *Science*, *327*(5973), 1653-1657.

Nobles, M., Benians, A., & Tinker, A. (2005). Heterotrimeric G proteins precouple with G protein-coupled receptors in living cells. *Proceedings of the National Academy of Sciences*, *102*(51), 18706-18711.

Noel, J. P., Hamm, H. E., & Sigler, P. B. (1993). The 2.2 Å crystal structure of transducin-α complexed with GTPγS. *Nature*, *366*(6456), 654-663.

Van Noord, J. A., Smeets, J. J., Custers, F. L. J., Korducki, L., & Cornelissen, P. J. G. (2002). Pharmacodynamic steady state of tiotropium in patients with chronic obstructive pulmonary disease. *European Respiratory Journal*, *19*(4), 639-644.

Norris, D. O., & Carr, J. A. (2020). *Vertebrate endocrinology*. Academic Press.

Núñez, S., Venhorst, J., & Kruse, C. G. (2012). Target–drug interactions: first principles and their application to drug discovery. *Drug discovery today*, *17*(1-2), 10-22.

O'Hayre, M., Eichel, K., Avino, S., Zhao, X., Steffen, D. J., Feng, X., ... & Gutkind, J. S. (2017). Genetic evidence that β-arrestins are dispensable for the initiation of β2-adrenergic receptor signaling to ERK. *Science signaling*, *10*(484), eaal3395.

Oakley, R. H., Laporte, S. A., Holt, J. A., Barak, L. S., & Caron, M. G. (1999). Association of β-arrestin with G protein-coupled receptors during clathrin-mediated endocytosis dictates the profile of receptor resensitization. *Journal of Biological Chemistry*, *274*(45), 32248-32257.

Oakley, R. H., Laporte, S. A., Holt, J. A., Caron, M. G., & Barak, L. S. (2000). Differential affinities of visual arrestin, βarrestin1, and βarrestin2 for G protein-coupled receptors delineate two major classes of receptors. *Journal of Biological Chemistry*, *275*(22), 17201-17210.

Oh-Hashi, K., Furuta, E., Fujimura, K., & Hirata, Y. (2017). Application of a novel HiBiT peptide tag for monitoring ATF4 protein expression in Neuro2a cells. *Biochemistry and biophysics reports*, *12*, 40-45.

Ohmuro-Matsuyama, Y., Chung, C. I., & Ueda, H. (2013). Demonstration of protein-fragment complementation assay using purified firefly luciferase fragments. *BMC biotechnology*, *13*(1), 1-9.

Okashah, N., Wan, Q., Ghosh, S., Sandhu, M., Inoue, A., Vaidehi, N., & Lambert, N. A. (2019). Variable G protein determinants of GPCR coupling selectivity. *Proceedings of the National Academy of Sciences*, *116*(24), 12054-12059.

Oldham, W. M., & Hamm, H. E. (2006). Structural basis of function in heterotrimeric G proteins. *Quarterly reviews of biophysics*, *39*(2), 117-166.

Oldham, W. M., & Hamm, H. E. (2008). Heterotrimeric G protein activation by G-protein-coupled receptors. *Nature reviews Molecular cell biology*, *9*(1), 60-71.

Pan, A. C., Borhani, D. W., Dror, R. O., & Shaw, D. E. (2013). Molecular determinants of drug–receptor binding kinetics. *Drug discovery today*, *18*(13-14), 667-673.

Park, P. S. H., Lodowski, D. T., & Palczewski, K. (2008). Activation of G protein–coupled receptors: beyond two-state models and tertiary conformational changes. *Annu. Rev. Pharmacol. Toxicol.*, *48*, 107-141.

Paronis, C. A., Chopda, G. R., Vemuri, K., Zakarian, A. S., Makriyannis, A., & Bergman, J. (2018). Long-lasting in vivo effects of the cannabinoid CB1 antagonist AM6538. *Journal of Pharmacology and Experimental Therapeutics*, *364*(3), 485-493.

Paulmurugan, R., Umezawa, Y., & Gambhir, S. S. (2002). Noninvasive imaging of protein–protein interactions in living subjects by using reporter protein complementation and reconstitution strategies. *Proceedings of the National Academy of Sciences*, *99*(24), 15608-15613.

Peach, C. J., Mignone, V. W., Arruda, M. A., Alcobia, D. C., Hill, S. J., Kilpatrick, L. E., & Woolard, J. (2018). Molecular pharmacology of VEGF-A isoforms: binding and signalling at VEGFR2. *International journal of molecular sciences*, *19*(4), 1264.

Peach, C. J., Kilpatrick, L. E., Woolard, J., & Hill, S. J. (2019). Comparison of the ligand-binding properties of fluorescent VEGF-A isoforms to VEGF receptor 2 in living cells and membrane preparations using NanoBRET. *British journal of pharmacology*, *176*(17), 3220-3235.

Peach, C. J., Kilpatrick, L. E., Woolard, J., & Hill, S. J. (2021). Use of NanoBiT and NanoBRET to monitor fluorescent VEGF-A binding kinetics to VEGFR2/NRP1 heteromeric complexes in living cells. *British Journal of Pharmacology*, *178*(12), 2393-2411.

Pedersen, M. H., Pham, J., Mancebo, H., Inoue, A., Asher, W. B., & Javitch, J. A. (2021). A novel luminescence-based β-arrestin recruitment assay for unmodified receptors. *Journal of Biological Chemistry*, *296*.

Peercy, B. E., Sherman, A. S., & Bertram, R. (2015). Modeling of glucose-induced cAMP oscillations in pancreatic β cells: cAMP rocks when metabolism rolls. *Biophysical journal*, *109*(2), 439-449.

Peterson, Y. K., & Luttrell, L. M. (2017). The diverse roles of arrestin scaffolds in G protein–coupled receptor signaling. *Pharmacological reviews*, *69*(3), 256-297.

Pierce, K. L., Premont, R. T., & Lefkowitz, R. J. (2002). Seven-transmembrane receptors. *Nature reviews Molecular cell biology*, *3*(9), 639-650.

Pihlavisto, M., Sjöholm, B., Scheinin, M., & Wurster, S. (1998). Modulation of agonist binding to recombinant human α2-adrenoceptors by sodium ions. *Biochimica et Biophysica Acta (BBA)-Molecular Cell Research*, *1448*(1), 135-146.

Purcell, R. H., Toro, C., Gahl, W. A., & Hall, R. A. (2017). A disease-associated mutation in the adhesion GPCR BAI2 (ADGRB2) increases receptor signaling activity. *Human mutation*, *38*(12), 1751-1760.

Qian, M., Vasudevan, L., Huysentruyt, J., Risseeuw, M. D., Stove, C., Vanderheyden, P. M., ... & Van Calenbergh, S. (2018). Design, synthesis, and biological evaluation of bivalent ligands targeting Dopamine D2-Like Receptors and the μ-Opioid Receptor. *ChemMedChem*, *13*(9), 944-956.

Raehal, K. M., Schmid, C. L., Groer, C. E., & Bohn, L. M. (2011). Functional selectivity at the μ-opioid receptor: implications for understanding opioid analgesia and tolerance. *Pharmacological reviews*, *63*(4), 1001-1019.

Rankovic, Z., Brust, T. F., & Bohn, L. M. (2016). Biased agonism: An emerging paradigm in GPCR drug discovery. *Bioorganic & medicinal chemistry letters*, *26*(2), 241-250.

Rasmussen, S. G., Choi, H. J., Rosenbaum, D. M., Kobilka, T. S., Thian, F. S., Edwards, P. C., ... & Kobilka, B. K. (2007). Crystal structure of the human β2 adrenergic G-protein-coupled receptor. *Nature*, *450*(7168), 383-387.

Rasmussen, S. G., Choi, H. J., Fung, J. J., Pardon, E., Casarosa, P., Chae, P. S., ... & Kobilka, B. K. (2011a). Structure of a nanobody-stabilized active state of the β2 adrenoceptor. *Nature*, *469*(7329), 175-180.

Rasmussen, S. G., DeVree, B. T., Zou, Y., Kruse, A. C., Chung, K. Y., Kobilka, T. S., ... & Kobilka, B. K. (2011b). Crystal structure of the β2 adrenergic receptor–Gs protein complex. *Nature*, *477*(7366), 549-555.

Rasmussen, S. G., Jensen, A. D., Liapakis, G., Ghanouni, P., Javitch, J. A., & Gether, U. (1999). Mutation of a highly conserved aspartic acid in the β2 adrenergic receptor: constitutive activation, structural instability, and conformational rearrangement of transmembrane segment 6. *Molecular pharmacology*, *56*(1), 175-184.

Regan, D., Williams, J., Borri, P., & Langbein, W. (2019). Lipid bilayer thickness measured by quantitative DIC reveals phase transitions and effects of substrate hydrophilicity. *Langmuir*, *35*(43), 13805-13814.

Reinartz, M. T., Kälble, S., Littmann, T., Ozawa, T., Dove, S., Kaever, V., ... & Seifert, R. (2015). Structure-bias relationships for fenoterol stereoisomers in six molecular and cellular assays at the β2-adrenoceptor. *Naunyn-Schmiedeberg's archives of pharmacology*, *388*(1), 51-65.

Remy, I., & Michnick, S. W. (2006). A highly sensitive protein-protein interaction assay based on Gaussia luciferase. *Nature methods*, *3*(12), 977-979.

Rengo, G., Zincarelli, C., Femminella, G. D., Liccardo, D., Pagano, G., De Lucia, C., ... & Leosco, D. (2012). Myocardial β2-adrenoceptor gene delivery promotes coordinated cardiac adaptive remodelling and angiogenesis in heart failure. *British journal of pharmacology*, *166*(8), 2348-2361.

Reyes-Alcaraz, A., Lee, Y. N., Yun, S., Hwang, J. I., & Seong, J. Y. (2018). Conformational signatures in β-arrestin2 reveal natural biased agonism at a G-protein-coupled receptor. *Communications biology*, *1*(1), 1-12.

Ribrault, C., Sekimoto, K., & Triller, A. (2011). From the stochasticity of molecular processes to the variability of synaptic transmission. *Nature Reviews Neuroscience*, *12*(7), 375-387.

Riddy, D. M., Valant, C., Rueda, P., Charman, W. N., Sexton, P. M., Summers, R. J., ... & Langmead, C. J. (2015). Label-free kinetics: exploiting functional hemi-equilibrium to derive rate constants for muscarinic receptor antagonists. *Molecular Pharmacology*, *88*(4), 779-790.

Ring, A. M., Manglik, A., Kruse, A. C., Enos, M. D., Weis, W. I., Garcia, K. C., & Kobilka, B. K. (2013). Adrenaline-activated structure of β2-adrenoceptor stabilized by an engineered nanobody. *Nature*, *502*(7472), 575-579.

Ritter, S. L., & Hall, R. A. (2009). Fine-tuning of GPCR activity by receptor-interacting proteins. *Nature reviews Molecular cell biology*, *10*(12), 819-830.

Roberts, D. J., Lin, H., & Strange, P. G. (2004). Mechanisms of agonist action at D2 dopamine receptors. *Molecular pharmacology*, *66*(6), 1573-1579.

Robishaw, J. D., & Berlot, C. H. (2004). Translating G protein subunit diversity into functional specificity. *Current opinion in cell biology*, *16*(2), 206-209.

Rose, R. H., Briddon, S. J., & Holliday, N. D. (2010). Bimolecular fluorescence complementation: lighting up seven transmembrane domain receptor signalling networks. *British journal of pharmacology*, *159*(4), 738-750.

Rosenbaum, D. M., Cherezov, V., Hanson, M. A., Rasmussen, S. G., Thian, F. S., Kobilka, T. S., ... & Kobilka, B. K. (2007). GPCR engineering yields high-resolution structural insights into β2-adrenergic receptor function. *science*, *318*(5854), 1266-1273.

Rosenbaum, D. M., Zhang, C., Lyons, J. A., Holl, R., Aragao, D., Arlow, D. H., ... & Kobilka, B. K. (2011). Structure and function of an irreversible agonist-β2 adrenoceptor complex. *Nature*, *469*(7329), 236-240.

Rosenbaum, D. M., Rasmussen, S. G., & Kobilka, B. K. (2009). The structure and function of G-protein-coupled receptors. *Nature*, *459*(7245), 356-363.

Rosethorne, E. M., Bradley, M. E., Gherbi, K., Sykes, D. A., Sattikar, A., Wright, J. D., ... & Charlton, S. J. (2016). Long receptor residence time of C26 contributes to super agonist activity at the human β2 ADrenoceptor. *Molecular Pharmacology*, *89*(4), 467-475.

Rosier, N., Grätz, L., Schihada, H., Möller, J., Işbilir, A., Humphrys, L. J., ... & Pockes, S. (2021). A Versatile Sub-Nanomolar Fluorescent Ligand Enables NanoBRET Binding Studies and Single-Molecule Microscopy at the Histamine H3 Receptor. *Journal of Medicinal Chemistry*, *64*(15), 11695-11708.

Rößler, P., Mayer, D., Tsai, C. J., Veprintsev, D. B., Schertler, G. F., & Gossert, A. D. (2020). GPCR activation states induced by nanobodies and mini-G proteins compared by NMR spectroscopy. *Molecules*, *25*(24), 5984.

Rovati, G. E., Capra, V., Shaw, V. S., Malik, R. U., Sivaramakrishnan, S., & Neubig, R. R. (2017). The DRY motif and the four corners of the cubic ternary complex model. *Cellular Signalling*, *35*, 16-23.

Samama, P., Cotecchia, S., Costa, T., & Lefkowitz, R. J. (1993). A mutation-induced activated state of the beta 2-adrenergic receptor. Extending the ternary complex model. *Journal of Biological Chemistry*, *268*(7), 4625-4636.

Samama, P., Pei, G., Costa, T., Cotecchia, S., & Lefkowitz, R. J. (1994). Negative antagonists promote an inactive conformation of the beta 2-adrenergic receptor. *Molecular pharmacology*, *45*(3), 390-394.

Sandoval, A., Eichler, S., Madathil, S., Reeves, P. J., Fahmy, K., & Böckmann, R. A. (2016). The molecular switching mechanism at the conserved D (E) RY motif in class-A GPCRs. *Biophysical journal*, *111*(1), 79-89.

Sassone-Corsi, P. (2012). The cyclic AMP pathway. *Cold Spring Harbor perspectives in biology*, *4*(12), a011148.

Scheer, A., Fanelli, F., Costa, T., De Benedetti, P. G., & Cotecchia, S. (1996). Constitutively active mutants of the alpha 1B-adrenergic receptor: role of highly conserved polar amino acids in receptor activation. *The EMBO Journal*, *15*(14), 3566-3578.

Schiele, F., Ayaz, P., & Fernández-Montalván, A. (2015). A universal homogeneous assay for high-throughput determination of binding kinetics. *Analytical biochemistry*, *468*, 42-49.

Schiffmann, A., & Gimpl, G. (2018). Sodium functions as a negative allosteric modulator of the oxytocin receptor. *Biochimica et Biophysica Acta (BBA)-Biomembranes*, *1860*(6), 1301-1308.

Schmidtke, P., Luque, F. J., Murray, J. B., & Barril, X. (2011). Shielded hydrogen bonds as structural determinants of binding kinetics: application in drug design. *Journal of the American Chemical Society*, *133*(46), 18903-18910.

Scholes, G. D. (2003). Long-range resonance energy transfer in molecular systems. *Annual review of physical chemistry*, *54*(1), 57-87.

Schreiber, G., & Fersht, A. R. (1996). Rapid, electrostatically assisted association of proteins. *Nature structural biology*, *3*(5), 427-431.

Schuetz, D. A., Richter, L., Amaral, M., Grandits, M., Grädler, U., Musil, D., ... & Ecker, G. F. (2018). Ligand desolvation steers on-rate and impacts drug residence time of heat shock protein 90 (Hsp90) inhibitors. *Journal of Medicinal Chemistry*, *61*(10), 4397-4411.

Schwartz, T. W., Frimurer, T. M., Holst, B., Rosenkilde, M. M., & Elling, C. E. (2006). Molecular mechanism of 7TM receptor activation—a global toggle switch model. *Annu. Rev. Pharmacol. Toxicol.*, *46*, 481-519.

Scimemi, A., & Beato, M. (2009). Determining the neurotransmitter concentration profile at active synapses. *Molecular neurobiology*, *40*(3), 289-306.

Scola, A. M., Loxham, M., Charlton, S. J., & Peachell, P. T. (2009). The long-acting β-adrenoceptor agonist, indacaterol, inhibits IgE-dependent responses of human lung mast cells. *British journal of pharmacology*, *158*(1), 267-276.

Seifert, R., Lee, T. W., Lam, V. T., & Kobilka, B. K. (1998). Reconstitution of β2-adrenoceptor−GTP-binding-protein interaction in Sf9 cells: High coupling efficiency in a β2-adrenoceptor-Gsα fusion protein. *European journal of biochemistry*, *255*(2), 369-382.

Seifert, R., Gether, U., Wenzel-Seifert, K., & Kobilka, B. K. (1999). Effects of guanine, inosine, and xanthine nucleotides on β2-adrenergic receptor/Gs interactions: evidence for multiple receptor conformations. *Molecular Pharmacology*, *56*(2), 348-358.

Selley, D. E., Sim, L. J., Xiao, R., Liu, Q., & Childers, S. R. (1997). μ-Opioid receptor-stimulated guanosine-5'-O-(γ-thio)-triphosphate binding in rat thalamus and cultured cell lines: signal transduction mechanisms underlying agonist efficacy. *Molecular pharmacology*, *51*(1), 87-96.

Sengmany, K., Singh, J., Stewart, G. D., Conn, P. J., Christopoulos, A., & Gregory, K. J. (2017). Biased allosteric agonism and modulation of metabotropic glutamate receptor 5: Implications for optimizing preclinical neuroscience drug discovery. *Neuropharmacology*, *115*, 60-72.

Sergeev, E., Hansen, A. H., Bolognini, D., Kawakami, K., Kishi, T., Aoki, J., ... & Milligan, G. (2017). A single extracellular amino acid in Free Fatty Acid Receptor 2 defines antagonist species selectivity and G protein selection bias. *Scientific reports*, *7*(1), 1-15.

Shao, Z., Yin, J., Chapman, K., Grzemska, M., Clark, L., Wang, J., & Rosenbaum, D. M. (2016). High-resolution crystal structure of the human CB1 cannabinoid receptor. *Nature*, *540*(7634), 602-606.

Shea, L., & Linderman, J. J. (1997). Mechanistic model of G-protein signal transduction determinants of efficacy and effect of precoupled receptors. *Biochemical pharmacology*, *53*(4), 519-530.

Shenoy, S. K., Drake, M. T., Nelson, C. D., Houtz, D. A., Xiao, K., Madabushi, S., ... & Lefkowitz, R. J. (2006). β-Arrestin-dependent, G protein-independent ERK1/2 activation by the β2 adrenergic receptor. *Journal of Biological Chemistry*, *281*(2), 1261-1273.

Shiina, T., Kawasaki, A., Nagao, T., & Kurose, H. (2000). Interaction with β-arrestin determines the difference in internalization behavior between β1-and β2-adrenergic receptors. *Journal of Biological Chemistry*, *275*(37), 29082-29090.

Shukla, A. K., Singh, G., & Ghosh, E. (2014). Emerging structural insights into biased GPCR signaling. *Trends in biochemical sciences*, *39*(12), 594-602.

Simon, M. I., Strathmann, M. P., & Gautam, N. (1991). Diversity of G proteins in signal transduction. *Science*, *252*(5007), 802-808.

Slack, R. J., & Hall, D. A. (2012). Development of operational models of receptor activation including constitutive receptor activity and their use to determine the efficacy of the chemokine CCL17 at the CC chemokine receptor CCR4. *British journal of pharmacology*, *166*(6), 1774-1792.

Smith, J. S., & Rajagopal, S. (2016). The β-arrestins: multifunctional regulators of G protein-coupled receptors. *Journal of Biological Chemistry*, *291*(17), 8969-8977.

Smith, J. S., Lefkowitz, R. J., & Rajagopal, S. (2018). Biased signalling: from simple switches to allosteric microprocessors. *Nature reviews Drug discovery*, *17*(4), 243-260.

Soave, M., Heukers, R., Kellam, B., Woolard, J., Smit, M. J., Briddon, S. J., & Hill, S. J. (2020). Monitoring allosteric interactions with CXCR4 using NanoBiT conjugated nanobodies. *Cell chemical biology*, *27*(10), 1250-1261.

Soave, M., Kellam, B., Woolard, J., Briddon, S. J., & Hill, S. J. (2020). NanoBiT complementation to monitor agonist-induced adenosine A1 receptor internalization. *SLAS DISCOVERY: Advancing the Science of Drug Discovery*, *25*(2), 186-194.

Soergel, D. G., Subach, R. A., Burnham, N., Lark, M. W., James, I. E., Sadler, B. M., ... & Webster, L. R. (2014). Biased agonism of the μ-opioid receptor by TRV130 increases analgesia and reduces on-target adverse effects versus morphine: a randomized, double-blind, placebo-controlled, crossover study in healthy volunteers. *PAIN®*, *155*(9), 1829-1835.

Sorkin, A., & Von Zastrow, M. (2009). Endocytosis and signalling: intertwining molecular networks. *Nature reviews Molecular cell biology*, *10*(9), 609-622.

Sparre-Ulrich, A. H., Hansen, L. S., Svendsen, B., Christensen, M., Knop, F. K., Hartmann, B., ... & Rosenkilde, M. M. (2016). Species-specific action of (Pro3) GIP–A full agonist at human GIP receptors, but a partial agonist and competitive antagonist at rat and mouse GIP receptors. *British journal of pharmacology*, *173*(1), 27-38.

Sposini, S., & Hanyaloglu, A. C. (2017). Spatial encryption of G protein-coupled receptor signaling in endosomes; Mechanisms and applications. *Biochemical pharmacology*, *143*, 1-9.

Sprang, S. R. (1997). G protein mechanisms: insights from structural analysis. *Annual review of biochemistry*, *66*(1), 639-678.

Stefan, E., Aquin, S., Berger, N., Landry, C. R., Nyfeler, B., Bouvier, M., & Michnick, S. W. (2007). Quantification of dynamic protein complexes using Renilla luciferase fragment complementation applied to protein kinase A activities in vivo. *Proceedings of the National Academy of Sciences*, *104*(43), 16916-16921.

Stephenson, R. P. (1956). A modification of receptor theory. *British journal of pharmacology and chemotherapy*, *11*(4), 379.

Steyaert, J., & Kobilka, B. K. (2011). Nanobody stabilization of G protein-coupled receptor conformational states. *Current opinion in structural biology*, *21*(4), 567-572.

Stoddart, L. A., Johnstone, E. K., Wheal, A. J., Goulding, J., Robers, M. B., Machleidt, T., ... & Pfleger, K. D. (2015). Application of BRET to monitor ligand binding to GPCRs. *Nature methods*, *12*(7), 661-663.

Stoddart, L. A., White, C. W., Nguyen, K., Hill, S. J., & Pfleger, K. D. (2016). Fluorescence-and bioluminescence-based approaches to study GPCR ligand binding. *British journal of pharmacology*, *173*(20), 3028-3037.

Stoddart, L. A., Kilpatrick, L. E., & Hill, S. J. (2018). NanoBRET approaches to study ligand binding to GPCRs and RTKs. *Trends in pharmacological sciences*, *39*(2), 136-147.

Storme, J., Cannaert, A., Van Craenenbroeck, K., & Stove, C. P. (2018). Molecular dissection of the human A3 adenosine receptor coupling with β-arrestin2. *Biochemical pharmacology*, *148*, 298-307.

Stott, L. A., Hall, D. A., & Holliday, N. D. (2016). Unravelling intrinsic efficacy and ligand bias at G protein coupled receptors: A practical guide to assessing functional data. *Biochemical pharmacology*, *101*, 1-12.

Strasser, R. H., Sibley, D. R., & Lefkowitz, R. J. (1986). A novel catecholamine-activated adenosine cyclic 3', 5'-phosphate independent pathway for. beta.-adrenergic receptor phosphorylation in wild-type and mutant S49 lymphoma cells: mechanism of homologous desensitization of adenylate cyclase. *Biochemistry*, *25*(6), 1371-1377.

Stryer, L. (1978). Fluorescence energy transfer as a spectroscopic ruler. *Annual review of biochemistry*, *47*(1), 819-846.

Stryer, L., & Haugland, R. P. (1967). Energy transfer: a spectroscopic ruler. *Proceedings of the National Academy of Sciences of the United States of America*, *58*(2), 719.

Suen, J. Y., Cotterell, A., Lohman, R. J., Lim, J., Han, A., Yau, M. K., ... & Fairlie, D. (2014). Pathway-selective antagonism of proteinase activated receptor 2. *British journal of pharmacology*, *171*(17), 4112-4124.

Suzuki, T., Nguyen, C. T., Nantel, F., Bonin, H., Valiquette, M., Frielle, T., & Bouvier, M. (1992). Distinct regulation of beta 1-and beta 2-adrenergic receptors in Chinese hamster fibroblasts. *Molecular pharmacology*, *41*(3), 542-548.

Swaminath, G., Xiang, Y., Lee, T. W., Steenhuis, J., Parnot, C., & Kobilka, B. K. (2004). Sequential binding of agonists to the β2 adrenoceptor: kinetic evidence for intermediate conformational states. *Journal of Biological Chemistry*, *279*(1), 686-691.

Swaminath, G., Deupi, X., Lee, T. W., Zhu, W., Thian, F. S., Kobilka, T. S., & Kobilka, B. (2005). Probing the β2 adrenoceptor binding site with catechol reveals differences in binding and activation by agonists and partial agonists. *Journal of Biological Chemistry*, *280*(23), 22165-22171.

C Swinney, D., A Haubrich, B., Van Liefde, I., & Vauquelin, G. (2015). The role of binding kinetics in GPCR drug discovery. *Current Topics in Medicinal Chemistry*, *15*(24), 2504-2522.

Sykes, D. A., Dowling, M. R., Leighton-Davies, J., Kent, T. C., Fawcett, L., Renard, E., ... & Charlton, S. J. (2012). The influence of receptor kinetics on the onset and duration of action and the therapeutic index of NVA237 and tiotropium. *Journal of Pharmacology and Experimental Therapeutics*, *343*(2), 520-528.

Sykes, D. A., Parry, C., Reilly, J., Wright, P., Fairhurst, R. A., & Charlton, S. J. (2014). Observed drug-receptor association rates are governed by membrane affinity: the importance of establishing "micro-pharmacokinetic/pharmacodynamic relationships" at the β2-adrenoceptor. *Molecular pharmacology*, *85*(4), 608-617.

Sykes, D. A., Bradley, M. E., Riddy, D. M., Willard, E., Reilly, J., Miah, A., ... & Charlton, S. J. (2016). Fevipiprant (QAW039), a slowly dissociating CRTh2 antagonist with the potential for improved clinical efficacy. *Molecular pharmacology*, *89*(5), 593-605.

Sykes, D. A., Moore, H., Stott, L., Holliday, N., Javitch, J. A., Lane, J. R., & Charlton, S. J. (2017). Extrapyramidal side effects of antipsychotics are linked to their association kinetics at dopamine D2 receptors. *Nature communications*, *8*(1), 1-11.

Sykes, D. A., Stoddart, L. A., Kilpatrick, L. E., & Hill, S. J. (2019). Binding kinetics of ligands acting at GPCRs. *Molecular and cellular endocrinology*, *485*, 9-19.

Grünewald, S., Haase, W., Reiländer, H., & Michel, H. (1996). Glycosylation, palmitoylation, and localization of the human D2S receptor in baculovirus-infected insect cells. *Biochemistry*, *35*(48), 15149-15161.

Szabo, M., Klein Herenbrink, C., Christopoulos, A., Lane, J. R., & Capuano, B. (2014). Structure–activity relationships of privileged structures lead to the discovery of novel biased ligands at the dopamine D2 receptor. *Journal of medicinal chemistry*, *57*(11), 4924-4939.

Szpakowska, M., Nevins, A. M., Meyrath, M., Rhainds, D., D'huys, T., Guité-Vinet, F., ... & Chevigné, A. (2018). Different contributions of chemokine N-terminal features attest to a different ligand binding mode and a bias towards activation of ACKR3/CXCR7 compared with CXCR4 and CXCR3. *British journal of pharmacology*, *175*(9), 1419-1438..

Taylor, S. S., Ilouz, R., Zhang, P., & Kornev, A. P. (2012). Assembly of allosteric macromolecular switches: lessons from PKA. *Nature reviews Molecular cell biology*, *13*(10), 646-658.

Tehan, B. G., Bortolato, A., Blaney, F. E., Weir, M. P., & Mason, J. S. (2014). Unifying family A GPCR theories of activation. *Pharmacology & therapeutics*, *143*(1), 51-60.

Teitler, M., Toohey, N., Knight, J. A., Klein, M. T., & Smith, C. (2010). Clozapine and other competitive antagonists reactivate risperidone-inactivated h5-HT7 receptors: radioligand binding and functional evidence for GPCR homodimer protomer interactions. *Psychopharmacology*, *212*(4), 687-697.

Tevaearai, H. T. (2002). Eckhart AD, Walton GB, Keys JR, Wilson K, Koch WJ. *Myocardial gene transfer and overexpression of beta2-adrenergic receptors potentiates the functional recovery of unloaded failing hearts. Circulation*, *106*, 124-129.

Tewson, P., Westenberg, M., Zhao, Y., Campbell, R. E., Quinn, A. M., & Hughes, T. E. (2012). Simultaneous detection of Ca2+ and diacylglycerol signaling in living cells.

Thompson, G. L., Lane, J. R., Coudrat, T., Sexton, P. M., Christopoulos, A., & Canals, M. (2015). Biased agonism of endogenous opioid peptides at the μ-opioid receptor. *Molecular pharmacology*, *88*(2), 335-346.

Thompson, G. L., Lane, J. R., Coudrat, T., Sexton, P. M., Christopoulos, A., & Canals, M. (2016). Systematic analysis of factors influencing observations of biased agonism at the mu-opioid receptor. *Biochemical pharmacology*, *113*, 70-87.

Thorsen, T. S., Matt, R., Weis, W. I., & Kobilka, B. K. (2014). Modified T4 lysozyme fusion proteins facilitate G protein-coupled receptor crystallogenesis. *Structure*, *22*(11), 1657-1664.

Tian, W. N., Duzic, E., Lanier, S. M., & Deth, R. C. (1994). Determinants of alpha 2-adrenergic receptor activation of G proteins: evidence for a precoupled receptor/G protein state. *Molecular pharmacology*, *45*(3), 524-531.

Trzaskowski, B., Latek, D., Yuan, S., Ghoshdastider, U., Debinski, A., & Filipek, S. (2012). Action of molecular switches in GPCRs-theoretical and experimental studies. *Current medicinal chemistry*, *19*(8), 1090-1109.

Tsai, C. J., Pamula, F., Nehmé, R., Mühle, J., Weinert, T., Flock, T., ... & Schertler, G. F. (2018). Crystal structure of rhodopsin in complex with a mini-Go sheds light on the principles of G protein selectivity. *Science advances*, *4*(9), eaat7052.

Tschammer, N., Bollinger, S., Kenakin, T., & Gmeiner, P. (2011). Histidine 6.55 is a major determinant of ligand-biased signaling in dopamine D2L receptor. *Molecular pharmacology*, *79*(3), 575-585.

Unett, D. J., Gatlin, J., Anthony, T. L., Buzard, D. J., Chang, S., Chen, C., ... & Gaidarov, I. (2013). Kinetics of 5-HT2B receptor signaling: profound agonist-dependent effects on signaling onset and duration. *Journal of Pharmacology and Experimental Therapeutics*, *347*(3), 645-659.

Unsicker, K., Huber, K., Schütz, G., & Kalcheim, C. (2005). The chromaffin cell and its development. *Neurochemical research*, *30*(6), 921-925.

Urban, J. D., Vargas, G. A., Von Zastrow, M., & Mailman, R. B. (2007). Aripiprazole has functionally selective actions at dopamine D2 receptor-mediated signaling pathways. *Neuropsychopharmacology*, *32*(1), 67-77.

Urban, J. D., Clarke, W. P., Von Zastrow, M., Nichols, D. E., Kobilka, B., Weinstein, H., ... & Mailman, R. B. (2007). Functional selectivity and classical concepts of quantitative pharmacology. *Journal of Pharmacology and Experimental Therapeutics*, *320*(1), 1-13.

Valentin-Hansen, L., Groenen, M., Nygaard, R., Frimurer, T. M., Holliday, N. D., & Schwartz, T. W. (2012). The arginine of the DRY motif in transmembrane segment III functions as a balancing micro-switch in the activation of the β2-adrenergic receptor. *Journal of Biological Chemistry*, *287*(38), 31973-31982.

Vauquelin, G. (2010). Rebinding: or why drugs may act longer in vivo than expected from their in vitro target residence time. *Expert opinion on drug discovery*, *5*(10), 927-941.

Vauquelin, G., Bostoen, S., Vanderheyden, P., & Seeman, P. (2012). Clozapine, atypical antipsychotics, and the benefits of fast-off D2 dopamine receptor antagonism. *Naunyn-Schmiedeberg's archives of pharmacology*, *385*(4), 337-372.

Vauquelin, G. (2016). Effects of target binding kinetics on in vivo drug efficacy: koff, kon and rebinding. *British journal of pharmacology*, *173*(15), 2319-2334.

Vauquelin, G., & Charlton, S. J. (2010). Long-lasting target binding and rebinding as mechanisms to prolong in vivo drug action. *British journal of pharmacology*, *161*(3), 488-508.

Vauquelin, G., & Van Liefde, I. (2006). Slow antagonist dissociation and long-lasting in vivo receptor protection. *Trends in pharmacological sciences*, *27*(7), 355-359.

Vauquelin, G., Van Liefde, I., & Vanderheyden, P. (2002). Models and methods for studying insurmountable antagonism. *Trends in pharmacological sciences*, *23*(11), 514-518.

Vauquelin, G., & Packeu, A. (2009). Ligands, their receptors and… plasma membranes. *Molecular and cellular endocrinology*, *311*(1-2), 1-10.

Vauquelin, G., & Szczuka, A. (2007). Kinetic versus allosteric mechanisms to explain insurmountable antagonism and delayed ligand dissociation. *Neurochemistry international*, *51*(5), 254-260.

van der Velden, W. J., Smit, F. X., Christiansen, C. B., Møller, T. C., Hjortø, G. M., Larsen, O., ... & Rosenkilde, M. M. (2021). GLP-1 Val8: A Biased GLP-1R Agonist with Altered Binding Kinetics and Impaired Release of Pancreatic Hormones in Rats. *ACS pharmacology & translational science*, *4*(1), 296-313.

Roesch, E. A., Nichols, D. P., & Chmiel, J. F. (2018). Inflammation in cystic fibrosis: An update. *Pediatric pulmonology*, *53*(S3), S30-S50.

Vernall, A. J., Hill, S. J., & Kellam, B. (2014). The evolving small-molecule fluorescent-conjugate toolbox for C lass A GPCRs. *British journal of pharmacology*, *171*(5), 1073-1084.

Vilardaga, J. P., Bünemann, M., Krasel, C., Castro, M., & Lohse, M. J. (2003). Measurement of the millisecond activation switch of G protein–coupled receptors in living cells. *Nature biotechnology*, *21*(7), 807-812.

Chavatte, L., Brown, B. A., & Driscoll, D. M. (2005). Ribosomal protein L30 is a component of the UGA-selenocysteine recoding machinery in eukaryotes. *Nature structural & molecular biology*, *12*(5), 408-416.

Villalobos, V., Naik, S., Bruinsma, M., Dothager, R. S., Pan, M. H., Samrakandi, M., ... & Piwnica-Worms, D. (2010). Dual-color click beetle luciferase heteroprotein fragment complementation assays. *Chemistry & biology*, *17*(9), 1018-1029.

Violin, J. D., Ren, X. R., & Lefkowitz, R. J. (2006). G-protein-coupled receptor kinase specificity for β-arrestin recruitment to the β2-adrenergic receptor revealed by fluorescence resonance energy transfer. *Journal of Biological Chemistry*, *281*(29), 20577-20588.

Wacker, D., Fenalti, G., Brown, M. A., Katritch, V., Abagyan, R., Cherezov, V., & Stevens, R. C. (2010). Conserved binding mode of human β2 adrenergic receptor inverse agonists and antagonist revealed by X-ray crystallography. *Journal of the American Chemical Society*, *132*(33), 11443-11445.

Wacker, D., Stevens, R. C., & Roth, B. L. (2017). How ligands illuminate GPCR molecular pharmacology. *Cell*, *170*(3), 414-427.

Walker, C. S., Raddant, A. C., Woolley, M. J., Russo, A. F., & Hay, D. L. (2018). CGRP receptor antagonist activity of olcegepant depends on the signalling pathway measured. *Cephalalgia*, *38*(3), 437-451.

Wan, Q., Okashah, N., Inoue, A., Nehmé, R., Carpenter, B., Tate, C. G., & Lambert, N. A. (2018). Mini G protein probes for active G protein–coupled receptors (GPCRs) in live cells. *Journal of Biological Chemistry*, *293*(19), 7466-7473.

Wang, M., Zhang, S., Zheng, G., Huang, J., Songyang, Z., Zhao, X., & Lin, X. (2018). Gain-of-function mutation of Card14 leads to spontaneous psoriasis-like skin inflammation through enhanced keratinocyte response to IL-17A. *Immunity*, *49*(1), 66-79.

Warne, T., Edwards, P. C., Doré, A. S., Leslie, A. G., & Tate, C. G. (2019). Molecular basis for high-affinity agonist binding in GPCRs. *Science*, *364*(6442), 775-778.

Warne, T., & Tate, C. G. (2013). The importance of interactions with helix 5 in determining the efficacy of β-adrenoceptor ligands. *Biochemical Society Transactions*, *41*(1), 159-165.

Watson, S. J., Brown, A. J., & Holliday, N. D. (2012). Differential signaling by splice variants of the human free fatty acid receptor GPR120. *Molecular pharmacology*, *81*(5), 631-642.

Wei, H., Ahn, S., Shenoy, S. K., Karnik, S. S., Hunyady, L., Luttrell, L. M., & Lefkowitz, R. J. (2003). Independent β-arrestin 2 and G protein-mediated pathways for angiotensin II activation of extracellular signal-regulated kinases 1 and 2. *Proceedings of the National Academy of Sciences*, *100*(19), 10782-10787.

Wei, X. F., Gan, C. Y., Cui, J., Luo, Y. Y., Cai, X. F., Yuan, Y., ... & Hu, J. L. (2018). Identification of compounds targeting hepatitis B virus core protein dimerization through a split luciferase complementation assay. *Antimicrobial agents and chemotherapy*, *62*(12), e01302-18.

Weis, W. I., & Kobilka, B. K. (2018). The molecular basis of G protein–coupled receptor activation. *Annual review of biochemistry*, *87*, 897-919.

Weiss, J. M., Morgan, P. H., Lutz, M. W., & Kenakin, T. P. (1996). The cubic ternary complex receptor–occupancy model I. Model description. *Journal of theoretical biology*, *178*(2), 151-167.

Wess, J. (1998). Molecular basis of receptor/G-protein-coupling selectivity. *Pharmacology & therapeutics*, *80*(3), 231-264.

Westfield, G. H., Rasmussen, S. G., Su, M., Dutta, S., DeVree, B. T., Chung, K. Y., ... & Skiniotis, G. (2011). Structural flexibility of the Gαs α-helical domain in the β2-adrenoceptor Gs complex. *Proceedings of the National Academy of Sciences*, *108*(38), 16086-16091.

van der Westhuizen, E. T., Breton, B., Christopoulos, A., & Bouvier, M. (2014). Quantification of ligand bias for clinically relevant β2-adrenergic receptor ligands: implications for drug taxonomy. *Molecular pharmacology*, *85*(3), 492-509.

White, C. W., Caspar, B., Vanyai, H. K., Pfleger, K. D., & Hill, S. J. (2020). CRISPR-mediated protein tagging with nanoluciferase to investigate native chemokine receptor function and conformational changes. *Cell chemical biology*, *27*(5), 499-510.

Wilden, U., Hall, S. W., & Kühn, H. (1986). Phosphodiesterase activation by photoexcited rhodopsin is quenched when rhodopsin is phosphorylated and binds the intrinsic 48-kDa protein of rod outer segments. *Proceedings of the National Academy of Sciences*, *83*(5), 1174-1178.

Williams, J. T., Ingram, S. L., Henderson, G., Chavkin, C., von Zastrow, M., Schulz, S., ... & Christie, M. J. (2013). Regulation of μ-opioid receptors: desensitization, phosphorylation, internalization, and tolerance. *Pharmacological reviews*, *65*(1), 223-254.

Wingler, L. M., & Lefkowitz, R. J. (2020). Conformational basis of G protein-coupled receptor signaling versatility. *Trends in cell biology*, *30*(9), 736-747.

Wisler, J. W., DeWire, S. M., Whalen, E. J., Violin, J. D., Drake, M. T., Ahn, S., ... & Lefkowitz, R. J. (2007). A unique mechanism of β-blocker action: carvedilol stimulates β-arrestin signaling. *Proceedings of the National Academy of Sciences*, *104*(42), 16657-16662.

de Witte, W. E., Danhof, M., van der Graaf, P. H., & de Lange, E. C. (2016). In vivo target residence time and kinetic selectivity: the association rate constant as determinant. *Trends in pharmacological sciences*, *37*(10), 831-842.

de Witte, W. E. A., Vauquelin, G., van der Graaf, P. H., & de Lange, E. C. M. (2017). The influence of drug distribution and drug-target binding on target occupancy: the rate-limiting step approximation. *European Journal of Pharmaceutical Sciences*, *109*, S83-S89.

Woodroffe, P. J., Bridge, L. J., King, J. R., & Hill, S. J. (2009). Modelling the activation of G-protein coupled receptors by a single drug. *Mathematical biosciences*, *219*(1), 32-55.

Wright, S. C., Lukasheva, V., Le Gouill, C., Kobayashi, H., Breton, B., Mailhot-Larouche, S., ... & Bouvier, M. (2021). BRET-based effector membrane translocation assay monitors GPCR-promoted and endocytosis-mediated Gq activation at early endosomes. *Proceedings of the National Academy of Sciences*, *118*(20).

Xanthou, G., Williams, T. J., & Pease, J. E. (2003). Molecular characterization of the chemokine receptor CXCR3: evidence for the involvement of distinct extracellular domains in a multi-step model of ligand binding and receptor activation. *European journal of immunology*, *33*(10), 2927-2936.

Xia, L., de Vries, H., IJzerman, A. P., & Heitman, L. H. (2016). Scintillation proximity assay (SPA) as a new approach to determine a ligand's kinetic profile. A case in point for the adenosine A1 receptor. *Purinergic Signalling*, *12*(1), 115-126.

Xiao, R. P., Avdonin, P., Zhou, Y. Y., Cheng, H., Akhter, S. A., Eschenhagen, T., ... & Lakatta, E. G. (1999). Coupling of β2-adrenoceptor to Gi proteins and its physiological relevance in murine cardiac myocytes. *Circulation research*, *84*(1), 43-52.

Yano, H., Cai, N. S., Javitch, J. A., & Ferré, S. (2018). Luciferase complementation based-detection of G-protein-coupled receptor activity. *BioTechniques*, *65*(1), 9-14.

Yao, X., Parnot, C., Deupi, X., Ratnala, V. R., Swaminath, G., Farrens, D., & Kobilka, B. (2006). Coupling ligand structure to specific conformational switches in the β2-adrenoceptor. *Nature chemical biology*, *2*(8), 417-422.

Yao, X. Q., Malik, R. U., Griggs, N. W., Skjærven, L., Traynor, J. R., Sivaramakrishnan, S., & Grant, B. J. (2016). Dynamic coupling and allosteric networks in the α subunit of heterotrimeric G proteins. *Journal of Biological Chemistry*, *291*(9), 4742-4753.

Yao, X. J., Ruiz, G. V., Whorton, M. R., Rasmussen, S. G., DeVree, B. T., Deupi, X., ... & Kobilka, B. (2009). The effect of ligand efficacy on the formation and stability of a GPCR-G protein complex. *Proceedings of the National Academy of Sciences*, *106*(23), 9501-9506.

Yen, H. Y., Hoi, K. K., Liko, I., Hedger, G., Horrell, M. R., Song, W., ... & Robinson, C. V. (2018). PIP2 stabilises active states of GPCRs and enhances the selectivity. *Nature*, *559*.

Zeilinger, M., Pichler, F., Nics, L., Wadsak, W., Spreitzer, H., Hacker, M., & Mitterhauser, M. (2017). New approaches for the reliable in vitro assessment of binding affinity based on high-resolution real-time data acquisition of radioligand-receptor binding kinetics. *EJNMMI research*, *7*(1), 1-13.

Zhan, X., Kook, S., Gurevich, E. V., & Gurevich, V. V. (2014). Arrestin-dependent activation of JNK family kinases. In *Arrestins-Pharmacology and Therapeutic Potential* (pp. 259-280). Springer, Berlin, Heidelberg.

Zhang, D., Gao, Z. G., Zhang, K., Kiselev, E., Crane, S., Wang, J., ... & Wu, B. (2015). Two disparate ligand-binding sites in the human P2Y1 receptor. *Nature*, *520*(7547), 317-321.

Zhang, Q., Okamura, M., Guo, Z. D., Niwa, S., & Haga, T. (2004). Effects of partial agonists and Mg2+ ions on the interaction of M2 muscarinic acetylcholine receptor and G protein Gαi1 subunit in the M2-Gαi1 fusion protein. *Journal of biochemistry*, *135*(5), 589-596.

Zhang, R., & Xie, X. (2012). Tools for GPCR drug discovery. *Acta Pharmacologica Sinica*, *33*(3), 372-384.

Zhang, X., Stevens, R. C., & Xu, F. (2015). The importance of ligands for G protein-coupled receptor stability. *Trends in biochemical sciences*, *40*(2), 79-87.

Zhang, Y. L., Moran, S. P., Allen, A., Baez-Nieto, D., Xu, Q., Wang, L. A., ... & Pan, J. Q. (2022). Novel Fluorescence-Based High-Throughput FLIPR Assay Utilizing Membrane-Tethered Genetic Calcium Sensors to Identify T-Type Calcium Channel Modulators. *ACS Pharmacology & Translational Science*, *5*(3), 156-168.

Zhu, X., Finlay, D. B., Glass, M., & Duffull, S. B. (2019). Model-free and kinetic modelling approaches for characterising non-equilibrium pharmacological pathway activity: Internalisation of cannabinoid CB1 receptors. *British journal of pharmacology*, *176*(14), 2593-2607.

Zou, Y., Weis, W. I., & Kobilka, B. K. (2012). N-terminal T4 lysozyme fusion facilitates crystallization of a G protein coupled receptor.

Chapter IX: Professional Industrial Placement Reflective Statement

In February to April 2021, I spent 3 months on a research placement at OMass Therapeutics in Oxford, UK. There, I acted as a junior scientist based on a GPCR project under the supervision of Hsin Yung Yen, with day to day guidance given by Paarth Kapoor. The initial stage of my time at OMass was focused on training with protein engineering of both membrane and cytosolic proteins, advancing my knowledge beyond the training I experienced at the University Of Nottingham. This was followed by training and guidance in how to use native mass spectrometry to interrogate GPCR – cellular protein interactions.

I thoroughly enjoyed and thrived in the protein engineering department, working with both bacterial and insect expression system, and using tools that would not have been available to me at the University Of Nottingham, such as analytical size exclusion chromatography. I found the mass spectrometry highly challenging, which was compounded by a difficult project, and whilst I am glad I was given the opportunity to be exposed to the mass spectrometry techniques, I currently do not want to work as a mass spectrometry scientist. However, the exposure allowed for a greater appreciation of the techniques available and how they can be used in the GPCR research field.

The placement provided me with the opportunity to work within a drug discovery environment, driven by individual drug targets. The discussion with colleagues and within project meetings I attended allowed me to gain insight into the similarities and differences in how academia and industry approach drug discovery. I was excited to see that the company took a positive approach to collaborations, with the focus on the best way to access the suitable experimental expertise.

From the placement I was able to form connections with new scientists from within the protein engineering and mass spectrometry field, with whom I have maintained contact.

Due to the pandemic, I was required to adhere to a strict risk assessment set forward by the University Of Nottingham during my 3 month placement. This required me to live alone and restrict social contact other than the time spent at work. Whilst this was a challenging experience, I believe it provided an opportunity to focus on my career and my future aspirations and expectations following my doctoral completion.